THE PHYSICAL REVIEW

VOLUME 90 Second Series NUMBER 6

JUNE 15, 1953

Published for the

AMERICAN PHYSICAL SOCIETY

by the

AMERICAN INSTITUTE OF PHYSICS

LANCASTER, PA., AND NEW YORK, N. Y.

[illegible]

A journal of [illegible]

Published by the American Institute of [illegible]
for the

AMERICAN PHYSICAL SO[illegible]

Officers

President

Enrico Fermi
Institute for Nuclear Studies
University of Chicago
Chicago 37, Illinois

Vice-President

H. A. Bethe
Cornell University
Ithaca, New York

Secretary

K. K. Darrow
Bell Telephone Laboratories
Office:
Columbia University
New York 27, New York

Treasurer

G. B. Pegram
Columbia University
New York 27, New York

Local Secretary
for the Pacific Coast

J. Kaplan
University of California
Angeles
Los Angeles, California

Managing Editor

S. A. Goudsmit
Brookhaven National Laboratory
Upton, Long Island
New York

[illegible]

[illegible]

[illegible]

THE
PHYSICAL REVIEW

A journal of experimental and theoretical physics established by E. L. Nichols in 1893

SECOND SERIES, VOL. 90, NO. 6 JUNE 15, 1953

The Small Angle Scattering of X-Rays from Cold-Worked Solids

D. L. DEXTER
Institute of Optics, University of Rochester, Rochester, New York
(Received March 6, 1953)

The small angle scattering of x-rays or thermal neutrons from cold-worked crystals is calculated on the basis of two models, according to which the scattering arises predominantly from the density variation associated either with small cavities or with edge-type dislocations. The elastic distortions surrounding the cavities are unimportant, so that the scattering from cavities in a uniform medium of density n is the same, to a good approximation, as that from partices (in vacuum) of density n of the same size as the cavities. Thus the usual formulas of small angle scattering obtain, the scattered intensity has the familiar Gaussian-like dependence on scattering angle, and earlier results on multiple scattering may be applied. Around edge-type dislocations, on the other hand, the density variation is proportional to $\sin\xi/r$, where ξ is the angle measured from the slip direction in the plane perpendicular to the dislocation line and r is the distance from the dislocation line. This angular variation results in a complete modification of the usual formulas, and, in fact, all of the terms ordinarily present disappear for this case, and conversely. The scattering shows a parabolic increase from zero at small angles, a maximum, and finally a monotonic decrease with increasing scattering angle. There is a large degree of anisotropy in the scattering, depending on the direction of the incident beam relative to the slip and dislocation axes. Multiple scattering from an array of dislocations in even a thick specimen is shown to be negligible. The theory is compared with Blin and Guinier's preliminary experimental results, and it is concluded that dislocations are incapable of explaining their data, although it is expected that under suitable conditions the measurement of the scattering from dislocations should be experimentally feasible.

I. INTRODUCTION

ACCORDING to current interpretations, the process of cold-working leads to the introduction of considerable imperfection into a crystal. For the last dozen or so years it has been generally believed that much of this imperfection may be described in terms of dislocations of the lattice, and more recently, Seitz[1] has suggested that vacancies are produced as a result of the motion of dislocations during cold-work. The concentrations of dislocations involved are perhaps of the order 10^7 or 10^8 dislocation line-cm per cm^3 in a "perfect" crystal, increasing to 10^{12} lines per cm^2 in a heavily cold-worked specimen.

Associated with imperfection of these types, there is a variation in the density of the lattice and a variation in the scattering power and potential within the material. These variations will, of course, affect the electrical conductivity, measurements of which are proving an important tool in the investigation of crystalline imperfection.[2] Conductivity measurements, combined with stored energy experiments on cold-worked metals, suggest that the observed resistivity change per unit stored energy q may be too large to be explained by dislocations or perhaps even by isolated vacancies. A more advantageous ratio q is expected for clusters of vacancies.[2c]

The density variations will also result in a scattering of x-rays or thermal neutrons. The small angle scattering of x-rays (wavelength $\sim$1A) has developed in the past 15 years into an accurate and powerful technique for the investigation[3] of small particles of linear dimensions $L>10\lambda$. Although the most striking successes have dealt with biological materials,[4] Blin and Guinier[5] have recently made preliminary measure-

[1] F. Seitz, Phil. Mag. Supplement **1**, 43 (1952).

[2] For discussion of the effects of (a) dislocations, (b) isolated vacancies, and (c) clustered vacancies or cavities on the resistance, see, respectively, the following papers and references contained therein: (a) D. L. Dexter, Phys. Rev. **86**, 447 (1952); (b) D. L. Dexter, Phys. Rev. **87**, 768 (1952); J. W. Kauffman and J. S. Koehler, Phys. Rev. **88**, 149 (1952); (c) D. L. Dexter (to be published).

[3] A. Guinier, Ann. phys. **12**, 161 (1939) and many subsequent papers.

[4] The reader is referred to a series of papers in J. Chem. Phys. by W. W. Beeman and his co-workers on the scattering from protein molecules in aqueous solution, for example, Ritland, Kaesberg, and Beeman, J. Chem. Phys. **18**, 1237 (1950). See also Kaesberg, Ritland, and Beeman, Phys. Rev. **74**, 71 (1948).

[5] J. Blin and A. Guinier, Compt. rend. **233**, 1288 (1951). Professor Guinier has kindly informed the writer in a private communication that the concentration of scatterers mentioned in their paper was too large by about a factor of 10.

ments of the scattering from cold-worked metals, and it seems probable that small angle scattering will become useful also in the investigation of crystalline imperfection. It is, therefore, the purpose of this paper to compute the scattering to be expected from clustered vacancies, or cavities, and from dislocations.

II. SCATTERING FROM CAVITIES

We consider an effectively infinite medium consisting of a solid of electron density n_e and atomic density n_a. For the sake of definiteness we shall speak throughout of x-ray scattering and shall consequently be concerned with the electron density and the Thompson scattering coefficient I_e. It is clear that our conclusions will likewise apply to neutron scattering, if we replace n_e by n_a and the x-ray scattering cross section per electron by the neutron scattering cross section per atom.

The coherent scattering by the perfect infinite medium will, of course, all be in the forward direction and will be indistinguishable from the direct, unscattered beam. Thus only the deviations from the density n_e will be of interest to us. If we introduce into the medium a number N of randomly arranged identical regions of constant electron density n_e', the coherent scattered intensity will be

$$I(\epsilon)=I_e N[V(n_e'-n_e)]^2\{1-\tfrac{1}{3}(2\pi\rho\epsilon/\lambda)^2+\cdots\}, \quad (1)$$

where ϵ is the angle of deviation from the incident beam, I_e the intensity scattered by a single electron, V the volume of one of the identical regions of electron density n_e', and ρ is the radius of gyration defined by

$$\rho^2=V^{-1}\int r^2 d\tau, \quad (2)$$

where the integration is carried out over a single region. Thus the scattering is a maximum in the forward direction. It should be noted that $I(\epsilon)$ is proportional to the square of the difference between the electron densities. Thus a number N of cavities of density zero scatter exactly as N particles in vacuum of the same shape and of density n_e. The small angle approximation in Eq. (1) requires that $\sin(\epsilon/2)$ be replaceable by $\epsilon/2$ and that $\frac{1}{3}(2\pi\rho\epsilon/\lambda)^2$ be less than 1. Thus we may not treat the scattering of 1-A x-rays from isolated vacancies by this approximation, since the radiation will be scattered over large angles where $\sin(\epsilon/2)$ is not $\sim\epsilon/2$. For large cavities, however, Eq. (1) is valid out to the angle of half-maximum intensity, in so far as the model is adequate. All of the above follows directly from well-known results.

The above model is certainly applicable if the elastic distortions surrounding a cavity are sufficiently small. According to the theory[6] of elasticity of an isotropic continuum, the displacement of the medium surrounding a spherical cavity of radius a at the center of a sphere of radius R is of the form

$$\mathbf{U}(\mathbf{r})=A\mathbf{r}/r^3+B\mathbf{r}, \quad (3)$$

where

$$B=2A(1-2\nu)/R^3(1+\nu), \quad (4)$$

ν is Poisson's ratio and A is determined by the boundary condition at the surface of the cavity. The fractional change in the density of the medium associated with the distortions resulting from N cavities is then given approximately by $(\delta D/D)\sim -N\nabla\cdot\mathbf{U}$, and since the divergence of the first term in Eq. (3) vanishes, we obtain a density change

$$\frac{\delta D}{D}=-6\frac{NA}{R^3}\frac{(1-2\nu)}{(1+\nu)}. \quad (5)$$

Since the density change is roughly independent of position, the lattice surrounding the cavity does not contribute to the scattering, and the radius of gyration is determined solely by the size of the cavity. Thus the primary effect of the distortions is to change the factor $[V(n_e'-n_e)]^2$ by an amount that will be seen to be negligible, and the radius of gyration determined by experiment will correspond in the usual way to the geometrical size of the cavity.

If the magnitude of the displacement at the surface of a cavity is γ, then $A=a^3(\gamma/a)$, so that Eq. (5) becomes, on setting $\nu\sim\frac{1}{3}$, $\delta D/D\sim-\frac{3}{2}(Na^3/R^3)(\gamma/a)$. The factor Na^3/R^3 is the fractional volume of the sphere occupied by cavities and is less than or about equal to 10^{-3} for all cases in which we shall be interested. Likewise, γ/a is in all cases much less than unity. Thus we may certainly neglect the effects of distortion in the surrounding medium, and we may treat the cavities in a medium of initial density n_e as small particles of the same size and shape and of the same density n_e dispersed in vacuum.

Blin and Guinier[5] found that their experimental data on copper, heavily cold-worked at room temperature, are characterized in angular dependence by a radius of gyration of about 6.6A. This experimental figure is, of course, determined independently of any model which may be chosen to interpret the data and corresponds to the spatial extent of whatever regions may be present in which the electron density differs from that of the surrounding medium. If these regions be spherical and of a constant density, they correspond to a volume of 2.6×10^{-21} cm^3, or about 200 times the atomic volume of copper. If the density is constant but the regions are nonspherical, the volume is correspondingly less. Blin and Guinier[5] likewise made a preliminary measurement of the absolute intensity of the scattered x-radiation. From comparison with Eq. (1), therefore, the total number of scattering regions may be determined for any specific model consistent with the measured radius of gyration. For example, if one assumes the scattering regions are spherical cavities of radius of gyration 6.6A

[6] S. Timoshenko, *Theory of Elasticity* (McGraw-Hill Book Company, Inc., New York, 1934).

and electron density zero, the concentration of cavities turns out to be about 7×10^{17} per cm^3.[5] The fractional volume of the copper occupied by cavities would then be 1.8×10^{-3}. If one chooses cylindrical cavities in the shape of a pancake, of thickness $L=3$A, radius $a=9.25$A $[\rho=(a^2/2+L^2/12)^{\frac{1}{2}}=6.6\text{A}]$, the concentration becomes 7.3×10^{18} cm^{-3}, and the fractional volume occupied by the cavities is 5.9×10^{-3}. Similarly for cylindrical rods of $L=22.6$A, $a=1.5$A ($\rho=6.6$A), the concentration would be 1.8×10^{20} cm^{-3}, and the fractional volume occupied would be 2.9×10^{-2}. (The above shapes for the cylinders were not selected as reasonable physical models but were chosen as limiting cases.)

It is clear that if one employs too thick a scattering sample, a given photon may be scattered more than once. Such multiple scattering would broaden the scattering curve and would result in too small a radius of gyration, if the interpretation were made on the basis of Eq. (1). There exists an alternative procedure for obtaining the radius of gyration, however, in cases where multiple scattering is present, a method depending on the variation of the width of the scattering curve with sample thickness.[7] As will be seen below, this method is not practicable for the systems of interest here.

The condition that multiple scattering have negligible effect is given by $\mu_s t<1$, where μ_s, the linear scattering coefficient, is equal to

$$\mu_s=27r_0^2\lambda^2[V(n_e'-n_e)]^2\mathfrak{N}/(40\pi\rho^2), \tag{6}$$

where r_0 is the classical electron radius e^2/mc^2, λ the x-ray wavelength, $V(n_e-n_e')$ the deficit of electrons in each scattering region, $\mathfrak{N}$ the number density of the regions, and where t is the thickness of the scattering sample. Thus, for example, in the first case mentioned above for copper, with $\lambda=1.54$A, $V=2.6\times10^{-21}$ cm^3, $n_e=2.4\times10^{24}$ cm^{-3}, $n_e'=0$, $\mathfrak{N}=7\times10^{17}$ cm^{-3}, and $\rho=6.6$A, the condition for negligible multiple scattering is

$$t<40 \text{ cm}.$$

Since V varies as ρ^3, μ_s appears to vary as the fourth power of the radius of gyration. It must be recalled, however, that the fractional volume of a cold-worked specimen occupied by cavities cannot become greater than about 10^{-3}, since the fractional density change of cold-worked crystals is of this order of magnitude. Hence, we must add the condition that $\mathfrak{N}V\lesssim10^{-3}$, so that μ_s varies linearly with ρ for samples in which $\mathfrak{N}V$ has reached its maximum value of $\sim10^{-3}$. Thus we see that for very small cavities $\rho\lesssim100$A, multiple scattering need not be considered at all. Alternatively, we may say that the condition for the experimental practicability of the multiple scattering method[7] for determining particle size is given by

$$\mu_s>\mu_a, \tag{7}$$

where μ_a is the linear absorption coefficient of the bulk medium. For spherical cavities, we may solve the inequality (7) for the radius of gyration, first inserting the relation $V\mathfrak{N}\leqslant10^{-3}$. We find as a necessary condition that appreciable multiple scattering occur,

$$\rho>2\times10^4\tau_a\Delta/Z\lambda^2, \tag{8}$$

where τ_a is the mass absorption coefficient, Δ the atomic volume, and Z the atomic number of the bulk medium. In obtaining Eq. (8), we have taken the atomic weight as approximately twice the atomic number. All quantities in Eq. (8) are expressed in cgs units. It is clear that Eq. (8) cannot be satisfied and that the multiple scattering method cannot practicably be applied to cold-worked specimens by means of x-rays.

For neutron scattering the linear scattering coefficient is given by Eq. (6) with $n_e'-n_e$ replaced by $n_a'-n_a$ and with r_0^2 replaced by $\sigma_s/4\pi$, the coherent scattering cross section per unit solid angle for neutrons of wavelength λ. With $n_a'-n_a$ of the order 10^{23} cm^{-3} and σ_s of the order one barn, the condition for negligible multiple scattering becomes

$$t<2\times10^4 \text{ cm},$$

a condition that indicates the experimental impracticability of a multiple scattering measurement with neutrons.

III. SCATTERING FROM DISLOCATIONS

In this section we shall compute, on the basis of certain approximations, the coherent, diffuse, small angle scattering to be expected from dislocations in a heavily cold-worked crystal. Since the separation of dislocations in heavily cold-worked metals is believed to be of the order of 100A,[2] it perhaps seems impossible at first sight to attempt to explain with dislocations the scattering observed by Blin and Guinier[6] which was characteristic of a linear dimension of 17A (for spherical regions). Nevertheless, the peculiar distribution function for electrons surrounding a dislocation [see Eq. (9)] would be expected to reduce the "effective" characteristic length for the distorted region about a dislocation. It will be seen below that this is indeed the case but that the reduction is insufficient to explain the observed data.

We shall ignore the effects of vacancies in this section; we shall likewise ignore the scattering from the screw-type component of the dislocations, since to a first approximation, there is no electronic density change associated with this type of imperfection.[8] It is assumed that the dislocation lines do not remain straight for macroscopic distances, but rather are frequently bent, that the principal component changes from screw to edge type over distances of the order of the mean spacing of the dislocations, and that only small coherence occurs in the scattering from regions surround-

[7] D. L. Dexter and W. W. Beeman, Phys. Rev. **76**, 1782 (1949).

[8] A. J. C. Wilson, Research **2**, 541 (1949); **3**, 387 (1950).

ing neighboring edge-type sections. This assumption of random phase from one such region to the next certainly is not exactly valid; quantitatively correct results can perhaps be obtained by the calculation of corrections for coherence, when more is known about the detailed geometry of interacting dislocations. (Such corrections would be expected to reduce the scattering at very small scattering angles, as in the scattering from concentrated solutions. As will be seen below, however, the scattering has a minimum in the forward direction anyway, so it seems certain that interference corrections will not change the qualitative aspects of the scattering curves.) A further approximation, which is closely related to the others, is the neglect of end effects at the termination of an edge-type component of the dislocation line. Now, according to the theory of elasticity for a homogeneous isotropic medium, the density change at a point in a lattice is equal to[9]

$$\Delta n = n_e\left(\frac{1-2\nu}{1-\nu}\right)\frac{a}{2\pi}\frac{\sin\xi}{r} \equiv \kappa\frac{\sin\xi}{r}. \tag{9}$$

In this expression ν is the Poisson ratio (approximately equal to $\frac{1}{3}$ for most materials), a is the unit slip distance, r is the distance from the point to the dislocation line (Z axis), i.e., $r=(x^2+y^2)^{\frac{1}{2}}$, and ξ is the angle from the slip direction (X axis) measured in the XY plane, i.e., $\xi=\tan^{-1}(y/x)$. (The "extra plane" of atoms, according to this notation, in the YZ plane, and XZ is the slip plane.) It will be noted that, since the density change below the slip plane is the negative of that above, there is no excess or deficit of matter in a symmetrical region region surrounding the dislocation axis. This fact has important consequences on the shape of the x-ray scattering curve.

Following the assumptions described above, we take as our model for the elementary, coherently scattering region, the lattice surrounding a length L of edge-type dislocation, out to a distance R equal to about half the average separation between dislocations. We shall arbitrarily cut off our unit scattering region by considering only that volume enclosed in a right circular cylinder of radius R and length L; the scattering we calculate with this model will be very similar to that obtained from any cylinder of length L and of symmetrical cross section, for example, a square. The matter outside the cylinder is considered to contribute to the scattering associated with neighboring dislocations, and, in accord with the assumptions discussed above, the total scattered intensity will be taken to be the sum of the intensities scattered from the individual cylinders.

The scattered intensity from one of these cylinders is given by

$$I = I_e\int\Delta n(\mathbf{r})d\tau\int\Delta n(\mathbf{r}')d\tau'\cos k(l-l'), \tag{10}$$

where $k\equiv(4\pi/\lambda)\sin(\epsilon/2)$.[10] In the usual small angle approximation, we set k equal to $2\pi\epsilon/\lambda$ throughout the following. The lengths l and l' are defined in the customary way as follows. We consider an incident x-ray AB, having a given orientation with respect to the cylinder, and consider a particular ray BC scattered through an angle ϵ. The angle bisector of the supplementary angle ABC will be referred to as L, and the angle between L and the axis of the dislocation Z will be called θ. We now define a plane Π perpendicular to L, which passes through the geometrical center of the cylinder. The quantities l and l' are the perpendicular distances from the points $\mathbf{r}$ and $\mathbf{r}'$ to Π. The value of these definitions is a result of the fact that all of the electrons on a given plane parallel to Π scatter in phase with each other. Let the projection of L on the XY plane make an angle φ with the X axis. Then the perpendicular distance from a point to Π is given by

$$l(r,\xi,z)=r\sin\theta\cos\varphi\cos\xi+r\sin\theta\sin\varphi\sin\xi+z\cos\theta, \tag{11}$$

in terms of the location of the points and the orientation of the angle bisector. Inserting Eqs. (9) and (11) into Eq. (10), we find

$$\begin{aligned}\frac{I}{\kappa^2 I_e}=&\left[\int_{-L/2}^{L/2}dz\int_0^{2\pi}d\xi\sin\xi\int_0^R dr\right.\\&\left.\times\cos k\{r\sin\theta(\cos\varphi\cos\xi+\sin\varphi\sin\xi)+z\cos\theta\}\right]^2\\&+\left[\int_{-L/2}^{L/2}dz\int_0^{2\pi}d\xi\sin\xi\int_0^R dr\right.\\&\left.\times\sin k\{r\sin\theta(\cos\varphi\cos\xi+\sin\varphi\sin\xi)+z\cos\theta\}\right]^2.\end{aligned} \tag{12}$$

In most scattering problem the density function is an even function of ξ and the second term of this sum vanishes by symmetry. In the present case, however, the reverse is true, since the presence of $\sin\xi$ in the density makes the first term vanish. Performing the integrations indicated in Eq. (12), we obtain

$$I=\frac{I_e\kappa^2 16\pi^2\sin^2(\frac{1}{2}kL\cos\theta)\sin^2\varphi}{k^4\cos^2\theta\sin^2\theta}[1-J_0(kR\sin\theta)]^2. \tag{13}$$

Let us now define an axial ratio $\alpha\equiv L/2R$ and a reduced scattering angle $\gamma\equiv 2\pi\epsilon R/\lambda=kR$. If the dislocations are distributed with random orientation in the cold-worked specimen, the average intensity scat-

[9] J. S. Koehler, Phys. Rev. **60**, 397 (1941).

[10] See, for example, A. Guinier, *Radiocristallographie* (Dunod, Paris, 1945), p. 229.

tered from each is equal to

$$\bar{I}(\gamma,\alpha)=\frac{I_e(\pi R^2 L n_e)^2}{32\pi^2\alpha^2}\left(\frac{a}{R}\right)^2\left(\frac{1-2\nu}{1-\nu}\right)^2 F(\gamma,\alpha), \quad (14)$$

where $F(\gamma,\alpha)$ is a dimensionless quantity having a maximum of about $\frac{3}{2}$:

$$F(\gamma,\alpha)=\frac{16}{\gamma}\int_0^{\gamma_0} dx\frac{\sin^2(\alpha x)}{x^2(\gamma^2-x^2)}[1-J_0((\gamma^2-x^2)^{\frac{1}{2}})]^2. \quad (15)$$

For small scattering angles, i.e., $\gamma\ll 1$, we may expand expand Eq. (15) and obtain a quadratic dependence on scattering angle,

$$\bar{I}=\frac{I_e}{48\pi^2}\left(\frac{1-2\nu}{1-\nu}\right)^2(\pi R^2 L n_e)^2\left(\frac{a}{R}\right)^2 \times\{\gamma^2-\tfrac{1}{10}\gamma^4(1+\tfrac{2}{3}\alpha^2)+\cdots\}. \quad (16)$$

This result is in striking contrast with the shape of the usual small angle scattering curves, which have a maximum in the forward direction. The absence of scattering at very small angles in the present case is a result of the fact that no net material has been added to the lattice, but the material has merely been displaced from one side of the slip plane to the other. Thus at very small angles, where all the electrons scatter approximately in phase, the scattering takes no account of inhomogeneities in the sample.[11]

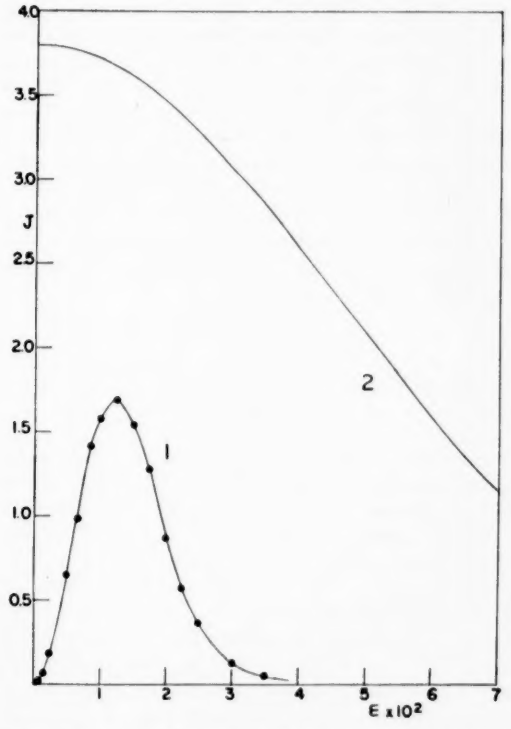

FIG. 1. Curve 1 represents the intensity scattered from an edge-type dislocation of $2R=L=98$A, as a function of scattering angle ϵ. Curve 2 is proportional to the scattered intensity from the cavities of radius of gyration 6.6A present in a volume $\pi R^2 L$, if the concentration of cavities is 7×10^{17} cm^{-3}. For both curves $\lambda=1.54$A. The ordinate scale for both curves is equal to the scattered intensity times 10^{42} $(n_e^2 I_e)^{-1}$.

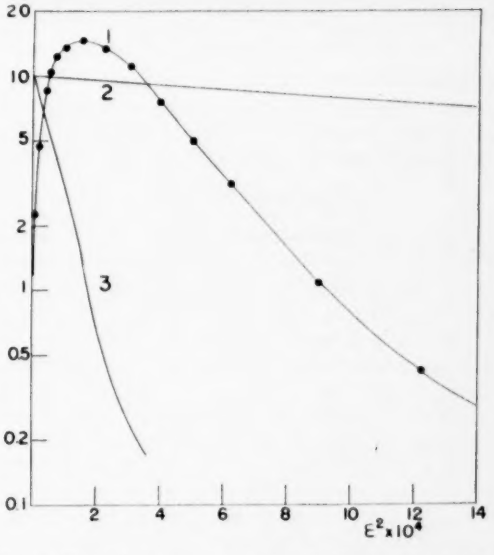

FIG. 2. These three curves represent the shape of the familiar plots of log intensity *versus* angle squared. Curve 1 is proportional to curve 1 of Fig. 1 for the scattering by dislocations; curve 2 is proportional to curve 2 of Fig. 1 for spherical cavities; and curve 3 is for solid cylinders of the same dimensions as those of the cylinders taken to approximate the effects of dislocations. The relative ordinates for the three curves are of no significance.

It is interesting to compare Eq. (16) with the intensity scattered in vacuum from a solid cylinder of the same dimensions and of electron density n_e:

$$\bar{I}=I_e(\pi R^2 L n_e)^2\{1-\tfrac{1}{6}\gamma^2(1+\tfrac{2}{3}\alpha^2)+\cdots\}. \quad (17)$$

Since in both Eqs. (16) and (17) the quantities in curly brackets have maximum values of the order unity, we see that the ratio of the peak scattered intensities is of the order one to one million for $\alpha=1$ and R equal to 50A, i.e., for dislocation concentrations of the order 10^{12} cm^{-2}.

It is also of interest to compare the absolute intensities of the scattering observed by Blin and Guinier[5] with that to be expected from edge-type dislocations. For $L=2R=100$A, $\nu\sim\frac{1}{3}$ and $a=2.55$A (for Cu), the intensity scattered from a volume $(\pi R^2 L)$ has a maxi-

[11] Professor W. W. Beeman has kindly called the attention of the writer to a paper by A. Guinier [Metallkunde **43**, 217 (1952)], who has measured the x-ray scattering from silver-rich clusters in an alloy of Al: 6 percent Ag. Since each Ag-rich cluster is surrounded by a Ag-poor shell, for this system also there is no net excess of scattering power in each scattering unit, and the scattered intensity is observed to have a minimum in the forward direction.

mum of

$$\bar{I}_{\max}\sim 1.7\times 10^{-42} n_c^2 I_e. \tag{18}$$

On the other hand, from Eq. (1), the absolute intensity scattered from the cavities (of radius of gyration 6.6A and of concentration 7×10^{17} cm^{-3}) contained within this volume would be equal to about twice this value,

$$I_{\max}\sim 3.8\times 10^{-42} n_c^2 I_e. \tag{19}$$

However, the total scattered intensity is much smaller for the dislocations than that observed, as indicated in Fig. 1. The upper curve of Fig. 1 corresponds to Eq. (19), the scattering from 7×10^{17} spherical cavities per cm^3, of radius of gyration 6.6A, as estimated by Blin and Guinier with Cu $K\alpha$ radiation. On the same absolute intensity scale, the lower curve corresponds to a numerical integration of Eqs. (14) and (15) for axial ratio equal to unity. To fit the absolute abscissa scale of Fig. 1, λ is set equal to 1.54A and R equal to 49A, so that γ becomes 200ϵ. The quantity plotted vertically in Fig. 1 is the absolute intensity scattered from a sample of volume $(\pi R^2 L)$, multiplied by $10^{42}(n_c^2 I_e)^{-1}$.

Figure 2 shows the customary curves of the log of the intensity *versus* the square of the scattering angle for (1) dislocations of $2R=L=98$A, (2) spherical cavities of radius of gyration 6.6A, and (3) solid cylinders of $2R=L=98$A. The relative heights of the three curves are of no significance. It will be noticed that curve (1) is accurately represented by a straight line for more than a full cycle on the log scale and that, if experimental data were lacking for angles smaller than that of the maximum, the data would ordinarily be interpreted as representing the scattering from homogeneous regions of radius of gyration $0.542R$, or 26.5A. Note also that this "effective" radius of gyration is 41 percent smaller than that for the solid cylinder of the same dimensions, 44.8A.

It will also be observed that dislocations of this size clearly cannot be responsible for the scattering observed[5] by Blin and Guinier. Furthermore, if one should attempt to interpret their data on the angular variation on the basis of suitably reduced cylinders of this type, namely, $2R=L=24.4$A, the absolute scattered intensity would be too small by a factor of 8.

If the scattering observed by Blin and Guinier should indeed be a result of clustered vacancies, as they tentatively suggest, it may be possible to observe the scattering from dislocations by cold-working and measuring the scattering at liquid nitrogen temperatures, where isolated vacancies are not sufficiently mobile to cluster. The extremely characteristic minimum in the scattered intensity at zero scattering angle should enable the effects of dislocations to be observed even above a background of diffuse scattering which is due to a large number of isolated vacancies. The expected counting rates ($\lesssim 3$ sec^{-1}) with apparatus similar to that in use by Beeman and co-workers,[4] should be high enough above room background (~ 0.5 sec^{-1}) to make the experiment feasible. It is possible, however, that some geometrical mechanism not as yet understood favors the production of high concentrations of vacancies in localized regions such that clustering is possible even at extremely low temperatures. If such is the case, it may prove impossible sufficiently to reduce the background scattering due to vacancies to isolate the effects of dislocations. Certainly the variation with temperature of the scattering curves for samples cold-worked at nitrogen temperatures should be most interesting.

From the discussion given in Sec. II it is clear that multiple scattering can have an appreciable influence on the scattering from dislocations. The scattering coefficients for solid cylinders is more than a million times larger than that for our model of the dislocation [see Eqs. (16) and (17)] and even a solid cylinder would have to be hundreds of angstroms in size for multiple scattering to become experimentally significant.[7]

Another point of interest in the scattering from dislocations is the large degree of anistropy in the scattering, as can be seen from Eq. (13). For example, if x-rays are incident along the dislocation axis (Z axis), the scattered intensity in the slip plane (XZ plane) is zero, but that in the plane of extra atoms (YZ plane) is relatively large. On the other hand, the scattered intensity in either the YZ plane or the YX plane from x-rays incident along the Y axis is of the order $\epsilon^2/4$ times the latter. If we let the first subscript denote the direction of incidence of the x-ray beam and the two subscripts together indicate the plane of scattering, the anisotropy relations may be summarized as follows, for very small angles:

$$\begin{aligned} &I_{ZX}=I_{XZ}\equiv 0,\\ &I_{ZY}=I_{XY}=\tfrac{1}{4}\kappa^2\pi^2 I_e L^2 R^4 k^2,\\ &I_{YZ}=I_{YX}=\tfrac{1}{4}\epsilon^2 I_{ZY}. \end{aligned} \tag{20}$$

The anistropy of the x-ray scattering may prove useful in the investigation of kinking phenomena, where dislocations may be oriented primarily in one direction.

Another possible imperfection of interest is the collapsed vacancy disk, similar in some respects to an edge dislocation and in others to a flat cylinder of vacancies of the type discussed in Sec. II. Since there is a net absence of matter in the vicinity of the disk, we would expect that the scattering would be a maximum in the forward direction and that by a suitable choice of size and concentration of the collapsed disks, it should be possible to fit Blin and Guinier's results.

A Neutron Diffraction Study of Magnesium Ferrite*

L. M. CORLISS AND J. M. HASTINGS, *Chemistry Department, Brookhaven National Laboratory, Upton, New York*

AND

F. G. BROCKMAN, *Philips Laboratories, Irvington-on-Hudson, New York*

(Received Februrary 18, 1953)

Neutron diffraction patterns have been obtained for polycrystalline magnesium ferrite. Application of a suitably oriented strong magnetic field has made possible a separation of the coherent scattering into its nuclear and magnetic parts. The magnetic scattering is found to be in good agreement with the Néel model of ferrimagnetism. The form factor for the magnetic scattering is found to be, within experimental error, identical with that previously obtained in the case of nickel ferrite. Analysis of the nuclear scattering permits a simultaneous determination of the degree of inversion, which for the specimen used was 0.88 ± 0.01, and the u space group parameter to which the value 0.381 ± 0.001 was assigned.

INTRODUCTION

MAGNESIUM ferrite belongs to a class of compounds having the general formula $M^{+2}Fe_2^{+3}O_4$ and crystallizing with the spinel structure. The structure may be characterized as a slightly distorted cubic close-packed array of oxygen atoms containing metal ions in prescribed interstitial positions. The lattice sites occupied by metal ions are of two types, commonly designated as A and B, and distinguished by the way in which the nearest oxygen neighbors are arranged. The configuration of the surrounding oxygens is tetrahedral in the case of A sites and octahedral in the case of B sites. The unit cell contains eight molecules, with twenty-four metal ions distributed among sixteen octahedral or B sites and eight tetrahedral or A sites. In the so-called *normal* or *regular* spinel the divalent metal ions occupy the A sites and the trivalent metal ions the B sites. Without violating the symmetry requirements it is possible for the divalent ions on A sites to exchange places with trivalent ions on B sites. The extent to which this process of inversion occurs depends in some cases on the method of preparation. The *inverted* spinel is then one in which the A sites are occupied solely by trivalent metal ions and the B sites by equal numbers of trivalent and divalent metal ions. Figure 1 shows the atomic agreement for both the normal and inverted spinel.

Ferrites in which the divalent ion is Mn^{+2}, Fe^{+2}, Co^{+2}, Ni^{+2} all have the inverted spinel structure[1] and are ferromagnetic with saturation moments[1a] appropriate to the divalent ions alone. According to the Néel theory[2] there exists a strong negative exchange coupling between the atoms on A sites and the atoms on B sites. This results in a spin alignment in which the A moments are all oriented antiparallel to the B moments. In the case of an inverted ferrite the iron moments on A sites just cancel those on B sites, leaving the crystal with a net moment equal to that of the divalent ion. Zinc and cadmium ferrites, on the other hand, are normal spinels[1] and are observed to be paramagnetic over a wide temperature range in agreement with the predictions of Néel. The validity of the Néel model as well as the conclusions of earlier x-ray workers regarding inversion in the spinels have been recently verified by neutron diffraction studies on Fe^{+2}, Ni^{+2}, and Zn^{+2} ferrites.[3,4]

The case of magnesium ferrite is somewhat exceptional. Its structure was originally reported[5] to be

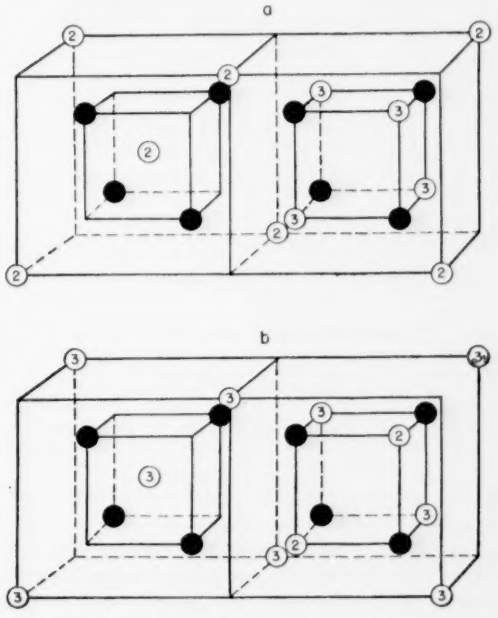

FIG. 1. (a) Two octants of the regular spinel structure. Open circles with numbers refer to di- and trivalent metal ions. Solid circles refer to oxygen ions; (b) same for inverted spinel.

* Research carried out under the auspices of the U. S. Atomic Energy Commission.

[1] E. J. W. Verwey and E. L. Heilmann, J. Chem. Phys. **15**, 174 (1947).

[1a] Added in proof.—E. W. Gorter, Nature **165**, 798 (1950).

[2] L. Néel, Ann. phys. **3**, 139 (1948).

[3] Shull, Wollan, and Koehler, Phys. Rev. **84**, 912 (1951).

[4] J. M. Hastings and L. M. Corliss, Revs. Modern Phys. **25**, 114 (1953).

[5] T. F. W. Barth and E. Posnjak, Krist. **82**, 325 (1932).

inverted, i.e., to possess the same number of magnetic atoms on A sites as on B sites. On the basis of the Néel coupling scheme magnesium ferrite would then be expected to have zero saturation moment. However, this is not what is observed experimentally. The saturation moment is found[6,7] to vary within the limits of 1–2.4 Bohr magnetons depending on the conditions of preparation. This discrepancy has been explained on the assumption that magnesium ferrite is

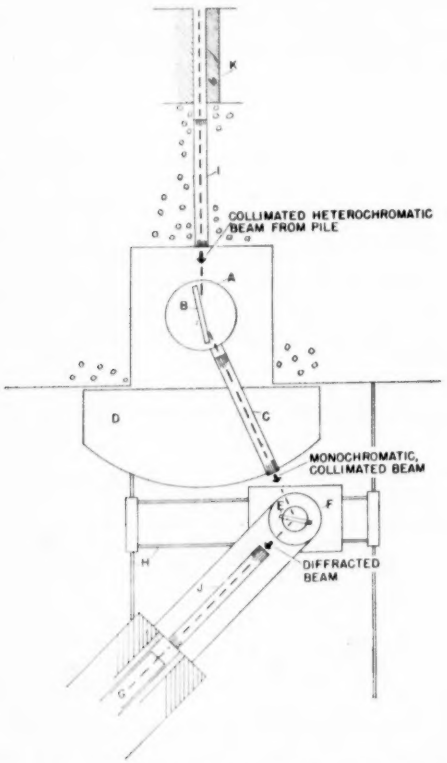

FIG. 2. Schematic diagram of neutron diffraction apparatus. A is the first spectrometer table, set in a niche in the reactor shield, and carries the lead monochromating crystal B. F is the second crystal table and is mounted on a set of crossed tracks H. E is the sample and G is a BF_3 counter set in a paraffin—B_4C shield. K is a steel shutter, and the Soller slit collimators are represented by I, C, J. The direct beam from the reactor is caught in the shield D.

incompletely inverted; the number of iron atoms on B sites thus exceeding the number on A sites. The departure from complete inversion need only be of the order of 10–15 percent to account for the saturation moment by means of the Néel model, and thus might very easily have escaped detection in the original x-ray work. More recent investigations by Guillaud[6] and by Bertaut[8] have indeed shown that magnesium ferrite is partially inverted to an extent which is qualitatively in accord with the saturation moment measurements. The present neutron diffraction study is aimed at checking the Néel theory not only by a determination of the degree of inversion but also by direct observation of the coherent scattering from the aligned magnetic moments.

PREPARATION OF $MgFe_2O_4$

The samples of magnesium ferrite for the neutron diffraction studies were prepared by the sintering techniques described by Snoek.[9] Because rather large solid specimens (about $10\times6.3\times1$ cm) are desirable and because magnesium ferrite is the most refractory of the ferrites (mp 1760°C),[10] more than the usual difficulties were encountered in the sintering process. In order to prepare the specimen with laboratory scale equipment the specimen was made of four pieces, $6.3\times2.5\times1.3$ cm. These were stacked together to furnish the larger specimen required.

Mechanically good specimens were prepared in the following way. Basic magnesium carbonate which assayed 41.39 percent MgO was thoroughly mixed with the stoichiometric amount of ferric oxide (assay: 99.55 percent Fe_2O_3). This mixing was accomplished in a steel ball mill using ethyl alcohol as the milling fluid. After filtering and drying, the powder mixture was heated for one hour at 1040°C. Following this treatment the material was ground again in the ball mill as above. After drying, the partly reacted powder was pressed in 100-gram quantities after the addition of 2.5 grams of a natural gum binder (gum acacia) and 10 cc of water to each 100 grams of powder. The die used was about 7.5×3 cm (3.00 in.$\times1.25$ in.) in cross section and the total force applied in pressing was 10 tons. These "bricks" were dried at 120°C and then crushed and graded by sieving. After this the granules were moistened with 1 cc of distilled water and repressed in the same die with 10 tons total force applied. The samples were dried overnight at 120°C and were then fired at 1315°C (2400°F) for 2 hours on temperature, using a temperature rise of 30°C per hour in the initial heating.

SATURATION MAGNETIZATION OF $MgFe_2O_4$

The saturation magnetization was determined at room temperature by a yoke method. The applied field was as high as 9000 oersteds. Above a field of about 2000 oersteds, the intrinsic induction ($4\pi I$) was constant at 1400 gauss. The apparent density (calculated from the mass of the piece and its volume obtained from its linear dimensions) was 4.12 g/cm³. These two data together with the molecular weight of magnesium ferrite, 200, lead to an effective number of Bohr magnetons per molecule of 0.96. Guillaud[11] has shown that

[6] C. Guillaud, J. phys. et. radium **12**, 239 (1951).
[7] R. Pauthenet and L. Bochirol, J. phys. et. radium **12**, 249 (1951).
[8] E. F. Bertaut, J. phys. et. radium **12**, 252 (1951).
[9] J. L. Snoek, *New Development in Ferromagnetic Materials* (Elsevier Publishing Company, Inc., New York, 1947).
[10] van Arkel, Verwey, van Bruggen, Rec. trav. chim. **55**, 331 (1936).
[11] C. Guillaud, Compt. rend. **232**, 944 (1951).

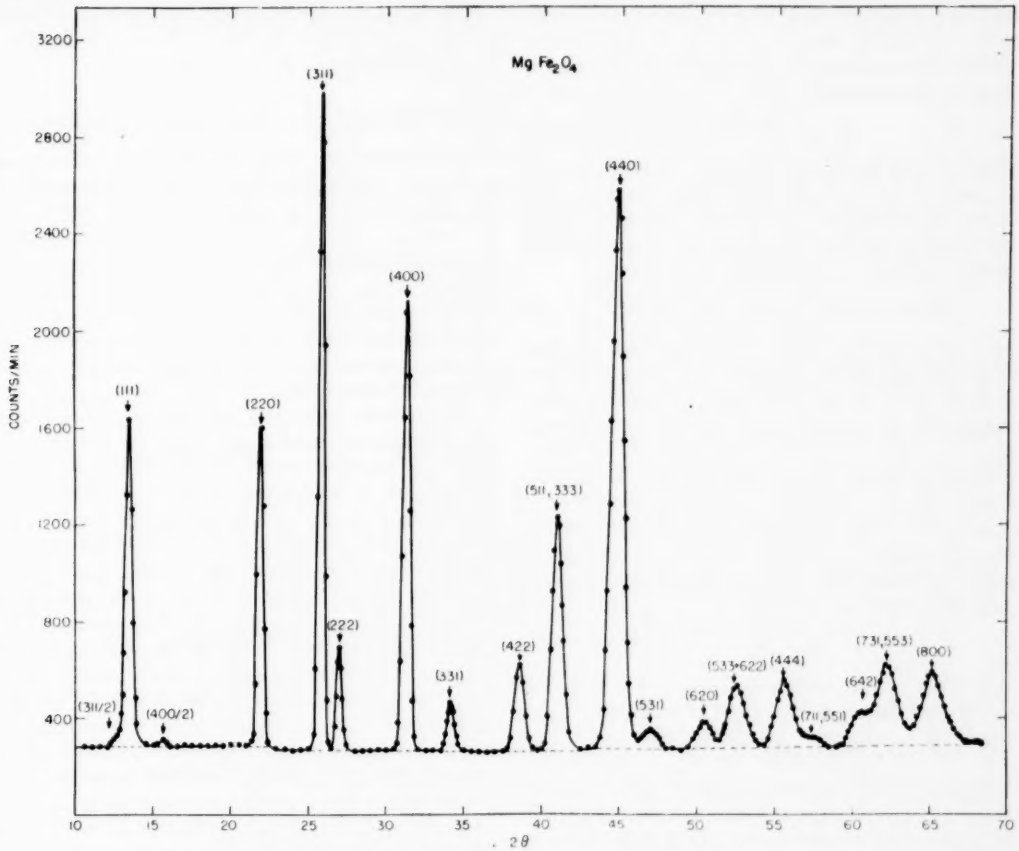

FIG. 3. Neutron diffraction pattern of polycrystalline $MgFe_2O_4$.

the ratio of the saturation magnetization at room temperature to that at absolute zero is 0.8. Using this value, the magnetic moment per molecule is computed to be 1.2 Bohr magnetons.

APPARATUS AND METHOD OF COMPUTATION

The neutron diffraction apparatus consists essentially of two spectrometers. The first of these holds a lead monochromating crystal which selects a narrow band of neutron wavelengths from the broad distribution incident upon it from the nuclear reactor. The second spectrometer table holds both the sample whose diffraction pattern is sought and a BF_3 counter for detecting the scattered radiation. Suitable collimation is provided both before and after the monochromating crystal and in front of the BF_3 detector by means of Soller slits constructed by stacking 0.010-in. wall steel tubing of dimensions $\frac{1}{8}$ in.$\times\frac{1}{2}$ in.$\times$22 in. to an over-all cross section of 2 in.$\times$2 in. A schematic diagram of the apparatus is shown in Fig. 2. Figure 3 shows the diffraction pattern obtained with polycrystalline $MgFe_2O_4$ using neutrons of wavelength 1.132A.

The integrated intensity for a flat powder specimen of thickness h and linear absorption coefficient μ, observed in transmission, is given by the expression

$$P_{hkl}=kj_{hkl}F_{hkl}^2e^{-\mu h\sec\theta}/\sin^2 2\theta, \quad (1)$$

where θ is the Bragg angle, j_{hkl} the multiplicity, and F_{hkl} the structure factor for a reflection corresponding to Miller indices (hkl). The constant k is given by the expression

$$k=(P_0\lambda^3 l/4\pi r)(N^2h\rho'/\rho),$$

in which P_0 is the incident beam power, λ the wavelength, l the counter slit height, and r the distance from the counter slit to the sample. N is the number of unit cells per unit volume, ρ' the apparent density of the powder, and ρ the true density of the solid.

Halpern and Johnson[12] have shown that the differential scattering cross section of a magnetic atom can be written

$$b^2+2bp\boldsymbol{\lambda}\cdot\mathbf{q}+q^2p^2, \quad (2)$$

[12] O. Halpern and M. H. Johnson, Phys. Rev. 55, 898 (1939).

where b is the nuclear scattering amplitude and p the magnetic scattering amplitude. $\boldsymbol{\lambda}$ is a unit vector describing the polarization state of the neutron and $\mathbf{q}$ is given by the expression

$$\mathbf{q}=\mathbf{e}(\mathbf{e}\cdot\mathbf{k})-\mathbf{k}, \tag{3}$$

in which $\mathbf{e}$ is the unit scattering vector and $\mathbf{k}$ is a unit vector parallel to the magnetic moment of the scattering atom. For an ion whose magnetic moment is determined solely by its total spin quantum number S, the magnetic scattering amplitude takes the form

$$p=(e^2/mc^2)\gamma Sf=0.539\times10^{-12}Sf\text{ cm}, \tag{4}$$

where e and m are the charge and mass of the electron and γ is the magnetic moment of the neutron in nuclear magnetons; f is the magnetic form factor describing the variation of magnetic amplitude with scattering angle.

In order to compute the structure factor for a given (hkl) reflection we must take into account the fact that the various magnetic moments in the unit cell need not all have the same orientation. As long as we restrict ourselves to coherent phenomena, the effective scattering amplitude may be written

$$b\boldsymbol{\lambda}+p\mathbf{q}. \tag{5}$$

In this notation the structure factor for a reflection whose Miller indices are h, k, l can be written

$$\mathbf{F}_{hkl}=\Sigma_i(b_i\boldsymbol{\lambda}+p_i\mathbf{q}_i)e^{2\pi i(hx_i+ky_i+lz_i)}. \tag{6}$$

In computing the scattered intensity for *unpolarized* neutrons we must average the quantity $|F|^2$ over both polarization states of the neutron. Thus no cross terms of the form $b_ip_i(\boldsymbol{\lambda}\cdot\mathbf{q}_i)$ appear in the final result and for all practical purposes the nuclear and magnetic parts of the structure factor can be calculated separately. A typical calculation is shown in the appendix.

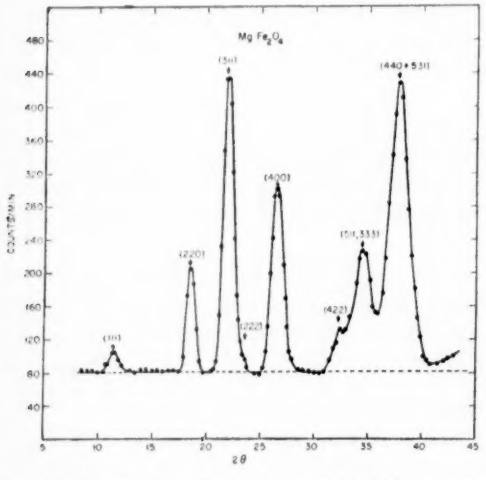

FIG. 4. Neutron diffraction pattern of $MgFe_2O_4$ caused by nuclear scattering alone. The magnetic scattering has been eliminated by application of a strong magnetic field (~10 000 oersteds) parallel to the scattering vector. Lower resolution was employed to enhance the scattered intensity.

ANALYSIS OF DIFFRACTION PATTERNS

The complete interpretation of the diffraction pattern requires a knowledge of the following quantities: (1) the degree of inversion, which we define as the fraction of A sites occupied by Fe^{+3} ions; (2) the u space group parameter (the deviation of this parameter from the value 0.375 is a measure of the distortion of the oxygen arrangement from cubic close-packing); (3) the Debye-Waller temperature factor; (4) the orientation and magnitude of atomic moments; and (5) the form factor for magnetic scattering.

The first two quantities, the degree of inversion and the u parameter, which depend only on the "chemical" structure, were determined simultaneously in the following manner. A diffraction pattern was obtained for a small sample of $MgFe_2O_4$ so placed in a magnetic field as to remove the coherent magnetic scattering contribution which at this stage of the analysis was unknown. This was accomplished by orienting the external field parallel to the scattering vector, thus making q^2 equal to zero. The pattern is shown in Fig. 4. It will be noted that the resolution in this case is much poorer than that shown in Fig. 3. The reason for this is the following. It is necessary that the sample be magnetically saturated and hence a strong external field must be employed. This limits the gap size and hence the sample size so that it was necessary to compensate for the loss in scattered intensity by increasing the incident flux. This was done by replacing the Soller slit system previously described by a coarser slit system which gave greater intensity but poorer resolution.

An examination of the calculated nuclear structure factors for the various reflections shows that there are some which are strongly dependent upon either the degree of inversion or the choice of the u parameter but not upon both. In addition, the sum $(F_{311}^2+F_{222}^2)$ is almost independent of the choice of either of these variables. A series of parameter plots were therefore constructed in which the computed ratio $F_{hkl}^2/(F_{311}^2+F_{222}^2)$ was plotted as a function of the u parameter for various values of the degree of inversion. The experimentally observed ratio for a given peak, drawn as a horizontal line on such a plot, determines by its intersections the u parameter appropriate to a given degree of inversion. The dependence of the degree of inversion upon the u parameter as determined in this way for several reflections is shown in Fig. 5. The intersection of these curves fixes the degree of inversion and the u parameter common to all the reflections. Examination of Fig. 5 shows the degree of inversion to be 0.88 ± 0.01 and the u parameter to be 0.381 ± 0.001.

The degree of inversion can be used to calculate the

saturation magnetization of this particular preparation according to the Néel coupling scheme. This gives a value of 1.2 Bohr magnetons per molecule which is in exact agreement with the observed value. The agreement may be considered somewhat fortuitous inasmuch as the computed saturation magnetization is very sensitive to small changes in the degree of inversion. A one percent change in the degree of inversion corresponds to a ten percent change in the saturation magnetization.

The third quantity to be determined is the Debye-Waller temperature factor. This was done by the usual method of plotting $\ln(F_{obs}^2/F_{calc}^2)$ against $\sin^2\theta/\lambda^2$ for the nuclear scattering alone.

With the determination of the foregoing quantities, it is now possible to deal with the magnetic scattering

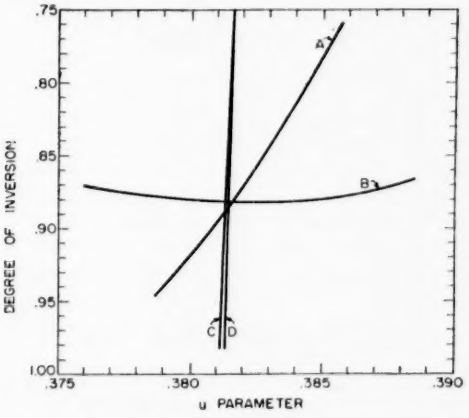

FIG. 5. Dependence of the degree of inversion upon the u parameter as determined for several peak combinations. (a) $F_{220}^2/(F_{311}^2+F_{222}^2)$; (b) $F_{400}^2/(F_{311}^2+F_{222}^2)$; (c) $(F_{422}^2+F_{511}^2+F_{333}^2)/(F_{311}^2+F_{222}^2)$; (d) $(F_{511}^2+F_{333}^2)/F_{311}^2$ (from data of Fig. 3). The intersection of these curves determines the parameter values appropriate to the specimen studied. Peak intensities used in the computations were corrected for temperature effects by a process of successive approximations.

as an isolated diffraction pattern. The interpretation of this pattern involves a knowledge of the magnitude and orientation of the atomic moments as well as the form factor for magnetic scattering. At present the form factor cannot be calculated and must be determined by experiment. However, from the intensity of the magnetic (111) reflection it is possible to deduce a great deal about the moments without a detailed knowledge of the form factor. It is shown in the appendix [Eq. (A-7)] that the magnetic structure factor for the reflection can be written

$$|\mathbf{F}_{111}|_{mag}^2=\tfrac{2}{3}p_{Fe^{+3}}^2|4.5\langle\mathbf{k}\rangle_{B'}-5.0\langle\mathbf{k}\rangle_{A'}|^2,$$

where $\mathbf{k}$ is a unit vector in the direction of the atomic magnetic moment and $\langle\mathbf{k}\rangle_{A'}$ and $\langle\mathbf{k}\rangle_{B'}$ are vector averages for the magnetic ions on A and B sites,

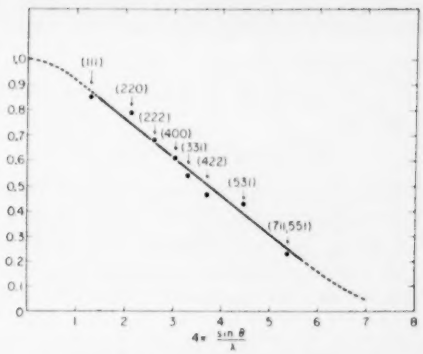

FIG. 6. Form factor $MgFe_2O_4$ (points). The solid line represents the experimental form factor for $NiFe_2O_4$.

respectively. Using the observed value for $|F_{111}|_{mag}^2$ and denoting by the symbol $|\mathbf{K}|^2$ the expression $|4.5\langle\mathbf{k}\rangle_{B'}-5.0\langle\mathbf{k}\rangle_{A'}|^2$, we have

$$|\mathbf{K}|=8.2/f. \tag{7}$$

In obtaining this expression the magnetic moment of Fe^{+3} has been taken to be 5.0 Bohr magnetons. Since $f\leq 1$, Eq. (7) can be written as the inequality

$$|\mathbf{K}|\geq 8.2. \tag{8}$$

For the Néel model we have $\langle\mathbf{k}\rangle_{A'}=-\langle\mathbf{k}\rangle_{B'}$ and $|\langle\mathbf{k}\rangle_{A'}|=1$. The computed value of $|\mathbf{K}|$ is thus 9.5, and the inequality is satisfied. If we reverse as much as one of each of the A and B moments, the saturation moment is unchanged but the value of $|\mathbf{K}|$ is reduced to 7.1, thus violating the inequality. Clearly, the orientation of the moments must be very close to the Néel model for the inequality in Eq. (8) to hold. On the basis of experiments carried out with iron group elements and compounds, the form factor appropriate to the (111) reflection may be expected to be in the range 0.8–0.9. The inequality can then be made somewhat stronger, for then $|\mathbf{K}|\geq 9.1$.[13]

Having shown qualitatively that the essential features of the Néel model are required to explain the magnetic (111) reflection, we can now reverse the procedure and use the model to compute the magnetic scattering and hence the form factor. The factor determined in this way as a function of scattering angle is shown by the series of points in Fig. 6. A further check on the model is provided by the fact that the form factor is smooth and has the expected general shape. The solid line represents the form factor deduced previously[4] from measurements on $NiFe_2O_4$ and is seen to be in good agreement with the experimental points for $MgFe_2O_4$. A comparison of the observed and calculated integrated intensities for $MgFe_2O_4$ based upon the Néel model is given in Table I.

[13] These considerations do not, however, eliminate the possibility that the moments have a slightly "staggered" configuration.

APPENDIX: CALCULATION OF THE MAGNETIC STRUCTURE FACTOR FOR THE (111) PEAK

Following the discussion on scattering amplitudes the magnetic structure factor for a general (hkl) reflection can be written

$$\mathbf{F}=\Sigma_i p_i \mathbf{q}_i e^{2\pi i(hx_i+ky_i+lz_i)}, \quad \text{(A1)}$$

where the summation is taken over all sites in the unit cell. Only the magnetic atoms contribute to the sum in (1) since the p_i vanish for diamagnetic ions. Since the diffraction pattern shows no evidence of superlattice formation we may assume that the octahedral magnetic ions are distributed at random over the octahedral sites and that the tetrahedral magnetic ions are located at random on the tetrahedral sites. Thus, breaking up the sum into two parts for convenience of summation, we have

$$\mathbf{F}=\langle p\mathbf{q}\rangle_B \Sigma_B e^{2\pi i(hx_B+ky_B+lz_B)} + \langle p\mathbf{q}\rangle_A \Sigma_A e^{2\pi i(hx_A+ky_A+lz_A)}, \quad \text{(A2)}$$

where the subscripts B and A refer to octahedral and tetrahedral positions, respectively, and the individual amplitudes have been replaced by the appropriate vector averages. Denoting the indicated summations by β and α, one obtains

$$|\mathbf{F}|^2=|\beta\langle p\mathbf{q}\rangle_B+\alpha\langle p\mathbf{q}\rangle_A|^2. \quad \text{(A3)}$$

Noting that the vector $\mathbf{q}$ is linear in $\mathbf{k}$, the spin unit vector, we can write this result in the form

$$|\mathbf{F}|^2=|\mathbf{e}(\mathbf{e}\cdot\{\beta\langle p\mathbf{k}\rangle_B+\alpha\langle p\mathbf{k}\rangle_A\})-\{\beta\langle p\mathbf{k}\rangle_B+\alpha\langle p\mathbf{k}\rangle_A\}|^2 = |\beta\langle p\mathbf{k}\rangle_B+\alpha\langle p\mathbf{k}\rangle_A|^2\sin^2\theta, \quad \text{(A4)}$$

where θ is the angle between the scattering vector $\mathbf{e}$ and the "structure weighted" mean spin vector, $\beta\langle p\mathbf{k}\rangle_B+\alpha\langle p\mathbf{k}\rangle_A$. For an unmagnetized specimen in which the direction of spontaneous domain magnetization is random we must also average the above result over all values of θ. Thus

$$\langle|\mathbf{F}|^2\rangle_{\text{domains}}=\tfrac{2}{3}|\beta\langle p\mathbf{k}\rangle_B+\alpha\langle p\mathbf{k}\rangle_A|^2. \quad \text{(A5)}$$

For the (111) peak of $MgFe_2O_4$, $\beta=8$ and $\alpha=-4\sqrt{2}$. Furthermore, we have only one species of magnetic ion, and so $p=p_{Fe}$. Thus Eq. (5) becomes

$$\langle|\mathbf{F}_{111}|^2\rangle_{\text{domains}}=\tfrac{2}{3}p_{Fe}{}^2|8\langle\mathbf{k}\rangle_B-4\sqrt{2}\langle\mathbf{k}\rangle_A|^2. \quad \text{(A6)}$$

It is to be noted that $\langle\mathbf{k}\rangle_B$ and $\langle\mathbf{k}\rangle_A$ represent averages of the spin vectors taken over *all* of the B and A sites, respectively. We are interested, however, in knowing the averages for the magnetic ions alone. Thus if the degree of inversion is 0.88, the fraction of A sites occupied by Fe^{+3} ions is 0.88 and the fraction of B sites occupied by Fe^{+3} is 0.56. Equation (6) then becomes

$$\langle|\mathbf{F}_{111}|^2\rangle_{\text{domains}}=\tfrac{2}{3}p_{Fe}{}^2|4.5\langle\mathbf{k}\rangle_{B'}-5.0\langle\mathbf{k}\rangle_{A'}|^2, \quad \text{(A7)}$$

where the primed subscripts indicate that the averages are to be taken only over the magnetic ions.

TABLE I. Calculated and observed integrated intensities for $MgFe_2O_4$ relative to (311).

($h\,k\,l$)	Calculated intensities: Nuclear[a]	Magnetic[b]	Total	Observed intensity
(111)	230	3270	3500	3370
(220)	1911	788	2700	2800
(311)	6370		6370 ↔	6370
(222)	560	429	990	1000
(400)	4830	720	5550	5500
(331)	11	828	840	634
(422)	1260	334	1590	1470
(511), (333)	4530		4530	4660
(440)	13 250		13 250	13 110
(531)	59	639	700	520
(620)	752		752	771
(533), (622)	2184		2180	2230
(444), (711), (551)	2534	162	2700	2670
(642), (731), (553)	4883		4880	4910

[a] The nuclear amplitudes used in the computation are $b_{Fe}=0.96\times10^{-12}$, $b_{Mg}=0.55\times10^{-12}$, and $b_O=0.58\times10^{-12}$.
[b] The magnetic contributions were computed using a smoothed form factor curve obtained from the points shown in Fig. 6.

The authors are indebted to Dr. D. A. Kleinman for helpful discussions in the course of this work.

Note added in proof.—Since the completion of this work, a report[14] of neutron diffraction studies of magnesium ferrite has been published by Bacon and Roberts. The nuclear scattering was separated from the magnetic scattering by comparison of room temperature data with data taken above the Curie point. For a degree of inversion consistent with the observed moment, a value of 0.382×0.002 was obtained for the U parameter in agreement with the present work in which both the U parameter and the degree of inversion were determined simultaneously from the diffraction data. Although a complete analysis of the magnetic scattering was not attempted, the intensities of the (111) and (220) peaks were found to be consistent with the Néel model.

[14] G. E. Bacon and F. F. Roberts, Acta Cryst. **6**, 57 (1953).

Broadening and Shift of the Second Doublet of the Rubidium Absorption Series Under Different Pressures of Argon and Helium*

SHANG-YI CH'EN AND DONALD A. KOHLER
Department of Physics, University of Oregon, Eugene, Oregon

(Received February 13, 1953)

The shift and broadening of the second doublet of the principal series of rubidium produced by argon and by helium were studied for pressures up to 123.5 atmospheres (rd 52) and up to 97.5 atmospheres (rd 44), respectively. The red shift produced by argon gives a linear relationship with its relative density, rd. The slopes for both components of the doublet are 2.95 cm^{-1}/rd. The violet shift produced by helium in the high pressure range is greater than linear with the rd. The $^2P_{\frac{1}{2}}$ component is shifted more than the $^2P_{\frac{3}{2}}$ component.

Argon shows a nicely linear broadening for both components over the entire range of rd. For the $^2P_{\frac{1}{2}}$ component the broadening is 2.28 cm^{-1}/rd and for the $^2P_{\frac{3}{2}}$ component it is 2.11 cm^{-1}/rd. Helium appears to give a definite quadratic broadening, particularly for the $^2P_{\frac{1}{2}}$ component.

INTRODUCTION

PRESSURE effects of N_2 (with rd up to 8) upon the second doublet of the principal series of potassium, and those of He, Ne, A, H_2, and N_2 (rd = 3) upon the second doublet of caesium have been reported by Watson and Margenau[1] and Füchtbauer and Gossler,[2] respectively. The latter observers reported the same shift and broadening (except for H_2) for the two doublet components, and showed that the shift or broadening *vs* relative density curves should be accurately linear. The former two observers found some difference in shifts for the doublet components, and the shift showed a tendency of higher than linear relationship with the relative density. They obtained the same values in broadening for the two doublet components and found a linear relationship with the relative density. The corresponding data for He, Ne, and A upon the second member of the rubidium principal series have been obtained by Ny and Ch'en[3] for pressures up to 12 atmospheres (rd 8). They were the first to emphasize the presence of the so-called "fine-structure pressure effects," i.e., the difference in behavior of shifts and broadening of the two doublet components, and showed that the relationship between shift and relative density was more than linear within that restricted pressure range.

These varied results of different observers on various foreign gas-alkali combinations at limited pressure ranges have not presented a clear picture for the consideration of theoretical physicists interested in the

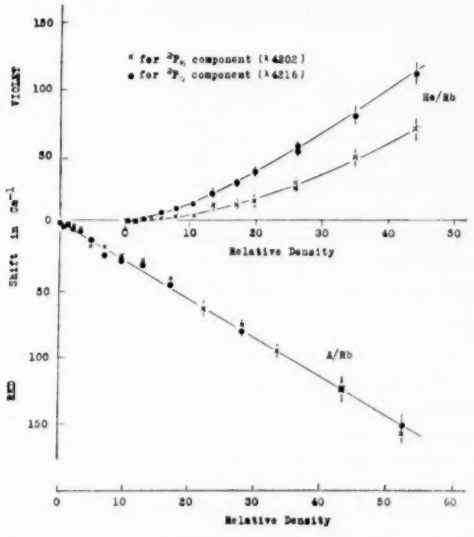

FIG. 1. Shift *vs* rd.

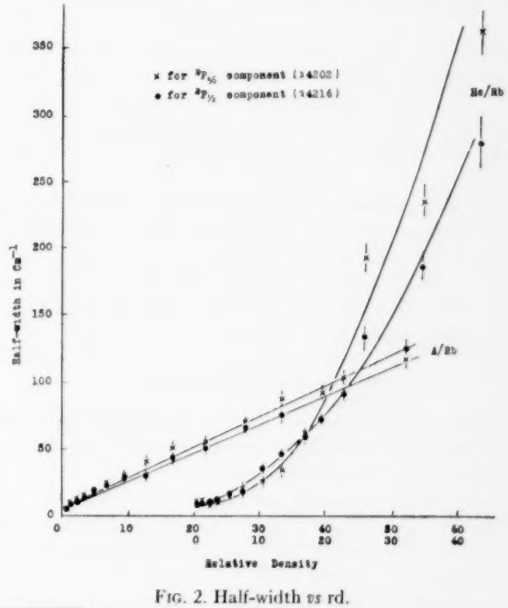

FIG. 2. Half-width *vs* rd.

* This work was first supported by a Frederick Gardner Cottrell grant from the Research Corporation, and then by the National Science Foundation.

[1] W. Watson and H. Margenau, Phys. Rev. **44**, 748 (1933).

[2] C. Füchtbauer and F. Gossler, Z. Physik **87**, 89 (1934).

[3] T. Z. Ny and S. Y. Ch'en, Phys. Rev. **52**, 1158 (1937).

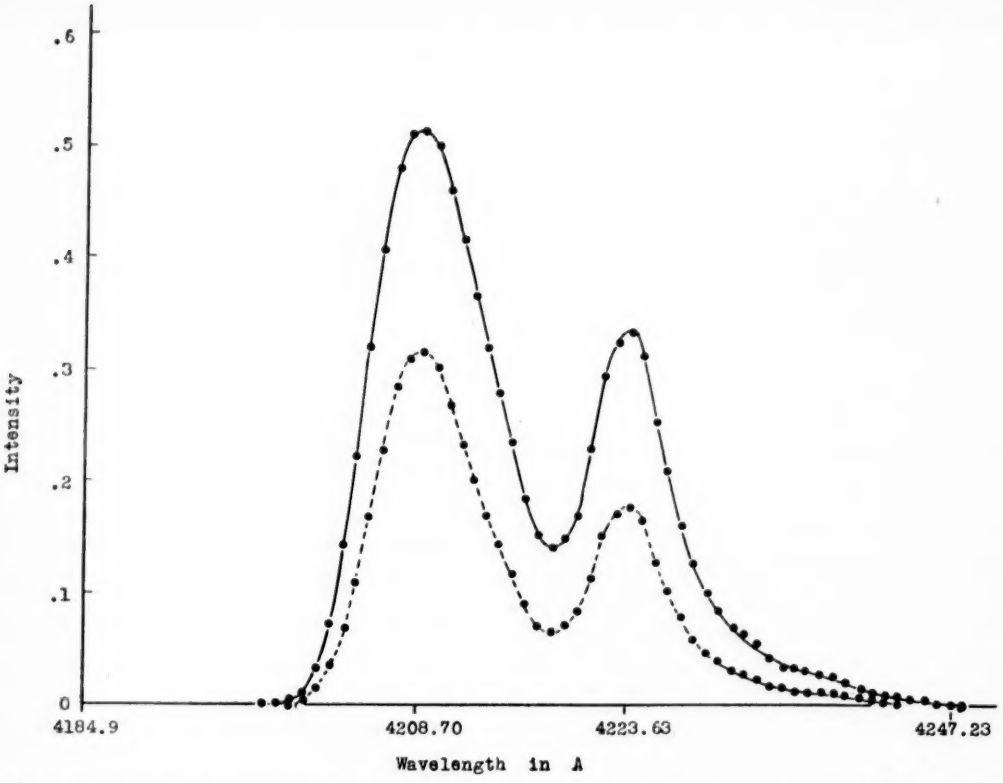

FIG. 3. The absorption line contour of the λλ4202 and 4216 lines of Rb under 34.8 atmos of argon (T=288°C, rd=16.91). The length of the absorbing column=6.66 cm. The ordinate of the solid curve is $(E_0-E_\lambda)/E_0$ and that for the dotted curve $\log_{10}(E_\lambda/E_0)$.

problem. Recent work by the Robins[4] has produced interesting results, showing the difference in behavior of shift and broadening for the resonance lines of rubidium, but this work gives little information regarding the behavior of the components of the second doublet.

In the present work observations were made for pressures up to 97.5 atmospheres (rd=44) for helium and up to 123.5 atmospheres (rd=52) for argon. More light is thrown on the general behavior of broadening and shifts of these spectral lines under these pressures of foreign gases.

EXPERIMENTAL RESULTS

The experimental set up, the instrument and the foreign gases used have been described previously.[5] Six-in. type supergauges, obtained from the U. S. Gauge Company, with pressure ranges 600, 2000, and 3000 lb/in.^{2} were used. The continuous spectrum source of constant intensity was a General Electric 30-amp 7.5-v tungsten ribbon lamp. The length of the rubidium vapor column was maintained at 6.66 cm. The temperatures ranged from 232° to 372°C and 238° to 333°C for argon and helium, respectively. As a result of the rather low dispersion of the Bausch and Lomb, large, quartz Littrow spectrograph in this region (12.4 A/mm), the graininess of the Eastman 103-0 plates used as shown by the microphotometer traces, and the overlapping of the lines for high pressures, the readings may have an error as indicated in Figs. 1 and 2.

(a) Shift

As shown in Fig. 1, the red shift produced by argon exhibits a linear relationship with its rd. The straight line drawn according to readings for the $^2P_{\frac{1}{2}}$ component (λ4216) has the same slope as the straight line drawn according to the readings for the $^2P_{\frac{3}{2}}$ component (λ4202). The slopes for both components are thus 2.95 cm^{-1} per unit rd. The shift for argon at lower pressures may possibly be nonlinear, as also pointed out in the previous article,[3] but when the entire pressure range is considered the shift is definitely linear.

In contrast, the violet shift produced by helium in the same pressure range appears to be according to a

[4] J. Robin and S. Robin, Compt. rend. **233**, 1019 (1951).
[5] E. D. Clayton and S. Y. Ch'en, Phys. Rev. **85**, 68 (1952).

power somewhat less than the quadratic and greater than linear in rd. In the lower pressure range the nonlinearity is quite evident, but the plot seems to approach a straight line at a higher pressure range. The $^2P_{\frac{1}{2}}$ component is shifted more than the $^2P_{\frac{3}{2}}$ component by an appreciable amount.

(b) The Broadening

Figure 2 shows the relationship between the halfwidths of the two components and the relative density of argon or helium. Argon gives again a nicely linear broadening for both components over the entire range of relative density. The $^2P_{\frac{1}{2}}$ component exhibits very slightly greater broadening than the $^2P_{\frac{3}{2}}$ component. The slope for the $^2P_{\frac{1}{2}}$ component is 2.28 cm^{-1}/rd and that for the $^2P_{\frac{3}{2}}$ component is 2.11 cm^{-1}/rd. To exemplify the exact shape of the broadened doublet under a particular pressure of argon, Fig. 3 is given. For the convenience of the reader the curve is plotted with two quantities as vertical coordinate, $(E_0-E_\lambda)/E_0$ and $\log_{10}(E_\lambda/E_0)$, E_0 being the incident intensity, and E_λ the energy transmitted after absorption by the vapor at wavelength λ. Thus, $(E_0-E_\lambda)/E_0$ is the absorption of light intensity by the chamber of vapor of 6.66-cm length at wavelength λ per unit incident intensity.

Helium appears to give a definite quadratic broadening, particularly for the $^2P_{\frac{1}{2}}$ component. For the $^2P_{\frac{3}{2}}$ component the broadening appears to be rather less than quadratic.

DISCUSSION

It is to be noted that results in Figs. 1 and 2 agree very well with those in reference 3 within that small rd range. Although no data are available yet to compare the present results with results for the second doublets of the other alkali atoms under pressures of argon or helium, it is expected that curves in Figs. 1 and 2 should represent quite closely the corresponding (unobserved) readings for the second member of the principal series of other alkali atoms perturbed by argon and helium.

It is also to be noted that although the general trend of the curve in Fig. 1 for argon is definitely linear, there are indications of an irregular behavior at low rd region, the significance of which is not yet clear. The temperature differences of these readings are not responsible for the irregularity because the temperature was increased with pressure increase in a fairly uniform manner. The small temperature effect would be regularly added.

The fact that the shift and the broadening produced by argon for the two components is the same (or nearly the same for broadening), while that produced by helium is different is probably attributable to the difference in the distance of closest collision and, thus, the difference in perturbation of the wave functions of the two doublet components being more perceptible for closer distance of collision.

The broadening of the $^2P_{\frac{1}{2}}$ component was a little greater than that of the $^2P_{\frac{3}{2}}$ component when the pressure was below 45 atmos (rd about 19) in agreement with previous observations.[3] This exception to the general behavior of fine-structure pressure broadening, as pointed out in reference 5, was removed when the pressure was higher than this value, *viz.*, the broadening of the $^2P_{\frac{1}{2}}$ component turned out to be comparatively greater than that of the $^2P_{\frac{3}{2}}$ component.

PHYSICAL REVIEW VOLUME 90, NUMBER 6 JUNE 15, 1953

The Forces Between Hydrogen Molecules

ARTHUR A. EVETT AND HENRY MARGENAU
Yale University, New Haven, Connecticut

(Received March 2, 1953)

Earlier calculations of the H_2-H_2 interaction, based on the use of screening-constant functions, seemed to lead to reasonable answers only with the use of a nuclear charge much greater than the correct value for the isolated molecule, $Z_0=1.166$. The present work is a recalculation of the exchange forces for $Z=Z_0$. A small numerical error in the earlier work is eliminated, and the exchange energy, instead of being slightly negative as reported previously, is actually positive. This removes all perplexing features from the problem and yields results in substantial agreement with experiments.

The total interaction, consisting of exchange, van der Waals, and quadrupole energies, is plotted for different relative orientations of the molecules in Fig. 2. A weighted average over all orientations is shown in Fig. 3 and compared with the semi-empirical curve of Hirschfelder, Bird, and Spotz, which was derived by fitting viscosity data.

THE theory of the total interaction between hydrogen molecules, based on the Wang treatment for a single molecule, was published in 1943.[1] Unlike the simpler work of De Boer,[2] it included all exchange integrals (though some of them had to be approximated); but the results were discouraging inasmuch as an

[1] H. Margenau, Phys. Rev. **64**, 131 (1943). This will be referred to as I hereafter.

[2] J. De Boer, Physica **9**, 363 (1942). See also T. Nagamiya and H. Kishi, Researches Chem. Phys. (Japan) **39**, 64 (1951).

unreasonable choice of the screening constant Z had to be made in order to obtain a satisfactory interaction. We now wish to report a numerical error in the computation of the exchange energy for the case $Z=1.166$ which, instead of being slightly negative as given in I, is actually positive. Indeed, recalculation of this one instance has removed all perplexing features from this important problem and yields results in substantial agreement with experiments.

The symbols used in the present note are defined in I; in particular, the exchange energy η is given by Eq. (22). A simple generalization in the treatment of the problem will be made: While previously the same Z was used for all distances of interaction, this will now be allowed

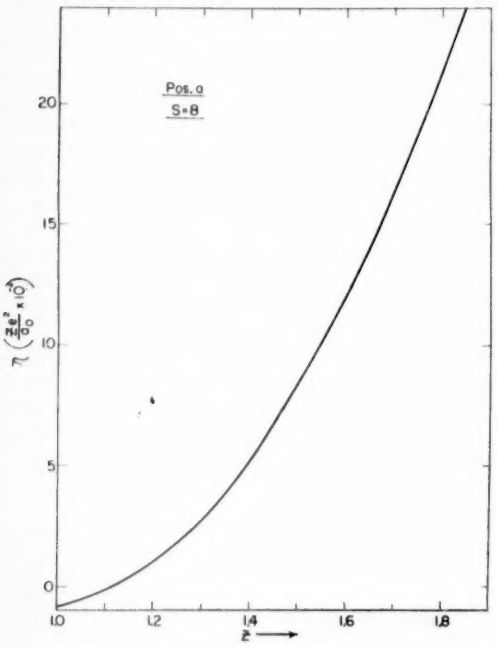

FIG. 1. Exchange energy η *vs* screening constant Z.

to vary. For fixed Z the first-order energy of two interacting molecules is

$$E=4D(Z)+2E_m(Z)+\eta(Z, R), \qquad (1)$$

provided D is the energy of a hydrogen-like atom of charge Z, E_m the molecular energy ($=\frac{1}{2}E_0'$ in the notation of reference 1), and η the intermolecular energy. The value of Z which minimizes $2D+E_m$ is $1.166=Z_0$. If we allow Z to change, we must define a new exchange interaction:

$$\bar{\eta}(Z, R)=4D(Z)+2E_m(Z)+\eta(Z, R) -4D(Z_0)-2E_m(Z_0). \qquad (2)$$

For $Z=Z_0$, $\bar{\eta}=\eta$. At any given intermolecular distance R and for a particular orientation of the molecules, the best value of Z is the one which minimizes $\bar{\eta}$.

To show in a general way how η depends on Z we present in Fig. 1 a graph of η at constant ZR. The points are taken from the earlier work, except for the recalculated one at $Z=1.166$. It is seen that η turns negative at $Z=1.12$ and is still positive at Z_0. This correction, though not very large in magnitude, removes the difficulties of interpretation and the artificialities in the previous treatment.

In the region $1.0<Z<1.4$, Eq. (2) is closely approximated by $\bar{\eta}(Z, R)=\eta(Z, R)+6.34(Z-Z_0)^2(Z+7.202)$ ev. If Z differs from Z_0 by more than 0.01, the second term on the right becomes dominant in the region $R>3.0$A. Hence the best value of Z must lie in the immediate neighborhood of Z_0. The choice of 1.428 in I, while yielding an acceptable η on the fixed Z interpretation, leads to values of $\bar{\eta}$ entirely too large because of the change in the molecular energy.

More extensive calculations have now been made for $Z=1.166$. Instead of the three relative orientations of the molecules considered in I, we have chosen four, labeled as follows.

Case (a): Both molecular axes are parallel to R, the line joining the centers.

Case (b): One axis is parallel, the other perpendicular to R.

Case (c): Both axes are perpendicular to R and parallel to each other.

Case (d): Both axes are perpendicular to R and perpendicular to each other. Case (d) was not treated in the earlier paper.

Figure 1 refers to position (a) only; but analogous results are obtained for the other cases, and the conclusion regarding the value of Z at which η becomes negative is generally true.

Table I shows the exchange energy $\bar{\eta}=\eta$ as a function of the intermolecular separation R for $Z=1.166$. This is the interaction energy exclusive of the dispersion energy E_d and the quadrupole energy E_Q.

The latter two contributions are taken from our earlier work.[3] As was shown,

$$E_d=-15.4\frac{e^2}{a_0}\left(\frac{a_0}{R}\right)^6=-\frac{9030}{R^6}\ \text{millivolts}, \qquad (3)$$

the latter if R is in A. This formula includes a correction

TABLE I. Exchange energy as a function of the intermolecular separation (R) for $Z=1.166$.

S	R (in A)	η (in millivolts) Pos. (a)	Pos. (b)	Pos. (c)	Pos. (d)
5	2.27	154.2	150.7	138.46	139.90
6	2.72	38.08	34.20	30.45	30.37
7	3.18	8.364	7.304	6.306	6.262
8	3.63	1.680	1.402	1.202	1.151

[3] The values for E_Q listed in Table VI of I are too small by a factor 16/3. We are grateful to Professor J. O. Hirschfelder for calling this to our attention.

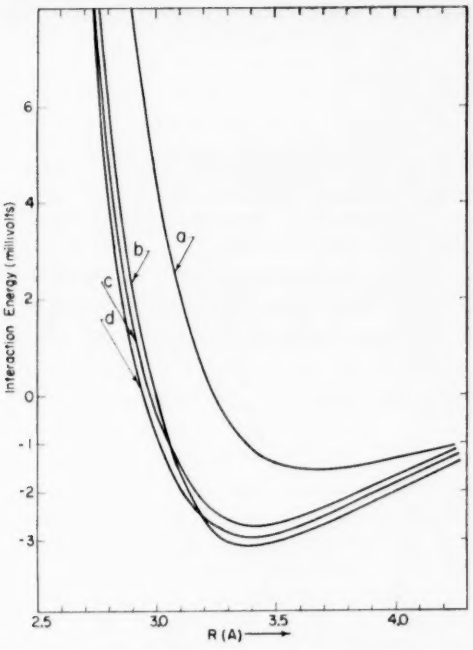

FIG. 2. Total energy of interaction for different molecular orientations as function of intermolecular distance.

for the instantaneous dipole-quadrupole component of the van der Waals force.

The energy resulting from the interaction of the permanent quadrupoles carried by the molecules is [see Eq. (26)]

$$E_Q=\frac{3}{25}\left(\frac{\Delta^2}{1+\Delta^2}\right)^2\frac{e^2d^4}{R^5}f(\theta_1,\theta_2,\varphi), \tag{4}$$

d being the separation of the atoms in a molecule, and Δ the overlap integral. The smaller Z used here makes Δ much greater than in I, and therefore the quadrupole energy is much more important. The function f, which depends on the relative orientations of the molecules, has the values 8, -4, 3, 1 for positions (a), (b), (c), (d), respectively. In the present instance $\Delta=0.685$, $d=1.406\,a_0$, and

$$E_Q=\tfrac{3}{4}([0.252)^2/R^5]e^2a_0^4\cdot f. \tag{5}$$

In Fig. 2 are shown the results of compounding $\bar{\eta}$ and the quantities represented by Eqs. (3) and (5). The curves of b, c, and d now fall quite close together, the main reason being the opposite signs of a more effective E_Q in cases (b) and (c). The crossing of the curves b, c, and d is hardly meaningful, for the simple form (5) is not very accurate at these small values of R.

For comparison with semi-empirical data it is necessary to compute an average over cases (a) to (d). This average curve was obtained by the following procedure. Assuming that all orientations of one molecule with respect to the intermolecular axis are equally probable, we find the volume of configuration space for two molecules in which the molecular axes depart by not more than 45° from our schematized four cases. These cases then exhaust the configuration space, and if the volumes thus specified are taken as statistical weights, then the factors multiplying curves a, b, c, d in the averaging process turn out to be 0.085, 0.415, 0.25, and 0.25, respectively.

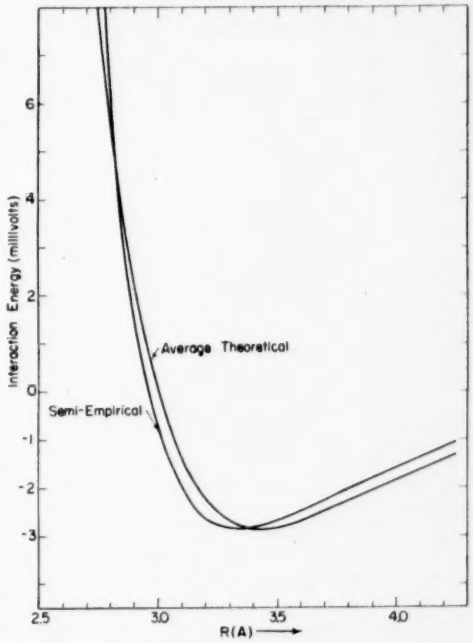

FIG. 3. Comparison of theoretical interaction (averaged over molecular orientations) with empirical curve of Hirschfelder, Bird, and Spotz.

The curve obtained is plotted in Fig. 3, together with the results derived by Hirschfelder, Bird, and Spotz[4] from viscosity data. The work of De Boer and Michels,[5] based on an evaluation of second virial coefficients and including quantum effects, leads to points slightly lower than Hirschfelder's. The essential agreement of our interaction, which relies on no empirical parameters, with both of these seems gratifying.

[4] Hirschfelder, Bird, and Spotz, J. Chem. Phys. **16**, 968 (1948).
[5] J. De Boer and A. Michels, Physica **5**, 945 (1938).

Absorption Line Width in the Infrared Spectrum of Atmospheric Carbon Dioxide*

ARTHUR ADEL
Arizona State College, Flagstaff, Arizona
(Received January 7, 1953)

Line width in the 15-micron band of atmospheric carbon dioxide has been determined by direct observation of line contour. The influence of finite width of slit has been eliminated by numerical correction. 0.12 cm^{-1} is an upper limit for the CO_2 absorption coefficient half-width at half-height.

I. INTRODUCTION

As is well known, the absorption coefficient half-width, D_0, is an important parameter in the problem of the thermal balance of the atmosphere. It is thus important that D_0 be determined for the radiatively significant constituents of the atmosphere. These are

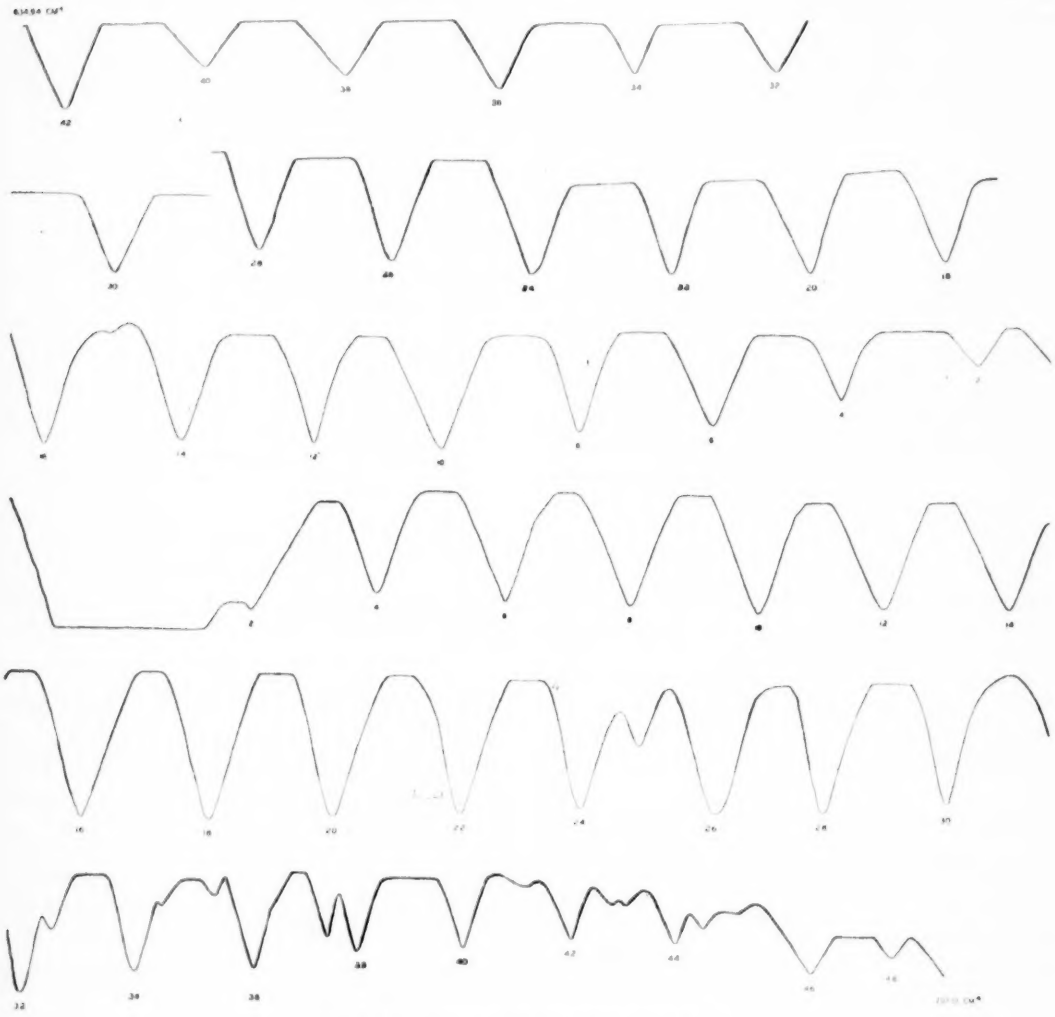

FIG. 1. Line contours in the 15-micron band of CO_2.

* This work was supported in part by a contract with the United States Air Force, through sponsorship of the Geophysical Research Division, Air Force Cambridge Research Center, Air Research and Development Command.

mainly the polyatomic molecules. D_0 is now known for nitrous oxide and water vapor,[1] and the present report deals with the carbon dioxide molecule.

Line width may be measured quite directly by exploring the absorption line with a sufficiently narrow slit and then making a correction for slit influence.

Infrared lines are generally exceedingly narrow. For example, the directly observed absorption line half-width in N_2O, at a pressure of 30 cm Hg, prior to correction for slit width, was found to be but 0.09 cm^{-1}. The need for narrow slits is evident, for one may hope to explore a line significantly only if the slit is of the order of narrowness of the line itself.

The details of the methods of achieving narrow effective slits and making the correction for finite width of slit are given in reference 1 and so will not be repeated here.

II. EXPERIMENTAL

The second fundamental of atmospheric CO_2 was explored from 634.94 cm^{-1} to 707.51 cm^{-1}, and all lines in between were mapped, from number 42 in the *P* branch through number 48 in the *R* branch. A Pfund-type spectrometer of one meter focal length equipped with a 2400 lines per inch grating, fore-prism, and Nernst glower provided a total atmospheric path of six meters. The effective slit half-width was maintained at 0.14 cm^{-1} over the band.

The lines, arranged in sequence from *P* branch through *Q* and *R* branches, are presented in Fig. 1. Their positions are given by the expression

$$\tilde{\nu}_J = 667.5 \pm 0.780J + 0.00045J^2 \text{ cm}^{-1}.$$

III. REDUCTION

The analysis, reference 1, is valid only for weak lines because of the assumption

$$e^{-k(\nu)t} \cong 1 - k(\nu)t.$$

[1] Arthur Adel, Phys. Rev. **71**, 806 (1947).

TABLE I. Apparent half-widths.

P branch		*R* branch	
Line No.	Apparent half-width *D* (cm^{-1})	Line No.	Apparent half-width *D* (cm^{-1})
42	0.221	2	...
40	0.221	4	0.232
38	0.218	6	0.266
36	0.223	8	0.283
34	0.140	10	0.292
32	0.193	12	0.318
30	0.204	14	0.272
28	0.221	16	0.304
26	0.222	18	0.292
24	0.238	20	0.291
22	0.186	22	0.274
20	0.232	24	0.225
18	0.201	26	0.367
16	0.213	28	0.257
14	0.245	30	0.240
12	0.204	32	0.209
10	0.260	34	0.219
8	0.197	36	0.227
6	0.263	38	0.179
4	0.169	40	0.182
2	0.181	42	0.176
		44	0.151

Application of the analysis to lines of even moderate strength will yield conservative values; that is, values slightly in excess of the true D_0. For this reason the very deep lines, numbers 6 through 30 in the *R* branch, have been excluded from the final reduction (see Table I).

The reduction of the remaining lines was effected by averaging the *apparent* line half-widths (Table I): $D_{Av} = 0.208$ cm^{-1}, and applying the analysis of reference 1. The ratio of average *apparent* line half-width to slit half-width is 1.5, whence the analysis[1] yields $D_0 = D/1.7 = 0.12$ cm^{-1}.

The conservative value 0.12 cm^{-1} is notably smaller than the values heretofore assumed for the absorption coefficient half-width of the rotation-vibration lines of carbon dioxide under atmospheric conditions, and will thus require a re-examination of existing calculations bearing on the thermal structure of the atmosphere.

Polarization of Bremsstrahlung Radiation

R. L. GLUCKSTERN, M. H. HULL, JR., AND G. BREIT
Yale University, New Haven, Connecticut*
(Received February 25, 1953)

The dependence of the differential cross section for bremsstrahlung on photon polarization is calculated in the same approximation as the Bethe-Heitler formula for the sum over polarizations. The radiation is found to consist of a mixture of an unpolarized and a linearly polarized component. The relation of the method of intermediate states to the method of transitions between stationary states is explicitly stated.

I. INTRODUCTION

IT is well known that x-rays produced when an electron strikes a solid target are polarized. Sommerfeld[1] has treated this process on the basis of nonrelativistic quantum mechanics and showed the correspondence with the classical picture of the radiation being due to the acceleration of a charged particle in the electric field of a nucleus.

The cross section for bremsstrahlung summed over photon polarization has been treated on the Dirac theory of the electron by Heitler[2,3] and by Bethe and Heitler.[4] The cross section for arbitrary photon polarization was obtained by May and Wick[5] by means of the Weizsäcker-Williams method[6] and by May[7] as an extension of the Bethe-Heitler formula for extreme relativistic energies ($\gg 137Z^{-\frac{1}{2}}mc^2$). All of these calculations presuppose the validity of the first Born approximation in the calculation of the effect of the Coulomb field on the electron wave function, namely $Ze^2/\hbar v \ll 1$. Maximon and Bethe[8] and Bess[9] have investigated the change in the Bethe-Heitler formula for large Z using the more exact wave function of Furry[10] and of Sommerfeld and Maue.[11] The exact answer for the first nonvanishing term in the interaction with transverse photons has not been obtained even for the intensity summed over polarizations.

The assumptions involved in the derivation of the differential cross section formula[7,12] for arbitrary photon polarizations are analyzed below in Sec. II. Stationary states of matter are considered as being perturbed by radiation and the first-order effects in $e^2/\hbar c$ are calculated, reducing the problem to the consideration of Einstein's spontaneous emission probability. Comparison with other treatments shows the equivalence of this consideration and that of intermediate states. In Sec. III some symmetry considerations regarding the nature of photon polarization are discussed.

Symbols and Notation

$\mathbf{p}_0$, $\mathbf{p}$ = Initial and final momentum of the electron.
E_0, E = Initial and final total energy of the electron.
$\mathbf{k}$, k = Momentum and energy of the emitted photon.
θ_0, θ = Angle of $\mathbf{p}_0$ and $\mathbf{p}$ with respect to $\mathbf{k}$.
$d\Omega_0$, $d\Omega$ = Element of solid angle in the directions $\mathbf{p}_0$ and $\mathbf{p}$, taken with respect to $\mathbf{k}$.
Ψ_0, Ψ = Dirac wave functions of the initial and final states of the electron in the field of the nucleus.
Φ_0, Φ = Initial and final states of the radiation field.
$\boldsymbol{\alpha}$ = Dirac matrix vector.
α_l = Component of $\boldsymbol{\alpha}$ in the direction of polarization.
a, $a^\dagger$ = Creation and destruction operators for the electron.
$\mathcal{U}$ = Fundamental volume for normalization.
$\mathbf{A}_R$ = Vector potential of the radiation field.
φ_0, φ = Time independent 4-component Dirac spinors for the initial and final electron states.
α, S = Direction of spin and sign of energy.
Z = Nuclear charge.
H = Dirac Hamiltonian ($H=-\boldsymbol{\alpha}\cdot\mathbf{p}-\beta m$).
$\mathbf{q}$ = Momentum transferred to the nucleus ($\mathbf{q}=\mathbf{p}_0-\mathbf{p}-\mathbf{k}$).
$\epsilon'^2 = -2(kE-\mathbf{k}\cdot\mathbf{p}) = -2k\Delta$.
$\epsilon''^2 = 2(kE_0-\mathbf{k}\cdot\mathbf{p}_0) = 2k\Delta_0$.
$\Delta_0 = E_0 - p_0\cos\theta_0$.
$\Delta = E - p\cos\theta$.
γ^μ = Matrix four-vector $(\boldsymbol{\gamma}, \gamma^4)$; $\boldsymbol{\gamma} = -i\beta\boldsymbol{\alpha}$, $\gamma^4 = -\beta$.
γ^l = Component of $\boldsymbol{\gamma}$ in the direction of polarization.
$p_{0\mu}$, p_μ = Momentum energy four vectors $(\mathbf{p}_0, iE_0)$ and $(\mathbf{p}, iE)$ for initial and final electron states.
$\gamma A = \gamma^\mu A_\mu$.

The constants $\hbar$ and c will be taken as 1 throughout the paper except where the meaning may be clearer with the explicit use of $\hbar$ and c.

* Assisted by the joint program of the U. S. Office of Naval Research and the U. S. Atomic Energy Commission.

[1] A. Sommerfeld, Ann. Physik **11**, 257 (1931).
[2] W. Heitler, Z. Physik **84**, 145 (1933).
[3] W. Heitler, *The Quantum Theory of Radiation* (Oxford University Press, London, 1949), second edition, p. 161.
[4] H. A. Bethe and W. Heitler, Proc. Roy. Soc. (London) **A146**, 83 (1934).
[5] M. May and G. C. Wick, Phys. Rev. **81**, 628 (1951).
[6] C. F. Weizsäcker, Z. Physik **88**, 612 (1934); E. J. Williams, Kgl. Danske Videnskab. Selskab. Mat.-fys. Medd. **13**, No. 4 (1935); Phys. Rev. **45**, 729 (1934).
[7] M. May, Phys. Rev. **84**, 265 (1951).
[8] L. C. Maximon and H. A. Bethe, Phys. Rev. **87**, 156 (1952).
[9] L. Bess, Phys. Rev. **77**, 550 (1950).
[10] W. H. Furry, Phys. Rev. **46**, 391 (1934).
[11] A. Sommerfeld and A. W. Maue, Ann. Physik **22**, 629 (1935).
[12] Gluckstern, Hull, and Breit, Science **114**, 480 (1951).

II. DIFFERENTIAL CROSS SECTION

The radiation field is treated as a perturbation between states of the electron in the field of the nucleus. Thus if Ψ_0 and Ψ are the Dirac wave functions of the initial and final states of the electron in the field of the nucleus, and if Φ_0 and Φ are the initial and final states of the radiation field, the matrix element for the emission of a photon with momentum $\mathbf{k}$ is given by

$$\mathfrak{M}=\{\Phi\Psi,\ e(\boldsymbol{\alpha}\cdot\mathbf{A}_R)\Phi_0\Psi_0\},\tag{1}$$

where $\boldsymbol{\alpha}$ is the Dirac matrix vector and $\mathbf{A}_R$ is the vector potential of the radiation field. It is convenient to make use of Heisenberg and Pauli's second form of quantum electrodynamics, employing the choice of gauge enabling the elimination of the electrostatic field and leaving the radiation variables only in the description of transverse waves. This is the form of radiation theory which has proved especially useful in nonrelativistic quantum mechanics. The interaction energy with the radiation field may be written as[13]

$$(\boldsymbol{\alpha}\cdot\mathbf{A}_R(\mathbf{r}))=\sum_{\text{states}}\alpha_l(\mathcal{U}k/2\pi)^{-\frac{1}{2}}\times\{a\exp(-i\mathbf{k}\cdot\mathbf{r})+ia^\dagger\exp(i\mathbf{k}\cdot\mathbf{r})\},\tag{2}$$

where α_l is the component of $\boldsymbol{\alpha}$ in the direction of polarization, and $\mathcal{U}$ is the fundamental volume used for normalization. Only the creation operator a contributes to spontaneous emission, and the matrix element becomes

$$\mathfrak{M}=e(\mathcal{U}k/2\pi)^{-\frac{1}{2}}\{\Psi,\ \alpha_l\exp(-i\mathbf{k}\cdot\mathbf{r})\Psi_0\}.\tag{3}$$

If exact wave functions of the continuous spectrum were used for Ψ_0 and Ψ in Eq. (3), one would have the true cross section except for radiative corrections, the treatment of which is not attempted in the present paper. The success of the Bethe-Heitler formula indicates that the treatment of matter waves by the first Born approximation should be good enough for many purposes, and all of the work below is carried out by means of this simplifying device. One then has

$$\mathcal{U}^{\frac{1}{2}}\Psi_0(\mathbf{r})=\varphi_0\exp(i\mathbf{p}_0\cdot\mathbf{r})-\left(\frac{Ze^2}{2\pi^2\mathcal{U}^{\frac{1}{2}}}\right)\times\int\sum_{\alpha'S'}\frac{\varphi'\exp(i\mathbf{p}'\cdot\mathbf{r})(\varphi',\varphi_0)d\mathbf{p}'}{(E'-E_0)|\mathbf{p}'-\mathbf{p}_0|^2},\tag{4.1}$$

$$\mathcal{U}^{\frac{1}{2}}\Psi(\mathbf{r})=\varphi\exp(i\mathbf{p}\cdot\mathbf{r})-\left(\frac{Ze^2}{2\pi^2\mathcal{U}^{\frac{1}{2}}}\right)\times\int\sum_{\alpha''S''}\frac{\varphi''\exp(i\mathbf{p}''\cdot\mathbf{r})(\varphi'',\varphi)d\mathbf{p}''}{(E''-E)|\mathbf{p}''-\mathbf{p}|^2},\tag{4.2}$$

where φ_0, φ, φ', and φ'' are the Dirac 4-vectors for the various electron states, α denotes the spin orientation, and S the sign of the energy in the perturbed states with moments $\mathbf{p}'$ and $\mathbf{p}''$ and energy E' and E''.

If Eqs. (4.1) and (4.2) are inserted into Eq. (3), the lowest order nonvanishing terms are the two linear in Z. The integration over $\mathbf{r}$ in Eq. (3) gives a delta-function for each of these terms, in one case giving $\delta(\mathbf{p}'-\mathbf{p}-\mathbf{k})$ and in the other $\delta(\mathbf{p}''-\mathbf{p}_0+\mathbf{k})$. The $\mathbf{p}'$ and $\mathbf{p}''$ integration then yields an expression of the form

$$\sum_{\alpha\alpha_0}\left|\sum_{\alpha'S'}\frac{(\varphi,\alpha_l\varphi')(\varphi',\varphi_0)}{E'-E_0}+\sum_{\alpha''S''}\frac{(\varphi,\varphi'')(\varphi'',\alpha_l\varphi_0)}{E''-E}\right|^2.\tag{5}$$

The sums over α', α'', S'' may be performed with the aid of the factors $(H'+E)/(E'+E)$ and $(H''+E_0)/(E''+E_0)$ which make the denominators independent of the sign of the energy in the perturbed electron state. Here $H'=-\boldsymbol{\alpha}\cdot\mathbf{p}'-\beta m$ and $H''=-\boldsymbol{\alpha}\cdot\mathbf{p}''-\beta m$. The resulting expression is of the form

$$\sum_{\alpha,\alpha_0}|(\varphi,(A+B)\varphi_0)|^2,\tag{6}$$

where

$$A=\alpha_l(H'+E_0)/\epsilon'^2;\quad B=(H''+E)\alpha_l/\epsilon''^2,$$

$$\epsilon'^2=E'^2-E_0^2=(\mathbf{p}+\mathbf{k})^2+m^2-E_0^2=-2(kE-\mathbf{k}\cdot\mathbf{p}),\tag{6.1}$$

$$\epsilon''^2=E''^2-E^2=(\mathbf{p}_0-\mathbf{k})^2+m^2-E^2=2(kE_0-\mathbf{k}\cdot\mathbf{p}_0).$$

The average over the initial spin states and sum over the final spin states is carried out by using the projection operators $(H+E)/2E$ and $(H_0+E_0)/2E_0$ in the usual way. The cross section then becomes

$$d\sigma=(Z^2e^6/8\pi^2)(p/p_0)(kdk/q^4)\times\mathrm{Tr}\{(\bar{A}^*+\bar{B}^*)(H+E)(A+B)(H_0+E_0)\}d\Omega d\Omega_0,\tag{7}$$

where the symbols $\bar{A}^*$ and $\bar{B}^*$ represent the Hermitian conjugates of the matrices A and B, and the momentum transferred to the nucleus is given by

$$\mathbf{q}=\mathbf{p}_0-\mathbf{p}-\mathbf{k}.\tag{7.1}$$

Equation (7) may also be reached formally by use of Feynman diagrams. The terms A and B in Eq. (7) correspond to the two diagrams in which the photon emitted "after" and "before" the interaction of the electron with the field of the nucleus, and may be written down directly according to Feynman's prescription.[14] However, the relationship to the nonrelativistic emission probability calculations employing exact nonrelativistic functions is not immediately clear in the method of Feynman diagrams.

The evaluation of the trace in Eq. (7) can lead to an unreasonable amount of work unless it is properly arranged and a few of the intermediate steps will be outlined therefore. It is convenient to introduce the matrices

$$\gamma^\mu=(\boldsymbol{\gamma},\gamma^4),\quad \boldsymbol{\gamma}=-i\beta\boldsymbol{\alpha},\quad \gamma^4=-\beta.\tag{8}$$

[13] The notation used is similar to that of G. Breit, Revs. Modern Phys. **4**, 504 (1932).

[14] R. P. Feynman, Phys. Rev. **76**, 749, 769 (1949).

The functions $H+E$ and H_0+E_0 may be written in terms of the momentum energy four-vectors as

$$H+E=-i(\gamma p+im)\gamma^4, \quad H_0+E_0=-i(\gamma p_0+im)\gamma^4, \tag{9}$$

where γp stands for $\Sigma_\mu \gamma^\mu p_\mu$ and

$$p_\mu=(\mathbf{p}, iE), \quad p_{0\mu}=(\mathbf{p}_0, iE_0). \tag{9.1}$$

The quantities A, B, $\bar{A}^*$, and $\bar{B}^*$ in Eq. (7) may similarly be written as

$$A=\gamma^l\gamma^4(\gamma p+im)\gamma^4/\epsilon'^2, \quad \bar{A}^*=(\gamma p'+im)\gamma^4\gamma^l\gamma^4/\epsilon'^2,$$
$$B=(\gamma p''+im)\gamma^4\gamma^l\gamma^4/\epsilon''^2, \quad \bar{B}^*=\gamma^l\gamma^4(\gamma p''+im)\gamma^4/\epsilon''^2, \tag{10}$$

where

$$p_\mu'=p_\mu+k_\mu=p_{0\mu}-q_\mu$$

and

$$p_\mu''=p_{0\mu}-k_\mu=p_\mu+q_\mu, \tag{10.1}$$

with

$$k_\mu=(\mathbf{k}, ik) \quad \text{and} \quad q_\mu=(\mathbf{q}, 0).$$

The γ-matrices obey the usual commutation rule

$$\gamma^\mu\gamma^\nu+\gamma^\nu\gamma^\mu=2\delta_{\mu\nu}, \tag{11}$$

and γ^l, the component of $\boldsymbol{\gamma}$ in the direction of polarization, having only a space component, anticommutes with γ^4.

The terms arising in Eq. (7) separate naturally into those proportional to $(\epsilon')^{-4}$, $(\epsilon'\epsilon'')^{-2}$, and $(\epsilon'')^{-4}$. For example, the term proportional to $(\epsilon')^{-4}$ is

$$-(\epsilon')^{-4}\,\mathrm{Tr}\{(\gamma p_0+im)\gamma^4(\gamma p'+im)\gamma^l \times(\gamma p+im)\gamma^l(\gamma p'+im)\gamma^4\}. \tag{12}$$

In the evaluation of the trace, the commutation rule is conveniently written in the form

$$(\gamma A)(\gamma B)=2\textstyle\sum_\mu A_\mu B_\mu-(\gamma B)(\gamma A). \tag{11.1}$$

Since a trace is invariant under a cyclic permutation of its factors, one can arrange for the second factor $\gamma p'+im$ to occur first, having first removed the free factors γ^4, γ^l by means of Eq. (11.1). Employing next relations such as

$$(im+\gamma p)(im-\gamma p)=-m^2-\textstyle\sum_\mu p_\mu p_\mu=0,$$
$$(im+\gamma p')(im-\gamma p')=-m^2-\textstyle\sum_\mu p_\mu' p_\mu'=-\epsilon'^2, \tag{13}$$
$$\mathrm{Tr}[1]=4, \quad \mathrm{Tr}[(\gamma A)(\gamma B)]=4\textstyle\sum_\mu A_\mu B_\mu,$$

one obtains the term displayed in Eq. (12) after some simple manipulation as

$$8p_l^2(4E_0^2-q^2)(\epsilon')^{-4}+8(p_lq_l-E_0k)(\epsilon')^{-2} +2(\epsilon'')^2(\epsilon')^{-2}. \tag{14.1}$$

In a similar manner the term containing the factor $(\epsilon'')^{-4}$ is found to be the result of changing p to p_0, ϵ' to ϵ'', E to E_0, k to $-k$, q to $-q$ in Eq. (14.1). The part of the trace containing $(\epsilon'\epsilon'')^{-2}$ is similarly found to be

$$16p_lp_0(4EE_0-q^2)(\epsilon'\epsilon'')^{-2}+8(p_{0l}q_l-kE)(\epsilon'')^{-2} -8(p_lq_l-kE_0)(\epsilon')^{-2}-8k^2q^2+4. \tag{14.2}$$

Combining these three contributions, one obtains

$$d\sigma=(Z^2e^6/4\pi^2)(p/p_0)(dk/kq^4)d\Omega d\Omega_0 \times\{(4E_0^2-q^2)(p_l^2/\Delta^2)+(4E^2-q^2)(p_{0l}^2/\Delta_0^2) -2(4EE_0-q^2)(p_lp_{0l}/\Delta\Delta_0) -k^2[\Delta/\Delta_0+\Delta_0/\Delta-2-(q^2/\Delta\Delta_0)]\}, \tag{15}$$

where

$$\epsilon'^2=-2k\Delta, \quad \Delta=E-p\cos\theta,$$
$$\epsilon''^2=2k\Delta_0, \quad \Delta_0=E_0-p_0\cos\theta_0, \tag{15.1}$$

and θ and θ_0 are the angles of $\mathbf{p}$ and $\mathbf{p}_0$ measured with respect to $\mathbf{k}$. This expression was reported previously[12] and was also given by May[7] who then went on to treat the extreme relativistic case. If a sum over polarization is taken, Eq. (15) goes over directly into the Bethe-Heitler differential cross section for bremsstrahlung.

In the nonrelativistic limit Eq. (15) becomes

$$d\sigma_{\mathrm{N.R.}}=(Z^2e^6/\pi^2)(p/p_0)(dk/kq^4)d\Omega d\Omega_0(p_l-p_{0l})^2. \tag{16}$$

Since on the classical picture $\mathbf{p}-\mathbf{p}_0$ is in the direction of the average acceleration of the electron, Eq. (16) states that the radiation has its electric vector parallel to the direction of acceleration, as expected from the preservation of form of classical equations of motion in quantum theory.

III. POLARIZATION FOR FIXED ELECTRON RECOIL DIRECTION

In an adjoining paper Eq. (15) will be used to obtain the intensity of radiation with specified directions of polarization l and photon propagation $\mathbf{k}/k$, integrating $d\sigma$ of Eq. (15) over all directions of the recoil electron momentum $\mathbf{p}$. The present note is being concluded by a few observations concerning the intensity of the elementary process, averaging over spin directions of the electron in the initial and final states but with a specified direction of the electron recoil momentum $\mathbf{p}$.

Introducing an azimuthal angle φ_l for the direction l measured in a plane perpendicular to $\mathbf{k}$ Eq. (15) can be verified to be of the form

$$d\sigma=[\mathfrak{A}+\mathfrak{B}\cos2\varphi_l+\mathfrak{C}\sin2\varphi_l]d\Omega d\Omega_0, \tag{17}$$

i.e.,

$$d\sigma=[\mathfrak{A}+\mathfrak{D}\cos(2\varphi_l-2\varphi_l^0)]d\Omega d\Omega_0, \tag{17.1}$$

where

$$\mathfrak{D}=(\mathfrak{B}^2+\mathfrak{C}^2)^{\frac{1}{2}}, \quad \tan(2\varphi_l^0)=\mathfrak{C}/\mathfrak{B}. \tag{17.2}$$

Replacing $\cos2\epsilon$ by $2\cos^2\epsilon-1$ in Eq. (17.1), one sees an intensity variation with φ_l of the form

$$\mathfrak{A}-\mathfrak{D}+2\mathfrak{D}\cos^2(\varphi_l-\varphi_l^0), \tag{18}$$

which is such as would be obtained if the radiation consisted of a superposition of unpolarized radiation of

relative intensity $\mathfrak{A}-\mathfrak{D}$ and of linearly polarized radiation of relative intensity $2\mathfrak{D}$. The direction of the electric vector of the linearly polarized component is $\varphi_l=\varphi_l^0$. Intensity measurements with a device capable of measuring the intensity having a given direction of linear polarization cannot give more specific information regarding the composition of the radiation than is contained in Eq. (18). As is well known linearly polarized light may be resolved into circularly or elliptically polarized components and it is impossible to claim on the basis of Eq. (17) that the radiation cannot be analyzed in other terms than the unpolarized intensity $\mathfrak{A}-\mathfrak{D}$ and the linearly polarized $2\mathfrak{D}$. Thus, for example, Eq. (18) is consistent with supposing a part or all of $\mathfrak{A}-\mathfrak{D}$ to be circularly polarized. In optics one is able to distinguish between circular and unpolarized radiations by means of a quarter-wave plate while a Nicol prism by itself corresponds only to Eq. (18). A quarter-wave plate between crossed Nicols when rotated through 90° distinguishes between right- and left-handed polarization. It is thus possible to distinguish between $\mathfrak{A}-\mathfrak{D}$ being composed of unpolarized radiation and consisting at least partly of photons having a preferentially right- or left-handed polarization. Since the $\mathbf{p}$, $\mathbf{p}_0$ plane is one of symmetry and since averages of intensity over electron spin directions are taken, one suspects that there can be no net preference for a sense of rotation around $\mathbf{k}$. A proof of the correctness of this surmise will now be given.

Elliptically polarized photons in the general case can be described by means of Eqs. (135), (136), page 103 of the continuation[15] of a previously quoted paper.[13] The propriety of physical identification in terms of elliptic polarizations follows from an examination of absorption or emission effects as on page 102 of the same reference. Changing φ to $(\pi/2)-\varphi$, the right- and left-handed ellipses of Fig. 2 on page 102 are seen to interchange. Calling the radiation variables thus obtained a_1''', a_2''' and comparing them with variables a_1^{iv}, a_2^{iv} obtained by changing i to $-i$ in the formulas expressing the a_s'', $a_s''^\dagger$ in terms of the a_s', $a_s'^\dagger$, one finds

$$a_s^{iv}=ia_s''', \quad (a_s^{iv})^\dagger=-i(a_s''')^\dagger, \quad (s=1,2) \tag{19}$$

which shows that these variables are equivalent, since the factors i, $-i$ correspond only to a contact transformation involving one s at a time. It is thus seen that one can analyze the radiation in terms of elliptic polarizations with reversed directions of rotation simply by reversing the sign of i in the defining formulas for the a''.

The calculation of the intensity of elliptic polarization takes place through the introduction of the variables a_1'', a_2'' with the result that the α_l in Eq. (5) becomes replaced by expressions of the type $\alpha_l\cos\varphi-i\alpha_m\sin\varphi$ with m standing for a direction perpendicular to $\mathbf{k}$ and l. According to the discussion of elliptic polarizations in connection with Eq. (19) the change to the opposite direction of rotation can be made by changing from $\alpha_l\cos\varphi-i\alpha_m\sin\varphi$ to $\alpha_l\cos\varphi+i\alpha_m\sin\varphi$. The intensity difference between the two directions of rotation can be ascertained therefore by substituting $\alpha_l+i\lambda\alpha_m$ for α_l in Eq. (5) and ascertaining the difference caused by a change of sign of λ. It may be shown in several ways that the sign of λ does not matter. One way of doing so is to transform the sum in Eq. (5) by means of projection operators which gives an expression of the form $F/(4E_0E)$, with

$$F=\sum_{\gamma,\,\gamma_0}|(\varphi')^*(H+E)[\alpha_\lambda(H'+E_0)/\epsilon'^2 + (H''+E)\alpha_\lambda/\epsilon''^2](H_0+E_0)\varphi_0|^2, \tag{20}$$

where

$$\gamma=\alpha, S; \quad \gamma_0=\alpha_0, S_0; \tag{20.1}$$

and

$$\alpha_\lambda=\alpha_l+i\lambda\alpha_m. \tag{20.2}$$

On employing completeness relations for φ and φ_0 one obtains an expression for F in the form of a trace of products of four-row matrices. The coefficient of $i\lambda$ is also such an expression and the matrices occurring in the product are Dirac's α_1, α_2, α_3, and β. The trace of a product of any number of such matrices is real or zero. Therefore the coefficient of $i\lambda$ is real or zero. If the coefficient were not zero the quantity F would have a nonvanishing imaginary part which contradicts Eq. (20). Hence the coefficient of λ is zero and a change in the sign of λ does not affect F. By working with Eq. (5) one can show by explicit calculation that a change in the direction of the electron spin in the initial, intermediate, and final states leads to a change in the sense of rotation of the polarization which can be represented by a change in the sign of λ. It is probable therefore that polarized electrons can produce elliptically polarized bremsstrahlung. The lack of ellipticity for unpolarized electrons is the result of compensation of right by left-handed components somewhat as in the Zeeman pattern of optical lines. The part $\mathfrak{A}-\mathfrak{D}$ of Eq. (18) has no net right-handedness. This part of the intensity is thus neutral to all tests for polarization. The whole radiation may be considered therefore as consisting of an unpolarized part with intensity proportional to $\mathfrak{A}-\mathfrak{D}$ and a linearly polarized part with intensity proportional to $2\mathfrak{D}$. The proofs as given refer specifically to the approximations used in obtaining Eq. (5). The symmetry involved is that of the time reversal transformation.[16]

[15] G. Breit, Revs. Modern Phys. **5**, 91 (1933).

[16] Unpublished work of L. C. Biedenharn and G. Breit.

Polarization Dependence of the Integrated Bremsstrahlung Cross Section

R. L. Gluckstern and M. H. Hull, Jr.
Yale University, New Haven, Connecticut*

(Received February 25, 1953)

The differential cross section for bremsstrahlung derived in the previous paper is integrated over the direction of the emerging electron. It is found that regions of appreciable polarization occur near both the low energy and high energy ends of the photon spectrum. Calculations are performed for the polarization dependence of the radiation for incident electrons of about 0.1, 0.5, 2.5 Mev with and without approximate shielding corrections calculated for aluminum. The polarization dependence of the differential cross section for pair production and of the cross section integrated over either the electron or positron direction is obtained from the results for bremsstrahlung by the well-known procedure of changes from positive to negative energy state.

I. INTRODUCTION

IN the preceding paper[1] the differential cross section for bremsstrahlung is given in Eq. (16) as a function of photon polarization for a specified photon momentum $\mathbf{k}$ and for the electron emerging in a direction within the element of solid angle $d\Omega$. In the present paper this cross section is integrated over the direction of the emerging electron. One obtains, in this way, the angular and energy distribution and the polarization of the photons emitted in the bremsstrahlung process.

The considerations in Sec. III of the preceding paper regarding the nature of the photon polarization are not necessary for the integrated cross section. The symmetry with respect to reflections in the $\mathbf{p}_0\mathbf{k}$ plane is sufficient to eliminate the possibility of an elliptically polarized component of the radiation.

The notation used is the same as that of the preceding paper and reference to equations and references in the preceding paper will be made by inserting I- in front of the appropriate equation or reference number.

II. INTEGRATED BREMSSTRAHLUNG CROSS SECTION

The integration of the cross section given in Eq. (I-15) over the direction of the emerging electron is rather lengthy, and only a brief outline of the method will be given. A few intermediate steps are described in Appendix I.

The integrals to be evaluated are of the general form

$$\int q^{-2m}\Delta^{-n}d\Omega; \quad m=0,\,1,\,2; \quad n=-1,\,0,\,1,\,2,$$

where $\Delta=E-p\cos\theta$. If one writes

$$q^2=(\mathbf{p}_0-\mathbf{p}-\mathbf{k})^2=(T^2+p^2)(1-\mathbf{p}\cdot\mathbf{a}), \tag{1}$$

with

$$\mathbf{a}=2\mathbf{T}/(T^2+p^2), \quad \mathbf{T}=\mathbf{p}_0-\mathbf{k}, \tag{1.1}$$

and

$$\Delta=E(1-\mathbf{p}\cdot\mathbf{b}), \tag{2}$$

with

$$\mathbf{b}=\mathbf{k}/kE, \tag{2.1}$$

the integrals

$$I_{m,n}=\int(d\Omega/2\pi)(1-\mathbf{p}\cdot\mathbf{a})^{-m}(1-\mathbf{p}\cdot\mathbf{b})^{-n} \tag{3}$$

are nontrivial for $m=1, 2$ and $n=1, 2$. These integrals are discussed further in Appendix I.

It suffices to consider two conditions of polarization referred to below as Cases I and II. Case I corresponds to a sum of cross sections over polarizations. In Case II the polarization vector is taken to lie in the $\mathbf{p}_0\mathbf{k}$ plane and may be expressed as

$$(2kp_0\sin\theta_0)^{-1}[k(T^2+p^2)\mathbf{a}+E(T^2-p^2-2kE)\mathbf{b}].$$

After considerable algebraic manipulation involving the integrals $I_{m,n}$, the photon cross section for each polarization as a function of θ_0, the angle between the photon and incoming electron directions, is found to be

$$\begin{aligned}d\sigma_{\mathrm{I}}=&(Z^2e^6/8\pi)(dk/k)(p/p_0)d\Omega_0\\
&\times\{8m^2\sin^2\theta_0(2E_0^2+m^2)/(p_0^2\Delta_0^4)\\
&-2(5E_0^2+2EE_0+3m^2)/(p_0^2\Delta_0^2)\\
&-2(p_0^2-k^2)/(T^2\Delta_0^2)+4E/(p_0^2\Delta_0)\\
&+(L/pp_0)[4E_0m^2\sin^2\theta_0(3km^2-p_0^2E)/(p_0^2\Delta_0^4)\\
&+(4E_0^2(E_0^2+E^2)\\
&-2m^2(7E_0^2-3EE_0+E^2)+2m^4)/(p_0^2\Delta_0^2)\\
&+2k(E_0^2+EE_0-m^2)/(p_0^2\Delta_0)]\\
&+(\epsilon^T/pT)[4m^2/\Delta_0^2-6k/\Delta_0\\
&\quad-2k(p_0^2-k^2)/(T^2\Delta_0)]-4\epsilon/(p\Delta_0)\},\end{aligned} \tag{4.1}$$

$$\begin{aligned}d\sigma_{\mathrm{II}}=&(Z^2e^6/8\pi)(dk/k)(p/p_0)d\Omega_0\\
&\times\{8m^2\sin^2\theta_0(2E_0^2+m^2)/(p_0^2\Delta_0^4)\\
&-(5E_0^2+2EE_0+5m^2)/(p_0^2\Delta_0^2)\\
&-(p_0^2-k^2)/(T^2\Delta_0^2)+2(E+E_0)/(p_0^2\Delta_0)\\
&+(L/pp_0)[4E_0m^2\sin^2\theta_0(3km^2-p_0^2E)/(p_0^2\Delta_0^4)\\
&+(2E_0^2(E_0^2+E^2)\\
&-m^2(9E_0^2-4EE_0+E^2)+2m^4)/(p_0^2\Delta_0^2)\\
&+k(E_0^2+EE_0)/(p_0^2\Delta_0)]\\
&+(\epsilon^T/pT)[4m^2/\Delta_0^2-7k/\Delta_0-k(p_0^2-k^2)/\\
&(T^2\Delta_0)-4]-4\epsilon/(p\Delta_0)+(1/p_0^2\sin^2\theta_0)\\
&\times[(2L/pp_0)(2E_0^2-EE_0-m^2-(m^2k/\Delta_0))\\
&\quad-4\epsilon^T(\Delta_0-E)^2/(pT)-2\epsilon(\Delta_0-E)/p]\},\end{aligned} \tag{4.2}$$

* Assisted by the joint program of the U. S. Office of Naval Research and the U. S. Atomic Energy Commission.

[1] Gluckstern, Hull, and Breit (preceding paper), Phys. Rev. 90, 1026 (1953).

$$d\sigma_{III}=(Z^2e^6/8\pi)(dk/k)(p/p_0)d\Omega_0$$
$$\times\{-(5E_0^2+2EE_0+m^2)/(p_0^2\Delta_0^2)$$
$$-(p_0^2-k^2)/(T^2\Delta_0^2)-2k/(p_0^2\Delta_0)$$
$$+(L/pp_0)[(2E_0^2(E_0^2+E^2)$$
$$-m^2(5E_0^2-2EE_0+E^2))/(p_0^2\Delta_0^2)$$
$$+k(E_0^2+EE_0-2m^2)/(p_0^2\Delta_0)]$$
$$+(\epsilon^T/pT)[k/\Delta_0-k(p_0^2-k^2)/(T^2\Delta_0)+4]$$
$$-(1/p_0^2\sin^2\theta_0)[(2L/pp_0)$$
$$\times(2E_0^2-EE_0-m^2-(m^2k/\Delta_0))$$
$$\times 4\epsilon^T(\Delta_0-E)^2/(pT)-2\epsilon(\Delta_0-E)/p]\}. \quad (4.3)$$

Here

$$T=|\mathbf{p}_0-\mathbf{k}|,$$

$$L=\ln[(EE_0-m^2+pp_0)/(EE_0-m^2-pp_0)],$$

$$\epsilon=\ln[(E+p)/(E-p)], \quad \epsilon^T=\ln[(T+p)/(T-p)],$$

$$\Delta_0=E_0-p_0\cos\theta_0.$$

The polarization vector in Case III is perpendicular to both $\mathbf{p}_0$ and $\mathbf{k}$ and $d\sigma_{III}=d\sigma_I-d\sigma_{II}$. As a check, $d\sigma_I$ was integrated over $d\Omega_0$ and agreed with the integrated form of the Bethe-Heitler bremsstrahlung formula.[2]

The limits of validity of Eqs. (4.1), (4.2) and (4.3) are the usual ones made in treatments of the bremsstrahlung process (references [I-3] and [I-4]). Due to the limitations of the first Born approximation the low energy limit of validity is

$$(Ze^2/\hbar v)\ll 1; \quad (\text{kinetic energy}/mc^2)\gg(Z/137)^2. \quad (5)$$

As previously mentioned the situation may be improved by using more accurate electron wave functions in Eq. (I-3). This has been done by Sommerfeld [I-1] in the nonrelativistic limit and by Maximon and Bethe [I-8] and Bess [I-9] as an improvement on the Bethe-Heitler relativistic formula.

The other limit of validity occurs for low energy photons or for extremely high energy electrons and is due to screening of the (Ze/r) potential by the atomic electrons. The effect of screening may be taken into account roughly by using[3]

$$V(r)=(Ze/r)\exp(-r/a), \quad (6)$$

where $a=108Z^{-\frac{1}{3}}(\hbar/mc)$ is chosen such that in the high energy limit the total cross section agrees with that obtained using the numerical values of the form factor of a Thomas-Fermi atom.[4] The potential in Eq. (6) simulates screening by reducing the Coulomb interaction for distant collisions. The effect is to replace q^{-2} in the Fourier transform of (Ze/r) by $(q^2+\alpha^2)^{-1}$ with $\alpha=(Z^{\frac{1}{3}}m/108)$. This then changes the factor (dk/kq^4) in Eq. (I-15) to $[dk/k(q^2+\alpha^2)^2]$, leaving the remainder of Eq. (I-15) unchanged. The integration over $d\Omega$ is more complex when shielding is included in this way, but may be carried out exactly. However, it seems sufficient to assume that α can be neglected with respect to q except for very low energy photons. The case of electrons of sufficiently high energy ($E_0\gg 137mc^2$) to make shielding important for all photon energies has been treated by May [I-7]. Except for the corrections due to shielding, the present results, Eqs. (4.1), (4.2), (4.3), agree with those of May in the extreme relativistic low angle range. Equation (4.1) is also in agreement with calculations of Schiff[5] who obtained the angular distribution of high energy photons summed over polarizations.

The expressions (4.1), (4.2), and (4.3) are therefore approximately valid as long as the electron energy is not too high ($E_0\ll 137Z^{-\frac{1}{3}}mc^2$) and the photon energy is not too low ($k\sim mc^2$). The modified expression for $k\ll mc^2$ may be obtained[6] by taking the limit $k\to 0$ in Eq. (I-15), retaining the first nonvanishing term. The main contribution to the integral over $d\Omega$ occurs near $\theta=\theta_0$ and $\varphi=\varphi_0$, and all quantities are expanded in powers of $\theta-\theta_0$, $\varphi-\varphi_0$, and k/p_0. *The azimuthal angles φ and φ_0 used here should not be confused with the 4-component Dirac spinors φ and φ_0 used in the previous paper.* One obtains the approximation

$$q^2\cong(k^2/p_0^2)(E_0-p_0\cos\theta_0)^2+[p_0(\theta-\theta_0)-k\sin\theta_0]^2$$
$$+p_0^2\sin^2\theta_0(\varphi-\varphi_0)^2, \quad (7)$$

and similar expressions for the other quantities in Eq. (I-15). If one makes the substitutions,

$$u=\theta-\theta_0-k\sin\theta_0/p_0, \quad w=(\varphi-\varphi_0)\sin\theta_0,$$
$$\delta=k\Delta_0/p_0, \quad \Delta_0=E_0-p_0\cos\theta_0, \quad \bar{\Delta}_0=E_0\cos\theta_0-p_0, \quad (8)$$

the integral over $d\Omega$ in Eq. (I-15) assumes the form

$$\int du\int dw[u^2\bar{\Delta}_0^2+w^2\Delta_0^2-2u\delta\bar{\Delta}_0m^2\sin\theta_0/p_0E_0$$
$$+m^2\sin^2\theta_0\delta^2/E_0^2]/[u^2+w^2+(\alpha^2+\delta^2)/p_0^2]^2 \quad (9)$$

for Case I and similar forms for Cases II and III. The integral over u and w in Eq. (9) is logarithmically divergent for large u and w even though no such difficulty existed before the approximations $\theta\approx\theta_0$, $\varphi\approx\varphi_0$ were made. In order to avoid getting an infinite answer, cutoffs of order of magnitude unity are used for u and w corresponding to similar cutoffs for θ and φ. This procedure is not intended as an exact evaluation of the effect of shielding, but rather it is hoped that the main effect will be given sufficiently well by the leading term thus obtained. In this approximation the leading term arises from the terms in the numerator proportional to

[2] See W. Heitler, *The Quantum Theory of Radiation* (Oxford University Press, London, 1949), second edition, p. 165, Eq. (16).
[3] See, for example H. A. Bethe, Proc. Cambridge Phil. Soc. **30**, 538 (1934).
[4] L. H. Thomas, Proc. Cambridge Phil. Soc. **23**, 542 (1926); E. Fermi, Z. Physik **48**, 73 (1928).
[5] L. I. Schiff, Phys. Rev. **83**, 252 (1951).
[6] No account is taken of multiple photon emission and the related infrared catastrophe.

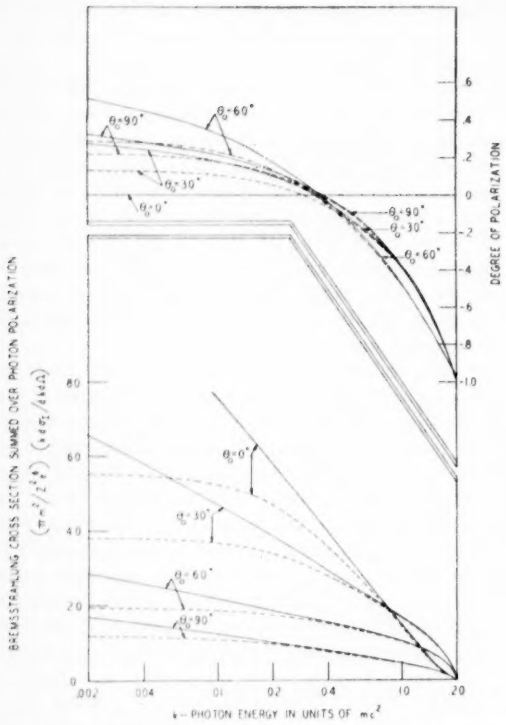

FIG. 1. Bremsstrahlung cross section (lower half of figure) and degree of polarization (upper half of figure) for incident electrons with $E_0=1.2mc^2$ ($\approx$0.1 Mev) *vs* photon energy for photon angles $\theta_0=0°$, 30°, 60°, 90°. The solid curves are without shielding, and the dashed curves are with shielding for $Z=13$.

u^2 and w^2 and leads to the following result:

$$(d\sigma_{\rm I})_{k\to 0}=(d\sigma_{\rm II})_{k\to 0}+(d\sigma_{\rm III})_{k\to 0}, \tag{10.1}$$

$$(d\sigma_{\rm II})_{k\to 0}\approx(Z^2e^6/2\pi)(pE_0^2/p_0^3)(dk/k)d\Omega_0\bar{\Delta}_0^2\Delta_0^{-4}\times\{\ln[p_0^2/(\delta^2+\alpha^2)]+O_{\rm II}(1)\}, \tag{10.2}$$

$$(d\sigma_{\rm III})_{k\to 0}\approx(Z^2e^6/2\pi)(pE_0^2/p_0^3)(dk/k)d\Omega_0\Delta_0^{-2}\times\{\ln[p_0^2/(\delta^2+\alpha^2)]+O_{\rm III}(1)\}, \tag{10.3}$$

where $O_{\rm II}(1)$ and $O_{\rm III}(1)$ stand for terms of order of magnitude unity.

If one instead takes the limit $k\to 0$ in Eqs. (4.1), (4.2), and (4.3), which do not include shielding, the result is

$$(d\sigma_{\rm I})'_{k\to 0}=(d\sigma_{\rm II})'_{k\to 0}+(d\sigma_{\rm III})'_{k\to 0}, \tag{11.1}$$

$$(d\sigma_{\rm II})'_{k\to 0}\approx(Z^2e^6/2\pi)(pE_0^2/p_0^3)(dk/k)d\Omega_0\bar{\Delta}_0^2\Delta_0^{-4}\times\{\ln(p_0^2/\delta^2)+O_{\rm II}(1)\}, \tag{11.2}$$

$$(d\sigma_{\rm III})'_{k\to 0}\approx(Z^2e^6/2\pi)(pE_0^2/p_0^3)(dk/k)d\Omega_0\Delta_0^{-2}\times\{\ln(p_0^2/\delta^2)+O_{\rm III}(1)\}. \tag{11.3}$$

As expected, the leading terms in Eqs. (11.1), (11.2), and (11.3) agree with those in Eqs. (10.1), (10.2), and (10.3) for $\alpha=0$. The main effect of the shielding is to replace $\delta^2=k^2\Delta_0^2p_0^{-2}$ by $\delta^2+\alpha^2=(k^2+\alpha^2p_0^2\Delta_0^{-2})\Delta_0^2p_0^{-2}$ in Eqs. (11.1), (11.2), and (11.3). A rough estimate of the effect of the shielding may therefore be obtained by using Eqs. (4.1), (4.2), (4.3), and replacing k^2 by $k^2+\alpha^2p_0^2\Delta_0^{-2}$ in the logarithmically divergent terms,

$$L=\ln[(EE_0-m^2+pp_0)^2/m^2k^2] \tag{12.1}$$

and

$$2\epsilon^T=2\ln[(T+p)^2/(T^2-p^2)]=\ln[(T+p)^4/(4k^2\Delta_0^2)], \tag{12.2}$$

giving

$$L\to\ln[(EE_0-m^2+pp_0)^2/(m^2k^2+m^2\alpha^2p_0^2\Delta_0^{-2})] \tag{13.1}$$

and

$$2\epsilon^T\to\ln[(T+p)^4/(4k^2\Delta_0^2+4\alpha^2p_0^2)]. \tag{13.2}$$

An exact analysis would most likely show that other changes occur, but the most important ones, namely those which make $k(d\sigma/dk)$ finite as $k\to 0$, have been taken into account by the changes indicated in Eqs. (13.1) and (13.2).

Calculations have been performed to determine the polarization effect for $E_0=1.2\ m$, $2m$, $6m$, corresponding to incident electrons of kinetic energy $mc^2/5$, mc^2, $5mc^2$.

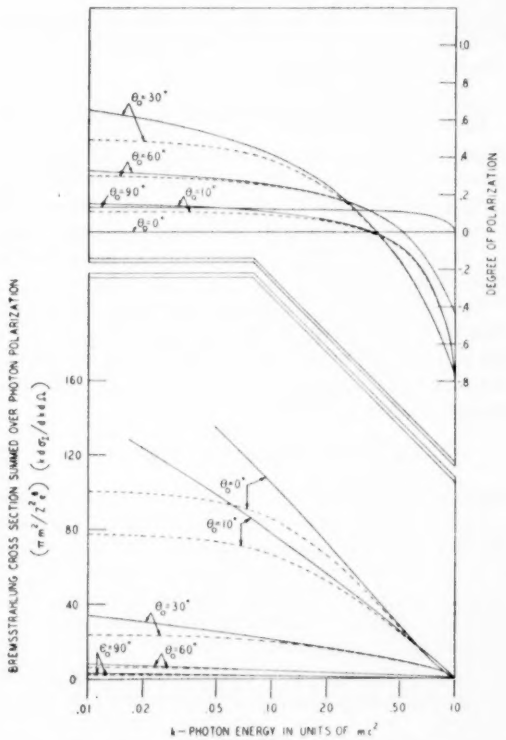

FIG. 2. Bremsstrahlung cross section (lower half of figure) and degree of polarization (upper half of figure) for incident electrons with $E_0=2mc^2$ ($\approx$0.5 Mev) *vs* photon energy for photon angles $\theta_0=0°$, 10°, 30°, 60°, 90°. The solid curves are without shielding, and the dashed curves are with shielding for $Z=13$.

The photon spectrum summed over polarization $(\pi m^2/Z^2e^6)(kd\sigma_I)/(dkd\Omega_0)$ is shown in Figs. 1–3 for each value of E_0, and in each case for various values of θ_0, the angle between the photon and incoming electron directions. In each figure the degree of polarization,

$$P=(d\sigma_{III}-d\sigma_{II})/(d\sigma_I), \tag{14}$$

is also plotted against the photon energy k for the same values of θ_0. The dotted curves represent the approximate effects of shielding, calculated for $Z=13$ (aluminum).

The main features of the results are that the polarization effect is appreciable both for low and high energy photons, with P having a different sign in the two cases. At the low energy end of the photon spectrum $d\sigma_{II}<d\sigma_{III}$, and the effect is most pronounced for high electron energies with $\theta_0\sim m/E_0$. This can be seen from Eq. (10.2) where in the low energy photon limit $d\sigma_{II}\to 0$ for the particular angle given by $\cos\theta_0=p_0/E_0$ or $\sin\theta_0=m/E_0$. This also happens to be the angular region in which the bremsstrahlung cross section is important. As has been pointed out by May and Wick [I-5], the fact that an appreciable polarization effect occurs in the range $\theta_0\sim m/E_0$ may be seen by using the Weizsäcker-Williams method [I-6].

The other region of appreciable polarization occurs at the high end of the photon spectrum, as can be seen in Figs. 1–3, with $d\sigma_{II}>d\sigma_{III}$, but this effect decreases with increasing electron energy. The factor (p/p_0) in Eqs. (4.1), (4.2), and (4.3) causes the cross section to tend to zero as $(k_0-k)^{\frac{1}{2}}$ at the upper end of the spectrum $(E=m,\ p=0,\ k_0=E_0-m)$. In addition the first Born approximation limitation given by Eq. (5) is no longer satisfied as $p\to 0$. However, these limitations are serious only in the immediate vicinity of the high end of the photon spectrum. Condition (5) for aluminum is equivalent to $Z=13$, $k_0-k\gg 0.005mc^2\approx 2.5$ kev. The factor (p/p_0) which tends to zero at the high energy end of the photon spectrum has the values 0.21, 0.18 and 0.12 for $E_0=1.2m$, $2m$, and $6m$, respectively, for a photon energy 95 percent of the available energy. Therefore an appreciable cross section may be obtained for photon energies up to about 95 percent of the maximum.

The reason for the presence of a polarization effect at the high end of the spectrum may be seen from Eq. (I-16), where for $p\to 0$ the acceleration of the electron on the classical picture is in the direction of motion of the incident electron. In this nonrelativistic limit $d\sigma_{III}=0$ for the direction of polarization perpendicular to $\mathbf{p}_0$ and $\mathbf{k}$, and the degree of polarization approaches -1. The effect diminishes as the other terms in Eq. (I-15) enter for higher energies.

The limiting forms for $d\sigma_I$, $d\sigma_{II}$, and $d\sigma_{III}$ near $p=0$

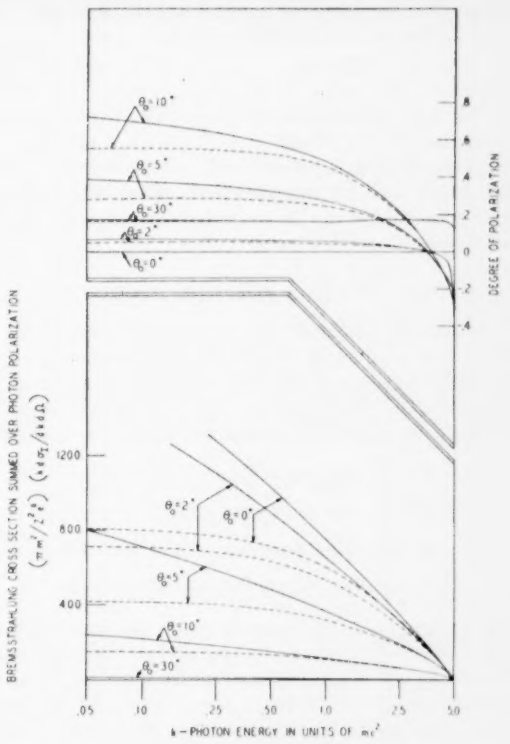

FIG. 3. Bremsstrahlung cross section (lower half of figure) and degree of polarization (upper half of figure) for incident electrons with $E_0=6mc^2$ (≈ 2.5 Mev) *vs* photon energy for photon angles $\theta_0=0°$, 2°, 5°, 10°, 30°. The solid curves are without shielding, and the dashed curves are with shielding for $Z=13$.

may be easily obtained from Eq. (I-15) and are

$$(d\sigma_I)_{p\to 0}=(d\sigma_{II})_{p\to 0}+(d\sigma_{III})_{p\to 0}, \tag{15.1}$$

$$(d\sigma_{II})_{p\to 0}\approx(Z^2e^6/4\pi)(p/p_0)(dk/k)d\Omega_0 \times(p_0^2\sin^2\theta_0/mk^2\Delta_0^4)(k^2\Delta_0+4m^3-2mk\Delta_0), \tag{15.2}$$

$$(d\sigma_{III})_{p\to 0}\approx(Z^2e^6/4\pi)(p/p_0)(dk/k)d\Omega_0 \times(p_0^2\sin^2\theta_0/mk^2\Delta_0^4)(k^2\Delta_0), \tag{15.3}$$

$$P=(mk\Delta_0-2m^3)/(k^2\Delta_0-mk\Delta_0+2m^3). \tag{15.4}$$

For small values of θ_0, the degree of polarization, in the limit $p\to 0$, is -0.99, -0.87, and -0.43 for $E_0=1.2m$, $2m$ and $6m$, respectively.

The results including the shielding calculated from the corrections indicated in Eqs. (13.1) and (13.2), are shown as the dotted curves in the figures. The effect on the cross sections is to flatten out $k(d\sigma/dk)$ near $k=0$, and the effect on the degree of polarization is to decrease the values calculated without shielding at the low energy end of the photon spectrum.

The formulas given in Eqs. (4.1), (4.2), and (4.3) with the changes indicated in Eqs. (13.1) and (13.2) give the bremsstrahlung cross section with approximate

corrections for shielding by the atomic electrons. In practice one would also like to know the effect of multiple electron scattering on the bremsstrahlung angular distribution in order to be able to predict the cross section for targets of finite thickness. This has been done approximately by Schiff[5] and May [I-7]. The experimental measurements of Lanzl and Hanson[7] and Rosengren[8] indicate that the effects of multiple electron scattering should not be neglected for practical target thicknesses.

III. CROSS SECTION FOR PAIR PRODUCTION

As has been pointed out by several authors [I-3], [I-4], pair production differs from bremsstrahlung only in that the energy of the initial state of the electron is negative. The cross section for pair production may be obtained from that of bremsstrahlung by the changes:

$E_0 \rightarrow E_-$, the total energy of the electron,

$-E \rightarrow E_+$, the total energy of the positron,

$\mathbf{p}_0 \rightarrow \mathbf{p}_-$, the momentum of the electron,

$-\mathbf{p} \rightarrow \mathbf{p}_+$, the momentum of the positron.

The final state of the system is now an electron-positron pair instead of a photon and an electron, and the factor describing the density of final states must be changed accordingly. The differential cross section for the production of an electron-positron pair of energy E_-, E_+ and momenta $\mathbf{p}_-$, $\mathbf{p}_+$ by a photon of momentum $\mathbf{k}$ may then be obtained from Eq. (I-15) as

$$d\sigma=(Z^2e^6/4\pi^2)(p_+p_-dE_-/k^3q^4)d\Omega_+d\Omega_-$$
$$\times\{(q^2-4E_-^2)(p_+t^2/\Delta_+^2)+(q^2-4E_+^2)(p_-t^2/\Delta_-^2)$$
$$-2(q^2+4E_+E_-)(p_+tp_-t/\Delta_+\Delta_-)$$
$$+k^2[(q^2/\Delta_+\Delta_-)-\Delta_+/\Delta_--\Delta_-/\Delta_+-2]\}, \quad (16)$$

where

$$\mathbf{q}=\mathbf{p}_-+\mathbf{p}_+-\mathbf{k}, \quad \Delta_-=E_--p_-\cos\theta_-, \quad (16.1)$$
$$\Delta_+=E_+-p_+\cos\theta_+,$$

and θ_- and θ_+ are the angles of $\mathbf{p}_-$ and $\mathbf{p}_+$ measured with respect to $\mathbf{k}$.

This expression was obtained by Berlin and Madanky[9] and was discussed by Wick[10] in the high energy limit by means of the Weizsäcker-Williams virtual photon method [I-6]. As in the case of bremsstrahlung, Wick[10] and May [I-7] showed that for high energies, an appreciable polarization effect was obtained only at angles of the order $\theta\sim m/k$.

Since the terms in the braces in Eqs. (4.1), (4.2), and (4.3) do not depend on the sign of p, the pair production cross section may be integrated over $d\Omega_+$ by replacing E_0 by E_- and E by $-E_+$ in Eqs. (4.1), (4.2), and (4.3), giving

$$d\sigma_{\rm I}=(Z^2e^6/8\pi)(p_+p_-dE_-/k^3)d\Omega_-$$
$$\times\{-4m^2\sin^2\theta_-(2E_-^2+m^2)/(p_-^2\Delta_-^4)$$
$$+(5E_-^2-2E_+E_-+3m^2)/(p_-^2\Delta_-^2)$$
$$+(p_-^2-k^2)/(T^2\Delta_-^2)+2E_+/(p_-^2\Delta_-)$$
$$+(L/p_-p_+)[2E_-m^2\sin^2\theta_-(3km^2+p_-^2E_+)/$$
$$(p_-^2\Delta_-^4)+(2E_-^2(E_-^2+E_+^2)$$
$$-m^2(7E_-^2+3E_-E_++E_+^2)+m^4)/(p_-^2\Delta_-^2)$$
$$+k(E_-^2-E_-E_+-m^2)/(p_-^2\Delta_-)]$$
$$-(\epsilon_+^T/p_+T)[2m^2/\Delta_-^2-3k/\Delta_-$$
$$-k(p_-^2-k^2)/(T^2\Delta_-)]-2\epsilon_+/(p_+\Delta_-)\}. \quad (17.1)$$

$$d\sigma_{\rm II}=(Z^2e^6/8\pi)(p_+p_-dE_-/k^3)d\Omega_-$$
$$\times\{-8m^2\sin^2\theta_-(2E_-^2+m^2)/(p_-^2\Delta_-^4)$$
$$+(5E_-^2-2E_+E_-+5m^2)/(p_-^2\Delta_-^2)$$
$$+(p_-^2-k^2)/(T^2\Delta_-^2)-2(E_--E_+)/(p_-^2\Delta_-)$$
$$+(L/p_-p_+)[4E_-m^2\sin^2\theta_-(3km^2+p_-^2E_+)/$$
$$(p_-^2\Delta_-^4)+(2E_-^2(E_-^2+E_+^2)$$
$$-m^2(9E_-^2+4E_-E_++E_+^2)+2m^4)/(p_-^2\Delta_-^2)$$
$$+k(E_-^2-E_-E_+)/(p_-^2\Delta_-)]$$
$$-(\epsilon_+^T/p_+T)[4m^2/\Delta_-^2-7k/\Delta_-$$
$$-k(p_-^2-k^2)/(T^2\Delta_-)-4]-4\epsilon_+/(p_+\Delta_-)$$
$$+(1/p_-^2\sin^2\theta_-)[(2L/p_+p_-)(2E_-^2+E_-E_+$$
$$-m^2-(m^2k/\Delta_-))$$
$$+4\epsilon_+^T(\Delta_-+E_+)^2/(p_+T)-2\epsilon_+(\Delta_-+E_+)/p_+]\}. \quad (17.2)$$

$$d\sigma_{\rm III}=(Z^2e^6/8\pi)(p_+p_-dE_-/k^3)d\Omega_-$$
$$\times\{(5E_-^2-2E_-E_++m^2)/(p_-^2\Delta_-^2)$$
$$+(p_-^2-k^2)/(T^2\Delta_-^2)+2k/(p_-^2\Delta_-)$$
$$+(L/p_-p_+)[(2E_-^2(E_-^2+E_+^2)$$
$$-m^2(5E_-^2+2E_-E_++E_+^2))/(p_-^2\Delta_-^2)$$
$$+k(E_-^2-E_-E_+-2m^2)/(p_-^2\Delta_-)]$$
$$-(\epsilon_+^T/p_+T)][k/\Delta_--k(p_-^2-k^2)/(T^2\Delta_-)+4]$$
$$-(1/p_-^2\sin^2\theta_-)[(2L/p_+p_-)$$
$$\times(2E_-^2+E_-E_+-m^2-(m^2k/\Delta_-))$$
$$+4\epsilon_+^T(\Delta_-+E_+)^2/(p_+T)-2\epsilon_+(\Delta_-+E_+)/p_+]\}. \quad (17.3)$$

Here

$$T=|\mathbf{p}_--\mathbf{k}|,$$

$$L=\ln[(E_-E_++m^2+p_-p_+)/(E_-E_++m^2-p_-p_+)], \quad (17.4)$$

$$\epsilon_+=\ln[(E_++p_+)/(E_+-p_+)],$$

$$\epsilon_+^T=\ln[(T+p_+)/(T-p_+)], \quad \Delta_-=E_--p_-\cos\theta_-.$$

The cross sections in Eqs. (17.1), (17.2), and (17.3) give the energy and angular distribution of the electron

[7] L. H. Lanzl and A. O. Hanson, Phys. Rev. **83**, 959 (1951).
[8] J. W. Rosengren, University of California Radiation Laboratory Report UCRL 1999, Nov. 3, 1952, unpublished.
[9] T. H. Berlin and L. Madanky, Phys. Rev. **78**, 623 (1950).
[10] G. C. Wick, Phys. Rev. **81**, 467 (1951).

for: (I) average over photon polarization, (II) electron created in the plane of polarization, (III) electron emitted perpendicular to the direction of polarization. For pair production $d\sigma_I=(d\sigma_{II}+d\sigma_{III})/2$.

Since Eq. (16) is symmetric in the electron-positron pair, Eqs. (17.1), (17.2), and (17.3) hold equally well terms of the angular distribution of the emitted positrons instead of electrons. The approximate expression may be obtained by interchanging + and − signs in Eqs. (17.1), (17.2), and (17.3).

The considerations on the validity of Eqs. (16), (17.1), (17.2), and (17.3) remain essentially unchanged. The expressions are valid for $(Ze^2/\hbar v_+\ll 1$ and $(Ze^2/\hbar v_-)\ll 1$. Shielding becomes important for photon energies of the order of $137Z^{-\frac{1}{3}}mc^2$ and can be taken into account approximately by replacing $(p_+p_-dE_-/k^3q^4)$ in Eq. (16) by $[p_+p_-dE_-/k^3(q^2+\alpha^2)^2]$, as previously discussed. Since the photon energy is now always greater than $2mc^2$, the previous considerations for low energy photons are no longer needed. Equations (16), (17.1), (17.2), and (17.3) are therefore approximately valid as long as the photon energy is not too large $(k\ll 137Z^{-\frac{1}{3}}mc^2)$. The extreme relativistic range is treated by May [I-7] together with the similar limit for bremsstrahlung as previously mentioned.

APPENDIX I

The integral,

$$I_{m,n}=\int (d\Omega/2\pi)(1-\mathbf{p}\cdot\mathbf{a})^{-m}(1-\mathbf{p}\cdot\mathbf{b})^{-n},$$

in Eq. (3) must be evaluated for the cases $I_{0,1}$, $I_{1,0}$, $I_{0,2}$, $I_{2,0}$, $I_{1,1}$, $I_{1,2}$, $I_{2,1}$, $I_{2,2}$, $I_{2,-1}$. The integral $I_{2,-1}$ may be expressed in terms of the others by choosing $\mathbf{a}$ as the polar axis for the integration over $d\Omega$ and performing the azimuthal integration, giving

$$I_{2,-1}=\int d(\cos\theta_{pa})(1-\mathbf{p}\cdot\mathbf{a})^{-2}\{1-[(\mathbf{p}\cdot\mathbf{a})(\mathbf{a}\cdot\mathbf{b})/a^2]\}$$
$$=\{(\mathbf{a}\cdot\mathbf{b})/a^2\}I_{1,0}+\{1-[(\mathbf{a}\cdot\mathbf{b})/a^2]\}I_{2,0}. \quad (18)$$

The integrals for $m=0$ or $n=0$ may be readily evaluated by choosing $\mathbf{b}$ or $\mathbf{a}$ as the polar axis for the integration over $d\Omega$, giving

$$I_{1,0}=\int_{-1}^{1} d(\cos\theta_{pa})(1-\mathbf{p}\cdot\mathbf{a})^{-1}$$
$$=(pa)^{-1}\ln[(1+pa)/(1-pa)], \quad (19.1)$$

$$I_{2,0}=\int_{-1}^{1} d(\cos\theta_{pa})(1-\mathbf{p}\cdot\mathbf{a})^{-2}=2(1-p^2a^2)^{-1}, \quad (19.2)$$

$$I_{0,1}=(pb)^{-1}\ln[(1+pb)/(1-pb)], \quad (19.3)$$

$$I_{0,2}=2(1-p^2b^2)^{-1}. \quad (19.4)$$

The integrals $I_{1,1}$, $I_{1,2}$, $I_{2,1}$, $I_{2,2}$ may be easily carried out with the aid of the identity

$$(\alpha\beta)^{-1}=\int_0^1 [\alpha x+\beta(1-x)]^{-2}dx, \quad (20)$$

and those obtained by differentiating Eq. (20) with respect to α and β. For example,

$$I_{1,1}=\int (d\Omega/2\pi)(1-\mathbf{p}\cdot\mathbf{a})^{-1}(1-\mathbf{p}\cdot\mathbf{b})^{-1}$$
$$=\int_0^1 dx\int (d\Omega/2\pi)[1-\mathbf{p}\cdot\mathbf{g}]^{-2},$$

where $\mathbf{g}=\mathbf{a}x+\mathbf{b}(1-x)$. If $\mathbf{g}$ is now used as the polar axis, the integration over $d\Omega$ may be performed, giving

$$I_{1,1}=2\int_0^1 X^{-1}dx,$$

where X is a quadratic in x given by

$$X=1-p^2g^2=1-p^2b^2-2xp^2(\mathbf{a}\cdot\mathbf{b}-b^2)-x^2p^2(\mathbf{a}-\mathbf{b})^2.$$

Using $\mathbf{a}=2\mathbf{T}/(T^2+p^2)$, $\mathbf{b}=\mathbf{k}/kE$ from Eqs. (1.1) and (2.1) and $2\mathbf{k}\cdot\mathbf{T}=p_0^2-T^2-k^2$, one obtains

$$I_{1,1}=2\int_0^1 X^{-1}dx=Ek(T^2+p^2)(pp_0)^{-1}(T^2-p^2)^{-1}L, \quad (21.1)$$

where

$$L=\ln[(EE_0-m^2+pp_0)/(EE_0-m^2-pp_0)], \quad (21.2)$$

as defined by Heitler.[11] In a similar way one also obtains

$$I_{1,2}=\int_0^1 4(1-x)X^{-2}dx, \quad (21.3)$$

$$I_{2,1}=\int_0^1 4xX^{-2}dx, \quad (21.4)$$

$$I_{2,2}=\int_0^1 16x(1-x)X^{-3}dx-\int_0^1 4x(1-x)X^{-2}dx. \quad (21.5)$$

These integrals, involving quadratic forms in x, are elementary but lead to long algebraic expressions for $I_{1,2}$, $I_{2,1}$, $I_{2,2}$.

The authors would like to express their gratitude to Professor G. Breit for many helpful suggestions and conversations. They also wish to acknowledge the assistance of Miss Jacqueline Gibson and Miss Cecilie Smolen who performed the numerical calculations.

[11] See reference 2, p. 165, Eq. (16′).

Production of Polarized Particles in Nuclear Reactions*

A. SIMON AND T. A. WELTON
Oak Ridge National Laboratory, Oak Ridge, Tennessee
(Received March 4, 1953)

A general calculation of the polarization resulting from nuclear reactions is made by means of the S matrix and Racah formalisms. All sums over magnetic quantum numbers are performed; and the resulting polarization is expressed as a series in associated Legendre polynomials, each coefficient being manifestly real. All selection rules follow immediately from the requirements for the nonvanishing of the Racah and X coefficients. The only restriction required is to a two-body break-up.

Higher spin tensor moments are required for the complete specification of the state of polarization of a beam of particles of spin greater than $\frac{1}{2}$. A general expression is given for arbitrary spin moments resulting from a nuclear reaction. The result is expressed as a series in the spherical harmonics with all coefficients being manifestly real. The previous results of Blatt and Biedenharn for the angular distribution follow as a special case of the result. A generalization of the Eisner-Sachs rules for the complexity of angular distributions is also given.

I. INTRODUCTION

SCHWINGER[1] has shown that polarized neutrons may be obtained by the elastic scattering of neutrons from He^4. This is a special case of a more general theorem, first stated by Blin-Stoyle,[2] to the effect that, under suitable conditions, the products of any nuclear reaction will be polarized. As a result it should be possible to use resonant charged particle reactions to obtain directly (rather than by an intervening elastic scattering) high intensity beams of polarized neutrons, with energies variable over a considerable range.

In Sec. II of this paper, we write down a *general* expression for the polarization of particles emerging from a reaction (the term reaction includes the special case of elastic scattering). The expression includes the elements of the nuclear scattering matrix as well as a sum over magnetic quantum numbers, since the incident beam and target nucleus are taken to be unpolarized. The sums over the magnetic quantum numbers are essentially geometrical in nature, since the elements of the nuclear scattering matrix are independent of all magnetic quantum numbers. These sums are eliminated in Sec. III, and the final result is expressed completely in terms of the nuclear scattering matrix and the Racah coefficients.

From the properties of the Racah coefficients, it is possible to read off the selection rules governing the polarization. These are listed in Sec. IV.

In Sec. V two illustrative examples are given. In one case the nuclear parameters given by Peshkin and Siegert[3] for the $Li^6(n,\alpha)H^3$ reaction are used to estimate the polarization of the emitted tritons. In the second case the formula given by Lepore[4] for the polarization of neutrons resulting from elastic scattering from He^4 is rederived using the general result. A rough rule of thumb is also given in this section for the angles at which polarization is most likely to be observed.

If the particle produced in a nuclear reaction has a spin, complete information on its final state can be obtained by giving all its irreducible spin tensor moments. In essence the angular distribution is the expectation value in the scattered wave of the spin tensor of rank zero; namely, unity. The polarization, similarly, is simply the expectation value of the tensor of rank unity formed by the spin operator $\mathbf{i}'$. In general, however, an outgoing particle of spin i' will have nonzero irreducible tensor moments up to a maximum tensor rank given by $2i'$. For example, a deuteron produced in a reaction will have a Legendre second moment $[3(i_z')^2-i'(i'+1)]$ which will usually differ from zero. Lakin and Wolfenstein[5] have recently pointed out the possible importance of the deuteron second-rank tensor in analyzing reactions.

A reduction of the magnetic sums, similar to that for the polarization, should be possible for this generalized spin tensor expectation value. This reduction is performed in Sec. VI. The resulting general expression yields the previous formula for the polarization upon specializing to tensor rank unity. The expression of Blatt and Biedenharn[6] for the angular distribution of scattering and reaction cross sections is also obtained immediately by specializing to tensor rank zero.

A generalization of the rules for the complexity of angular distributions results from the properties of the Racah and X coefficients. These rules are given in Sec. VI.

It is interesting to note that even a single level of definite J ($\neq\frac{1}{2}$ or 0) and parity will produce polarization if more than one subchannel (l value or final

* This paper is based on work performed for the U. S. Atomic Energy Commission at the Oak Ridge National Laboratory.

[1] J. Schwinger, Phys. Rev. **69**, 681 (1946).

[2] R. J. Blin-Stoyle, Proc. Phys. Soc. (London) **64**, 700 (1951). An explicit formula for the polarization of spin $\frac{1}{2}$ particles is given in this paper. A previous Letter to the Editor of *The Physical Review* was submitted before the authors became aware of this earlier work.

[3] M. Peshkin and A. J. F. Siegert, Phys. Rev. **87**, 735 (1952).

[4] J. V. Lepore, Phys. Rev. **79**, 137 (1950).

[5] W. Lakin and L. Wolfenstein, Bull. Am. Phys. Soc. **28**, No. 1, 36 (1953).

[6] J. M. Blatt and L. C. Biedenharn, Revs. Modern Phys. **24**, 258 (1952); references to this paper will be designated by BB.

channel spin) contribute. Several known reactions offer promise. In particular, analyses[7] of the angular distributions of (p,n) neutrons resulting from resonances in C^{13}, B^{11}, Li^7, and H^3 indicate that p waves or higher and opposite parities are interfering. It, in fact, seems likely that many neutron sources, hitherto considered unpolarized, may actually exhibit partial polarization. Such partial polarization could introduce systematic errors in the measurement of differential scattering cross sections for neutrons, if care is not taken.

The present paper is restricted to the case of an unpolarized initial beam and target. The general case of the spin tensor moments resulting from an arbitrarily polarized initial beam has been solved and will be reported on at a later time.

II. NOTATION AND GENERAL EXPRESSION FOR THE POLARIZATION

In the following sections the notation of BB will be closely adhered to. We consider the reaction

$$a+X=Y+b, \tag{2.1}$$

in which particle a collides with nucleus X. Particle b emerges at an angle θ to the direction of the incident beam, and Y is the residual nucleus. All quantities are measured in the center-of-gravity system. As in BB, *the formulas derived below are applicable to any collision process in which two particles collide and two particles emerge.*

The system before collision is described by the channel index α which defines the type of incoming particle (neutron, proton, etc.) as well as the state of the target nucleus, the channel spin s, and l the orbital angular momentum. The channel spin s is the total spin angular momentum in the entrance channel and is formed by the vector addition of the intrinsic spin i of the incoming particle and the spin I of the target nucleus. The state of the system after the reaction will be described by primed quantities.

The asymptotic form of the outgoing wave can be written [see BB (3.12)]

$$\psi(\alpha's')=i\lambda_\alpha\left(\frac{v_\alpha}{v_{\alpha'}}\right)^{\frac{1}{2}}\frac{\exp(ik_{\alpha'}r_{\alpha'})}{r_{\alpha'}}\phi_{\alpha'} \times\sum_{m_{s'}=-s'}^{s'} q(\alpha's'm_{s'};\alpha sm_s;\theta,\varphi)\chi(s'm_{s'}), \tag{2.2}$$

where v_α and k_α are the relative velocity and wave number, respectively, in entrance channel α; $\phi_{\alpha'}$ is the product of internal wave functions of nucleus Y and particle b corresponding to the specification α'; $\chi^{s'm_{s'}}$ is the final channel spin wave function; and[8]

$$q(\alpha's'm_{s'};\alpha sm_s;\theta,\varphi) =(\pi)^{\frac{1}{2}}\sum_{J=0}^{\infty}\sum_{l=|J-s|}^{J+s}{}'\sum_{l'=|J-s'|}^{J+s'}{}'\sum_{\pi=\pm1} i^{l-l'}(2l+1)^{\frac{1}{2}} \times(ls0m_s|lsJm_s)(l's'\mu'm_{s'}|l's'Jm_s) \times[\delta(\alpha',\alpha)\delta(s',s)\delta(l',l) -S(\alpha's'l';\alpha sl;J\pi)]Y_{l',\mu'}(\theta,\varphi). \tag{2.3}$$

The quantity $(ls0m_s|lsJm_s)$ is the Clebsch-Gordan coefficient defined as in Condon and Shortley.[9] With this choice of phase, we have $Y_{l,-m}=(-1)^mY_{l,m}{}^*$. Here $S(\alpha's'l';\alpha sl;J\pi)$ is an element of the scattering matrix representing the probability of a colliding system having a total angular momentum J and a parity π to go from an incident state described by the quantities αsl to a final state described by $\alpha's'l'$. The good quantum numbers for this reaction are Jm_J and π. The prime on the summation symbol for the orbital angular momenta indicates that only those values of l and l' are to be chosen which will satisfy the parity condition. For pure elastic scattering S is related to the phase shift δ by the relation $S=\exp(2i\delta)$. Note that Eq. (2.2) is written for a definite incident channel spin s and channel spin direction m_s. The differential cross section for the process $\alpha\rightarrow\alpha'$ can be written

$$d\sigma_{\alpha'\alpha}=\sum_{s=|I-i|}^{I+i}\sum_{s'=|I'-i'|}^{I'+i'}\sum_{m_s=-s}^{s}\sum_{m_{s'}=-s'}^{s'}\frac{\lambda_\alpha{}^2}{(2I+1)(2i+1)} \times|q(\alpha's'm_{s'};\alpha sm_s;\theta,\varphi)|^2d\Omega. \tag{2.4}$$

Since the scattering matrix is independent of magnetic quantum numbers, the sums over all magnetic quantum numbers are essentially geometrical in character and can be performed without any detailed knowledge of the collision process. The elegant reduction of these sums has been performed in BB. A similar reduction will be performed for the case of the polarization (as well as any higher spin moments of interest).

We define the *differential polarization* in the outgoing channel α' to be

$$d\mathbf{P}_{\alpha'\alpha}=\langle\textstyle\sum(\psi(\alpha's')|\,\mathbf{i}'\,|\psi(\alpha's''))r_{\alpha'}{}^2v_\alpha{}^{-1}v_{\alpha'}\rangle_{\mathrm{Av}}d\Omega, \tag{2.5}$$

where the sum is over all final channel spins and final channel spin directions and an average is taken over the initial states. Here $\mathbf{i}'$ is the spin operator for the outgoing particle b whose polarization is to be measured. The *polarization* will be defined to be

$$f(\theta)=(i')^{-1}d|\mathbf{P}|/d\Omega,$$

[7] H. B. Willard, private communication.

[8] Note that the separation of the final wave function into a channel spin function and an internal function is an idealization. Since, however, only angular properties of the wave functions are of interest, the final answer will be unaffected.

[9] E. U. Condon and G. H. Shortley, *The Theory of Atomic Spectra* (Cambridge University Press, Cambridge, 1951).

and such that f has a maximum value of unity for a completely polarized beam.

It is more convenient in the calculations to evaluate first the expectation values of those linear combinations of the components of the spin operator $\mathbf{i}'$ which transform as spherical harmonics. In particular, for the polarization, we will evaluate the quantities $T_\kappa^{(1)}$ where

$$T_{\pm 1}^{(1)} = \mp (i_x' \pm i i_y')/[2i'(i'+1)]^{\frac{1}{2}},$$
$$T_0^{(1)} = i_z'/[i'(i'+1)]^{\frac{1}{2}}. \tag{2.6}$$

These definitions are chosen so as to agree with the definition of a tensor given by Racah.[10]

Using Eqs. (2.6), (2.5), (2.3), and (2.2), we can now write the polarization intensity as

$$\begin{aligned} dT_{\kappa,\alpha'\alpha}^{(1)} &= \pi\lambda_\alpha^2 (2I+1)^{-1}(2i+1)^{-1} \sum i^{l_2-l_1+l_1'-l_2'} \\ &\times [(2l_1+1)(2l_2+1)]^{\frac{1}{2}} [\delta(\alpha',\alpha)\delta(s_1's)\delta(l_1',l_1) \\ &-S(\alpha' s_1' l_1';\alpha s l_1;J_1\pi_1)]^* [\delta(\alpha',\alpha)\delta(s_2',s)\delta(l_2',l_2) \\ &-S(\alpha' s_2' l_2';\alpha s l_2;J_2\pi_2)] d\Omega \\ &\times \sum_{m_s}\sum_{m_1'}\sum_{m_2'} [(l_1 s 0 m_s | l_1 s J_1 m_s)(l_2 s 0 m_s | l_2 s J_2 m_s) \\ &\times (l_1' s_1' \mu_1' m_1' | l_1' s_1' J_1 m_s)(l_2' s_2' \mu_2' m_2' | l_2' s_2' J_2 m_s) \\ &\times Y^*{}_{l_1'\mu_1} Y_{l_2'\mu_2'} (\chi(s_1'm_1') | T_\kappa^{(1)} | \chi(s_2'm_2'))], \end{aligned} \tag{2.7}$$

where the first sum is over the quantities $J_1 J_2 \pi_1 \pi_2 l_1 l_2 l_1' l_2' s_1' s_2'$ and s. For simplicity we have written $m_{s1}' = m_1'$; $m_{s2}' = m_2'$.

The expression in the square brackets may be expressed entirely in terms of Clebsch-Gordan coefficients by the use of two theorems. One relates the product of two spherical harmonics to a linear superposition of spherical harmonics.

$$Y^*{}_{l_1\mu_1} Y_{l_2\mu_2} = (-1)^{\mu_1} \sum_{L=|l_1-l_2|}^{l_1+l_2} \left[\frac{(2l_1+1)(2l_2+1)}{4\pi(2L+1)}\right]^{\frac{1}{2}}$$
$$\times (l_1 l_2 00 | l_1 l_2 L0)(l_1 l_2 -\mu_1\mu_2 | l_1 l_2 L \mu_2 - \mu_1) Y_{L,\mu_2-\mu_1}. \tag{2.8}$$

The other expresses the matrix element of $T_\kappa^{(1)}$ in terms of the Clebsch-Gordan and Racah coefficients. By the use of the Eckart-Wigner theorem and the Racah formalism we obtain the following result, which is derived in Appendix A:

$$\begin{aligned} &(\chi(s_1'm_1') | T_\kappa^{(1)} | \chi(s_2'm_2')) \\ &= (-1)^{I'-i'+m_1'-\kappa} [(2i'+1)(2s_1'+1)(2s_2'+1)/(3)]^{\frac{1}{2}} \\ &\times (s_1's_2' - m_1'm_2' | s_1's_2' 1 - \kappa) W(i's_1'i's_2'; I'1), \end{aligned} \tag{2.9}$$

where $W(abcd;ef)$ is the usual Racah coefficient.

[10] G. Racah, Phys. Rev. **62**, 442 (1942); references to this paper will be denoted by R.

Combining Eqs. (2.7), (2.8), and (2.9) we obtain

$$\begin{aligned} dT_{\kappa,\alpha'\alpha}^{(1)} &= [\lambda_\alpha^2/(2I+1)(2i+1)][\pi(2i'+1)/12]^{\frac{1}{2}} \\ &\times \sum (-1)^{I'-i'-\kappa} i^{l_2-l_1-l_2'+l_1'} [\delta(\alpha',\alpha)\delta(s_1',s)\delta(l_1',l_1) \\ &-S(\alpha' s_1' l_1';\alpha s l_1;J_1\pi_1)]^* [\delta(\alpha'\alpha)\delta(s_2's)\delta(l_2'l_2) \\ &-S(\alpha' s_2' l_2';\alpha s l_2;J_2\pi_2)][(2l_1+1)(2l_2+1) \\ &\times (2l_1'+1)(2l_2'+1)(2s_1'+1)(2s_2'+1)]^{\frac{1}{2}}(2L+1)^{-\frac{1}{2}} \\ &\times (l_1'l_2'00 | l_1'l_2'L0) W(i's_1'i's_2';I'1) Y_{L,\kappa}(\theta,\varphi) d\Omega \\ &\times \sum_{m_s}\sum_{m_1'}\sum_{m_2'} [(-1)^{m_s} (l_1 s 0 m_s | l_1 s J_1 m_s) \\ &\times (l_2 s 0 m_s | l_2 s J_2 m_s)(l_1' s_1' \mu_1' m_1' | l_1' s_1' J_1 m_s) \\ &\times (l_2' s_2' \mu_2' m_2' | l_2' s_2' J_2 m_s)(l_1' l_2' - \mu_1' \mu_2' | l_1' l_2' L\kappa) \\ &\times (s_1's_2' - m_1'm_2' | s_1's_2' 1 - \kappa)], \end{aligned} \tag{2.10}$$

where the sum now includes the index L. Note that by the properties of the Clebsch-Gordan coefficients, $\mu_1' = m_s - m_1'$, $\mu_2' = m_s - m_2'$ and $m_1' - m_2' = \kappa$. Hence the sum m_2' is purely formal and actually reduces to only one term: $m_2' = m_1' - \kappa$.

The remaining geometrical sums over the magnetic quantum numbers can be eliminated by the use of some Racah identities which have been recently summarized in a review paper by Biedenharn *et al.*[11]

III. ELIMINATION OF THE MAGNETIC SUMS

By use of BBR (1) and (18) we find that

$$\begin{aligned} &(l_1 s 0 m_s | l_1 s J_1 m_s)(l_2 s 0 m_s | l_2 s J_2 m_s) \\ &= (-1)^{s+2J_1-m_s} [(2J_1+1)(2J_2+1)]^{\frac{1}{2}} \sum_f [(l_1 l_2 00 | l_1 l_2 f 0) \\ &\times (J_1 J_2 - m_s m_s | J_1 J_2 f 0) W(l_1 J_1 l_2 J_2; s f)]. \end{aligned}$$

Using this reduction once again, there results

$$\begin{aligned} &(J_1 J_2 m_s - m_s | J_1 J_2 f 0)(l_1' s_1' \mu_1' m_1' | l_1' s_1' J_1 m_s) \\ &= (-1)^{J_1+f+s_1'-m_s+m_1'} [(2f+1)(2J_1+1)/(2l_1'+1)]^{\frac{1}{2}} \\ &\times \sum_g [(2g+1)^{\frac{1}{2}} (f s_1' 0 m_1' | f s_1' g m_1') \\ &\times (J_2 g - m_s m_1' | J_2 g l_1' - \mu_1') W(J_2 f l_1' s_1'; J_1 g)]. \end{aligned}$$

The sum over m_s by BBR (1) can now be written as

$$\begin{aligned} &\sum_{m_s} [(g J_2 - m_1' m_s | g J_2 l_1' \mu_1')(l_1' l_2' \mu_1' - \mu_2' | l_1' l_2' L - \kappa) \\ &\times (J_2 l_2' m_s - \mu_2' | J_2 l_2' s_2' m_2')], \end{aligned}$$

which by BBR (19) becomes

$$\begin{aligned} &= [(2l_1'+1)(2s_2'+1)]^{\frac{1}{2}} (g s_2' - m_1' m_2' | g s_2' L - \kappa) \\ &\times W(g J_2 L l_2'; l_1' s_2'). \end{aligned}$$

Finally, the sum on m_1' can be put in the form

$$\begin{aligned} &\sum_{m_1'} [(f s_1' 0 m_1' | f s_1' g m_1')(g s_2' m_1' - m_2' | g s_2' L \kappa) \\ &\times (s_1' s_2' m_1' - m_2' | s_1' s_2' 1 \kappa)], \end{aligned}$$

which again by BBR (19) becomes

$$= [3(2g+1)]^{\frac{1}{2}} (f 10\kappa | f 1 L\kappa) W(f s_1' L s_2'; g 1).$$

[11] Biedenharn, Blatt, and Rose, Revs. Modern Phys. **24**, 249 (1952); references to this paper will be designated by BBR.

Hence, the entire magnetic sum can be written as

$$= (-1)^{-s-l_2'-J_2+\kappa-1}\sqrt{3}(2J_1+1)(2J_2+1)$$
$$\times\sum_f (-1)^f(2f+1)^{\frac{1}{2}}(l_1l_200|l_1l_2f0)(f10\kappa|f1L\kappa)$$
$$\times W(l_1J_1l_2J_2;sf)\sum_g[(-1)^g(2g+1)W(J_2fl_1's_1';J_1g)$$
$$\times W(gJ_2Ll_2';l_1's_2')W(fs_1'Ls_2';g1)].$$

Finally, by BBR (14), the sum over g can be written in terms of the X function defined in Appendix B and originally introduced by Fano and Racah.[12] As a result the magnetic sum becomes

$$= (-1)^{-s-s_1'+J_1-l_2'+L+\kappa}\sqrt{3}(2J_1+1)(2J_2+1)$$
$$\times\sum_f[(2f+1)^{\frac{1}{2}}(l_1l_200|l_1l_2f0)(f10\kappa|f1L\kappa)$$
$$\times W(l_1J_1l_2J_2;sf)X(J_1l_1's_1';J_2l_2's_2';fL1). \quad (3.1)$$

In the particular case of the polarization tensor, which is of rank one, the sum over f reduces to a single term which is $f=L$. To see this, recall that by conservation of parity $l_1+l_2+l_1'+l_2'=$ even integer. In addition, the Clebsch-Gordan coefficient $(ab00|abc0)$ vanishes unless $a+b+c=$ even integer [see BBR (5)]. The corresponding coefficients in Eqs. (3.1) and (2.10) now show that $L+f=$ even integer. However, by the properties of $(f10\kappa|f1L\kappa)$ we must have $f=L$ or $f=L\pm1$. Hence there follows the result $f=L$.

The final result for the polarization intensity may now be written in a very simple form by noting that the entire dependence on κ of dP_κ is contained in the terms $(L10\kappa|L1L\kappa)Y_{L,\kappa}$ where we have set f equal to L. Hence

$$dP_z\equiv dP_0=0,$$

$$dP_x=(dP_{-1}-dP_1)/\sqrt{2}\sim\tfrac{1}{2}(Y_{L,-1}+Y_{L,1})$$
$$\sim -i\sin\varphi\bar{P}_L^1(\theta),$$

$$dP_y=i(dP_1+dP_{-1})/\sqrt{2}\sim-\tfrac{1}{2}i(Y_{L,1}-Y_{L,-1})$$
$$\sim i\cos\varphi\bar{P}_L^1(\theta),$$

where $\bar{P}_L^1$ is the normalized associated Legendre polynomial. This result clearly shows that the polarization is always normal to the plane formed by the directions of the incoming and outgoing particles. In terms of the unit vector $\mathbf{n}=(\mathbf{k}_\alpha\times\mathbf{k}_{\alpha'})/|\mathbf{k}_\alpha\times\mathbf{k}_{\alpha'}|$ we have the final result:

$$d\mathbf{P}_{\alpha'\alpha}=\mathbf{n}(\lambda_\alpha^2/4)(2I+1)^{-1}(2i+1)^{-1}[2(2i'+1)]^{\frac{1}{2}}$$
$$\times\sum i^{l_2-l_1+l_1'-l_2'}\text{R.P.}[i\{\delta(\alpha',\alpha)\delta(l_1',l_1)\delta(s_1',s)$$
$$-S(\alpha'l_1's_1';\alpha l_1s;J_1\pi_1)\}^*\{\delta(\alpha',\alpha)\delta(l_2',l_2)\delta(s_2',s)$$
$$-S(\alpha'l_2's_2';\alpha l_2s;J_2\pi_2)\}](-1)^{I'-i'-s+l_1'+J_1-s_1'}$$
$$\times[(2l_1+1)(2l_2+1)(2l_1'+1)(2l_2'+1)(2s_1'+1)$$
$$\times(2s_2'+1)]^{\frac{1}{2}}(2J_1+1)(2J_2+1)(l_1l_200|l_1l_2L0)$$
$$\times(l_1'l_2'00|l_1'l_2'L0)W(i's_1'i's_2';I'1)W(l_1J_1l_2J_2;sL)$$
$$\times X(J_1l_1's_1';J_2l_2's_2';LL1)\bar{P}_L^1(\theta)d\Omega. \quad (3.2)$$

[12] U. Fano and G. Racah, unpublished. See also U. Fano, National Bureau of Standards Report 1214, p. 48.

where the sum is over $J_1J_2\pi_1\pi_2l_1l_2l_1'l_2's_1's_2's$ and L. The final expression for $d\mathbf{P}$ has been written entirely in terms of real quantities by use of the symmetry property of the X coefficient for interchange of two rows (see Appendix B). This form of the expression clearly shows that the polarization is an interference phenomenon.[13]

IV. SELECTION RULES

The fact that the polarization is always normal to the scattering plane has been demonstrated in the previous paragraph. All other selection rules follow from the requirements for the nonvanishing of the Racah and Clebsch-Gordan coefficients [see BBR (5) and (13)] and are listed below:

(a) If only S waves are effective in the reaction, for either the incident or the final states, there can be no polarization.

(b) If only levels of the compound nucleus having $J=\frac{1}{2}$ and a single parity (or $J=0$ with any parity) are effective, there will be no polarization.

(c) If only channel spin 0 is effective for the final channel spin, the polarization vanishes.

(d) Polarization results from the interference of different subchannels (i.e., partial waves or final channel spins) contributing to the reaction. (The state of the residual nucleus must always be the same, of course.) Hence, if there is only a single nonzero element of the scattering matrix, the polarization will vanish.

(e) If there is no spin-orbit coupling, the polarization is zero.

(f) If there is a largest effective incident orbital wave l, final orbital wave l' or total angular momentum J, there will be a largest value of L in Eq. (3.2) given by the simultaneous conditions

$$L\leq 2l;\ 2l';\ 2J. \quad (4.1)$$

In addition, one must remember that L must be even if the interfering states have the same parity. These rules are identical to the rules for the limitation of the complexity of angular distributions.[14] Selection rules (a) and (b) are actually special cases of (f). Some of these rules have been given before by Wolfenstein[15] for the special case of reactions involving polarized particles of spin $\frac{1}{2}$.

[13] F. Coester [Phys. Rev. **89**, 619 (1953)] has recently conjectured that the elements of the scattering matrix $S(s_1l;s'l';J\pi)$ having the same J and π have the same phase. If this were so, polarization could only result from the interference of levels of different J or parity and not from the possible interference of different subchannels of a single level, as stated in Sec. I. The existence or nonexistence of this type of polarization would then constitute an experimental check of Coester's hypothesis. In this connection it should also be noted that the matrix elements resulting from the use of perturbation theory or the Born approximation are all real. Hence in these approximations there can be no polarization (or higher odd tensor moments). This implies the absence of circular polarization in γ-rays resulting from nuclear reactions.

[14] C. N. Yang, Phys. Rev. **74**, 764 (1948).

[15] L. Wolfenstein, Phys. Rev. **75**, 1664 (1949).

It is important to note that, if the observed angular distribution in a nuclear reaction is not isotropic, we are assured that selection rules (a) and (b) are not operating. Furthermore, if the distribution is not symmetric about 90° in the center-of-mass system, then selection rule (d) is also not operating.

In many nuclear reactions the largest incident or final orbital angular momentum is often either a p wave or a d wave. In such cases the polarization will vary with angle as $P_1^1(\theta)$ or $P_2^2(\theta)$ or a combination of these. In the absence of more detailed information, it would then seem most profitable to search for polarization in the vicinity of 45° or 135° in the center-of-gravity system.

V. ILLUSTRATIVE EXAMPLES

Any calculation of the polarization, as well as any other spin moments, requires a knowledge of the scattering matrix. In practice only a few levels contribute to a reaction at a given energy and hence the formidable sum of Eq. (3.2) reduces to only a few terms. However, even this limited information is practically nonexistent.

Recently, Peshkin, and Siegert[3] have analyzed the $Li^6(n,\alpha)H^3$ reaction and obtained some information on the nuclear parameters. In addition, Lepore[4] has given a formula for the neutron polarization resulting from He^4 scattering. We will make a numerical estimate of the polarization of the triton in the Li^6 reaction and also rederive Lepore's formula as a special case of our general result.

$Li^6(n,\alpha)H^3$ Reaction

The relative angular distribution of the tritons at 270 kev has been found to be[16]

$$I(\theta)=103+83\cos\theta+192\cos^2\theta.$$

Absorption cross-section measurements[17] show a resonance maximum of 3.1 barns, 2.5 barns of which is actually due to the resonance, at 250 kev with a width at half-maximum of about 100 kev. Peshkin and Siegert have shown that these measurements can be fitted by assuming that the resonance is of total angular momentum $J=\frac{3}{2}$ formed by a p wave with the entrance channel spin $s=\frac{1}{2}$. In addition there is interference with the two distant levels formed by s waves. One being of $s=J=\frac{1}{2}$ and the other of $s=J=\frac{3}{2}$. If we now define the corresponding scattering matrix elements in terms of the notation in reference 3, we have

$$S(1\tfrac{1}{2};1\tfrac{1}{2};\tfrac{3}{2}-)\equiv\tau/\sqrt{2},$$
$$S(0\tfrac{1}{2};0\tfrac{1}{2};\tfrac{1}{2}+)\equiv b,$$
$$S(2\tfrac{1}{2};0\tfrac{3}{2};\tfrac{3}{2}+)\equiv a.$$

The resultant angular distribution then agrees with that of Peshkin and Siegert and is

$$d\sigma(\theta)=\tfrac{1}{6}\lambda^2[|a|^2+\tfrac{1}{2}|b|^2+\tfrac{1}{4}|\tau|^2+(1/\sqrt{2})(b^*\tau+b\tau^*)\times\cos\theta+\tfrac{3}{4}|\tau|^2\cos^2\theta]d\Omega.$$

Comparing with the experimental cross sections, we find the relative values

$$|\tau|^2=256,\quad |a|^2+\tfrac{1}{2}|b|^2=39,\quad (b^*\tau+b\tau^*)=83\sqrt{2}. \quad (5.1)$$

The expression for the polarization may now be written down almost immediately from Eq. (3.2). Since different entrance channel spins are incoherent, the only contributing term is that due to interference between the reactions denoted by τ and b. For this case, the sum on L reduces to a single term, $L=1$. Tables of the Racah coefficients have been published by Biedernharn.[18] Using these, we find

$$W(\tfrac{1}{2}\tfrac{1}{2}\tfrac{1}{2}\tfrac{1}{2},01)=\tfrac{1}{2},$$
$$W(1\tfrac{3}{2}0\tfrac{1}{2};\tfrac{1}{2}1)=6^{-\frac{1}{2}},$$
$$X(\tfrac{3}{2}1\tfrac{1}{2};\tfrac{1}{2}0\tfrac{1}{2};111)=(216)^{-\frac{1}{2}},$$

and the final result which is

$$d\mathbf{P}=\mathbf{n}\lambda^2(864)^{-\frac{1}{2}}i(\tau b^*-\tau^*b)\bar{P}_1^1(\theta)d\Omega.$$

By Eq. (5.1) we have $|b|\leq(78)^{\frac{1}{2}}$ and $|\tau|=16$, and thus $|\tau^*b|\leq 141.3$. Now $\tau b^*+\tau^*b=2|\tau^*b|\cos\phi=83\sqrt{2}$ where ϕ is the modulus. Hence

$$|i(\tau b^*-\tau^*b)|=2|\tau^*b|\sin\phi=[4|\tau^*b|^2-4|\tau^*b|^2\cos^2\phi]^{\frac{1}{2}}\leq[4(141.3)^2-2(83)^2]^{\frac{1}{2}}=257.1.$$

Depending on the unknown phase which is not determined by the angular distribution, there will be a polarization of the triton which may vary from zero to a maximum value given by

$$f=105\bar{P}_1^1(\theta)/[103+83\cos\theta+192\cos^2\theta]. \quad (5.2)$$

This expression has a maximum value of 0.95 at an angle $\theta=100°$. Conversely, a determination of the polarization would establish the value of this phase.

Scattering of Neutrons by He^4

The general formalism has been used to rederive Eq. (2.9) in reference 4. The only nonzero elements of the scattering matrix are those referring to S and P wave scattering. In terms of the notation of Lepore, these scattering elements are

$$1-S(0\tfrac{1}{2};0\tfrac{1}{2};\tfrac{1}{2}+)=-2i\exp(i\delta_0)\sin\delta_0,$$
$$1-S(1\tfrac{1}{2};1\tfrac{1}{2};\tfrac{1}{2}-)=-i\Gamma/(E_{\frac{1}{2}}-E-\tfrac{1}{2}i\Gamma),$$
$$1-S(1\tfrac{1}{2};1\tfrac{1}{2};\tfrac{3}{2}-)=-i\Gamma/(E_{\frac{3}{2}}-E-\tfrac{1}{2}i\Gamma).$$

Note that $\alpha'=\alpha$, $l'=l$ and $s'=s$ in all cases.

Equation (2.9) in reference 4 was found to have two misprints. The sign of the first term in the numerator should be negative. The last term in the denominator

[16] Roberts, Darlington, and Haugsnes, Phys. Rev. **82**, 299 (951).
[17] J. M. Blair and R. E. Holland (to be published).
[18] L. C. Biedenharn, Oak Ridge National Laboratory Report No. 1098, 1952.

should read in part $(x_1x_1+\frac{1}{4})$ rather than $(x_1+x_1+\frac{1}{4})$. When these corrections are made, complete agreement is reached.

VI. HIGHER SPIN MOMENTS

The previous sections have been specialized to the problem of the polarization of the outgoing particle i'. In essence this quantity is just the expectation value in the scattered wave of the tensor of rank unity formed out of the spin operators $\mathbf{i}'$. In general however, an outgoing particle will have nonzero irreducible tensor moments up to a maximum tensor rank given by $2i'$.

The previous results can be made completely general by a few slight changes. Instead of considering the expectation value of a tensor of rank unity $T_\kappa^{(1)}$, we ask for the expectation value of the general irreducible tensor operator of rank q, $T_\kappa^{(q)}$, which is formed out of the spin operators $\mathbf{i}'$.[19] We define the *differential tensor moment* to be

$$dT_{\kappa,\alpha'\alpha}^{(q)} = \langle\sum(\psi(\alpha's')|T_\kappa^{(q)}|\psi(\alpha's'))r_{\alpha'}{}^2v_\alpha{}^{-1}v_{\alpha'}\rangle_{Av}d\Omega, \quad (6.1)$$

where the sum is over all final channel spins and final channel spin directions, and an average is taken over the initial states. By Eq. (A.2) we have

$$\begin{aligned}(\chi(s_1'm_1')|T_\kappa^{(q)}|\chi(s_2'm_2')) &= (-1)^{I'-i'-\kappa+m_1'}[(2s_1'+1)(2s_2'+1)]^{\frac{1}{2}} \\ &\times[(2i')!]^{-1}[(2i'-q)!(2i'+q+1)!/(2q+1)]^{\frac{1}{2}} \\ &\times(s_1's_2'-m_1'm_2'|s_1's_2'q-\kappa)W(i's_1'i's_2';I'q) \\ &\times P_q([i'/(i'+1)]^{\frac{1}{2}}). \quad (6.2)\end{aligned}$$

which replaces Eq. (2.9). Here P_q is the usual Legendre polynomial. The magnetic sums proceed as before with the only change being the replacement of 1 by q.

As a result, we obtain the following *general* expression for the differential tensor moment:

$$\begin{aligned}dT_{\kappa,\alpha'\alpha}^{(q)} &= \frac{(\pi)^{\frac{1}{2}}\lambda_\alpha{}^2[(2i'-q)!(2i'+q+1)!]^{\frac{1}{2}}}{2(2I+1)(2i+1)(2i')!} \\ &\times P_q\left(\left[\frac{i'}{i'+1}\right]^{\frac{1}{2}}\right)\sum(-1)^{I'-i'-\kappa+J_1-\kappa_1'+l_1'}\,i^{l_2-l_1+l_1'-l_2'} \\ &\times[\delta(\alpha',\alpha)\delta(s_1',s)\delta(l_1',l_1)-S(\alpha's_1'l_1;\alpha sl_1;J_1\pi_1)]^* \\ &\times[\delta(\alpha',\alpha)\delta(s_2',s)\delta(l_2',l_2)-S(\alpha's_2'l_2';\alpha sl_2;J_2\pi_2)] \\ &\times[(2f+1)(2l_1+1)(2l_2+1)(2l_1'+1)(2l_2'+1) \\ &\times(2s_1'+1)(2s_2'+1)/(2L+1)]^{\frac{1}{2}}(2J_1+1)(2J_2+1) \\ &\times(l_1'l_2'00|l_1'l_2'L0)(l_1l_200|l_1l_2f0)W(l_1J_1l_2J_2;sf) \\ &\times W(i's_1'i's_2';I'q)X(J_1l_1's_1';J_2l_2's_2';fLq) \\ &\times(fq0\kappa|fqL\kappa)Y_{L,\kappa}(\theta,\varphi)d\Omega, \quad (6.3)\end{aligned}$$

where the sum is over $J_1J_2\pi_1\pi_2l_1l_2l_1'l_2's_1's_2'sL$ and f. Note that for tensors of rank higher than unity, the sum over f does not necessarily reduce to a single term.

[19] All tensor operators are to be defined so as to agree with the definition given in R. For definiteness we take

$$T_0^{(q)} = P_q(i_z'/[i'(i'+1)]^{\frac{1}{2}}).$$

Selection rules (a), (b), and (d) of Sec. IV are now seen to apply to *all* odd values of q. Selection rules (c) and (e) apply to all values of q greater than zero.

A generalization of the rules[14] for the complexity of the angular distribution also follows from the properties of the Racah coefficients. If there is a maximum effective *final* orbital angular momentum l', a maximum *initial* orbital momentum l, or a maximum total angular momentum J, then a maximum value of L in Eq. (6.3) is given by the simultaneous conditions

$$\begin{aligned}L &\leq 2l';\ 2l+q;\ 2J+q \quad (q \text{ even}) \\ &\leq 2l';\ 2l+q-1;\ 2J+q-1 \quad (q \text{ odd})\end{aligned} \quad (6.4)$$

along with the condition that L must be even if the interfering levels have the same parity.

Equation (6.3) is the general expression for the components of the spin tensor with respect to the direction of the incident beam. It is also convenient to have these components expressed relative to the direction of scattering (θ, φ). If the incident beam direction is denoted by $\mathbf{k}$ and the scattered direction by $\mathbf{k}'$, let us choose a new coordinate system with z' axis along $\mathbf{k}'$, and with the y' axis along $\mathbf{k}\times\mathbf{k}'$. The Euler angles of this rotation are then $(\varphi, \theta, 0)$ relative to the original coordinate system.

The spin tensor operator $T_\mu^{(q)}$ in the new system is then related to the spin tensor operators $T_\kappa^{(q)}$ in the original coordinate system by the relation[20]

$$T_\mu^{(q)} = \sum_\kappa D_{\kappa,\mu}^{(q)}(\varphi,\theta,0)T_\kappa^{(q)}, \quad (6.5)$$

where $D_{\kappa,\mu}^{(q)}$ is an element of the three-dimensional rotation group. The complete dependence on κ of Eq. (6.3) is contained in the factors $(fq0\kappa|fqL\kappa)Y_{L,\kappa}(\theta,\varphi)$. Hence, the new tensor moment contains the transformed factors

$$\sum_\kappa D_{\kappa,\mu}^{(q)}(\varphi,\theta,0)Y_{L,\kappa}(\theta,\varphi)(fq0\kappa|fqL\kappa).$$

Using the relation

$$(-1)^\kappa Y_{L,\kappa}(\theta,\varphi) = [(2L+1)/4\pi]^{\frac{1}{2}}D_{-\kappa,0}^{(L)}(\varphi,\theta,0),$$

as well as the following expansion of the product of two rotation matrices,[21]

$$\begin{aligned}D_{\alpha\beta}^{(S)}(R)D_{\gamma\delta}^{(T)}(R) &= \sum_U(ST\alpha\gamma|STU\alpha+\gamma) \\ &\times(ST\beta\delta|STU\beta+\delta)D^{(U)}{}_{\alpha+\gamma,\beta+\delta}(R),\end{aligned}$$

and performing the sum over κ by R (20a), we obtain for the transformed factors

$$\begin{aligned}&(-1)^q[(2L+1)/(2f+1)]^{\frac{1}{2}}(Lq0\mu|Lqf\mu) \\ &\times[(2L+1)/4\pi]^{\frac{1}{2}}D_{0,\mu}^{(f)}(\varphi,\theta,0).\end{aligned}$$

[20] E. Wigner, *Gruppentheorie und ihre Anwendung auf die Quantenmechanik der Atomspektren* (F. Vieweg, Braunschweig, 1931), p. 165.

[21] This is derived in reference 20, p. 203.

In addition,

$$D_{0,\mu}{}^{(f)}(\varphi,\theta,0)=D_{0,\mu}{}^{(f)}(0,\theta,0)$$
$$=(-1)^{\mu}[4\pi/(2f+1)]^{\frac{1}{2}}Y_{f,\mu}(\theta,0).$$

This result yields the following simple recipe for converting Eq. (6.3) so as to give the tensor moments relative to the scattered axis.

(a) Replace the expressions $(fq0\kappa|fqL\kappa)Y_{L,\kappa}(\theta,\varphi)$ by $(Lq0\kappa|Lqf\kappa)Y_{f,\kappa}(\theta,0)$.

(b) Multiply by the factors

$$(-1)^{q+\kappa}(2L+1)(2f+1)^{-1}.$$

The component κ now refers to the scattered axis. Note carefully that the angle θ is still measured relative to the incident direction and that our result is now independent of φ. Note also that f and L have interchanged their roles since the complexity of the angular distribution is now determined by f. This clarifies the physical meaning of the parameter f and leads to an alternative form of the generalized rule for the complexity of the angular distribution. Instead of Eq. (6.4) we have

$$\begin{aligned} f&\leq 2l,\ 2J,\ 2l'+q \qquad (q \text{ even})\\ &\leq 2l,\ 2J,\ 2l'+q-1 \qquad (q \text{ odd}) \end{aligned} \tag{6.6}$$

along with the condition that f must be even if the interfering levels have the same parity.

Angular Distribution of Nuclear Reactions

It is interesting to note that the results given in BB for the angular distribution of nuclear reactions now appear immediately as a special case of our general result. Since the angular distribution is essentially the expectation value of the unit operator in the final state, we obtain this result by taking $q=\kappa=0$ in Eq. (6.3). An immediate consequence is that $f=L$ and $s_1'=s_2'=s'$. In addition, by Eqs. (B.1) and BBR (14) and (30),

$$X(J_1l_1's';J_2l_2's';LI0)=(-1)^{L+S'-J_1+l_2'}$$
$$\times W(l_1'J_1l_2'J_2;s'L)[(2L+1)(2s'+1)]^{-\frac{1}{2}},$$

$$W(i's'i's';I'0)=(-1)^{i'+s'-I'}[(2i'+1)(2s'+1)]^{-\frac{1}{2}},$$

and $Y_{L,0}=[(2L+1)/4\pi]^{\frac{1}{2}}P_L(\theta)$. The result follows immediately.

The authors wish to thank Dr. Ugo Fano for permission to see the manuscript by Fano and Racah in advance of publication and for the information that the X coefficient was also introduced by Wigner in an earlier unpublished manuscript.

APPENDIX A. REDUCTION OF THE SPIN MATRIX ELEMENT

Consider the matrix element $(\chi(s_1m_1)|T_\kappa{}^{(q)}|\chi(s_2m_2))$, where s_1 and s_2 are channel spins resulting from the vector addition of the spins i and I. The magnetic quantum numbers of s_1 and s_2 are m_1 and m_2, respectively. The tensor operator $T_\kappa{}^{(q)}$ operates only on the particle with spin i and is so normalized that

$$T_0{}^{(q)}=P_q(i_z'/[i'(i'+1)]^{\frac{1}{2}}),$$

where P_q is the usual Legendre polynomial. By the use of the Wigner-Eckart theorem and the Racah formalism [see R (44) and (16′)] we have[22]

$$(\chi(s_1m_1)|T_\kappa{}^{(q)}|\chi(s_2m_2))=(-1)^{I-\kappa-i+m_1}$$
$$\times[(2s_1+1)(2s_2+1)/(2q+1)]^{\frac{1}{2}}W(is_1is_2;Iq)$$
$$\times(s_1s_2-m_1m_2|s_1s_2q-\kappa)(i\|T^{(q)}\|i), \tag{A.1}$$

where the reduced matrix element $(i\|T^{(q)}\|i)$ is independent of κ, m_1, m_2, I, s_1, and s_2. To evaluate this matrix element then, we can choose special values of the parameters which allow a solution of Eq. (A.1). Let us choose $\kappa=I=0$ and $m_1=m_2=i$. Then $s_1=s_2=i$ and

$$(\chi(ii)|T_0{}^{(q)}|\chi(ii))=P_q([i'/(i'+1)]^{\frac{1}{2}}),$$
$$W(iiii;0q)=(-1)^{2i-q}/(2i+1),$$

and, by BBR (1) and R (16),

$$(ii-ii|iiq0)=(-1)^{2i-q}(iii-i|iiq0)$$
$$=(-1)^{2i-q}(2i)!(2q+1)^{\frac{1}{2}}[(2i-q)!(2i+q+1)!]^{-\frac{1}{2}}.$$

Substituting these in Eq. (A.1) we obtain

$$(i\|T^{(q)}\|i)$$
$$=P_q([i/(i+1)]^{\frac{1}{2}})[(2i)!]^{-1}[(2i-q)!(2i+q+1)!]^{\frac{1}{2}}.$$

Hence the general result is

$$(\chi(s_1m_1)|T_\kappa{}^{(q)}|\chi(s_2m_2))$$
$$=(-1)^{I-\kappa-i+m_1}(2q+1)^{-\frac{1}{2}}[(2i)!]^{-1}$$
$$\times[(2s_1+1)(2s_2+1)(2i-q)!(2i+q+1)!]^{\frac{1}{2}}$$
$$\times W(is_1is_2;Iq)(s_1s_2-m_1m_2|s_1s_2q-\kappa)$$
$$\times P_q([i/(i+1)]^{\frac{1}{2}}). \tag{A.2}$$

For the particular value of $q=1$,

$$(\chi(s_1m_1)|T_\kappa{}^{(1)}|\chi(s_2m_2))=(-1)^{I-\kappa-i+m_1}W(is_1is_2;I1)$$
$$\times[(2s_1+1)(2s_2+1)(2i+1)/3]^{\frac{1}{2}}$$
$$\times(s_1s_2-m_1m_2|s_1s_21-\kappa). \tag{A.3}$$

APPENDIX B. SOME PROPERTIES OF THE X COEFFICIENT

The X coefficient is defined by Fano and Racah[12] in terms of Racah functions as

$$X\begin{pmatrix} a & b & c\\ d & e & f\\ g & h & i\end{pmatrix}=(-1)^S\sum_z[(2z+1)W(bdcg;za)$$
$$\times W(dbfh;ze)W(gchf;zi)].$$

[22] For the spin moments of rank greater than zero it is necessary to specify the scattering matrix more completely than the definition given in BB (3.3) and (3.2). The phase of the channel spin wave function must be fixed. We take

$$\chi_{s,m}=\sum(il m_i m-m_i|il sm)\chi_{i,m_i}\chi_{I,\,m-m_i}.$$

Where $S=a+b+\cdots+i$. Fano and Racah have shown than an interchange of two rows or columns multiplies X by $(-1)^S$ and that the interchange between rows and columns leaves X invariant. It should also be noted that the elements of each row and each column must form a possible triad.

For simplicity in printing, we have written the X function as $X(abc;def;ghi)$. The special value

$$X(abc;dec;gg0) = (-1)^{c+g-a-e}W(abde;cg)/[(2c+1)(2g+1)]^{\frac{1}{2}} \quad \text{(B.1)}$$

is often useful.

PHYSICAL REVIEW VOLUME 90, NUMBER 6 JUNE 15, 1953

The Azimuthal Distribution of Photoelectrons Produced by 0.5-Mev Polarized Photons*

FRANK L. HEREFORD AND JEROME P. KEUPER†
Department of Physics, University of Virginia, Charlottesville, Virginia
(Received January 22, 1953)

The azimuth angular distribution of photoelectrons ejected from lead by linearly polarized 0.51-Mev photons has been studied. The known correlation between polarization states of annihilation quanta was employed in preparation of the incident beam of polarized photons. Results indicate that for emission from the K shell, the most probable direction is in the plane containing the momentum and polarization vectors of the incident photon. The asymmetry in the distribution thereby produced is slightly greater than that expected from the relativistically computed differential cross section.

EARLY measurements of the spatial distribution of photoelectrons produced by linearly polarized photons were carried out by Wilson,[1] Bubb,[2] and Kirkpatrick.[3] These measurements were confined to photons of energy less than 40 kev because of the difficulty of preparing a polarized beam at higher energies. The results confirmed the $\cos^2\phi$ azimuthal distribution deduced from classical considerations by Auger and Perrin,[4] and from nonrelativistic quantum mechanics by Sommerfeld and Schur.[5] Here ϕ is the angle between the plane containing the momentum vectors of the photon and ejected photoelectron and that containing the polarization and momentum vectors of the incident photon. Thus the most probable electron emission is along the polarization vector.

This result is valid only for electrons ejected from the K shell, those from higher levels showing complete azimuthal symmetry. The K shell electrons normally comprise approximately 80 percent of all electrons ejected for moderately hard quanta.[6] Actually the computed distribution for L electrons contains a term yielding an azimuthal asymmetry.[7] However, this component represents a small fraction of the 20 percent of total intensity deriving from higher levels and can be neglected for our purposes.

For relativistic energies, Sauter[8] has computed the distribution for K electrons with the following factor in the differential cross section giving the angular distribution,

$$d\sigma\sim\frac{\sin^2\theta}{(1-\beta\cos\theta)^4}\{\tfrac{1}{4}(\gamma-1)^2(1-\beta\cos\theta) + [1/\gamma-\tfrac{1}{2}(\gamma-1)(1-\beta\cos\theta)]\cos^2\phi\}, \quad (1)$$

where β is the photoelectron velocity in units of c, $\gamma=(1-\beta^2)^{-\frac{1}{2}}$, and θ is the angle $(\mathbf{k}_0, \mathbf{p})$ between the incident photon and photoelectron. For the case of importance here ($\theta=\pi/2$), this factor reduces to

$$d\sigma\sim\tfrac{1}{4}(\gamma-1)^2+[1/\gamma-\tfrac{1}{2}(\gamma-1)]\cos^2\phi. \quad (2)$$

In the nonrelativistic limit the second term predominates in agreement with the previously stated results. For $\beta=0.87$ (K.E.$=0.51$ Mev) the second term vanishes yielding azimuthal symmetry, and for higher energies this term is negative. Moreover, in this region the first term, containing the square of the energy, predominates. Thus for $\beta>0.87$ the preferred K electron emission is orthogonal to the polarization vector of the incident photon. It can be presumed that the 20 percent of the photoelectrons from higher levels show azimuthal symmetry for all energies, although no calculations on this point have been performed.

No experimental results in the region of higher energies were available until recently when the cross-polarization property[9] of electron-positron annihilation quanta was used to investigate the azimuthal distribution of photoelectrons ejected by the 0.51-Mev anni-

* Supported in part by the Navy Bureau of Ordnance, Contract NOrd 7873.
† Now with Remington Arms Company, Bridgeport, Connecticut.
[1] C. T. R. Wilson, Proc. Roy. Soc. (London) **A104**, 11 (1923).
[2] F. W. Bubb, Phys. Rev. **23**, 137 (1924).
[3] P. Kirkpatrick, Phys. Rev. **38**, 1938 (1931).
[4] P. Auger and F. Perrin, J. phys. et radium **8**, 93 (1927).
[5] A. Sommerfeld and G. Schur, Ann. Physik **4**, 409 (1930).
[6] W. Heitler, *Quantum Theory of Radiation* (Oxford University Press, London, 1944), p. 127.
[7] G. Schur, Ann. Physik **4**, 433 (1930).
[8] F. Sauter, Ann. Physik **11**, 454 (1931).
[9] J. A. Wheeler, Ann. N. Y. Acad. Sci. **48**, 219 (1946).

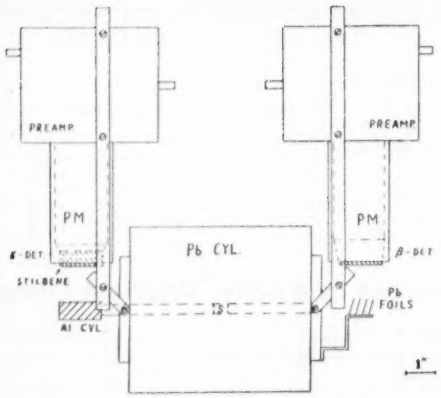

FIG. 1. The arrangement of the Na^{22} source (S), Pb collimator, Al and Pb foil scatterers, and stilbene crystals for detection of scattered photons on the left (γ-det.) and photoelectrons on the right (β-det.).

hilation quanta.[10] The results of this experiment yielded an azimuthal asymmetry considerably greater than that predicted by a calculation employing Sauter's photoelectron cross section and the method of Snyder *et al.*[11] for analyzing experiments involving the polarization states of annihilation quanta. Two undesirable features of this experiment were (1) the lack of experimental information on the possible influence of photons and electrons scattered from the edge of the Pb collimator (which themselves exhibit a known angular correlation[11,12]) and (2) the inability of the experimental method to distinguish between asymmetry due to preferred photoemission in the polarization plane and asymmetry due to emission orthogonal to this plane. Either case would yield asymmetry in this experiment.

EXPERIMENT

A more suitable arrangement is that employed in the experiment described here. A source of annihilation quanta (3 Mc of Na^{22}) was sealed in an aluminum capsule and placed at the center of a $\frac{3}{8}$-in. hole drilled through a 7 in. by 6 in. diameter lead cylinder (Fig. 1). The photon beam emerging from one end was scattered by a 1 in.$\times\frac{1}{2}$ in. diameter aluminum cylinder and detected by a $\frac{1}{4}$ in.$\times$1 in.$\times$1 in. stilbene crystal. The oppositely directed beam impinged upon four $\frac{1}{2}$ in. square by 0.01 in. thick lead foils. Photoelectrons ejected from these foils were detected by a $\frac{1}{2}$-in. diameter by 0.020 in. thick stilbene crystal covered by 0.0005-in. aluminum foil. The computed efficiency of this crystal for 0.25-Mev photons was 2.0 percent, whereas the electron efficiency was very nearly 100 percent for any electron entering the crystal. Scintillations from the crystals were detected by RCA 5819 photomultipliers and coincident pulses counted by a fast coincidence circuit of 2×10^{-8} sec resolving time. Coincidence rates were recorded for relative azimuth angles between detectors of 0°, 90°, 180°, and 270°.

THEORY

We consider now the expected result of these measurements. The correlation between polarization states of annihilation quanta follows from selection rules in Dirac theory which allow two-photon annihilation to proceed only from a singlet state positronium system.[9] Conservation of angular momentum then demands that the two annihilation quanta be in an eigenstate of zero total angular momentum for which eigenstate the polarization vectors must be crossed. The polarization of either photon is completely undetermined. However, observation of the polarization state of one performs a partial analysis of the polarization state of the other.[13]

Photons $\mathbf{k}_0$ and $-\mathbf{k}_0$ can be arbitrarily analyzed into orthogonal eigenstates of linear polarization 1 and 2 as shown for photon $\mathbf{k}_0$ in Fig. 2. Let the direction 1 contain the axis of the γ-counter detecting photons scattered at an angle ϕ_1 with respect to some direction

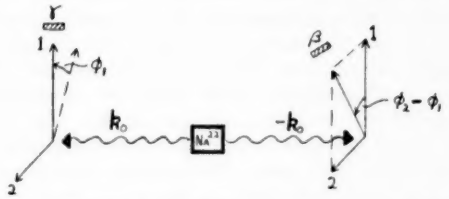

FIG. 2. Coordinate systems for resolution of photons into orthogonal eigenstates of linear polarization (1 and 2).

$\phi=0$. Following Snyder *et al.*,[11] the Schrödinger wave functional for the photon pair may be written

$$\Psi=\frac{1}{\sqrt{2}}\{\psi_1(\cdots 1_{\mathbf{k}_0 1}, 0_{\mathbf{k}_0 2}\cdots 0_{-\mathbf{k}_0 1}, 1_{-\mathbf{k}_0 2}\cdots) +\psi_2(\cdots 0_{\mathbf{k}_0 1}, 1_{\mathbf{k}_0 2}\cdots 1_{-\mathbf{k}_0 1}, 0_{-\mathbf{k}_0 2}\cdots)\},$$

where $\psi(N_{\mathbf{k}\lambda}\cdots)$ is the wave functional for N photons of momentum $\mathbf{k}$ and polarization λ. An observation of the polarization state of one photon forces the pair into either state ψ_1 or ψ_2. Thus component 1 of photon $\mathbf{k}_0$ is associated with component 2 of $-\mathbf{k}_0$, and component 2 of $\mathbf{k}_0$ with component 1 of $-\mathbf{k}_0$.

Assume now that the photon into which $\mathbf{k}_0$ is scattered is detected by the γ-counter and the photoelectron

[10] F. L. Hereford, Phys. Rev. **81**, 482 (1951); **81**, 627 (1951).
[11] Snyder, Pasternack, and Hornbostel, Phys. Rev. **73**, 440 (1948).
[12] E. Bleuler and H. L. Bradt, Phys. Rev. **73**, 1938 (1948); R. C. Hanna, Nature **162**, 332 (1948); C. S. Wu and I. Shaknov, Phys. Rev. **77**, 136 (1950).
[13] The experiment is analagous to the hypothetical experiment of Einstein, Podolsky, and Rosen [Phys. Rev. **47**, 777 (1935)], purporting to show the incompleteness of the quantum-mechanical description of the physical world. Their argument has been refuted, and the experiment described here can be analyzed from the standpoint of the quantum theory of measurement in a manner similar to that employed in analysis of their proposed experiment. See, for example, D. Bohm, *Quantum Theory* (Prentice-Hall, Inc., New York, 1951) for a similar analysis.

ejected by $-\mathbf{k}_0$ detected by the β-counter oriented at some angle, $\phi_2-\phi_1$, with respect to the γ-counter. We seek the expected dependence of coincidence rate upon $\phi_2-\phi_1$. The Klein-Nishina formula predicts an angular distribution of the scattered photon given by the factor,

$$k_0/k+k/k_0-2+4\cos^2\Theta,$$

where Θ is the angle between the polarization vectors of the incident and scattered photons.

Averaging over all directions of the polarization of the scattered photon this becomes

$$k_0/k+k/k_0-2\sin^2\theta\cos^2\phi,$$

where θ=angle $(\mathbf{k}_0, \mathbf{k})$, and ϕ=angle between the $(\mathbf{e}_0, \mathbf{k}_0)$ and $(\mathbf{k}_0, \mathbf{k})$ planes.

The angular distribution of the photoelectron ejected by photon $-\mathbf{k}_0$ in the $\theta=\pi/2$ plane is given by Eq. (2) which may be written $A+B\cos^2\phi$.

Now component 1 of $\mathbf{k}_0$ will produce a counting rate in the γ-detector given by $P^{(1)}\sim k_0/k+k/k_0-2$. This will be associated with a rate produced by component 2 of $-\mathbf{k}_0$: $P^{(2)}\sim A+B\sin^2(\phi_2-\phi_1)$. The coincidence rate due to these two components is then

$$C^{(1)}\sim(k_0/k+k/k_0-2)[A+B\sin^2(\phi_2-\phi_1)].$$

Similarly the other two associated components yield a rate

$$C^{(2)}\sim(k_0/k+k/k_0)[A+B\cos^2(\phi_2-\phi_1)].$$

The total coincidence rate is then

$$C\sim(k_0/k+k/k_0)(2A+B)-2A-2B\sin^2(\phi_2-\phi_1). \quad (3)$$

In substituting appropriate values for k_0, k, etc. it must be recalled that Eq. (2) is valid only for K electrons comprising approximately 80 percent of the total electrons ejected. Hence, it must be multiplied by a weighting factor 0.8 and a symmetrical term of weight 0.2 added to account for the electrons from higher levels. Also, in computation of the velocity of the photoelectrons, the K shell binding energy must be considered. Taking into account these factors for the experiment under consideration, one finds for the coincidence rate in arbitrary units,

$$C\sim1-0.27\sin^2(\phi_1-\phi_2). \quad (4)$$

This expression must be corrected for the finite geometry of the detectors by integrating with respect to ϕ_1 and ϕ_2 over the azimuth angles subtended by the crystals. Strictly speaking, the integration should also be carried out over the variable θ_1 and θ_2. However, the further correction so obtained is small. This is due mainly to the appearance of $\cos\theta$ in the bracketed term in Eq. (1). Since $\cos\theta$ changes sign at $\pi/2$, integration of the term from $\pi/2-\theta_0$ to $\pi/2$ will introduce an increased asymmetry in azimuth which is just compensated by the decreased asymmetry introduced in integration from $\pi/2$ to $\pi/2+\theta_0$. The effect of the factor before the bracket can be shown to be small (about 4 percent) relative to the experimental errors to be given. For these reasons the rather tedious integration over θ_1 and θ_2 has not been performed.

Carrying out the integration over ϕ_1 and ϕ_2 for the case at hand where the half-span in azimuth of each detector is 20°, one can compute the expected ratio of the coincidence rates with detectors orthogonal and coplanar. If Sauter's relativistic cross section is employed, using Eq. (4), deduced from Sauter's cross section, one finds $C_\perp/C_\parallel=0.77$. If the nonrelativistic cross section for the photoelectric effect is employed, the result is $C_\perp/C_\parallel=0.37$. It should be noted that this ratio is less than unity, whereas in the previous experiments in which either the scattered quanta[12] or photoelectrons[10] are detected at both ends, the ratio is greater than unity.

EXTRANEOUS EFFECTS

Before discussion of results, the possible influence of a number of extraneous contributions to the observed coincidence rates should be considered. Accidental coincidences were suppressed by the use of a coincidence circuit of resolving time 2×10^{-8} sec. The accidental rates constituted at the most 40 percent of the total coincidence rates in each of the four independent runs to be reported. The contribution of cosmic-ray showers was negligible.

Possible coincidences between an annihilation quantum and the 1.3-Mev gamma-ray following the Na^{22} beta-transition were also of negligible consequence for the geometry employed. This follows from the fact that while the relative angle of emission of an annihilation photon pair is $\pi\pm1/137$ radians, the 1.3-Mev gamma-ray emission is spherically symmetric. This argument has been confirmed experimentally.[10]

The extremely low photon efficiency of the thin β-crystal (about 2.0 percent) discriminated strongly against detection of photons scattered from the lead foils. A subsidiary experiment confirmed the negligibility of coincidences caused by these photons. Detection of Compton electrons produced in the lead foils was also improbable for several reasons. In the first place it should be noted that for 0.51-Mev photons in lead the photoelectron cross section exceeds the Compton cross section by a factor of about 1.3. More im-

TABLE I. Coincidence rates for a typical single run with and without lead foils in place.

	Coin.	$C_\parallel$ (counts/hr)	$C_\perp$ (counts/hr)
Pb in	Total	18.10	16.04
	Chance	7.18	7.28
	Genuine	10.92	8.72
Pb out	Total	9.52	9.35
	Chance	4.30	4.32
	Genuine	5.22	5.03
Produced in Pb foils		5.70±0.9	3.69±0.8

portant, the energy of Compton electrons at the minimum angle for detection by the β-crystal were of energy less than 30 kev, which was insufficient for penetration of the thin reflector foil which covered the crystal.

Actually the most probable spurious events detected by the β-crystal were photoelectrons and Compton electrons produced at the edge of the lead collimator. However, the scattered photon-electron coincidence rate so produced could be observed by removing the lead foils. This rate was subtracted from the observed coincidence rate with the foils in place as shown in Table I.

It should be noted that it was not possible to shield the β-crystal from these extraneous radiations since the shield would act as a converter for stray photons thereby enhancing the over-all photon efficiency of this detector. The extent to which single counts in each detector were the result of radiation actually produced in the aluminum or lead scatterer can be seen from the following typical rates:

$C_\beta = 10\,200$ counts/min, Pb foils in;

$C_\beta = 5600$ counts/min, Pb foils out;

$C_\gamma = 13\,300$ counts/min, Al scatterer in;

$C_\gamma = 9400$ counts/min, Al scatterer out.

TABLE II. Net coincidence rates for four runs and computed values of the ratio $C_\perp/C_\parallel$.

Run	$C_\perp$ (counts/hr)	$C_\parallel$ (counts/hr)	$C_\perp/C_\parallel$
1	3.69	5.70	0.65±0.13
2	2.75	3.73	0.73±0.15
3	3.62	5.32	0.68±0.13
4	4.15	6.56	0.64±0.13
Average exp. value			0.68±0.06
Computed (relativistic)			0.77
Computed (nonrelativistic)			0.37

RESULTS

Since the measured total coincidence rates were only 16 to 20 counts per hour, several days were required to obtain satisfactory statistical accuracy. The difficulties involved in prolonged measurements with scintillation counters necessitated a series of independent 40-hr runs rather than a single run of several days duration.

The results of a typical single run are shown in Table I, where total, accidental, and genuine coincidence rates with and without the lead foils in place are given. The collected data from four such runs are given in Table II with the average value of the ratio $C_\perp/C_\parallel$. The ratios computed from both the relativistic and nonrelativistic photoelectric cross sections are also shown for comparison.

The agreement is probably satisfactory in view of the fact that the computed ratio would be decreased somewhat if integration over θ_1 and θ_2 had been performed. Actually the relativistic cross section should not be expected to yield correct results in the case at hand because of the approximate nature of Sauter's calculation. In particular, he approximates the quantity $(l^2-\alpha^2Z^2)^{\frac{1}{2}}$ by l, where l is the orbital angular momentum quantum number, α the fine structure constant, and Z the atomic number of the absorber. While a good approximation for small Z, it is hardly valid for small values of l in the case of a lead absorber ($\alpha Z=0.6$). Sauter estimates that the computed total cross section for lead differs by no more than 15 percent from the correct value as a result of the approximation. It seems likely, however, that the angular distribution may be more seriously affected.[14]

The computed result may be further in error from neglect of the symmetrical component in the cross section for L electrons which was mentioned above. The The uncertainty of the available information on cross sections for ejection from different shells[15] makes it difficult to estimate the contribution of this component.

We plan to extend these measurements to other values of θ in the near future. Incorporation of pulse height analysis of the pulses from the β-crystal will allow discrimination against Compton electrons and detection of photoelectrons emitted in the forward hemisphere. Preliminary results for $\theta=45°$ indicate a decrease in $C_\perp/C_\parallel$ in qualitative agreement with Sauter's cross section.

[14] This possibility has been confirmed by Prof. H. A. Bethe in a private communication.

[15] Gladys R. White, National Bureau of Standards Report 1003, May 13, 1952 (unpublished).

The Isotopic Constitution of Silicon, Germanium, and Hafnium

JOHN H. REYNOLDS
Department of Physics, University of California, Berkeley, California
(Received February 25, 1953)

The isotopic constitutions of silicon, germanium, and hafnium have been measured with a mass spectrometer by techniques which are described. Results for silicon are in good agreement with certain of the earlier determinations but are in poor agreement with the values adopted in the recent compilation by Bainbridge and Nier. Results for germanium do not differ significantly from earlier determinations. Results for hafnium differ only slightly from the one previous determination in which electrical detection was used, but in such a way as to suggest that determinations on hafnium which has been fractionally purified with respect to zirconium may not be faithfully representative of the true abundances. An upper limit of 0.003 percent has been placed on the abundance in nature of Hf^{182}.

THE isotopic constitution of the elements silicon, germanium, and hafnium has been measured with a 9-in. radius, 60-degree deflection, single-focusing mass spectrometer recently constructed at Berkeley. In each case the trifluoride ion from electron bombardment of the tetrafluoride was examined. The tetrafluorides were prepared by thermal decomposition of the barium or ammonium complex fluorides, a technique[1] which ensures no isotopic fractionation in the chemistry since the yield of all reactions involved is 100 percent. Prior to all runs, the spectrometer envelope was baked overnight at 350°C so as to reduce the residual hydrocarbon background to a negligible fraction of the peaks measured at any mass position. The ion source was of conventional design, but no source magnet was employed. Magnetic sweep was employed throughout, the ion accelerating voltage being held fixed at 4200 volts. Secondary electrons were repelled to the final collector by application of -45 volt to a repelling electrode. Ion currents were measured by recording the voltage across a 5×10^{10} ohm resistor in the input to a Model 30 Applied Physics vibrating reed electrometer which drove a Brown recording potentiometer. The entire detection system, including input resistor, was checked and found to be perfectly voltage linear within the sensitivity of the procedure which was 0.2 percent. Scale changing multipliers were calibrated with a type K-2 potentiometer.

For analyses of silicon and germanium, the gaseous tetrafluoride was admitted to the ion source through a leak consisting of a 0.001-in. hole in a 0.001-in. aluminum foil from a reservoir wherein the pressure was always such as to ensure pure molecular flow through the leak. The collector slit was adjusted for flat-topped, fully resolved ion peaks and the rate of sweep was kept sufficiently slow that a constant ion current was recorded on the peak top for at least 8 seconds, a precaution which effectively eliminates any errors due to variable sweep speed. A single determination consisted in ten successive sweeps of the spectrum under completely stable conditions. The mean deviation within the sets of 10 ratios so obtained was always less than 0.1 percent.

The data for silicon are presented in Table I and reflect measurements of the ratios of peak intensities to that for Si^{28}. The silicon used was from olivine from dunite (Jackson County, North Carolina). Subsequent research[2] on the variations in isotopic constitution of silicon from various geological sources has detected maximum deviations in the Si^{30}/Si^{28} ratio of only 0.2 percent from that for olivine. It is worthy of mention that in the latter research the mean deviation in the Si^{30}/Si^{28} ratio for olivine, for 39 determinations of this quantity, was 0.05 percent, the determinations extending over a period of several months within which the machine was baked several times and the ion source disassembled and reassembled twice. It is the result of this extreme constancy that the low probable error of about 0.5 percent for the silicon abundance ratios is quoted. Most of this error resides in undetermined, inherent mass discrimination of the spectrometer. Nier[3]

TABLE I. Silicon isotope abundances.

Observer	Ion used	Abundance, atomic percent Si^{28}	Si^{29}	Si^{30}
Present work	SiF_3^+ from SiF_4	92.18±0.03	4.71±0.02	3.12±0.02
Hibbs,[a] 1949	SiF_3^+ from SiF_4	92.19±0.06	4.70±0.03	3.12±0.04
White and Cameron,[a] 1946	SiF_3^+ from SiF_4	92.16±0.06	4.71±0.03	3.13±0.04
Adopted average:[a] Ney and McQueen, Williams, and Yuster, Inghram, 1946	SiF_3^+ from SiF_4	92.27±0.09	4.68±0.05	3.05±0.03

[a] As reported in reference 4.

[1] J. H. Reynolds and T. J. Ypsilantis, Phys. Rev. **90**, 378A (1953).
[2] J. Reynolds and J. Verhoogen, Geochim. Cosmochim. Acta (to be published).
[3] A. O. Nier, Phys. Rev. **79**, 450 (1950).

TABLE II. Germanium isotope abundances.

Observer	Ion used	Abundance, atomic percent Ge^{70}	Ge^{72}	Ge^{73}	Ge^{74}	Ge^{76}
Present work	GeF_3^+ from GeF_4	20.52±0.17	27.43±0.21	7.76±0.08	36.54±0.23	7.76±0.08
Hibbs, Redmond, Gwinn, and Harman,[a] 1949	GeF_3^+ from GeF_4	20.60±0.06[b]	27.38±0.08	7.83±0.06	36.40±0.10	7.78±0.05
Hibbs, Redmond, Gwinn, and Harman,[a] 1949	GeI^+ from GeI_4	20.65±0.04[b]	27.43±0.02	7.86±0.04	36.34±0.05	7.72±0.01
Inghram, Hayden, and Hess,[a] 1947	Ge^+ from Ge	20.55	27.37	7.67[c]	36.74	7.67

[a] As reported in reference 4.
[b] Statistical errors only.
[c] The value 7.61 appearing in reference 4 is the result of a misprint in the original publication of this assay.

reports this to be of the order of 0.4 percent per mass unit in the region of mass 85 for a similar instrument, but using a capillary leak and voltage sweep; it is felt that in the present investigation, using a molecular flow leak and magnetic sweep, the inherent discrimination should be lower. It will be noted that the present results on silicon are in good agreement with determinations made at Oak Ridge by Hibbs and by White and Cameron, but are in rather poor agreement with the values adopted by Bainbridge and Nier[4] in a recent compilation, although the last represent the average of three distinct investigations which were in good agreement with each other.

The data for germanium are presented in Table II and reflect measurements of the ratios of peak intensities to that for Ge^{74}. Shelf germanium dioxide* was the source material. Somewhat higher probable errors in the abundance ratios are quoted because of the fact that fewer determinations were made with this element. Reference to Table II shows that the present results are in slightly better agreement with the GeF_3^+ results of Hibbs than with the other determinations listed there. Discrepancies appear to be random, i.e., not systematic with mass.

For the analysis of hafnium, HfF_4 was sublimed into the electron beam from a stainless steel crucible which was initially loaded with a solid $(NH_4)_2HfF_6$. This compound, when preheated in vacuum, dissociates to form the tetrafluoride. Techniques were those described above except that with the small solid samples used, ion currents were considerably less stable than with the gas samples. This required a faster rate of sweep in order that the time between successive observations of the Hf^{178} reference peak would not be overlong and thus preclude making meaningful corrections, when reading the charts, for drift in ion intensity. Source material was hafnium oxide, 99 percent pure obtained from Research Chemicals, Inc. The data are presented in Table III and reflect measurements of the ratios of peak intensities to that for Hf^{178}. A correction proportional to $(M)^{\frac{1}{2}}$ has been applied to compensate for nonselective evaporation from the solid HfF_4. In addition to the abundance measurements, an upper limit of 0.003 percent, was placed on the abundance in nature of Hf^{182}. Reference to Table III shows random disagreement with the abundances reported by Mattauch and Ewald but systematic disagreement with those reported by Hibbs. The differences with the latter can be improved partially by application of an $(M)^{\frac{1}{2}}$ correction to Hibbs' values (which may be appropriate since he sublimed solid $HfCl_4$ into the ion source) but considerable systematic differences remain. These are possibly attributable to differences in the chemical procedure by which the source hafnium was separated from zirconium. Fractional crystallizations, precipitations, or distillations are the rule in such separations and, depending upon the method used, there would be opportunity for enrichment of either the heavy or the light isotopes in the final hafnium fractions. An unambiguous hafnium assay should probably be made from hafnium which

TABLE III. Hafnium isotope abundances.

Observer	Ion used	Abundance, atomic percent Hf^{174}	Hf^{176}	Hf^{177}	Hf^{178}	Hf^{179}	Hf^{180}
Present work	HfF_3^+ from HfF_4	$0.199\pm^{0.003}_{0.010}$	5.23±0.05	18.55±0.17	27.23±0.22	13.73±0.13	35.07±0.24
Hibbs,[a] 1949	Hf^+ from $HfCl_4$	0.18±0.01[b]	5.15±0.02	18.39±0.01	27.08±0.04	13.78±0.02	35.44±0.06
Mattauch and Ewald,[a] 1944	Hf^+ and Hf^{++} from HfO_2 and Hf (spark)	0.18±0.01	5.30±0.11	18.47±0.06	27.10±0.08	13.84±0.07	35.11±0.14

[a] As reported in reference 4.
[b] Statistical errors only.

[4] K. T. Bainbridge and A. O. Nier, Prelim. Report No. 9, Nuc. Science Ser., National Research Council, 1950 (unpublished).
* Fairmount Chemical Company, "As-free, purest."

has not been highly purified with respect to zirconium.

Note Added in Proof.—Since this article was prepared, there has come to my attention the careful work of Graham[5] and co-workers on the isotopic constitution of germanium. These workers found that, with the exception of one sample, germanium from various ores was isotopically indistinguishable. Their averaged results for the isotopic constitution of six germanium ores, excluding the anomalous sample, can be brought into total agreement with results given here (except at mass 73 where the residual discrepancy is 0.25 percent of the abundance quoted) by application of a factor which reduces their abundances for heavier isotopes relative to the lighter, which is linear with mass, and which amounts to 0.24 percent per mass unit. This factor in all probability represents the relative discrimination of the two mass spectrometers involved. An attempt has been made to detect mass discrimination in this mass region in the Berkeley instrument by comparing measurements on atmospheric xenon with those of Nier,[3] which latter have been corrected for spectrometer discrimination. Agreement was such as to indicate that the mass discrimination of the Berkeley instrument is less than 0.025 percent per mass unit at mass 130.

[5] Graham, Macnamara, Crocker, and MacFarlane, Can. J. Chem. **29**, 89 (1951).

PHYSICAL REVIEW VOLUME 90, NUMBER 6 JUNE 15, 1953

The Angular Distribution of $Li^6(n,\alpha)H^3$ for Neutrons of 200, 270, 400, and 600 kev*

LILLIAN E. DARLINGTON, JACK HAUGSNES, HARRY M. MANN, AND JAMES H. ROBERTS
Department of Physics, Northwestern University, Evanston, Illinois

(Received March 9, 1953)

The angular distribution of $Li^6(n,\alpha)H^3$ has been measured for neutron energies of 200, 270, 400, and 600 kev by determining the distribution of triton tracks from this reaction in Ilford *C2* plates loaded with enriched Li^6. The results fit a series of the type $A+B\cos\phi_0+C\cos^2\phi_0$, where ϕ_0 is the neutron-triton angle in the center-of-mass system. This indicates that the *s* and *p* components of the incident neutron wave predominate in the interaction.

(1) INTRODUCTION

THERE are two reasons why an investigation of $Li^6(n,\alpha)H^3$ was undertaken. (1) The use of this reaction to study neutron spectra[1] requires that the differential cross section be known as a function of neutron energy. (2) Basic data of theoretical importance can be obtained.[2] Preliminary results have been reported.[3]

The technique used is to expose Ilford *C2* plates loaded with enriched Li^6 to unidirectional monoergic neutrons from an electrostatic generator and to measure the distribution of tracks as a function of the neutron-triton angle. Further measurements are now in progress to determine the absolute differential cross section of the reaction for neutron energies from 100 to 2000 kev. These results will be published at a later date.

(2) PLATE EXPOSURE AND PROCESSING

The 100-micron Ilford *C2* plates loaded with enriched Li^6 were exposed to neutrons from $Li^7(p,n)$ at the electrostatic generator of the Argonne National Laboratory. The exposure geometry is shown in Fig. 1. Each plate was inside a cadmium box during exposure to shield it from the thermal neutron background. Integrated neutron fluxes of approximately 10^9 neutrons/cm^2 were used except for the exposure at 270 kev at the peak of the resonance where approximately 10^8 neutrons/cm^2 were used. All lithium targets were about 30 kev thick. The proton energy was selected so that the neutron groups would peak at 200, 270 kev, etc.

The plates were stored for at least two weeks and then given additional latent-image fading for 24 hours in an atmosphere saturated with water vapor at 22°C. The plates were processed by the technique outlined by Keepin in University of California Radiation Laboratory Report UCRL 790 (unpublished). Some of the plates were also treated with glycerine so as to be

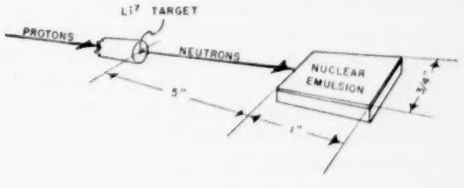

FIG. 1. Exposure geometry for Li^6 loaded plates. Each plate was inside a Cd box to shield it from the thermal neutron background due to room scattering.

* Work supported by the U. S. Atomic Energy Commission.

[1] G. R. Keepin, Jr., and J. H. Roberts, Phys. Rev. **76**, 154 (1949); Rev. Sci. Instr. **21**, 163 (1950).

[2] M. Peshkin and A. Siegert, Phys. Rev. **87**, 735 (1952); W. Solano and J. Roberts, Phys. Rev. **89**, 892 (1953).

[3] Roberts, Darlington, and Haugsnes, Phys. Rev. **82**, 299 (1951); J. Roberts and H. Mann, Phys. Rev. **83**, 202 (1951).

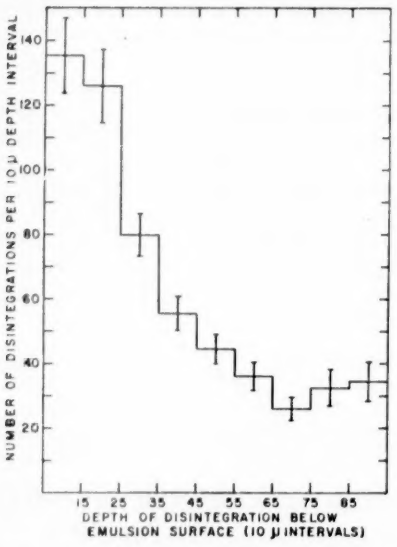

FIG. 2. Distribution of Li^6 atoms with depth below the top emulsion surface. To obtain this plot 979 tracks were measured. The vertical projection of the tritons was $\leq 20\mu$ in a glycerine treated plate. Corrections were made for the probability that a track would go through either emulsion surface. A curve of this type was determined for each plate; all were similar to this one.

restored approximately to their original thickness at the time of exposure.[4]

(3) TRACK MEASUREMENTS

All tracks were measured by use of Leitz Ortholux and Bausch and Lomb model CTB microscopes. 2-mm 90× apochromatic oil immersion objectives were used throughout. A protractor scale was attached to one eyepiece for the measurement of angles. Observers were trained as outlined in a previous report.[5]

For each track the following quantities were measured: the vertical projection of the alpha and triton tracks; the horizontal projection of the triton track, the alpha-track, the neutron-triton angle, and the neutron-alpha-angle. As the measurements progressed it was observed that the distribution of Li^6 atoms with depth was not uniform; measurements were therefore made of this distribution. (See Fig. 2.)

Some tracks were difficult if not impossible to interpret correctly. In such cases the observer made the most reasonable interpretation. If a track was misinterpreted this could frequently be determined from its total length, assuming it was produced by a neutron of full energy coming directly from the lithium target of the electrostatic generator. The observers were given a rough guide as an aid for such tracks. If the triton was obviously placed at the wrong end of the track the neutron-triton angle was reflected through 180°. This introduced some random error and loss in angular resolution because of scattering of the alpha and triton particles in the emulsion.

(4) CORRECTIONS FOR GEOMETRICAL SELECTION CRITERIA

The plates were scanned parallel to the direction of neutron incidence. Any track projecting into the field of view was not measured if its point of disintegration was outside the width of the scanning path. This was to prevent the selection of tracks between two scanning paths in such a way as to favor tracks making a large angle with the neutron direction.

Since the emulsion thickness was of the same order of magnitude as the track lengths, the probability that a track would go through the emulsion surface and thus be rejected was appreciable. Also, since steeply diving tracks were difficult to interpret, it was expedient to put an upper limit δ (35 microns in a 100-micron plate) on the vertical projection of an acceptable triton track. These considerations made it necessary to correct the data to what one would obtain if all tracks in a 4π solid angle had been measured.[6] In order to simplify these corrections a minimum distance from the emulsion surfaces to either end of the triton track was imposed. This distance (15 microns in a 100-micron plate) was such that the alpha-track of an otherwise acceptable disintegration could not go out of the emulsion. This minimum distance defines "effective emulsion surfaces" inside of which all parts of acceptable triton tracks must lie.

From the data we find the triton range R_T, the alpha-range R_α, and the neutron-triton angle ϕ in the laboratory system for every track. We also have a histogram giving the distribution of Li^6 atoms with depth below the emulsion surface. Let $W(\gamma)d\gamma$ = the probability that a disintegration will occur at a height between γ

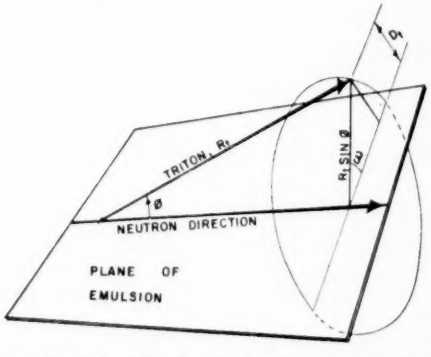

FIG. 3. The orientation of a typical triton track with respect to the emulsion plane and the direction of the incident neutrons. D_T is the vertical projection of the triton track.

[4] Details of this treatment are discussed in a separate paper to be published in the Review of Scientific Instruments.

[5] J. Haugsnes and J. H. Roberts, Los Alamos Report LA-1303, 1951 (unpublished).

[6] For a more complete discussion see G. R. Keepin and A. J. Siegert, Los Alamos Report 937, 1949 (unpublished).

and $\gamma+d\gamma$ above the lower effective emulsion surface. This function was obtained by drawing a smooth curve through the depth distribution histogram of Li^6 atoms (Fig. 2). Any azimuth ω (Fig. 3) is equally probable because of symmetry around the neutron direction. Then $W(\gamma)d\gamma d\omega/2\pi$ is the probability that a given disintegration will lie in the interval γ to $\gamma+d\gamma$, and ω to $\omega+d\omega$. The integral of this probability over all values of ω and γ compatible with the selection criteria will give the probability that the track will be accepted for measurement. This probability is given by

$$P(R_T,\phi)=\frac{1}{\pi}\int_0^{\omega_0} d\omega\left[\int_0^{a-R_T\sin\phi\sin\omega} W(\gamma)d\gamma + \int_{R_T\sin\phi\sin\omega}^{a} W(\gamma)d\gamma\right], \quad (1)$$

where a is the distance from the lower effective emulsion surface to the upper, and $\omega_0=\pi/2$ if $R_T\sin\phi\leq\delta$, and $\omega_0=\arcsin(\delta/R_T\sin\phi)$ if $R_T\sin\phi>\delta$.

Now $R_T=R_T(\phi,E_n)$. From the neutron energy E_n, $Q=4.78$ Mev for $Li^6(n,\alpha)$, and the range-energy curve for tritons in $C2$ emulsions, we can obtain an expression $P(\phi,E_n)$ from $P(\phi,R_T)$. $P^{-1}(\phi,E_n)$ for a typical plate is shown in Fig. 4. Each track was given a statistical weight $P^{-1}(\phi,E_n)$.

(5) DATA AND RESULTS

Table I gives the number of tracks measured on each plate and the neutron energy to which it was exposed. The total track length, $R_\alpha+R_T$, and the angle ϕ between the neutron and the triton were calculated for each track. The tracks were divided into ϕ_0 intervals, usually 15° (ϕ_0 is the neutron-triton angle in the center-of-mass system). Figure 5 shows typical histograms of the number of tracks as a function of $R_\alpha+R_T$ for some of these intervals. The triangle in each group shows where the track distribution should peak on the basis of $Q=4.78$ Mev for $Li^6(n,\alpha)$ and the Ilford range-energy curves. The "satellite" peaks appearing in some of the groups result from tracks for which the point of disintegration has been misinterpreted and from the background of epithermal neutrons. The epithermal background was estimated by calculating[7] the alpha-triton

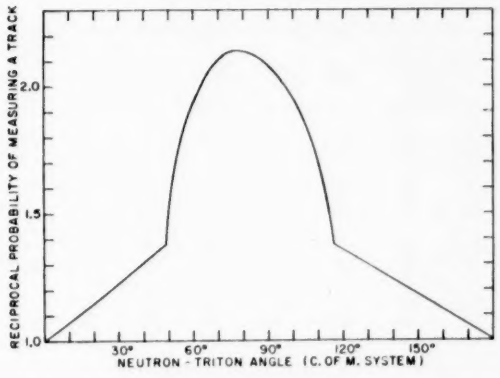

FIG. 4. Chart for determining $P^{-1}(\phi,E_n)$ for each track. This particular plot is for $E_n=600$ kev for plates 8 and 9 (see Table I).

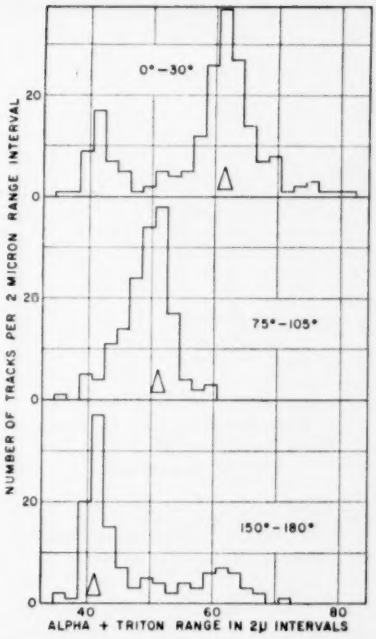

FIG. 5. Typical histograms of tracks in a few ϕ_0 intervals for $E_n=600$ kev. The arrow indicates the expected position of the peak on the basis of $Q=4.78$ Mev for $Li^6(n,\alpha)$, and the Ilford range-energy curves.

TABLE I. Tracks measured and differential cross-section coefficients.

Neutron energy (kev)	Plate number	Observer	No. of tracks measured	Capture[a] cross section (barns/atom of Li^6)	Differential capture cross-section coefficients (barns/steradian) A	B	C
200[b]	1-S	3	1000	2.1	0.10	0.08	0.18
200	2	1	948	2.1	0.09	0.11	0.23
200	3	3	996	2.1	0.08	0.14	0.26
270[b,c]	4	—	—	3.0	0.17	0.060	0.22
270	5	13	988	3.0	0.17	0.065	0.21
270	5	9	650	3.0			
400	6	3	438	1.2	0.06	0.040	0.11
400	7	1	1005	1.2	0.065	0.047	0.09
600[b]	8-S	21	1097	0.5	0.031	0.007	0.024
600	8	3	786	0.5	0.029	0.017	0.032
600	9	7	595	0.5	0.032	0.012	0.023

[a] From data of Blair and Holland (reference 8).
[b] Data from glycerine-treated plates.
[c] See 2nd paper, reference 2.

[7] M. L. Boas, Rev. Sci. Instr. (to be published).

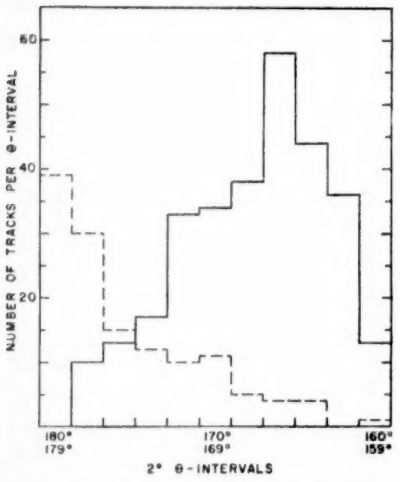

FIG. 6. Distribution of tracks as a function of the alpha-triton angle θ. The solid curve is for tracks in the interval $60° \leqslant \phi_0 \leqslant 120°$ for $E_n = 600$ kev in plate 8-S. (See Table I.) The broken curve is for tracks in a glycerine treated plate exposed to thermal neutrons.

angle θ for tracks in the region $60° \leqslant \phi_0 \leqslant 120°$ in glycerine treated plates. A plot of the number of tracks per two-degree θ-interval as a function of θ for $E_n = 600$ kev is shown in Fig. 6. The distribution in θ for tracks obtained from a glycerine treated plate exposed to thermal neutrons is shown in the broken histogram in the same figure. Since this latter distribution peaks $\sim\theta = 180°$, and since the distribution for $E_n = 600$ kev shows no rise in this region, the epithermal background must be low. Also, since the angular distribution at $E_n = 400$ and 600 kev was similar to that at $E_n = 270$ kev, any small number of unresolved tracks resulting from a neutron background in the vicinity of this resonance would introduce a very small correction. All background corrections would be somewhat less than the statistical accuracy of the data; therefore no such corrections were made.

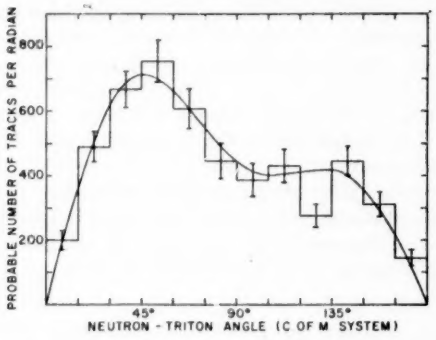

FIG. 7. Histogram showing distribution of tracks per 15° ϕ_0 interval for $E_n = 200$ kev from plate 1-S (see Table I) corrected for geometrical selection criteria. The smooth curve is a plot of $2\pi Y(E_n, \phi_0) \sin\phi_0$, where $Y(E_n, \phi_0)$ is defined in Eq. (2).

The tracks in the "satellite" peaks were reflected through 180° in the laboratory system. However, these reflections proved to be of such a nature (i.e., random), that the effect was again somewhat less than the statistical accuracy of the data. The main effect of these misinterpretations was to decrease the angular resolution because of scattering of the tracks in the plate.

Each track was weighted with the factor $P^{-1}(\phi, E_n)$ as discussed in Sec. 4. A plot of $\Sigma P^{-1}(\phi, E_n)$ for all tracks in each 15° ϕ_0 interval in the c.m. system as a function of ϕ_0 for $E_n = 200$ kev is shown in Fig. 7. The data for each E_n as obtained by each observer are given in Table II. The observer agreement is seen to be reasonably satisfactory in most cases. Since the observers had received more experience and more complete instruction by the time the tracks were measured in the glycerine treated plates, it is probable that these data are the most reliable. The over-all correctness of the method of analyzing the data was checked by determining the angular distribution for collimated

TABLE II. ΣP^{-1} for tracks in 15° intervals.[a]

Neutron energy (kev)	Plate number	Observer	Neutron-triton angle interval 0–15°	15°–30°	30°–45°	45°–60°	60°–75°	75°–90°	90°–105°	105°–120°	120°–135°	135°–150°	150°–165°	165°–180°	Actual ΣP^{-1} 0–180°
200[b]	1-S	3	39	95	129	146	118	86	75	84	54	86	60	28	1355
200	2	1	45	124	154	140	90	105	50	85	53	67	70	21	1325
200	3	3	56	156	159	141	110	114	49	30	42	62	57	25	1315
270	5	13	34	103	150	112	113	106	77	73	79	84	45	25	1417
270	5	9	35	90	118	143	174	83	73	76	82	64	42	18	975
400	6	3	52	103	112	132	103	129	56	72	72	79	60	31	619
400	7	1	54	88	128	125	150	130	76	28	41	84	59	36	1560
600[b]	8-S	21	23	77	107	113	124	107	100	92	103	78	52	24	1746
600	8	3	42	80	123	138	106	128	99	69	60	69	58	30	1227
600	9	7	32	94	109	109	120	87	138	81	82	68	67	13	914

[a] For all the data except at $E_n = 270$ kev, the intervals are in the center-of-mass system. The data at 270 kev are grouped in the corresponding intervals in the laboratory system. The total sum of P^{-1} from 0° to 180° is adjusted to 1000 for convenience in comparing the data of the different observers.
[b] Data from glycerine treated plates.

thermal neutrons; it was found to be spherically symmetric, as it should be.

If the s and p components of the incident neutron wave are contributing to the reaction, the angular distribution giving the relative triton yield per unit solid angle will be of the form:

$$Y(E_n, \phi_0) = A' + B' \cos\phi_0 + C' \cos^2\phi_0, \qquad (2)$$

where A', B', and C' are constants for a given E_n. If we write $Y(E_n, \phi_0) = dN/d\Omega$, where dN is the number of tritons between Ω and $\Omega + d\Omega (d\Omega = 2\pi \sin\phi_0 d\phi_0)$, and integrate between the limits ϕ_{01} and ϕ_{02}, we have

$$\frac{1}{2\pi}\int_{\phi_{01}}^{\phi_{02}} dN = \left[A' \cos\phi_0 + \frac{B'}{2}\cos^2\phi_0 + \frac{C'}{3}\cos^3\phi_0\right]_{\phi_{02}}^{\phi_{01}}. \qquad (3)$$

If the data in Table II are divided into three equal ϕ_0 intervals, three simultaneous equations are obtained to evaluate A', B', and C' above for each E_n. If we normalize $\int_0^{4\pi} Y(E_n, \phi_0) d\Omega$ to the total capture cross section as measured by Blair and Holland,[8] we obtain directly the differential cross section $d\sigma(E_n, \phi_0)/d\Omega = A + B\cos\phi_0 + C\cos^2\phi_0$. The values of A, B, and C thus determined from the data of each observer are shown in Table I. The statistical accuracy of these coefficients is of the order of 12 percent for the A's and B's, and 20 percent for the C's. The agreement is seen to be reasonably satisfactory in most cases. A series of the type given in Eq. (2) fits the data from the glycerine treated plates more smoothly than it does the data from untreated plates, except for $E_n = 270$ kev, where excellent agreement was obtained throughout. Furthermore the data from the glycerine-treated plates were obtained after the observers had acquired more experience. They were therefore arbitrarily given twice as much weight as the data from untreated plates in determining the average value of the coefficients given in Table III. The statistical accuracy of these average coefficients is better than 10 percent for the A's and B's and 15 percent for the C's. A plot of $Y = A + B\cos\phi_0 + C\cos^2\phi_0$ using the values of A, B, and C in Table III is shown in Fig. 8.

TABLE III. Average value of the coefficients of the differential cross section of $Li^6(n,\alpha)$.

E_n kev	Coefficients (barns/steradian) A	B	C
200	0.096	0.105	0.215
270	0.17	0.063	0.22
400	0.064	0.043	0.095
600	0.031	0.0095	0.026

[8] J. M. Blair and R. E. Holland, data reproduced in *Neutron Cross Sections*, Atomic Energy Commission Report 2040 (Office of Technical Services, Washington, D. C., 1952).

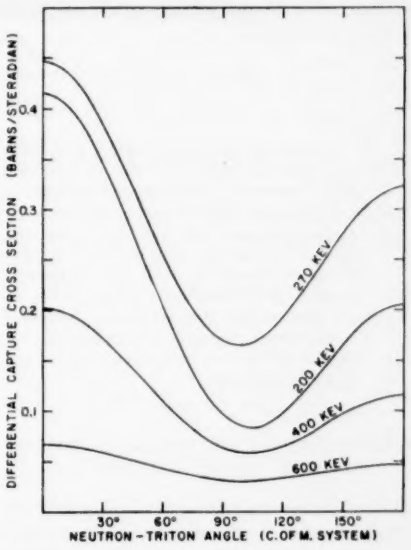

FIG. 8. The differential cross section of $Li^6(n,\alpha)H^3$ for $E_n = 200$, 270, 400, and 600 kev. The curves are plotted by using the average coefficients given in Table III.

Measurements of $d\sigma/d\Omega$ for $E_n = 100$, 1100, 1500, and 2000 kev are now in progress and will be published later. It is planned also to check some of the measurements with plates loaded with specks of lithium glass. The latter measurements should yield improved accuracy, since the visible specks of glass should make possible a more unique determination of the point of disintegration.

The authors wish to thank Franklin Peterson, Kate Rymer, Margaret Steele, and Elizabeth Stephenson for their patience in measuring most of the tracks and for helping with some of the calculations. We also wish to thank Hubert Billington for developing the plates. Appreciation is also expressed to Alexander Langsdorf and his group at the Argonne Laboratory for valuable assistance in exposing the plates and for the use of their electrostatic generator.

Production of Fissionable Isotopes in a Thermal Reactor*†

LAWRENCE BAYLOR ROBINSON‡
Atomic Energy Research Department, North American Aviation, Downey, California
(Received December 2, 1952)

Differential equations representing isotopic production and decay schemes are discussed. The Bateman equations are suitable for the description of naturally occurring processes. Van Wye and Beckerly have given equations which describe processes occurring in a thermal reactor, if feedback is neglected. Their equations are modified so that feedback might be included.

Examples are given which show the role and the origin of feedback. In a conversion reactor, the phenomenon of resonance capture and the operation of the reactor at criticality are responsible for feedback. An example is also given of the appearance of feedback resulting from the production of Pu^{239} from neutron capture by U^{235} and neutron capture by, and beta-decay of Pu^{239} products. This latter example is of more use conceptually than practically. A method of accounting for fuel replacements is also discussed.

Some special systems may be treated as general dynamical systems; a method is shown which will determine whether they are conservative or nonconservative. Such information is of both practical and theoretical importance.

I. REPRESENTATION OF ISOTOPIC PRODUCTION AND DECAY SCHEMES

NUCLEAR production and decay schemes have been known for some time. The mathematical description of typical processes is given in the so-called Bateman equations.[1] These equations are

$$dN_{i+1}/dt=\lambda_i N_i-\lambda_{i+1}N_{i+1}, \tag{1}$$

where the subscript i takes on all values from unity to one less than the number which characterizes the stable end product. The solution, for a typical case, in which all of the N_i, except N_1, are zero at $t=0$ (and from which the solution for any other initial conditions can be constructed by superposition) is

$$N_s=N_1(0)\lambda_1\lambda_2\lambda_3\cdots\lambda_{s-1}\sum_{i=1}^{s}\frac{e^{-\lambda_i t}}{\prod_{j\neq i}(\lambda_j-\lambda_i)}. \tag{2}$$

The subscript s represents any member of the production chain. The symbol $\prod_{j\neq i}$ means the product of all $(\lambda_j-\lambda_i)$ except the one for which $j=i$. These equations are descriptive of processes occurring naturally or of a process whereby radioactivity is induced in a particular species followed by leaving this species to itself.

The above equations are inadequate in accounting for processes occurring within nuclear reactors. In a reactor, activity is induced in the products as well as a given precursor species; the species will in general disappear by neutron capture as well as by beta-disintegration. A system of equations, with solutions, to represent such processes has been given by Van Wye and Beckerley.[2] They found it convenient to use two subscripts (one for mass number and the other for atomic number) to characterize a given nucleus. The Van Wye-Beckerley equations are

$$dN_{ij}/dt=(b_{i,j-1}N_{i,j-1}+c_{i-1,j}N_{i-1,j})-k_{ij}N_{ij}, \tag{3}$$

where

$$\begin{aligned} k_{ij}&=b_{ij}+c_{ij}+f_{ij},\\ b_{ij}&=\lambda_{ij}\ \text{(beta-disintegration constant)},\\ c_{ij}&=\phi\sigma_c(ij),\\ f_{ij}&=\phi\sigma_f(ij). \end{aligned} \tag{4}$$

The subscript c refers to capture and f to fission; ϕ is the thermal neutron flux, and σ is the microscopic cross section. The symbol i refers to mass number and j to atomic number. Equation (3) lists the various contributions to the net rate of change of the amount of a given nuclear species. The positive contributions are a result of beta-disintegration of a nucleus of the same mass number but atomic number smaller by one and of neutron capture by a nucleus of the same atomic number but mass number smaller by one; negative contributions to the rate of change of the species result from beta-disintegration of or neutron capture by the nucleus in question. *An important characterization of Eq. (3) is that each subscript on the right-hand side is either equal to or less than those on the left.* Van Wye and Beckerley give solutions representing various species in the production chain. The solutions are combinations of exponentials where the decay constant α in the various terms $(e^{-\alpha t})$ are simply the coefficients of the various N_{ij} on the right-hand side of Eq. (3). These solutions are somewhat lengthy expressions and will not be reproduced herein.

* Description of elementary reactor theory may be found in H. Soodak and E. C. Campbell, *Introduction to Pile Theory* (John Wiley and Sons, Inc., New York, 1950); C. Goodman, *Science and Engineering of Nuclear Power* (Addison-Wesley Press, Cambridge, 1949 and 1952), Vols. I and II; S. Glasstone and M. C. Edlund, *The Elements of Nuclear Reactor Theory* (D. Van Nostrand Company, Inc., New York, 1952).

† This report is based upon studies conducted for the U. S. Atomic Energy Commission.

‡ Now at Naval Research Laboratory, Washington, D. C.

[1] Rutherford, Chadwick, and Ellis, *Radiations from Radioactive Substances* (Cambridge University Press, New York, 1930 and 1951), pp. 11–31. Also most books on radioactivity and nuclear physics. H. Bateman, Proc. Cambridge Phil. Soc. **15**, 423 (1910).

[2] R. F. Van Wye and J. G. Beckerley, Nucleonics **9**, No. 10, 17 (1951).

The formulation, and hence solution, of systems (1) and (3) assumes that the fate of the product has no effect on the behavior of the precursor. There are processes which may occur in a nuclear reactor in which a given nuclear species may be regenerated through several intermediate steps. Hence, the fate of the total amount of some precursors is linked to that of their products. It is usual to call this phenomenon "feedback." A review of the neutron economy in a typical thermal reactor will show that the phenomenon of nuclear resonances makes for feedback in the production of heavy isotopes. Since the terms representing resonance capture involve more than one isotope, the equations representing the processes will in general be nonlinear (as will be shown later); nevertheless, for many practical cases (when the resonance escape probability of the reactor changes negligibly with time) a linearized version of the equations is adequate. The following modification of the Van Wye-Beckerley equations makes them adequate to represent the processes involving feedback:

$$dN_{ij}/dt=(b_{i,j-1}N_{i,j-1}+c_{i-1,j}N_{i-1,j})-\sum_k\sum_l h_{kl}N_{kl}. \quad (5)$$

In Eq. (5) the subscripts on the right may be larger numerically than those on the left; this differs from Eq. (3) and is an essential characterization of feedback in nuclear production schemes. The specific form of the h_k will be given later. The solutions of Eq. (5) differ from those of Eq. (3) in that the coefficients of time in the exponential functions are not the coefficients of the various N_{ij} in the differential equations [as in case (3)].

In the general problem of interest, Eq. (5) may be written as a homogeneous matrix differential equation as

$$d\mathbf{N}/dt=\mathbf{AN}. \quad (6)$$

Two examples will be developed in some detail mainly to show the specific role of feedback which has not been heretofore emphasized. One can characterize the individual nuclear species by only one subscript. The method of accounting for fuel replacements will be considered in a third example. No numerical results will be included.

II. EXAMPLES

A. Conversion Reactors

The first example to be discussed is a typical process occurring in a thermal reactor designed for the production of fissionable material. In a reactor which uses U^{235} in combination with U^{238} as fuel, some of the U^{238} is converted into Pu^{239}. A net gain of fissionable material would result if for every U^{235} atom undergoing fission, one of the neutrons produced would serve to carry on the reaction chain but more than one (on the average) would be captured in U^{238} to produce Pu^{239}. A reactor which can produce a net gain of fissionable material is called a "breeder."[3] This term has also been applied to the type of reactor in which the same element is regenerated as is the case when the fuel is a mixture of Pu^{239} and U^{238}. The term "converter" is more generally applied to the reactor in which some fissionable material, say U^{235}, is used up and some fertile material U^{238} becomes plutonium.

Thorium-232 is also a possible fertile material. Glasstone describes the reactions as:[4] "By the (n,γ) capture of a slow neutron, the latter (*thorium-232*) is converted into Th^{233}, which is a negative beta-emitter with a half-life of 23 minutes, the product being protactinium-233; this is also beta-active with a half-life of 27.4 days. The reaction and disintegration scheme is thus

$$_{90}Th^{232}+n\rightarrow{}_{90}Th^{233}\xrightarrow[23\text{ min}]{\beta}{}_{91}Pa^{233}\xrightarrow[27.4\text{ days}]{\beta}{}_{92}U^{233},$$

the U^{233} being a long-lived alpha-emitter of 1.63×10^5 years half life." U^{233} is fissionable by slow neutrons and hence is a possible fuel for sustaining a chain reaction.

The mathematical description of the scheme illustrated above is interesting. In setting up the differential equations for the Th-U^{233} system, one uses the following considerations. In the steady state, the nuclear species U^{235}, Th^{232}, Th^{233}, Pa^{233}, and U^{233} are present. The number of nuclei/cm³ of these may be designated, respectively, as N_1, N_2, N_3, N_4, and N_5. In addition to these, fission products and structural materials contribute absorbing nuclei. It will be assumed that the resonance absorption in all species, except Th^{232}, is negligible in comparison with thermal absorption. The number of thermal neutrons/cm² sec absorbed in U^{235} is $\phi\sigma_1N_1$; this is also the rate of change of U^{235} nuclei/cm³, since each absorption destroys a U^{235} nucleus and there are no significant processes[5] which produce U^{235}. Above, ϕ is the thermal flux in neutrons/cm² sec, σ_1 is the microscopic absorption cross section in cm². The absorption of $\phi\sigma_1N_1$ thermal neutrons in U^{235} will yield $\eta_1\phi\sigma_1N_1$ fast neutrons; η_1 is the number of fast neutrons released per thermal absorption in U^{235}. One may write the corresponding quantities for U^{233} as $\phi\sigma_5N_5$ and $\eta_5\phi\sigma_5N_5$. As the result of the capture of $\phi(\sigma_1N_1+\sigma_5N_5)$ thermal neutrons/cm³/sec in fissile material $\phi(\eta_1\sigma_1N_1+\eta_5\sigma_5N_5)$ fast neutrons are produced. These neutrons undergo several reactions in the process of being slowed down. In the first place, some leak out as fast neutrons. Secondly, some are captured in the thorium resonances in the process of slowing down. Thirdly, some of those which are slowed down to thermal energies are captured in each of the nuclear species within the reactor. Finally, the rest leak out of the reactor as thermal neutrons.

A quantitative accounting for these processes may be given as follows. One may let L represent the probability

[3] S. Glasstone, *Sourcebook on Atomic Energy* (D. Van Nostrand Company, Inc., New York, 1950), p. 401.

[4] Reference 4, pp. 400–401.

[5] Uranium-235 could be produced by two successive neutron captures by a U^{233} nucleus but this small contribution will be neglected.

that fast neutrons do not leak from the reactor and p represent the probability that they escape capture in the thorium resonances. It will be assumed that these probabilities are the same for the fast neutrons from U^{235} and U^{233}. Hence, the number of neutrons/cm³/sec absorbed in the thorium resonances is $(1-p)\phi L[\eta_1\sigma_1 N_1+\eta_5\sigma_5 N_5]$, and the number μ becoming thermal is $(\eta_1\sigma_1 N_1+\eta_5\sigma_5 N_5)pL\phi$. If l is the thermal nonleakage probability, then $\mu(1-l)$ leak thermally from the core and $\mu l\sum_i/\sum$ are absorbed in each of the ith species. $\sum_i$ represents $N_i\sigma_i$ and $\sum$ is the sum of all $N_i\sigma_i$ in the reactor. A total of μl neutrons are therefore absorbed thermally in the reactor, and this must be equal to $\sum\phi$; hence $\mu l/\sum\phi=1$. This is the condition of criticality under which the reactor operates. Because of criticality, the role of resonance capture in thorium is different from that of thermal capture in an essential manner. *The rate at which thorium is destroyed by resonance capture depends on the amount of U^{233} (a product of Th^{232}) which has been produced.* Although the amount of U^{233} appears in the expression for the thermal capture, it is in combination with other factors such that the combination is always equal to unity. There would be no difference in these two types of capture (i.e., resonance and thermal) if the system were imbedded in an infinite sea of neutrons. The fact that the system is closed (i.e., neutrons produce fissionable material and are in turn produced by the fissionable material while the reactor is always at criticality) is the physical basis for this type of feedback.

The equations describing these processes do not have as simple a solution as those indicated in reference 3. The λ_i will refer to the beta-disintegration constants; capture processes involving cross sections, such that the product σ_i and any reasonable ϕ is negligible, will not be indicated. The equations are

$$dN_1/dt=-\phi\sigma_1 N_1, \tag{7}$$

$$dN_2/dt=-\phi\sigma_2 N_2-\eta_1\phi\sigma_1 N_1(1-p)L-\eta_5\phi\sigma_5 N_5(1-p)L, \tag{8}$$

$$dN_3/dt=\phi\sigma_2 N_2+\eta_1\phi\sigma_1 N_1(1-p)L+\eta_5\phi\sigma_5 N_5(1-p)L-(\lambda_3+\phi\sigma_3)N_3, \tag{9}$$

$$dN_4/dt=\lambda_3 N_3-(\lambda_4+\phi\sigma_4)N_4, \tag{10}$$

$$dN_5/dt=\lambda_4 N_4-\phi\sigma_5 N_5, \tag{11}$$

$$dN_6/dt=y(\sigma_1 N_1\phi+\sigma_5 N_5\phi)-(\lambda_6+\sigma_6\phi)N_6. \tag{12}$$

The subscript 6 refers to the fission products (actually it may be more convenient to treat some of them separately) and y (the yield of fission products) is taken as a constant for a given flux. It is apparent that the system of Eqs. (7) through (12) may be written in the form of Eq. (6).

B. Direct Feedback

A second example will now be considered, in which feedback may be seen to enter. In this example, feedback enters more directly, although it plays a much less significant part. The first step is the successive absorption of neutrons by U^{235} and its products to become U^{238}. Further absorption by the U^{238} is followed by beta-disintegration of the U^{239} to produce neptunium (Np), followed in turn by beta-disintegration to yield plutonium (Pu); some of the plutonium undergoes alpha-disintegration to regenerate U^{235}. Designating U^{235}, U^{236}, U^{237}, U^{238}, U^{239}, Np^{239}, and Pu^{239} as species 1, 2, 3, 4, 5, 6, and 7, respectively, one may write the differential equations as

$$dN_1/dt=-\phi\sigma_1 N_1+\alpha N_7, \tag{13}$$

$$dN_{k+1}/dt=\phi\sigma_k N_k-(\lambda_{k+1}+\phi\sigma_{k+1})N_{k+1} \tag{14}$$

(k takes on values from 1 through 4, and some of the λ_i may be zero),

$$dN_6/dt=\lambda_5 N_5-\phi\sigma_6 N_6, \tag{15}$$

$$dN_7/dt=\lambda_6 N_6-(\alpha+\phi\sigma_7)N_7. \tag{16}$$

In Eq. (16) α represents the alpha-disintegration constant of plutonium. Feedback is evident here in that the total rate of change of U^{235} depends to some extent on the amount of its product Pu^{239}. The above process is of more use conceptually than practically.

Each of the systems may be represented as the matrix Eq. (6). The solution is

$$\mathbf{N}=\mathbf{N}_0\exp(\mathbf{A}t), \tag{17}$$

where $\mathbf{N}_0$ is the matrix describing the initial conditions. The meaning of $\exp(\mathbf{A}t)$ is well known from the Cayley-Hamilton theorem, a result of which may be written

$$\exp(\mathbf{B})=\sum_{i=1}^{n} e^{\lambda_i}\mathbf{G}_i, \tag{18}$$

where n is the order of the square matrix $\mathbf{B}$ and the λ_i are the distinct roots of the characteristic equation. The $\mathbf{G}_i$ are given by

$$\mathbf{G}_1=\prod_{j\neq i}(\lambda_j\mathbf{E}-\mathbf{B})/\prod_{j\neq i}(\lambda_j-\lambda_i), \tag{19}$$

where $\mathbf{E}$ is the unit matrix. Practical considerations often render other methods more useful than the evaluation of the $\mathbf{G}_i$. This is particularly so if some of the λ_i are approximately equal.

The Laplace transform technique may be conveniently applied to Eq. (6). The solutions may be found in well-known texts.[6]

C. Replacement of Fuel

In conversion reactors, operating for long times, additional fuel is added to compensate for that which has been consumed and product is withdrawn. The

[6] F. D. Murnaghan, *Introduction to Applied Mathematics* (John Wiley and Sons, Inc., New York, 1948), pp. 356–374; C. R. Wylie, *Advanced Engineering Mathematics* (McGraw-Hill Book Company, Inc., New York, 1952), pp. 191–194.

total change in the material can become a significant portion of the total. A satisfactory manner in which this can be taken into account is as follows. One may use the derivation given by Churchill[7] for systems in which replacements are made. Let $N_i(t)$ be the number gf atoms (per unit volume) of the ith species (in the reactor); the atoms are destroyed by neutron capture and other processes such that out of $N_i(0)$ atoms introduced at time $t=0$, the number $N_i(t)$ in existence at any subsequent time t is given by

$$N_i(t)=N_i(0)H_i(t). \tag{20}$$

In Eq. (20), $H_i(t)$ is the survival function for the ith species. $H_i(0)=1$. In conversion reactors, replacements (positive and negative) are usually effected through the insertion or withdrawal of shim rods. If $R_i(\tau)$ is the total number of atoms/cm^3 introduced in (or withdrawn from) the reactor up to time τ, then $R_i'(\tau)d\tau$ is the total number of replacements between $t=\tau$ and $t=\tau+d\tau$; the number of survivals out of these which were added in $d\tau$ at any future time t is $R_i'(\tau)H_i(t-\tau)d\tau$. Hence, the total number of atoms of the ith kind at any time t is the sum of the survivals from those on hand at time $t=0$ increased by the survivals from the replacements during every time interval $d\tau$ between $\tau=0$ and $\tau=t$. Therefore,

$$N_i(t)=N_i(0)H_i(t)+\int_0^t R_i'(\tau)H_i(t-\tau)d\tau. \tag{21}$$

The determination of the survival factor $H_i(t)$ is effected through the solution of the basic Eq. (5). If the replacements are made at a predetermined rate, then $R_i(\tau)$ is known and the indicated integration is immediate. However, if the number of atoms $N_i(t)$ that are required to be in service at each instant is known, then Eq. (21) is an integral equation (since the unknown appears under the integral sign) of the convolution type in R_i'. The rate R_i' at which replacements must be made to maintain the required $N_i(t)$ may then be determined. In either case, the Laplace transform techniques is useful in the solution of Eq. (21).

III. REMARKS

One may isolate from such systems as have been described the basic processes and obtain essential information in a general fashion as is described below; in some instances the results may not be immediately obtainable by physical considerations. One may consider the essential processes occurring in a reactor using U^{235} as feed and Pu^{239} as fuel in an attempt to obtain true breeding. Since resonance capture is important in such a case, it is desirable to consider the resonance capture probability in U^{238} as being proportional to the amount of U^{238} present and consider the nonlinear differential equations. It is also convenient to consider the capture of the neutrons in U^{238} as giving Pu^{239} directly. If one writes the amount of U^{238} as N_1 and that of Pu^{239} as N_2, then (for constant thermal flux),

$$dN_1/dt=-a_1N_1-a_{12}N_1N_2, \tag{22}$$

$$dN_2/dt=a_1N_1+a_{12}N_1N_2-a_2N_2. \tag{23}$$

This system may be considered as a generalized dynamical system from which the examination of a certain function of N_1 and N_2 will yield information which, in some instances, may not be obtained otherwise.[8]

An exact integral for the system is found from Eqs. (22) and (23). These equations give

$$\frac{dN_1}{dt}+\frac{dN_2}{dt}-\frac{a}{N_1}\frac{dN_1}{dt}-b=0, \tag{24}$$

where $a=a_2/a_{12}$ and $b=a_1a_2/a_{12}$. Integration of Eq. (24) yields

$$N_1+N_2+\ln N_1^{-a}-bt=K, \tag{25}$$

which may be written as

$$F(N_1, N_2)=e^{N_1}e^{N_2}N_1^{-a}=Ae^{bt}. \tag{26}$$

It is evident that some systems in which feed is supplied, as the reactions occur, could yield $F(N_1, N_2)=$constant. Equation (26) represents what may be called a generalized nonconservative system, whereas $F(N_1, N_2)=C$ is conservative. The phase plane representation of the latter, for some values of C, yields closed trajectories, which means oscillatory phenomena. In such cases both N_1 and N_2 will increase and decrease periodically with time. It is apparent that such information is important for practical as well as theoretical reasons.

One final remark might be made in regard to Eq. (26). One notices that as time increases indefinitely $F(N_1, N_2)$ approaches infinity ($b>0$). This can be true only by N_1 approaching zero (since $a>0$). This is known from physical considerations as Eqs. (25) and (26) imply no replenishing of the U^{238}.

The writer would like to thank Dr. E. Richard Cohen for many helpful suggestions in the preparation of this article.

[7] R. V. Churchill, *Modern Operational Mathematics in Engineering* (McGraw-Hill Book Company, Inc., New York, 1944), pp. 79–80; see also H. Branson, Cold Spring Harbor Symposia on Quantitative Biology **13**, 35 (1948).

[8] A. A. Androvow and C. E. Chaikin, *Theory of Oscillations* (Princeton University Press, Princeton, 1949), pp. 94–101.

Nuclear Hyperfine Structure of Mn^{++}†

MENDEL SACHS
University of California, Los Angeles, California
(Received December 29, 1952; revised manuscript received March 2, 1953)

A theoretical calculation of the nuclear hyperfine splitting in Mn^{++} is made on the assumption that the ground state is composed of a mixture of the normal electronic configuration and a state created by moving an inner $3s$ electron to the $4s$ state. The ground-state wave function is then written as

$$\Psi=(1-\alpha^2)^{\frac{1}{2}}\psi(3s^23d^5)+\alpha\psi(3s3d^54s).$$

The numerical calculation of α is limited primarily by the inaccuracy of the values of the $3s$ and $4s$ radial wave functions at the nucleus. The observed splitting is obtained for the value $\alpha^2\simeq 4.41\times10^{-4}$.
The calculation was carried out by assuming a jj coupling model.

I. INTRODUCTION

THE paramagnetic resonance spectra of Mn^{++} diluted in powdered samples of phosphor crystals has been observed in this laboratory.[1] The normal electronic configuration and ground state of Mn^{++} are $(1s)^2\cdots(3s)^2(3p)^6(3d)^5$ and $^6S_{\frac{5}{2}}$, respectively. The nuclear hyperfine structure arises from an interaction between electronic and nuclear spins. This interaction is a function of $(3\cos^2\theta-1)$. Since the normal configuration of Mn^{++} corresponds to a spherically symmetric charge distribution around the nucleus, the average value of $(3\cos^2\theta-1)$ is zero, and there should be no observable hyperfine structure. It was pointed out by Abragam and Pryce[2] that a reduction of the spherical symmetry by a crystalline field would result in a very small splitting, and this splitting would show a characteristic anisotropy with respect to the direction of the external magnetic field. However, observations in this laboratory, and in many other laboratories reveal a large isotropic splitting.

It has been suggested by Abragam and Pryce that the observed hyperfine structure may be due to an admixture to the normal electronic configuration of a configuration in which one of the inner electrons is in a higher state. The unpaired electrons in the admixed state should then produce an isotropic hyperfine splitting.

Configurational coupling will only couple states with the same L, S, and parity,[3] so that the higher state must also be a state with $L=0$, $J=5/2$, and $g=2$. Abragam and Pryce suggest that the most probable higher state which will couple with the original ^6S state is the state in which a $3s$ electron is moved to the $4s$ state. The wave function for the ground state of Mn^{++} may now be written as

$$\Psi=(1-\alpha^2)^{\frac{1}{2}}\psi(3s^23d^5)+\alpha\psi(3s3d^54s). \quad (1)$$

It is the purpose of this paper to calculate the fraction α which would account for the experimentally observed nuclear hyperfine splitting.

II. INTERACTION HAMILTONIAN

By means of an expansion of the electronic field into multipoles, it is found that the interaction energy between the electron cloud and the nuclear magnetic moment is $\boldsymbol{\mu}_N\cdot\mathbf{H}_0$, where H_0 is the magnetic field of the electron cloud at the nucleus, and μ_N is the magnetic moment of the nucleus. The vector potential of the electron cloud is $\mathbf{A}=\boldsymbol{\mu}\times\mathbf{r}/r^3$ and the magnetic field is $\mathbf{H}=\nabla\times\mathbf{A}=[3\mathbf{r}(\boldsymbol{\mu}\cdot\mathbf{r})r^{-2}-\boldsymbol{\mu}]r^{-3}$. The magnetic moment of the electron cloud is $\boldsymbol{\mu}=\mu(\mathbf{L}+2\mathbf{S})$, and the nuclear magnetic moment is $\boldsymbol{\mu}_N=\gamma\mu_N\mathbf{I}$.

The ground state of Mn^{++} has an orbital angular momentum $L=0$; therefore our Hamiltonian operator is $\mathcal{H}_{hfs}=2\gamma\mu_N\mu[3(\mathbf{I}\cdot\mathbf{r})(\mathbf{S}\cdot\mathbf{r})r^{-2}-(\mathbf{S}\cdot\mathbf{I})]r^{-3}$.

If the unit vector $\mathbf{r}/r$ is located at an angle (θ,φ), then

$$[3(\mathbf{I}\cdot\mathbf{r})(\mathbf{S}\cdot\mathbf{r})r^{-2}-\mathbf{S}\cdot\mathbf{I}](m,m)=[S_zI_z(3\cos^2\theta-1)](m,m),$$

and the Hamiltonian is

$$\mathcal{H}_{hfs}=2\gamma\mu_N\mu S_zI_z(3\cos^2\theta-1)r^{-3}. \quad (2)$$

III. EIGENFUNCTIONS

The eigenfunctions for the $(3s3d^54s)$ wave function were calculated by a method described by Gray and Wills.[4]

Using the notation

$$\Psi[LSM_LM_S]\equiv[^{2S+1}LM_LM_S],$$

and denoting the eigenfunction product states by $(m_{l_1}{}^{\pm}m_{l_2}{}^{\pm}\cdots m_{l_7}{}^{\pm})$, the eigenfunctions are

$$[^6S\ 0\ \pm5/2]=2^{-\frac{1}{2}}[(0^+0^-)-(0^-0^+)](2^+-2^+\ 1^+-1^+\ 0^+), \quad (3a)$$

$$[^6S\ 0\ \pm3/2]=10^{-\frac{1}{2}}[(0^+0^-)-(0^-0^+)]\sum_{i=1}^{5}x_i{}^{\pm}, \quad (3b)$$

$$[^6S\ 0\ \pm1/2]=20^{-\frac{1}{2}}[(0^+0^-)-(0^-0^+)]\sum_{i=1}^{10}y_i{}^{\pm}. \quad (3c)$$

† This work was supported in part by the U. S. Office of Naval Research.

[1] W. D. Hershberger and H. Leifer, Phys. Rev. **88**, 714 (1952).
[2] A. Abragam and M. H. L. Pryce, Proc. Roy. Soc. (London) **A205**, 135 (1951).
[3] E. U. Condon and G. H. Shortley, *Theory of Atomic Spectra* (Cambridge University Press, Cambridge, 1935).
[4] N. M. Gray and L. A. Wills, Phys. Rev. **38**, 248 (1931).

The first bracket represents the antisymmetrized wave function for the two nonequivalent s electrons; the second bracket represents the $3d^5$ part of the wave function. The eigenfunctions $x_i^{\pm}$ and $y_i^{\pm}$ are written down explicitly in Appendix I.

IV. MATRIX ELEMENTS

We will now calculate the matrix elements $(JM|\mathcal{H}|JM)$, where the Hamiltonian is given by Eq. (2). In terms of the ground-state wave function (1) the energy eigenvalue $\mathcal{H}_{hfs}'$ is

$$\mathcal{H}_{hfs}'=((1-\alpha^2)^{\frac{1}{2}}\psi(3s^23d^5)+\alpha\psi(3s3d^54s)|\mathcal{H}| \times(1-\alpha^2)^{\frac{1}{2}}\psi(3s^23d^5)+\alpha\psi(3s3d^54s)),$$

or

$$\mathcal{H}_{hfs}'=2\alpha^2\gamma\mu_N\mu(m|I_z|m) \times([^6S\,0\,M]|S_z(3\cos^2\theta-1)r^{-3}|[^6S\,0\,M]). \quad (4)$$

Since we are dealing with an S state, the eigenfunctions in the M_LM_S and MJ representations are equivalent. M and m denote the electronic and nuclear magnetic quantum numbers, respectively.

The radial, spin, and orbital parts of the Hamiltonian operator will be treated separately.

(a) Recalling that the interaction between the magnetic field due to the electron cloud and the nuclear moment takes place at the nucleus, and that the $3s$ and $4s$ unpaired electrons are the cause of the hyperfine splitting, we can write

$$\begin{aligned}&([^6S\,0\,M]|S_z(3\cos^2\theta-1)r^{-3}|[^6S\,0\,M])\\&=([^6S\,0\,M]|S_z(3\cos^2\theta-1)|[^6S\,0\,M])\\&\quad\times(R_{3s}(1)R_{4s}(2)-R_{3s}(2)R_{4s}(1)|r_1^{-3}+r_2^{-3}|\\&\quad\times R_{3s}(1)R_{4s}(2)-R_{3s}(2)R_{4s}(1))\\&=A(\theta,\varphi)\Re(r),\end{aligned} \quad (5)$$

where $A(\theta,\varphi)$ is the angular part of the integral, $\Re(r)$ is the radial part of the integral, and 1 and 2 represent the coordinate positions $(r_1\theta_1\varphi_1)$ and $(r_2\theta_2\varphi_2)$, respectively.

It turns out[5] that

$$\Re(r)=2[R_{3s}^2(0)+R_{4s}^2(0)]. \quad (6)$$

From Eqs. (5) and (6) we have

$$\mathcal{H}_{hfs}'=4\alpha^2\gamma\mu_N\mu(R_{3s}^2(0)+R_{4s}^2(0)) \times([^6S\,0\,M]|S_z(3\cos^2\theta-1)|[^6S\,0\,M])m. \quad (7)$$

(b) Operation with $S_z=s_{z1}+s_{z2}+\cdots+s_{z7}$, on the wave function $[^6S\,0\,M]$ gives

$$\mathcal{H}_{hfs}'=4\alpha^2\gamma\mu_N\mu(R_{3s}^2(0)+R_{4s}^2(0)) \times([^6S\,0\,M]|(3\cos^2\theta-1)|[^6S\,0\,M])Mm. \quad (8)$$

(c) Operation with $(3\cos^2\theta-1)$.

Since the ground state of Mn^{++} corresponds to the state $J=S$, we can write in the jj scheme:[6]

$$(3\cos^2\theta-1)=\frac{3}{S(S+1)}[j_1(j_1+1)\cos^2\theta_1+\cdots +j_7(j_7+1)\cos^2\theta_7-\tfrac{1}{3}S(S+1)], \quad (9)$$

plus terms whose matrix elements vanish.

It is shown in Appendix II that the average value of $\langle j(j+1)\cos^2\theta\rangle(m,m)$ is

$$\langle j(j+1)\cos^2\theta\rangle_{As}(m,m) =\frac{[2(l+m_l)(l-m_l)+(2l-1)][4l(l+1)+3]}{4(2l+3)(2l-1)}. \quad (10)$$

The values in Table I were calculated by means of Eq. (10).

TABLE I. Matrix elements of $j(j+1)\cos^2\theta$.

l	m_l	$\langle j(j+1)\cos^2\theta\rangle_{As}(m,m)$
2	±2	27/28
2	±1	81/28
2	0	99/28
0	0	7/28

If we write the total Hamiltonian as

$$\mathcal{H}=\mathcal{H}_{hfs}+\mathcal{H}_Z,$$

where $\mathcal{H}_Z$ denotes the Zeeman energy term, and calculate $\mathcal{H}_{hfs}'$ by means of Eqs. (8), (9), and (10), then the energy eigenvalues are

$$\mathcal{H}_{\frac{5}{2},m}'=(24936/1715)\alpha^2\gamma\mu_N\mu[R_{3s}^2(0)+R_{4s}^2(0)]m +(5/2)g\mu H, \quad (11a)$$

$$\mathcal{H}_{\frac{3}{2}m}'=\tfrac{3}{5}\mathcal{H}_{\frac{5}{2}m}', \quad (11b)$$

$$\mathcal{H}_{\frac{1}{2}m}'=\tfrac{1}{5}\mathcal{H}_{\frac{5}{2}m}'. \quad (11c)$$

The selection rules for paramagnetic resonance absorption are $\Delta M=-1$, $\Delta m=0$. Therefore, the transition energy is

$$\begin{aligned}(\hbar\omega)_m&=\mathcal{H}_{M,m}'-\mathcal{H}_{M-1,m}'\\&=5.814\alpha^2\gamma_{\mu N}\mu[R_{3s}^2(0)+R_{4s}^2(0)]m+g\mu H.\end{aligned} \quad (12)$$

The hyperfine splitting constant is equal to

$$\begin{aligned}A&=[(\hbar\omega)_m-(\hbar\omega)_{m-1}]/g\mu\\&=2.907\alpha^2\gamma\mu_N[R_{3s}^2(0)+R_{4s}^2(0)]\text{ gauss.}\end{aligned}$$

V. NUMERICAL CALCULATIONS

The value of α can now be computed from the values of A obtained by Hershberger and Leifer.[1]

The radial functions were taken to be the Hartree functions for $Cr^{++}(Z=24)$,[7] assuming that their values are not far removed from those of $Mn^{++}(Z=25)$.

[5] E. Fermi, Z. Physik **60**, 320 (1930).

[6] For a discussion of the validity of a jj coupling approximation see reference 3, Chapter 13, 5.

[7] R. L. Mooney, Phys. Rev. **55**, 557 (1939).

Using the values $a=5.28\times10^{-9}$ cm, $\gamma=3.47$, $\mu_N=5.05\times10^{-24}$ erg gauss^{-1}, and $A=76.2$ gauss, we obtain $\alpha^2=4.409\times10^{-4}$.

VI. CONCLUSIONS

Owing to the inaccuracy with which the radial function R_{nl} was estimated, the numerical calculation given here merely gives an order of magnitude for α.

The laboratory is now making use of the proton resonance method for measuring magnetic fields. A program of evaluating R_{nl} for many-electron atoms is now under way at the Massachusetts Institute of Technology.[8] If the radial wave function for Mn^{++} becomes available, then in conjunction with the more accurate field measurement, a much more accurate estimation of α can be made.

Assuming that the theory of the mixture of states is the reason for the large nuclear hyperfine splitting of Mn^{++}, ground-state wave function for Mn^{++} is approximately given by

$$\Psi=0.999\psi(3s3d^5)+0.021\psi(3s3d^54s).$$

The author wishes to thank Professor W. D. Hershberger, Professor D. Saxon, Professor R. J. Finkelstein, and Mr. M. Melkanoff for many helpful discussions.

APPENDIX I. EIGENFUNCTIONS

$$({}^6S\,0\,\pm5/2)=2^{-\frac{1}{2}}[(0^+0^-)-(0^-0^+)](2^\pm-2^\pm\,1^\pm-1^\pm\,0^\pm),$$

$$({}^6S\,0\,\pm3/2)=10^{-\frac{1}{2}}[(0^+0^-)-(0^-0^+)]\sum_{i=1}^{5}x_i{}^\pm,$$

$$({}^6S\,0\,\pm1/2)=20^{-\frac{1}{2}}[(0^+0^-)-(0^-0^+)]\sum_{i=1}^{10}y_i{}^\mp.$$

$$x_1{}^\pm=(2^\mp-2^\pm\,1^\pm-1^\pm\,0^\pm)\qquad y_4{}^\pm=(2^\mp-2^\pm\,1^\pm-1^\pm\,0^\mp)$$
$$x_2{}^\pm=(2^\pm-2^\mp\,1^\pm-1^\pm\,0^\pm)\qquad y_5{}^\pm=(2^\pm-2^\mp\,1^\mp-1^\pm\,0^\pm)$$
$$x_3{}^\pm=(2^\pm-2^\pm\,1^\mp-1^\pm\,0^\pm)\qquad y_6{}^\pm=(2^\pm-2^\mp\,1^\pm-1^\mp\,0^\pm)$$
$$x_4{}^\pm=(2^\pm-2^\pm\,1^\pm-1^\mp\,0^\pm)\qquad y_7{}^\pm=(2^\pm-2^\mp\,1^\pm-1^\pm\,0^\mp)$$
$$x_5{}^\pm=(2^\pm-2^\pm\,1^\pm-1^\pm\,0^\mp)\qquad y_8{}^\pm=(2^\pm-2^\pm\,1^\mp-1^\mp\,0^\pm)$$
$$y_1{}^\pm=(2^\mp-2^\mp\,1^\pm-1^\pm\,0^\pm)\qquad y_9{}^\pm=(2^\pm-2^\pm\,1^\mp-1^\pm\,0^\mp)$$
$$y_2{}^\pm=(2^\mp-2^\pm\,1^\mp-1^\pm\,0^\pm)\qquad y_{10}{}^\pm=(2^\pm-2^\pm\,1^\pm-1^\mp\,0^\mp)$$
$$y_3{}^\pm=(2^\mp-2^\pm\,1^\pm-1^\mp\,0^\pm)$$

[8] A. J. Freeman, Quarterly Progress Report No. 6, Solid State and Molecular Theory Group MIT.

APPENDIX II. MATRIX ELEMENTS OF $\cos^2\theta$

$$(jm|\cos^2\theta|jm)$$
$$=\{\sum_{m_l,\,m_s}(jm|m_lm_s)(m_lm_s|\cos^2\theta|m_lm_s)$$
$$\times(m_lm_s|jm)\}\delta(m,m_l+m_s)$$
$$=(jm|m_l+\tfrac{1}{2})(m_l+\tfrac{1}{2}|\cos^2\theta|m_l+\tfrac{1}{2})(m_l+\tfrac{1}{2}|jm)$$
$$+(jm|m_l-\tfrac{1}{2})(m_l-\tfrac{1}{2}|\cos^2\theta|m_l-\tfrac{1}{2})(m_l-\tfrac{1}{2}|jm). \quad (1)$$

$$(m_lm_s|\cos^2\theta|m_lm_s)$$
$$=\int_{-1}^{+1}\bar{P}_l{}^m(\cos\theta)\cos^2\theta\bar{P}_l{}^m(\cos\theta)d(\cos\theta)$$
$$=[2(l^2-m_l^2)+(2l-1)]/(2l+3)(2l-1), \quad (2)$$

where $\bar{P}_l{}^m(x)$ is the normalized associated Legendre function. $(jm|m_lm_s)$ is the Wigner coefficient and has the values

$$\begin{array}{c|cc} j\backslash m_s & +\frac{1}{2} & -\frac{1}{2} \\ \hline l+\frac{1}{2} & \left[\dfrac{l+m_l+1}{2l+1}\right]^{\frac{1}{2}} & \left[\dfrac{l-m_l+1}{2l+1}\right]^{\frac{1}{2}} \\ l-\frac{1}{2} & -\left[\dfrac{l-m_l}{2l+1}\right]^{\frac{1}{2}} & \left[\dfrac{l+m_l}{2l+1}\right]^{\frac{1}{2}} \end{array} \quad (3)$$

Since we do not know whether $j=l+\frac{1}{2}$ or $j=l-\frac{1}{2}$, we shall assume that both cases are equally probable. The matrix element is therefore averaged over both states of the electron.

From Eqs. (1), (2), and (3) we have

$$\langle j(j+1)\cos^2\theta\rangle_{lm}$$
$$=\frac{[2(l+m_l)(l-m_l)+(2l-1)][4l(l+1)+3]}{4(2l+3)(2l-1)}. \quad (4)$$

Continuous Gamma-Radiation Accompanying Internal Conversion in Ba^{137m}

HARRY B. BROWN AND ROBERT STUMP
Department of Physics and Astronomy, University of Kansas, Lawrence, Kansas
(Received March 9, 1953)

A weak continuous gamma-radiation accompanying internal conversion has been observed from the decay of the isomeric state of Ba^{137}. The probability of this emission is $(1.17\pm0.27)\times10^{-3}$ photons in the energy range 50 to 100 kev per conversion electron, and $(3.4\pm0.8)\times10^{-3}$ photons in the energy range 50 to 200 kev per conversion electron. The angular distribution of the continuous radiation in the energy range 50 to 200 kev has been measured at angles from 90° to 160° with the electron direction. There appears to be no deviation from isotropy.

I. INTRODUCTION

WHEN a nucleus decays by the emission of a high energy electron, it is to be expected that there will also be a weak continuum of γ-rays. This continuum is explained classically as the radiation arising from the large acceleration of the electron as it receives energy from the nucleus. Wang Chang and Falkoff[1] have shown that the radiation accompanying β-decay calculated by a second-order perturbation calculation does not differ markedly from the semiclassical result. Experimental measurements of both the radiation probability and the angular distribution of the γ-radiation accompanying β-decay are in good agreement with the theory.[2,3]

The continuous γ-radiation accompanying internal conversion is, on the basis of the semiclassical theory, identical with that accompanying β-decay. It is of some importance to determine how closely the effect agrees with the theory, if for no other reason than that it is necessary to take the continuous radiation into account when measuring internal conversion coefficients. This experiment was performed to determine the amount of continuous radiation, as well as its angular distribution, in the case of the conversion electrons from the isomeric state of Ba^{137}.

II. EXPERIMENTAL DETAILS

Cs^{137}, obtained from Oak Ridge National Laboratory, was used as a source of conversion electrons. The most probable contamination of this source is Cs^{134}.[4] The decay schemes of these isotopes are shown in Fig. 1.[5]

The transition from the isomeric state of Ba^{137} is about 10 percent internally converted. Thus the source produces a very considerable background of γ-rays, x-rays, and continuous γ-rays accompanying the β-decay. In the presence of this background, the continuous radiation accompanying the internal conversion was identified by means of a coincidence experiment. The conversion electrons are in coincidence only with x-rays and with the continuous radiation.

Scintillation counters with RCA 5819 photomultiplier tubes were used to detect both γ-rays and electrons. The crystal for the electron counter was of anthracene, $\frac{1}{16}$-in. thick, $\frac{1}{2}$-in. in diameter. The γ-ray counter used a $\frac{1}{8}$-in. thick, 1-in. diameter thallium activated sodium iodide crystal. The sodium iodide crystal was shielded from electrons by a $\frac{3}{16}$-in. Lucite cover.

The pulses from the counters were amplified and sorted by means of single-channel pulse-height selectors. Those pulses which were accepted by the pulse-height selectors went to a coincidence circuit. The number of counts from each pulse-height selector and from the coincidence circuit were recorded.

III. RESULTS

In a preliminary experiment to establish the existence of continuous radiation accompanying internal conversion, the two counters were placed about $\frac{1}{4}$ in. apart with the source on a Nylon film between them. The β-counter was set to count only electrons of energy greater than 530 kev and the γ-counter to count only quanta of energy above 50 kev. The range of energy of the continuous radiation which could be observed was then roughly from 50 to 100 kev. The lower limit was set by the γ-counter, the upper by the fact that the β-counter would not observe electrons which had lost more than 100 kev to the continuous radiation.

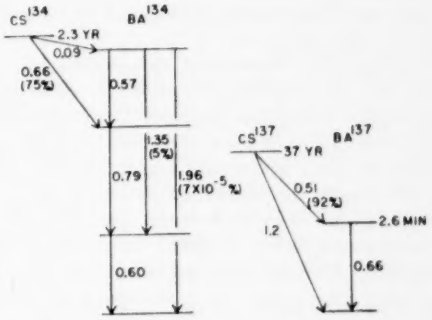

FIG. 1. Decay scheme of Cs^{137} and Cs^{134}.

[1] C. S. Wang Chang and D. L. Falkoff, Phys. Rev. **76**, 365 (1949).
[2] L. Madansky and F. Rasetti, Phys. Rev. **83**, 187 (1951).
[3] T. B. Novey, Phys. Rev. **84**, 145 (1951).
[4] F. R. Metzger, private communication.
[5] M. Goldhaber and R. D. Hill, Revs. Modern Phys. **24**, 179 (1952).

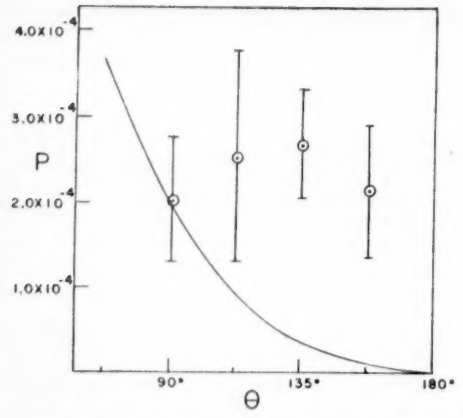

FIG. 2. Angular correlation between direction of conversion electron from Ba^{137m} and of the photon of the continuous radiation. Circled points represent experimental measurements; the solid curve is the value predicted on the basis of semiclassical theory. P: Probability of emission of a photon of the continuous radiation with energy between 50 and 200 kev into a unit solid angle. θ: Angle between the electron and photon directions.

Assuming no angular correlation between the direction of the electron and of the γ-ray, the rate of continuous radiation was found to be $(1.17\pm0.27)\times10^{-3}$ quanta in the energy range 50 to 100 kev per conversion electron. This is in fair agreement with the corresponding theoretical value from the semiclassical formula of Wang Chang and Falkoff of 2.04×10^{-3} quanta per electron.

An additional measurement of the radiation probability was made using 1 in. of lead between the two counters. With this arrangement, it was possible to lower the energy detected in the β-counter without adding spurious coincidences caused by scattering between the crystals. The angle between the two counters and the source was 135°. The β-counter was set to detect particles of energy greater than about 430 kev, and the γ-ray counter to detect those of energy greater than 50 kev. Thus continuous radiation in the range 50 to 200 kev could be detected, together with the coincident electron.

Assuming the radiation to be isotropic, the rate of radiation was found to be $(3.4\pm0.8)\times10^{-3}$ quanta in the energy range 50 to 200 kev per conversion electron. The corresponding theoretical value from the semiclassical formula is 3.24×10^{-3} quanta per electron.

The angular correlation between the direction of the electron and of the continuous radiation in the range 50 to 200 kev was measured for angles from 90° to 160°, using the energy discrimination described above and with 1-inch lead absorber between the counters. The results are shown in Fig. 2. Within the accuracy of the measurement, there is no deviation from isotropy. This is in marked disagreement with the results of the semiclassical theory. The calculated results are shown as a full curve in the figure.

IV. SOURCES OF ERROR

In addition to the coincidences between the conversion electrons and the continuous γ-radiation, there were several other sources of coincidences which could interfere with the experiment.

(1) Electron x-ray coincidences. About 75 percent of the K conversion electrons are in coincidence with x-rays of barium. Since the energy of the K x-ray of barium is about 32 kev, setting the γ-detector to count only those pulses which correspond to γ-ray energies above 50 kev effectively eliminates this source of coincidences.

(2) $\beta-\gamma$ or $\gamma-\gamma$-coincidences from source contamination. If $\beta-\gamma$-coincidences were observed due to source contamination by Cs^{134}, the coincidence rate should vary with setting of the β-counter pulse-height selector, according to the number of β-particles counted at each setting. With the β-detector set to count particles of energy 430 to 570 kev and the γ-ray counter to count only quanta of energy above 50 kev, a coincidence rate above chance of 0.077 ± 0.032 was observed. With the γ-ray detector unchanged, and the β-detector set to count particles in the range 140 to 280 kev, the coincidence rate was 0.00 ± 0.057. This is in contradiction with the fact that the number of β-particles from the 660-kev transition of Cs^{134} is about three times as great in the lower energy range as in the higher. No appreciable number of coincidences is attributable to $\beta-\gamma$-source contamination. Likewise, the possibility of $\gamma-\gamma$-coincidences is ruled out by the fact that the γ-ray efficiency of the β-detector increases at lower energy settings, whereas the coincidence rate decreases.

(3) Scattering between the crystals. If a γ-ray makes a Compton collision in the β-detector, and the γ-ray is counted by the γ-detector, a coincidence would be observed. In the preliminary experiment, this source of coincidences was eliminated by setting the β-detector to count only particles of energy above 500 kev. Since the maximum energy given an electron in a Compton collision by a 661-kev γ-ray is 475 kev, no spurious coincidences should occur. In all later experiments, this source of coincidences was eliminated by placing at least 1 in. of lead between the counters.

(4) β-continuous γ-ray coincidences. The high energy β-transition of Cs^{137} contributes a weak source of continuous γ-radiation in coincidence with the high energy β-particles. Calculations of the coincidence rate were made and all coincidence counts were corrected for this effect. Coincidences due to the low energy β of Cs^{137} and its continuous γ-radiation were not observed, because of energy considerations.

As a further check on the energy of the γ-rays which contributed to the coincidences, aluminum and lead γ-ray coincidence absorption measurements were made. The results were in agreement with the assignment of coincidences to γ-rays of energy between 50 kev and 200 kev.

V. CONCLUSIONS

There appears to be little doubt that internal conversion electrons are accompanied by a weak continuous γ-radiation. The probability of this effect is of the same order of magnitude as given by the semiclassical theory. The angular distribution of the radiation seems to be quite different from that predicted. However, there is some reason to expect that the quantum-mechanical calculation might give results in poorer agreement with the semiclassical calculation in the case of internal conversion than in the case of β-decay, where the agreement is very good. This arises from the consideration of the nature of the calculation. In the case of β-decay the second-order calculation involves a single intermediate state, i.e., the first step of the transition is the emission of an electron from the nucleus, and the second step is then the emission of a photon of the continuous radiation. On the other hand, there are two possible intermediate states involved in the calculation for internal conversion: the first step may be the emission of either an electron or of a photon; the second step then supplies, respectively, a photon or an electron.

PHYSICAL REVIEW VOLUME 90, NUMBER 6 JUNE 15, 1953

The Photodisintegration Cross Section of Beryllium at 2.185 Mev

BERNARD HAMERMESH AND CLYDE KIMBALL
Argonne National Laboratory, Lemont, Illinois
(Received March 9, 1953)

The cross section for the photodisintegration of Be^9 at 2.185 Mev has been measured using gamma-rays which follow the beta-decay of Pr^{144}. A value of 3.9×10^{-28} cm^2 was found, in reasonably good agreement with the valence neutron model. This value is lower than the values at 1.81 Mev and 2.50 Mev, in agreement with the theoretical prediction that a minimum value of the cross section should be found near 2.2 Mev.

THE cross section for the photodisintegration of Be^9 has been measured at several energies.[1,2] The cross section increases from zero at the threshold (1.66 Mev) to a value of 10×10^{-28} cm^2 at 1.70 Mev (Sb^{124}). At 1.81 Mev (Mn^{56}) it has decreased to 6×10^{-28} cm^2. At 2.50 Mev (La^{140}) its value is 5×10^{-28} cm^2, while at 2.76 Mev (Na^{24}) it has increased one again to 7×10^{-28} cm^2. These results are shown in Fig. 1. It is clear that there is a minimum value of the cross section in the region between 1.81 and 2.50 Mev. The first maximum in the cross section can be ascribed to S neutrons whereas the second increase in the cross section is caused by the emission of higher angular momentum (D) neutrons. Measurements of the angular distribution of the neutrons[3] indicate that the distribution is spherically symmetric near the first peak and is of the form $a+b\sin^2\theta$ near the region of the second increase in cross section.

Guth and Mullin[4] have calculated the cross section and angular distribution as a function of gamma-ray energy using a valence neutron model. The Be^9 nucleus is pictured as consisting of a neutron moving in the field of a Be^8 core. Although Be^8 is unstable against decay into two alpha-particles by about 120 kev, the lifetime is very long compared to the time required to emit a neutron from Be^9. The cross section is calculated for $P\rightarrow S$ and $P\rightarrow D$ transitions. The former is the major contributor to the cross section near threshold whereas the latter interaction is more important at higher energies, i.e., near the second maximum. Guth's curve is shown in Fig. 1.

The cross-section data and angular distributions agree with the theoretical predictions made with the valence neutron model. However, no data have been available to check the theory in the region of the minimum. There is a scarcity of gamma-ray emitters with useful half-lives having energies near 2.2 Mev. When the presence of a line near this energy[5] was reported in the fission product chain $Ce^{144}-Pr^{144}$, a study of the $Be(\gamma,n)$ cross section was undertaken using these isotopes.

METHOD

Approximately one curie of 282-day[6] Ce^{144} was obatined from Oak Ridge as a sulfate in solution; it was treated with $6M$ NH_4OH and precipitated as $Ce(OH)_4$. The precipitate was ignited to CeO_2, which was canned in a 0.030-inch-wall stainless steel cylinder, one centimeter in diameter and one centimeter in height. The capsule was placed in a cavity in a beryllium sphere. The sphere had an outer diameter of 1.5 inches and was made in two sections and was assembled by screwing

[1] Russell, Sachs, Wattenberg, and Fields, Phys. Rev. **73**, 545 (1948).
[2] A. Wattenberg, *Photoneutron Sources, Preliminary Report No. 6*, Nuclear Science Series, Division of Mathematics and Physical Sciences, National Research Council (unpublished).
[3] Hamermesh, Hamermesh, and Wattenberg, Phys. Rev. **76**, 611 (1949).
[4] E. Guth and C. J. Mullin, Phys. Rev. **76**, 234 (1949).
[5] M. Goldhaber and E. der Mateosian, Brookhaven National Laboratory Report No. 51, (S-5), 1950 (unpublished).
[6] R. P. Schuman and A. Camilli, Phys. Rev. **84**, 158 (1951).

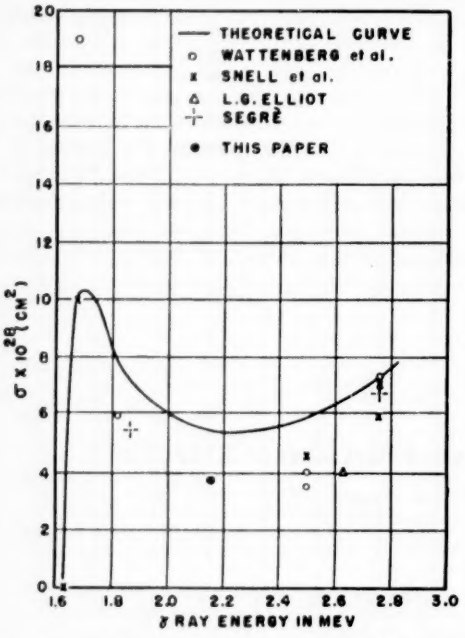

FIG. 1. The photodisintegration cross section of Be^9 [from E. Guth and C. J. Mullin, Phys. Rev. **76**, 234 (1949), and including result found in present experiment].

the two threaded pieces together. The neutron measurements were made one year after the preparation of the sample.

The detector was an enriched BF_3 pulse-ion chamber imbedded in a paraffin cylinder 20 centimeters in diameter. The response of the detector to neutrons was relatively independent of energy. The Ce–Be neutron yield was determined by comparison with a Ra–Be source of identical geometry whose strength was found by comparison with Argonne source No. 38 in the Argonne uranium-graphite pile by the method described by Hughes.[7]

The decay schemes of Ce^{144} and Pr^{144} have recently been studied.[8,9] Figure 2 shows Alburger's decay scheme. The major difference between this and Porter and Cook's result is in the intensity of the beta-branch leading to the 2.185-Mev level. Porter and Cook indicate that the branching ratio is the order of one percent.[10] The strength of the 2.185-Mev line could be determined by comparison with a source of known strength having a gamma-ray of nearly the same energy. Because of the difficulty mentioned previously in finding useful gamma-rays in this energy region, the comparison was made between the 1.48-Mev line from Nd^{144} and the 1.38-Mev line from Na^{24}. A NaI(Tl) crystal and a 5819 phototube were used in conjunction with a very stable twenty-channel pulse-height analyzer in order to make the comparison. Assuming that the efficiencies of detection by the crystal were identical for the 1.38 and 1.48-Mev lines and using the relative intensities of the 1.48 to 2.185-Mev lines as given in reference 8, the strength of the 2.185 lines was determined. The standard sodium source used for the comparison was prepared by irradiating a small sample of NaF in a known flux in the Argonne heavy water—moderated reactor; the size of sample and the duration of irradiation were chosen so that the activity of the 1.38-Mev line of the Na^{24} was approximately the same as that of the 1.48-Mev line in Nd^{144}. The value of the sodium cross section used was 0.505 barn.[11] The energy region around 1.5 Mev was scanned with the twenty-channel pulse-height discriminator. The data were plotted and a planimeter was used to compare the areas under the respective curves, which areas gave the relative intensities of the 1.38 to 1.48-Mev lines.

RESULTS AND CONCLUSIONS

The strength of the Ra–Be source was 1.38×10^6 neutrons/second. Relative to this the Ce–Be source gave a neutron yield of 4.3×10^3 neutrons/second. Using 2.185-Mev γ-rays (see Fig. 2 and reference 8), the strength of the 2.185-Mev line was 6.0×10^7 disintegrations/second.

The following formula (1) for the neutron yield was obtained by assuming that the cylinder in which the cerium was contained could be replaced by a sphere of the same volume located at the center of the beryllium and also assuming radial symmetry in the γ-ray emission:

$$\text{neutrons/second} = \sigma\rho q(0.6/\text{M.W.})(R-R'), \quad (1)$$

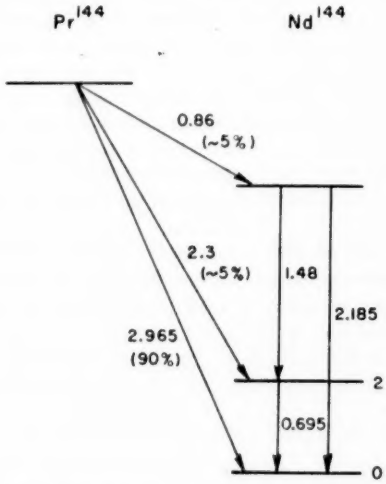

FIG. 2. The decay scheme of Pr^{144} according to D. Alburger and J. Kraushaar, Phys. Rev. **87**, 448 (1952).

[7] D. J. Hughes, Nucleonics **6**, No. 6, 50 (1950).
[8] D. E. Alburger and J. J. Kraushaar, Phys. Rev. **87**, 448 (1952).
[9] F. T. Porter and C. S. Cook, Phys. Rev. **87**, 464 (1952).
[10] Private communication with C. S. Cook indicates that their result is not less than 0.6 percent for this ratio.
[11] D. Rose (unpublished).

where σ is the photoneutron cross section in barns; ρ is the density of beryllium; q is the strength of the 2.185-Mev line; R is the outer diameter of the beryllium sphere; R' is the diameter of the equivalent spherical cavity in the beryllium; and M.W. is the molecular weight of beryllium.

Substituting the experimental data into the above formula, we found $\sigma=4.1\times10^{-28}$ cm^2.

This result requires one important correction, since some photoneutrons arise from the bremsstrahlung from the 2.96-Mev β-rays. A calculation was made to determine the relative importance of this yield of neutrons compared to the yield of neutrons from the 2.185-Mev γ-ray. This depends on the relative intensities of the 0.86-Mev β-rays to the 2.96-Mev β-rays. Assuming that the branching ratios of the 0.86 and the 2.3-Mev β-branches are equal and neglecting the bremsstrahlung photoneutron yield from the 2.3-Mev β-rays compared to the 2.96-Mev β-rays, Eq. (1) is corrected to

$$\frac{\text{neutrons}}{\text{second}}=\rho q\frac{0.6}{\text{M.W.}}(R-R')\times\left[\sigma+22\times10^{-8}\times\frac{1.5}{1.1}\times\frac{1-2B}{B}\right], \quad (2)$$

TABLE I. Change in σ caused by correction for bremsstrahlung yield of photoneutrons.

B (percent)	0.6	1	2	3	4	5
$\Delta\sigma(10^{-28}$ cm$^2)$	−0.5	−0.29	−0.14	−0.09	−0.07	−0.05

where σ is in barns and B is the above-mentioned branching ratio. The correction decreases the value of σ. Table I gives the calculated change in cross section as a function of B.

Table I shows that if we use Alburger's decay scheme, there is a negligible correction to the cross section. On the other hand, if we use Porter and Cook's value for B of about one percent, then the cross section would be 3.8×10^{-28} cm^2.

Comparing these values with Fig. 1, it can be seen that there is a minimum value of the cross section in the region of 2.185 Mev. Furthermore, the experimental value of about 3.9×10^{-28} cm$^2\pm15$ percent is in reasonably good agreement with the predictions of the valence neutron model.

It gives us great pleasure to thank Dr. M. Hamermesh for the calculation of the bremsstrahlung yield of photoneutrons.

PHYSICAL REVIEW VOLUME 90, NUMBER 6 JUNE 15, 1953

Fourth-Order Corrections to the Scattering of Pions by Nonrelativistic Nucleons*

J. S. BLAIR† AND G. F. CHEW
Department of Physics, University of Illinois, Urbana, Illinois

(Received March 9, 1953)

Fourth-order corrections to the field theoretical phase shifts for pion nucleon scattering have been calculated for a linear and extended coupling and no nucleon recoil. The results support the use of the "Dancoff approximation," since those processes passing through intermediate states which contain three pions turn out to be much less important than processes involving only one and two pions.

I. INTRODUCTION

A BROAD program of theoretical calculations is being carried out at the University of Illinois to see to what extent the experimental information on the pion-nucleon interaction at energies less than 1 Bev can be correlated on the basis of a Yukawa theory in which nucleon recoil is relatively unimportant. The qualitative arguments for the supposition that at these low energies the nucleon may be approximately regarded as a fixed "source" have been summarized by Blair and Chew.[1] These same arguments also lead to the conclusion that the pion-nucleon interaction is linear in the pion field and not very strong and that, therefore, an essentially weak-coupling calculational technique is in order. The purpose of this paper then is to present the results of a calculation, up to the fourth order in the coupling constant, of the pion-nucleon scattering phase shifts, when the nucleon is regarded as infinitely heavy. Our conclusions here form the basis for the more satisfactory method of calculation reported by Chew.[2] The notation of reference 2 will be used throughout.

II. PROCEDURE

With the neglect of nucleon recoil, pions interact with nucleons only in P states.[1] With charge inde-

* This research was supported by the U. S. Office of Naval Research.

† Now at the Department of Physics, University of Washington, Seattle, Washington.

[1] J. S. Blair and G. F. Chew, *Annual Review of Nuclear Science* (Annual Reviews, Inc., Stanford, 1952), Vol. II, p. 163 (1952).

[2] G. F. Chew, Phys. Rev. **89**, 591 (1953).

pendence, the cross sections for scattering can then be expressed in terms of four phase shifts, denoted α_{33}, α_{31}, α_{13}, and α_{11}, where the first index corresponds to isotopic spin $\frac{3}{2}$ or $\frac{1}{2}$, and the second index refers to $P_{\frac{3}{2}}$ or $P_{\frac{1}{2}}$ states, respectively.

It is convenient to evaluate the reaction (or reactance) matrix element,[3] K_{f0}, between plane wave states, and then relate K_{f0} to the phase shifts. The reaction matrix may be separated into spin-flip and nonspin-flip contributions, so that, for example, the reaction matrix for the scattering of positive pions by protons is written

$$K_{f0}(\pi^+p)=B(\pi^+p)\cos\theta+A(\pi^+p)i\boldsymbol{\sigma}\cdot\mathbf{n}\sin\theta, \quad (1)$$

where θ is the angle between $\mathbf{k}_0$ and $\mathbf{k}_f$, the incident and final pion momenta, and $\mathbf{n}$ is the unit vector in the direction $\mathbf{k}_f\times\mathbf{k}_0$. Similarly, we will write the reaction matrix for the elastic scattering of negative pions by protons as

$$K_{f0}(\pi^-p)_{el}=B(\pi^-p)_{el}\cos\theta+A(\pi^-p)_{el}i\boldsymbol{\sigma}\cdot\mathbf{n}\sin\theta.$$

It is then easily verified that

$$K_{33}=\tfrac{1}{3}[B(\pi^+p)-A(\pi^+p)], \quad (2a)$$

$$K_{31}=\tfrac{1}{3}[B(\pi^+p)+2A(\pi^+p)], \quad (2b)$$

$$K_{13}=\tfrac{1}{2}[B(\pi^-p)_{el}-A(\pi^-p)_{el}]-\tfrac{1}{2}K_{33}, \quad (2c)$$

$$K_{11}=\tfrac{1}{2}[B(\pi^-p)_{el}+2A(\pi^-p)_{el}]-\tfrac{1}{2}K_{31}. \quad (2d)$$

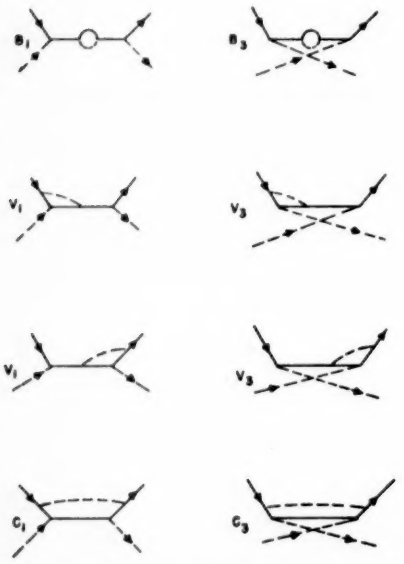

FIG. 1. Feynman diagrams for the fourth-order matrix elements in pion-nucleon scattering. The nucleon lines are solid and the pion lines dashed.

[3] Following B. A. Lippmann and J. Schwinger, Phys. Rev. **79**, 469 (1950), we mean by the reaction operator K a matrix which obeys equations identical in form to those obeyed by the transition matrix T, except that principal values are to be taken whenever poles are encountered.

The phase shifts are to be obtained from Eqs. (2) by the relation, $\tan\alpha_{ij}=-(k_0\omega_0/2\pi)K_{ij}$.

The fourth-order perturbation theory contribution to the reaction matrix is given by[4]

$$K_{f0}^{(4)}=\sum_{l,m,n\neq 0,f}\frac{H_{fn}H_{nm}H_{ml}H_{l0}}{(E_0-E_n)(E_0-E_m)(E_0-E_l)}$$
$$-\tfrac{1}{2}\sum_{l,m}\frac{H_{fm}H_{m0}}{(E_0-E_m)}\left\{\frac{H_{0l}H_{l0}}{(E_0-E_l)^2}+\frac{H_{fl}H_{lf}}{(E_f-E_l)^2}\right\}$$
$$-\tfrac{1}{2}\sum_{l,m}\frac{H_{fm}H_{m0}}{(E_0-E_m)^2}\left\{\frac{H_{0l}H_{l0}}{E_0-E_l}+\frac{H_{fl}H_{lf}}{E_f-E_l}\right\}, \quad (3)$$

where one is to take principal parts of any integrals over intermediate momenta. It is apparent that the second bracket is a part of the nucleon self-energy; this term compensates for a self-energy buried in the expression on the first line. The first bracket is part of the factor renormalizing f^2:

The interaction Hamiltonian density is taken to be[5]

$$H(\mathbf{x})=(4\pi)^{\frac{1}{2}}(f/\mu)\sum_{i=1}^{3}\rho(x)\boldsymbol{\sigma}\cdot\boldsymbol{\nabla}\tau_i\varphi_i(\mathbf{x}), \quad (4)$$

where the symbols are conventional. The Fourier transform of the source density $\rho(x)$ will be denoted by $v(k)$, which is normalized to unity at $k=0$. There are eight possible diagrams describing the ordering of transitions and these are sketched in Fig. 1.[6] The evaluation of the matrix elements is straightforward.

III. RESULTS

The resulting phase shifts through fourth order may be written as

$$\tan\alpha_{33}=2y(1-\delta+2\Delta_-+4\Delta_+), \quad (5a)$$

$$\tan\alpha_{31}=\tan\alpha_{13}=-y(1-\delta-\Delta_-+\Delta_+), \quad (5b, c)$$

$$\tan\alpha_{11}=-4y(1-\delta-4\Delta_--2\Delta_+), \quad (5d)$$

where

$$y=(2/3)(f/\mu)^2(k_0^3/\omega_0)v^2(k_0), \quad (6)$$

$$\delta=(16/3\pi)(f/\mu)^2\int^{\infty}dk(k^4/\omega^3)v^2(k), \quad (7)$$

$$\Delta_{\pm}=(2/3\pi)(f/\mu)^2\int^{\infty}dk(k^4/\omega^2)[\omega_0/(\omega\pm\omega_0)]v^2(k). \quad (8)$$

Even though all contributions are finite, it is desirable to separate out those terms which merely renormalize

[4] See, for example, E. Corinaldesi and G. Field, Phil. Mag. **40**, 1159 (1949).

[5] W. Pauli, *Meson Theory of Nuclear Forces* (Interscience Publishers, Inc., New York, 1946), p. 12.

[6] Our notation here follows Ashkin, Simon, and Marshak, Progr. Theoret. Phys. **5**, 684 (1950), who have considered fourth-order scattering in the relativistic theory.

the second-order calculation. Thus, the recurring quantity $(1-\delta)$ should be interpreted as a factor renormalizing f^2. It may be noted that $(9/16)\delta$ is simply the weak coupling probability for a one pion configuration in the self-field of a single physical nucleon.

The above results can be compared with those resulting from the "Dancoff approximation:"[2]

$$\tan\alpha_{33}=2y(1-2\Delta_-)^{-1}, \tag{9a}$$

$$\tan\alpha_{31}=\tan\alpha_{13}=-y(1+\Delta_-)^{-1}, \tag{9b, c}$$

$$\tan\alpha_{11}=-4y(1+4\Delta_-)^{-1}. \tag{9d}$$

It is readily seen that the expansion of Eqs. (9) to fourth order in f^2 is equivalent to Eqs. (5) except for the contributions of Δ_+. The terms in Δ_- arise only from diagrams in which the number of pions in the second intermediate state is one (i.e., the diagrams of Fig. 1 with subscript 1); those in Δ_+ appear when this number is three (i.e., diagrams with subscript 3). A measure of the validity of the "Dancoff approximation" then is the relative magnitude of Δ_- and Δ_+. It is qualitatively expected that Δ_- should outweigh Δ_+ because of the possible smallness of the denominator in Δ_-.

The term Δ_-/f^2 is shown as the solid curve in Fig. 2, as a function of ω_0/μ for the case of a "square" momentum distribution $v(k)$, with several choices of ω_{max}.[2] Δ_+/f^2 is similarly plotted in Fig. 2 and in the range shown is seen to be substantially smaller than Δ_-/f^2. On the other hand, if the cut-off energy is made very large compared to ω_0 (i.e., the source radius is made very small compared to the pion wavelength) it is seen by inspection of formula (8) that $\Delta_+\to\Delta_-$ and the Dancoff approximation loses its validity. Fortunately, it appears that the experimental data, up to now at least, can be fitted with a relatively low cut-off. Using the values of $f^2=0.2$ and $\omega_{max}=3.2\mu$, deduced in reference 2, it is seen that the Δ_+ contributions to formulas (5) are generally less than 20 percent in the low energy region, while at the same time the contributions from Δ_- are large. (It is perhaps worth noting that in the important phase shifts, α_{33} and α_{11}, the effect of Δ_+ reinforces that of Δ_-; so even if the cutoff were too large to allow the neglect of Δ_+, the fourth-order contributions would still be in the right direction to fit experiment.)

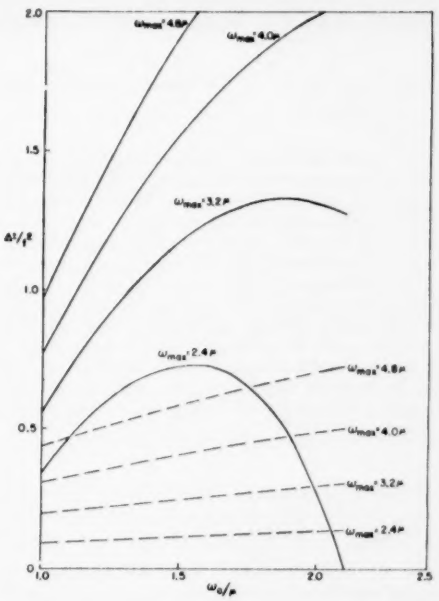

FIG. 2. The quantities, $\Delta_\pm$, given by Eq. (8), as functions of ω_0 for various choices of ω_{max}. The solid curves represent Δ_-/f^2 and the dashed curves Δ_+/f^2.

In conclusion, we believe that our results here support the validity of the Dancoff approximation, *provided that intermediate virtual pions at very high energy do not play a dominant role in the scattering.* This is another way of saying that as a source of pions the nucleon must effectively be extended over a region appreciably larger than its own Compton wavelength.

Properties of the Low Energy Nucleonic Component at Large Atmospheric Depths*

J. A. SIMPSON AND W. C. FAGOT
Institute for Nuclear Studies, University of Chicago, Chicago, Illinois
(Received February 13, 1953)

This is a report on the absorption properties of the cosmic radiation low energy nucleonic component measured by detectors of disintegration product neutrons as the nucleonic cascade develops deep within the atmosphere. The air absorption mean free path L of the star- or neutron-producing radiation was measured as a function of atmospheric depth x (in g-cm^{-2} atmosphere) at the geomagnetic latitudes $\lambda=0°$, 41°, 52°. $L(x,\lambda)$ was obtained for carbon or free atmosphere and for a lead plus carbon pile geometry. As reported earlier, for small x the absorption mfp, L, is dependent upon λ (L is a function of the average energy of the primary nucleons which initiate the nucleonic chain or cascade). However, it is shown by the present measurements that, for $x>600$ g-cm^{-2}, $L\rightarrow\sim140$ g-cm^{-2} *independent* of latitude λ.

The latitude dependence of neutron component intensity was measured at $x=680$ g-cm^{-2} (11 200 ft) between $\lambda=0°$ and 58°N. The latitude factor of intensity increase is 2.55. In view of the independence of $L(x)$ on λ at large atmospheric depths this latitude effect is nearly constant down to sea level ($x=1030$). It is shown that at large atmospheric depths neutron production is observed from primary protons with energies as low as ~1 Bev. The specific yield of neutrons at 11 200 ft has been computed taking into account protons, alpha-particles, and heavier primary nuclei.

These measurements resolve discrepancies reported in the literature between high altitude measurements and measurements between sea level and mountain altitudes for the low energy nucleonic component.

ALTHOUGH extensive measurements of the absorption of the star-producing radiations and fast neutrons from the nucleonic component have been obtained at both small and large atmospheric depths numerous discrepancies appear to exist among the measurements reported in the literature. For example, (a) extrapolations of the high altitude neutron or star intensity curves to sea level yield results inconsistent with the reported altitude dependence of stars in the lower atmosphere,[1,2] and (b) the pressure coefficient for a neutron or low energy star detector as derived from intensity *vs* atmospheric pressure variations yields an equivalent absorption mean free path for the incident radiation which differs from intensity-altitude measurements higher in the atmosphere.[3] In an attempt to resolve these difficulties and to extend the use of neutron detectors employed to measure nucleonic component intensity-time variations at low latitudes, we have investigated some properties of the nucleonic component as a function of atmospheric depth. We have defined the low energy nucleonic component as the secondary component which is propagated by nucleons capable of producing nuclear disintegrations and which generates a cascade or chain of nucleons and nuclear disintegrations within the atmosphere. Each nuclear disintegration predominantly yields protons, neutrons, and alpha-particles. We shall measure nucleonic component intensity by detection of the disintegration product neutrons since the neutron intensity closely represents nucleonic component intensity and is easily measured.

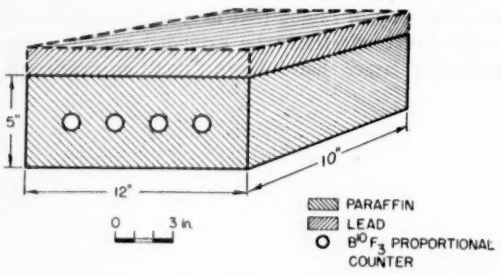

FIG. 1. Perspective view of detector. This is a pile geometry containing four $B^{10}F_3$ counters. Local production of neutrons from lead may be measured with the addition of a layer of lead as shown. This pile geometry was mounted in the nose section of an RF-80 aircraft. (See Fig. 2.)

Specifically, we shall report upon the absorption behavior of the nucleonic component in air as measured by fast disintegration neutron detectors as the nucleonic cascade or chain develops deep within the atmosphere of the earth. The study consists of measurements of the absorption mean free path L of the star-producing or neutron-producing radiation as a function of atmospheric depth x (in g-cm^{-2}) and geomagnetic latitude λ. The measurements of $L(x,\lambda)$ were obtained for local production in carbon (equivalent to free atmosphere measurements[4]) and for local neutron production in a lead-carbon pile geometry. We also report on the latitude dependence over the range $\lambda=0°-58°$ for atmospheric depths between 11 000 ft and sea level. From these data we have computed the average neutron specific yield near sea level from incident primary particles of momentum-to-charge ratio P/Z.

I. DETECTORS AND INSTRUMENTATION

All the measurements, with the exception of one series of high altitude measurements at $\lambda=52°$, were obtained with the geometry shown in Fig. 1. The geometry consisted of a paraffin block 5 in.×10 in.×12

* Assisted by the Office of Scientific Research, Air Research and Development Command, U. S. Air Force, Baltimore, Maryland.
[1] For example, M. Teucher, Z. Naturforsch. **7a**, 61 (1952).
[2] H. Yagoda, Proceedings of the Echo Lake Conference on Cosmic Rays (1949); J. G. Roederer, Z. Naturforsch. **7a**, 765 (1952).
[3] V. Tongiorgi, Phys. Rev. **76**, 517 (1949); N. Adams and H. J. J. Braddick, Z. Naturforsch. **6a**, 592 (1951).
[4] J. Simpson and R. B. Uretz, Phys. Rev. **90**, 44 (1953); J. Simpson, Phys. Rev. **83**, 1175 (1951).

in. in which four $B^{10}F_3$ proportional counters were distributed. Plates of lead 10 in.×12 in. were placed above the paraffin geometry as shown in Fig. 1 for measurements of local production in lead. For the measurements reported here the lead thickness was 59 g-cm^{-2}. Details on the behavior of pile geometries for measuring the local production of neutrons have been discussed in an earlier paper.[4] We refer to local production within the paraffin block as production in carbon.

The detector system and associated electronic and recording apparatus were located in the nose section

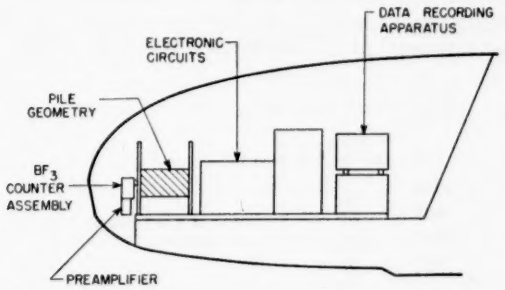

FIG. 2. Vertical view through mid-section of the RF-80 jet aircraft nose showing the location of the pile geometry (see Fig. 1) and related apparatus.

of a type RF-80 jet aircraft as shown in Fig. 2. Special aluminum ballast replaced the usual lead ballast required to balance the aircraft; there was no effect resulting from variable fuel loads.

The subminiature electronic circuits were designed specially for these measurements and will be described in detail elsewhere. By using a dual electronic and recording system the chance for component failure or loss of data was greatly reduced. All high potential circuits were maintained at sea level atmospheric pressure during all flights. Atmospheric pressure, accumulated counts, time and temperature were recorded at one minute intervals on film. An extra recorder was located in the cockpit so that the pilot could report preliminary results to a ground observer at specified intervals. The temperature in the nose section was controlled by a heated air stream from the aircraft heat-exchanger.

TABLE I. The measurements of the air absorption mean free path $L(x)$ of the neutron-producing radiations at $\lambda=41°$N.

Range of atmospheric depth, x g-cm^{-2}	Flight No.	$L(x)$ carbon	$L(x)$ lead (59 g-cm^{-2})
240–380	257		162±3
	262	175±3	
	263		166±3
	265	174±3	
580–770	256		135±3
	258		147±3
	264	144±4	

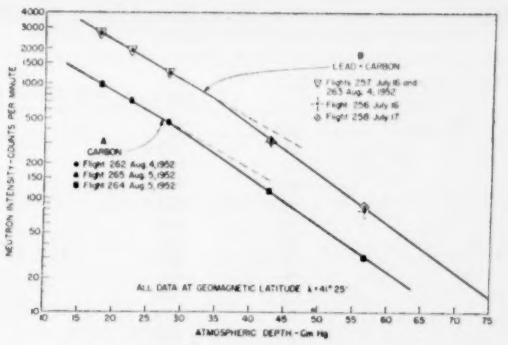

FIG. 3. The altitude dependence of the disintegration product neutron intensity at $\lambda=41°25'$ (Mobile, Alabama). From these data it is shown that the absorption mean free path L of the incident radiation is a function of atmospheric depth x. The experimental geometry for curve B is shown in Fig. 1 with lead thickness 59 g-cm^{-2}.

The pressure altimeter was modified to eliminate back lash or hysteresis effects and was calibrated to the N.A.C.A. standard atmosphere.

Before and after each flight the detector efficiency was checked with a Ra–Be neutron source. Since the counting rate of the detector at high altitude is the order of 1000–2500 events per minute, the neutron intensity at approximately 3–4 different altitudes may be obtained within the ~2-hour fuel supply of the aircraft. Hence, the data for computing L from a single flight need not be corrected for intensity—time variations. For data assembled over extended periods of time the intensity corrections are obtained from our continuously operating pile detectors.[5]

II. DEGRADATION OF NUCLEON AVERAGE ENERGY WITH INCREASING ATMOSPHERIC DEPTH

We select first the intensity measurements at geomagnetic latitude $\lambda=41°$N. The absorption of the neutron-producing radiation was computed on the assumption that over a small interval of atmospheric depth the omnidirectional intensity may be represented by $I=I_0e^{-x/L}$. The results are presented in Table I, and the data are plotted in Fig. 3 after correcting for the changes of primary intensity which occurred in July and August 1952. Curve A represents local production in carbon, air, and aircraft aluminum; curve B represents the addition of local production from lead 59 g-cm^{-2} thick. (See Fig. 1.)

At $\lambda=52°$N we report measurements of L in the range of $x=175$ to $x=750$ g-cm^{-2} atmosphere in Table II from a series of 32 flights. The average values of $L(x)$ for four ranges of x, with both the carbon and the lead geometries, are summarized in Table III.

For $\lambda=0°$ values for L have been reported[4] only for small values of x, i.e., $L=212$ g-cm^{-2} for $x\approx200$ to $x\approx500$ g-cm^{-2}. Although measurements in aircraft

[5] Simpson, Fonger, and Treiman, Phys. Rev. **90**, 934 (1953).

TABLE II. The measurements of the air absorption mean free path $L(x)$ of the neutron-producing radiations at $\lambda = 52°$N.

Range of atmospheric depth, x g-cm^{-2}	Flight No.	$L(x)$ carbon	$L(x)$ lead (59 g-cm^{-2})
175–300	60[a]	166	
	61	177	
	62	164	
	63	165	
	64	171	
	66	162	
	68	172	
	69	166	
	70	168	
	71	169	
	74	173	
	75	162	
	76	168	
	77	170	
	78	168	
	79	167	
	247		165
	248		155
	249		163
	251		158
230–530	138		148
	203	153	
	225	151	
	235		147
	266		150
	267		148
300–530	134	149	
	139	151	
	141	145	
530–750	144		136
	239		143
	240		139

[a] A cylindrical paraffin geometry was used for Flights 60–79.

were not obtained for large x at the equator, L has been determined[6] from intensity measurements of carbon and carbon-plus-lead piles at two mountain altitudes in the range of $x = 600$–700 g-cm^{-2}, with the results shown in Table IV.

We conclude from these experimental results that the absorption mean free path L for the neutron-producing radiation is a function of atmospheric depth x and that $L(x) \rightarrow 140$ g-cm^{-2} near $x = 700$ g-cm^{-2}. For example, in Fig. 3 at $\lambda = 41°$ $L(x)$ changes by 20 percent between $x \approx 300$ and $x = 600$ for the free atmosphere and $L(x)$ changes by ~ 15 percent for local production in a lead-carbon pile. This latter result is a consequence of the reported anomalous measurements of L by using the local neutron production from elements of high atomic weight at small atmospheric depth.[4]

TABLE III. Summary of the data in Table II for $\lambda = 52°$N.

Range of atmospheric depth, x g-cm^{-2}	$L(x)$ carbon	$L(x)$ lead
175–300	168±3	158±2.3
230–530	152±2	148±2
300–530	148±2	
530–750		141±2

A crude plot of $L(x)$ *vs* x with λ as a parameter is given in Fig. 4. We conclude from these results that, in first approximation, $L(x)$ *becomes independent of geomagnetic latitude at large atmospheric depths* x.

Since it is known from cyclotron experiments with nucleons in the energy range of 50–450 Mev that L decreases with decreasing nucleon energy, it is clear that the change of L with x in the atmosphere is a consequence of the development of a nucleon cascade or chain. The nucleon average energy is degraded by nucleon collisions and nuclear disintegrations as the cascade develops deep within the atmosphere. These results are consistent with and an extension of the measurements of $L(\lambda)$ at small x, which show that as

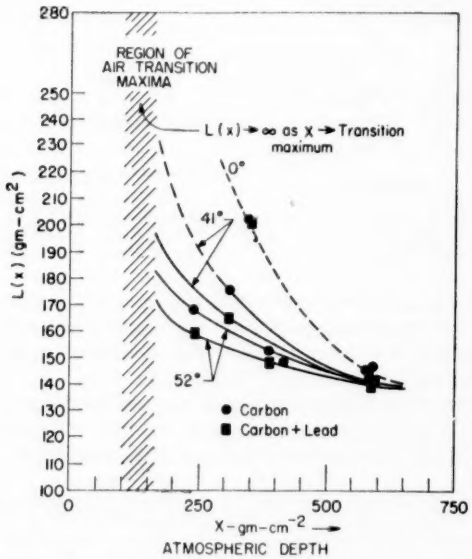

FIG. 4. The *air* absorption mean free path L as a function of atmospheric depth x at geomagnetic latitudes $\lambda = 0°$, 41°N and 52°N. The anomalous values of $L(x)$ at high altitude measured by determining local production rates in lead are shown. This phenomenon was discussed in reference 4.

the average *primary* particle nucleon energy is decreased, L decreases. We believe that any detailed theory providing for a description of the nucleonic cascade must account for this behavior of $L(x)$.

III. INTERPRETATION OF RELATED MEASUREMENTS

We may now explain the apparent anomaly between the atmospheric pressure coefficient ("barometric" coefficient) and the absorption mean free path measurements for neutron production by the nucleonic component. Several observers have reported measurements of the pressure coefficient for neutron production. All the measurements were at high latitudes and at altitudes below 14 000 ft pressure altitude. The values obtained

are in the range -0.92 to -1.1 percent/mm Hg, which leads to an absorption mean free path of $L \approx 140$ g-cm^{-2}.[3] This L is now in agreement with the free air absorption measurements in the *lower atmosphere*. Further, we conclude that within experimental errors the pressure coefficient for local neutron production in the lower atmosphere is *not* a function of λ. This result is of interest where the local neutron production is used as a monitor of intensity variations at low latitudes, but where the small tropical pressure variations have made it difficult to obtain an accurate pressure coefficient for $\lambda = 0°$.[5]

Photographic plate measurements in the lower atmosphere yield $L = 130$–145 g-cm^{-2} for the star-producing radiation. Our measurements also explain the observations of Yagoda and Roederer[2] at low altitudes, in which the altitude dependence of star production was approximately independent of λ.

The recent low altitude measurements of fast neutron production at $\lambda = 20°$ by Curtiss and Gill[6] are now clearly related to the high altitude neutron production at this latitude.

IV. LATITUDE DEPENDENCE OF NEUTRON PRODUCTION IN THE LOWER ATMOSPHERE

For $x > 600$ g-cm^{-2} we have shown that $L(x)$ is independent of λ in first approximation. We therefore report I *vs* λ measurements for $x > 600$, since this latitude effect will be essentially constant with x in the lower atmosphere. The results are given in Fig. 5 for $x = 681$ g-cm^{-2}, where measurements above 40° were obtained with the carbon plus 59 g-cm^{-2} thick lead pile in the jet aircraft. All data are corrected for variations with time and normalized to the average intensity observed October 6, 1952. The points at 0°, 29°, 42°, and 48° are obtained from the ratios of neutron production in "standard" piles[5] employed for observing intensity-time variations near 11 000 ft; these points are normalized to the pressure $x = 681$ g-cm^{-2}. These data are then fitted to the aircraft results at $\lambda = 48°$N. Since $L(x)$ is independent of λ for $x > 600$, we conclude that at $x = 681$ the neutron production increases by the factor 2.55 from the geomagnetic equator to $> 58°$ and the increase is only slightly less at *sea level* ($x = 1030$). The shape of the latitude curve, Fig. 5, for intermediate latitudes is determined by the *longitude* dependence of the neutron intensity. We therefore note that the intermediate point at 29° was determined at 99° west longitude. The only reported latitude measurement of stars in photographic emulsions near this altitude is in agreement with this neutron latitude effect.[7]

Although the exact shape of the curve in Fig. 5 has not been determined above 52°, we observe that $dI/d\lambda \to 0$ as $\lambda \to 56°$N. From this fact we estimate the *minimum* momentum-to-charge ratio of a primary particle producing secondary particles which contributes to the total neutron production at sea level. For a centered dipole geomagnetic field this value is ~ 1 Bev/c for vertically incident primary protons. This observed low momentum cutoff is either: (1) due to atmospheric absorption of the primary particles of lowest momenta and their secondaries, or (2) due to a cutoff in the primary particle spectrum. Recent evidence discussed in reference 5 favors a primary spectrum cutoff.

[6] L. F. Curtiss and P. S. Gill, Phys. Rev. **85**, 309 (1952).
[7] S. Lattimore, Phil. Mag. **41**, 961 (1950).

TABLE IV. The measurements of the air absorption mean free path $L(x)$ of the neutron-producing radiations at $\lambda = 0°$N.

Range of atmospheric depth, x g-cm^{-2}	$L(x)$ carbon or lead g-cm^{-2}
200–500	212±4
600–700	145±9

V. SPECIFIC YIELD OF NEUTRONS AT LOW ALTITUDES

The specific yield for neutrons has been defined in reference 5 as a function $S(P/Z, x)$ which gives the observed time-averaged neutron counting rate at atmospheric depth x arising from a unity flux of vertically incident primary particles of momentum-to-charge ratio P/Z. We may rewrite Eq. (2) in reference 5 in terms of particle kinetic energy per nucleon as follows:

$$I_v(\lambda, x, t) = \sum_Z \int_{E_Z(\lambda,t)}^{\infty} S_Z(E, x) j_Z(E, t) dE \qquad (1)$$

at time t, where I_v is the neutron intensity at λ, x, t arising from the vertically incident primary particles. Since for $x > 600$ gm-cm^{-2} $L(x)$ is independent of lati-

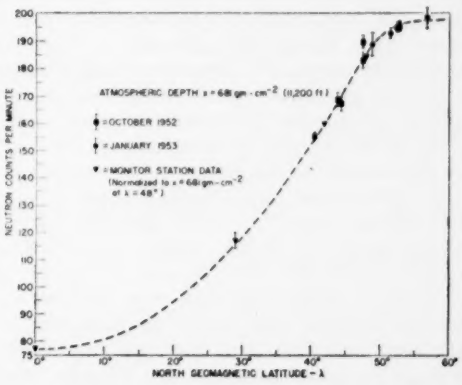
NEUTRON COUNTS PER MINUTE
ATMOSPHERIC DEPTH x = 681 gm-cm⁻² (11,200 ft)
= OCTOBER 1952
= JANUARY 1953
= MONITOR STATION DATA
(Normalized to x = 681 gm-cm⁻² at λ = 48°)
NORTH GEOMAGNETIC LATITUDE - λ

FIG. 5. Disintegration product neutron intensity (low energy nucleonic component intensity) as a function of geomagnetic latitude λ. This is the approximate curve for all greater atmospheric depths including sea level. The monitor station data are obtained from continuous recording piles described in reference 5. The shape of the curve near 20–35°N is determined by the longitude effect.

tude λ, we have from Eq. 3, reference 5, $I_v \propto I$, where I is the counting rate of the omnidirectional detector.

If we separate $S_Z(E, x)$ to form the product of two functions, one dependent on Z, the other dependent on E and x, then

$$S_Z(E, x) = k_Z S(E, x), \tag{2}$$

where $k_Z \approx A$, the atomic weight of the primary particle.[6] Accordingly,

$$I_v = (\lambda, x, t) = \sum_Z k_Z \int_{E_Z(\lambda,t)}^{\infty} S(E, x) j_Z(E, t) dE. \tag{3}$$

Fonger[8] has fitted the function $S(E, x)$ to the experimental data shown in Fig. 5 for the omnidirectional detector at 0° and above 40° for $x = 680$ g-cm^{-2}. The primary differential spectra are obtained from Kaplon *et al.*[9] The results are as follows:

$$S(E, 680) = \begin{cases} 0 & \text{for } E < E_0, \\ 9.64 \ln[(1+E)/(1+E_0)] & \text{for } E > E_0, \end{cases} \tag{4}$$

where E_0 is 0.83 Bev. The computed detector counting rate was normalized to unity at $\lambda = 0°$.

This function will generate an intensity *vs* latitude curve which falls below the experimental curve in Fig. 5 at intermediate latitudes since we do not take account of the longitude effect.

We are indebted to the many pilots, ground crews, and the staff at the Flight Test Division, Wright Air Development Center, U.S.A.F. for their generous cooperation and expert assistance in this work. We also wish to express our thanks to L. Wilcox, K. Benford, W. H. Fonger, R. Baron, and Dr. S. B. Treiman for assistance.

[8] W. H. Fonger, thesis, University of Chicago, 1953 (unpublished).

[9] Kaplon, Peters, Reynolds, and Ritson, Phys. Rev. **85**, 295 (1952).

PHYSICAL REVIEW VOLUME 90, NUMBER 6 JUNE 15, 1953

A Note on Meson-Nucleon Scattering

ROBERT KARPLUS, MARGARET KIVELSON, AND PAUL C. MARTIN*
Harvard University, Cambridge, Massachusetts

(Received March 3, 1953)

A relativistic meson-nucleon two-body equation applicable to the elastic nonexchange scattering of negative pions by protons is solved using the lowest order interaction kernel. The scattering matrix which this equation yields is shown to be unitary. The total cross section calculated from this scattering matrix is finite at threshold and relatively independent of the coupling constant. A plot of the cross section as a function of energy is included.

THE relativistic two-body equation[1,2] has proved useful[3] in discussing the behavior of two-nucleon systems. With this equation one may attempt to get approximate solutions by using terms from the expansion of the interaction operator in powers of the coupling constant, but not assuming such an expansion for the meson-nucleon Green's function itself.[4] The three-dimensional approximation to the resulting equation is equivalent to the configuration space or generalized Tamm-Dancoff method.[3] The latter has the disadvantage that self-energy terms cannot be readily recognized and removed. In the case of negative pion proton elastic nonexchange scattering that part of the lowest order kernel which leads to divergences is so simple that with this term alone we may solve the four-dimensional integral equation directly. Renormalization may then be carried out in the usual manner. The scattering matrix for the process calculated from this Green's function can be shown to be unitary. For meson energies above a few hundred Mev the calculated cross section is almost independent of the coupling constant; even at low energies the s wave scattering is insensitive to the choice of coupling constant in the usual range of values.

We begin with the relativistic meson-nucleon two-body equation. Using the notation of the previous papers,[2,4,5] this may be written

$$[(\gamma p + M)(k^2 + \mu^2 + \Pi) - I_{MN}] G_{MN} = 1. \tag{1}$$

We retain only that part of the interaction operator which gives rise to the above-mentioned divergence difficulty,

$$(x\xi | I_{MN} | y\eta) = -ig^2 \gamma_5 \tau^\xi G_+^{(0)}(x - x') \gamma_5 \tau^\eta \times \delta(x - \xi) \delta(y - \eta). \tag{2}$$

* National Science Foundation Predoctoral Fellow.

[1] H. A. Bethe and E. E. Salpeter, Phys. Rev. **84**, 1232 (1951).

[2] J. Schwinger, Proc. Natl. Acad. Sci. U. S. **37**, 452, 455 (1951).

[3] M. Levy, Phys. Rev. **88**, 441 (1952); A. Klein, Phys. Rev. **90**, 1101 (1953).

[4] S. Deser and P. Martin, preceding paper [Phys. Rev. **90**, 1075 (1953)].

[5] S. F. Edwards, Phys. Rev. **90**, 284 (1953).

The superscript 0 on the nucleon Green's function is used to indicate that it is the Green's function for a noninteracting field. In the absence of an external field, we may replace the inherently one-body radiative corrections M and Π by m and 0, so that our equation becomes, in the integral form appropriate to scattering:

$$G_{MN}=G_+^{(0)}\Delta_+^{(0)}+G_+^{(0)}\Delta_+^{(0)}I_{MN}G_{MN}, \tag{3a}$$

$$G_{MN}(x,y;\xi_i,\eta_-)=G_+^{(0)}(x,y)\Delta_+^{(0)}(\xi_i,\eta_-)$$
$$-ig^2\int G_+^{(0)}(x,\xi')\Delta_+^{(0)}(\xi_i,\xi_k')\gamma_5\tau_k G_+^{(0)}(\xi',\xi'')\gamma_5\tau_j$$
$$\times G_{MN}(\xi'',y;\xi_j''\eta_-)d\xi'd\xi'', \tag{3b}$$

where we have written the isotopic spin indices, 1, 2, 3, + or −, explicitly as subscripts on the arguments of the $\Delta_+^{(0)}$ function.

The solution to this equation may be found formally. It is

$$G_{MN}=G_+^{(0)}\Delta_+^{(0)}-ig^2G_+^{(0)}\Delta_+^{(0)}\gamma_5\tau G_+^{(1)}\gamma_5\tau G_+^{(0)}\Delta_+^{(0)}, \tag{4a}$$

or, with indices,

$$G_{MN}(x,y;\xi_i,\eta_-)=G_+^{(0)}(x,y)\Delta_+^{(0)}(\xi_i,\eta_-)$$
$$-ig^2\int d\xi'd\xi''G_+^{(0)}(x,\xi')\Delta_+^{(0)}(\xi_i,\xi_j')$$
$$\times\gamma_5\tau_j G_+^{(1)}(\xi',\xi'')\gamma_5\tau_k$$
$$\times G_+^{(0)}(\xi'',y)\Delta_+^{(0)}(\xi_k'',\eta_-). \tag{4b}$$

$G_+^{(1)}$ is the solution of the one-body equation

$$(\gamma p+m+ig^2Tr[\gamma_5\tau G_+^{(0)}\gamma_5\tau\Delta_+^{(0)}])G_+^{(1)}=1. \tag{5}$$

It is the nucleon Green's function obtained by using the first approximation to the mass operator. In momentum space, operation with $\gamma p+M^{(1)}$ becomes merely multiplication by a function of p, whence the inverse operator, $G_+^{(1)}$, may be determined by taking Fourier transforms. We obtain[6]

$$G_+^{(1)}(x,x')=\frac{1}{(2\pi)^4}\int d^4p e^{ip(x-x')}G^{(1)}(p), \tag{6a}$$

$$G^{(1)}(p)=\left[\gamma p+m+\frac{ig^2}{(2\pi)^4}\int\gamma_5\tau_j G_+^{(0)}(p-k)\right.$$
$$\left.\times\gamma_5\tau_j\Delta_+^{(0)}(k)d^4k\right]^{-1}. \tag{6b}$$

The integral in $G_+^{(1)}(p)$ may be evaluated by procedures identical with those used in the corresponding electrodynamic calculation[7] with trivial modifications due to the use of a $\gamma_5\tau$-vertex operator instead of a γ_μ. Incorporating the renormalization terms appropriately, we have

$$\delta M=\frac{3g^2}{16\pi^2}\int_0^1 du\left\{[(u-1)\gamma p-m]\right.$$
$$\times\ln\left[\frac{(1-u)\mu^2+um^2+u(1-u)p^2}{(1-u)\mu^2+u^2m^2}\right]$$
$$\left.+(\gamma p+m)\frac{2m^2u^2(1-u)}{m^2u^2+(1-u)\mu^2}\right\} \tag{7}$$

where

$$\delta M(p)=M^{(1)}(p)-m. \tag{7'}$$

Since G_{MN} is the vacuum expectation value of the ordered product[4] $-[\psi(x)\bar\psi(y)\varphi(\xi)\varphi(\eta)]_+\epsilon(x-y)$, the **S** matrix elements are obtained by integrating G_{MN} between eigenvalues of the momenta conjugate to ϕ, $\bar\psi$, and ψ, namely, $\chi=n_u\partial_u\phi$, $-in_u\gamma_u\psi=n_u\partial_u\bar\psi$, and $i\bar\psi n_u\gamma_u=n_u\partial_u\psi$. The **S** matrix element between eigenfunctions $\psi_i'(y)$ and $\chi_i'(\eta)$ on a space-like surface prior to the interaction and $\bar\psi_f'(x)$ and $\chi_f'(\xi)$ on such a surface subsequent to the interaction is given by the expression[8]

$$(\bar\psi_f'\chi_f'|\mathbf{S}|\psi_i'\chi_i')$$
$$=-\int_{\sigma_{-\infty}}d\sigma_y\int_{\sigma_{-\infty}}d\sigma_\eta\int_{\sigma_\infty}d\sigma_x\int_{\sigma_\infty}d\sigma_\xi\,\bar\psi_f'(x)\chi_f'(\xi)$$
$$\times\gamma_0 G_{MN}(x,y;\xi,\eta)\gamma_0\chi_i'(\eta)\psi_i'(y). \tag{8}$$

In particular, if at large times we assume the fields to be adiabatically decoupled, the eigenvalues of the momenta may be taken to be plane waves satisfying noninteracting field equations, and we may determine matrix elements from the meson state with momentum and charge denoted by $(\mathbf{k}, i)$ and the proton state of momentum and spinor index described by $(\mathbf{p}, \lambda)$ to the state described by $(\mathbf{k}', i')$ and $(\mathbf{p}', \lambda')$. The **S** matrix element then becomes

$$(\psi_{\lambda'\mathbf{p}'}\chi_{\mathbf{k}'i'}'|\mathbf{S}-\mathbf{1}|\psi_{\lambda\mathbf{p}}'\chi_{\mathbf{k}i}')$$
$$=ig^2\int d^4xd^4x'\bar\psi_{\lambda'\mathbf{p}'}'(x)\chi_{i'\mathbf{k}'}'(x)\gamma_5\tau_{i'}$$
$$\times G_+^{(1)}(x-x')\gamma_5\tau_i\chi_{i\mathbf{k}}'(x')\psi_{\lambda\mathbf{p}}'(x'). \tag{9}$$

Expressing all quantities in terms of their Fourier transforms and performing the usual integrations, we get

$$(p'k'|\mathbf{S}-\mathbf{1}|pk)=C_{\mathbf{pk}}C_{\mathbf{p}'\mathbf{k}'}(2\pi)^4\delta(p'+k'-p-k)$$
$$\times ig^2\bar u_{\lambda'\mathbf{p}'}(e_{i'}\cdot\tau)^\dagger\gamma_5 G^{(1)}(p+k)\gamma_5(e_i\cdot\tau)u_{\lambda\mathbf{p}}. \tag{10}$$

The quantity $C_{\mathbf{pk}}$ is the normalization factor for a

[6] We are indebted to Dr. S. D. Drell for furnishing us helpful information about K. Brueckner's recent discussion of this Green's function and its bearing on the two nucleon problem.

[7] R. Karplus and N. M. Kroll, Phys. Rev. **77**, 536 (1950).

[8] J. Schwinger, Lectures on quantum field theory, Harvard, 1952 (unpublished).

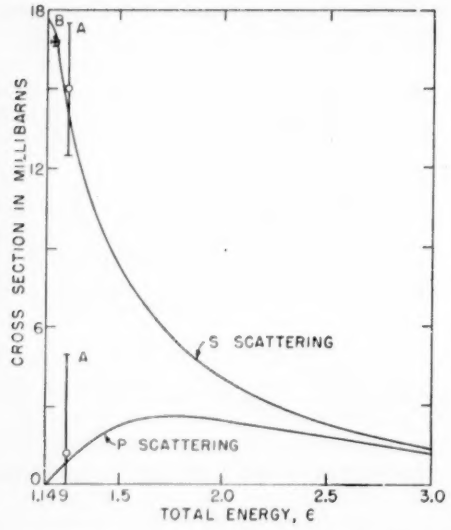

FIG. 1. S and p scattering cross sections as functions of total energy ϵmc^2 in the center-of-mass system. ϵmc^2 is related to T, the kinetic energy of the incident meson in the nucleon rest system, by $T=c^2(2m)^{-1}[m^2c^4-(m+\mu)^2]$. The experimental data are those of Anderson *et al.* (A) and Barnes *et al.* (B). The experimental error for the latter was not available.

meson-nucleon function and is given by[9]

$$C_{\mathrm{pk}}=\left(\frac{1}{(2\pi)^6}\frac{m}{E(\mathbf{p})}\frac{1}{2\omega(\mathbf{k})}d\mathbf{p}d\mathbf{k}\right)^{\frac{1}{2}}. \tag{11}$$

The meson amplitudes and Dirac spinors have been normalized so that

$$(e^*\cdot e)=1, \quad \text{and} \quad \sum_{\lambda=1}^{4}\bar{u}_{\lambda\mathrm{p}}u_{\lambda\mathrm{p}}=1. \tag{12}$$

Unlike the Born approximation to the **S** matrix, the approximate **S** matrix here obtained is unitary. We demonstrate this fact directly by proving that the matrix $\mathbf{S}-\mathbf{1}$ satisfies the relation

$$(a|(\mathbf{S}-\mathbf{1})^\dagger(\mathbf{S}-\mathbf{1})|a)=-2\,\mathrm{Re}(a|\mathbf{S}-\mathbf{1}|a). \tag{13}$$

The evaluation of $(a|(\mathbf{S}-\mathbf{1})^\dagger(\mathbf{S}-\mathbf{1})|a)$ by summation over intermediate states is accomplished with the use of the identities

$$\sum_{\lambda=1}^{2}u_{\lambda\mathrm{p}}\bar{u}_{\lambda\mathrm{p}}=\frac{m+\gamma_0E(\mathbf{p})}{2m} \quad \text{and} \quad \sum_{i=1}^{3}(e_i\cdot\tau)^\dagger(e_i\cdot\tau)=3 \tag{14}$$

and integration over $\mathbf{p}'$ and $\mathbf{k}'$ in the frame in which $\mathbf{p}'+\mathbf{k}'=0$ and $p_0'+k_0'=P_0$. If, in this frame, $\mathbf{q}$ is the momentum for which $P_0=E(\mathbf{q})+\omega(\mathbf{q})$ and VT is the magnitude of the space-time region in which the interaction takes place, then the l.h.s. of Eq. (13) becomes

$$C_{\mathrm{pk}}{}^2\frac{3g^4}{4\pi}VT\bar{u}_{\lambda\mathrm{p}}(e_i\cdot\tau)^\dagger\gamma_5G^{(1)}(P_0)^\dagger\left(\frac{-m+\gamma_0E(\mathbf{q})}{E(\mathbf{q})+\omega(\mathbf{q})}|\mathbf{q}|\right)$$
$$\times G^{(1)}(P_0)\gamma_5(e_i\cdot\tau)u_{\lambda\mathrm{p}}. \tag{15}$$

$G^{(1)}(P_0)^\dagger$ is the adjoint of the Fourier transform of $G^{(1)}(P_0)$. This is to be compared with $-2\,\mathrm{Re}(a|\mathbf{S}-\mathbf{1}|a)$,

$$-2\,\mathrm{Re}(a|\mathbf{S}-\mathbf{1}|a)=-2VT\,\mathrm{Re}\Big[ig^2\bar{u}_{\lambda\mathrm{p}}(e_i\cdot\tau)^\dagger\gamma_5$$
$$\times\frac{\delta M^*(P_0)}{|-\gamma_0P_0+M(P_0)|^2}\gamma_5(e_i\cdot\tau)u_{\lambda\mathrm{p}}\Big], \tag{16}$$

where δM^* is the complex conjugate of δM. Only the imaginary part of the mass operator need be evaluated to demonstrate the desired equality. This imaginary part arises from integration over the logarithm in Eq. (7). The sign of the imaginary part may be determined by explicitly including a negative imaginary addition to the mass. The integral in $\delta M(P_0)$ is evaluated in the appendix. The imaginary part is stated in Eq. (A.3). The substitution of Eq. (A.3) into Eq. (16) makes the latter identical with Eq. (15).

The cross section σ is obtained from (15) by multiplying by the density of final states and dividing by the relative velocities in the center-of-mass system. Since the scattering matrix has been expressed in terms of γ_0 and the unit matrix, there is no mixing of small and large components of the spin wave functions, and σ divides into cross sections for s and p wave scattering. Denoting δM evaluated with $\gamma_0=1$ and -1 by δM_+ and δM_-, respectively, we find

$$\sigma_s=\frac{4}{3}\frac{g^2}{|\mathbf{q}|\epsilon}\frac{[1+E(\mathbf{q})/m](\mathrm{Im}\,\delta M_-)}{(\mathrm{Im}\,\delta M_-/m)^2+(1+\epsilon+\mathrm{Re}\,\delta M_-/m)^2} \tag{17a}$$

and

$$\sigma_p=\frac{4}{3}\frac{g^2}{|\mathbf{q}|\epsilon}\frac{[1-E(\mathbf{q})/m](\mathrm{Im}\,\delta M_+)}{(\mathrm{Im}\,\delta M_+/m)^2+(1-\epsilon+\mathrm{Re}\,\delta M_+/m)^2}, \tag{17b}$$

where $\mathbf{q}$ is defined as in Eq. (15). A factor of 2, arising from the isotopic spin matrices which enter explicitly, and an additional factor of 2/3, required to select only those final states in which a negative meson is present, account for the 4/3 in the expressions above. The dependence of the cross section on the kinetic energy of the incoming meson is shown in Fig. 1. The value of 10 has arbitrarily been selected for the coupling constant $g^2/4\pi$. Two experimental values have been included.[10,11]

Naturally, a calculation based on one leading term of an expansion of the interaction in powers of the coupling

[9] $E(\mathbf{p})=(m^2+\mathbf{p}^2)^{\frac{1}{2}}$ and $\omega(\mathbf{k})=(\mu^2+\mathbf{k}^2)^{\frac{1}{2}}$.

[10] Anderson, Fermi, Nagel, and Yodh, Phys. Rev. **86**, 793 (1952).

[11] Barnes, Roberts, and Tinlot, Summer School Newsletter No. 3 (unpublished).

constant is not much sounder than a similar assumption for the Green's function. However, the fact that the partial **S** matrix here obtained is unitary makes us feel that this covariant calculation presents some progress over the Born approximation applied to this term.

APPENDIX

In this section we evaluate the integral appearing in Eq. (9),

$$\delta M=\frac{3g^2}{16\pi^2}\int_0^1 du\Big\{[(u-1)\gamma P-m]\times\ln\Big[\frac{(1-u)\mu^2+um^2+u(1-u)P^2}{(1-u)\mu^2+u^2m^2}\Big]+(\gamma P+m)\frac{2m^2u^2(1-u)}{m^2u^2+(1-u)\mu^2}\Big\}. \quad (9)$$

The integration is carried out in the reference frame in which the spatial components of P are zero and the dimensionless quantities $\alpha=\mu/m$ and $\epsilon=P_0/m$ are introduced. The real part of δM is obtained by straightforward integration with absolute value signs placed on the argument of the logarithm:

$$\begin{aligned}\mathrm{Re}\,\delta M=(3g^2/16\pi^2)m\{&-1+2\alpha^2+(1+3\alpha^2-2\alpha^4\\&+(\alpha^2-1)/\epsilon^2)\ln\alpha+\alpha^3(2\alpha^2-7)(4-\alpha^2)^{-\frac{1}{2}}\\&\times\tan^{-1}\alpha(4-\alpha^2)^{\frac{1}{2}}-\tfrac{1}{2}B(\epsilon)\ln F(\epsilon)\\&+\tfrac{1}{2}\gamma_0\epsilon[1-3\alpha^2+(1-\alpha^2)/\epsilon^2-(1+4\alpha^2\\&-3\alpha^4+2\alpha^2/\epsilon^2-(1-\alpha^2)^2/\epsilon^4)\ln\alpha\\&-\alpha^3(3\alpha^2-10)(4-\alpha^2)^{-\frac{1}{2}}\tan^{-1}\alpha(4-\alpha^2)^{-\frac{1}{2}}\\&+(1-(\alpha^2-1)/\epsilon^2)\tfrac{1}{2}B(\epsilon)\ln F(\epsilon)]\}. \quad (A.1)\end{aligned}$$

Here

$$B(\epsilon)=(1-2(1+\alpha^2)/\epsilon^2+(1-\alpha^2)^2/\epsilon^4)^{\frac{1}{2}} \quad (A.1a)$$

FIG. 2. Path of integration for the variable u.

and

$$F(\epsilon)=\frac{1-(1+\alpha^2)/\epsilon^2-B(\epsilon)}{1-(1+\alpha^2)/\epsilon^2+B(\epsilon)}. \quad (A.1b)$$

To obtain the imaginary part of δM, we note that the polynomial $\alpha^2(1-u)+u-\epsilon^2u(1-u)$ which appears in the numerator of the logarithm in Eq. (9) has two roots in the region of integration $0\leqslant u\leqslant 1$,

$$u=(\epsilon^2-1+\alpha^2)/2\epsilon^2\pm\tfrac{1}{2}B(\epsilon). \quad (A.2)$$

and that it is negative between these roots. The values of the logarithm appropriate to the three segments of the interval may be inferred from the path of integration shown in Fig. 2, which follows from the choice of Green's functions for outgoing waves. The imaginary part of the mass operator is therefore

$$\mathrm{Im}\delta M=-(3g^2/16\pi)m\times\{-1+\tfrac{1}{2}\gamma_0\epsilon[1+(1-\alpha^2)/\epsilon]\}B(\epsilon). \quad (A.3)$$

The numerical value of $\alpha^{-1}=M/\mu=6.70$ may be used to simplify the expressions in Eqs. (A.1) and (A.3) to

$$\begin{aligned}\delta M=\frac{3g^2m}{16\pi^2}\{&-2.998+1.862/\epsilon^2-\tfrac{1}{2}B(\epsilon)\ln F(\epsilon)\\&+\gamma_0\epsilon[1.504+0.531/\epsilon^2-0.910/\epsilon^4\\&+\tfrac{1}{4}(1+0.9778/\epsilon^2)B(\epsilon)\ln F(\epsilon)]\\&+i\pi[-1+\tfrac{1}{2}\gamma_0\epsilon(1+0.9778/\epsilon^2)]B(\epsilon)\}. \quad (A.4)\end{aligned}$$

PHYSICAL REVIEW VOLUME 90, NUMBER 6 JUNE 15, 1953

A Covariant Meson-Nucleon Equation

STANLEY DESER* AND PAUL C. MARTIN*
Harvard University, Cambridge, Massachusetts

(Received March 9, 1953)

A relativistic meson-nucleon two-body equation is derived in a form suitable for carrying out renormalization. Methods for determining the interaction kernel and classifying its terms are discussed. A reduction of the equation to three dimensions is carried out and the approximations involved in this procedure are examined. The resulting equation agrees with a corresponding one derived by Tamm-Dancoff methods.

INTRODUCTION

SEVERAL investigations[1] have been undertaken recently with the aim of improving the Born approximation results for pion-nucleon scattering. It is the purpose of this note to point out that such a boson-fermion system may be described to advantage by means of a covariant two-body equation akin to the one employed in the two-nucleon problem.[2-4] We shall derive such an equation for the pion-nucleon Green's

* National Science Foundation Predoctoral Fellow.
[1] Dyson, Schweber, and Visscher, Phys. Rev. **90**, 372 (1953).
[2] J. Schwinger, Proc. Natl. Acad. Sci. U.S. **37**, 452 (1951); also unpublished lectures at Harvard.
[3] H. A. Bethe and E. E. Salpeter, Phys. Rev. **84**, 1232 (1951).
[4] M. Gell-Mann and F. Low, Phys. Rev. **84**, 350 (1951).

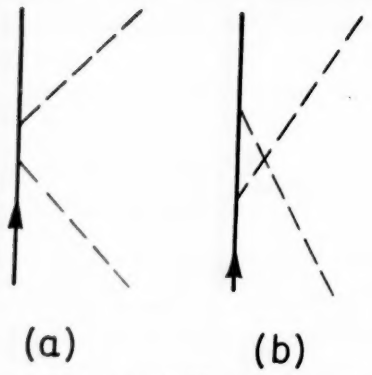

FIG. 1. The lowest order "Compton" interactions.

function, the latter being defined in a manner analogous to the two-nucleon Green's function. A symbolic equation for the interaction kernel of this problem yields on iteration all the irreducible[3] terms of the kernel to any desired order. Approximations to the meson-nucleon (M.N.) equation may be based on approximations to this interaction kernel. For a given kernel, the M.N. equation may be reduced to three-dimensional form[5–7] with the aid of certain assumptions. In particular, it is possible to reduce the equation for the M.N. Green's function with the interaction corresponding to the two simplest "Compton" terms (Fig. 1). The equation obtained is the same as one previously derived using a Fock space representation.[1]

DERIVATION OF FOUR-DIMENSIONAL EQUATION

We shall employ the notation and results of Schwinger[2] as modified for pseudoscalar meson theory,[8] but including the isotopic spin matrix in the $\gamma_5(\xi)$ or $\Gamma_5(\xi)$ vertex operators. The M.N. Green's function is defined by

$$G_{\mathrm{MN}}(xx',\xi_1\xi_2)=(x\xi_1|G_{\mathrm{MN}}|x'\xi_2)$$
$$=-\langle(\psi(x)\bar{\psi}(x')\phi(\xi_1)\phi(\xi_2))_+\rangle\epsilon(x-x'). \quad (1)$$

The desired form for the M.N. equation is

$$(FE-I_{\mathrm{MN}})G_{\mathrm{MN}}$$
$$=[(\gamma p+M)(k^2+\mu^2+\Pi)-I_{\mathrm{MN}}]G_{\mathrm{MN}}=1, \quad (2)$$

where M is the nucleon mass operator and Π the meson polarization operator. It is apparent from this equation that renormalization of the separate particle propagation functions may be carried out in the usual manner; this leaves only the finite parts of the M and Π operators which we shall neglect hereafter. The extra renormalization needed in pseudoscalar theory, that of direct meson-meson scattering, is to be included in the renormalization of Δ_+ and offers no special difficulty. This renormalization, like those of Γ_5 and G_+, must be carried out when these terms occur in I_{MN}. A further complication arises due to the dual role of the meson as particle and virtual field quantum; that is, after I_{MN} has been renormalized, its iterates may still diverge. In that case, the divergences arising in the "ladder" process must be renormalized as well. It is only with such a prescription that the meson-nucleon equation yields finite solutions.

Two alternative methods may be used to determine I_{MN}. The first employs the fact that given the Green's function for one nucleon in an external meson field, it is possible to determine the one-nucleon n-meson Green's function;[9] the second method is closer to that employed in the two nucleon problem and treats the particles on a more equal footing.

In the first method, we note that the M.N. Green's function is related to that of one nucleon in an external meson field by

$$G_{\mathrm{MN}}(xx',\xi_1\xi_2)=\Delta_+(\xi_1,\xi_2)G_+(x,x')$$
$$+\frac{1}{i}\frac{\delta^2G_+(x,x')}{\delta K(\xi_1)\delta K(\xi_2)}\bigg|_{K=0}, \quad (3)$$

where K is the external meson source, set equal to zero after differentiation. This follows immediately from Eq. (1) and the identities

$$\frac{1}{i}\frac{\delta^2G_+(x,x')}{\delta K(\xi_1)\delta K(\xi_2)}\bigg|_{K=0}$$
$$=-\langle(\psi(x)\bar{\psi}(x')\phi(\xi_1)\phi(\xi_2))_+\rangle\epsilon(x-x')$$
$$+\langle(\psi(x)\bar{\psi}(x'))_+\rangle\epsilon(x-x')\langle(\phi(\xi_1)\phi(\xi_2))_+\rangle \quad (4)$$

and

$$\Delta_+(\xi_1,\xi_2)=i\langle(\phi(\xi_1)\phi(\xi_2))_+\rangle-i\langle\phi(\xi_1)\rangle\langle\phi(\xi_2)\rangle. \quad (5)$$

The variational derivative may be evaluated symbolically:

$$\frac{\delta^2G_+}{\delta K(\xi_1)\delta K(\xi_2)}\bigg|_{K=0}$$
$$=g^2\Big[G_+\Delta_+(\xi_1,\xi')\Gamma_5(\xi')G_+\Gamma_5(\xi'')\Delta_+(\xi'',\xi_2)G_+$$
$$+G_+\Delta_+(\xi_2,\xi')\Gamma_5(\xi')G_+\Gamma_5(\xi'')\Delta_+(\xi'',\xi_1)G_+$$
$$+G_+\frac{\delta\Gamma_5(\xi')}{\delta gK(\xi_2)}\Delta_+(\xi',\xi_1)G_+$$
$$+G_+\Gamma_5(\xi')\frac{\delta\Delta_+(\xi',\xi_1)}{\delta gK(\xi_2)}G_+\Big]_{K=0}. \quad (6)$$

Matrix notation has been employed in the above for only the nucleon coordinates, and a summation con-

[5] E. E. Salpeter, Phys. Rev. **87**, 328 (1952).
[6] M. M. Levy, Phys. Rev. **88**, 72, 725 (1952).
[7] A. Klein, Phys. Rev. **90**, 1090 (1953).
[8] S. F. Edwards, Phys. Rev. **90**, 284 (1953).

[9] The possibility of treating Compton scattering by use of variational derivatives of the one fermion Green's function has also been noted by R. Utiyama *et al.*, Progr. Theoret. Phys. (Japan) **8**, 77 (1952).

vention has been introduced for the meson coordinates including isotopic spin indices. The last term in Eq. (6) may be seen to vanish since $\langle(\phi\phi\phi)_+\rangle_{K=0}$ and $\langle\phi\rangle_{K=0}$ are zero. In the former case this is on account of a generalized Furry theorem for pseudoscalar symmetric theory. Thus G_{MN} may be obtained formally in closed form in terms of G_+, Δ_+, Γ_5, and $\delta\Gamma_5/\delta K$; unfortunately, these quantities themselves are known only in series expansion. I_{MN} also may be obtained in closed form by substituting Eq. (6) into Eq. (2). Here again, only expansion is practicable, but a given approximation to I_{MN} may be inserted into Eq. (2) to yield a solution for G_{MN} which is not a power series approximation to G_{MN}.

In the second method, the equation for I_{MN} is recast into a form more in correspondence with the two nucleon problem. From the definition of G_{MN} and the equation of motion for the operator ψ, it will be seen that

$$\tilde{\delta}G_{MN}=(\gamma p+M-g\gamma_5\langle\phi\rangle+ig\gamma_5\delta/\delta K)G_{MN}=\Delta_+ +\langle\phi\rangle\langle\phi\rangle, \quad (7)$$

and that therefore

$$E\tilde{\delta}G_{MN}=1+E\langle\phi\rangle\langle\phi\rangle. \quad (8)$$

Comparing Eq. (8) with the desired form, Eq. (2), and using $\delta G_{MN}/\delta K$ as obtained by differentiating Eq. (2), we find a symbolic equation for I_{MN} of the form

$$(I_{MN}G_{MN})(\xi_1,\xi_2)=-ig\gamma_5(\xi)G_+\frac{\delta}{\delta K(\xi)}(I_{MN}G_{MN})(\xi_1,\xi_2)+ig\gamma_5(\xi)\frac{\delta E(\xi_1,\xi')}{\delta K(\xi)}G_{MN}(\xi',\xi_2)+E(\xi_1,\xi)\langle\phi(\xi)\rangle\langle\phi(\xi_2)\rangle. \quad (9)$$

This equation may be iterated to obtain $I_{MN}G_{MN}$ to any desired order by substituting the last two terms of the right-hand side into $-ig\gamma_5(\xi)G_+(\delta/\delta K(\xi))I_{MN}G_{MN}$. Indefinite repetition of this procedure generates two distinct groups of terms: the first series, arising from $E\langle\phi\rangle\langle\phi\rangle$ consists of generalized "Compton" terms, in which at least one of the real mesons interacts directly with the nucleon; the other series, typified by Fig. 2, contains "indirect" types of interaction in which the real mesons and nucleon affect each other only through the nucleon's virtual meson cloud. This latter sequence results from the middle term on the right hand side of Eq. (9). Had we derived the interaction using Eq. (6) we would have found this series of processes along with some of those of the first series included in the expansion of $\delta\Gamma/\delta K$.

It is easy to verify that the lowest order nonvanishing terms in the Compton and indirect series are, respectively,[10]

$$I_C^{(0)}(\xi,\xi')=-ig^2[\gamma_5(\xi)G_+^{(0)}\gamma_5(\xi')+\gamma_5(\xi')G_+^{(0)}\gamma_5(\xi)], \quad (10a)$$

[10] A superscript zero is used to denote the propagation function of a noninteracting field.

(or explicitly,

$$I_C^{(0)}(x,x';\xi_i,\xi_f')=-ig^2[\gamma_5\tau_i\delta(x-\xi)G_+^{(0)}(x,x')\gamma_5\tau_f\delta(x'-\xi')+\gamma_5\tau_f\delta(x-\xi')G_+^{(0)}(x,x')\gamma_5\tau_i\delta(x'-\xi)], \quad (10b))$$

and

$$I_I^{(0)}(\xi_1,\xi_2)=-ig^6\gamma_5(\xi)\Delta_+^{(0)}(\xi,\eta)\gamma_5(\xi')\Delta_+^{(0)}(\xi',\eta')\times\mathrm{Tr}[\gamma_5(\xi_1)G_+^{(0)}\gamma_5(\eta')G_+^{(0)}\gamma_5(\eta)G_+^{(0)}\gamma_5(\xi_2)G_+^{(0)}+\gamma_5(\xi_1)G_+^{(0)}\gamma_5(\eta)G_+^{(0)}\gamma_5(\xi_2)G_+^{(0)}\gamma_5(\eta')G_+^{(0)}+\gamma_5(\xi_1)G_+^{(0)}\gamma_5(\eta)G_+^{(0)}\gamma_5(\eta')G_+^{(0)}\gamma_5(\xi_2)G_+^{(0)}]+\text{terms with } \xi_1 \text{ and } \xi_2 \text{ interchanged}. \quad (11)$$

As in the two-nucleon problem,[4] only irreducible terms contribute to I_{MN}. Since radiative corrections to the nucleon propagation function and to $\gamma_5(\xi')$ yield reducible graphs, the terms from Fig. 1(a) will take the form $\gamma_5(\xi)G_+^{(0)}\gamma_5(\xi')$ in higher order approximations.

REDUCTION TO THREE DIMENSIONS

By adaptation of now standard techniques,[5-7] the four-dimensional Eq. (2) may be reduced to three-dimensional form with an interaction operator correct to any order. Equation (2) may be written in momentum space in terms of the total four-momentum P and one-half the difference of the nucleon and meson momenta, p,

$$(\gamma(\tfrac{1}{2}P+p)+M)((\tfrac{1}{2}P-p)^2+\mu^2)G_{MN}(p,p';P)\times\int I_{MN}(p,p'';P)dp''G_{MN}(p'',p';P)+\delta(p-p'). \quad (12)$$

The first step in the derivation employs the adiabatic approximation; we assume that the three-dimensional Green's function,

$$G(\mathbf{p},\mathbf{p}';P)=\frac{1}{(2\pi)^{\frac{1}{2}}}\int dp_0 G(p,\mathbf{p}';P)=\frac{1}{2\pi}\int dp_0 dp_0' G_{MN}(p,p';P), \quad (13)$$

is related to $G(p,\mathbf{p}';P)$ by

$$G(p,\mathbf{p}';P)=(2\pi)^{-\frac{1}{2}}i\Omega(p,P)2\omega_p[(P_0-E_p-\omega_p)\Lambda_+(\mathbf{p})+(P_0+E_p+\omega_p)\Lambda_-(\mathbf{p})]G(\mathbf{p},\mathbf{p}';P), \quad (14)$$

where, in the reference frame in which $\mathbf{P}=0$,

$$\Lambda_\pm(\mathbf{p})=[E_p\pm(\alpha\cdot\mathbf{p}+\beta M)]/2E_p, \qquad E_p=(\mathbf{p}^2+M^2)^{\frac{1}{2}}, \quad \omega_p=(\mathbf{p}^2+\mu^2)^{\frac{1}{2}},$$

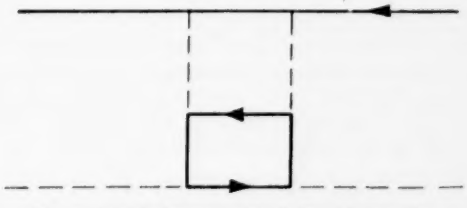

FIG. 2. A typical lowest order indirect interaction.

and

$$\Omega(p,P)=[\alpha\cdot\mathbf{p}+\beta M-(\tfrac{1}{2}P_0+p_0)]^{-1}[\omega_p{}^2-(\tfrac{1}{2}P_0-p_0)^2]^{-1}$$
$$=\left[\frac{\Lambda_+(\mathbf{p})}{E_p-\frac{1}{2}P_0-p_0}-\frac{\Lambda_-(\mathbf{p})}{E_p+\frac{1}{2}P_0+p_0}\right]$$
$$\times\frac{1}{2\omega_p}\left[\frac{1}{\omega_p-\frac{1}{2}P_0+p_0}+\frac{1}{\omega_p+\frac{1}{2}P_0-p_0}\right]. \quad (15)$$

Inserting Eq. (14) into Eq. (12), we obtain

$$G(\mathbf{p},\mathbf{p}';P_0)=(2\pi i)^{-1}\int\Omega(p,P_0)dp_0\gamma_0 I(p,p'';P_0)\gamma_0 dp''$$
$$\times\Omega(p'',P_0)G(p'',\mathbf{p}';P_0)$$
$$+(2\pi)^{-1}\int dp_0\Omega(p,P_0)\gamma_0\delta(\mathbf{p}-\mathbf{p}') \quad (16)$$

as the equation for the Green's function.[11] In scattering problems, the quantities of interests are matrix elements of G between free particle states at times prior and subsequent to the interaction. At these times, we require that one nucleon and one meson be present, the meson having positive frequencies. This means that we need only be concerned with that part of the Green's function which has nonvanishing matrix elements between such states, and desire an equation for this part alone. We denote it by ${}_+G_+$ where the plus sign on either side indicates the restriction of G to those matrix elements on that side which satisfy the above criteria. In other words, ${}_+G_+=\Lambda_+(\mathbf{p})\omega_+(\mathbf{p})G(\mathbf{p},\mathbf{p}';P)\Lambda_+(\mathbf{p}')\omega_+(\mathbf{p}')$, where the ω_+ operators select that part of G_{MN} which contains the proper meson frequencies. With these restrictions, Eq. (16) becomes

$${}_+G_+(\mathbf{p},\mathbf{p}';P_0)=(2\pi i)^{-1}\int(E_p-\tfrac{1}{2}P_0-p_0)^{-1}$$
$$\times\Lambda_+(\mathbf{p})(2\omega_p)^{-1}(\omega_p-\tfrac{1}{2}P_0+p_0)^{-1}dp_0$$
$$\times\gamma_0 I(p,p'';P_0)\gamma_0 dp''\Omega(p'',P_0)G_+(p'',\mathbf{p}';P_0)$$
$$+(2\omega_p i)^{-1}\Lambda_+(\mathbf{p})\gamma_0\delta(\mathbf{p}-\mathbf{p}')\Lambda_+(\mathbf{p}'). \quad (17)$$

It is clear that this argument cannot be used to eliminate the factors

$$(E_{p''}+\tfrac{1}{2}P_0+p_0'')^{-1}\Lambda_-(\mathbf{p}'')$$

and

$$(\omega_{p''}+\tfrac{1}{2}P_0-p_0'')^{-1}$$

occurring in $\Omega(p'')$ on the right-hand side of Eq. (17). However as long as we have G_+ and not ${}_+G_+$ on the right-hand side of Eq. (17), the reduction made in going from Eq. (16) to Eq. (17) does not suffice for our purpose. The simplest assumption, rigorous only when there is no interaction, is to replace G_+ by ${}_+G_+$, or equivalently, to replace I_+ by ${}_+I_+$. The portions of I that are thereby excluded may be reinserted to any desired extent through the use of more complex effective interaction operators (which are reducible in a four-dimensional sense). These are obtained by iteration processes described elsewhere and are of higher order than the covariant kernel from which they arise; hence this procedure has been carried out[6,7] together with the inclusion of irreducible interaction terms of comparable order in g^2. Clearly, at any stage of the three-dimensional procedure, only part of the initial kernel will be included so that the three-dimensional effective interaction of a given order will in some sense contain less than the four-dimensional kernel to that order. This is not to say that there is mathematical justification for preferring the latter, since for neither approximation is the error involved known.

Since it is not our aim to solve Eq. (17) in any approximation, we shall not dwell on the more involved aspects of this procedure. We merely illustrate it by reduction of Eq. (12) with the lowest order interaction, Eq. (10), and with the approximation $I_+\rightarrow{}_+I_+$.[12] In the coordinate system of Eq. (12), this interaction is

$$I_C{}^{(0)}(p,p';P_0)=$$
$$-\frac{ig^2}{(2\pi)^4}\gamma_5\left[\frac{\tau\tau'}{-\gamma_0P_0+M}+\frac{\tau'\tau}{\gamma(p+p')+M}\right]\gamma_5. \quad (18)$$

Insertion of Eq. (18) into the ${}_+I_+$ version of Eq. (17) and integration over the relative energy variables yields

$$(P_0-E_p-\omega_p)G_{ik}(\mathbf{p},\mathbf{p}';P_0)$$
$$=\frac{-g^2}{(2\pi)^3}\int\left[\frac{(1-\gamma_0)\tau_i\tau_j}{2(P_0-M)}+\frac{(1+\gamma_0)\tau_i\tau_j}{2(P_0+M)}\right.$$
$$\left.+\frac{\Lambda_-(\mathbf{p}+\mathbf{p}'')\tau_j\tau_i}{P_0-E_{p+p''}-\omega_p-\omega_{p''}}+\frac{\Lambda_+(\mathbf{p}+\mathbf{p}'')\tau_j\tau_i}{P_0-E_{p+p''}-E_p-E_{p''}}\right]$$
$$\times\frac{d\mathbf{p}''}{2\omega_p}G_{jk}(\mathbf{p}'',\mathbf{p}';P_0)+(2\omega_p i)^{-1}\delta(\mathbf{p}-\mathbf{p}')\delta_{ik}. \quad (19)$$

In wave function form, this equation is the same as that obtained by a Tamm-Dancoff procedure previously.[1] The "uncrossed" term is troublesome in this three-dimensional formulation on account of its contact nature; however, precisely for this reason, the M.N. equation containing only this term has been solved directly in four dimensions.[13] For charge and spin $\frac{3}{2}$ states, only the "crossed" term contributes and the contact term may be dropped in the three-dimensional investigations.

We are grateful to Professor R. Karplus, Professor J. Schwinger, and Dr. A. Klein for illuminating conversations and constructive criticism.

[11] In contrast to the result in the two-nucleon problem, this equation is an equation for G and not for certain Dirac spinor components of G.

[12] This approximation implies that no more than three nucleons may be present at a given time and restricts the number of permitted meson states.

[13] Karplus, Kivelson, and Martin, following paper [Phys. Rev. **90**, 1072 (1953)].

Mass of Cosmic-Ray Mesons at Mountain Altitudes*

GIULIO ASCOLI
Massachusetts Institute of Technology, Cambridge, Massachusetts and University of Illinois, Urbana, Illinois
(Received January 22, 1953)

Mass measurements of cosmic-ray particles have been carried out by cloud-chamber observations at 3240-meters' elevation to determine the relative rate of occurrence of mesons of different types, in particular of μ-mesons of the hard component and of π-mesons produced locally above the apparatus. From momentum and range observations, the mass of individual particles could be obtained with a probable error of 5 percent, thus allowing accurate resolution between μ- and π-mesons.

The results of 48 observations indicate that all of the particles were very probably μ-mesons. The data yield a μ-meson mass value of 207.4 ± 2.4 electron masses, where the probable error includes an estimate of systematic errors. The observed absence of π-mesons in the experiment is in agreement with the results of observations in photographic plates.

In addition, a single cloud-chamber observation was obtained which suggests the existence of a particle having a positive charge twice the elementary charge and a mass roughly equal to that of a nucleon. Alternative interpretations of the observation are discussed in detail.

I. INTRODUCTION

THE work reported in this paper grew from an attempt to carry out measurements of momentum and range of cosmic-ray mesons by means of a cloud chamber with the precision required to differentiate among mesons of different masses in single observations. The accuracy needed to resolve pions from muons was in fact maintained in a series of measurements at Echo Lake, Colorado (3240-meters elevation). However, the results of mass measurements on 48 particles show that all of these particles were muons. The absence of pions among the observed mesons is in agreement with more recent work with photographic plates. A calculation, based on the results obtained by the Bristol group[1,2] on the rate of production of pions, their distribution in energy and mean free path against nuclear collisions, predicts a relative rate of only about one positive pion among ninety muons in our apparatus. The original evaluation had been based on too high a rate of pion production and too long a mean free path, each error leading to an overestimate by a factor of about 3. Since no pions were observed we omit a detailed discussion of the apparatus as a reliable pion detector. A fairly detailed account of those features of the experiment which affect the accuracy of mass measurement is given, since the results yield an independent estimate of the mass of the muon of accuracy comparable to that obtained in recent observations on π-μ-decays in flight.[3]

In addition to the μ-meson traversals, several events were observed in the cloud chamber, which were probably caused by the occurrence of nuclear interactions in the materials surrounding the chamber. In one such event, (Sec. VI) a particle traversing the chamber appears to be a doubly charged proton.

II. GENERAL

The mass of the mesons was obtained from the simultaneous observation of their momentum and range in the apparatus shown in Fig. 1. The momentum of the particles was obtained by observing in a cloud chamber their curvature in a magnetic field of about 7500 gauss, while their range was essentially fixed by the selection of events which triggered the chamber expansions. The chamber was triggered by a "down" sequence, consisting of a prompt $B+C-D$ coincidence, followed by a delayed discharge of tray D, 1 to 6 μsec after firing of the BC telescope. Such a sequence should be the result, in most instances, of a meson which moves downward through the chamber, is slowed down by ionization losses in the aluminum absorber a-3 and comes to rest in the carbon layer a-4 to decay with emission of an electron. Since the final absorber is of low atomic

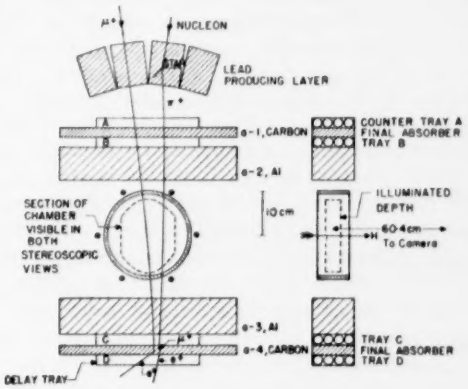

FIG. 1. General arrangement of the apparatus.

* The material presented here is taken from a thesis submitted in 1951 to the Physics Department, Massachusetts Institute of Technology, based on work carried out at Massachusetts Institute of Technology with the assistance of the U. S. Office of Naval Research and completed at the University of Illinois.

[1] Brown, Camerini, Fowler, Heitler, King, and Powell, Phil. Mag. **40**, 862 (1949).

[2] Camerini, Fowler, Lock, Muirhead, and Tobin, Phil. Mag. **41**, 413 (1950).

[3] Lederman, Booth, Byfield, and Kessler, Phys. Rev. **83**, 685 (1951).

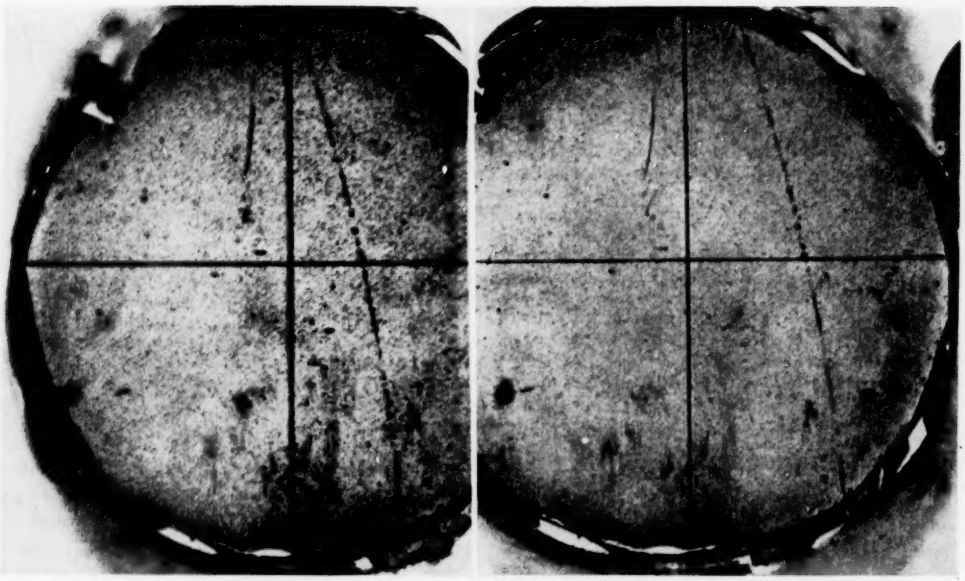

FIG. 2. Typical μ-meson track, M-6-6281.

number, muons of either sign as well as positive pions can be detected. Production of pions can take place either in the 10-cm lead layer above the apparatus, or in the aluminum layer a-2 located immediately above the chamber (in the second case a charged primary is required to fire tray B). The apparatus selects muons with kinetic energies of about 280 Mev (before entering the lead blocks), while the selected pions would have energies at production in the interval from 90 to 290 Mev, depending on their place of birth. In addition to the events described, one anticipates that a certain number of "spurious" events will contribute to the observations. Some will result from random delayed coincidences of independent particles, while others will be caused by single fast particles through the spurious delay of a Geiger counter pulse. Other spurious observations will result from nuclear interactions taking place below the chamber. In the great majority of these events, as one can easily show, the observed particles would have such high momenta that the observations can be ruled out unambiguously. A final source of spurious observations would occur for events in which several mesons are produced, because in such cases it may happen that a meson of the appropriate range, after traversing the chamber outside the illuminated region, gives rise to the delayed firing of tray D, while another meson of lower momentum is seen in the chamber. Again, most of these events can be ruled out unambiguously. A small fraction of all of these events may be expected to result in the observation of particles having momenta close enough to those of stopped particles so that they cannot be ruled out unambiguously and may be interpreted as "heavy" or "light" mesons. As a control on the method of selection, the cloud chamber was also triggered by an "up" sequence, $(B+C-A)_{\text{prompt}}+A_{\text{delay}}$. Since the true events in this control channel would be attributable to mesons travelling upward through the chamber, most of the events in this channel should be spurious. The counting rates and the classification of the corresponding observations are given in Table I.

In the main channel, only single tracks of minimum ionization were observed. Fourteen percent of these

TABLE I. Counting rates and classification of observed events.

	Main channel (down)	Control channel (up)
Counting rate	18.6 ± 0.6 day^{-1}	3.8 ± 0.3 day^{-1}
Type of event		
No tracks observed[a]	367 (75 percent)[b]	80 (75 percent)[b]
Single minimum ionization tracks		
Positive	61 (12.5 percent)	0
Negative	43 (8.8 percent)	0
Straight	17[c] (3.5 percent)	21 (20 percent)
Other	0	6[d] (5 percent)
Total	488	107

[a] These include irrelevant tracks such as: (1) tracks too short to be identified, (2) tracks not of counter age, (3) slow α-particles, (4) electrons, (5) tracks obviously not through counters.

[b] This is consistent with the geometry of the telescope and the chamber. A rough calculation shows that only about one-third of the particles passing through the telescope could yield tracks illuminated and visible from both cameras.

[c] Thirteen of these tracks were suitable for measurement. The observed moments extended from 700 to 6000 Mev/c, corresponding to mass of 2000 m_e, or more, if the particles had actually stopped.

[d] 2 pairs of lightly ionizing straight tracks, 1 deuteron or proton, 1 shower of several hundreds of particles, 1 moderate shower, and 1 event discussed in Sec. VI.

were almost straight, with measured momenta corresponding to masses of 2000 m_e or more for stopped particles. The number of such straight tracks in the control channel was the same within statistical fluctuations, while no curved tracks were recorded. Among 49 curved tracks measured in the main channel we found no "light" mesons and one "heavy" meson, the latter being probably caused by a spurious event.

III. MOMENTUM MEASUREMENTS

The cloud chamber used was of the conventional, cylindrical, diaphragm-expansion type, filled with argon and saturated alcohol-water vapor to a pressure of 76 cm of Hg, with an expansion ratio of 1.081. A system of filters fore and aft of the rubber diaphragm insured uniform motion of the diaphragm and of the gas during the fast (0.006 second) expansion. Suitable circulation of water kept the temperature of the chamber uniform to minimize thermal currents. Stereoscopic photographs of the tracks were taken with a delay of 0.05 second through a 14-cm cylindrical hole in the magnet pole, since the required accuracy made it necessary to take into account changes in photographic magnification and magnetic field with depth. Both images of the tracks were then measured on a travelling stage microscope, and the parameters required to reconstruct the track in space obtained by least square fitting of parabolas to the measured track coordinates.

The accuracy of the momentum measurements depends on experimental factors affecting the curvature measurements (residual turbulence, photographic distortion, accuracy of track location), on the Coulomb scattering and on the precision with which the magnetic field is known. Table II gives a summary of the estimated errors from the various sources, classified into three groups: random errors on single measurements, systematic errors affecting particles of either sign, and systematic errors having opposite effect on particles of opposite signs (for technical reasons it was not practical to reverse the direction of the field).

TABLE II. Probable errors in momentum measurements on μ- or π-mesons.

Type	Source	Percent error
Random errors	Turbulence	1.8
	Curvature measurement	0.9
	Scattering	1.5
	Other	0.5
	Total	2.5
Systematic errors on particles of either sign	Magnetic field	0.3
	Magnification	0.1
	Location of chamber	0.2
	Total	0.4
Systematic error affecting the mass difference of positive and negative particles	Possible systematic distortion	1.0

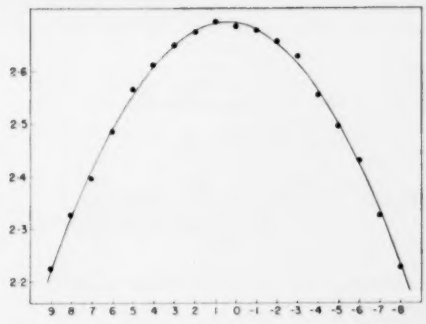

FIG. 3. Measurements of coordinates along track of Fig. 2. The ordinate gives the deviation of the track from its chord, at a scale 25 times larger than that of the abscissa, which shows the position along the chord.

The errors affecting curvature measurements, from all sources, were determined by the examination of tracks of high energy particles taken with the magnetic field removed for a very short time (to avoid changes in the prevailing thermal conditions). The measured curvatures of 33 such no-field tracks taken throughout the experiment appeared to be normally distributed with a probable curvature of 0.032 meter^{-1} (equivalent to a momentum of 7×10^9 ev/c in a field of 7500 gauss), and a mean value of 0.008 ± 0.006 m^{-1}. This error is caused largely (0.026 m^{-1}) by residual turbulence, with a measured contribution of 0.006 m^{-1}, from photographic distortion and nonuniform motion of the diaphragm and a contribution of 0.018 m^{-1} from the errors in locating track coordinates. The last error, estimated both from the scatter of measured coordinates from the fitted circle, and from the consistency of repeated measurements, is about 50 percent higher than the lower limit set by ion diffusion. Figure 2 shows a typical μ-meson track, while Fig. 3 shows some of the coordinates measured on one of the two images of the same track.

The process of translating the image coordinates back into the original trajectory is one of straightforward geometry and introduces no additional errors (except for the small experimental uncertainty in the measured photographic magnification), provided adequate account is taken of the exact nature of the object-image transformation as well as of the backward motion of the gas. When this is done, several corrections appear, which are not all immediately obvious, but which are nevertheless quite straightforward and rather small.

The magnetic field was measured with flip coils which were calibrated using as a primary standard the field of a permanent magnet, kindly made available by R. V. Pound of Harvard University, which was known to 0.01 percent in terms of the proton moment. The results of seven independent measurements with two flip coils and four intermediate standards were all well within the adopted probable error and gave a value

TABLE III. Probable errors on range measurements.

Type of error	Source	Percent error
Random	Final thickness of absorber	2.8
	Scattering[a]	2.1
	Straggling in range[b]	1.8
	Total	4.0
Systematic	Uncertainty in mass of absorbers	0.3
	Uncertainty in average ionization potential	0.4
	Total	0.5

[a] See appendix I.
[b] See appendix II.

TABLE IV. Probable errors in mass measurements.

Type of error	Source	Percent error
Random	Momentum	4.5
	Mass	3.0
	Total	5.5
Systematic, for particles of either sign	Momentum	0.7
	Range	0.4
	Total	0.8
Error in difference between mass of positive and negative particles	Systematic distortion of tracks	0.8

of 8140±20 gauss at a particular reference point in the gap, the quoted error including hysteresis effects of ±10 gauss. The time variation of the field was kept to a negligible value (±5 gauss) throughout the experiment by electronic regulation of the magnet current. The space variations of the field within the used region of the chamber were, on the contrary, quite large (±500 gauss). The resulting error was, however minimized by mapping the variation from point to point of the axial component of the field, and by using for each particle the value of the magnetic field corresponding to the actual position of the trajectory (averaged along the track by a suitable process). The final uncertainty from this source in the field appropriate to a particular measurement is about 20 gauss, arising largely from the error in locating the track. The large gradient in the axial field component implies the existence of an appreciable radial component of the field. A map of the latter (computed by means of $\nabla \cdot \mathbf{H} = 0$) shows values as high as 500 gauss. One can compute the average effect of this component on the observation, and this turns out to be quite small (equivalent to a random error of about 5 gauss in the longitudinal field).

IV. RANGE MEASUREMENTS

The average equivalent aluminum thickness traversed by mesons moving perpendicularly to the absorber was 27.54 g-cm^{-2}, the conversion to equivalent aluminum thickness of other absorbers (about 6 g-cm^{-2} of glass, brass, water, carbon) being made by use of the Bethe-Bloch equation, taking into account the velocity of the mesons at the location of each material. The average range given above includes two small corrections; one is for the increase in path length due to scattering (0.4_4 g-cm^{-2}), and the other takes into account that the average point of stopping of mesons will be a short distance (0.1_3 g-cm^{-2}) below the midpoint of the final absorber because of a slight change in probability of detection of the decay electrons with position. An appropriate averaging of the Geiger-tube wall thickness traversed was similarly included. In estimating the range of individual mesons account had, of course, to be taken of the angle of traversal of the absorber, which differed (by about 6°) from the angle at the end of the visible track, because of the fringing magnetic field. Fortunately, the magnetic field and momentum of particles dropped at nearly the same rate throughout the absorber, resulting in nearly constant curvature.

Table III gives the source and estimated magnitude of the errors in range, for random errors and for systematic errors affecting all measurements. In the latter group, we have included the effect of possible inaccuracies in the range-energy relation used. The latter was based on the assumption that the Bethe-Bloch equation is valid in the pertinent range of velocities ($p/mc < 1.6$) and on the adoption of an average ionization potential for aluminum of 150±5 volts, from measurements of Mather and Segrè on 340-Mev protons.[4] To justify the neglect of polarization effects, we have estimated the reduction in energy loss by the

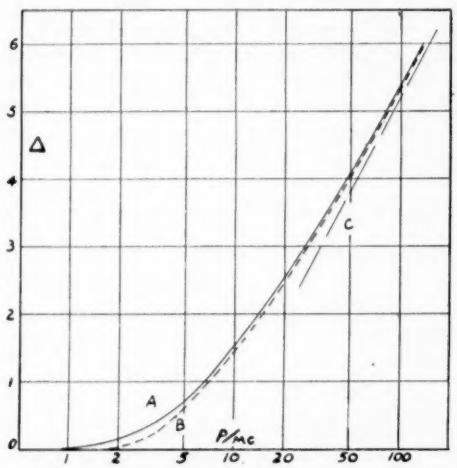

FIG. 4. Density effect in aluminum. Δ is the difference between the loss predicted by extrapolation of the Bethe-Bloch equation from low energy data and the actual loss, measured in units of $2\pi N_{el} e^4 / m_{el} v^2$ according to the theory of Wick (*A*) and of Halpern and Hall (*B*). *C* is the asymptotic result predicted by all theories.

[4] R. L. Mather and E. Segrè, Phys. Rev. **84**, 191 (1951).

method of Wick.[5] With an assumed distribution of atomic frequencies from x-ray data which turned out to give the correct ionization potential, the result shown in Fig. 4 was obtained.[6] According to this result, the density effect should be negligible at the velocities encountered in this experiment and in the Mather-Segrè measurements, at least within the assigned uncertainty on the ionization potential.

Table IV shows the estimated errors on the mass measurements of μ- (or π-) mesons obtained by compounding the errors on momentum and range. The expected distribution of mass values is not quite Gaussian, partly because the mass does not depend linearly on momentum and range and partly because of the fact that while it is reasonable to expect a normal distribution of errors in the curvature measurements, this is certainly not the case for the range measurements. In the latter case, none of the sources yield Gaussian errors. We have estimated the departure of the expected mass distribution from a normal curve by computing its moments from the various sources. The result of the computation yields the somewhat asymmetric curve shown in Fig. 5, and shows that a small correction should be applied to the arithmetic mean of individual mass values ($-0.6\ m_e$ in the case of μ-mesons).

V. RESULTS OF THE MASS MEASUREMENTS

Forty-nine out of a total of one hundred and four curved tracks were selected for detailed measurement, the remaining tracks being rejected for one of the following reasons: (a) Tracks shorter than 9 cm. (b) Tracks partially hidden by reference marks or large blobs of condensation. (c) Tracks separated as a result of the persistence of clearing field. (d) Tracks where it was not absolutely certain that they were oriented toward the counter trays C and D. (e) Tracks with probable single scattering.

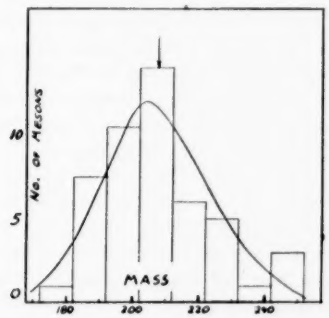

FIG. 5. Distribution of observed meson masses, in units of the electron mass. The curve is the distribution calculated for a unique mass on the basis of the estimated experimental errors.

[5] G. C. Wick, Nuovo cimento **1**, 302 (1943).
[6] The Halpern-Hall method yields even smaller corrections at low energies.

TABLE V. Results of mass measurements.

Corrected[a] average of 28 positive mesons: 204.3 m_e.
Corrected average of 20 negative mesons: 210.5 m_e.
Difference: $6.2\pm5.0\ m_e$.
Average of positive and negative mesons: 207.4 m_e.

Track	Number	Sign	$H\rho$, gauss-cm $\times10^5$	Range, g cm^{-2}	Mass/electron mass
M-1	2049	+	4.831	28.31	187
M-2	352	+	4.933	27.85	196
	1508	+	4.784	27.76	186
M-4	101	+	5.514	29.40	230
	597	−	5.257	28.14	218
	799	+	5.374	28.12	227
	1374	+	5.084	28.66	203
	2145	+	5.236	29.98	206
	2404	+	4.933	29.97	185
M-5	266	+	5.003	28.69	197
	569	+	4.861	27.56	193
	779	−	5.269	27.53	223
	1960	−	5.165	29.19	205
	3381	−	5.645	27.83	249
	2027	+	9.05	28.53	530
	3623	+	5.671	28.73	245
M-6	4814	−	4.962	28.90	193
	4926	+	5.160	30.55	198
	6281	+	5.060	27.54	207
	6350	+	5.121	28.04	209
	7304	−	5.260	28.76	215
	7702	−	5.219	28.21	215
	7971	+	4.952	30.21	186
	8326	+	5.054	27.57	207
	9605	+	4.881	28.28	190
	9653	−	5.397	28.88	224
	10 732	−	5.061	27.64	207
	11 026	+	5.434	31.70	211
M-8	756	−	5.070	28.00	205
	1558	−	4.826	29.39	181
	2289	+	4.821	28.38	186
	2497	−	5.327	29.44	216
	3248	+	5.074	32.00	185
	5091	+	5.011	27.94	202
	5701	+	5.117	27.95	209
	6754	−	5.159	28.45	210
	6910	−	4.871	27.92	192
	7454	−	5.262	27.87	220
A-1	2348	−	5.165	27.95	213
	5057	+	5.046	27.53	207
	7815	+	5.347	27.61	228
	8474	−	4.997	27.62	202
	8484	−	4.972	27.90	199
	8889	+	4.976	27.56	201
	9132	−	5.047	28.61	200
	9181	+	6.214	34.68	250
	14 453	−	5.711	31.18	234
	15 377	+	4.990	27.86	201
	15 598	+	5.063	27.89	206

[a] Includes a correction of $-0.6\ m_e$ for the asymmetry of the distribution

Table V gives a summary of the measurements. With the exception of a single track yielding a mass of 530 m_e, the other observed mass values range uniformly from 181 to 249 m_e. These 48 tracks appear to be consistent with a single mass, the observed spread of values corresponding to a probable deviation of $11\pm1\ m_e$ in agreement with the *a priori* estimate of 11.6 m_e. The average of these measurements yields a muon mass of 208.0 m_e, with a probable statistical error of 1.7 m_e. When a small correction is made for the asymmetry of the distribution and the estimated probable systematic error of 1.6 m_e is taken into

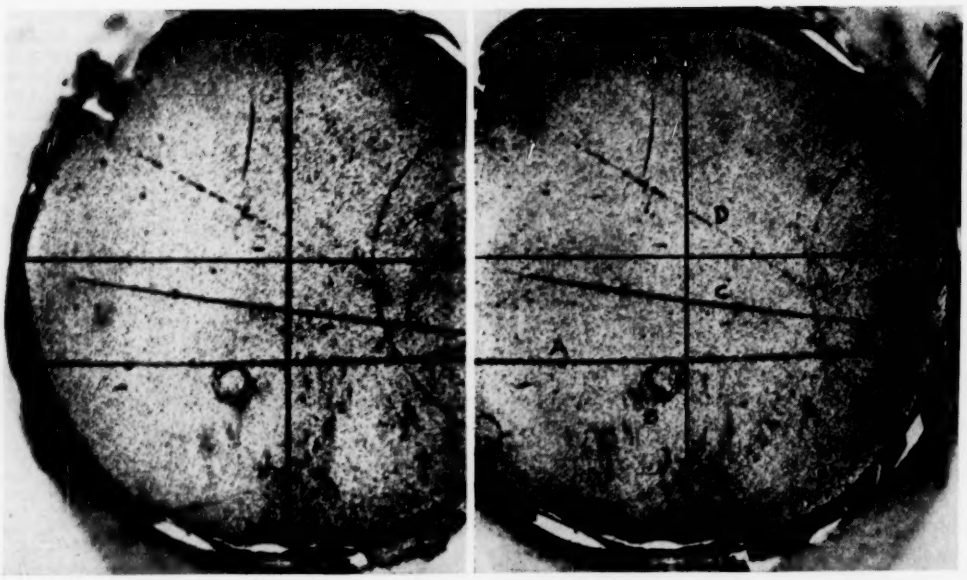

FIG. 6. Event *M*-6-6971. A lighted bulb—not shown—indicates that the event fired the "up" sequence. Track *A* is interpreted as a doubly charged proton from its ionization and momentum, and from the momentum of the knock-on electron *B*.

account, we get a final value of $207.4\pm2.4\ m_e$ for the muon mass. This value agrees within the probable error with the values of 209.8 ± 2.2 obtained by observation of the decay in flight of pions[3] and of 209.0 ± 1.2 obtained from the range in photographic plates of muons from the decay of pions at rest, both obtained under the assumption of decay of the pion into a muon and a neutrino, using a pion mass of 276 ± 1 electron masses.

VI. A DOUBLY CHARGED PROTON?

During the course of the experiment, one event was photographed which gives tentative evidence for the existence of a doubly charged positive particle with mass close to that of a nucleon. Figure 6 shows stereoscopic views of the event and Table VI gives a summary of the measurements. The cloud-chamber expansion was triggered by a delayed coincidence in the upper tray *A*, so that a meson probably came to rest in the carbon absorber *a*-1 above the chamber; however, none of the particles visible in the photograph travels in a direction to reach tray *A*. Two of the tracks, *A* and *C*, meet at a common point in the glass wall of the chamber and if they are taken to originate at that point they must both be positive. Track *B* is that of an electron originating in the gas and spiraling slowly toward the back of the chamber; since the loops are close to each other the origin of the track cannot be fixed beyond a doubt: however, the stereoscopic views are consistent with its origin being located on the trajectory of *A* (within the resolution of observation, i.e., 1 mm in height and 3 mm in depth), in which case *B* is emitted essentially in the direction of travel of *A* (within at most 20 degrees). We assume for the moment that *B* is an electron in the gas set in motion by a close collision of *A* which can be treated as a two-body process, and discuss alternative interpretations of *B* toward the end of the section. If *B* is a knock-on electron, knowledge of its momentum can be used to calculate the velocity of *A*, and we obtain

$$p_A/m_Ac=0.78^{+0.07}_{-0.10},$$

where the assigned uncertainties are essentially limit of errors obtained by calculating the momentum of *B* from the radius of the inner and outer envelope of the tight spiral formed by the projection of track *B*. The errors caused by scattering and location of drops were very much smaller than the assigned limits of error. This measurement of the velocity of *A* would be inconsistent with the observed ionization of *A*, if *A* were singly charged, since $p_A/m_Ac=0.68$ corresponds to a probable ionization 2.5 times minimum, and the observed ionization (obtained by comparison with that of the electron track *E* in the same photograph) is definitely higher than 3.5 times minimum. This value of the ionization is an upper limit of error, which is obtained when no attempt is made to resolve cluster of droplets along the very dense track of *A*; the uncertainty caused by statistical fluctuations, background and so on is quite small. The ionization of *A* is probably much higher (5 or more times minimum). It appears out of the question to attribute the discrepancy between the

two measurements to experimental error. With $z=2$ the discrepancy is removed,[7] since the calculated value of the ionization (about 7 times minimum) is consistent with the observed ionization. If a value of $z=2$ is assumed p/mc from the kinematics of the knock-on collision together with p/z from the observed curvature in the magnetic field yield the mass of the particle. For $z=2$, we obtain

$$m_A c^2 = (780\pm 50) \Big/ \left(0.78 \begin{matrix}+0.07\\-0.10\end{matrix}\right) = 1000 \begin{matrix}+230\\-140\end{matrix} \text{ Mev.}$$

It seems extremely improbable that A be a known multiply charged particle such as He^{3++} or He^{4++}, since this would require an error in curvature measurement attributable to turbulence about 12 times the probable error and about 4 times the largest spurious curvature observed in about one hundred photographs.

There remains to discuss alternative interpretations of track B. If B is not an electron from a two-body collision of A with an electron at rest in the gas, there is, of course, no discrepancy to explain and A is in all likelihood a proton. The following possibilities have been considered: (a) B is a heavy electron of mass $2m_e$. This does not seem a very attractive alternative and we do not consider it further. (b) B is a knock-on electron, but momentum is not conserved between A and B alone, the atom to which B was originally bound taking up the excess momentum. (c) B is an internal conversion electron from a radiative transition of a nucleus in the gas excited by a collision with A. (d) B is a Compton electron formed in the gas by a photon produced in the same nuclear collision in which A and C originate. (e) B is a Compton electron formed in the gas by an unrelated photon.

The probabilities, P, of b, c, d, e giving rise to an electron B at the observed position and time and with the observed energy have been estimated and are given below expressed as a ratio to the probability that a δ-ray of the energy of B be produced along the track of A, if A is a doubly charged proton.[8] We obtained the following results:

(b) A calculation of the probability of δ-ray emission with recoil (see Appendix III) gives $P_b \sim 5\times 10^{-8}$.

(c) We require a nuclear collision of a proton with a nucleus in the gas (probability—with geometric cross section—2.4×10^{-4}) in which the nucleus is excited and the proton loses little energy (probability $\lesssim 10^{-2}$),[9] that the resulting photon be internally converted (probability $\lesssim 10^{-2}$)[9] and that the electron be emitted within 20 degrees (probability 3×10^{-2}). The over-all relative probability is $P_c \lesssim 2\times 10^{-8}$.

[7] $z \gtrsim 2$ cannot, of course, be excluded. For any $z \gtrsim 2$ our measurement yields $m_A c^2 \sim 500z$ Mev.

[8] The probability that in 12 cm of track of a doubly charged proton of the observed energy a δ-ray be emitted having an energy high enough to identify the doubly charged proton is about 5 percent.

[9] These estimates are given by J. M. Blatt.

TABLE VI. Resumé of measurements on doubly charged proton event.

Track	A	B	C	D	E
Sign	+	−	+	±	±
Momentum/z, Mev/c	390 ± 30	$1.02 \begin{matrix}+0.11\\-0.19\end{matrix}$	520 ± 80	400	12 ± 2
Ionization/minimum ionization	>3.5		3 ± 1	~1	1.22[a]
Identification	doubly charged proton	electron	proton	meson or electron	electron (±)

[a] Calculated. The observed drop count on this trcak is used as calibration for other measurements.

(d) We have calculated the probability of (d) with the generous assumption that 10 neutral pions are created in the primary interaction. After averaging the Klein-Nishina cross section over the photon spectrum resulting from neutral pion decay and taking into account geometrical factors we get $P_d \sim 2\times 10^{-8}$.

(e) To calculate the probability of such a random coincidence the rate at which Compton electrons are created in the cloud-chamber gas by photons of the soft component is required. With the photon and electron energy distributions of Richards and Nordheim[10] and the flux of the soft component given by Rossi,[11] the number of such electrons in the energy range 0.17 to 0.63 Mev[12] turns out to be about 3.5×10^{-6} electrons sec^{-1} cm^{-3}. With a resolving time of 0.03 second and an effective cloud-chamber volume of 10^3 cm^3 this gives 10^{-4} such electron per picture, in agreement with the fact that none were observed in 500 pictures. The requirement that the electron track be tangent to A within the experimental error reduces the probability that B be due to this source so that $P_e \sim 4\times 10^{-6}$.

It appears from these considerations that the alternative interpretations of track B are improbable enough to make the hypothesis of a new particle reasonably attractive, even though an observation of the type reported does not carry as much weight as that of an observed disintegration. If such a doubly charged proton exists it may possibly disintegrate in a manner similar to that of a V particle, giving rise to a proton and a positive pion, perhaps with a comparable lifetime. In the present observation, the time of flight of A from its assumed origin to the point where it disappears, was 6×10^{-10} second in the rest frame of the particle.

ACKNOWLEDGMENTS

The author is grateful to Bruno Rossi and George Valley for their interest and guidance. He is very much indebted to Richard W. Safford who was associated

[10] J. A. Richards and L. W. Nordheim, Phys. Rev. **74**, 1106 (1948).

[11] B. Rossi, Revs. Modern Phys. **20**, 567 (1948).

[12] 0.17 Mev is the maximum energy of a knock-on electron if A is a proton; 0.63 Mev is the observed electron energy.

with and who made important contributions to the early phases of the work.

APPENDIX I. INCREASE IN RANGE CAUSED BY SCATTERING

We have calculated the various moments of the distribution in actual path length of particles which are stopped by a slab of absorber of thickness t when the angle of incidence is α. We have done this under the usual small angle approximation, assuming the simplest type of scattering cross section, i.e.:

$$\sigma(\theta)d\theta=(\text{constant})\theta^{-3}d\theta \text{ for } \theta_1<\theta<\theta_2$$
$$=0 \text{ for } \theta<\theta_1=\lambda/r_{\text{atom}} \text{ and for } \theta>\theta_1=\lambda/r_{\text{nucleus}}.$$

We obtain the following moments for $\Delta=$(actual path length $-t$):

$$\langle\Delta\rangle=\tfrac{1}{2}\alpha^2 t+\tfrac{1}{2}\int_0^t r\theta_s^2 dr,$$

$$\langle(\Delta-\langle\Delta\rangle)^2\rangle=\tfrac{1}{2}\int_0^t \theta_s^2 dr\int_0^r r'^2\theta_s^2 dr'$$
$$+\tfrac{1}{4}\int_0^t r^2 dr\theta_2^2\theta_s^2/\log(\theta_2^2/\theta_1^2)$$
$$+\tfrac{1}{2}\alpha^2\int_0^t r^2 dr\theta_s^2,$$

where $\theta_s^2\{=E_s^2/(p^2v^2x_0)(E_s=21\cdot10^6 \text{ ev}; x_0=\text{radiation length})\}$ is a function of the residual range r or r'. The higher moments which are given by rather complicated expressions show that the distribution is far from normal.

APPENDIX II. STRAGGLING IN RANGE

We simplify the problem by neglecting the fluctuations in the total number of collisions suffered by a particle in a certain path length and by use of a simplified expression for the probability of a collision loss ϵ in $d\epsilon$:

$$P(\epsilon)d\epsilon=\frac{\text{constant}}{\beta^2\epsilon^2}d\epsilon(1-\beta^2\epsilon/\epsilon_2) \text{ for } \epsilon_0<\epsilon<\epsilon_2$$
$$=0 \qquad \text{for } \epsilon<\epsilon_0 \text{ or } \epsilon>\epsilon_2,$$

where ϵ_2 is the maximum energy loss in a single collision and ϵ_0 is a sharp low energy cutoff, which may be substituted to the actual smooth cutoff, since it is the fluctuation in large energy losses (near ϵ_2) that contributes to the straggling, and for $\epsilon_0\ll\epsilon_2$, ϵ_0 disappears from the results. We further simplify the problem to the extent required to make the different collisions statistically independent, by assuming the energy at any point along the path to be essentially equal to the average energy at the point. With these approximations (valid for $\epsilon_0\ll\epsilon_2$) we get the following values for the "Hermitian" moments $h^{(n)}(R)$:

$$h^{(n)}(R)=2m_e c^2 C(n-1)^{-1}(-)^n$$
$$\times\int_0^E \epsilon_2^{n-1}K^{-(n+1)}\beta^{-2}[1-(n-1)\beta^2/n]dE,$$

where $m_e c^2$ is the rest energy of the electron, C is the classical cross section of the electrons in a unit volume of absorber, K is the average energy loss of the particle per unit path length and the moments $h^{(n)}(R)$ are defined by

$$h^{(2)}(R)\equiv\langle(R-\langle R\rangle)^2\rangle\equiv\sigma^2, \quad h^{(3)}(R)\equiv\langle(R-\langle R\rangle)^3\rangle,$$
$$n\geqslant 3, \quad h^{(n)}(R)\equiv\sigma^n\left\langle H_n\left(\frac{R-\langle R\rangle}{\sigma}\right)\right\rangle,$$

with

$$H_n(Z)=(-)^n\exp(Z^2/2)\frac{d^n}{dZ^n}\exp(-Z^2/2).$$

APPENDIX III. COLLISION OF A CHARGED PARTICLE WITH A BOUND ELECTRON[13]

When a charged particle (total energy U_0, momentum p_0, velocity β_0,[14] mass m, charge ze) collides with a free electron (mass m_e) at rest, the probability that the electron acquire an energy E_e in dE_e is given by the well-known Rutherford-type cross section:

$$d\sigma=2\sigma_0 z^2 f m_e dE_e/\beta_0^2 E_e^2, \tag{1}$$

where f is a factor of the order unity, provided that the energy E_e of the electron does not exceed the maximum value E_m, consistent with conservation of energy and momentum.

If the electron is originally bound in an atom this limitation does not apply and the electron can acquire an energy in excess of E_m while the atom recoils. We have calculated the cross section for such a collision by the usual perturbation methods, considering the electron to be originally in an s orbit and neglecting the binding energy and the recoil energy compared to other energies. The result can be expressed in the form of Eq. (1) with

$$f=\frac{64}{\pi}m_e^2E_e^2p_B^5\int_{p_0-p_F}^{p_0+p_F}\frac{dq}{(q^2-E_e^2)^2}$$
$$\times\int_{|q-p_e|}^{q+p_e}\frac{sds}{(s^2+p_B^2)^4}F(s,q), \tag{2}$$

where the subscript F refers to the motion of the incident particle after collision, $B=p_B^2/2m_e$ is the binding energy of the electron, q is the momentum transferred by the incident particle (i.e., $\mathbf{q}=\mathbf{p}_0-\mathbf{p}_F$) and s is the recoil momentum of the atom.

[13] The author is indebted to G. F. Chew for a discussion of this problem in the nonrelativistic limit.

[14] We use units such that $c=1$.

The function F is given by

$$F(s,q)=1-\beta_0^2E_e/E_m+\tfrac{1}{2}[(U_0+U_F)/2U_0]^2 [(q^2+s^2-p_e^2)/q^2](E_e/m_e)+\delta,$$

$$\delta=(4m_e^2+p_e^2-q^2)E_e/8m_eU_0^2 \text{ for spin 0,} \quad (3)$$

$$\delta=\{(4m_eE_e-s^2)E_e+(q^2-p_e^2)(E_e-2m_e)\}/8m_eU^2 \text{ for spin } \tfrac{1}{2}.$$

The term δ, which depends on the spin of the incident particle, is negligible unless the energy of the electron is comparable to the energy of the incident particle. The integration of Eq. (2) leads to very unwieldy expressions and is best performed numerically. As a check one can easily verify that in the limit $B=0$, f goes over into the well-known expressions of Bhabha.[15]

[15] H. J. Bhabha, Proc. Roy. Soc. (London) **A164**, 247 (1938).

PHYSICAL REVIEW VOLUME 90, NUMBER 6 JUNE 15, 1953

The Production of Heavy Mesons

L. S. KOTHARI*
Cavendish Laboratory, Cambridge, England
(Received February 24, 1953)

Using Fermi's theory of multiple production, the production of heavy mesons in a nucleon-nucleon collision (with primary energy $<20Mc^2$) is studied. One obtains the result that heavy mesons should be produced singly about 10 times more frequently than in pairs. Creation of mesons in a meson-nucleon collision is also considered, and it is found that mesons of energy $E<Mc^2$ would, most likely, pass through nuclear matter without further creation of mesons, while for $E>2Mc^2$ the probability of multiplication is large. In a qualitative way, the results deduced seem to agree rather well with experiments.

I. INTRODUCTION

RECENTLY a number of different theories have been developed to explain the multiple production of mesons in nucleon-nucleon collisions,[1] for which quite convincing evidence now exists. Fermi[2] has proposed a theory based upon statistical considerations which seems to be in fair agreement with the experimental data so far obtained. We propose to consider here the production of heavy mesons of the basis of his theory.[3] Application of Fermi's theory to this problem implies the assumption that the heavy mesons—like the π-mesons—are "strongly" coupled to the nucleons. This assumption is fairly well born out by experiment.[4]

In the next section, the production of heavy mesons in a nucleon-nucleon collision is considered. Meson-nucleon collisions are studied in a later section. Though we have confined ourselves mainly to primary energies $E<20Mc^2$, in the last section extremely high energy collisions have also been briefly discussed.

II. NUCLEON-NUCLEON COLLISION

In high energy collisions between nucleons the production of mesons heavier than π-mesons is well established. Using Fermi's theory, we calculate the probability for the creation of a heavy meson in a collision process. The collision is studied in the center-of-mass system of the colliding particles, and it is assumed that W, the total energy in the center-of-mass system, is suddenly released in a small volume Ω,

$$\Omega=4\pi/3(\hbar/\mu c)^3(2Mc^2/W), \quad (1)$$

surrounding the nucleons. (M is the mass of the nucleon and μ is the mass of the π-meson.) One then calculates statistically the probability that a certain number of mesons are present in the final state.

With a suitable modification of Fermi's result [Eqs. (20) and (21) of reference 2], we find that the probability for r nucleons, s heavy mesons (of mass κ), and n π-mesons being present in the final state of the collision is given by

$$P(r,s,n)=\frac{2r^{\frac{1}{2}}}{(r+s)^{\frac{1}{2}}}\frac{(29.3/\omega)^{s/2}}{\alpha!}\left\{\frac{6.31}{\omega^{\frac{1}{4}}}(\omega-r-\tfrac{2}{3}s)\right\}^{\alpha} \times\exp\left\{-\frac{6.31}{\omega^{\frac{1}{4}}}(\omega-r)\right\}, \quad (2)$$

where

$$\alpha=\{3n+\tfrac{3}{2}(r+s)-\tfrac{5}{2}\},$$

$\omega=W/Mc^2$, and we have taken $\kappa/M=\frac{2}{3}$, $\mu/M=0.15$. In deriving the above result the nucleons and the heavy mesons have been treated in the nonrelativistic approximation, whereas the π-mesons have been treated in the extreme relativistic approximation. Further, the conservation of angular momentum has not been con-

* On Government of India scholarship.

[1] See Lewis, Oppenheimer, and Wouthuysen, Phys. Rev. **73**, 127 (1948); W. Heisenberg, Z. Physik **126**, 509 (1949); K. A. Brueckner, Phys. Rev. **82**, 590 (1951); R. Glauber, Phys. Rev. **84**, 395 (1951); see also H. W. Lewis, Revs. Modern Phys. **24**, 241 (1953).

[2] E. Fermi, Progr. Theoret. Phys. (Japan) **5**, 570 (1950).

[3] L. S. Kothari, Jr., Nature **171**, 309 (1953).

[4] A. Pais, Phys. Rev. **86**, 663 (1952).

sidered, and the spins of the particles have been neglected.

In a nucleon-nucleon collision $r=2$ (neglecting nucleon pair production). Taking this value for r, we have from Eq. (2)

$$P(2,s,n)=\frac{8.5}{(2+s)^{\frac{1}{2}}}\frac{(29.3/\omega)^{s/2}}{[(6n+3s+1)/2]!}\times\left\{\frac{6.31}{\omega^{\frac{1}{2}}}(\omega-2-\tfrac{2}{3}s)\right\}^{(6n+3s+1)/2}\times\exp\left\{-\frac{6.31}{\omega^{\frac{1}{2}}}(\omega-2)\right\}. \quad (3)$$

The result calculated from this formula is given in Table I.

It will be noticed that in collisions involving primary energies up to about $20Mc^2$, the possibility of a heavy meson being observed is fairly small, though very much within the experimental reach. In nucleon-nucleus collisions the probability of observing a heavy meson will be still less, because of the fact that the heavy meson in colliding with other nucleons inside the nucleus will, most likely, change over into a π-meson. This point is discussed further in Sec. IV.

The slightly higher ratio of heavy mesons to π-mesons near the threshold energy for the creation of a heavy meson will also be observed. This arises because, according to this theory, the probability of creation of a heavy meson varies more slowly with increasing energy than does the average number of π-mesons created.

The heavy mesons will mostly be created singly, though in some collisions one may expect to get two or more of them. For primary energies in the neighborhood of $15Mc^2$, the ratio of the number of collisions in which a single heavy meson is produced to those in which a pair of heavy mesons appear would be nearly 10.

III. MESON-NUCLEON COLLISIONS

Another related problem, which is of importance, is the production of mesons in a meson-nucleon collision. Apart from the fact that this type of process has been observed in photographic emulsions,[5] it is of importance in considering nucleon-nucleus collisions. If the nucleus considered is heavy, the π-mesons produced inside the nucleus in a single event would multiply still further when they interact with other nucleons present.

The initial meson responsible for the collision may be either a π-meson or a heavy meson. We assume, however, that in the final state no heavy meson is emitted. (If in the final state a heavy meson is also present then, since we are neglecting the spins of the particles, the result for a given ω would not be much different from that of a nucleon-nucleon encounter. Some difference would arise, however, when we transform ω back into the energy of the primary particle in the laboratory frame.) This assumption implies that, for the same total energy in the center-of-mass system, the collision process is independent of the primary meson. However, when we calculate the energy of the incoming meson in the laboratory frame from a given total energy in the center-of-mass system, the two types of mesons would give different results.

The probability, that in the final state of collision, we have 1 nucleon and $(1+n)$ π-mesons is given by

$$P(1,1+n)=\frac{3}{[(6n+7)/2]!}\left\{6.31\frac{\omega-1}{\omega^{\frac{1}{2}}}\right\}^{(6n+7)/2}\times\exp\left(-6.31\frac{\omega-1}{\omega^{\frac{1}{2}}}\right), \quad (4)$$

where n represents the number of π-mesons created in the collision. The nucleon has again been considered in the nonrelativistic approximation and the π-mesons in the extreme relativistic approximation. Table II gives, for various total energies ω, the relative probabilities for different number of mesons being produced, as calculated from Eq. (4).

On comparing these results with those of Fermi, one finds that for a given ω, the average number of mesons produced is more in the meson-nucleon collision than in the nucleon-nucleon collision. Thus, at these comparatively low energies, the multiplicity of mesons produced in a collision depends upon the nature of the primary particle. One also observes that incident mesons with energy $E<Mc^2$ will, on the whole, not produce any further mesons in a collision with a nucleon. However, the probability for mesons of energy $E>2Mc^2$ to lead to the creation of further mesons is fairly high. This seems to agree rather well with experiment.[5]

TABLE I. The relative probability for the production of heavy mesons in a nucleon-nucleon collision. ω' is the energy of the primary particle in the laboratory system divided by Mc^2. $\bar{n}_i$ $(i=0, 1, 2\cdots)$ is the average number of π mesons produced when i heavy mesons are also created in the collision. $\Sigma_n P(r,n)$, $(r=0, 1, 2)$ is the probability for the production of r heavy mesons. $\Sigma_n P(0,n)$ has been taken to be 100. σ is the ratio of heavy mesons to π-mesons produced in the collision. The other symbols are defined in the text.

ω	ω'	$\bar{n}_0$	$\Sigma_n P(1,n)$	$\bar{n}_1$	$\Sigma_n P(2,n)$	$\bar{n}_2$	σ
3	3.5	1.2	7				~1/17
4	7.0	2.5	9	1.0	0.5	0	1/26
5	11.5	3.5	11	2.2	1.2	0.9	1/28
6	16.9	4.4	12	2.3	1.4	1.8	1/31

IV. DISCUSSION

So far, we have considered mainly nucleon-nucleon or meson-nucleon collisions. If an incident nucleon collides with a nucleus, then besides multiple production, plural

[5] J. G. Wilson, *Progress in Cosmic Ray Physics* (North-Holland Publishing Company, Amsterdam, 1952), Chap. I.

production of mesons would also play a great role. In a "light" nucleus the probability of a daughter meson colliding with another nucleon inside the nucleus is comparatively small, and one would not expect much deviation from the results predicted by the multiple theory. In "heavy" nuclei, the case is different. If one assumes that in a single multiple collision the total energy is equally shared between the various particles in the center-of-mass system, then the heavy mesons have a rather small chance of coming out of the nucleus. In a subsequent collision, the probability of their transforming themselves into π-mesons is fairly large. Thus, for primary energies in the neighborhood of $15Mc^2$ it seems that one should expect a larger number of heavy mesons to come from collisions of a nucleon with the lighter nuclei.

The recoil nucleons may also produce further mesons in subsequent collisions, but for the energy range that we have considered, these will not be very significant.

Though we have so far confined ourselves to the energy region in which nucleons can be treated in the nonrelativistic approximation, it is of interest to note a few points about the high energy region, where the heavy mesons and the nucleons also have to be treated in the extreme relativistic approximation. It follows from thermodynamic considerations[2] that the ratio of the number of heavy mesons to the number of π-mesons produced in any collision is governed only by the ratio of their respective statistical weight factors. If the heavy meson has spin 1, then this ratio is $9/3=3$. For a scalar heavy meson this ratio would be $3/3=1$. The possibility of determining the spin of the heavy particle by studying the collisions appears, however, to be very small. The collisions usually observed are of the nucleon-nucleus type and are far more complicated than the simple nucleon-nucleon collisions which we have considered.

A further point to observe is that in these energy regions the final result of the collision does not depend upon the nature of the primary particle. Thus the heavy mesons could very well be produced in a collision between a high energy π-meson and a nucleon. There is some experimental evidence to show that such processes actually do occur.[6]

TABLE II. The relative probabilities for different number of mesons being produced in a meson-nucleon collision. According as the incident particle is a π-meson or a heavy meson, ω' or ω'' give the energy of the primary particle in the laboratory frame of reference, divided by Mc^2. $\bar{n}$ represents the average number of mesons created.

ω	ω'	ω''	$n=0$	1	2	3	4	5	6	$\bar{n}$
1.25	0.3		98	2						0
1.5	0.6		89	11	0					0.1
1.75	1.0	0.8	70	27	3					0.3
2.0	1.5	1.3	50	40	9	1				0.6
2.5	2.6	2.4	20	48	26	6	0			1.1
3.0	4.0	3.8	8	34	38	16	4	0		1.7
4.0	7.5	7.3	1	10	30	33	19	6	1	2.8

[6] Leighton, Wanlass, and Anderson, Phys. Rev. **89**, 148 (1953).

The Continuum in Special Relativity. II

BORIS LEAF
Department of Physics, Kansas State College, Manhattan, Kansas
(Received September 8, 1952)

A covariant description is given of the properties, relative to an arbitrary secondary frame, of an element of anisotropic continuum composed of a single chemical species. These properties are measured by an observer in a primary reference frame relative to which the motion of the secondary frame is constant. This is a generalization of an earlier formalism in which the secondary frame coincided with the rest frame of the element. The equation of continuity of mass in the classical sense is formulated, and Gauss' theorem for transformation of volume integrals of space divergences into surface integrals is stated for the secondary reference frame. If the equation of motion relative to the secondary frame is assumed given by the statement that the divergence in the secondary frame of the energy-momentum tensor vanishes, then the equation for the first law of thermodynamics, the equation of continuity of energy, the dynamical equations of motion including the force equation and the kinetic energy equation, and the equation of continuity of momentum result; each equation is formulated for motion of an element of continuum relative to an arbitrary secondary frame as measured by a primary observer. The divergence in the secondary frame of the entropy tensor is assumed to be a time vector whose projection upon the four-vector velocity of the element relative to the primary frame is non-negative; this is shown to imply the second law of thermodynamics relative to the secondary frame, and, in the reversible case, an equation of continuity of entropy. The equation defining the reversible stress in the element of continuum is introduced. The chemical potential function which appears in this equation has the properties of the specific Helmholtz free energy in the thermodynamic consequences of this equation and the properties of the specific Gibbs free energy in the dynamical consequences, a circumstance which obviates the necessity of formulating a Gibbs free energy for anisotropic media. The conditions for reversibility of a process in the continuum are found to be independent of the secondary reference frame chosen for description of the process. Finally, a covariant theory of transport processes is given for a one-component, anisotropic medium. It is shown that in the theory of diffusion and thermal conduction the motion of every element of the continuum must satisfy a special transport condition relative to a secondary frame; in the theory of viscosity this condition need not be met.

A. MATHEMATICAL FORMALISM

IN a preceding paper,[1] a formalism was developed for resolving four-dimensional tensors into space and time components by means of the unit space tensor $\bar{\bar{\delta}}_{\sigma\tau}$ and unit time vector $\hat{u}_\sigma$. We consider the case of two reference frames, one attached momentarily to the physical system whose properties are to be measured, the rest frame, and the other a frame relative to which the rest frame has a four-velocity $u_\sigma = c\hat{u}_\sigma$, where c is the speed of light. We call the latter frame a primary frame. Any four-vector whose components in the rest frame are $P_\sigma{}^0$ will have co nponents in the primary frame,

$$P_\sigma = L_{\sigma\tau} P_\tau{}^0. \tag{1}$$

$L_{\sigma\tau}$ is the general Lorentz transformation.

The transformation $L_{\sigma\tau}$ may be expressed as

$$L_{\sigma\tau} = A_{\sigma\mu} l_{\mu\nu} A_{\tau\nu}{}^0. \tag{2}$$

If the velocity in space of the rest frame relative to the primary frame is represented by the three-vector $\mathbf{v}$, then the matrices on the right side of Eq. (2) have the following meanings: $A_{\tau\nu}{}^0$ is an orthogonal space rotation with Euler angles θ^0, ϕ^0, ψ^0 which transforms a coordinate system in the rest frame whose Z^0 axis is parallel to $\mathbf{v}$ into an arbitrarily oriented coordinate system in the rest frame; $A_{\sigma\mu}$ is a similar rotation with Euler angles θ, ϕ, ψ which transforms a coordinate system in the primary frame whose Z axis is parallel to $\mathbf{v}$ into an arbitrarily oriented coordinate system in the primary frame; $l_{\mu\nu}$ is a simple Lorentz transformation from a coordinate system in the rest frame whose Z^0 axis is parallel to $\mathbf{v}$ to a coordinate system in the primary frame whose Z axis is parallel to $\mathbf{v}$. Accordingly, $L_{\sigma\tau}$ transforms one arbitrarily oriented coordinate system in the rest frame into another arbitrarily oriented coordinate system in the primary frame.

In Paper I, we used the Hermitian matrix $a_{\sigma\tau}$ of Abraham and Becker in place of $L_{\sigma\tau}$. It may be obtained as a special case of $L_{\sigma\tau}$ by letting $\theta=\theta^0$, $\phi=\phi^0$, $\psi=\psi^0$. However, $a_{\sigma\tau}$ does not possess the group property under conditions general enough for our purposes. In fact, if $a_{\sigma\tau}'$ and $a_{\sigma\tau}{}^*$ represent successive transformations associated with relative velocities $\mathbf{v}'$ and $\mathbf{v}^*$, their product cannot be written as a single transformation $a_{\sigma\tau}$ associated with a velocity $\mathbf{v}$ unless the velocities $\mathbf{v}'$, $\mathbf{v}^*$ and $\mathbf{v}$ are parallel. The generality of $a_{\sigma\tau}$ over the simple Lorentz transformation $l_{\sigma\tau}$ consists only in the fact that whereas the direction of $\mathbf{v}'$, $\mathbf{v}^*$, and $\mathbf{v}$ in the former case is unspecified, in the latter case it must coincide with the common direction of the Z axes of the three reference frames involved. In addition, in either case, as is well known, the magnitude of $\mathbf{v}$ must be obtained from that of $\mathbf{v}'$ and $\mathbf{v}^*$ by the Einstein addition law.

The requirement that the general Lorentz matrix $L_{\sigma\tau}$ possess the group property imposes the following conditions on the velocities: Let β' be the magnitude of the velocity $\mathbf{v}'$ of the first reference frame relative to a second frame, β^* be the magnitude of the velocity $\mathbf{v}^*$ of the second frame relative to a third frame, and β be the magnitude of the resultant velocity $\mathbf{v}$ of the first frame relative to the third frame, all magnitudes measured in

[1] B. Leaf, Phys. Rev. **84**, 345 (1951) (referred to in the following as Paper I).

units of the speed of light. Then,

$$(1)\quad \beta/(1-\beta^2)^{\frac{1}{2}}=(\beta^{*2}+\beta'^2+2\beta^*\beta'\cos\theta_2 -\beta^{*2}\beta'^2\sin^2\theta_2)^{\frac{1}{2}}/(1-\beta^{*2})^{\frac{1}{2}}(1-\beta'^2)^{\frac{1}{2}}.$$

Here θ_2 is the angle between $\mathbf{v}'$ and $\mathbf{v}^*$ as measured by an observer in the second frame. If $\theta_2=0$, this equation reduces to the Einstein addition law. This relation is the relativistic form of the trigonometric law of cosines, to which it reduces for small velocities.

$$(2)\quad \sin\theta_2(1-\beta^2)^{\frac{1}{2}}/\beta=\sin\theta_1(1-\beta^{*2})^{\frac{1}{2}}/\beta^* =-\sin\theta_3(1-\beta'^2)^{\frac{1}{2}}/\beta'.$$

Here θ_1 is the angle between $\mathbf{v}$ and $\mathbf{v}'$ as measured by an observer in the first frame; θ_3 is the angle between $\mathbf{v}$ and $\mathbf{v}^*$ as measured by an observer in the third frame. This relation is the relativistic form of the law of sines.

(3) We also have the relationships:

$$\cos\theta_2=\cos\theta_1\cos\theta_3+\sin\theta_1\sin\theta_3/(1-\beta^2)^{\frac{1}{2}},$$
$$\sin\theta_2/(1-\beta^{*2})^{\frac{1}{2}}=-\cos\theta_1\sin\theta_3+\sin\theta_1\cos\theta_3/(1-\beta^2)^{\frac{1}{2}},$$
$$\sin\theta_2/(1-\beta'^2)^{\frac{1}{2}}=\cos\theta_3\sin\theta_1-\sin\theta_3\cos\theta_1/(1-\beta^2)^{\frac{1}{2}},$$

which reduces for small velocities to well-known trigonometric equations for $\theta_1=\theta_2+\theta_3$.

(4) As in the classical case, the vector $\mathbf{v}$ must be coplanar with $\mathbf{v}'$ and $\mathbf{v}^*$.

In Paper I the group property was not essentially employed so that the results appearing there are not significantly affected by the use of the Abraham and Becker transformation $a_{\sigma\tau}$ in place of $L_{\sigma\tau}$. Only Eqs. (23) and (24) of Paper I depend on the particular transformation matrix used, and must be modified for the general case. In the present paper we shall utilize the group property in an essential way and will, therefore, require $L_{\sigma\tau}$. The transformation $L_{\sigma\tau}$ is orthogonal but not, in general, Hermitian. Its determinant equals unity.

Let us return to the case of two reference frames, the rest frame and the primary frame. Introducing the unit vectors in the rest frame,

$$\bar{\imath}_\sigma{}^0=(1,0,0,0)\quad \bar{\jmath}_\sigma{}^0=(0,1,0,0),$$
$$\bar{k}_\sigma{}^0=(0,0,1,0),\quad \hat{u}_\sigma{}^0=(0,0,0,i),$$

into Eq. (1), we find their values in the primary frame,

$$\bar{\imath}_\sigma=L_{\sigma 1},\quad \bar{\jmath}_\sigma=L_{\sigma 2},\quad \bar{k}_\sigma=L_{\sigma 3},\quad \hat{u}_\sigma=iL_{\sigma 4}.$$

Accordingly, $u_\sigma=icL_{\sigma 4}$, and we find, on using the values of $L_{\sigma 4}$ given by Eq. (2), that

$$u_k=v_k(1-v^2/c^2)^{-\frac{1}{2}}\text{ for }k=1,2,3,\text{ and }u_4=ic(1-v^2/c^2)^{-\frac{1}{2}}. \tag{3}$$

In terms of unit vectors, the Kronecker delta $\delta_{\sigma\tau}$ and the unit space tensor $\bar{\delta}_{\sigma\tau}$ become

$$\delta_{\sigma\tau}=\bar{\delta}_{\sigma\tau}-\hat{u}_\sigma\hat{u}_\tau,\quad \bar{\delta}_{\sigma\tau}=\bar{\imath}_\sigma\bar{\imath}_\tau+\bar{\jmath}_\sigma\bar{\jmath}_\tau+\bar{k}_\sigma\bar{k}_\tau. \tag{4}$$

In Paper I, we defined the space component of a vector P_σ as $\bar{\delta}_{\sigma\tau}P_\tau$ an the time component as $-\hat{u}_\sigma\hat{u}_\tau P_\tau$. Since

$$\bar{\delta}_{\sigma\tau}P_\tau=\bar{\imath}_\sigma P_1{}^0+\bar{\jmath}_\sigma P_2{}^0+\bar{k}_\sigma P_3{}^0=L_{\sigma k}P_k{}^0,$$

we see that the space component of P_σ is the value of $(P_1{}^0, P_2{}^0, P_3{}^0, 0)$ after Lorentz transformation; it is the space component of P_σ relative to the rest frame as measured by a primary observer. Similarly, since

$$-\hat{u}_\sigma\hat{u}_\tau P_\tau=-i\hat{u}_\sigma P_4{}^0=L_{\sigma 4}P_4{}^0,$$

the time component of P_σ is the value of $(0,0,0,P_4{}^0)$ after Lorentz transformation; it is the time component of P_σ relative to the rest frame as measured by a primary observer.

Let us consider some examples of space and time components. If x_σ is the position vector of an element of the physical system along its trajectory as measured by a primary observer, then

$$x_\sigma-x_\sigma(0)=L_{\sigma\tau}x_\tau{}^0=\bar{\imath}_\sigma x_1{}^0+\bar{\jmath}_\sigma x_2{}^0+\bar{k}_\sigma x_3{}^0-i\hat{u}_\sigma x_4{}^0, \tag{5}$$

where $x_\sigma(0)$ is the initial position of the origin of the coordinate system in the rest frame as measured by the primary observer, and $x_\sigma{}^0$ is the position vector of the element relative to a coordinate system in the rest frame. The time component of $x_\sigma-x_\sigma(0)$ is $-i\hat{u}_\sigma x_4{}^0=u_\sigma t^0$; the space component, $\bar{\imath}_\sigma x_1{}^0+\bar{\jmath}_\sigma x_2{}^0+\bar{k}_\sigma x_3{}^0$. It may be observed that the whole trajectory is plotted by the primary observer who uses a single coordinate system in the primary frame, but not by the succession of rest observers each of whom records only one position of the element along the trajectory. The coordinate systems which the rest observers employ need have no relation to each other either in point of origin or in orientation in space. Any vector having components $P_\sigma{}^0$ in such an arbitrary coordinate system of a rest frame will have components P_σ as measured by a primary observer when the appropriate value of $L_{\sigma\tau}$ is used in Eq. (1).

Despite the arbitrary variability of $x_\sigma{}^0$ along the trajectory according to the rest observers' choices of origin and orientation of coordinate systems, the change in $x_\sigma{}^0$ as the physical system moves relatively to any one such coordinate system may be defined. This is the change in position along the tangent at a point on the trajectory as measured by a rest observer at that point using a single coordinate system. Thus

$$dx_k{}^0=0\text{ for }k=1,2,3;\quad dx_4{}^0=icdt^0.$$

The corresponding change in dx_σ along the tangent, measured by the primary observer, is obtained by differentiating Eq. (5). We find

$$dx_\sigma=u_\sigma dt^0. \tag{6}$$

The "proper" time interval dt^0 is read on a clock fixed in the rest frame. Since $dx_4=icdt$, we see that

$$dt=-i\hat{u}_4dt^0=(1-v^2/c^2)^{-\frac{1}{2}}dt^0. \tag{7}$$

Consequently, $dx_k=u_k(1-v^2/c^2)^{\frac{1}{2}}dt$ for $k=1,2,3$. Comparison with Eq. (3) gives $v_k=dx_k/dt$. The time interval

dl is measured as the difference in readings of two synchronized clocks fixed in the primary frame, one at the initial point, the other at the final point of the displacement dx_k. Accordingly, dl is an interval associated with the trajectory.

The four-vector velocity $u_\sigma = dx_\sigma/dl^0$ is itself a time vector since $\bar{\delta}_{\sigma\tau}u_\tau = 0$. The space component of velocity of an object relative to its own rest frame is zero when measured by any primary observer. The four-vector acceleration du_σ/dl^0 is a space vector, since $u_\sigma du_\sigma/dl^0 = 0$. The time component of acceleration of an object relative to its own rest frame is zero when measured by any primary observer.

The symbol ∂_σ represents the gradient operator, whose time and space components are $-\hat{u}_\sigma\hat{u}_\tau\partial_\tau$ and $\bar{\delta}_{\sigma\tau}\partial_\tau$. The factor $u_\tau\partial_\tau$ in the time component is the operator, $d/dl^0 = u_\tau\partial_\tau$. This operator was designated as $d/d\tau$ in Paper I, but we shall reserve this symbol for a more general operator defined in Eq. (20) of which this is a special case.

In Paper I, any symmetric, second-order tensor $\psi_{\sigma\tau}$ was resolved as follows

$$\psi_{\sigma\tau} = -(1/c^2)(\chi_{\rho\rho}u_\sigma u_\tau + u_\sigma Q_\tau + u_\tau Q_\sigma) + \phi_{\sigma\tau}, \qquad (8)$$

where the combinations of space and time components for each tensor index are

$$\begin{aligned}
\phi_{\sigma\tau} &= \bar{\delta}_{\sigma\mu}\bar{\delta}_{\tau\nu}\psi_{\mu\nu},\\
-u_\tau Q_\sigma/c^2 &= \bar{\delta}_{\sigma\mu}(-\hat{u}_\tau\hat{u}_\nu)\psi_{\mu\nu},\\
-u_\sigma Q_\tau/c^2 &= -\hat{u}_\sigma\hat{u}_\mu\bar{\delta}_{\tau\nu}\psi_{\mu\nu},\\
\chi_{\rho\rho}\hat{u}_\sigma\hat{u}_\tau &= (-\hat{u}_\sigma\hat{u}_\mu)(-\hat{u}_\tau\hat{u}_\nu)\psi_{\mu\nu}.
\end{aligned}$$

Here, if we identify $\psi_{\sigma\tau}$ as the energy-momentum tensor, we find that Q_σ and $\phi_{\sigma\tau}$ are the components of heat flux and stress relative to the rest frame as measured by a primary observer, whereas $\chi_{\rho\rho}$ is the scalar invariant energy density relative to the rest frame, (i.e., nonkinetic energy) which will appear the same to any primary observer.

In all the resolutions of vectors and tensors into space and time components which we have performed up to this point, we have in every case obtained the components relative to the rest frame as measured by the primary observer. But in many physical experiments the primary observer does not measure the properties of an element of continuum relative to the rest frame of the element, but relative to some other arbitrary frame. We call such a frame a secondary frame. Let the secondary frame have a three-vector velocity $\mathbf{v}^*$ relative to the primary frame as measured by a primary observer; and let the rest frame have a three-vector velocity $\mathbf{v}'$ relative to the secondary frame as measured by a secondary observer. Then, subject to the conditions stated previously on the magnitude and direction of the resultant velocity $\mathbf{v}$ of the rest frame relative to the primary frame, we may write the group property of the Lorentz transformation $L_{\sigma\tau}$ of Eq. (2) as

$$L_{\sigma\tau} = L_{\sigma\rho}{}^*L_{\rho\tau}{}'. \qquad (9)$$

The transformation $P_\sigma{}' = L_{\sigma\tau}{}'P_\tau{}^0$ gives the values $P_\sigma{}'$ of measurements made upon the rest frame by a secondary observer and $P_\sigma = L_{\sigma\tau}{}^*P_\tau{}'$ gives the values P_σ of measurements made upon the rest frame by a primary observer. Also

$$P_\sigma{}^* = L_{\sigma\tau}{}^*P_\tau{}^0 \qquad (10)$$

gives the values $P_\sigma{}^*$ of measurements made by the primary observer upon physical systems at rest in the secondary frame. Introducing the unit vectors in the secondary frame, $\bar{\imath}_\sigma{}^0$, $\bar{\jmath}_\sigma{}^0$, $\bar{k}_\sigma{}^0$, $\hat{u}_\sigma{}^0$, into Eq. (10) we find their values in the primary frame, $\bar{\imath}_\sigma{}^* = L_{\sigma 1}{}^*$, $\bar{\jmath}_\sigma{}^* = L_{\sigma 2}{}^*$, $\bar{k}_\sigma{}^* = L_{\sigma 3}{}^*$, $\hat{u}_\sigma{}^* = iL_{\sigma 4}{}^*$. The four-vector velocities $u_\sigma{}'$ and $u_\sigma{}^*$ are related to the corresponding three-vector velocities $\mathbf{v}'$ and $\mathbf{v}^*$ by equations similar to Eq. (3). We may now write the Kronecker delta $\delta_{\sigma\tau}$ and a unit relative space tensor $\bar{\delta}_{\sigma\tau}{}^*$ as

$$\delta_{\sigma\tau} = \bar{\delta}_{\sigma\tau}{}^* - \hat{u}_\sigma{}^*\hat{u}_\tau{}^*, \quad \bar{\delta}_{\sigma\tau}{}^* = \bar{\imath}_\sigma{}^*\bar{\imath}_\tau{}^* + \bar{\jmath}_\sigma{}^*\bar{\jmath}_\tau{}^* + \bar{k}_\sigma{}^*\bar{k}_\tau{}^*, \quad (11)$$

and define the relative space component of P_σ as $\bar{\delta}_{\sigma\tau}{}^*P_\tau$ and the relative time component as $-\hat{u}_\sigma{}^*\hat{u}_\tau{}^*P_\tau$. We readily find that

$$\begin{aligned}
\bar{\delta}_{\sigma\tau}{}^*P_\tau &= \bar{\imath}_\sigma{}^*P_1{}' + \bar{\jmath}_\sigma{}^*P_2{}' + \bar{k}_\sigma{}^*P_3{}' = L_{\sigma k}{}^*P_k{}',\\
-\hat{u}_\sigma{}^*\hat{u}_\tau{}^*P_\tau &= -i\hat{u}_\sigma{}^*P_4{}' = L_{\sigma 4}{}^*P_4{}'.
\end{aligned}$$

Thus $\bar{\delta}_{\sigma\tau}{}^*P_\tau$ is the value of the space component, $(P_1{}', P_2{}', P_3{}', 0)$, relative to the secondary frame as measured by a primary observer, and $-\hat{u}_\sigma{}^*\hat{u}_\tau{}^*P_\tau$ is the time component, $(0, 0, 0, P_4{}')$, relative to the secondary frame as measured by the primary observer. If the secondary frame and the momentary rest frame are at rest relative to each other, then we revert to the case considered previously, with $\bar{\delta}_{\sigma\tau}{}^*P_\tau = \bar{\delta}_{\sigma\tau}P_\tau$ and $-\hat{u}_\sigma{}^*\hat{u}_\tau{}^*P_\tau = -\hat{u}_\sigma\hat{u}_\tau P_\tau$. On the other hand, if the secondary frame is at rest relative to the primary frame, then the primary observer is measuring the properties of the physical system relative to his own coordinate system in the primary frame. In this case, $L_{\sigma\tau}{}^*$ becomes a mere space rotation in the primary frame, so that

$$\bar{\delta}_{\sigma\tau}{}^*P_\tau = (P_1, P_2, P_3, 0), \quad -\hat{u}_\sigma{}^*\hat{u}_\tau{}^*P_\tau = (0, 0, 0, P_4).$$

For example, let $P_\sigma = u_0$, the velocity vector. Then the relative space component, $\bar{\delta}_{\sigma\tau}{}^*u_\tau$, equals zero when the secondary frame coincides with the rest frame, but it equals $(u_1, u_2, u_3, 0)$ when the secondary frame coincides with the primary. At the same time, the relative time component, $-\hat{u}_\sigma{}^*\hat{u}_\tau{}^*u_\tau$, equals u_σ in the first case, and $(0, 0, 0, u_4)$ in the latter.

We now define the four-vector v_σ,

$$v_\sigma = u_\sigma/(-\hat{u}_\tau\hat{u}_\tau{}^*). \qquad (12)$$

The invariant quantity $-\hat{u}_\tau\hat{u}_\tau{}^*$ will appear frequently in the following and will be represented by k'. We find

$$k' = -i\hat{u}_4{}' = L_{44}{}' = (1-\beta'^2)^{-\frac{1}{2}}.$$

The relative space component of v_σ is $\bar{\delta}_{\sigma\tau}{}^*v_\tau = L_{\sigma k}{}^*v_k{}'$, which when measured by a secondary observer is equal

to $(v_1', v_2', v_3', 0)$ in which the three space components constitute the three-vector velocity $\mathbf{v}'$ of the rest frame relative to the secondary frame. The relative time component of v_σ is $-\hat{u}_\sigma^*\hat{u}_\tau^* v_\tau = u_\sigma^*$, which when measured measured by a secondary observer is equal to $(0, 0, 0, ic)$. The vector v_σ differs quantitatively from u_σ only by the factor $1/k'$. But a fundamental qualitative difference appears between them. In the case of u_σ it will be noted that u_σ' is the value measured by a secondary observer of the vector $u_\sigma^0 = (0, 0, 0, ic)$ associated with the rest frame. But in the case of v_σ there is no property of the rest frame which when measured by the secondary observer yields $v_\sigma' = (v_1', v_2', v_3', ic)$. When the primary observer, therefore, measures $v_\sigma = L_{\sigma\tau}^* v_\tau'$ he is measuring a property of the secondary frame. This is particularly evident in the expression for the relative time component of v_σ, $-\hat{u}_\sigma^*\hat{u}_\tau^* v_\tau = u_\sigma^*$.

We conclude this section with a result which we shall find very useful. If A_σ is a space vector and B_σ a time vector, then

$$(\bar{\delta}_{\sigma\rho}^* A_\rho)(\bar{\delta}_{\sigma\tau}^* B_\tau) + (-\hat{u}_\sigma^*\hat{u}_\rho^* A_\rho)(-\hat{u}_\sigma^*\hat{u}_\tau^* B_\tau) = 0,$$

so that

$$A_\rho \hat{u}_\rho^* = \bar{\delta}_{\sigma\rho}^* A_\rho B_\sigma / B_\tau \hat{u}_\tau^*,$$

or

$$A_\rho u_\rho^* = -\bar{\delta}_{\sigma\rho}^* A_\rho v_\sigma. \tag{13}$$

B. EQUATION OF CONTINUITY AND GAUSS' THEOREM

The secondary frames used in physical experiments have certain special properties which we now formulate. While the velocity u_σ of the rest frame relative to the primary may vary in space because of the differing velocities of the various elements of the physical system relative to the primary, and may vary in time because of the acceleration of these elements, this is not the case for a secondary frame. The velocity u_σ^* of the secondary frame relative to the primary must have the same value throughout space; that is, the secondary frame is a rigid reference frame. A necessary condition for the uniformity in space of u_σ^* is $\bar{\delta}_{\rho\tau}^* \partial_\tau^* u_\sigma^* = 0$. We shall require also that the secondary frame be unaccelerated, so that $\hat{u}_\tau^* \partial_\tau^* u_\sigma^* = 0$. These two conditions imply that

$$\partial_\rho^* u_\sigma^* = 0 \quad \text{and} \quad \partial_\sigma^* \bar{\delta}_{\sigma\tau}^* = 0. \tag{14}$$

The gradient operator ∂_σ^* indicates partial differentiation with respect to x_σ^*.

A formalism was presented in Paper I according to which the basic equations of dynamics and thermodynamics for an element of continuum appear, respectively, as space and time components of the same tensor relationships. However, the space and time components were in every case the values relative to the rest frame of the element. We shall now reformulate these equations in order to obtain the laws of dynamics and thermodynamics for an element relative to a secondary frame.

Consider first the equation of continuity of mass. This equation was stated in Paper I as $\partial_\sigma \rho u_\sigma = 0$, where ρ is the scalar invariant density of rest mass per unit volume in the rest frame. We now consider instead, the equation,

$$\partial_\sigma^* \rho u_\sigma = 0. \tag{15}$$

We shall see that this equation describes conservation of rest mass in motion relative to the secondary frame as measured by any primary observer. It includes the earlier formulation as a special case when the secondary frame coincides with the rest frame.

Resolving the vectors u_σ and ∂_σ^* in Eq. (15) into relative space and time components and using Eq. (14), we find that

$$-\hat{u}_\sigma^*\hat{u}_\mu^*\partial_\mu^*(-\hat{u}_\sigma^*\hat{u}_\nu^*\rho u_\nu) = -\bar{\delta}_{\sigma\mu}^*\partial_\mu^*(\bar{\delta}_{\sigma\nu}^*\rho u_\nu),$$

or

$$\partial\rho k'/\partial\tau^* = -\bar{\delta}_{\sigma\mu}^*\partial_\mu^*\rho u_\sigma, \tag{16}$$

where we have written

$$\partial/\partial\tau^* = u_\sigma^*\partial_\sigma^*. \tag{17}$$

Comparison with the operator $u_\sigma\partial_\sigma = d/dt^0$ shows that $\partial/\partial\tau^*$ gives the rate of change with respect to time as read on a clock fixed in the secondary frame. Evidently, $u_\sigma\partial_\sigma$ and $u_\sigma^*\partial_\sigma^*$ are the same invariant operator according to the primary observer, which implies that the rate of flow of time is the same in every reference frame when measured by a clock at rest in that frame.

From Eq. (15) we also obtain

$$u_\sigma\partial_\sigma^*\rho = -\rho\partial_\sigma^* u_\sigma. \tag{18}$$

The left side of this equation can be written as

$$u_\sigma\partial_\sigma^*\rho = k'(\partial\rho/\partial\tau^* + \bar{\delta}_{\sigma\mu}^* v_\mu \partial_\sigma^*\rho).$$

It is evident that the operator,

$$d/d\tau^* = \partial/\partial\tau^* + \bar{\delta}_{\sigma\mu}^* v_\mu \partial_\sigma^* = v_\sigma\partial_\sigma^*, \tag{19}$$

is the usual hydrodynamic "mobile" time differentiation operator which follows the motion of the physical element relative to the secondary frame. We now define the operator,

$$d/d\tau = u_\sigma\partial_\sigma^* = k'd/d\tau^*. \tag{20}$$

This definition supersedes that given in Paper I where $d/d\tau$ was identified with $d/dt^0 = u_\tau\partial_\tau$, and includes it as a special case when the secondary frame coincides with the momentary rest frame.

It is important to understand the four operators, $d/d\tau^*$, $d/d\tau$, d/dt', and d/dt^0. We shall see that the two latter ones are special cases of the two former. Writing

$$v_\sigma\partial_\sigma^* = v_\sigma'\partial_\sigma^0 = \lim_{\Delta t' = 0} \Delta x_\sigma'\partial_\sigma^0/\Delta t',$$

$$u_\sigma\partial_\sigma^* = u_\sigma'\partial_\sigma^0 = \lim_{\Delta t^0 = 0} \Delta x_\sigma'\partial_\sigma^0/\Delta t^0,$$

we find that $d/d\tau^*$ expresses rate of change relative to the secondary frame along the trajectory per unit of

time interval $\Delta t'$; and $d/d\tau$, rate of change relative to the secondary frame along the trajectory per unit of time interval Δt^0. The proper time interval Δt^0 is read on a clock fixed in the rest frame, whereas $\Delta t' = k'\Delta t^0$ is the difference in readings of two synchronized clocks fixed in the secondary frame, one having the same position as the rest clock at the beginning at Δt^0; the other, the same position as the rest clock at the end of Δt^0. We may write similarly

$$d/dt' = \lim_{\Delta t'=0} \Delta x_\sigma{}^0 \partial_\sigma{}^0/\Delta t'; \quad d/dt^0 = \lim_{\Delta t^0=0} \Delta x_\sigma{}^0 \partial_\sigma{}^0/\Delta t^0.$$

Accordingly, d/dt' gives rate of change relative to the rest frame along the trajectory per unit of $\Delta t'$; and d/dt^0, rate of change relative to the rest frame along the trajectory per unit of Δt^0. Obviously $d/d\tau^*$ and $d/d\tau$ reduce to d/dt' and d/dt^0, respectively, in the special case that the secondary frame coincides with the rest frame.

The rate of dilatation of an element of continuum as it moves relatively to the secondary frame is $-d\ln\rho k'/d\tau^*$ which, according to Eqs. (16) and (19), equals $\bar{\delta}_{\sigma\tau}{}^*\partial_\sigma{}^* v_\tau$. The quantity $\rho k'$ is the density of rest mass per unit volume fixed on the secondary frame. The factor k' appears because of the Lorentz contraction of volume in motion relative to the observer. If $\rho k'$ is constant, then the dilatation rate vanishes, and $\bar{\delta}_{\sigma\tau}{}^*\partial_\sigma{}^* v_\tau = 0$. However, this does not describe the case of an incompressible material. For this case, ρ is constant which, according to Eq. (18), requires $\partial_\sigma{}^* u_\sigma = 0$; dilatation occurs at the rate $-d\ln k'/d\tau^*$.

Volume integrals of space divergences of the form $\bar{\delta}_{\sigma\tau}{}^*\partial_\sigma{}^* P_\tau$ may be transformed by Gauss' theorem into integrals over the surface enclosing the volume. In covariant form, Gauss' theorem is

$$\int_{V^*} (\bar{\delta}_{\sigma\tau}{}^*\partial_\sigma{}^* P_\tau)(-i\hat{u}_4{}^* dV^*) = \int_{\Sigma^*} P_\sigma dn_\sigma{}^*, \qquad (21)$$

where $dn_\sigma{}^* = \bar{\delta}_{\sigma\tau}{}^* dn_\tau{}^*$ is a space vector having the direction of the normal drawn outwardly to the boundary surface Σ^* and magnitude equal to an element of area of Σ^*. The invariance of $-i\hat{u}_4{}^* dV^*$ follows according to the argument given in Paper I, Eq. (72); it represents the differential volume of a region at rest in the secondary frame. The conditions of Eq. (14) upon the secondary frame are essential for this formulation; for this reason, the theorem is not applicable to an integral of a space divergence $\bar{\delta}_{\sigma\tau}\partial_\sigma P_\tau$ in the rest frame.

Forming the volume integral of Eq. (16) over a region fixed in the secondary frame and applying Gauss' theorem, we have

$$\partial m/\partial\tau^* = -\int \rho k' v_\sigma dn_\sigma{}^*, \qquad (22)$$

where $m = \int \rho k'(-i\hat{u}_4{}^* dV^*$. Equation (22) is the statement of the classical law of conservation of rest mass contained in a region V^* fixed in the secondary frame. A similar integration shows that the integral over the region V^* of the dilatation rate is equal to the surface integral $\int v_\sigma dn_\sigma{}^*$.

The symbol ρ can also be interpreted as the quantity of electrical charge per unit volume of the rest frame, in which case Eq. (15) represents the equation of continuity of charge. In a molecular theory the equation of continuity expresses conservation of number of particles rather than of rest mass or charge; conservation of the latter results from the fixed quantity of rest mass or charge per particle. It is obvious that Eq. (15) applies only when a single chemical species is considered and chemical reaction excluded, since in the course of chemical transformation the number of particles of a species is not conserved.

C. EQUATIONS OF MOTION

The basic dynamical and thermodynamic hypothesis of Paper I, $\partial_\sigma \psi_{\sigma\tau} = 0$, is replaced here by the more general assumption,

$$\partial_\sigma{}^* \psi_{\sigma\tau} = 0. \qquad (23)$$

The tensor $\psi_{\sigma\tau}$ is the energy-momentum tensor of Eq. (8) so that, accordingly,

$$\partial_\sigma{}^*[(\chi_{\rho\rho} u_\sigma + Q_\sigma)u_\tau/c^2] = \partial_\sigma{}^*(\phi_{\sigma\tau} - u_\sigma Q_\tau/c^2). \qquad (24)$$

Four equations can be obtained from Eq. (23) by equating to zero the time components and the space components of $\partial_\sigma{}^*\psi_{\sigma\tau}$ relative to the rest frame and the secondary frame. We consider these in turn.

Multiplying Eq. (24) by $-u_\tau$, we obtain the time component equation relative to the rest frame,

$$\partial_\sigma{}^*(\chi_{\rho\rho} u_\sigma + Q_\sigma) = \phi_{\sigma\tau}\partial_\sigma{}^* u_\tau - (Q_\tau/c^2)(du_\tau/d\tau). \qquad (25)$$

Resolving the gradient operator into space and time components, and using Eq. (13), we find

$$\begin{aligned}(\partial/\partial\tau^*)(\chi_{\rho\rho}k' + \bar{\delta}_{\sigma\tau}{}^* Q_\sigma v_\tau/c^2) + \bar{\delta}_{\sigma\tau}{}^*\partial_\sigma{}^*(\chi_{\rho\rho}u_\tau + Q_\tau) \\ = (1/c^2)(\bar{\delta}_{\sigma\rho}{}^* v_\rho \phi_{\sigma\tau} - k' Q_\tau)(\partial u_\tau/\partial\tau^*) \\ + (\phi_{\sigma\tau} - k' Q_\tau v_\sigma/c^2)\bar{\delta}_{\sigma\rho}{}^*\partial_\rho{}^* u_\tau. \qquad (25')\end{aligned}$$

Neglecting terms which vanish in the classical limit, $c \to \infty$, we recognize the first law of thermodynamics relative to a secondary frame. On the left side appear the rate of increase of energy density $\chi_{\rho\rho}k'$ which is the rest energy per unit volume in the secondary frame, and the space divergence of the flux of heat and convected rest energy, $Q_\tau + \chi_{\rho\rho}u_\tau$. On integration over a volume fixed in the secondary frame, the integral of the space divergence term can be transformed by Gauss' theorem into the surface integral, $\int(Q_\sigma + \chi_{\rho\rho}k' v_\sigma)dn_\sigma{}^*$. On the right side appears the rate at which thermodynamic work is performed on unit volume of the secondary frame.

Multiplying Eq. (24) by $-u_\tau{}^*$, we obtain the time component equation relative to the secondary frame,

$$\partial_\sigma{}^*[k'(\chi_{\rho\rho}u_\sigma + Q_\sigma)] = \partial_\sigma{}^*[(\phi_{\sigma\tau} - u_\sigma Q_\tau/c^2)\bar{\delta}_{\tau\mu}{}^* v_\mu], \qquad (26)$$

which may be written as

$$(\partial/\partial\tau^*)[k'(\chi_{\rho\rho}k'+\bar{\delta}_{\sigma\tau}{}^*Q_\sigma v_\tau/c^2)]+\bar{\delta}_{\sigma\tau}{}^*\partial_\sigma{}^*[k'(\chi_{\rho\rho}u_\tau+Q_\tau)]$$
$$=(1/c^2)(\partial/\partial\tau^*)[(\phi_{\sigma\tau}v_\rho\bar{\delta}_{\sigma\rho}{}^*-k'Q_\tau)\bar{\delta}_{\tau\mu}{}^*v_\mu]$$
$$+\bar{\delta}_{\sigma\mu}{}^*\partial_\sigma{}^*[(\phi_{\mu\tau}-u_\mu Q_\tau/c^2)\bar{\delta}_{\tau\rho}{}^*v_\rho]. \quad (26')$$

Equation (26) has the form of a continuity equation for energy relative to a secondary frame. In the classical limit, there appear on the left side of Eq. (26′) the rate of increase of energy density, $\chi_{\rho\rho}k'/(1-\beta'^2)^{\frac{1}{2}}$ which includes the kinetic energy density relative to the secondary frame, and the space divergence of heat and convected energy flux, also augmented by the factor $k'=(1-\beta'^2)^{-\frac{1}{2}}$ as compared to the flux in the corresponding term of Eq. (25′). On the right side appears the rate at which total work, both thermodynamic and dynamical, is performed on unit volume. Equation (26) is equivalent to

$$\partial_\sigma{}^*(\psi_{\sigma\tau}u_\tau{}^*)=\partial_\sigma{}^0(ic\psi_{\sigma 4}')=0. \quad (26'')$$

Thus in Eq. (26′) the operator $\partial/\partial\tau^*$ differentiates $\psi_{44}'=-\psi_{\sigma\tau}\hat{u}_\sigma{}^*\hat{u}_\tau{}^*$.

$$\psi_{44}'=\chi_{\rho\rho}k'^2+2\bar{\delta}_{\sigma\tau}{}^*Q_\sigma u_\tau/c^2-\phi_{\sigma\tau}\bar{\delta}_{\sigma\rho}{}^*v_\rho\bar{\delta}_{\tau\mu}{}^*v_\mu/c^2.$$

It is because of Eq. (26″) that it is customary to interpret ψ_{44}' as the total energy density and $ic\psi_{m4}'$ as the three-vector of total energy flux relative to the secondary frame.[2]

Multiplying Eq. (24) by $\bar{\delta}_{\alpha\tau}$, we obtain the space component equation relative to the rest frame,

$$(1/c^2)(\chi_{\rho\rho}du_\alpha/d\tau+Q_\sigma\partial_\sigma{}^*u_\alpha)=K_\alpha, \quad (27)$$

where K_α is a Minkowski force density,

$$K_\alpha=\bar{\delta}_{\alpha\tau}\partial_\sigma{}^*(\phi_{\sigma\tau}-u_\sigma Q_\tau/c^2). \quad (28)$$

Obviously, K_α is a space vector, so that $K_\alpha u_\alpha=0$ and, according to Eq. (13), $-u_\alpha{}^*K_\alpha=\bar{\delta}_{\alpha\beta}{}^*K_\alpha v_\beta$. Equation (27) is the basic equation of dynamics relative to a secondary frame. It may be resolved in turn into two equations. Multiplication by $\bar{\delta}_{\alpha\beta}{}^*$ gives the relative space component equation,

$$(1/c^2)(\chi_{\rho\rho}du_\alpha\bar{\delta}_{\alpha\beta}{}^*/d\tau+Q_\sigma\partial_\sigma{}^*u_\alpha\bar{\delta}_{\alpha\beta}{}^*)=\bar{\delta}_{\alpha\beta}{}^*K_\alpha, \quad (29)$$

which is the force equation; multiplication by $-u_\alpha{}^*$ gives the relative time component equation,

$$\chi_{\rho\rho}dk'/d\tau+Q_\sigma\partial_\sigma{}^*k'=\bar{\delta}_{\alpha\beta}{}^*K_\alpha v_\beta, \quad (30)$$

which is the kinetic energy equation. Thus, the product of the space component of force relative to the secondary frame, $\bar{\delta}_{\alpha\beta}{}^*K_\alpha$, by the relative space component of velocity, $\bar{\delta}_{\rho\beta}{}^*v_\rho$, gives the rate of performance of dynamical work, $\bar{\delta}_{\alpha\beta}{}^*K_\alpha v_\beta$, which according to Eq. (30) equals the rate of increase of kinetic energy. We may readily show that

$$\bar{\delta}_{\alpha\beta}{}^*K_\alpha v_\beta=\partial_\sigma{}^*[(\phi_{\sigma\tau}-u_\sigma Q_\tau/c^2)\bar{\delta}_{\tau\mu}{}^*v_\mu]$$
$$-k'(\phi_{\sigma\tau}-u_\sigma Q_\tau/c^2)\partial_\sigma{}^*u_\tau,$$

so that, according to Eqs. (25) and (26), the rate of performance of dynamical work per unit volume in the secondary frame is equal to the excess of the rate of performance of total work over that of thermodynamic work per unit volume.

Multiplying Eq. (24) by $\bar{\delta}_{\alpha\tau}{}^*$, we obtain the space component equation relative to the secondary frame

$$\partial_\sigma{}^*[(\chi_{\rho\rho}u_\sigma+Q_\sigma)u_\tau\bar{\delta}_{\alpha\tau}{}^*/c^2]$$
$$=\partial_\sigma{}^*[(\phi_{\sigma\tau}-u_\sigma Q_\tau/c^2)\bar{\delta}_{\alpha\tau}{}^*]. \quad (31)$$

This is the equation of continuity of momentum relative to the secondary frame. It is equivalent to

$$\partial_\sigma{}^*(\psi_{\sigma\tau}\bar{\delta}_{\alpha\tau}{}^*)=\partial_\sigma{}^0\psi_{\sigma m}'=0, \quad m=1,2,3. \quad (31')$$

Here we have the basis for the usual interpretation of $ic\psi_{4m}'$ as the total momentum density three-vector and ψ_{km}' as the total stress three-tensor relative to the secondary frame.

Just as Eqs. (25) and (26) yielded Eqs. (25′) and (26′), respectively, when the gradient operator was resolved into its space and time components, similarly each of Eqs. (27) to (31), inclusive, may be written in more detail. These equations will not be given here. However, an important case arises, the condition of the steady state, the covariant requirement for which is that the application of operator $\partial/\partial\tau^*$ to any quantity characterizing the continuum produce a derivative whose value is zero. Since the operator $\partial/\partial\tau^*$, as we have seen, is equal to d/dt^0, the steady-state condition does not depend on the choice of secondary frame to which the motion of the physical medium is referred. For example, the kinetic energy equation, Eq. (30), gives for the steady state

$$\chi_{\rho\rho}k'\bar{\delta}_{\sigma\tau}{}^*v_\sigma\partial_\tau{}^*k'+\bar{\delta}_{\sigma\tau}{}^*Q_\sigma\partial_\tau{}^*k'=\bar{\delta}_{\sigma\tau}{}^*K_\sigma v_\tau,$$

where the terms in the expression for K_σ, Eq. (28), which contain $\partial/\partial\tau^*$ also vanish.

The equations of this section all stem from Eq. (23), which we have seen implies, among other things, the expression for the first law of thermodynamics. They will appear more familiar as a description of the continuum after being modified by the statement of the second law and the equation for the stress in the system. They will be employed in the following discussion only in considering the case of a continuum composed of a single chemical species in the absence of chemical reaction.

D. ENTROPY TENSOR AND SECOND LAW OF THERMODYNAMICS

As in Paper I we write the entropy tensor,

$$S_{\sigma\tau}=-(1/c^2)(S_{\rho\rho}u_\sigma u_\tau+S_\sigma u_\tau+S_\tau u_\sigma), \quad (32)$$

where $S_{\rho\rho}$ is the scalar entropy density in the rest frame and S_σ is the entropy flux vector given by the heat flux vector divided by the scalar temperature T.

$$S_\sigma=Q_\sigma/T. \quad (33)$$

[2] See, for example, R. Tolman, *Relativity, Thermodynamics and Cosmology* (Oxford University Press, London, 1934), p. 73.

It was shown in Paper I that $S_{\rho\rho}$ and T have the properties, respectively, of the Clausius entropy and Kelvin temperature. We shall now require that the vector $\partial_\sigma^* S_{\sigma\tau}$ be a time vector. Accordingly,

$$\bar{\delta}_{\sigma\tau}\partial_\sigma^* S_{\sigma\tau}=0. \tag{34}$$

Furthermore, we require

$$u_\tau \partial_\sigma^* S_{\sigma\tau} \geq 0. \tag{35}$$

Equation (35) is a generalization of Eq. (55) of Paper I, but Eq. (34) is a new condition, of a dynamical rather than thermodynamic nature, which completes the specification of $\partial_\sigma^* S_{\sigma\tau}$.

Equation (35) is the statement of the second law of thermodynamics relative to a secondary frame. It may be written

$$\partial_\sigma^*(S_{\rho\rho}u_\sigma+S_\sigma)+(S_\tau/c^2)(du_\tau/d_\tau)\geq 0, \tag{35'}$$

or, in more detail,

$$(\partial/\partial\tau^*)(S_{\rho\rho}k'+S_\sigma v_\tau \bar{\delta}_{\sigma\tau}^*/c^2)+\bar{\delta}_{\sigma\tau}^*\partial_\sigma^*(S_{\rho\rho}u_\tau+S_\tau) +(S_\tau/c^2)(du_\tau/d\tau)\geq 0. \tag{35''}$$

Apart from terms which vanish in the classical limit, $c\to\infty$, these equations state that the local entropy production rate per unit volume in the secondary frame is non-negative. A process occurring in the continuum for which the equality in Eq. (35) holds at every point will be called a reversible process relative to the secondary frame.

Equation (34) may be written

$$S_{\rho\rho}du_\alpha/d\tau+S_\sigma\partial_\sigma^* u_\alpha=-\bar{\delta}_{\alpha\tau}\partial_\sigma^*(S_\tau u_\sigma). \tag{34'}$$

From this equation two component equations may be derived. Multiplying by $-u_\alpha^*$ gives the time component equation,

$$S_{\rho\rho}dk'/d\tau+S_\sigma\partial_\sigma^* k'=-\bar{\delta}_{\alpha\beta}^* v_\beta \bar{\delta}_{\alpha\tau}\partial_\sigma^*(S_\tau u_\sigma), \tag{36}$$

or multiplying by $\bar{\delta}_{\alpha\beta}^*$ gives the space component equation,

$$S_{\rho\rho}du_\alpha\bar{\delta}_{\alpha\beta}^*/d\tau+S_\sigma\partial_\sigma^*(u_\alpha\bar{\delta}_{\alpha\beta}^*)=-\bar{\delta}_{\alpha\beta}^*\bar{\delta}_{\alpha\tau}\partial_\sigma^*(S_\tau u_\sigma). \tag{37}$$

These equations describe a sort of entropy dynamics, a consequence of Eq. (34).

If $\partial_\sigma^* S_{\sigma\tau}$ is multiplied by u_τ^*, we find that

$$\partial_\sigma^*(S_{\sigma\tau}u_\tau^*)=k'u_\tau\partial_\sigma^* S_{\sigma\tau}\geq 0, \tag{38}$$

since k' is non-negative. This may also be written as

$$\partial_\sigma^*[k'(S_{\rho\rho}u_\sigma+S_\sigma+\bar{\delta}_{\alpha\beta}^* S_\alpha v_\beta v_\sigma/c^2)]\geq 0. \tag{38'}$$

In a reversible process for which the equality holds, we find a continuity equation for entropy relative to a secondary frame. This result cannot be obtained from the second law, Eq. (35), alone without the use of Eq. (34). Equation (38) is equivalent to

$$\partial_\sigma^0(ic S_{\sigma 4}')\geq 0, \tag{38''}$$

which permits interpretation of S_{44}' as the total entropy density and S_{m4}' as the three-vector of total entropy flux relative to the secondary frame.

Similarly, if $\partial_\sigma^* S_{\sigma\tau}$ is multiplied by $\bar{\delta}_{\tau\alpha}^*$, we have

$$\partial_\sigma^*(S_{\sigma\tau}\bar{\delta}_{\tau\alpha}^*)=-(u_\tau\bar{\delta}_{\tau\alpha}^*/c^2)(u_\rho\partial_\sigma^* S_{\sigma\rho}), \tag{39}$$

which is equivalent to

$$\partial_\sigma^0 S_{\sigma m}'=-(u_m'/c^2)(u_\rho\partial_\sigma^* S_{\sigma\rho}) \text{ for } m=1,2,3. \tag{39'}$$

The right side vanishes in a reversible process, so that an additional continuity equation appears in this case,

$$\partial_\sigma^*[(S_{\rho\rho}u_\sigma u_\tau+S_\sigma u_\tau+S_\tau u_\sigma)\bar{\delta}_{\tau\alpha}^*]=0. \tag{40}$$

These equations which have been obtained from Eqs. (34) and (35) may be combined with those of the preceding section obtained from Eq. (23). We write, using Eq. (33),

$$\psi_{\sigma\tau}=-(1/c^2)(\chi_{\rho\rho}-TS_{\rho\rho})u_\sigma u_\tau+TS_{\sigma\tau}+\phi_{\sigma\tau}, \tag{41}$$

so that

$$-(1/c^2)\partial_\sigma^*[(\chi_{\rho\rho}-TS_{\rho\rho})u_\tau u_\sigma] =-T\partial_\sigma^* S_{\sigma\tau}-S_{\sigma\tau}\partial_\sigma^* T-\partial_\sigma^*\phi_{\sigma\tau}. \tag{42}$$

Letting

$$\rho A=\chi_{\rho\rho}-TS_{\rho\rho}-\rho c^2, \tag{43}$$

where A is the specific Helmholtz free energy, as in Paper I, and using the equation of continuity, Eq. (15), we have

$$-(\rho/c^2)d(A+c^2)u_\tau/d\tau =-T\partial_\sigma^* S_{\sigma\tau}-S_{\sigma\tau}\partial_\sigma^* T-\partial_\sigma^*\phi_{\sigma\tau}. \tag{44}$$

Equation (44) is an alternative formulation of Eq. (24) and yields equivalent thermodynamic and dynamical consequences when the time component and space component equations relative to the rest frame and the secondary frame are obtained. We shall list these in turn, each combined with the appropriate component equation derived from Eqs. (34) and (35).

Multiplying Eq. (44) by u_τ and using Eq. (35) gives

$$\rho dA/d\tau\leq -S_{\rho\rho}dT/d\tau-S_\sigma\partial_\sigma^* T+\phi_{\sigma\tau}\partial_\sigma^* u_\tau. \tag{45}$$

Multiplying Eq. (44) by u_τ^* and using Eq. (38) gives

$$\rho d(A+c^2)k'/d\tau\leq -k'(S_{\rho\rho}u_\sigma+S_\sigma)\partial_\sigma^* T -(S_\tau v_\sigma\bar{\delta}_{\sigma\tau}^*/c^2)(dT/d\tau)+\partial_\sigma^*(\phi_{\alpha\tau}v_\mu\bar{\delta}_{\tau\mu}^*). \tag{46}$$

Multiplying Eq. (44) by $-\bar{\delta}_{\alpha\tau}$ and using Eq. (34) gives

$$\rho(1+A/c^2)du_\alpha/d\tau=-(S_\alpha/c^2)(dT/d\tau)+\bar{\delta}_{\alpha\tau}\partial_\sigma^*\phi_{\sigma\tau}. \tag{47}$$

Equation (47), when multiplied by $-u_\alpha^*$, gives the kinetic energy equation,

$$\rho(A+c^2)dk'd\tau=-(S_\alpha v_\beta\bar{\delta}_{\alpha\beta}^*/c^2)(dT/d\tau)+v_\beta\bar{\delta}_{\alpha\beta}^*\bar{\delta}_{\alpha\tau}\partial_\sigma^*\phi_{\sigma\tau}, \tag{48}$$

or, when multiplied by $\bar{\delta}_{\alpha\beta}^*$, gives the force equation,

$$\rho(1+A/c^2)du_\alpha\bar{\delta}_{\alpha\beta}^*/d\tau =-S_\alpha(\bar{\delta}_{\alpha\beta}^*/c^2)(dT/d\tau)+\bar{\delta}_{\alpha\beta}^*\bar{\delta}_{\alpha\tau}\partial_\sigma^*\phi_{\sigma\tau}. \tag{49}$$

Finally, multiplying Eq. (44) by $-\bar{\delta}_{\alpha\tau}^*$ and using Eq. (39) gives

$$(\rho/c^2)d(A+c^2)u_\tau\bar{\delta}_{\alpha\tau}^*/d\tau = \partial_\sigma^*(\phi_{\sigma\tau}\bar{\delta}_{\tau\alpha}^*)-(\bar{\delta}_{\alpha\tau}^*/c^2)[(S_{\rho\rho}u_\tau+S_\tau)(dT/d\tau) +u_\tau S_\sigma\partial_\sigma^*T]-T(u_\tau\bar{\delta}_{\tau\alpha}^*/c^2)(u_\rho\partial_\sigma^*S_{\sigma\rho}), \quad (50)$$

in which the last term on the right side vanishes in a reversible process. These equations describe the thermodynamics and dynamics of an element of continuum composed of a single, chemically inert species, and conform to the requirements of the first and second laws of thermodynamics.

E. THE STRESS IN THE SYSTEM AND REVERSIBILITY

Let us now introduce the equations defining the reversible stress in the system. This is the stress determined by the properties of the element of continuum at a point in the physical system. It was denoted by $\phi_{\sigma\tau}'$ and defined by Eq. (38) or Eq. (46) in Paper I. We will denote it here by $\phi_{\sigma\tau}{}^r$ and replace Eq. (46) of Paper I by a more general form,

$$\partial_\sigma^*[(-1/c^2)\rho(A+c^2)u_\tau u_\sigma+\phi_{\sigma\tau}{}^r] = (\rho u_\sigma/c^2)[\partial_\tau^*(A+c^2)u_\sigma -\partial_\sigma^*(A+c^2)u_\tau]-S_{\rho\rho}\partial_\tau^*T. \quad (51)$$

With the help of the equation of continuity Eq. (15), we may reduce this equation to

$$-\rho\partial_\tau^*A-S_{\rho\rho}\partial_\tau^*T=\partial_\sigma^*\phi_{\sigma\tau}{}^r. \quad (51')$$

Consequences of this equation are obtained in the usual manner. Multiplying Eq. (51′) by $-u_\tau$ gives

$$\rho dA/d\tau+S_{\rho\rho}dT/d\tau=\phi_{\sigma\tau}{}^r\partial_\sigma^*u_\tau. \quad (52)$$

Multiplying Eq. (51′) by $-u_\tau^*$ gives

$$\rho\partial A/\partial\tau^*+S_{\rho\rho}\partial T/\partial\tau^*=\partial_\sigma^*(\phi_{\sigma\tau}{}^r v_\mu\bar{\delta}_{\tau\mu}^*). \quad (53)$$

Multiplying Eq. (51′) by $\bar{\delta}_{\alpha\tau}$ gives

$$-\rho\bar{\delta}_{\alpha\tau}\partial_\tau^*A-S_{\rho\rho}\bar{\delta}_{\alpha\tau}\partial_\tau^*T=\bar{\delta}_{\alpha\tau}\partial_\sigma^*\phi_{\sigma\tau}{}^r. \quad (54)$$

Multiplying Eq. (51′) by $\bar{\delta}_{\alpha\tau}^*$ gives

$$-\rho\bar{\delta}_{\alpha\tau}^*\partial_\tau^*A-S_{\rho\rho}\bar{\delta}_{\alpha\tau}^*\partial_\tau^*T=\partial_\sigma^*(\phi_{\sigma\tau}{}^r\bar{\delta}_{\alpha\tau}^*). \quad (55)$$

In Eq. (52), $dA/d\tau$ expresses the rate of change of specific Helmholz free energy, a point function of the variables specifying the properties of the element of continuum. In the special case that these properties are isotropic, $\phi_{\sigma\tau}{}^r$ reduces to the hydrostatic pressure, $-p\bar{\delta}_{\sigma\tau}$. We find with the aid of Eq. (18) in this case the usual thermodynamic formula,

$$\rho dA/d\tau=-S_{\rho\rho}dT/d\tau-\rho pd(1/\rho)/d\tau, \quad (52')$$

expressing A as a function of T and specific volume, $1/\rho$.

Equation (54) takes a particularly interesting form in the isotropic case,

$$\rho\bar{\delta}_{\alpha\tau}\partial_\tau^*A=-S_{\rho\rho}\bar{\delta}_{\alpha\tau}\partial_\tau^*T-\bar{\delta}_{\alpha\tau}\partial_\tau^*p-(p/c^2)(du_\alpha/d\tau). \quad (54')$$

But in the classical limit, $c\to\infty$, the right side is just the expression which would be expected to equal $\rho\bar{\delta}_{\alpha\tau}\partial_\tau^*F$, where F is the specific Gibbs free energy, rather than $\rho\bar{\delta}_{\alpha\tau}\partial_\tau^*A$, where A is the specific Helmholtz free energy. We see, therefore, that ∂_τ^*A in Eq. (51′) has the property that in its time component or thermodynamic aspect, A plays the role of the Helmholtz free energy, but in its space component or dynamical aspect, A has the nature of the Gibbs free energy. It will be seen in the following that the Helmholtz free energy will appear in our dynamical equations whereas in the corresponding classical equations for the isotropic case the Gibbs free energy would appear. This is particularly fortunate since it enables us to formulate equations for anisotropic media which cannot be written classically, because of the inability of classical theory to define an adequate Gibbs free energy for anisotropic media; we use the Helmholz function. In the following we shall refer to A as simply the chemical potential.

Similar remarks, of course, apply to the behavior of $\chi_{\rho\rho}/\rho$ in the equation,

$$-\rho\partial_\tau^*(\chi_{\rho\rho}/\rho)=-T\rho\partial_\tau^*(S_{\rho\rho}/\rho)+\partial_\sigma^*\phi_{\sigma\tau}{}^r. \quad (56)$$

In the time component of $\partial_\tau^*(\chi_{\rho\rho}/\rho)$ this quantity appears as the specific thermodynamic energy, whereas in the space component it appears as the specific enthalpy. Classical theory is likewise unable to define an enthalpy function for anisotropic media.

Since the change in A in a physical process depends only on the end points of the process and not on the path, therefore, in the reversible case described by the equality in Eq. (45), the expression for $\rho dA/d\tau$ in Eqs. (45) and (52) must be identical. This is the case if we take as conditions for reversibility,

$$S_\sigma=0 \quad \text{and} \quad \phi_{\sigma\tau}=\phi_{\sigma\tau}{}^r. \quad (57)$$

Following Paper I, Eq. (67), we could have chosen the condition $\bar{\delta}_{\sigma\tau}\partial_\tau^*T=0$ instead of $S_\sigma=0$, offering Fourier's law of heat conduction as evidence that the two conditions are equivalent. However, Fourier's law, as we shall see in the discussion of transport processes which concludes this paper, does not possess the degree of generality which has been assumed in our formulation to this point. It seems preferable to take $S_\sigma=0$ as the condition of reversibility with $\bar{\delta}_{\sigma\tau}\partial_\tau^*T=0$ as equivalent to it when the motion of the medium conforms to the requirements of the theory of transport processes. It is important to note that the conditions stated in Eq. (57) are independent of the choice of secondary reference frame to which the motion of the continuum is referred.

Equations (45) and (52) give, in the general case,

$$-S_\sigma\partial_\sigma^*T+(\phi_{\sigma\tau}-\phi_{\sigma\tau}{}^r)\partial_\sigma^*u_\tau\geq 0, \quad (58)$$

which is the dissipation equation corresponding to Eq. (57) of Paper I, while Eq. (45) itself corresponds to Eq. (58) of Paper I.

In the remainder of this section we shall consider the dynamical consequences of Eq. (51′), appearing in the space component equation, Eq. (54). If we combine the dynamical equation, Eq. (47), with Eq. (54), we find

$$\rho(1+A/c^2)du_\alpha/d\tau+(S_\alpha/c^2)(dT/d\tau)$$
$$=-S_{\rho\rho}\bar{\delta}_{\alpha\tau}\partial_\tau{}^*T-\rho\bar{\delta}_{\alpha\tau}\partial_\tau{}^*A-\bar{\delta}_{\alpha\tau}\partial_\sigma{}^*(\phi_{\sigma\tau}-\phi_{\sigma\tau}{}^r), \quad (59)$$

corresponding to Eq. (78) of Paper I, the difference arising from our present assumption of Eq. (34). On multiplying by $\bar{\delta}_{\alpha\beta}{}^*$ we obtain the force equation,

$$\rho(1+A/c^2)du_\alpha\bar{\delta}_{\alpha\beta}{}^*/d\tau+(S_\alpha\bar{\delta}_{\alpha\beta}{}^*/c^2)(dT/d\tau)$$
$$=-S_{\rho\rho}\bar{\delta}_{\alpha\beta}{}^*\bar{\delta}_{\alpha\tau}\partial_\tau{}^*T-\rho\bar{\delta}_{\alpha\beta}{}^*\bar{\delta}_{\alpha\tau}\partial_\tau{}^*A$$
$$+\bar{\delta}_{\alpha\beta}{}^*\bar{\delta}_{\alpha\tau}\partial_\sigma{}^*(\phi_{\sigma\tau}-\phi_{\sigma\tau}{}^r). \quad (60)$$

On the right-hand side, the following force densities may be recognized:

(1) $\bar{\delta}_{\alpha\beta}{}^*\bar{\delta}_{\alpha\tau}\partial_\sigma{}^*(\phi_{\sigma\tau}-\phi_{\sigma\tau}{}^r)$
$$=(1/c^2)(\partial/\partial\tau^*)[(\phi_{\sigma\alpha}-\phi_{\sigma\alpha}{}^r)\bar{\delta}_{\alpha\beta}{}^*\bar{\delta}_{\sigma\rho}{}^*v_\rho]$$
$$+\bar{\delta}_{\sigma\rho}{}^*\partial_\sigma{}^*[(\phi_{\rho\alpha}-\phi_{\rho\alpha}{}^r)\bar{\delta}_{\alpha\beta}{}^*]$$
$$-(u_\alpha\bar{\delta}_{\alpha\beta}{}^*/c^2)(\phi_{\sigma\tau}-\phi_{\sigma\tau}{}^r)\partial_\sigma{}^*u_\tau.$$

In the classical limit, $c\to\infty$, only the space divergence term remains on the right. On integration over a volume fixed in the secondary frame, the integral of this space divergence can be converted into a surface integral, $\int(\phi_{\sigma\alpha}-\phi_{\sigma\alpha}{}^r)\bar{\delta}_{\alpha\beta}{}^*dn_\sigma{}^*$, proportional to the area of the boundary surface. This force density corresponds to the classical surface force density of hydrodynamics.

(2) $-\rho\bar{\delta}_{\beta\alpha}{}^*\bar{\delta}_{\alpha\tau}\partial_\tau{}^*A$ is a body force density arising from the gradient of chemical potential. As we know, other forces such as electromagnetic forces and gravitational forces are included among the possible body forces of classical hydrodynamics. The absence of such forces in Eq. (60) indicates the limitation of our present treatment to a single-component chemical system without external body forces. Equation (59) may be written in the form

$$\rho du_\alpha/d\tau+(S_\alpha/c^2)(dT/d\tau)$$
$$=(\rho u_\tau/c)(\partial_\alpha{}^*A\hat{u}_\tau-\partial_\tau{}^*A\hat{u}_\alpha)$$
$$-S_{\rho\rho}\bar{\delta}_{\alpha\tau}\partial_\tau{}^*T+\bar{\delta}_{\alpha\tau}\partial_\sigma{}^*(\phi_{\sigma\tau}-\phi_{\sigma\tau}{}^r). \quad (59')$$

The term containing the skew-symmetric tensor, $\partial_\alpha{}^*A\hat{u}_\tau-\partial_\tau{}^*A\hat{u}_\alpha$, suggests the electromagnetic Lorentz force, $(\rho u_\tau/c)(\partial_\alpha{}^*A_\tau-\partial_\tau{}^*A_\alpha)$, where A_τ is a four-vector potential. Inclusion of such an electromagnetic force would be accomplished by simply replacing the chemical four-vector potential $A\hat{u}_\sigma$ by the electrochemical potential $A\hat{u}_\sigma+A_\sigma$. A general investigation of electrical processes in continuous media will no doubt reveal such quantities, but this will not be undertaken here.

(3) $-S_{\rho\rho}\bar{\delta}_{\beta\alpha}{}^*\bar{\delta}_{\alpha\tau}\partial_\tau{}^*T$ is the force density arising from the presence of entropy in a temperature gradient. This force is exerted on the matter with which the entropy is associated.

The sum of these three force densities constitutes the single force density $\bar{\delta}_{\beta\alpha}{}^*\bar{\delta}_{\alpha\tau}\partial_\sigma{}^*\phi_{\sigma\tau}$ on the right-hand side of Eq. (49), the total force density exerted on an element of continuum relative to the secondary reference frame.

On multiplying Eq. (59) by $-u_\alpha{}^*$ we obtain the kinetic energy equation,

$$\rho(A+c^2)dk'/d\tau+v_\beta\bar{\delta}_{\alpha\beta}{}^*S_\alpha dT/d\tau$$
$$=-S_{\rho\rho}v_\beta\bar{\delta}_{\alpha\beta}{}^*\bar{\delta}_{\alpha\tau}\partial_\tau{}^*T-\rho v_\beta\bar{\delta}_{\alpha\beta}{}^*\bar{\delta}_{\alpha\tau}\partial_\tau{}^*A$$
$$+v_\beta\bar{\delta}_{\alpha\beta}{}^*\bar{\delta}_{\alpha\tau}\partial_\sigma{}^*(\phi_{\sigma\tau}-\phi_{\sigma\tau}{}^r). \quad (61)$$

Each term on the right, representing a rate of performance of work per unit volume, is simply the product of the corresponding force density term of Eq. (59) by the relative space velocity $v_\rho\bar{\delta}_{\beta\rho}{}^*$. The last term on the right, attributable to surface forces, may be written as

$$v_\beta\bar{\delta}_{\alpha\beta}{}^*\bar{\delta}_{\alpha\tau}\partial_\sigma{}^*(\phi_{\sigma\tau}-\phi_{\sigma\tau}{}^r)=\partial_\sigma{}^*[(\phi_{\sigma\alpha}-\phi_{\sigma\alpha}{}^r)\bar{\delta}_{\alpha\beta}{}^*v_\beta]$$
$$-k'(\phi_{\sigma\tau}-\phi_{\sigma\tau}{}^r)\partial_\sigma{}^*u_\tau. \quad (61')$$

Each term on the right side of this equation has an interpretation in the classical limit. The first yields a space divergence which gives the total rate of performance of work by the stress at the surface of the element in excess of that which the element can support. The other is the rate of dissipation accompanying the action of this excess stress. It is of interest that dissipative effects are associated with surfaces stresses, not with body forces.

For reversible processes the dynamical equations, Eqs. (47) and (59), give

$$\rho(1+A/c^2)du_\alpha/d\tau=\bar{\delta}_{\alpha\tau}\partial_\sigma{}^*\phi_{\sigma\tau}{}^r$$
$$=-S_{\rho\rho}\bar{\delta}_{\sigma\tau}\partial_\tau{}^*T-\rho\bar{\delta}_{\alpha\tau}\partial_\tau{}^*A, \quad (62)$$

or

$$\rho du_\alpha/d\tau=-S_{\rho\rho}\bar{\delta}_{\sigma\tau}\partial_\tau{}^*T+(\rho u_\tau/c)(\partial_\alpha{}^*A\hat{u}_\tau-\partial_\tau{}^*A\hat{u}_\alpha). \quad (62')$$

According to Eq. (62′), in the absence of a temperature gradient an element of continuum moves in a reversible process like a particle of rest mass density ρ in a field whose four-vector potential is $A\hat{u}_\sigma$. As a special case of reversible process we have the condition of unaccelerated motion relative to the secondary frame, for which $du_\alpha/d\tau$ vanishes. Equation (62) shows that in this case $\bar{\delta}_{\alpha\tau}\partial_\sigma{}^*\phi_{\sigma\tau}{}^r=0$. Since the operator $d/d\tau=u_\sigma\partial_\sigma{}^*$ depends on the choice of secondary frame, the vanishing of $du_\alpha/d\tau$ in one secondary frame does not guarantee its vanishing in all others, unless the secondary frame in which $du_\alpha/d\tau$ vanishes is also a rest frame.

Equations (52) and (62) can be used as a starting point for the formulation of the theory of elasticity. The stress which according to Hooke's law is proportional to the symmetric strain is $\phi_{\sigma\tau}{}^r$. The theory is essentially a theory of reversible strains. For example, in the derivation of the Laplace formula for the velocity

of sound in a gas, the equations for reversible, adiabatic compressions are employed.

F. TRANSPORT PROCESSES IN A ONE-COMPONENT MEDIUM

In the description of the transport processes of conduction and diffusion the motion of every element of the continuum is referred to the same secondary frame. It is necessary to find a secondary frame relative to which the continuum everywhere satisfies a special condition, which may be formulated as

$$\partial_\sigma^*[(\phi_{\sigma\tau}-\phi_{\sigma\tau}{}^r)v_\mu\bar{\delta}_{\tau\mu}{}^*]=v_\beta\bar{\delta}_{\alpha\beta}{}^*\bar{\delta}_{\alpha\tau}\partial_\sigma^*\phi_{\sigma\tau}. \quad (63)$$

It is evident that the fact that Eq. (63) characterizes the motion relative to one secondary frame does not imply that a similar relation will hold for all other secondary frames. This, however, does not vitiate the covariance of Eq. (63) since this expression is the same for all primary observers; any primary observer recording the motion of the continuum relative to the special secondary frame will find that Eq. (63) is satisfied, if the motion is amenable to description by the theories of diffusion or conduction.

According to Eq. (63), the rate at which total work is performed upon each element of continuum by the excess of stress in its surroundings over that in the element is equal to the rate of dynamical work which increases the kinetic energy. Equation (48) gives

$$\partial_\sigma^*[(\phi_{\sigma\tau}-\phi_{\sigma\tau}{}^r)v_\mu\bar{\delta}_{\tau\mu}{}^*]=\rho(A+c^2)dk'/d\tau + (S_\alpha v_\beta\bar{\delta}_{\alpha\beta}{}^*/c^2)dT/d\tau. \quad (64)$$

On the other hand, Eqs. (61′) and (54) give

$$k'(\phi_{\sigma\tau}-\phi_{\sigma\tau}{}^r)\partial_\sigma^* u_\tau=v_\beta\bar{\delta}_{\alpha\beta}{}^*\bar{\delta}_{\alpha\tau}\partial_\sigma^*\phi_{\sigma\tau}{}^r =-\rho v_\beta\bar{\delta}_{\alpha\beta}{}^*\bar{\delta}_{\alpha\tau}\partial_\tau^* A-S_{\rho\rho}v_\beta\bar{\delta}_{\alpha\beta}{}^*\bar{\delta}_{\alpha\tau}\partial_\tau^* T, \quad (65)$$

so that the rate of dissipation $k'(\phi_{\sigma\tau}-\phi_{\sigma\tau}{}^r)\partial_\sigma^* u_\tau$ is maintained by a lowering of potential levels in the element. If this last equation is combined with Eq. (52), the rate of thermodynamic work performed by the surroundings upon the element is found to be

$$k'\phi_{\sigma\tau}\partial_\sigma^* u_\tau=\rho\partial A/\partial\tau^*+S_{\rho\rho}\partial T/\partial\tau^*; \quad (66)$$

whereas combination with Eq. (58) gives the dissipation equation,

$$-S_{\rho\rho}v_\beta\bar{\delta}_{\alpha\beta}{}^*\bar{\delta}_{\alpha\tau}\partial_\tau^* T-k'S_\sigma\partial_\sigma^* T -\rho v_\beta\bar{\delta}_{\alpha\beta}{}^*\bar{\delta}_{\alpha\tau}\partial_\tau^* A\geq 0. \quad (67)$$

Equation (67) will serve as starting point for a covariant theory of transport processes.

It is interesting that the alternative form of the transport condition appearing in Eq. (64) gives, in the classical limit, exactly the same equation as that which must be assumed in a nonrelativistic transport theory, the equation expressing the assumption that "the entire acceleration of any fluid element is produced by viscous forces alone, acting on the element as though it were rigid."[3] Equation (67) differs from the corresponding nonrelativistic equation in that the latter is limited to isotropic media since it employs the specific Gibbs free energy to represent the chemical potential. The theory developed here will describe transport processes in an anisotropic, one-component chemical continuum in the absence of external body forces. We follow the method used in the nonrelativistic theory.

Equation (67) can be written

$$-[S_{\rho\rho}v_\beta\bar{\delta}_{\alpha\beta}{}^*+k'S_\beta(\bar{\delta}_{\alpha\beta}{}^*-v_\rho\bar{\delta}_{\beta\rho}{}^*v_\sigma\bar{\delta}_{\alpha\sigma}{}^*/c^2)]\bar{\delta}_{\alpha\tau}\partial_\tau^* T -\rho v_\beta\bar{\delta}_{\alpha\beta}{}^*\bar{\delta}_{\alpha\tau}\partial_\tau^* A\geq 0. \quad (67')$$

We assume the linear relationships,

$$\begin{aligned}\rho v_\beta\bar{\delta}_{\alpha\beta}{}^* &= -a_{\alpha\beta}{}^*\bar{\delta}_{\beta\tau}\partial_\tau^* A-b_{\alpha\beta}{}^*\bar{\delta}_{\beta\tau}\partial_\tau^* T,\\ S_{\rho\rho}v_\beta\bar{\delta}_{\alpha\beta}{}^*+k'S_\beta(\bar{\delta}_{\alpha\beta}{}^*-v_\rho\bar{\delta}_{\beta\rho}{}^*v_\sigma\bar{\delta}_{\alpha\sigma}{}^*/c^2) &= -b_{\alpha\beta}{}^*\bar{\delta}_{\beta\tau}\partial_\tau^* A-c_{\alpha\beta}{}^*\bar{\delta}_{\beta\tau}\partial_\tau^* T,\end{aligned} \quad (68)$$

where, according to Onsager's reciprocal relations,[4] the tensors $a_{\alpha\beta}{}^*$, $b_{\alpha\beta}{}^*$, $c_{\alpha\beta}{}^*$ are symmetric. These tensors are pure space tensors in the secondary reference frame. For example,

$$a_{\alpha\beta}{}^*=\left\{\begin{array}{l}\bar{\imath}_\alpha{}^*\bar{\imath}_\beta{}^*a_{11}{}^0+\bar{\imath}_\alpha{}^*\bar{\jmath}_\beta{}^*a_{12}{}^0+\bar{\imath}_\alpha{}^*\bar{k}_\beta{}^*a_{13}{}^0\\ +\bar{\jmath}_\alpha{}^*\bar{\imath}_\beta{}^*a_{21}{}^0+\bar{\jmath}_\alpha{}^*\bar{\jmath}_\beta{}^*a_{22}{}^0+\bar{\jmath}_\alpha{}^*\bar{k}_\beta{}^*a_{23}{}^0\\ +\bar{k}_\alpha{}^*\bar{\imath}_\beta{}^*a_{31}{}^0+\bar{k}_\alpha{}^*\bar{\jmath}_\beta{}^*a_{32}{}^0+\bar{k}_\alpha{}^*\bar{k}_\beta{}^*a_{33}{}^0\end{array}\right\} =L_{\alpha m}{}^*L_{\beta n}{}^*a_{mn}{}^0,$$

where six coefficients, independent of the velocity components v_1', v_2', v_3' of the continuum relative to the secondary frame, appear. In an isotropic medium we should have

$$a_{\alpha\beta}{}^*=a\bar{\delta}_{\alpha\beta}{}^*, \quad b_{\alpha\beta}{}^*=b\bar{\delta}_{\alpha\beta}{}^*, \quad c_{\alpha\beta}{}^*=c\bar{\delta}_{\alpha\beta}{}^*.$$

Substituting Eq. (68) into Eq. (67′) gives

$$a_{\alpha\beta}{}^*\bar{\delta}_{\alpha\sigma}\partial_\sigma^* A\bar{\delta}_{\beta\tau}\partial_\tau^* A+2b_{\alpha\beta}{}^*\bar{\delta}_{\alpha\sigma}\partial_\sigma^* A\bar{\delta}_{\beta\tau}\partial_\tau^* T +c_{\alpha\beta}{}^*\bar{\delta}_{\alpha\sigma}\partial_\sigma^* T\bar{\delta}_{\beta\tau}\partial_\tau^* T\geq 0. \quad (69)$$

Since this relation must be valid for any choice of $\bar{\delta}_{\alpha\tau}\partial_\tau^* A$ and $\bar{\delta}_{\alpha\tau}\partial_\tau^* T$, the determinant

$$\begin{vmatrix} a_{11}{}^0, & a_{12}{}^0, & a_{13}{}^0, & b_{11}{}^0, & b_{12}{}^0, & b_{13}{}^0\\ a_{21}{}^0, & a_{22}{}^0, & a_{23}{}^0, & b_{21}{}^0, & b_{22}{}^0, & b_{23}{}^0\\ a_{31}{}^0, & a_{32}{}^0, & a_{33}{}^0, & b_{31}{}^0, & b_{32}{}^0, & b_{33}{}^0\\ b_{11}{}^0, & b_{12}{}^0, & b_{13}{}^0, & c_{11}{}^0, & c_{12}{}^0, & c_{13}{}^0\\ b_{21}{}^0, & b_{22}{}^0, & b_{23}{}^0, & c_{21}{}^0, & c_{22}{}^0, & c_{23}{}^0\\ b_{31}{}^0, & b_{32}{}^0, & b_{33}{}^0, & c_{31}{}^0, & c_{32}{}^0, & c_{33}{}^0\end{vmatrix}\geq 0, \quad (70)$$

and each of its principal minors must be non-negative. The conditions of reversibility of transport processes, under which the equality holds in Eq. (69), appear as

$$\bar{\delta}_{\alpha\tau}\partial_\tau^* T=0 \quad \text{and} \quad \bar{\delta}_{\alpha\tau}\partial_\tau^* A=0, \quad (71)$$

which may be compared to the more general conditions of Eq. (57). According to Eqs. (68) and (62), we must

[3] B. Leaf, Phys. Rev. **70**, 752 (1946), Eq. (42).
[4] L. Onsager, Phys. Rev. **37**, 405 (1931); **38**, 2265 (1931).

also have

$$v_\beta \bar{\delta}_{\alpha\beta}^* = 0, \quad du_\alpha/d\tau = 0, \quad S_\alpha = 0, \tag{72}$$

so that in this case the secondary frame to which the transport is referred is the rest frame for the entire continuum. The continuum is static throughout a reversible transport process, which is, therefore, a quasi-static process.

Let us write

$$b_{mn}^0 = \sigma_{mk}^0 a_{kn}^0, \tag{73}$$

so that

$$b_{\alpha\beta}^* = L_{\alpha m}^* L_{\beta n}^* \sigma_{mk}^0 a_{kn}^0 = (L_{\alpha m}^* L_{\nu k}^* \sigma_{mk}^0)(L_{\nu j}^* L_{\beta n}^* a_{jn}^0) = \sigma_{\alpha\nu}^* a_{\nu\beta}^*.$$

Then, according to Eq. (68),

$$k' S_\beta (\bar{\delta}_{\alpha\beta}^* - v_\rho \bar{\delta}_{\beta\rho}^* v_\sigma \bar{\delta}_{\alpha\sigma}^*/c^2) = -(\sigma_{\alpha\nu}^* - S_{\rho\rho} \bar{\delta}_{\alpha\nu}/\rho) a_{\nu\beta}^* \bar{\delta}_{\beta\tau} \partial_\tau^* A - (c_{\alpha\beta}^* - S_{\rho\rho} b_{\alpha\beta}^*/\rho) \bar{\delta}_{\beta\tau} \partial_\tau^* T$$
$$= (\rho \sigma_{\alpha\beta}^* - S_{\rho\rho} \bar{\delta}_{\alpha\beta}^*) v_\beta - (c_{\alpha\beta}^* - \sigma_{\alpha\mu}^* \sigma_{\mu\nu}^* a_{\nu\beta}^*) \bar{\delta}_{\beta\tau} \partial_\tau^* T.$$

Therefore,

$$k' Q_\beta (\bar{\delta}_{\alpha\beta}^* - v_\rho \bar{\delta}_{\beta\rho}^* v_\sigma \bar{\delta}_{\alpha\sigma}^*/c^2) = T(\rho \sigma_{\alpha\beta}^* - S_{\rho\rho} \bar{\delta}_{\alpha\beta}^*) v_\beta - \lambda_{\alpha\beta}^* \bar{\delta}_{\beta\tau} \partial_\tau^* T, \tag{74}$$

which, for $v_\beta \bar{\delta}_{\alpha\beta}^* = 0$, gives in the classical limit Fourier's law of heat conduction. Here $\lambda_{\alpha\beta}^* = L_{\alpha m}^* L_{\beta n}^* \lambda_{mn}^0$, where λ_{mn}^0 is the heat conductivity tensor for an anisotropic medium.

$$\lambda_{mn}^0 = T(c_{mn}^0 - \sigma_{mk}^0 \sigma_{kj}^0 a_{jn}^0). \tag{75}$$

Solving Eq. (73) for σ_{mk}^0 we find

$$\sigma_{mk}^0 = b_{mn}^0 A_{kn}^0 / |a_{ij}|,$$

where A_{kn}^0 is the cofactor of a_{kn}^0 in the determinant $|a_{ij}|$. Therefore,

$$|a_{ij}^0| \lambda_{mn}^0 / T = |a_{ij}^0| c_{mn}^0 - b_{mj}^0 A_{kj}^0 b_{kn}^0 = \begin{vmatrix} a_{11}^0, & a_{12}^0, & a_{13}^0, & b_{1n}^0 \\ a_{21}^0, & a_{22}^0, & a_{23}^0, & b_{2n}^0 \\ a_{31}^0, & a_{32}^0, & a_{33}^0, & b_{3n}^0 \\ b_{m1}^0, & b_{m2}^0, & b_{m3}^0, & c_{mn}^0 \end{vmatrix},$$

which is a minor of the determinant of Eq. (70). Accordingly, λ_{11}^0, λ_{22}^0, λ_{33}^0 are all non-negative. Clearly, λ_{mn}^0 is a symmetric tensor.

Equations (68) and (73) give

$$\rho v_\beta \bar{\delta}_{\alpha\beta}^* = -a_{\alpha\beta}^* (\bar{\delta}_{\beta\tau} \partial_\tau^* A + \sigma_{\rho\beta}^* \bar{\delta}_{\rho\tau} \partial_\tau^* T).$$

Therefore,

$$\bar{\delta}_{\rho\beta}^* \bar{\delta}_{\rho\tau} \partial_\tau^* A + \sigma_{\rho\beta}^* \bar{\delta}_{\rho\tau} \partial_\tau^* T = -r_{\alpha\beta}^* \rho v_\alpha; \tag{76}$$

where

$$r_{\alpha\beta}^* = L_{\alpha m}^* L_{\beta n}^* r_{mn}^0, \quad r_{mn}^0 = A_{mn}^0 / |a_{ij}|. \tag{77}$$

Substitution of Eq. (76) into Eq. (67′) gives, with the help of Eq. (74),

$$r_{\alpha\beta}^* (\rho v_\alpha)(\rho v_\beta) + (\lambda_{\alpha\beta}^*/T)(\bar{\delta}_{\alpha\sigma} \partial_\sigma^* T)(\bar{\delta}_{\beta\tau} \partial_\tau^* T) \geq 0. \tag{78}$$

These equations describe the transport processes in terms of the symmetric resistivity tensor r_{mn}^0. The quantity $r_{\alpha\beta}^* (\rho v_\alpha)(\rho v_\beta)$ is the analog of the Joule electrical dissipation rate in an anisotropic medium per unit volume in the secondary frame. Both determinants, $|r_{mn}^0|$ and $|\lambda_{mn}^0|$, and their principal minors are non-negative.

The condition for a transport process given in Eq. (63) requires that a secondary reference frame exist such that when the motion of every element of the continuum is referred to this same frame the condition should hold. All the equations for transport processes are formulated for motion relative to this frame. If this frame should coincide with the momentary rest frame of some element of the continuum, then $v_\beta \bar{\delta}_{\alpha\beta}^* = 0$; the transport process in that element would consist merely of heat conduction. According to Eqs. (67) and (78), for such an element the dissipation is given by

$$-S_\sigma \partial_\sigma T = (\lambda_{\alpha\beta}/T)(\bar{\delta}_{\alpha\sigma} \partial_\sigma T)(\bar{\delta}_{\beta\tau} \partial_\tau T) \geq 0,$$

and, according to Eq. (65), $(\phi_{\sigma\tau} - \phi_{\sigma\tau}{}^r) \partial_\sigma u_\tau = 0$. If the special secondary frame should coincide with the rest frame of every element of the continuum, then the entire transport process would consist only of heat conduction throughout the continuum and these equations would be valid everywhere. But consider some element whose motion satisfies the transport condition relative to a special secondary frame which does not coincide with its rest frame. Its dissipation will be given by Eqs. (58), (67′), (69), or (78). Its dissipation is also given relative to its rest frame as

$$-S_\sigma \partial_\sigma T + (\phi_{\sigma\tau} - \phi_{\sigma\tau}{}^r) \partial_\sigma u_\tau \geq 0, \tag{58′}$$

according to Eq. (58). It should be noted that, although in the reversible case the dissipation relative to every secondary frame vanishes, in an irreversible process the magnitude of the dissipation given in Eq. (58) depends on the choice of secondary frame. (The equation is nevertheless relativistically covariant since for a given secondary frame its form is the same for all primary observers.)

The theory of viscosity differs in method from the transport theories of diffusion and conduction. In the theory of viscosity the motion of each element of continuum is referred to its own rest frame. The transport condition of Eq. (63) need not be satisfied and no special secondary frame is employed. The dissipation rate is given by Eq. (58′). The linear relations assumed in this theory were stated in Paper I, Eq. (66), as

$$\phi_{\sigma\tau} - \phi_{\sigma\tau}{}^r = \eta_{\sigma\tau\mu\nu} \Sigma_{\mu\nu}, \tag{79}$$

$$\Sigma_{\mu\nu} = \tfrac{1}{2} \bar{\delta}_{\mu\alpha} \bar{\delta}_{\nu\beta} (\partial_\alpha u_\beta + \partial_\beta u_\alpha), \tag{80}$$

where the coefficients of viscosity $\eta_{\sigma\tau\mu\nu}$ relate the excess stress tensor to the symmetric part $\Sigma_{\mu\nu}$ of the tensor which represents rate of strain relative to the rest frame. Every index of the viscosity tensor is a space

index; all time components vanish in the rest frame. Substitution of Eq. (79) into Eq. (58′) gives

$$-S_\sigma\partial_\sigma T+\eta_{\sigma\tau\mu\nu}\Sigma_{\sigma\tau}\Sigma_{\mu\nu}\geq 0, \quad (81)$$

where $\frac{1}{2}\eta_{\sigma\tau\mu\nu}\Sigma_{\sigma\tau}\Sigma_{\mu\nu}$ is the Rayleigh dissipation rate for an anisotropic medium. In the case of a transport process consisting only of heat conduction this viscous dissipation must vanish, since as we have seen, the entire dissipation in this case is $-S_\sigma\partial_\sigma T\geq 0$. Accordingly, in this case $\Sigma_{\mu\nu}$ must vanish, and $\phi_{\sigma\tau}=\phi_{\sigma\tau}{}^r$ everywhere. Because of the symmetry of the stress and rate-of-strain tensors in Eqs. (79) and (81), only 21 independent viscosity coefficients exist in the general anisotropic case. In the isotropic case, in which the excess stress and the rate-of-strain tensors can be diagonalized simultaneously, the number is reduced to 2, according to the usual arguments; here $\phi_{\sigma\tau}{}^r=-p\bar{\delta}_{\sigma\tau}$, where p is the hydrostatic pressure.

PHYSICAL REVIEW VOLUME 90, NUMBER 6 JUNE 15, 1953

The Tamm-Dancoff Formalism and the Symmetric Pseudoscalar Theory of Nuclear Forces

ABRAHAM KLEIN*
Harvard University, Cambridge, Massachusetts
(Received February 11, 1953)

The general method of deducing the Tamm-Dancoff equal-times formalism, as generalized by Lévy, from the relativistic two-body equation of Bethe-Salpeter and Schwinger is given. Only processes which are finite *ab initio* are considered. The essence of the procedure is the relation between a set of conventional matrix elements of the Tamm-Dancoff formalism and the Feynman diagram which summarizes them; this relationship provides a convenient guide for enumerating all matrix elements of a specified type and precludes the possibility of omission of any members of the set. Rules are also given for writing down any matrix element. The method is then applied to the derivation of the fourth-, sixth-, and eighth-order adiabatic potentials on the symmetrical pseudoscalar-pseudoscalar theory. Some discrepancies with the results of Lévy are noted: In connection with the fourth-order potential these are first, that a more careful treatment of the energy denominators of the leading two-pair terms brings to light contributions that cancel with all other two-pair matrix elements that are of relative order μ/M compared to the leading ones; second, that the one-pair terms do not vanish but yield a repulsive interaction which substantially alters the qualitative picture of the fourth-order potential; third, that for the no-pair terms the result should agree with the previously calculated fourth-order potential for the pseudoscalar-pseudovector theory. The sixth- and eighth-order results are also in disagreement with Lévy. Finally, an analysis of the problem of many-particle forces is given and explicit results obtained for the leading terms of the three- and four-particle forces as well as for certain smaller contributions to the three-particle interaction.

I. INTRODUCTION

IN a pair of extremely interesting papers recently published Lévy[1] has derived a three-dimensional equation for the relative motion of two particles with an interaction kernel that, in principle, can be computed to any order in the coupling constant; he has used his formalism for the most thorough examination of the nuclear forces predicted by weak coupling theory so far attempted and from the results has give a plausible account of the low energy properties of the deuteron.

Lévy's approach is a hybrid one. It consists, first of all, in an extension of the Fock space method of Tamm[2] and Dancoff[3] to include higher order processes involving multiple meson exchange and pair creation, with the proviso, however, that all infinite matrix elements associated with "radiative" corrections be omitted. It is then possible to eliminate all amplitudes except that for the two bound nucleons and to obtain an equation for the latter, which is interpreted as the wave function of the two-particle system in momentum space. To incorporate radiative corrections Lévy turns to the relativistic two-body equation[4–6] (henceforth called R.E.). He shows that by an appropriate iteration suggested by the solution for an instantaneous interaction the finite terms of the R.E. can be placed in a one-to-one correspondence with those of the T.D. (Tamm-Dancoff) formalism. It is then possible to carry out all required renormalizations *before* the reduction to equal times for the two particles is effected, and the finite residues can be incorporated into the three-dimensional interaction kernel.

The present work, begun after the author's reading of L1, was motivated by the belief that the demonstration given there of the equivalence between the T.D. formalism and the appropriately reduced R.E., though undoubtedly concerned with a true result, lacked cogency in certain details and completeness. It was felt, moreover, that since the R.E. was required for the

* Junior Fellow, Society of Fellows.
[1] M. M. Lévy, Phys. Rev. **88**, 72, 725 (1952); hereafter referred to as L1 and L2, respectively.
[2] I. Tamm, J. Phys. U.S.S.R. **9**, 449 (1945).
[3] S. M. Dancoff, Phys. Rev. **78**, 382 (1950).
[4] J. Schwinger, Proc. Natl. Acad. Sci. U. S. **37**, 452, 455 (1951).
[5] E. Salpeter and H. A. Bethe, Phys. Rev. **84**, 1232 (1951), referred to as S.B.
[6] M. Gell-Mann and F. Low, Phys. Rev. **84**, 350 (1951).

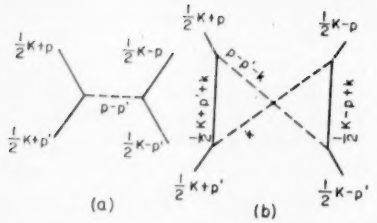

FIG. 1. Feynman diagrams for the interactions representing exchange of one or two quanta.

proper treatment of radiative corrections, it seemed reasonable, for the applications contemplated, to rest entirely within its frame work for the derivation of all results.

This paper is therefore concerned with a re-examination of some of the methods and results of L1 and L2. We shall confine ourselves completely to the parts of the theory that are finite *ab initio*, since we have nothing to add to Lévy's general prescription for treating renormalizations. In Sec. II we define the problem and indicate an apparent difficulty in generating an *equation* for equal times for the two particles using the form of unequal times wave function suggested by the solution for a static potential. There is no obstacle, however, to the derivation of such an equation for the projection of the wave function on the positive energy free-particle subspace. As in L1 and L2 it is this latter quantity that we shall designate as the wave function of the system.

Section III is devoted to a derivation of the complete interaction kernel up to the fourth order in the coupling constant. The main result of this section is the connection between a single covariant interaction term of a given order (as expressed by an appropriate four-dimensional integral and represented by a single Feynman diagram) and the number and kinds of more conventional matrix elements to which this "reduces" in the equal-times formalism. In fact, once this relationship is seen and expressed in complete generality, the equivalence of the result with the T.D. formalism becomes obvious. This relationship is undoubtedly understood by many physicists. From our present point of view, however, it becomes an extremely useful way of classifying matrix elements and of making symmetry relationships clear.

The remainder of the paper is concerned with the application of the formalism to the derivation of static nuclear potentials. In Sec. IV, we compute the leading contributions of the fourth-order adiabatic potential for the symmetric pseudoscalar theory. Our results are in disagreement with those of L2 for the two-pair, one-pair, and no-pair terms.[7] In Sec. V we outline, using our classification procedure, the derivation of the leading terms in the sixth- and eighth-order potentials. Again the results differ in detail from those of L2. The calculation of many-body forces is undertaken in Sec. VI. Explicit expressions are given for the most important terms of the three- and four-particle forces as well as contributions of one order of magnitude smaller to the three-body force. Appendix A contains a procedure for a concise derivation of the three-dimensional formalism from the R.E. and Appendix B points out that the theory contains spin-orbit forces.

The paper concludes in Sec. VII with a qualitative discussion of the status and significance of the Lévy theory. No numerical results are given, however.

[7] See reference 1, L2, Sec. III.

II. DEFINITION AND PRELIMINARY DISCUSSION OF THE PROBLEM

In this and in the following section we shall be dealing exclusively with some form of the equation

$$[\gamma(\tfrac{1}{2}K+p)+M]^{(1)}[\gamma(\tfrac{1}{2}K-p)+M]^{(2)}\psi(p_\mu) = \int d^4p' I(p,p';K)\psi(p_\mu'). \quad (1)$$

Before defining more closely the contents of Eq. (1) let us settle once and for all the matter of notation. In so far as it is possible, we shall follow the notation of S.B. and of S.[8] The Dirac matrices γ_μ are, however, the skew-symmetric ones defined by Schwinger,[9] and the reader should especially bear in mind that we shall use a γ_5 matrix whose square is minus one. However, when we pass to the α, β matrices, we shall employ the standard Dirac representation. For the necessary purposes of comparison, the notation of L1, 2 will also enter, especially from Sec. IV forward.

Thus, Eq. (1) is the two-body R.E. in momentum space for particles of equal mass M, total four-momentum K, and relative four-momentum p. For the kernel I we confine ourselves to the assumption that

$$I(p,p';K) = (2\pi i)^{-1}\lambda(\gamma_5\tau_i)^{(1)}(\gamma_5\tau_i)^{(2)}[(p-p')_\lambda{}^2 + \mu^2]^{-1} + (2\pi i)^{-2}\lambda^2\int d^4k[k_\lambda{}^2+\mu^2]^{-1}[(p-p'-k)_\nu{}^2 + \mu^2]^{-1}[\gamma_5\tau_i G(\tfrac{1}{2}K+p'+k)\gamma_5\tau_j]^{(1)} \times[\gamma_5\tau_j G(\tfrac{1}{2}K-p+k)\gamma_5\tau_i]^{(2)}, \quad (2)$$

representing the two Feynman diagrams shown in Fig. 1 for the symmetrical pseudoscalar theory with pseudoscalar coupling;[10] here

$$\lambda = g^2(2\pi)^{-3}, \quad G(p) = (\gamma p + M)^{-1}. \quad (3)$$

We shall not include in our discussion the terms of order λ^2 which are radiative corrections to the λ-term. Our problem is then as follows: We wish to derive from Eqs. (1) and (2) an equation for the three-dimensional function $\phi(\mathbf{p})$ defined by

$$\phi(\mathbf{p}) = \int_{-\infty}^{\infty}\psi(p_\mu)dp_0. \quad (4)$$

[8] E. Salpeter, Phys. Rev. **87**, 328 (1952), referred to as S.

[9] J. Schwinger, Phys. Rev. **82**, 664 (1951).

[10] In order to derive Eq. (2) and all other terms involving radiative corrections that have been omitted, we actually employed the technique of reference 4. See also R. Karplus and A. Klein, Phys. Rev. **87**, 848 (1952).

This is, in general, not possible, since we do not know the dependence of $\psi(p_\mu)$ on the relative energy variable p_0. Both S. and L1 have shown, however, that if one restricts oneself to the ladder approximation and assumes a static potential

$$[k_i^2-k_0^2+\mu^2]^{-1}\to[k_i^2+\mu^2]^{-1}, \tag{5}$$

then Eq. (1) yields a three-dimensional equation without further approximation [see S., Eq. (13) and sequel]. In terms of the solution $\phi_s(\mathbf{p})$ of this equation, $\psi(p_\mu)$ has the form:[11]

$$\psi_s(p_\mu)=[2\pi i\mathfrak{F}_W(\mathbf{p},p_0)]^{-1}\lambda\Gamma_i^{(1)}\Gamma_i^{(2)}\times\int\frac{d\mathbf{k}}{(k^2+\mu^2)}\phi_s(\mathbf{p}-\mathbf{k})$$
$$=-[2\pi i\mathfrak{F}_W(\mathbf{p},p_0)]^{-1}[W-H_1(\mathbf{p})-H_2(\mathbf{p})]\chi_s(\mathbf{p}) \tag{6}$$

with

$$\mathfrak{F}_W(\mathbf{p},p_0)=F_W^{(1)}(\mathbf{p},p_0)F_W^{(2)}(-\mathbf{p},-p_0)=[\tfrac{1}{2}W+p_0-H_1(\mathbf{p})][\tfrac{1}{2}W-p_0-H_2(\mathbf{p})] \tag{7}$$

and

$$\Gamma_i^{(r)}=(\gamma_0\gamma_5\tau_i)^{(r)}\equiv(\beta\gamma_5\tau_i)^{(r)},\ (r=1,2;\ i=1,2,3). \tag{8}$$

Equation (6) *defines* the function $\chi(\mathbf{p})$, which is then related in this approximation to $\phi(\mathbf{p})$ by the equation[12]

$$\phi(\mathbf{p})=\{\Lambda_+^{(1)}(\mathbf{p})\Lambda_+^{(2)}(\mathbf{p})-\Lambda_-^{(1)}(\mathbf{p})\Lambda_-^{(2)}(\mathbf{p})\}\chi(\mathbf{p}). \tag{9}$$

Up to this point everything in Eq. (6) is well defined, and it can, in fact, be used as the basis of a perturbation theory treatment of a "small" noninstantaneous interaction.[8,10] This is not our purpose, however; we are interested in deriving an improved *equation* for $\phi(\mathbf{p})$. Toward this end it is reasonable to adopt the second form of Eq. (6) as an *ansatz*, the physical content of which is the statement that the particles having propagated up to certain common time in a bound state, the propagation of one or the other of the particles "further" in time is according to free-particle behavior. [See Eq. (28) of S.B. for a nonrelativistic example.] We therefore insert Eq. (6) into the right-hand side (r.h.s.) of the ladder approximation

$$\mathfrak{F}_W(\mathbf{p},p_0)\psi(p_\mu)=(2\pi i)^{-1}\lambda\Gamma_i^{(1)}\Gamma_i^{(2)}\int\frac{d^4k}{k^2+\mu^2}\psi(p_\mu-k_\mu). \tag{10}$$

If we first carry out the integration over k_0 (with the usual hole theory definition of the poles), we obtain first of all an improved form for $\psi(p_\mu)$ which is a generalized version of L1, Eq. (35). We shall not record it here since we shall eventually find useful only a somewhat more limited version of the equation. Now, however, if we divide by $\mathfrak{F}_W(\mathbf{p},p_0)$ and carry out the p_0 integral, we obtain an equation which is precisely equivalent[13] to L1, Eq. (41), if, and only if, we establish the following correspondence between free-particle energy projections:

$$\phi_{++}=\chi_{++},\ \phi_{--}=-\chi_{--},\ \phi_{+-}=\chi_{+-},\ \phi_{-+}=\chi_{-+}. \tag{11}$$

The first original comment of this section is that Eq. (11) is *a priori* an incorrect identification. Though the plus-plus and minus-minus equalities are unobjectionable, since they follow from Eq. (6), the plus-minus and minus-plus equalities cannot be true, since in the adiabatic limit $\phi_{+-}=\phi_{-+}=0$, whereas χ_{+-} and χ_{-+} are finite well-defined functions.[14] The point is that the functions χ_{+-} and χ_{-+} are just not defined by anything which has been said or done up to this juncture. The resolution of the dilemma will be given below. As the final observation of this section we merely note that if one arbitrarily drops all terms of L1, Eq. (41) (or the equivalent equation which we have derived without writing down), which involve χ_{+-} and χ_{-+}, and if one eliminates ϕ_{--} in favor of ϕ_{++} as described in L1, one obtains to order λ^2 the equation

$$(W-2E_p)\phi_{++}(\mathbf{p})=\Lambda_+^{(1)}(\mathbf{p})\Lambda_+^{(2)}(\mathbf{p})\int d\mathbf{p}'[\lambda\Delta_2(\mathbf{p},\mathbf{p}')+\lambda^2\Delta_4(\mathbf{p},\mathbf{p}')]\phi_{++}(\mathbf{p}'), \tag{12}$$

where $\Delta_2(\mathbf{p},\mathbf{p}')$ recorded as Eq. (13) in the next section, is the kernel equivalent to that of L1, Eq. (36), and $\Delta_4(\mathbf{p},\mathbf{p}')$ is that equivalent to L2, Eq. (44). The latter, as we shall see in the next section is a small part of the entire fourth-order kernel or even of the pair effects to this order.

III. DERIVATION OF THE INTERACTION KERNEL TO FOURTH ORDER

The solution of the difficulty raised at the end of the previous section can be obtained by combining an observation with a more diligent job of computation. The observation is that our goal is precisely an equation of the form Eq. (12), whereby $\Delta_4(\mathbf{p},\mathbf{p}')$ we shall understand the complete T.D. interaction in fourth order. In other words, we interpret $\phi_{++}(\mathbf{p})$ as the bound state wave function in momentum space.[15] As we shall see

[11] Note that we are now working in the frame of reference defined by $K_\mu=(0,0,0,W)$; we have also used the relationship $\beta G^{-1}(p)=-F(p)$ so that we are working with the usual $\boldsymbol{\alpha},\beta$ matrices of Dirac. Note also that quantities referring to particle 2 such as $H_2(\mathbf{p})$, $\Lambda_+^{(2)}(\mathbf{p})$ are functions of $-\mathbf{p}$, though this dependence on $-\mathbf{p}$ is indicated explicitly for $F_W^{(2)}(-\mathbf{p},-\mathbf{p}_0)$.

[12] A nice logical point overlooked by S. is that having defined $\chi(\mathbf{p})$, say by Eq. (6), one can deduce therefrom by Eq. (9) the equation obeyed by the adiabatic $\phi(\mathbf{p})$, but because of the singularity of the operator involved in Eq. (9), one cannot proceed in the reverse direction.

[13] Lévy has already taken spin-matrix elements, whereas we prefer to leave our expressions in operator form until a later stage of the calculation.

[14] There appears to be an awareness of this difficulty in L2. There, the proper use of Eq. (52) can lead to no errors in the results sought, though formally it contains the incorrect statements that $\psi_{+-}(p_\mu)=\psi_{-+}(p_\mu)=0$ in the adiabatic case, whereas only their integrals with respect to p_0 have this property.

[15] See reference 1, L2, Sec. II, for a fuller and more precise statement of this connection.

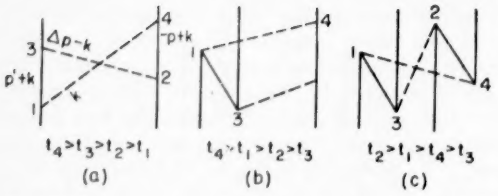

FIG. 2. Diagrams representing three typical conventional matrix elements of the twenty-four such contained in Fig. 1(b). The labeling of (a) accords with the variables used in Eq. (17).

shortly, an equation for this function can be obtained without having to be concerned directly about equations for ϕ_{++}, ϕ_{-+}, and ϕ_{--}. Before showing this, we record the form for $\Delta_2(\mathbf{p}, \mathbf{p}')$,

$$\Delta_2(\mathbf{p}, \mathbf{p}')=\frac{2\Gamma_i^{(1)}\Gamma_i^{(2)}}{2\omega(\mathbf{p}-\mathbf{p}')[W-E_p-E_{p'}-\omega(\mathbf{p}-\mathbf{p}')]}. \quad (13)$$

We have explicitly adjoined the factor of two to the quantity $\omega(\mathbf{p}-\mathbf{p}')$ in the denominator to show their joint origin in the Fourier analysis of the meson field and to point to the fact that Eq. (13) is the sum of the two possible matrix elements of the conventional type that can be associated with the exchange of a single field quantum. Since our task will later deteriorate into the mere enumeration of such matrix elements, it is well to establish good counting habits from the very beginning.

Now it is clear that if we are to derive the complete $\Delta_4(\mathbf{p}, \mathbf{p}')$, we must include both terms of Eq. (2) in Eq. (1). As a starting point we rewrite Eq. (1) as [see Eq. (7) and reference 11]

$$\begin{aligned}
&F_W^{(1)}(\mathbf{p}, p_0)F_W^{(2)}(-\mathbf{p}, -p_0)\psi(p_\mu)\\
&=(2\pi i)^{-1}\lambda\int d^4k\frac{\Gamma_i^{(1)}\Gamma_i^{(2)}}{k^2+\mu^2}\psi(p_\mu-k_\mu)\\
&+(2\pi i)^{-2}\lambda^2\int d^4k d^4p'\frac{1}{(k^2+\mu^2)[(p-p'-k)^2+\mu^2]}\\
&\times[\Gamma_i F_W^{-1}(\mathbf{p}'+\mathbf{k}, p_0+k_0)\Gamma_j]^{(1)}\\
&\times[\Gamma_j F_W^{-1}(-\mathbf{p}+\mathbf{k}, -p_0+k_0)\Gamma_i]^{(2)}\psi(p_\mu'). \quad (14)
\end{aligned}$$

In the explicit λ^2 term we can certainly approximate $\psi(p_\mu')$ by [see Eq. (6)]

$$\begin{aligned}
\psi(p_\mu)&\cong\psi_{++}^{(0)}(p_\mu)\\
&=-[2\pi i\delta_W{}_{++}(\mathbf{p}, p_0)]^{-1}[W-2E_p]\phi_{++}(\mathbf{p})\\
&=-(2\pi i)^{-1}[(\tfrac{1}{2}W+p_0-E_p)^{-1}\\
&\quad+(\tfrac{1}{2}W-p_0-E_p)^{-1}]\phi_{++}(\mathbf{p}), \quad (15)
\end{aligned}$$

an explicit form that permits us to start grinding out the integrations with respect to p_0', k_0, and p_0 successively. In the first term on the r.h.s. of Eq. (14) we require the next approximation for $\psi(p_\mu)$. This is obtained by dropping the second term on the r.h.s. of Eq. (14), writing $\psi_{++}^{(0)}(p_\mu-k_\mu)$ for $\psi(p_\mu-k_\mu)$ in the first term on the r.h.s. and solving for $\psi(p_\mu)$; thus,[16]

$$\begin{aligned}
\psi^{(1)}(p_\mu)&=[2\pi i F_W^{(1)}(\mathbf{p}, p_0)F_W^{(2)}(-\mathbf{p}, -p_0)]^{-1}\lambda\\
&\times\int d^4k\frac{\Gamma_i^{(1)}\Gamma_i^{(2)}}{k^2+\mu^2}\psi_{++}^{(0)}(p_\mu-k_\mu). \quad (16)
\end{aligned}$$

If we insert Eq. (16) into the first term on the r.h.s. of Eq. (14), take the positive energy projection of both sides, divide through by the p_0 dependent operator on the l.h.s. and finally integrate with respect to p_0, we obtain the equation

$$\begin{aligned}
&(W-2E_p)\phi_{++}(\mathbf{p})=\Lambda_+^{(1)}(\mathbf{p})\Lambda_+^{(2)}(\mathbf{p})(2\pi i)^{-2}\lambda^2\\
&\times\int d\mathbf{k}d\mathbf{p}'dp_0dk_0dp_0'[(\tfrac{1}{2}W+p_0-E_p)^{-1}+(\tfrac{1}{2}W\\
&-p_0-E_p)^{-1}][k^2+\mu^2]^{-1}[(p-p'-k)^2+\mu^2]^{-1}\\
&\times\{[\Gamma_i F_W^{-1}(\mathbf{p}-\mathbf{k}, p_0-k_0)\Gamma_j]^{(1)}[\Gamma_i F_W^{-1}(-\mathbf{p}+\mathbf{k},\\
&-p_0+k_0)\Gamma_j]^{(2)}+[\Gamma_i F_W^{-1}(\mathbf{p}'+\mathbf{k}, p_0+k_0)\Gamma_j]^{(1)}\\
&\times[\Gamma_j F_W^{-1}(-\mathbf{p}+\mathbf{k}, -p_0+k_0)\Gamma_i]^{(2)}\}\psi_{++}^{(0)}(p_\mu'). \quad (17)
\end{aligned}$$

Since the second term of the curly bracket is associated with the "crossed-quantum" diagram, Fig. 1(b), it is clear that the first term of the bracket, obtained by iteration based on Eq. (16), is nothing more than the iteration of Fig. 1(a). The dependence of the r.h.s. of Eq. (17) on the variables p_0, k_0, and p_0' is explicit; all poles are well defined, and therefore the integrations can be effected.

We now claim that the r.h.s. of Eq. (17) contains all of the T.D. $\Delta_4(\mathbf{p}, \mathbf{p}')$ [as well as the iteration of $\Delta_2(\mathbf{p}, \mathbf{p}')$]. We have verified this by actually performing the integrations over the relative energy variables and unscrambling the results. Whether it would have been possible to emerge from the labyrinth of algebraic manipulation involved without knowing the answer beforehand is a moot point. In any case, it is much more instructive to describe the answer than to reproduce the manipulations, since the description leads immediately to the generalization of the result to any order in the coupling constant, whereas actual computation by the means described starting from an equation like (17) becomes prohibitive for any order higher than λ^2. A more concise, and in a sense more physical, procedure for deriving the results described below is given in Appendix A.

Consider first the term in Eq. (17) corresponding to Fig. 1(b). It must contain all the matrix elements of fourth-order perturbation theory which describe the exchange of two mesons in the manner indicated, starting from a bound state of positive energy, ending with such a state, and proceeding *via* free-particle inter-

[16] Equation (16) is the immediate generalization, in our notation, of Eq. (35) of L1, though we have not given the explicit result of the integration with respect to k_0, for reasons of presentation that will become clear below. Note that although $\psi^{(0)}$ contains only a plus-plus part, $\psi^{(1)}$ contains both positive and negative free-particle energies.

mediate states of both positive and negative energy. There are 24 such matrix elements corresponding to the 4! time orderings of the interaction points of the figure. In the terminology of L1, 2 there are six two-pair terms, twelve one-pair terms, and six no-pair terms. Rather than record all twenty-four, we show in Fig. 2 diagrams of the type used by Lévy representing three typical matrix elements. They yield, in our notation, the following contributions to $\Delta_4(\mathbf{p}, \mathbf{p}')$ [in the context of Eq. (12)]:

$$\Delta_4^{(a)}(\mathbf{p}, \mathbf{p}') = \int d\mathbf{k} \frac{[\Gamma_i \Lambda_+(\mathbf{p}'+\mathbf{k})\Gamma_j]^{(1)}[\Gamma_j \Lambda_+(\mathbf{p}-\mathbf{k})\Gamma_i]^{(2)}}{4\omega_k\omega_{p-p'-k}(W-E_p-E_{p-k}-\omega_k)(W-E_{p-k}-E_{p'+k}-\omega_k-\omega_{p-p'-k})(W-E_{p'}-E_{p'+k}-\omega_k)}, \quad (18)$$

$$\Delta_4^{(b)}(\mathbf{p}, \mathbf{p}') = -\int d\mathbf{k} \frac{[\Gamma_i \Lambda_-(\mathbf{p}'+\mathbf{k})\Gamma_j]^{(1)}[\Gamma_j \Lambda_+(\mathbf{p}-\mathbf{k})\Gamma_i]^{(2)}}{4\omega_k\omega_{p-p'-k}(W-E_p-E_{p-k}-\omega_k)(W-E_p-E_{p'}-E_{p-k}-E_{p'+k})(-E_p-E_{p'+k}-\omega_{p-p'-k})}, \quad (19)$$

and

$$\Delta_4^{(c)}(\mathbf{p}, \mathbf{p}') = \int d\mathbf{k} \frac{[\Gamma_i \Lambda_-(\mathbf{p}'+\mathbf{k})\Gamma_j]^{(1)}[\Gamma_j \Lambda_-(\mathbf{p}-\mathbf{k})\Gamma_i]^{(2)}}{4\omega_k\omega_{p-p'-k}(-E_{p'}-E_{p'+k}-\omega_k)(-W-E_{p'+k}-E_{p-k}-\omega_k-\omega_{p-p'-k})(-E_p-E_{p-k}-\omega_k)}. \quad (20)$$

The rules for writing down Eqs. (18)–(20) are almost self-evident from the diagrams: The factors associated with the vertices, sums over intermediate spin states, and Fourier analysis of meson field are indeed so; there is a minus sign for an odd number of pairs, if all factors of the energy denominators are written as $W-E_I$, where E_I is the energy of the intermediate state. The apparently curious form of some of the energy denominators is explained, if we remark that whenever an intermediate state contains two nucleons in the initial or in the final state, their energy[17] is W and not $2E_{p'}$ or $2E_p$. Using these rules one can record all the contributions from Fig. 1(b) as they are actually provided by fairly elaborate calculation.

Turning to the contribution from the "ladder" diagram, the iteration of Fig. 1(a), there are again twenty-four physically distinct matrix elements which can be systematically enumerated. Here, however, a new but anticipated factor enters. Whereas in the previous case, no matrix element contained intermediate states in which only two nucleons are present, here one encounters four such elements, one of which is illustrated in Fig. 3, and with the remaining three obvious variants thereof. In terms of the present formalism, these are "reducible" diagrams, since one obtains their apparent contribution to Δ_4 by iterating Eq. (12) in which Δ_2 is given by Eq. (13). Clearly the correct procedure is to "uniterate" these terms. In this way we have derived the kernel $\lambda\Delta_2+\lambda^2\Delta_4$, the latter consisting of forty-four matrix elements of the conventional type.

Before proceeding, perhaps an additional word is in order justifying the process of "uniteration" beyond the purely formal reason that it leads to a known result. It should be noted that the energy denominator associated with an intermediate state in which only two nucleons are present can become small of the order of the binding energy in the nonrelativistic limit. On the other hand, the energy denominators of intermediate states in which there are mesons are no smaller than the order of μc^2 and those containing pairs of the order of Mc^2 in the nonrelativistic limit. Other things being equal (as is *not* the case in the pseudoscalar theory because of the properties of the γ_5 matrix), the iterated second-order terms would apparently give the largest contribution to the fourth-order potential, a result that would vary inversely with the binding energy. If one dropped all terms of the interaction kernel other than these, one would notice that one solution of the resulting equation could be obtained by "uniterating." This argument is equivalent to that already presented.

At this point, the formal generalization of our procedure to any order can be made. Suppose we were interested in the complete T.D. kernel correct through order $2n$. We could then easily write a generalized version of Eq. (17), which on the r.h.s. would contain n meson propagation functions and in the bracket the factors characteristic of the $n!$ Feynman diagrams (many of them reducible in the sense of S.B.) associated with the exchange of n field quanta and no radiative corrections. If we carried out the integration over all the relative energy variables, we should obtain $(2n)!\times n!$ matrix elements of the conventional type, many of them reducible in the sense defined above. These can all be recognized as arising from anywhere from 1 to $n-1$ iterations of a lower order equation according to the degree of reducibility of the matrix element. The latter is defined as the number of intermediate states with only two nucleons present.

In practice, we shall merely write down any set of matrix elements that may be of interest directly from the diagrams that represent them. This technique together with the underlying rules will be extensively

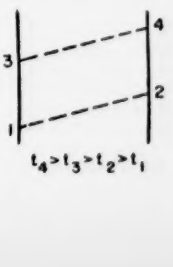

FIG. 3. Diagram representing one of four "reducible" matrix elements in fourth order. Others are $t_4>t_3>t_1>t_2$, $t_3>t_4>t_2>t_1$, $t_3>t_4>t_1>t_2$. All yield precisely the same matrix elements.

[17] This rule is clearly contained in the formalism. It is relevant only when pair production is considered.

used throughout the remainder of this paper. We turn first to a re-examination of the fourth-order potential.

IV. FOURTH-ORDER ADIABATIC NUCLEAR FORCES[18]

As shown in L2, the leading terms of the adiabatic fourth-order potential are of order (in the sense of expansion parameter) $(g^2/4\pi)^2(\mu/2M)^2$ and $(g^2/4\pi)^2(\mu/2M)^3$. To the former order one has strictly a static potential. To the next order, however, one must recognize the appearance of velocity-dependent forces. One can show, however, as in part C of this section (Lévy was undoubtedly aware of this) that such terms need not be considered in connection with the low energy properties of the two-nucleon system. Even omitting these terms we are in disagreement with the results of L2, as demonstrated in parts A and B. We preface the detailed discussion with a simplified formulation of the adiabatic limit.

To define the adiabatic potential one takes matrix elements of both sides of Eq. (12) with respect to positive energy free-particle Dirac spinors[19] and transforms back to coordinate space. The r.h.s. of Eq. (12) then takes the form[20]

$$V\psi(\mathbf{r})=\int d\mathbf{r}'[V_2(\mathbf{r},\mathbf{r}')+V_4(\mathbf{r},\mathbf{r}')]\psi(\mathbf{r}'), \quad (21)$$

where the quantity that now interests us, $V_4(\mathbf{r},\mathbf{r}')$, is given by the expression

$$V_4(\mathbf{r},\mathbf{r}')=\lambda^2(2\pi)^{-3}\int d\mathbf{p}d\mathbf{p}'e^{i\mathbf{p}\cdot\mathbf{r}}e^{-i\mathbf{p}'\cdot\mathbf{r}'} \times(\mathbf{p},-\mathbf{p}|\Delta_4(\mathbf{p},\mathbf{p}')|\mathbf{p}',-\mathbf{p}'), \quad (22)$$

and the matrix elements are between appropriately labelled Dirac spinors for the two particles. We further note that $\Delta_4(\mathbf{p},\mathbf{p}')$ has the form

$$\Delta_4(\mathbf{p},\mathbf{p}')=\int d\mathbf{k}_1 O_4(\mathbf{p},\mathbf{p}',\mathbf{k}_1). \quad (23)$$

To arrive at the adiabatic limit it is convenient to introduce the variable $\mathbf{k}_2$ by setting

$$\mathbf{p}'=\mathbf{p}-\mathbf{k}_1-\mathbf{k}_2. \quad (24)$$

In the limit in which p becomes vanishingly small Eq. (22) reduces to

$$V_4(\mathbf{r},\mathbf{r}')\to\delta(\mathbf{r}-\mathbf{r}')V_4(\mathbf{r}), \quad (25)$$

$$V_4(\mathbf{r})=\lambda^2\int d\mathbf{k}_1 d\mathbf{k}_2\exp[i(\mathbf{k}_1+\mathbf{k}_2)\cdot\mathbf{r}] \times(\mathbf{p},-\mathbf{p}|O_4(\mathbf{p},\mathbf{k}_1,\mathbf{k}_2)| \times\mathbf{p}-\mathbf{k}_1-\mathbf{k}_2,-\mathbf{p}+\mathbf{k}_1+\mathbf{k}_2)|_{p=0}. \quad (26)$$

[18] The results of this section and of the following one were reported by the author in Phys. Rev. **89**, 1158 (1953).

[19] As in reference 1, L1, Sec. III, 1. See also L2, Sec. II. Since we shall be interested only in the adiabatic potential, we need not be as elegant as in the latter reference.

[20] The differences between $\psi(\mathbf{r})$ and the function $\phi^{(0,0)}(\mathbf{r})$ of L2 are immaterial for our purposes.

A. Two-Pair Terms

According to our method of counting there are twelve distinct matrix elements of this type,[21] six having their origin in the ladder approximation (henceforth called M_1 matrix elements) and six in the diagram of Fig. 1(b) (henceforth called M_2 elements). A typical spin matrix element is

$$(\mathbf{p}|\Gamma_i^{(1)}\Lambda_-^{(1)}(\mathbf{p}-\mathbf{k})\Gamma_j^{(1)}|\mathbf{p}-\mathbf{k}_1-\mathbf{k}_2) =\tau_i^{(1)}\tau_j^{(1)}+O((\mu/M)^2), \quad (27)$$

since

$$\gamma_0\gamma_b\Lambda_-\gamma_0\gamma_b=\Lambda_+, \quad (28)$$

and the latter may be replaced by unity to the order indicated.[22] The isotopic spin operator associated with M_1 elements is $(\boldsymbol{\tau}^{(1)}\cdot\boldsymbol{\tau}^{(2)})^2=3-2\boldsymbol{\tau}^{(1)}\cdot\boldsymbol{\tau}^{(2)}$ whereas that associated with M_2 elements is $\tau_i^{(1)}\tau_j^{(1)}\tau_j^{(2)}\tau_i^{(2)}=3+2\boldsymbol{\tau}^{(1)}\cdot\boldsymbol{\tau}^{(2)}$.

Following Lüders,[23] we note that it is necessary to treat the energy denominators of the leading terms, involving at most one pair at a given time, with a little extra care. For example, M_1 contributes two denominators of the form (Fig. 1a$_1$ of L2)

$$(-E_p-E_{p-k_1}-\omega_1)(W-E_p-E_{p-k_1}-k_2-\omega_1-\omega_2) \times(-E_{p-k_1-k_2}-E_{p-k_1}-\omega_2)\cong-(2M)^2(\omega_1+\omega_2) \times\left\{1+\frac{\omega_1+\omega_2}{2M}+\frac{1}{(\omega_1+\omega_2)}\left[\frac{p^2+(p-k_1-k_2)^2}{2M}+\epsilon\right]\right\}, \quad (29)$$

where ϵ is the binding energy. Equation (29) is essentially an expansion in powers of (μ/M), and though objectionable from a strict mathematical point of view, it certainly has equal validity with the other approximations carried out in the nonrelativistic domain, for example, the manner of evaluation of spin matrix elements.

It is found that the elements of M_1 and M_2 contribute equally to the final result (the $\boldsymbol{\tau}^{(1)}\cdot\boldsymbol{\tau}^{(2)}$ dependence canceling). With a notation paralleling that of L2, we then find

$$V_4^{(a)}(\mathbf{r},\mathbf{r}')=-\frac{\lambda^2}{(2\pi)^3}\frac{3}{(2M)^2}\int d\mathbf{p}d\mathbf{k}_1 d\mathbf{k}_2 \times e^{i\mathbf{p}\cdot(\mathbf{r}-\mathbf{r}')}e^{i(\mathbf{k}_1+k_2)\cdot\mathbf{r}'}\frac{1}{\omega_1\omega_2(\omega_1+\omega_2)} \times\left\{1-\frac{\omega_1+\omega_2}{2M}-\frac{[p^2+(p-k_1-k_2)^2]/2M+\epsilon}{\omega_1+\omega_2}\right\}. \quad (30)$$

[21] See Fig. 1 of L2 for typical diagrams.

[22] It is shown in Appendix B that the terms neglected in Eq. (27) give rise to spin-orbit coupling.

[23] G. Lüders, Institute for Theoretical Physics, Copenhagen, Denmark (unpublished manuscript). However, Lüders does not include the binding energy terms in Eq. (29), which play an important role in the considerations of part C below.

In Eq. (30) the first term in the face brackets is the $V_4^{(a)}$ of L2; the second term, which results from expansion of denominators associated with intermediate states which contain a pair, precisely cancels the $V_4^{(b)}$ of L2; the third term is velocity dependent. The latter type of term always results from the expansion of an energy denominator in which there are no pairs and one or more mesons. It will be shown quite generally in part C that such terms need not be included in the treatment of the low energy properties of the two-nucleon system. We therefore assert that, except for corrections of relative order $(\mu/M)^2$, the adiabatic potential contributed by the two-pair terms has the form

$$V_4(r)=-3\left(\frac{g^2}{4\pi}\right)^2\left(\frac{\mu}{2M}\right)^2\frac{1}{\mu r^2}\frac{2}{\pi}K_1(2\mu r). \quad (31)$$

B. One-Pair Terms

Of the twenty-four one-pair matrix elements twelve are too small by a factor μ/M. The remaining twelve belong half to M_1 and half to M_2. Three of the diagrams for M_1 are shown in Fig. 4. The remaining contributions to M_1 result from interchange of the two particles and those of M_2 by uncrossing the meson lines. Beneath each diagram is indicated its energy denominator in the adiabatic limit. The first point to be emphasized is that each set of three matrix elements yields precisely the same set of energy denominators. The second fact to be noted is that the spin matrix element for one particle is unity, whereas for the other it has the typical form:[24]

$$[\mathbf{p}|\Lambda_-^{(r)}(\mathbf{p}-\mathbf{k}_1)|\mathbf{p}-\mathbf{k}_1-\mathbf{k}_2]$$
$$=-(2M)^{-2}\boldsymbol{\sigma}^{(r)}\cdot\mathbf{k}_1\boldsymbol{\sigma}^{(r)}\cdot\mathbf{k}_2+O((\mu/M)^4). \quad (32)$$

All the spin matrix elements have this form with the interchange of k_1 and k_2 the only alternative that arises. The remainder of each matrix element is symmetrical in the two momenta, so that this is not a significant change. In short, we claim that the M_1 and M_2 elements yield precisely the same contributions, except for the isotopic spin operators and when added together the $\boldsymbol{\tau}^{(1)}\cdot\boldsymbol{\tau}^{(2)}$ dependence cancels, but the remainder adds. In all we find that

$$V_4'(\mathbf{r})=-\frac{3\lambda^2}{(2M)^3}\int d\mathbf{k}_1 d\mathbf{k}_2\frac{e^{i(\mathbf{k}_1+\mathbf{k}_2)\cdot\mathbf{r}}}{4\omega_1\omega_2}4\mathbf{k}_1\cdot\mathbf{k}_2$$
$$\times\left[\frac{1}{\omega_1(\omega_1+\omega_2)}+\frac{1}{\omega_2(\omega_1+\omega_2)}+\frac{1}{\omega_1\omega_2}\right]$$
$$=-\frac{6\lambda^2}{(2M)^3}\left(\int\frac{\mathbf{k}d\mathbf{k}e^{i\mathbf{k}\cdot\mathbf{r}}}{\omega^2}\right)^2$$
$$=6(g^2/4\pi)^2(\mu/2M)^3(\mu r^2)^{-1}$$
$$\times[1+(\mu r)^{-1}]^2e^{-2\mu r}. \quad (33)$$

[24] The value of the first term of the matrix element is obtained without the adiabatic approximation.

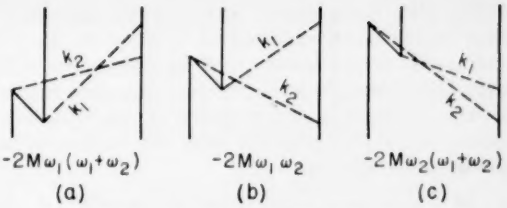

FIG. 4. Diagrams representing three of the six one-pair matrix elements belonging to M_1.

The net result is thus a repulsive potential, which at distances $r\lesssim\mu^{-1}$ is appreciably more significant than the second-order central potential. The neutral theory[25] yields a third of Eq. (33).

The fourth-order potential which we propose is the sums of Eqs. (31) and (33). It is hoped to report separately on the low energy properties of the two-nucleon system predicted by this potential used in conjunction with the well-known second-order result (and the hard-core model of L2). Further qualitative discussion of the model is given in Sec. VII.

C. Velocity Dependent Forces

We turn here to the proof of the assertion made in part A that a certain class of velocity dependent forces need not be included in a first treatment of the low energy properties of the two-nucleon system. The procedure to be employed is merely an adaptation to the present case of the proof given in L1 of the well-known result that there is a cancellation in the neutral scalar theory between the fourth-order potential and velocity dependent corrections to the second-order potential. For the sake of concreteness the discussion will be confined to the terms of actual interest, though it will be seen that the method of attack is widely applicable.

Consider the Schrödinger equation in momentum space with interaction terms consisting of the second-order terms plus the leading two-pair fourth-order terms,

$$\left(-\frac{p^2}{M}-\epsilon\right)\phi(\mathbf{p})=\lambda\int\frac{d\mathbf{k}\,\boldsymbol{\sigma}^{(1)}\cdot\mathbf{k}\boldsymbol{\sigma}^{(2)}\cdot\mathbf{k}}{\omega}\frac{}{(2M)^2}$$
$$\times\frac{\boldsymbol{\tau}^{(1)}\cdot\boldsymbol{\tau}^{(2)}}{W-E_p-E_{p-k}-\omega}\phi(\mathbf{p}-\mathbf{k})+\frac{\lambda^2}{(2M)^2}\int\frac{d\mathbf{k}_1d\mathbf{k}_2}{4\omega_1\omega_2}$$
$$\times\left[\frac{2(3-2\boldsymbol{\tau}^{(1)}\cdot\boldsymbol{\tau}^{(2)})}{W-E_p-E_{p-k_1-k_2}-\omega_1-\omega_2}\right.$$
$$\left.+\frac{2(3+2\boldsymbol{\tau}^{(1)}\cdot\boldsymbol{\tau}^{(2)})}{W-E_p-E_{p-k_1-k_2}-\omega_1-\omega_2}\right]$$
$$\times\phi(\mathbf{p}-\mathbf{k}_1-\mathbf{k}_2). \quad (34)$$

[25] See L2, reference 14, where the result should be multiplied by a factor of two. It is difficult to see how the symmetric and neutral theory can possibly differ other than in the isotopic spin operator dependence.

In Eq. (34), the adiabatic limit has been selectively taken in the fourth-order terms, namely, in the denominators corresponding to intermediate states with pairs. These denominators have been adequately treated in part *A*. If we now expand the remaining type of denominator about its adiabatic limit, the resulting equation can be written as

$$\left(-\frac{p^2}{M}-\epsilon\right)\phi(\mathbf{p})=-\lambda\boldsymbol{\tau}^{(1)}\cdot\boldsymbol{\tau}^{(2)}\int d\mathbf{k}\frac{\boldsymbol{\sigma}^{(1)}\cdot\mathbf{k}\boldsymbol{\sigma}^{(2)}\cdot\mathbf{k}}{(2M)^2}$$
$$\times\left\{\frac{1}{\omega^2}+\frac{1}{\omega^3}\left[\frac{(\mathbf{p}-\mathbf{k})^2-p^2}{2M}-\frac{(\mathbf{p}-\mathbf{k})^2}{M}-\epsilon\right]\right\}\phi(\mathbf{p}-\mathbf{k})$$
$$-\frac{3\lambda^2}{(2M)^2}\int\frac{d\mathbf{k}_1d\mathbf{k}_2}{\omega_1\omega_2}\left\{\frac{1}{\omega_1+\omega_2}+\frac{1}{(\omega_1+\omega_2)^2}\right.$$
$$\left.\times\left[\frac{(\mathbf{p}-\mathbf{k}_1-\mathbf{k}_2)^2-p^2}{2M}-\frac{(\mathbf{p}-\mathbf{k}_1-\mathbf{k}_2)^2}{M}-\epsilon\right]\right\}$$
$$\times\phi(\mathbf{p}-\mathbf{k}_1-\mathbf{k}_2). \quad (35)$$

The deliberate rearrangement of the velocity-dependent terms assumes significance, if we take the point of view that these terms are to be treated as a small perturbation to the problem defined by the static second plus fourth order potential. First of all then, we invoke the argument given in L1, Sec. 4.32, based on variational principle Eq. (49) of L1, to show that the terms proportional to the difference of the kinetic energies of initial and final momentum states vanish. We then iterate the remaining velocity-dependent terms by making use of the Schrödinger equation of the unperturbed problem. In this way the velocity dependent corrections to the second-order potential give rise to fourth- and sixth-order *static* potentials, whereas velocity-dependent corrections to the fourth-order potential give rise to sixth- and eighth-order *static* potentials. These potentials which we denote by $\delta V_4(r)$, $\delta V_6(r)$ and $\delta V_8(r)$, respectively, have the form (after Fourier transformation)

$$\delta V_4(r)=\frac{\lambda^2}{(2M)^4}(\boldsymbol{\tau}^{(1)}\cdot\boldsymbol{\tau}^{(2)})^2\int\frac{d\mathbf{k}_1d\mathbf{k}_2}{\omega_1^3\omega_2^2}\exp[i(\mathbf{k}_1+\mathbf{k}_2)\cdot\mathbf{r}]$$
$$\times\boldsymbol{\sigma}^{(1)}\cdot\mathbf{k}_1\boldsymbol{\sigma}^{(1)}\cdot\mathbf{k}_2\boldsymbol{\sigma}^{(2)}\cdot\mathbf{k}_1\boldsymbol{\sigma}^{(2)}\cdot\mathbf{k}_2, \quad (36)$$

$$\delta V_6(r)=\frac{3\lambda^2}{(2M)^4}\boldsymbol{\tau}^{(1)}\cdot\boldsymbol{\tau}^{(2)}\int\frac{d\mathbf{k}_1d\mathbf{k}_2d\mathbf{k}_3}{\omega_1\omega_2\omega_3}$$
$$\times\exp[i(\mathbf{k}_1+\mathbf{k}_2+\mathbf{k}_3)\cdot\mathbf{r}]\boldsymbol{\sigma}^{(1)}\cdot\mathbf{k}_1\boldsymbol{\sigma}^{(2)}\cdot\mathbf{k}_1$$
$$\times\left[\frac{1}{\omega_1^2(\omega_2+\omega_3)}+\frac{1}{\omega_1(\omega_2+\omega_3)^2}\right], \quad (37)$$

$$\delta V_8(r)=\frac{9\lambda^4}{(2M)^4}$$
$$\times\int\frac{d\mathbf{k}_1\cdots d\mathbf{k}_4\exp[i(\mathbf{k}_1+\mathbf{k}_2+\mathbf{k}_3+\mathbf{k}_4)\cdot\mathbf{r}]}{\omega_1\omega_2\omega_3\omega_4(\omega_1+\omega_2)^2(\omega_3+\omega_4)}. \quad (38)$$

Anticipating some of the results to be derived in the sections which follow, we note here that when we derive the no-pair terms of the fourth-order potential and the leading terms of the sixth- and eighth-order potentials, we shall find contributions which respectively cancel Eqs. (36)–(38). This phenomenon, in addition to the entire development of this section, points to the fact, previously remarked,[26] that in the low energy limit it is, in general, inconsistent to consider velocity-dependent corrections to the potential except in conjunction with static potentials of higher order.

D. No-Pair Terms

Here only two matrix elements are contributed by the ladder diagram (M_1), but there is the full complement of six of type M_2. (Four M_1 elements were of the reducible type.) The result we shall record differs from that given in L2, Eq. (20), in two respects. First, we omit the first term of the latter equation since it cancels, as promised, against $\delta V_4(r)$, Eq. (36). Secondly, we obtain an additional spin-independent, but charge-dependent term not found there. As the adiabatic no-pair term, we therefore take (some rearrangement is involved)

$$V_4''(r)=-\frac{\lambda^2}{(2M)^4}\int\frac{d\mathbf{k}_1d\mathbf{k}_2\exp[i(\mathbf{k}_1+\mathbf{k}_2)\cdot\mathbf{r}]}{\omega_1^2\omega_2(\omega_1+\omega_2)}$$
$$\times[2\boldsymbol{\tau}^{(1)}\cdot\boldsymbol{\tau}^{(2)}(\mathbf{k}_1\cdot\mathbf{k}_2)^2+3\boldsymbol{\sigma}^{(1)}\cdot(\mathbf{k}_1\times\mathbf{k}_2)$$
$$\times\boldsymbol{\sigma}^{(2)}\cdot(\mathbf{k}_1\times\mathbf{k}_2)]\left[\frac{2}{\omega_1}+\frac{1}{\omega_2}\right]. \quad (39)$$

We note parenthetically that if we multiply the equation above by $(2M/\mu)^4$, the resulting expression is just the *leading* term of the fourth-order potential of the pseudoscalar theory with pseudovector coupling. That the no-pair terms give the leading contribution in this case is a consequence, first of all, of the fact that for derivative coupling the spin matrix elements are of the same order of magnitude for no-pair, one-pair, and two-pair interactions. One then chooses for maximum contribution the terms with minimum energy denominators, i.e., the no-pair terms. The equivalence to the pseudoscalar result then follows from the observation that it is the spatial part of the coupling that is largest for the no-pair terms.

After a fairly laborious calculation we find for the potential of Eq. (39),

$$V_4''(\mathbf{r})=\mu(g^2/4\pi)^2(\mu/2M)^4[\boldsymbol{\tau}^{(1)}\cdot\boldsymbol{\tau}^{(2)}U_\tau(\mu r)$$
$$+\boldsymbol{\sigma}^{(1)}\cdot\boldsymbol{\sigma}^{(2)}U_\sigma(\mu r)+S_{12}U_T(\mu r)], \quad (40)$$

where

$$U_\tau(x)=(8/\pi)[-A_1+2A_2-4A_3+2A_4],$$
$$U_\sigma(x)=(8/\pi)[-2A_2+2A_3-A_4], \quad (41)$$
$$U_T(x)=(4/\pi)[2A_2-5A_3+4A_4],$$

[26] Y. Nambu, Progr. Theoret. Phys. **5**, 614 (1950).

and

$$A_1=K_0^{IV}(2x)/x, \qquad A_2=K_0'''(2x)/x^2,$$
$$A_3=K_0''(2x)/x^3, \qquad A_4=K_0'(2x)/x^4, \tag{42}$$

the superscripts indicating derivative. Equations (40) to (42) are in agreement with the work of previous authors who have considered the $ps-pv$ theory of nuclear forces.[27]

For the pseudoscalar coupling case we remark finally that, if we wish to include in a consistent fashion potentials of the order of magnitude of those considered in this section, we must also take into account terms arising from (a) velocity dependence in the spin-matrix elements of the two-pair diagrams; part of these are shown in Appendix B to lead to spin-orbit coupling; (b) corrections to the pair denominators of two-pair and one-pair matrix elements already included in lowest approximation; (c) one-pair matrix elements previously neglected.

V. SIXTH- AND EIGHTH-ORDER ADIABATIC POTENTIALS

A. Sixth-Order Results

The prescription given in Sec. III can be directly applied to the computation of any desired portion of the sixth-order potential. All matrix elements are contained in the six Feynman diagrams, shown in Fig. 5. There are $3!\times 6!=4320$ matrix elements in all; of these 8 from Fig. 5(a) merely contain Δ_2 three times, and 176 from Figs. 5(a), (b), (c) are combinations of Δ_2 and Δ_4 in either order. Only the remaining 4136 matrix elements are *bona fide* members of the sixth-order interaction kernel. Fortunately, only a small fraction of these (128 in all) contribute to the leading term of the adiabatic potential.

To see this we first look for contributions with the largest possible spin matrix elements. These are of the general form[28]

$$(\mathbf{p}_r|\Gamma^{(r)}\Lambda_+^{(r)}(\mathbf{p}_r-\epsilon_r\mathbf{k}_i)\Gamma^{(r)}\Lambda_\mp(\mathbf{p}_r-\epsilon_r\mathbf{k}_i-\epsilon_r\mathbf{k}_j)$$
$$\times\Gamma^{(r)}|\mathbf{p}_r-\epsilon_r(\mathbf{k}_1+\mathbf{k}_2+\mathbf{k}_3))=(\mathbf{p}_r|\Lambda_\mp^{(r)}(\mathbf{p}_r-\epsilon_r\mathbf{k}_i)$$
$$\times\Gamma^{(r)}\Lambda_\pm(\mathbf{p}_r-\epsilon_r\mathbf{k}_i-\epsilon_r\mathbf{k}_j)|\mathbf{p}_r-\epsilon_r(\mathbf{k}_1+\mathbf{k}_2+\mathbf{k}_3)), \tag{43}$$

admitting the restriction that in sixth order there can be at most one pair associated with each nucleon line, but insisting on that pair for maximum value of the matrix element. We shall designate the two matrix elements involved in Eq. (43) by $(+-)_{i+j}$ and $(-+)_i$. Then with $\Gamma^{(r)}=(\gamma_0\gamma_5)^{(r)}$ these have the general values

$$(+-)_{i+j}=(2M)^{-1}i\boldsymbol{\sigma}^{(r)}\cdot\epsilon_r\mathbf{k}_l, \quad (l\neq j\neq i), \tag{44}$$
$$(-+)_i=(2M)^{-1}i\boldsymbol{\sigma}^{(r)}\cdot\epsilon_r\mathbf{k}_i. \tag{45}$$

According to Fig. 5, for $r=1$, $i=1$ and $l=3$, whereas for $r=2$ the values which these indices assume varies from diagram to diagram but are the same for all matrix elements arising from a given diagram. Thus for each of the graphs a–f there are four possible spin elements consistent with our option of choosing a $(+-)$ or a $(-+)$ matrix element independently for each particle.

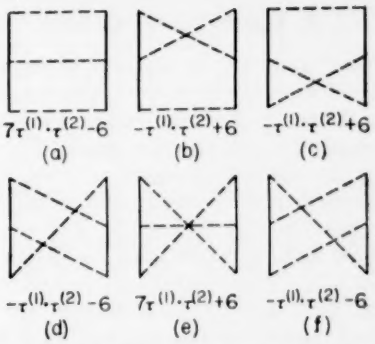

FIG. 5. Feynman diagrams for sixth-order interaction kernel. Beneath each figure stands the associated isotopic operator for matrix elements derived therefrom.

With this much settled and with the isotopic operators already designated in Fig. 5, one can begin the job of enumerating allowed matrix elements as soon as one recognizes that minimum energy denominators are associated with those processes in which a virtual pair created at a given point is annihilated at the next interaction point. (The restriction to one pair at a time is not sufficiently stringent here.) A typical diagram having its origin in our Fig. 3(f) is Fig. 3(a) of L2. A job of straightforward enumeration shows that twenty-four matrix elements of the specified type arise from each of Figs. 5(d), (e), (f), twenty (irreducible) elements each from (b), (c), and sixteen from (a), 128 in all. Counting up is simplified by the fact that (d) and (f) yield precisely the same set of matrix elements, as do (b) and (c). Further, for each Feynman diagram the matrix elements classify into sets associated with the different spin matrix elements, and when one takes advantage of symmetry properties in the meson momenta, there turns out to be in all only four distinct sets, comprising at most six matrix elements each. These then combine further into two sets. Of these one precisely cancels, as promised, the quantity $\delta V_6(r)$ of Eq. (37). The remainder which we take as the sixth-order adiabatic potential has the extremely simple appearance[29]

$$V_6(r)=-\left(\frac{g^2}{4\pi}\right)^3\left(\frac{1}{2M}\right)^4\boldsymbol{\tau}^{(1)}\cdot\boldsymbol{\tau}^{(2)}(2\pi^2)^{-3}\int\frac{d\mathbf{k}_1d\mathbf{k}_2d\mathbf{k}_3}{\omega_1^2\omega_2^2\omega_3^2}$$
$$\times\exp[i(\mathbf{k}_1+\mathbf{k}_2+\mathbf{k}_3)\cdot\mathbf{r}]4\boldsymbol{\sigma}^{(1)}\cdot\mathbf{k}_1\boldsymbol{\sigma}^{(2)}\cdot\mathbf{k}_3$$
$$=(4/3)(g^2/4\pi)^3(\mu/2M)^4\boldsymbol{\tau}^{(1)}\cdot\boldsymbol{\tau}^{(2)}(\mu^2r^3)^{-1}$$
$$\times[1+(\mu r)^{-1}]^2[\boldsymbol{\sigma}^{(1)}\cdot\boldsymbol{\sigma}^{(2)}+S_{12}]e^{-3\mu r}. \tag{46}$$

[27] K. Nishijima, Progr. Theoret. Phys. **6**, 815, 911 (1951). Taketani, Machida, and Onuma, Progr. Theoret. Phys. **6**, 638 (1951).

[28] Our notation parallels L1; thus $\mathbf{r}=1, 2$; $\mathbf{p}_1=-\mathbf{p}_2=\mathbf{p}$; $\epsilon_1=-\epsilon_2=1$. The isotopic dependence has been removed from the matrix element; $i, j, l=1, 2, 3$ each. One seeks the largest value of the spin matrix elements first because in the adiabatic region, these differ from one another by even powers of μ/M, whereas for energy denominators one progresses one power at a time.

[29] We obtain the result of L2, Eq. (23), if we include only those matrix elements which he explicitly stipulates, namely, those with two intermediate states in which there are two mesons present and one intermediate state with three mesons. There are many other possibilities, however.

B. Eighth-Order Results

We proceed as before: As the basis of our analysis, we use the twenty-four eighth-order Feynman diagrams involving the exchange of four mesons. The associated isotopic operators are easily computed. The leading terms of the adiabatic potential are the four-pair terms with no more than one pair present in any intermediate state (see Fig. 3(b) of L2). The spin matrix elements are unity to lowest order, as for the fourth-order potential. The conventional matrix elements associated with each Feynman diagram are readily enumerated—twenty of the diagrams yield six irreducible elements each, and the remaining four diagrams just two each. In the adiabatic limit, all these diagrams yield, aside from the charge dependence, just three distinct sets of matrix elements. Again it is found that a considerable part of the result cancels $\delta V_8(r)$ Eq. (38). The net result is then[30]

$$V_8(r)=-3\left(\frac{g^2}{2M}\right)^4(2\pi)^{-12}\int d\mathbf{k}_1\cdots d\mathbf{k}_4 \times\frac{\exp[i(\mathbf{k}_1+\mathbf{k}_2+\mathbf{k}_3+\mathbf{k}_4)\cdot\mathbf{r}]}{\omega_1\omega_2\omega_3\omega_4} \times\left[\frac{3}{(\omega_1+\omega_2)(\omega_1+\omega_3)(\omega_2+\omega_4)}+\frac{2}{(\omega_1+\omega_2)(\omega_1+\omega_3)(\omega_1+\omega_4)}\right]. \quad (47)$$

After extensive rearrangement it is found that the integral in Eq. (47) can be performed by methods analogous to those given in the Appendix of L2. It has the value

$$V_8(r)=-6\left(\frac{g^2}{4\pi}\right)^4\left(\frac{\mu}{2M}\right)^4\frac{1}{\mu^3r^4}\frac{2}{\pi}K_1(4\mu r). \quad (48)$$

As pointed out in L2, the effect of $V_6(r)$ and especially of $V_8(r)$ on the low energy properties of the two-nucleon system will provide a test of "convergence" of the asymptotic series for the nuclear potential.

VI. MANY-BODY FORCES

A. General Analysis of Leading Terms.

The analysis of many-body forces[31,32] could be carried out from first principles by deriving a many-particle relativistic equation and reducing this to a three-dimensional formalism. Such an undertaking, because of its length, is out of place here and will be reserved for a possible later publication. We begin our efforts, therefore, with the results of such an analysis, which for n particles is an equation of the form

$$(W-E_{p1}-E_{p2}-\cdots-E_{pn})\delta(\mathbf{p}_1+\mathbf{p}_2+\cdots+\mathbf{p}_n) \times\phi(\mathbf{p}_1\cdots\mathbf{p}_n)=\delta(\mathbf{p}_1+\cdots+\mathbf{p}_n)\Lambda_+^{(1)}(\mathbf{p}_1)\cdots\Lambda_+^{(n)}(\mathbf{p}_n) \times\int d\mathbf{p}_1'\cdots d\mathbf{p}_n'\Delta(\mathbf{p}_1\cdots\mathbf{p}_n;\mathbf{p}_1'\cdots\mathbf{p}_n') \times\delta(\mathbf{p}_1'+\cdots+\mathbf{p}_n')\phi(\mathbf{p}_1'\cdots\mathbf{p}_n'). \quad (49)$$

The kernel $\Delta(\mathbf{p}_1\cdots\mathbf{p}_n;\mathbf{p}_1'\cdots\mathbf{p}_n')$ contains interactions between $2, 3, \cdots n$ particles whose form is determined completely by the rules of perturbation theory as formulated in Sec. III of this paper. In particular, the adiabatic potentials can be defined in a manner precisely analogous to the definition given in Eq. (26).

The leading terms in the n-body force arise from Feynman diagrams involving n mesons in which two meson lines emanate from each nucleon line and in which there are n pairs but at most one pair at a time. Diagrams for typical matrix elements of the three- and four-particle forces are illustrated in Fig. 6. The expansion parameter is then $(g^2/4\pi)^n(\mu/2M)^n$. There are also n-particle forces involving $n-1$ mesons, but these can give rise to only $n-2$ pairs (see below for the three-particle case), and therefore the expansion parameter is $(g^2/4\pi)^{n-1}(\mu/2M)^n$, smaller roughly by an order of magnitude. By restricting our attention to the dominant n-pair terms a number of general statements can be made about the nature of the resulting potential in the adiabatic limit:

(1) All spin matrix elements are unity to lowest order. The resulting forces are spin independent.

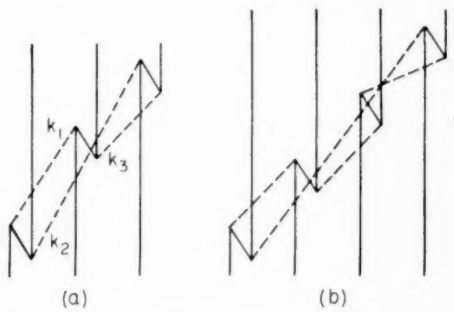

FIG. 6. Diagrams for typical matrix elements of leading contributions to three- and four-body forces.

[30] See Eq. (24) of L2. We obtain the result quoted there if we omit the considerable class of matrix elements which have at most two mesons in all intermediate states in which there are no pairs.

[31] The analytic form of the n-particle force was first given by G. Wentzel, Helv. Phys. Acta **XV**, 111 (1942), using equivalent pair theory methods. For the saturation problem see G. Wentzel, Helv. Phys. Acta **XXV**, 569 (1952).

[32] The major results of this section have been derived independently by S. D. Drell (private communication) using a method based on the canonical transformation of F. J. Dyson, Phys. Rev. **73**, 929 (1948). See also S. D. Drell and E. M. Henley, Phys. Rev. **88**, 1053 (1952). The problem of saturation of nuclear forces is under investigation by Drell and Huang. We wish to take this opportunity to thank Dr. Drell for an illuminating discussion of his work.

(2) The potential will consist of a sum of terms of the form $V(\{|\mathbf{r}_{i_1}-\mathbf{r}_{i_2}|+|\mathbf{r}_{i_2}-\mathbf{r}_{i_3}|+\cdots+|\mathbf{r}_{i_n}-\mathbf{r}_{i_1}|\})$, where $i_1, i_2, \cdots i_n$ is some permutation of $1, 2, \cdots n$. Aside from isotopic spin dependence to be dealt with in a moment, the number of distinct terms of this form is the number of ways of forming n-vector differences from n-distinct vectors, each vector being utilized twice. This number is $(n-1)!/2$. For there are $\frac{1}{2}n(n-1)$ choices for the pair $|\mathbf{r}_{i_1}-\mathbf{r}_{i_2}|$, then $n-2$ choices for $\mathbf{r}_{i_3}, \cdots$, one choice for $\mathbf{r}_{i_n}$. But then any of the n-coordinate differences can stand first in the sum and we must therefore divide by n. The number of Feynman diagrams contributing to one such ordering is 2^n, for having fixed on which particles are directly coupled by meson lines, we have still the possibility of interchanging the role of the two mesons which emerge from a given particle. And we can do this for n particles. The same result is obtained by dividing $(n-1)!/2$ into $2^{n-1}(n-1)!$, the total number of Feynman diagrams of the type under consideration.

(3) The contributions from each of the 2^n diagrams belonging to a given connection scheme differ only in isotopic spin dependence. The sum of the 2^n isotopic spin operators has the form

$$\{\tau_{\alpha_1}{}^{i_1}, \tau_{\alpha_n}{}^{i_1}\}\{\tau_{\alpha_1}{}^{i_2}, \tau_{\alpha_2}{}^{i_2}\}\{\tau_{\alpha_2}{}^{i_3}, \tau_{\alpha_3}{}^{i_3}\}\cdots\{\tau_{\alpha_{n-1}}{}^{i_n}, \tau_{\alpha_n}{}^{i_n}\}$$
$$=2^n\delta_{\alpha_n\alpha_1}\delta_{\alpha_1\alpha_2}\cdots\delta_{\alpha_{n-1}\alpha_n}=3\times 2^n. \quad (50)$$

The factor 2^n will cancel a similar factor in the denominator of the potential having its origin in the Fourier analysis of the meson field.

(4) One need calculate the analytic form of the potential for only a single connection scheme for the others will differ only by a relabelling of particle coordinates.

(5) We fix therefore on a standard connection scheme defined by $|\mathbf{r}_1-\mathbf{r}_2|+|\mathbf{r}_2-\mathbf{r}_3|+\cdots|\mathbf{r}_n-\mathbf{r}_1|$ and need consider only a single Feynman diagram associated with this connection. There will be just $n!$ time-ordered n-pair diagrams to compute corresponding to the permutation in time of the n pairs. Only half of these at most are distinct because of symmetry with respect to the inversion of the (vertical) time axis.

(6) The sign of the n-body force is $(-1)^{n-1}$ as follows from the fact that the matrix elements contain $2n-1$ negative energy denominators, but that there is an additional minus sign for an odd number of pairs.

Summarizing statements (1)–(6), we have reduced the problem to the evaluation of the quantity

$$V(\{|\mathbf{r}_1-\mathbf{r}_2|+\cdots+|\mathbf{r}_n-\mathbf{r}_1|\})$$
$$=(-1)^{n-1}6\left(\frac{g^2}{(2\pi)^3}\right)^n\left(\frac{1}{2M}\right)^n\int\frac{d\mathbf{k}_1\cdots d\mathbf{k}_n}{\omega_1\cdots\omega_n}$$
$$\times\exp[i\{\mathbf{k}_1\cdot(\mathbf{r}_1-\mathbf{r}_2)+\cdots k_n\cdot(\mathbf{r}_n-\mathbf{r}_1)\}]$$
$$\times[\quad], \quad (51)$$

where the square bracket is a sum of $n!/2$ terms, each comprising the adiabatic limit of the reciprocal of a product of energy denominators for the intermediate states without pairs

B. Three- and Four-Body Forces

We apply the general considerations given in the preceding section to the cases $n=3$ and $n=4$. In the former instance there are only three terms in the unspecified square bracket of Eq. (51). These are

$$[\quad]=\frac{1}{(\omega_1+\omega_2)(\omega_1+\omega_3)}+\frac{1}{(\omega_1+\omega_2)(\omega_2+\omega_3)}$$
$$+\frac{1}{(\omega_1+\omega_3)(\omega_2+\omega_3)}$$
$$=\frac{2\omega_1}{(\omega_2+\omega_3)(k_1^2-k_3^2)}+\frac{2\omega_3}{(\omega_1+\omega_2)(k_3^2-k_1^2)}, \quad (52)$$

the last form following from the observation that

$$\frac{1}{(\omega_1+\omega_2)(\omega_2+\omega_3)}=\frac{1}{(\omega_1-\omega_3)}\left[\frac{1}{\omega_2+\omega_3}-\frac{1}{\omega_1+\omega_2}\right]. \quad (53)$$

Using the last form of Eq. (52), the required integrations in Eq. (51) can be carried by methods indicated in the Appendix of L2. We find for the three-particle force the expression

$$V_{3p}=12\left(\frac{g^2}{4\pi}\right)^3\left(\frac{\mu}{2M}\right)^3\frac{2}{\pi}$$
$$\times\frac{K_1[\mu(|\mathbf{r}_1-\mathbf{r}_2|+|\mathbf{r}_2-\mathbf{r}_3|+|\mathbf{r}_3-\mathbf{r}_1|)]}{\mu^2|\mathbf{r}_1-\mathbf{r}_2||\mathbf{r}_2-\mathbf{r}_3||\mathbf{r}_3-\mathbf{r}_1|}. \quad (54)$$

For the four-particle force the bracket of Eq. (51) consists of twelve terms, which the reader can easily derive for himself from a set of diagrams. By extensive combination and rearrangement these can be brought into the useful form

$$[\quad]=\frac{4\omega_3\omega_4}{(\omega_1+\omega_2)(k_1^2-k_3^2)(k_2^2-k_4^2)}$$
$$+\frac{4\omega_1\omega_2}{(\omega_3+\omega_4)(k_1^2-k_3^2)(k_2^2-k_4^2)}$$
$$+\frac{4\omega_1\omega_4}{(\omega_2+\omega_3)(k_1^2-k_3^2)(k_4^2-k_2^2)}$$
$$+\frac{4\omega_2\omega_3}{(\omega_1+\omega_4)(k_3^2-k_1^2)(k_2^2-k_4^2)}. \quad (55)$$

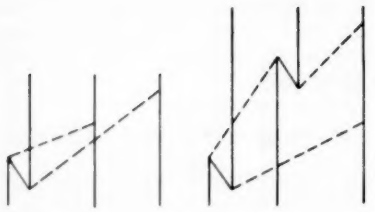

(a) (b)

FIG. 7. Diagrams for typical matrix elements of the three-particle force: (a) One-pair term involving interchange of two mesons. (b) Two-pair terms analogous to one-pair terms of two-particle fourth-order potential.

The integrations can now be carried out as before, and the total result for the four-particle potential given as

$$V_{4p}=-24\left(\frac{g^2}{4\pi}\right)^4\left(\frac{\mu}{2M}\right)^4\frac{2}{\pi}$$
$$\times\left\{\frac{K_1[\mu(|\mathbf{r}_1-\mathbf{r}_2|+|\mathbf{r}_2-\mathbf{r}_3|+|\mathbf{r}_3-\mathbf{r}_4|+|\mathbf{r}_4-\mathbf{r}_1|)]}{\mu^3|\mathbf{r}_1-\mathbf{r}_2||\mathbf{r}_2-\mathbf{r}_3||\mathbf{r}_3-\mathbf{r}_4||\mathbf{r}_4-\mathbf{r}_1|}\right.$$
$$+\frac{K_1[\mu(|\mathbf{r}_1-\mathbf{r}_3|+|\mathbf{r}_3-\mathbf{r}_2|+|\mathbf{r}_2-\mathbf{r}_4|+|\mathbf{r}_4-\mathbf{r}_1|)]}{\mu^3|\mathbf{r}_1-\mathbf{r}_3||\mathbf{r}_3-\mathbf{r}_2||\mathbf{r}_2-\mathbf{r}_4||\mathbf{r}_4-\mathbf{r}_1|}$$
$$\left.+\frac{K_1[\mu(|\mathbf{r}_1-\mathbf{r}_2|+|\mathbf{r}_2-\mathbf{r}_4|+|\mathbf{r}_4-\mathbf{r}_3|+|\mathbf{r}_3-\mathbf{r}_1|)]}{\mu^3|\mathbf{r}_1-\mathbf{r}_2||\mathbf{r}_2-\mathbf{r}_4||\mathbf{r}_4-\mathbf{r}_3||\mathbf{r}_3-\mathbf{r}_1|}\right\}. \quad (56)$$

We have not tried to push our diligence beyond this point, although it is conceivable that by sufficient searching one could obtain by these methods the general coefficient of the n-body force. The case of five particles, at any rate, is certainly amenable to direct calculation by these techniques.

C. Other Three-Body Forces

We consider briefly two types of three-body force which are roughly an order of magnitude smaller than the leading term. Of course these have their analogues in forces between any number of particles.

We turn first to the three-particle force which involves the total interchange of only two mesons, two mesons emanating from one of the particles, say, and each terminating on one of the others. There are six Feynman diagrams in all: for the particle which is the source of the two mesons we may interchange the role of the latter. The leading terms are one-pair terms, the pair subsisting only between neighboring interaction points as illustrated in Fig. 7(a). Six matrix elements of the specified type arise from each Feynman diagram. The calculation is straightforward and yields the result

$$V_{3p}'=2\left(\frac{g^2}{4\pi}\right)^2\left(\frac{\mu}{2M}\right)^3$$
$$\times\left[\tau^{(2)}\cdot\tau^{(3)}\frac{\sigma^{(2)}\cdot(\mathbf{r}_1-\mathbf{r}_2)}{|\mathbf{r}_1-\mathbf{r}_2|}\frac{\sigma^{(3)}\cdot(\mathbf{r}_1-\mathbf{r}_3)}{|\mathbf{r}_1-\mathbf{r}_3|}\right.$$
$$\times\left(1+\frac{1}{\mu|\mathbf{r}_1-\mathbf{r}_2|}\right)\left(1+\frac{1}{\mu|\mathbf{r}_1-\mathbf{r}_3|}\right)$$
$$\times\frac{\exp[-\mu(|\mathbf{r}_1-\mathbf{r}_2|+|\mathbf{r}_1-\mathbf{r}_3|)]}{\mu|\mathbf{r}_1-\mathbf{r}_2||\mathbf{r}_1-\mathbf{r}_3|}$$
$$\left.+1\leftrightarrow2+1\leftrightarrow3\right]. \quad (57)$$

We consider finally corrections of relative order μ/M to the leading three-pair terms computed in part B. The terms which contribute are as follows: corrections arise from the expansion of energy denominators of the leading three-pair terms. These are first the velocity-dependent terms supplied by the energy denominators for intermediate states without pairs. In accordance with previous results (see Sec. IV, C) these will not be given further consideration here since they must be regarded in connection with still higher order three-body forces. There are, however, the terms provided by pair denominators. In exact analogy to the situation which obtains in the case of fourth-order two-particle forces, these are canceled by the leading contribution from the three-pair terms which involve two pairs at a time.

There remains the leading two-pair terms. One easily enumerates twelve matrix elements for each Feynman diagram. A typical contribution is illustrated in Fig. 7(b). Calculation shows the result to be spin and charge independent and of the form

$$V_{3p}''=-12\left(\frac{g^2}{4\pi}\right)^3\left(\frac{\mu}{2M}\right)^4$$
$$\times\frac{\exp[-\mu(|\mathbf{r}_1-\mathbf{r}_2|+|\mathbf{r}_1-\mathbf{r}_3|+|\mathbf{r}_2-\mathbf{r}_3|)]}{\mu^2|\mathbf{r}_1-\mathbf{r}_2||\mathbf{r}_1-\mathbf{r}_3||\mathbf{r}_2-\mathbf{r}_3|}$$
$$\times\left[\frac{(\mathbf{r}_1-\mathbf{r}_2)\cdot(\mathbf{r}_1-\mathbf{r}_3)}{|\mathbf{r}_1-\mathbf{r}_2||\mathbf{r}_1-\mathbf{r}_3|}\left(1+\frac{1}{\mu|\mathbf{r}_1-\mathbf{r}_2|}\right)\right.$$
$$\left.\times\left(1+\frac{1}{\mu|\mathbf{r}_1-\mathbf{r}_3|}\right)+1\leftrightarrow2+1\leftrightarrow3\right]. \quad (58)$$

VII. CONCLUDING REMARKS

We have confined ourselves in this paper so far to the purely formal task of deriving static potentials with no radiative corrections. It is our opinion that Lévy's treatment of such corrections, aside possibly from ques-

tions of detail is qualitatively accurate. Quantitatively, one can say little more than that there is no *a priori* justification for equating the coupling constants associated with the second- and fourth-order potentials.[33] The relative values of the constants can only be adjusted by experiment. The result of Lévy that one obtains good agreement with experience by equating the two constants in no sense constitutes a proof of uniqueness. It is, in fact, almost self-evident that if one can obtain agreement by the use of two parameters only (coupling constant and cut-off radius), one should, within the present accuracy of experiment, be able to obtain as good or better agreement by the addition of an extra coupling parameter. In short, one must expect a range of acceptable relative values of the coupling constants.

Now, however, we must consider the alteration of the picture by the results of this paper. In particular, for equal values of the coupling constant the efficacy of the central force has been severely suppressed relative to the tensor force. Assuming a three-parameter scheme, there is again every reason to expect that there will be an arc of parameter space which gives agreement with experiment. Whether this arc passes through the plane determined by equating the values of the two coupling constants is a question that only detailed calculation can answer.

Another problem which requires further clarification is the exact nature of the role of the repulsive core. This problem has two facets. First, there is the field-theoretical task of establishing that the pseudoscalar theory actually predicts a hard core. The present methods of field theory are certainly not adequate to yield a definitive answer to this question and as Lévy himself is the first to admit, his arguments are only of the plausibility variety. Second, however, assuming the hard core as a useful *ad hoc* hypothesis, the question then arises as to the sensitivity of the results to the detailed form of the asymptotic potential. One is inclined to suspect that the answer, at least within the framework of a three-parameter theory, is that they are not very sensitive. One can quote in support of this contention the numerical results of Taketani *et al.*[34] for the low energy neutron-proton system using the second plus fourth potential of the $ps-pv$ theory and a cut-off. They find reasonable agreement with experiment (using only two parameters) for a theory in which for triplet even states the central force is repulsive and the tensor force much more strongly attractive than the tensor force of the second-order potential. There obviously remains then much work to be done before one can speak of a successful meson-theoretical model of nuclear forces. *Note added in proof:*—Numerical calculations show that the potential obtained in the paper does not agree with experiment. Further work, to be published, indicates moreover, that the perturbation theory doesn't even converge.

[33] We wish to make clear that there is no claim of originality for the observations of this section. Several of the ideas were brought to the author's attention during a series of discussions at the Cambridge meeting of the American Physical Society. The observation of the nonuniqueness of the numerical results of Lévy was variously attributed to R. Jastrow and J. Blatt.

[34] Taketani, Machida, and Onuma, Progr. Theoret. Phys. **7**, 45 (1952). It has also been brought to the author's attention that R. Jastrow has shown that using the Lévy potential, one can reduce V_4 by a factor of 4 and still obtain a decent fit with the $n-p$ data with a choice of $g^2/4\pi=15$.

APPENDIX A

The procedure described in Sec. III for reducing the R.E. to a three-dimensional equation, following closely the work of previous authors, depends on carrying out a sequence of integrations over energy variables. However, the interpretation of the resulting matrix elements is indissolubly tied to their representation by time-ordered Feynman diagrams. It makes more physical sense, therefore, and also renders the derivation more concise, if we reserve for last the sequence of time integrations. By appropriately breaking up the latter into a sum of terms defined by integrations over mutually exclusive subregions of time, we divide a given Feynman diagram automatically into the time-ordered regions corresponding to three-dimensional matrix elements.

We illustrate first by deriving the g^2 approximation in this manner, starting from the equation (for relative motion in center-of-mass system)

$$[\tfrac{1}{2}W+p_0-H_1(\mathbf{p})][\tfrac{1}{2}W-p_0-H_2(\mathbf{p})]\psi(x) = -ig^2\Gamma_1^{(1)}\Gamma_1^{(2)}\Delta(x)\psi_{++}(x). \quad (A.1)$$

Here p, p_0 will refer to momentum operators or momenta according to context, $x_\mu=x_{1\mu}-x_{2\mu}$; $\Delta(x)$, the meson propagation function, will be represented by its three-dimensional Fourier transform

$$\Delta(x)=\frac{i}{(2\pi)^3}\int\frac{\exp[i\mathbf{k}\cdot\mathbf{r}-i\omega|x_0|]}{2\omega}d\mathbf{k}. \quad (A.2)$$

Finally by $\psi_{++}(x)$ we mean the wave function which is the coordinate space transform of the wave function of Eq. (15) of the text,

$$\psi_{++}(x)=\frac{1}{(2\pi)^2}\int d^4p e^{ipx}(-2\pi i)^{-1}[(\tfrac{1}{2}W+p_0-E_p)^{-1} + (\tfrac{1}{2}W-p_0-E_p)^{-1}]\phi_{++}(\mathbf{p})=\frac{1}{(2\pi)^2}\int d\mathbf{p} \times\exp[i\mathbf{p}\cdot\mathbf{r}-i(E_p-\tfrac{1}{2}W)|x_0|]\phi_{++}(\mathbf{p}). \quad (A.3)$$

We insert Eqs. (A.2) and (A.3) into the r.h.s. of (A.1). For the l.h.s., we introduce the Fourier transform of $\psi(x)$,

$$\psi(x)=\frac{1}{(2\pi)^2}\int d^4p e^{ipx}\phi(\mathbf{p}), \quad (A.4)$$

project with respect to positive energies, and then integrate both sides with respect to p_0 in the manner al-

ready explained several times in the text. We thus obtain the equation

$$(W-2E_p)\phi_{++}(\mathbf{p})=-ig^2\frac{1}{(2\pi)^4}\frac{i}{(2\pi)^3}$$
$$\times\Lambda_+^{(1)}(\mathbf{p})\Lambda_+^{(2)}(\mathbf{p})\Gamma_i^{(1)}\Gamma_i^{(2)}\int d\mathbf{r}dx_0d\mathbf{k}d\mathbf{p}'dp_0$$
$$\times\frac{1}{2\omega}\left[\frac{1}{\frac{1}{2}W+p_0-E_p}+\frac{1}{\frac{1}{2}W-p_0-E_p}\right]e^{ip_0x_0}e^{i\mathbf{r}\cdot[\mathbf{k}-(\mathbf{p}-\mathbf{p}')]}$$
$$\times\exp[-i|x_0|(\omega+E_{p'}-\tfrac{1}{2}W)]\phi_{++}(p')$$
$$=-i\frac{g^2}{(2\pi)^3}\Lambda_+^{(1)}(\mathbf{p})\Lambda_+^{(2)}(\mathbf{p})\Gamma_i^{(1)}\Gamma_i^{(2)}\int dx_0d\mathbf{k}\frac{1}{2\omega}$$
$$\times\exp[-i|x_0|(\omega+E_p+E_{p-k}-W)]\phi_{++}(\mathbf{p}-\mathbf{k}). \quad (A.5)$$

The final step in the derivation is to break up the integral over x_0 into two regions defined by $x_0>0$ and $x_0<0$, and to use the relation

$$\int_0^\infty e^{-i\lambda x}dx=\int_{-\infty}^0 e^{i\lambda x}dx=\pi\delta(\lambda)-iP(1/\lambda), \quad (A.6)$$

noting that in application to Eq. (A.5) (and in all subsequent applications of the appendix) the delta-function does not contribute since its argument can never vanish. We finally obtain therefore, the equation

$$(W-2E_p)\phi_{++}(\mathbf{p})=\lambda\Lambda_+^{(1)}(\mathbf{p})\Lambda_+^{(2)}(\mathbf{p})\Gamma_i^{(1)}\Gamma_i^{(2)}$$
$$\times\int d\mathbf{k}\frac{2}{2\omega(W-E_p-E_{p-k}-\omega)}\phi_{++}(\mathbf{p}-\mathbf{k}), \quad (A.7)$$

which is just the Tamm-Dancoff approximation.

We turn next to the more complicated case of the diagram of Fig. 1(b). We add to the r.h.s. of Eq. (A.1) the term

$$(-ig^2)^2\int d^4x'd^4X'\exp[iW(X_0-X_0')]\Delta(X-X'-\tfrac{1}{2}(x+x'))\Delta(X-X'+\tfrac{1}{2}(x+x'))[\Gamma_iG(X-X'+\tfrac{1}{2}(x-x'))\tau_j\gamma_5]^{(1)}[\Gamma_jG(X-X'-\tfrac{1}{2}(x-x'))\tau_i\gamma_5]^{(2)}\psi_{++}(x'). \quad (A.8)$$

In Eq. (A.8), in addition to c.m. coordinates for the points x_1, x_2, we have introduced similar coordinates for x_3, x_4. To transform Eq. (A.8), we require, in addition to Eqs. (A.2) and (A.3), the representation

$$G(x)=\frac{i}{(2\pi)^3}\int d\mathbf{p}\exp[i\mathbf{p}\cdot\mathbf{r}-iE_p|x_0|]\times\frac{[H(\mathbf{p})+E_p\,\mathrm{sgn}x_0]\gamma_0}{2E_p}, \quad (A.9)$$

where $\mathrm{sgn}x_0$ means the sign of x_0. Incorporating Eqs. (A.2), (A.3), and (A.9) into (A.8) and carrying out the sequence of operations described prior to Eq. (A.5), the additional term in (A.5) contributed by (A.8) has the form

$$(-ig^2)^2\left(\frac{i}{(2\pi)^3}\right)^4\frac{1}{(2\pi)^4}\Lambda_+^{(1)}(\mathbf{p})\Lambda_+^{(2)}(\mathbf{p})$$
$$\times\int d^4xd^4x'd^4X'dp_0d\mathbf{k}_1d\mathbf{k}_2d\mathbf{p}_1d\mathbf{p}_2d\mathbf{p}'$$
$$\times\frac{1}{4\omega_1\omega_2}e^{-ipx}\left[\frac{1}{\frac{1}{2}W+p_0-E_p}+\frac{1}{\frac{1}{2}W-p_0-E_p}\right]$$
$$\times\exp[iW(X_0-X_0')]\exp[i\mathbf{k}_1\cdot(\mathbf{R}-\mathbf{R}'-\tfrac{1}{2}(\mathbf{r}+\mathbf{r}'))-i\omega_1|X_0-X_0'-\tfrac{1}{2}(x_0+x_0')|]$$
$$\times\exp[i\mathbf{k}_2\cdot(\mathbf{R}-\mathbf{R}'+\tfrac{1}{2}(\mathbf{r}+\mathbf{r}'))-i\omega_2|X_0-X_0'+\tfrac{1}{2}|x_0+x_0'|]\exp[i\mathbf{p}_1\cdot(\mathbf{R}-\mathbf{R}'+\tfrac{1}{2}(\mathbf{r}-\mathbf{r}'))-iE_{p1}|X_0-X_0'+\tfrac{1}{2}(x_0-x_0')|]\exp[i\mathbf{p}_2\cdot(\mathbf{R}-\mathbf{R}'-\tfrac{1}{2}(\mathbf{r}-\mathbf{r}'))-iE_{p2}|X_0-X_0'-\tfrac{1}{2}(x_0-x_0')|]$$
$$\times[\Gamma_i(H(\mathbf{p}_1)+E_{p1}\,\mathrm{sgn}(X_0-X_0'+\tfrac{1}{2}(x_0-x_0'))\Gamma_j]^{(1)}$$
$$\times\frac{1}{2E_{p1}}[\Gamma_j(H(\mathbf{p}_2)+E_{p2}\,\mathrm{sgn}(X_0-X_0'-\tfrac{1}{2}(x_0-x_0'))\Gamma_i]^{(2)}\frac{1}{2E_{p2}}\exp[i\mathbf{p}'\cdot\mathbf{r}'-i|x_0'|\times(E_{p'}-\tfrac{1}{2}W)]\phi_{++}(\mathbf{p}'). \quad (A.10)$$

As the next stage in the development, we record the result of performing the integrations with respect to p_0, $\mathbf{r}$, $\mathbf{r}'$, $\mathbf{R}'$, $\mathbf{p}_1$, $\mathbf{p}_2$, $\mathbf{p}'$. It is also useful to introduce the variable $x_0''=x_{20}-x_{30}=X_0-X_0'-\frac{1}{2}(x_0+x_0')$. Equation (A.10) now takes the somewhat simplified form

$$\lambda^2i\int\frac{d\mathbf{k}_1d\mathbf{k}_2}{4\omega_1\omega_2}\int_{-\infty}^{\infty}dx_0dx_0'dx_0''\exp\{iW[x_0''+\tfrac{1}{2}(x_0+x_0')]-i(E_p-\tfrac{1}{2}W)|x_0|-i\omega_1|x_0''|-i\omega_2|x_0''+x_0+x_0'|-iE_{p1}|x_0''+x_0|-iE_{p2}|x_0''+x_0'|-i(E_{p'}-\tfrac{1}{2}W)|x_0'|\}\times\left\{\Gamma_i\frac{[H(\mathbf{p}_1)+E_{p1}\,\mathrm{sgn}(x_0''+x_0)]}{2E_{p1}}\Gamma_j\right\}^{(1)}\times\left\{\Gamma_j\frac{[H(\mathbf{p}_2)+E_{p2}\,\mathrm{sgn}(x_0''+x_0')]}{2E_{p2}}\Gamma_i\right\}^{(2)}\times\phi_{++}(\mathbf{p}'), \quad (A.11)$$

where it is understood that

$$\mathbf{p}_1=\mathbf{p}-\mathbf{k}_2, \quad p_2=-\mathbf{p}+\mathbf{k}_1, \quad \mathbf{p}'=\mathbf{p}-\mathbf{k}_1-\mathbf{k}_2. \quad (A.12)$$

The final step in the derivation of the twenty-four matrix elements contained in Eq. (A.11) consists in

dividing the regions of integration with respect to x_0, x_0', x_0'' into appropriate subregions, each corresponding to a single three-dimensional matrix element. Contenting ourselves here with a sample indication, one easily verifies that the no-pair terms, six in all, are given by the six integrals

$$\Big[\int_0^\infty\int_0^\infty\int_0^\infty+\int_0^\infty\int_0^\infty\int_{-x_0''}^0+\int_0^\infty\int_{-x_0''}^0\int_0^\infty$$
$$+\int_0^\infty\int_{-x_0''}^0\int_{-x_0''}^{-x_0-x_0''}+\int_0^\infty\int_{-x_0''}^0\int_{-x_0-x_0''}^0$$
$$+\int_{-\infty}^0\int_{-x_0''}^\infty\int_{-x_0''}^\infty\Big]dx_0''dx_0dx_0'=(t_1>t_2>t_3>t_4)$$
$$+(t_1>t_2>t_4>t_3)+(t_2>t_1>t_3>t_4)+(t_2>t_4>t_1>t_3)$$
$$+(t_2>t_1>t_4>t_3)+(t_1>t_3>t_2>t_4). \quad \text{(A.13)}$$

The l.h.s. of Eq. (A.13) gives the ranges of integration variables corresponding to the matrix elements defined by the time orderings on the r.h.s. It is easily verified that the removal of the absolute value signs for the combinations of time variables found in Eq. (A.11) is well defined for each of the matrix elements in (A.13). The remaining matrix elements may be similarly derived. The same technique applies also to the ladder diagram.

The procedure described above appears to be the most concise means for extracting some small subset of desired matrix elements from higher order diagrams where the derivation of all matrix elements contained therein would be prohibitively laborious. In most of the applications in this paper, however, we have merely recorded the known results of such a derivation.

APPENDIX B

We wish to point out here that the existence of velocity-dependent corrections to the two-pair matrix elements of the same order of magnitude as the no-pair terms and in particular that one obtains from these terms a spin-orbit coupling. This follows from a more detailed consideration of the spin matrix element

$$(p_r|\Lambda_+^{(r)}(\mathbf{p}_r-\epsilon_r\mathbf{k}')|\mathbf{p}_r')=\frac{1}{2E_{p-k'}}\left[\frac{(E_p+M)(E_{p'}+M)}{2E_p2E_{p'}}\right]^{\frac{1}{2}}$$
$$\times\left[E_{p-k'}+M+\frac{\boldsymbol{\sigma}^{(r)}\cdot\mathbf{p}}{E_p+M}(E_{p-k}-M)\frac{\boldsymbol{\sigma}^{(r)}\cdot\mathbf{p}_r'}{E_{p'}+M}\right.$$
$$\left.+\boldsymbol{\sigma}^{(r)}\cdot(\mathbf{p}_r-\epsilon_r\mathbf{k}')\frac{(\boldsymbol{\sigma}^{(r)}\cdot\mathbf{p}_r')}{E_{p'}+M}+\frac{\boldsymbol{\sigma}^{(r)}\cdot\mathbf{p}_r}{E_p+M}\boldsymbol{\sigma}^{(r)}\cdot(\mathbf{p}_r-\epsilon_r\mathbf{k}')\right]$$
$$\rightarrow 1+(2M)^{-2}[\boldsymbol{\sigma}^{(r)}\cdot(\mathbf{p}_r-\epsilon_r\mathbf{k}')\boldsymbol{\sigma}^{(r)}\cdot p_r'+\boldsymbol{\sigma}^{(r)}\cdot p_r\boldsymbol{\sigma}^{(r)}$$
$$\cdot(\mathbf{p}_r-\epsilon_r\mathbf{k}')]\rightarrow 1+(2M)^{-2}i\boldsymbol{\sigma}^{(r)}\cdot(\mathbf{k}_1+\mathbf{k}_2)\times\mathbf{p}. \quad \text{(B.1)}$$

The successive simplifications indicated by the arrows consist at the first stage of discarding all terms beyond the leading one which do not contribute a spin-orbit coupling and at the second stage more of the same accompanied by substitution $p_r'=p_r-\epsilon_r(k_1+k_2)$. The result (B.1) is seen to depend on the particular particle involved only through its spin. Consequently, when we multiply the spin matrix elements for the two particles, the cross-term leads to an interaction that depends on the total spin of the system and is, in fact, of the spin-orbit type. If one inserts the latter into the leading two-pair terms, one finds easily an interaction,

$$V_4^{\text{S.O.}}=-6(g^2/4\pi)^2(\mu/2M)^4(\mu^3r)^{-1}(\partial/\partial r)$$
$$\times[K_1(2\mu r)/r^2]\mathbf{L}\cdot\mathbf{S}, \quad \text{(B.2)}$$

with

$$\mathbf{L}=\mathbf{r}\times\mathbf{p}, \qquad \mathbf{S}=\tfrac{1}{2}(\boldsymbol{\sigma}^{(1)}+\boldsymbol{\sigma}^{(2)}). \quad \text{(B.3)}$$

Since $K_1(x)$ is a monotonically decreasing function of its argument, the quantity multiplying $\mathbf{L}\cdot\mathbf{S}$ in Eq. (B.2) is positive. This is the sign required for the Case and Pais[35] interpretation of the $p-p$ scattering data at high energies. It is therefore of the wrong sign for application to the shell model of heavy nuclei. In the latter instance, however, there are many other mechanisms that can produce the desired result.

[35] K. M. Case and A. Pais, Phys. Rev. **80**, 203 (1950).

Letters to the Editor

PUBLICATION of brief reports of ***important*** *discoveries in physics may be secured by addressing them to this department. No proof will be sent to the authors. The Board of Editors does not hold itself responsible for the opinions expressed by the correspondents. Communications should not exceed 600 words in length and should be submitted in* ***duplicate****.*

Thermal Resistivity of Mercury in the Intermediate State

J. K. HULM
Institute for the Study of Metals, University of Chicago, Chicago, Illinois
(Received April 20, 1953)

THE thermal resistivity along the axis of a 5.2-mm diameter cylinder of approximately 99.99 percent pure mercury was measured as a function of transverse magnetic field at various temperatures between 4.2° and 1.3°K. At temperatures above about 2.1°K, the resistivity in the intermediate state ($0.5<\eta<1$, where η is the reduced field H/H_c) was quite well represented by

$$w=2(w_n-w_s)\eta+(2w_s-w_n), \tag{1}$$

where w_s and w_n are the resistivities in the pure superconducting and pure normal states, respectively. This result might have been anticipated for a specimen composed of alternate superconducting and normal laminas perpendicalar to the axis of the cylinder, which is probably a good first approximation to the structure in the intermediate state.[1]

Below 2.1°K, however, departures from Eq. (1) were observed corresponding to an additional component of resistivity $w_a(\eta)$ on the right-hand side, similar in character to that observed in pure lead by Webber and Spohr[2] and in pure tin and indium by Detweiler and Fairbank.[3] For mercury, w_a vanished at $\eta=0.5$ and 1.0 and passed through a maximum at an intermediate value of η which seemed to decrease somewhat with decreasing temperature, but which always lay between 0.74 and 0.70. As shown by Fig. 1, the maximum value of w_a was in good agreement with the empirical formula

$$(w_a)_{\max}=1.3\times10^{-3}t^{-5}\ \text{watt}^{-1}\ \text{cm deg},$$

where t is the reduced temperature T/T_c. The results of Detweiler and Fairbank[3] for two tin specimens of nearly the same diameter and impurity content also yield $(w_a)_{\max}$ values proportional to t^{-5} with a coefficient 7.9×10^{-4} watt^{-1} cm deg, which suggests that this type of behavior may be fairly general.

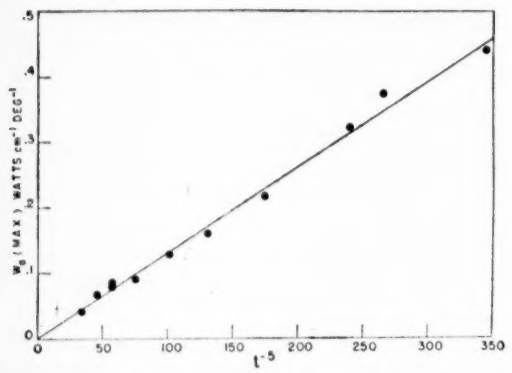

FIG. 1. Maximum additional thermal resistivity *versus* reduced temperature to the power −5, mercury.

It is worth noting that for the mercury specimen in the normal state the mean free path of electrons l_n at 2°K was about 4×10^{-4} cm. While this is small compared to the probable thickness of the normal laminas[1] for $\eta=0.72$, roughly 10^{-2} cm, it is greater than the estimated width of the superconducting-normal boundary layer,[1] about 5×10^{-5} cm. On the two-fluid model these figures seem to imply that as one crosses the boundary from a normal to a superconducting region, the equilibrium population of normal electrons decreases by a factor t^4 in a distance small compared to l_n. If it is assumed that a similar population decrease occurs for normal electrons actually crossing the boundary, a fraction $(1-t^4)$ of these electrons being in some way prevented from taking part in the heat transfer process, then a higher thermal resistivity w_nt^{-4} should occur in a normal layer of approximate thickness l_n in contact with the boundary. Although the reason for the existence of such a layer is not clear, it is interesting that for the specimen as a whole this assumption gives rise to an additional resistivity of the form

$$w_a\sim(w_{nc}l_{nc}/Z)t^{-5}, \tag{3}$$

where w_{nc} and l_{nc} are the values of w_n and l_n for $t=1$, and Z is the combined thickness of one superconducting and one normal lamina. Taking Z as about 10^{-2} cm, one obtains $w_a\sim5\times10^{-3}t^{-5}$ watt^{-1} cm deg, which is comparable with the observed $(w_a)_{\max}$.

I am grateful to Mr. R. J. Sladek for his cooperation in this experiment.

[1] D. Shoenberg, *Superconductivity* (Cambridge University Press, Cambridge, 1952).
[2] R. T. Webber and D. A. Spohr, Phys. Rev. **84**, 384 (1951).
[3] D. P. Detweiler and H. A. Fairbank, Phys. Rev. **88**, 1049 (1952).

The λ-Transition in Liquid Helium

R. P. FEYNMAN
California Institute of Technology, Pasadena, California
(Received April 29, 1953)

WE show why the interatomic potential does not alter the existence of an Einstein-Bose condensation[1] in He^4.

The partition function $Q=\Sigma_n\exp(-\beta E_n)$, with $\beta=1/kT$, is the trace of the operator $\exp(-\beta H)$. A coordinate representation of $\exp(-itH/\hbar)$ may be expressed in terms of an integral over trajectories.[2] An analogous situation applies to $\exp(-\beta H)$. For a system of N atoms of mass m interacting in pairs with a mutual potential $V(\mathbf{R})$ the partition function becomes

$$Q_B=(N!)^{-1}\int d^N\mathbf{z}_i\int_{tr}\exp\Big[-\int_0^\beta\Big\{\frac{m}{2\hbar^2}\sum_i\Big(\frac{d\mathbf{x}_i}{du}\Big)^2+\sum_{i,j}V(\mathbf{x}_i-\mathbf{x}_j)\Big\}du\Big]\mathfrak{D}^N\mathbf{x}_i(u). \tag{1}$$

The integral $\int_{tr}$ must be taken over all trajectories $\mathbf{x}_i(u)$, for $i=1$ to N, of the atoms such that initially they are in the same configuration $\mathbf{z}_i$ as finally, i.e., $\mathbf{x}_i(0)=\mathbf{z}_i$ and $\mathbf{x}_i(\beta)=\mathbf{z}_i$ [for we want the diagonal element of $\exp(-\beta H)$]. Also an integral is taken over all such configurations $\mathbf{z}_i$ (to obtain the trace). This Q_B is for atoms which obey Boltzmann statistics, and the $(N!)^{-1}$ is added, as is conventional. Actually He^4 obeys Bose statistics, the sum on states must only be over symmetrical states. This has the effect that the true Q for He^4 is

$$Q=(N!)^{-1}\sum_P\int d^N\mathbf{z}_i\int_{tr_P}\exp\Big[-\int_0^\beta\Big\{\frac{m}{2\hbar^2}\sum_i\Big(\frac{d\mathbf{x}_i}{du}\Big)^2+\sum_{i,j}V(\mathbf{x}_i-\mathbf{x}_j)\Big\}du\Big]\mathfrak{D}^N\mathbf{x}_i(u), \tag{2}$$

where in this case the integral $\int_{tr_P}$ is taken over all trajectories for which $\mathbf{x}_i(0)=\mathbf{z}_i$ and $\mathbf{x}_i(\beta)=P\mathbf{z}_i$.

That is, the final configuration may find the atoms permuted from the initial positions (signified by $P\mathbf{z}_i$), and we are to sum over all such permutations P.

The main effect of the potential is to limit the important trajectories and configurations $\mathbf{z}_i$ to those in which the atoms never overlap (radius of repulsion 2.6A).

In this note we will go into no further detail than is necessary to determine the reason for and character (order) of the transition. These features are not affected by smooth functions of the temperature. We assume Q_B would show no transition. Then we can write $Q=qQ_B$ and argue that the transition is contained in the factor q by which Q differs from Q_B.

Since for a free particle,[2]

$$\int \exp\Big(-\int_0^\beta \tfrac{1}{2}m\hbar^{-2}\dot{x}^2du\Big)\mathfrak{D}x(u) = (2\pi\hbar^2\beta/m)^{-\frac{1}{2}}\exp[-\tfrac{1}{2}m(x(0)-x(\beta))^2/\beta\hbar^2]$$

holds, a displacement by distance $x(0)-x(\beta)=d$ results in a factor

$$y=\exp(-\tfrac{1}{2}md^2/\beta\hbar^2) \tag{3}$$

relative to the case of a return to the original position $[x(\beta)=x(0)]$.

For He at the temperature of the transition (2.2°K), this factor is $1/e$ for $d=3.4$A. Hence, near the transition, displacements beyond nearest neighbors do not contribute effectively to Q. Only those permutations are important in which the atoms are either left in their original positions or moved to a neighboring atom. A permutation in which i goes to j's site must move j to, say, k's site, etc., until the rth atom in the cycle is adjacent to i's original position and moves over to occupy it. Such a cycle, or ring, of r adjacent atoms each moved to the position of the next contributes a factor y^r to q, if we use in (3) some mean atomic spacing for d.

The atoms are not free particles. But the potentials will not drastically alter the possibility of moving over to a nearest neighbor. At any rate we can expect such a factor y increasing with decreasing temperature, even though the exact temperature dependence may not be given correctly by[3] (3). The important configurations $\mathbf{z}_i$ in (2) (those with nonoverlapping atoms) are very much like the configurations for a classical fluid. Each permutation cycle corresponds to a ring or, if we consider lines joining atomic centers, to a polygon on this configuration. Therefore, roughly,

$$q=\Sigma_L\, g(L)y^L, \tag{4}$$

where $g(L)$ is the total number of ways that polygons can be drawn on the configuration so that the total number of sides of all the polygons together is L. The polygons must not cross.

A single large polygon of r sides contributes a very small amount y^r ($y<1$). But a large polygon can be drawn in more ways than a small one. Increasing the length r by one increases the number of polygons available by a factor, say s (perhaps 3 or 4), although the contribution of each is multiplied by y. Thus if $sy<1$ (high T) large polygons are unimportant. As T falls, suddenly when $sy=1$ the contributions from very large polygons (limited by the size of the container) begin to be important. This produces a transition in the behavior of q.

The theoretical determination of the order of the λ-transition in helium therefore can be reduced to a definite mathematical problem; namely, the behavior of the sum (4) as a function of y for a cubic lattice. For the character of the transition probably does not depend upon the long-range disorder of the actual configuration.

This idealized mathematical problem has not been solved. The difficulty is that the polygons must not intersect. A rough way of taking this into account is to assume that, when drawing polygons, if K sides are already drawn, the next atom site has a chance of $(N-K)/N$ of being unoccupied. This yields a third-order transition like the ideal Bose gas (for which, indeed, the above assumption is valid).

A solution of the idealized problem which more rigorously describes the geometrical correlations might well give a transition of a different order. (The experimental transition appears to be second order).

This work resulted from conversations with M. Kac.

[1] F. London, Phys. Rev. **54**, 947 (1938).
[2] R. P. Feynman, Revs. Modern Phys. **20**, 367 (1948).
[3] Actually (3) is essentially correct. Even for large displacements of a given atom i, the atoms which might hinder the motion can temporarily readjust their positions $\mathbf{x}(u)$ to permit i to pass more easily. The effect is just to change m to a somewhat higher effective mass. A more detailed account is being prepared.

Heat Pulses in Helium II between 0.1°K and 1.0°K

H. C. Kramers, F. A. W. van den Burg, and C. J. Gorter
Kamerlingh Onnes Laboratory, Leiden, Holland
(Received April 27, 1953)

THE propagation of heat pulses in helium II has been investigated at temperatures between 0.1°K and 1.0°K by the standard method of Pellam[1] and Atkins and Osborne.[2] The lengths of the cavities were 3 cm and 6 cm, and their diameter was 0.4 cm. The pulse duration was usually 20 microseconds. Special care was taken to ensure a good thermal contact between cooling agent and liquid. The warming-up times were of the order of one hour.

At the lowest temperatures the sharp start of the heat pulse was found to propagate with a velocity of 230 m/sec. In the 6-cm cavity this velocity decreased, the start becoming unsharp, from about 0.2°K. In the 3-cm cavity that did not occur until about 0.35°K. Between those temperatures and about 0.8°K the apparent velocity of the pulse decreased rapidly, being smaller in the 6-cm than in the 3-cm cavity.

The usual second sound was found above about 0.8°K. The velocities were the same for the two cavities and agreed with those reported by De Klerk, Pellam, and Hudson[3] and by Herlin.[4] The velocities of the start increase somewhat with rising heat input.[5]

The results suggest that the mean free path of the phonons traveling at the speed of normal sound is several centimeters at the lowest temperatures used and decreases to a few millimeters at most at the highest temperatures.[5,6] At temperatures of about 0.5°K the behavior of the pulse is rather similar to that of a heat pulse in a normal medium.[5]

Details will be published in *Physica* and the *Communications from the Kamerlingh Onnes Laboratory*.

[1] J. R. Pellam, Phys. Rev. **75**, 1183 (1949).
[2] D. V. Osborne, Nature **162**, 213 (1948); Proc. Phys. Soc. (London) **A64**, 114 (1951); K. R. Atkins and D. V. Osborne, Phil. Mag. **41**, 1048 (1950).
[3] de Klerk, Hudson, and Pellam, Phys. Rev. **89**, 326 (1953).
[4] R. D. Maurer and M. A. Herlin, Phys. Rev. **76**, 948 (1949).
[5] C. J. Gorter, Phys. Rev. **88**, 681 (1952).
[6] L. D. Landau and I. M. Khalatnikov, J. Exptl. Theoret. Phys. (U.S.S.R.) **19**, 637, 709 (1949).

Fountain Effect in Helium II below 1°K

G. J. C. Bots and C. J. Gorter
Kamerlingh Onnes Laboratory, Leiden, Holland
(Received April 27, 1953)

THE fountain effect in helium II was investigated below 1°K. A long vertical glass capillary, kept at a constant temperture of about 1.1°K, was connected by a tube filled with very fine Fe_2O_3 powder to a thermally insulated vessel which could be cooled down by adiabatic demagnetization. The vessel and the capillary were partly filled with helium II, and in the capillary fountain effects between 20 cm and 40 cm could be observed.

Below 0.8°K the observed fountain effect was smaller than is predicted by London's formula,[1]

$$dp/dT=\rho S, \tag{1}$$

where ρS is the entropy per unit volume.

As a matter of fact the integrated fountain effect between 0.5°K and 0.8°K was about 5 cm, while (1) predicts 7.3 cm. Below 0.5°K the integrated fountain effect is not more than a few millimeters, while (1) predicts 1.3 cm.[2]

Supposing that down to 0.6°K the formula

$$\rho_n = \rho_s T(dp/dT)^2/\rho^2 C_v V_{II}^2 \qquad (2)$$

may be applied, where C_v and V_{II} denote the specific heat[2] and the velocity of second sound,[3] while ρ_n and $\rho_s = \rho - \rho_n$ are the densities of the so-called normal fluid and superfluid, then ρ_n may be calculated. It is found to fall very steeply with decreasing temperature, remaining approximately proportional to C_v. In Landau's picture[4] this would confirm the rapid disappearance of the roton contribution to ρ_n below 1°K.

The original set-up for this investigation was made by Mr. G. J. de Vries.

Details will be published in *Physica* and the *Communications from the Kamerlingh Onnes Laboratory*.

[1] H. London, Proc. Roy. Soc. (London) **A171**, 484 (1939).
[2] Kramers, Wasscher, and Gorter, Physica **18**, 329 (1952); Communs. Kamerlingh Onnes Lab. Univ. Leiden No. 288c.
[3] Kramers, van den Burg, and Gorter, preceding letter [Phys. Rev. **90**, 1117 (1953)].
[4] L. D. Landau, J. Phys. (U.S.S.R.) **5**, 71 (1941).

OH in the Airglow at High Latitudes

JOSEPH W. CHAMBERLAIN AND NORMAN J. OLIVER
Geophysics Research Directorate, Air Force Cambridge Research Center, Air Research and Development Command, Cambridge, Massachusetts

(Received April 21, 1953)

IN November 1952 a brief expedition to Thule Air Force Base in northern Greenland resulted in a few spectra of the airglow north of the auroral belt. The spectrograph contains a grating ruled with 15 000 lines per inch and an $f/0.8$, five-inch, flat-field Schmidt camera. In the photographic infrared we used hypersensitized I-N plates in the first order of the grating with a dispersion of 138 A/mm, whereas the second order was used in the red-green region with the 103a-F(3) emulsion.

Our measured wavelengths are in fair agreement with those of other observers;[1-6] discrepancies of 1 or 2 angstroms are common, but this does not seem unusual in view of the resolving power and dispersion that have so far been employed. Also, wavelengths for the 6–2, 5–1, and 4–0 bands are consistent with those observed in oxy-acetylene flames under high dispersion.[7-10] Figure 1 illustrates microphotometer tracings in a region of the spectrum where the OH bands are relatively weak. In four bands that seemed to be free from distortion by overlapping images, the relative intensities of the rotational lines indicate temperatures between 300° and 350°K, which are somewhat higher than those determined from spectra made at intermediate latitudes.[2-4]

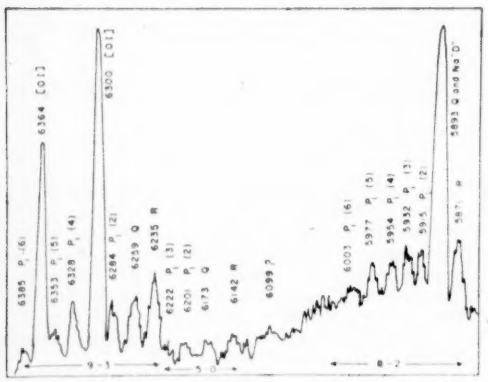

FIG. 1. The 9–3, 5–0, and 8–2 OH bands observed at Thule, Greenland. Note the blending of the 8–2 Q branch with Na "D"

Recently Herman and Hornbeck[10] have determined the rotational and vibrational constants of the ground ($^2\Pi$) state from their laboratory infrared bands and the data of Dieke and Crosswhite[11] on the ultraviolet OH bands. They find the usual power series involving ω_e, $\omega_e x_e$, etc., gives an excellent representation of the vibrational energy levels observed in the laboratory (i.e., $v \leq 6$) and have presented constants for three- and four-term power series. Their three-term solution, however, gives energy levels that are very discordant with the airglow data when $v' = 7$, 8, or 9. When $\omega_e z_e$ is considered, the agreement is much better, although small systematic residuals still exist for the higher levels.

In Table I are presented band origins determined from the strong P_1 lines ($^2\Pi_{\frac{1}{2}}$ state) in the airglow. In deriving these values of ν_0 we have used the rotational constants, B_v and D_v, of Herman and Hornbeck and the Hill and Van Vleck[12] formula for spin doubling. The five band origins marked with an asterisk (*) have been estimated from the measurements of other observers, whereas the data for the other seven bands were obtained from our own spectra. For comparison we have also listed band origins computed from Herman and Hornbeck's four-term constants.

TABLE I. Band origins, ν_0(vacuum), for OH in the airglow.

$v' - v''$	ν_0(obs)	ν_0(comp)
7–3	11 323*	11 329.9
6–2	11 985.0	11 984.5
5–1	12 637.2	12 636.9
9–4	12 896.4	12 911.3
4–0	13 291.7	13 291.5
8–3	13 731.8	13 746.2
7–2	14 562*	14 570.1
6–1	15 387*	15 388.4
9–3	15 980.5	15 989.0
5–0	16 204*	16 206.6
8–2	16 979.5	16 986.5
7–1	17 976*	17 974.0

A solution for the vibrational constants based on these airglow measurements gives results which are discordant with the more accurate laboratory data; previous determinations[1,3] based on airglow data also do not satisfactorily represent the lower vibrational levels. Since there may be significant errors in the wavelengths, arising from the iow resolving power, vibrational constants based only on airglow measurements are undoubtedly inferior to the laboratory constants. However, inasmuch as the term $\omega_e z_e$ becomes important only for $v > 6$, it would be very useful to have accurate measures of the high-excitation airglow bands, which unfortunately have not yet been observed in laboratory spectra. Thus a consolidation of precise measurements from various sources will be needed to give an accurate representation of the vibrational energy levels.

In the red and infrared there are a number of faint features whose origins are unknown. In view of some recent work[13] which indicates that starlight is much more important in the blue end of the spectrum than is generally believed, it seems likely that some of these features may be due to the continuous spectrum of the galactic starlight. That is, the background stellar radiation may produce the weak infrared and red continuum, in which case the intervals between stellar absorption lines would have the appearance of faint emissions.

We wish to acknowledge the cooperation of S. Wolnik, J. Scanlon, and C Sheehan, who assisted in various phases of this work. Thanks are also due Dr. R. C. Herman of The Johns

Hopkins University for supplying information on the laboratory analysis of OH.

[1] A. B. Meinel, Astrophys. J. **111**, 555 (1950).
[2] A. B. Meinel, Astrophys. J. **112**, 120 (1950).
[3] Cabannes, Dufay, and Dufay, Compt. rend. **230**, 1233 (1950).
[4] J. Dufay and M. Dufay, Compt. rend. **232**, 426 (1951).
[5] M. Dufay, Compt. rend. **232**, 2344 (1951).
[6] W. Petrie and R. Small, University of Saskatchewan Scientific Report No. AR-8, March, 1952 (unpublished).
[7] Dejardin, Janin, and Peyron, Compt. rend. **234**, 1866 (1952); **235**, 538 (1952).
[8] Dejardin, Janin, and Peyron, Phys. Rev. **90**, 359 (1953).
[9] G. A. Hornbeck and R. C. Herman, J. Chem. Phys. **19**, 512 (1951).
[10] R. C. Herman and G. A. Hornbeck, Astrophys. J. (to be published).
[11] G. H. Dieke and H. M. Crosswhite, Bumblebee Series Report No. 87, The Johns Hopkins University, 1948 (unpublished).
[12] E. L. Hill and J. H. Van Vleck, Phys. Rev. **32**, 250 (1928).
[13] J. W. Chamberlain and N. J. Oliver, Astrophys. J. (to be published); A. B. Meinel, Astrophys. J. (to be published).

Indications of the Interaction of Electric Field Gradients and Nuclear Electric Quadrupole Moments in Angular Correlation*

ROLF M. STEFFEN
Department of Physics, Purdue University, Lafayette, Indiana
(Received April 27, 1953)

THE influence of extranuclear fields on the angular correlation of successive nuclear radiation has been discussed by several authors.[1] It was generally assumed that the interaction between the nuclear magnetic dipole moment and magnetic fields, due to either the electron shell or the surrounding of the decaying atom, is mainly responsible for the reduction of the angular correlation. The dependence of this reduction on the source material was attributed to the difference in recovery time of the excited and ionized electron shell.

However, several directional correlations were reported recently, where the reduction of the anisotropy of the correlation could not be understood on the basis of the magnetic interaction alone, e.g., α-γ correlation of $RdTh^{228}$,[2] γ-γ correlation of Cd^{111},[3] and of Ta^{181}.[4] Abragam and Pound[5] were able to show that the coupling between the nuclear electric quadrupole moment in the intermediate state and the grad$E$ in axial crystals provides an explanation for the observed α-γ correlation of $RdTh^{228}$. It is well known that the Cd^{111} γ-directional correlation depends strongly on the chemical state[3, 6] and on the environment[1] of the decaying In^{111} atom. This was explained hitherto by magnetic interaction. However, magnetic decoupling experiments with a magnetic field of 7000 gauss applied in the direction of the propagation of one γ-ray showed no tendency to restore the maximum directional correlation (Table I). This field is probably too small for a complete decoupling of I and J (complete Paschen-Back effect of the hyperfine structure or Back-Goudsmit effect), but nevertheless it is large enough to cause a partial breaking of the (I, J) coupling (incomplete Back-Goudsmit effect). An increase in the anisotropy much larger than the experimental error of the measurements should have been observed if the magnetic coupling were the predominant cause for the attenuation of the correlation in the sources investigated. Similar results with even higher fields have been obtained by Heer *et al.*[7] This result seems to indicate that the attenuation of the Cd^{111} correlation in solid sources is due to the interaction between the crystalline grad$E$ field and the electric quadrupole moment of the 0.247-Mev excited state of Cd^{111}, for which a rather large value of the quadrupole moment is expected from shell model considerations.

The largest anisotropy found for nonmetallic solids is exhibited by In_2O_3 and $In(OH)_3$. Both are cubic crystals with relatively small values of grad$E$ at the position of the In, due to the high symmetry of their space groups: T_h^7 and T_h^5, respectively. As a result of the preceding decay, however, these atoms may be displaced from the original lattice point and may be in regions of larger grad$E$ values during a time comparable with the lifetime of the intermediate state.

TABLE I. Directional correlation of Cd^{111} with different sources and with application of a magnetic decoupling field.

Source	B gauss	Anisotropy: $A=\frac{W(\pi)}{W(\pi/2)}-1$
Solid sources:		
$InCl_3$, dry (20°C)	···	-0.012 ± 0.005
$InCl_3$, dry (20°C)	7000	-0.015 ± 0.005
$InCl_3$, dry (540°C)	···	-0.022 ± 0.006
InI_3, dry (20°C)	···	-0.020 ± 0.006
InI_3, dry (20°C)	7000	-0.019 ± 0.006
InI_3, dry (200°C)	···	-0.021 ± 0.006
$In(C_9H_6OH)_3$	···	-0.020 ± 0.006
In_2O_3	···	-0.045 ± 0.004
$In(OH)_3$, dry	···	-0.035 ± 0.006
$In(OH)_3$, dry	7000	-0.036 ± 0.007
In metal, electrodeposited (20°C)	···	-0.051 ± 0.005
In metal, electrodeposited (150°C)	···	-0.048 ± 0.006
In metal, electrodeposited (20°C)	7000	-0.056 ± 0.007
Liquid sources:		
$InCl_3$, aqueous solution	···	-0.221 ± 0.005
$InCl_3$, aqueous solution + 10^{21} Fe^{+++} ions/cc	···	-0.215 ± 0.006
InI_3, liquid salt (220°C)	···	$-0.19\ \pm0.02$
$In(C_9H_6ON)_3$ in $CHCl_3$ dissolved	···	$-0.20\ \pm0.01$
In, liquid metal (180°C)	···	$-0.20\ \pm0.01$

A further indication that the attenuation of the Cd^{111} correlation in the solid sources is caused by crystalline grad$E$ fields stems from the fact that, without exception, liquid In^{111} sources of very different character give the maximum correlation (Table I). In the liquids used the character of the local configuration around a nucleus and thus the gradient of the electric field changes in a time much smaller than the lifetime of the intermediate nuclear state. Consequently the average perturbation on the nuclear m substates due to the quadrupole interaction is zero over the lifetime of the nuclear state.

During the progress of this work a convincing proof for the electric quadrupole interaction on the Cd^{111} correlation has been given by the beautiful experiments of the Swiss group[7] by using single crystals of indium as sources.

Attenuation effects very similar to those exhibited by the Cd^{111} correlation have recently been measured by McGowan[4] on the Ta^{181} γ-cascade. Liquid sources of Hf^{181} also show a much more pronounced anisotropy than solid sources.[4] Moreover, there is evidence that the $P_4(\cos\theta)$ term in the angular correlation function is less attenuated than is the $P_2(\cos\theta)$ term, a result which is impossible with magnetic interaction alone.[8] Both effects, however, are explained easily if electric quadrupole interaction in the intermediate state of Ta^{181} is assumed. For this nucleus a very large electric quadrupole moment in the lower excited states is to be expected from shell model considerations, the ground state of Ta^{181} having one of the largest quadrupole moments known.

A more detailed account of this investigation will be submitted for publication in the near future.

* Supported by the U. S. Atomic Energy Commission.
[1] For references see H. Frauenfelder, *Annual Review of Nuclear Science* (Annual Reviews, Inc., Stanford, 1953), Vol. II.
[2] Beling, Feld, and Halpern, Phys. Rev. **84**, 155 (1951); Battey, Madansky, and Rasetti, Phys. Rev. **89**, 182 (1953).
[3] R. M. Steffen, Phys. Rev. **89**, 903 (1953).
[4] F. K. McGowan, Oak Ridge National Laboratory Quarterly Progress Report, Physics Division, ORNL—1365, —1415, and —1496 (unpublished).
[5] A. Abragam and R. V. Pound, Phys. Rev. **89**, 1306 (1953).
[6] J. C. Kluyver and M. Deutsch, Phys. Rev. **87**, 203 (1952).
[7] Albers, Schönberg, Hänni, Heer, Novey, and Scherrer, Phys. Rev. **90**, 322 (1953).
[8] K. Alder, Helv. Phys. Acta **25**, 235 (1952).

Search for 1-Mev Gamma from N^{16} Decay*

F. BOEHM, D. C. PEASLEE, AND V. PEREZ-MENDEZ†
Columbia University, New York, New York
(Received April 28, 1953)

IN the β-decay of N^{16} to the 1^- (7.1-Mev) and 3^- (6.1-Mev) excited states of O^{16}, respectively, a discrepancy exists between the branching ratio of about 1:1 determined from absorption measurements on the β-spectrum,[1] and the ratio of

about 1:12 from measurement of the associated γ-ray intensities.[2] If both measurements are to be reconciled, the most likely possibility is a strong $E2$ γ-ray transition from the 7.1-Mev to the 6.1-Mev level. The likelihood that this $E2$ could give serious competition to the normal 7.1-Mev $E1$ ground state transition is enhanced by the isotopic spin selection rule[3] forbidding $E1$ transitions with $\Delta T=N-Z=0$. In order to explain the quantitative discrepancy in this way, however, this selection rule would have to be much stronger[4] than suggested by simple estimates.

One check on this problem is to search for a strong 1-Mev γ-ray following N^{16} decay. The reaction $O^{16}(n,p)N^{16}$ was used to produce N^{16} in the Columbia cyclotron, using fast neutrons from $Be(d,n)$ on a water target. A flow system was installed to bring the water from a small chamber behind the Be cyclotron target to a measuring chamber. A 10-sec bombardment produced a very strong activity with the characteristic N^{16} half-life of 7 sec. After a waiting period of 5 sec to allow decay of any shorter activities, the γ-spectrum of N^{16} was measured with a scintillation counter consisting of a 1-inch NaI crystal. The pulse distribution from the crystal was photographed on a triggered oscilloscope.

A strong line was found in the 6-Mev region. In a weak exposure, a peak at 0.5 Mev is visible, owing to annihilation of positrons formed outside the crystal. Between these lines no γ-line can be seen. Assuming the scintillation to be caused by pair production for the 6-Mev line and photoelectric absorption for a hypothetical 1-Mev line, we find an upper intensity limit

$$I(1\text{ Mev})/I(6\text{ Mev})\leq 0.05. \quad (1)$$

To account for the above-mentioned discrepancy in the branching ratios, the ratio (1) should be 10 times larger than observed, which is certainly ruled out by the present measurements. An error in the β-decay branching ratio seems the most likely explanation, in view of the inherent inaccuracy of absorption methods. It is of interest to note that if we assume approximate equality of the β-decay matrix elements, the branching ratio is determined by the ratio of $(2J+1)f$. In this case the ratio is

$$3f(3.2)/7f(4.2)\sim 1/7, \quad (2)$$

in order of magnitude agreement with the intensity ratio of 7-Mev to 6-Mev γ-rays.

This measurement does not provide any information on the failure of the isotopic spin rule forbidding electric dipole transitions. The result (1) implies that $I(1\text{ Mev})/I(7\text{ Mev})\leq 0.6$. The ratio without restriction of the dipole transition is expected to be[5-7] of order 10^{-6} or 10^{-7}. Even if the isotopic spin selection rule reduces $I(7\text{ Mev})$ by a factor of 10^2, an increase of sensitivity of at least 10^3 is expected to be necessary before the 1-Mev line could be detected.

The authors thank Dr. V. L. Telegdi for discussions, Professor W. W. Havens for help with the cyclotron, and Mr. V. Fitch for loan of the NaI crystal.

* Work supported by the research program of the U. S. Atomic Energy Commission.

† Now at Project Whitney, Livermore, California.

[1] Bleuler, Scherrer, Walter, and Zünti, Helv. Phys. Acta **20**, 96 (1947).
[2] Millar, Bartholomew, and Kinsey, Phys. Rev. **81**, 150 (1951).
[3] L. A. Radicati, Phys. Rev. **87**, 521 (1952).
[4] M. Gell-Mann and V. L. Telegdi, Phys. Rev. (to be published).
[5] V. F. Weisskopf, Phys. Rev. **83**, 1073 (1951).
[6] M. Goldhaber and A. W. Sunyar, Phys. Rev. **83**, 906 (1951).
[7] D. H. Wilkinson, Phil. Mag. **44**, 450 (1953).

Alpha-Particle Ionization in Pure Gases and the Average Energy to Make an Ion Pair

WILLIAM P. JESSE AND JOHN SADAUSKIS
Argonne National Laboratory, Lemont, Illinois
(Received April 27, 1953)

FOR some time measurements have been in progress to determine the average energy required to make an ion pair by polonium alpha-particles in very carefully purified gases. Since some of the values obtained are in marked contrast to those found in the literature, it is hoped that the publication of them will be of interest to others working in the field.

In the measurements a short collimating system directed the polonium alpha-particles along the axis of a long cylindrical ionization chamber. The effective path length was about 20 cm. The ions produced by each alpha-particle were collected and measured by a method already described.[1,2] From a knowledge of the capacity of the system and the change of potential of the system produced by the ionization from each alpha-particle, the absolute number of ion pairs produced may be determined. The average energy W to produce an ion pair is, of course, the energy of the polonium alpha-particle (5.298 Mev) divided by this number. A very small correction is made for the energy lost in the collimating system.

The capacity of the chamber was determined at intervals by comparison with a standard double-ended capacitance. During the progress of the work this capacitance was calibrated twice at the National Bureau of Standards with concordant results. The estimated error in the final values of W, of the order of one-half percent, includes, of course, a consideration of errors in such auxiliary measurements.

Since previous work[2] had shown the marked effect of minute gaseous impurities, the greatest precautions were taken to insure the purity of the gases used. These, in general, were introduced from breaker flasks into the chamber and were continuously circulated during the progress of the readings over a purification system by means of a small metal-bellows pump. The chamber was initially baked and pumped for more than twelve hours at a temperature above 200°C.

In Table I are shown the values of W obtained for the various gases used and for comparison very recent results of three other investigators. Two of these determinations were with polonium alpha-particles, and the third, that of Sharpe, was with Pu^{239}. Two values of W are given for each gas. First is given the absolute value of W, and then in parentheses is given the value relative to argon as a standard. In general, the agreement in the table is good, particularly between our own results and those of J. Sharpe.

In the case of helium there is a wide disagreement between the Argonne value and the other two values shown.[3] As has been discussed elsewhere,[2] this is no doubt due to impurities in the gas samples used, since in the other two determinations no extraordinary precautions seem to have been adopted to insure extreme gas purity. By reaction with the impurities the metastable atoms of helium are discharged with the production of additional ion pairs. For the same reason the Argonne value for neon is much higher than the older values found in the literature (about 29 ev/ion pair).

The agreement for argon in the table is good, particularly for three of the determinations. The effect of impurities is much less marked in argon, since the ionization potentials of the common

TABLE I. Values of W, in ev/ion pair. Values relative to argon are given in parentheses.

Gas	Argonne	Sharpe[a]	Valentine and Curran[b]	Haeberli, Huber, and Baldinger[c]
He	42.7 (1.617)		31.7 (1.22)	30.86 (1.176)
Ne	36.8 (1.394)			
A	26.4 (1.000)	26.3 (1.000)	25.9 (1.000)	26.25 (1.000)
Kr	24.1 (0.913)			
Xe	21.9 (0.830)			
H_2	36.3 (1.375)		37.0 (1.43)	
CO_2	34.5 (1.307)	34.2 (1.300)		33.5 (1.276)
Air	35.5 (1.345)	35.6 (1.354)	35.2 (1.36)	
O_2	32.5 (1.231)	32.9 (1.251)	32.2 (1.24)	32.17 (1.226)
N_2	36.6 (1.386)	36.4 (1.384)	36.0 (1.39)	36.3 (1.383)
CH_4	29.2 (1.106)	29.1 (1.106)	29.0 (1.12)	
C_2H_2	27.5 (1.042)			
C_2H_6	26.6 (1.008)			
C_3H_4	28.0 (1.061)			

[a] J. Sharpe, Proc. Phys. Soc. (London) **A65**, 859 (1952).
[b] J. M. Valentine and S. C. Curran, Phil. Mag. **43**, 964 (1952).
[c] Haeberli, Huber, and Baldinger, Helv. Phys. Acta **25**, 467 (1952).

impurities, nitrogen and oxygen, are much above the energy available for the metastable state of argon (11.6 ev). However, by a well-chosen contaminant with an ionization potential below this value one can obtain a large increase in the ionization in argon. Thus, 0.2 percent of acetylene (ionization potential 11.2 ev) added to pure argon will produce an increase in ionization of 25 percent and a W of 21 ev/ion pair.

In view of the well-known difficulties of obtaining saturation for alpha-particle ionization measurements for air and probably oxygen, the corresponding values in the table may well be accepted with some degree of reserve. These difficulties have been emphasized by recent work,[4] where saturation was attained only at fields above 10 000 volts/cm. Alder, Huber, and Metzger,[5] also using fields of this order, employed a method of extrapolation to obtain a value of W for air at saturation of 34.7 ± 0.5 ev/ion pair.

A ratio often calculated is that of W to the ionization potential of the gas in question. Such ratios, based on the W values for the five noble gases in column two of Table I, yield for the first four gases values which are almost constant at about 1.71. The ratio for xenon is only slightly higher. All semblance of constancy is lost if one uses in this way the older values of W found in the literature for helium and neon.

[1] Jesse, Forstat, and Sadauskis, Phys. Rev. **77**, 782 (1950).
[2] W. P. Jesse and J. Sadauskis, Phys. Rev. **88**, 417 (1952).
[3] In a very recent letter, T. E. Bortnis and G. S. Hurst [Phys. Rev. **90**, 160 (1953)] give a value of W for helium of 46.0 ± 0.4 ev per ion pair. This is higher than our own value and much above the previously accepted value. Their values for argon, nitrogen, ethylene, and hydrogen agree well with those given above.
[4] Kimura, Ishiwari, Yuasa, Yamashita, Miyake, and Kimura, J. Phys. Soc. Japan **7**, 111 (1952).
[5] Alder, Huber, and Metzger, Helv. Phys. Acta **20**, 234 (1947).

The Neutron Activation of Ca^{46}

L. G. Cook and K. D. Shafer
Chemistry Branch, Atomic Energy of Canada, Limited, Chalk River, Ontario, Canada
(Received April 24, 1953)

THE natural abundance of Ca^{46} is low, and Ca^{47} has never been reported as observed in neutron-irradiated calcium. Sc^{47} has been observed as a product of $Ca(\alpha,p)$, (d,n), (p,γ),[1] $Ti(n,p)$,[2] $Ti(d,\alpha)$,[3] and Ca^{47} as a product of $Ca(d,p)$.[4] Ca^{47} has been observed directly in the calcium fraction from Cu spallation with 340-Mev protons, and the decay of Sc^{47} observed.[5] We have observed the decay of Ca^{47} in neutron-irradiated calcium indirectly, by observing the decrease in yield of Sc^{47} on successive milkings.

The irradiated calcium was spiked with Sc^{46} tracer, and the Sc fraction was removed, purified by T.T.A.-benzene extraction and ion exchange on Dowex-50, and estimated. This was repeated at weekly intervals for eight weeks.

The decrease in yield of Sc^{47} gave a half-life for Ca^{47} of 4.8 ± 0.5 days, agreeing with the half-life quoted by Batzel, Miller, and Seaborg,[6] but not with the 5.8 days quoted by Matthews and Pool.[4] The thermal neutron activation cross section $Ca^{46}\rightarrow Ca^{47}$ was $0.25\pm0.1\times10^{-24}$ cm^2/atom.

[1] C. T. Hebdon and M. L. Pool, Phys. Rev. **67**, 313 (1945).
[2] R. E. Hein and A. F. Voigt, Phys. Rev. **74**, 1265 (1948).
[3] N. L. Krisberg and M. L. Pool, Phys. Rev. **75**, 1693 (1949).
[4] D. E. Matthews and M. L. Pool, Phys. Rev. **72**, 163 (1947).
[5] Batzel, Miller, and Seaborg, Phys. Rev. **84**, 671 (1951).

Neutron Capture Cross Section of Em^{222}

A. P. Baerg
Chemistry Branch, Atomic Energy of Canada, Limited, Chalk River, Ontario, Canada
(Received April 24, 1953)

MEASUREMENTS have been made of the cross section of Em^{222}(Rn) for slow neutron capture in the NRX reactor, to form Em^{223} which has not been previously reported. This nuclide is expected to be a β-emitter with a calculated disintegration energy of 1.58 Mev,[1] and from this it may be estimated to have a half-life of about 5 minutes. Fr^{223}, the β-decay daughter of Em^{223}, is also short-lived but decays to Ra^{223}(AcX) which is an α-emitter with a half-life of 11.2 days. It seemed convenient to measure the production of Em^{223} by the growth of Ra^{223} during the neutron irradiation of the Em^{222}.

TABLE I. Data for cross-section calculation.

Expt.	$(Em^{222})_0$ mC	t hr	F n/cm^2/sec	$(Ra^{223})_t$ dis/min	$\sigma(n,\gamma)Em^{223}$ barn
1	0.32_7	239	4.8×10^{13}	2460	0.7_6
2	0.27_2	264	4.7	1640	0.6_2
3	0.36_4	222	5.19	3035	0.7_8

The Em^{222} was extracted from an acid solution of $RaCl_2$, purified and sealed in a small quartz bulb for irradiation. A slow stream of helium gas was used to sweep the Em^{223} from the heated $RaCl_2$ solution. The gas was passed through two dry ice traps to remove water vapor and through an Ascarite absorber to remove hydrochloric acid gas. The Em^{222} was then adsorbed in a charcoal trap in a dry ice—acetone mixture. The charcoal trap was then heated and a small volume of helium gas used to sweep the Em^{223} into a small U-shaped quartz bulb immersed in liquid nitrogen to condense the Em^{222}. The bulb was finally evacuated and quickly sealed with a small flame just above the liquid nitrogen level. Some of the Em^{223} was lost in the evacuation, but sufficient was retained for the irradiation.

After about ten days irradiation in a high-flux position of the NRX reactor, the quartz bulb was crushed in a vacuum system and the residual Em^{222} removed. The Ra^{223} and the decay products of Em^{222} were taken up in nitric acid. The Po, Bi, and Pb decay products were separated from the Ra^{223} by two sulfide precipitations using 1 mg each of Bi and Pb carrier. About 25 μg of Ba was used as holdback carrier for the Ra^{223}. The solution was evaporated on a platinum disk for α-counting. The sulfide precipitates were dissolved in nitric acid, and an aliquot was evaporated on platinum for α-counting of the Po^{210} to determine the initial quantity of Em^{222} sealed in the quartz bulb.

The Ra^{223} was identified by α-pulse analysis which showed the three α-groups with energies of 5.72, 5.61, and 5.53 Mev characteristic of Ra^{223}. The α-activity decayed with a half-life of 11.1 ± 0.2 days over a period of at least two half-lives.

The (n,γ) cross section of Em^{222} was calculated from the following equation:

$$\frac{(Ra^{223})_t}{(Em^{222})_0}=\frac{\sigma F\lambda_0}{(\lambda_0-\lambda_1)\lambda_1}(e^{-\lambda_1 t}-e^{-\lambda_0 t}),$$

where $(Em^{222})_0$ is the disintegration rate of the Em^{222} at the beginning of the irradiation, $(Ra^{223})_t$ that of Ra^{222} at the end, and λ_1 and λ_0 are the respective decay constants. F is the neutron flux during the time t of irradiation and was obtained from the calculated neutron distribution within the reactor and the reactor power log.

In three experiments an average value of 0.7_2 barn was found for the cross section σ of Em^{222}. The pertinent data are given in Table I.

The author is greatly indebted to B. G. Harvey for continued guidance and assistance throughout the course of this work.

[1] G. T. Seaborg, Lecture, Eta Chapter of Phi Lambda Upsilon, Ohio State University, March, 1952 (unpublished).

The β-Decay of Li^8

D. Sip. Bunbury
Department of Physics, Imperial College, London, England
(Received April 22, 1953)

THE β-decay of Li^8 is known to lead predominantly to the broad excited state of Be^8 at 3 Mev.[1] This provides an opportunity for studying the β-decay by observing the angular

correlation between the decay electrons and the α-particles from the subsequent break-up of Be^8.

This letter reports measurements which have been made on the angular correlation with a β-ray spectrometer,[2] to select electrons from the high energy part of the spectrum. The α-particles were detected with a thin-window proportional counter which could be rotated about the source.

Li^8 was produced by bombarding natural Li with 530-kev deuterons. The beam was interrupted periodically by deflecting it off the target by means of a 50-cps rectangular voltage wave applied to deflecting plates. The signals from the counters were passed through electronic gates which were opened only when the beam was off the target. The random coincidence rate was continuously monitored by counting delayed coincidences.

The spectrometer resolution was set at about 7 percent, and two sets of measurements were made, with the coil current set to select electrons of 9.8 Mev and 7.5 Mev, corresponding to 0.8 and 0.6 of the end-point energy of the β-spectrum, respectively. Measurements were made at five angles from 90° to 175°, and the results were fitted by least squares to the expression $(1+A\cos^2\theta)$. The values of A found in the two cases were, respectively (0.04 ± 0.2) and (0.12 ± 0.09).

These results are substantially in agreement with the recent measurements by Class and Hanna.[3]

An attempt was made to compute the theoretical angular correlation from the results of Falkoff and Uhlenbeck.[4] However, the results are uncertain, owing to the uncertainty as to the form of interaction involved in β-decay. This and the rather large experimental error make it impossible to arrive at any definite conclusion at present. The calculations of Gardner[5] for the angular correlation in this case appear to be in error. The above results can, however, be taken as confirming the nonzero spin of the 3-Mev level in Be^8, while they also rule out the possibility that the Li^8 β-decay is allowed.

A search was also made for γ-rays in coincidence with decay electrons of Li^8, since there is known to be a γ-ray emitting level at 4.9 Mev in Be^8.[6] In order to reduce as much as possible the effects of bremsstrahlung, the target was deposited at the end of a thin-walled aluminium tube, and the β-counter, which was also of very light construction, was placed as close to the target as possible. Two γ-counters were placed one on each side of the target, and glass walled β-counters, connected in anticoincidence with the other counters, were placed between the target and the γ-counters, to avoid spurious coincidences due to bremsstrahlung produced in the lead surrounding the latter. Bombardment and counting were carried out alternately, as described above, and the background coincidence rate was measured after each run of six minutes. The result obtained was that an upper limit of (0.8 ± 0.3) percent could be placed on the number of disintegrations leading to the 4.9-Mev level in Be^8. This is somewhat lower than the result of Vendryes[7] who obtained (2 ± 1) percent after making a correction for bremsstrahlung. If we take the spin of this level as one,[6] it is difficult to reconcile the above results with a spin of less than three for Li^8.

In the course of this work the half-life of Li^8 was also remeasured. The result obtained was (0.89 ± 0.01) sec, which is not in agreement with the recent measurement of Rall and McNeill[8] who obtained (0.825 ± 0.02) sec, but is in agreement with earlier measurements.[9-11]

The writer is indebted to Professor S. Devons for his interest and encouragement. He also wishes to thank the Senate of the University of London for a postgraduate studentship.

[1] W. F. Hornyak and T. Lauritsen, Phys. Rev. **77**, 160 (1950).
[2] R. L. Graham and O. Klemperer, Proc. Phys. Soc. (London) **B65**, 921 (1952).
[3] C. M. Class and S. S. Hanna, Phys. Rev. **89**, 877 (1953).
[4] D. L. Falkoff and G. E. Uhlenbeck, Phys. Rev. **79**, 323 and 334 (1950).
[5] J. W. Gardner, Phys. Rev. **82**, 283 (1951).
[6] F. Ajzenberg and T. Lauritsen, Revs. Modern Phys. **24**, 321 (1952).
[7] G. Vendryes, Compt. rend. **232**, 1549 (1951).
[8] W. Rall and K. G. McNeill, Phys. Rev. **83**, 1244 (1951).
[9] Lever, Burcham, and Chang, Nature **139**, 24 (1937).
[10] Hughes, Hall, Eggler, and Goldfarb, Phys. Rev. **72**, 646 (1947).
[11] G. C. Baldwin, Phys. Rev. **76**, 182 (1949).

An Unusual Example of V^0 Decay*

R. W. Thompson, A. V. Buskirk, L. R. Etter, C. J. Karzmark, and R. H. Rediker
Department of Physics, Indiana University, Bloomington, Indiana
(Received April 6, 1953).

THE object of this note is to report in detail a rather unusual V^0 decay recently observed in the new magnetic chamber.[1] Event R-118 is shown in Fig. 1. The V^0 particle, occurring with a penetrating shower, decays after traversing about one-eighth of the illuminated height of the chamber. The decay takes place

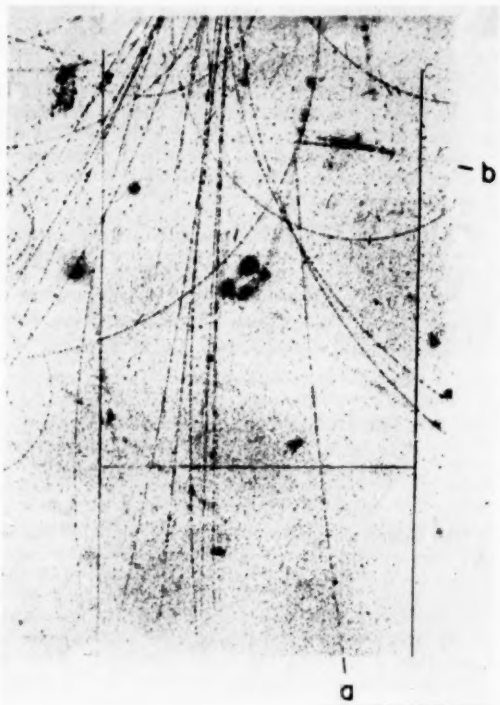

FIG. 1. Event R-118. The upper $\frac{3}{4}$ of the chamber is shown. The obscuration of track b, by an unrelated old track, is less in the other two stereoscopic views.

very near the center of the illuminated depth; the positive fragment (track a) is projected almost vertically down, and the negative fragment (track b) almost horizontally to the right.

The track of the positive fragment is 43 cm long and is well illuminated throughout its entire length. The comparator plot for the left eye is shown in Fig. 2. The corrected momentum, derived from the three eyes, is 0.67 ± 0.02 Bev/c, and the ionization is indistinguishable from that of electronic tracks nearby. A proton of this momentum would be heavily ionizing by a factor 2.3, which it is believed would not easily escape detection under these conditions. Thus it is probable that the positive fragment is lighter than a proton, which means that the disintegration is not of the type $V_1^0\rightarrow p+\pi$.

The track of the negative fragment, although relatively short, is highly curved and distinctly heavily ionizing. The track makes an angle of 26° with the plane of the chamber and crosses the front boundary of the illuminated depth near the right side of the chamber, as evidenced by the fading of track b in Fig. 1. The comparator plot for the left eye is shown in Fig. 2. The momentum is 0.094 ± 0.008 Bev/c, and the track is heavily

ionizing by an estimated factor of 2 or 3. A pion of this momentum would be heavily ionizing by a factor 2.5; and a muon by a factor 1.8; thus it is likely that the negative fragment is a pion or nuon. A τ-meson of this momentum would be heavily ionizing by a factor in the neighborhood of 15 and would not easily escape detection. We thus consider it unlikely that this event represents a decay of the type suggested by the California Institute of Technology group,[2] namely $V_2^0 \rightarrow (\tau^-$ or $\kappa^-) + \pi^+ + 60$ Mev.

The corrected angle between the tracks is $79.2° \pm 0.4°$, the relatively large error arising primarily from the shortness of the negative track. Although the orientation of the event with respect to the associated shower suggests that it represents the decay of a neutral V particle (the angle of decay being so large), the possibility that the event is grossly misinterpreted must not be overlooked. The possibility that the event represents the decay of a charged particle (track b) which enters the chamber from the right can be excluded on energetic grounds since the total energy indicated by track b is considerably less than the kinetic energy of track a. The possibility that the event represents the decay of a charged particle (track a) which enters the chamber from below is a possible but relatively improbable interpretation.

The $Q(\pi, \pi)$ value is 215 ± 7. The next most accurate cases[1] R-32 and R-39 give 212 ± 10 and 216 ± 7, and a recent unpublished event (R-151) gives 219 ± 15. Confirmation of individual $Q(\pi, \pi)$ values in the neighborhood of 214 Mev has not been forthcoming

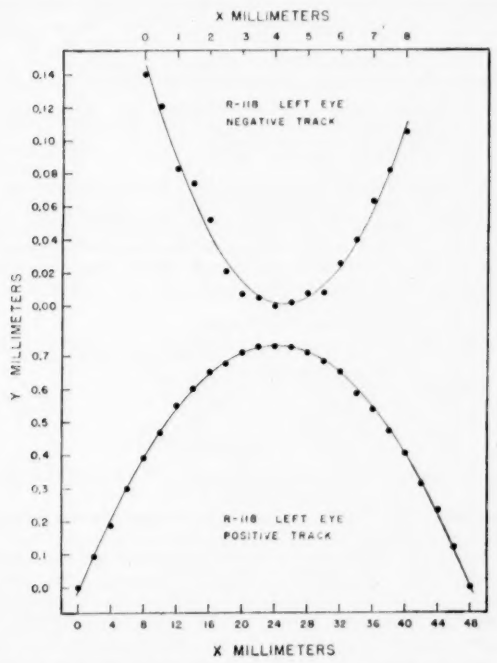

FIG. 2. Comparator plots of R-118 for the left eye. The plots for the other two stereoscopic views are of the same quality.

from other groups, and there is certainly no indication therefrom for the existence of either a line or a pronounced maximum in that neighborhood. We are inclined to consider that the values in the neighborhood of 214 determined as described above are incompatible with a value of 170 Mev,[3] limits of 115–185 Mev,[4] or a range of 100–130 Mev,[2] so that the present observations appear to be distinct from those of other investigators.

It may be that the experimental arrangement has biased[5] our observations in favor of a different type[6] of neutral V particle, $V_4^0 \rightarrow (\pi^+$ or $\mu^+) + (\pi^-$ or $\mu^-) + Q$, where $Q(\pi, \pi) = 214 \pm 5$ Mev.[7,8] In view of the limited statistics (7 cases of V_4^0), we cannot, of course, exclude a splitting of the V_4^0 structure in the Q-curve plot,[1] or a three-body decay. The latter might account for part of the differences with the results of other investigators, and for events[1] 328 and R65B.

* Assisted by the U. S. Office of Ordnance Research and by grant of the Frederick Gardner Cottrell Fund of the Research Corporation.

[1] Proceedings of the Third Rochester Conference. See Thompson, Buskirk, Etter, Karzmark, and Rediker, Phys. Rev. **90**, 329 (1953).

[2] Leighton, Wanlass, and Anderson, Phys. Rev. **89**, 148 (1953).

[3] We are indebted to Dr. Butler for recently informing us that the Manchester data has been remeasured to give $Q(\pi, \pi)$ values in the neighborhood of 170 Mev instead of 122 Mev as previously reported.

[4] We are indebted to Dr. Bridge for sending us a preprint of a forthcoming paper of the Massachusetts Institute of Technology group.

[5] With the new magnetic chamber, we find roughly equal numbers of V_1^0 and V_4^0 (see below).

[6] The Manchester group and the Massachusetts Institute of Technology group use the symbol V_2^0 to indicate the class of all neutral V particles other than $V_1^0 \rightarrow p + \pi$. In that usage, the V_2^0 symbol seems inappropriate here, in view of the large variety of decay schemes in that class which have been reported (see reference 2), but which we have not as yet observed.

[7] In case one or both fragments are muons, slight modification of the Q value would be necessary.

[8] The kinetic energy per pion in the c.m. system would be 107 Mev, very near $E_\pi = 115 \pm 10$ Mev for the χ-decay. See the excellent review paper of D. H. Perkins in the *Proceedings of the Third Annual Rochester Conference on High Energy Physics* (Interscience Publishing Company, New York, 1953).

The O^{14} β-Decay and the Fermi Interaction

M. E. ROSE
Oak Ridge National Laboratory, Oak Ridge, Tennessee
(Received April 20, 1953)

IN view of the results of the angular correlation measurements[1] in the He^6 decay it now appears that the Gamow-Teller (GT) part of the β-interaction is tensor or almost wholly so. It is clear that a measurement of the angular correlation or recoil momentum spectrum for an allowed transition with $\Delta J = 0$ could, in principle, provide corresponding information concerning the composition of the Fermi (F) interaction.[2,3] However, the analysis of transitions other than $J = 0 \rightarrow J = 0$ cases is complicated by the necessity of an accurate knowledge of the relative values of GT and F matrix elements and also by the fact that the He^6 angular correlation measurements, together with β-energy spectra of GT transitions, does not distinguish between pure tensor and an interaction containing an admixture of axial vector coupling. Specifically, if the GT interaction is $\mathcal{H}_{GT} = g(C_T \mathcal{H}_T + C_A \mathcal{H}_A)$ one can conclude only that $|C_A/C_T| \lesssim 0.1$.

In view of these remarks, the C^{10} and O^{14} decays become more interesting. Since the C^{10} decay is a 2 percent branch and is followed by two gamma-rays, the correlation or recoil experiment would be very difficult to carry out and interpret. In the O^{14} decay there is only the 2.31-Mev gamma-ray to consider. This does not interfere with the possibility of carrying out either of the experiments in question, since the recoil due to the gamma-ray is easily taken into account, as shown below.

It has been suggested[3] that the gamma-recoil can be taken into account by observing triple coincidences between the photon, positron, and recoil N^{14}. While this does serve the useful purpose of better definition of the effective source volume, it entails a severe reduction of intensity. It seems preferable to take the gamma-recoil into consideration by a direct and simple calculation. We have considered the recoil experiment since this involves the detection of only one particle. However, the difficulties of this experiment are recognized and similar considerations to those described below can be applied to the angular correlation experiment.

The nuclear recoil momentum is $\mathbf{P} = -(\mathbf{p}+\mathbf{q}+\mathbf{k}) = -(\mathbf{Q}+\mathbf{k})$, where $\mathbf{p}$, $\mathbf{q}$, and $\mathbf{k}$ are the momenta of positron, neutrino, and photon, respectively. Since the photon is isotropic with respect to $\mathbf{p}$ and $\mathbf{q}$, the distribution $N(P)dP$ of recoils with momentum between P and $P+dP$ is obtained essentially by integrating the spectrum of β-recoils (distribution in Q) over the appropriate Q limits. The analytic form of the result depends upon whether or

not $k>Q_{max}=(W_0^2-1)^{\frac{1}{2}}$. However, the shape of the spectrum changes continuously through this point. Present evidence gives $k=4.52$ and $Q_{max}=4.41$ (corresponding to 1.8 Mev for the maximum β-energy). Figure 1 exhibits the recoil momentum

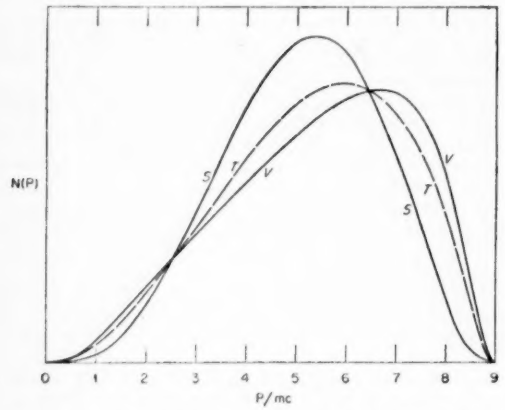

FIG. 1. The recoil momentum spectrum from the O^{14} β-decay, with the recoil due to the 2.31-Mev gamma-ray taken into account. The ordinate (arbitrary scale) is the number of recoils per dP and the abscissa is the recoil momentum in mc units (P_{max} corresponding to 791 ev). The curves labeled S, V, T refer to pure scalar, vector, and tensor interactions. The maximum kinetic energy of the β's is taken as 1.8 Mev, but for 1.7 Mev (curves not shown) the shapes of the spectra are changed rather little. The energy distributions are all symmetrical about $P=k$.

spectrum for this case and for pure S, V, and T interactions. The latter is included because of the slight chance that the first excited state of N^{14} has $J=1$. The experiment is thus capable of settling the question of whether or not the O^{14} decay is a $0\rightarrow 0$ transition. We consider only pure interactions because, on the evidence of linear Kurie plots in general, an admixture, if present, would change the spectrum by an amount too small to detect.

There is one possible difficulty which arises in connection with the O^{14} decay which has not yet been discussed. The decay results in the formation of an atomic ion N^{14-}, provided that the extra electron is not stripped off in the β-process itself. The electron affinity of N is not very well known, but a value of 0.04 ev has been obtained by uncertain extrapolation methods.[4] In any case, one would not expect a value of much more than a fraction per volt. With the value quoted, a rough calculation indicates a probability of only 3×10^{-4} that the sudden charge change will not strip off the extra electron. In this case, the feasibility of the experiment lies in the possibility that further electrons will be ejected resulting in a positive ion. While there will probably be many neutral atoms, these have the effect of reducing the intensity but do not distort the spectrum. In any case an e/M analysis of the residual N^{14} seems advisable.

[1] B. M. Rustad and S. L. Ruby, Phys. Rev. **89**, 880 (1953).
[2] D. C. Peaslee, Phys. Rev. **89**, 1148 (1953).
[3] J. M. Blatt, Phys. Rev. **89**, 83 (1953).
[4] H. S. W. Massey, *Negative Ions* (Cambridge University Press Cambridge, 1938), p. 15. According to preliminary calculations of Ta-You Wu (private communication), N^- is not even stable.

The Decay of Cr^{49}

BERND CRASEMANN AND HARRY T. EASTERDAY
Radiation Laboratory, Department of Physics, University of California, Berkeley, California
(Received April 24, 1953)

THE radioactive isotope Cr^{49} was first described by O'Connor, Pool, and Kurbatov,[1] who determined its half-life as 41.9±0.3 minutes and measured positrons of 1.45 Mev and gamma-rays of 1.55 and 0.18 Mev by absorption techniques. Huber, Lienhard, and Wäffler[2] measured the half-life of Cr^{49} as 45±5 minutes.

In the present work, titanium foils were bombarded for one hour with 40-Mev alpha-particles which produced Cr^{49} by the reactions $Ti^{48}(\alpha,3n)$ and $Ti^{47}(\alpha,2n)$.

The activated titanium foils were dissolved in hot concentrated nitric acid containing a few drops of hydrofluoric acid and 1-mg chromium carrier. Boric acid was added to complex the hydrofluoric acid. The solution was boiled with potassium bromate to oxidize the chromium to chromate. It was then neutralized with ammonium hydroxide and the precipitate redissolved by addition of a few drops of nitric acid. After chilling to $-5°C$, more potassium bromate was added to hold the chromium in the 6-state. Addition of a few drops of hydrogen peroxide formed peroxychromic acid, which was then extracted into prechilled di-isopropyl ketone. After washing with prechilled $\frac{1}{2}N$ nitric acid containing some potassium bromate, the peroxychromic acid was back-extracted into a dilute ammonium hydroxide solution. This was boiled down to near dryness and transferred to the thin Tygon film that served as source backing. The remaining moisture was then evaporated.

The half-life of Cr^{49}, followed on a trochoidal analyzer, was found to be 41.7±0.5 minutes.

The positron spectrum was determined using a thick lens β-spectrograph of two percent transmission and four percent resolution. Fermi plots were constructed that could be resolved into three components, as shown in Table I.

TABLE I. Positron spectrum of Cr^{49}.

Energy Mev	Abundance percent	logft
1.54±0.01	50	4.9
1.39±0.02	35	4.9
0.73±0.05	15	4.1

Photoelectrons ejected from a gold radiator were observed and yielded one set of energy values for the gamma-rays present. Conversion electrons belonging to the 153-kev line were also measured, whereas no conversion electrons could be detected for the 609-kev line. Table II shows measured gamma-energies and conversion coefficients.

TABLE II. Gamma-rays of Cr^{49}.

Energy from photoelectrons kev	Energy from conversion electrons kev	Conversion coefficient α_K	Type of transition
609		$<4\times10^{-4}$	$M1$
153	153	$(2.2\pm0.8)\times10^{-3}$	$M1$

No evidence of the 762-kev crossover transition could be found.

Figure 1 shows a suggested decay scheme, based on the present data. Cr^{49} is expected to have a $5/2-$ ground state. Since in the low Z region proton and neutron shells fill in the same order as given by the shell model,[3] Cr^{49} with 25 neutrons will have the same spin and parity as Mn^{55} with 25 protons. Mn^{55} has a measured spin of 5/2 resulting from the configuration $(f_{7/2})^5 p_{3/2}$.

V^{49} should have the same ground state spin and parity as V^{51}, which is $f_{7/2}$. Since all three beta-components are allowed, the first two excited states of V^{49} must have odd parity like its ground state. The conversion coefficient of the 153-kev gamma-ray identifies it as a magnetic dipole transition. The measured upper limit on the conversion coefficient of the 609-kev gamma-ray indicates that it is of multipole order one. Since its initial and its final state have the same parity, this transition must also be magnetic dipole. The first two excited states of V^{49} are assigned spins of 5/2 and 3/2, respectively, to account for the allowed nature of the three beta-components as well as for the two mag-

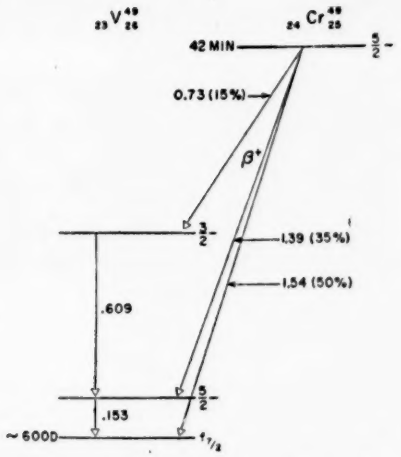

FIG. 1. Decay scheme for Cr^{49} (energies in Mev).

netic dipole gamma-rays. The lack of an observable crossover transition to the ground state agrees with this scheme. This assignment of spins and parities may well result from different coupling of the $(f_{7/2})^3$ proton configuration.

The authors wish to express their sincere thanks to Professor A. C. Helmholz for his interest in this work and his advice on the decay scheme. Dr. Harry G. Hicks' advice on the chemical separation involved is gratefully acknowledged. The authors also wish to thank Mr. G. B. Rossi, Mr. W. B. Jones, and the staff of the Crocker Laboratory cyclotron for making the bombardments.

[1] O'Connor, Pool, and Kurbatov, Phys. Rev. **62**, 413 (1942).
[2] Huber, Lienhard, and Wäffler, Helv. Phys. Acta **17**, 195 (1944).
[3] M. Mayer, Phys. Rev. **78**, 16 (1950).

The Scattering of Slow Neutrons by *Ortho*- and *Para*-Hydrogen

A. T. STEWART* AND G. L. SQUIRES†
Cavendish Laboratory, Cambridge, England
(Received May 4, 1953)

THE triplet and singlet scattering amplitudes of the neutron-proton interaction may be determined by measurement of the slow neutron cross sections of *ortho*- and *para*-hydrogen.[1] These cross sections, previously measured by Sutton *et al.*[2] and others,[3,4] have been remeasured at the Cavendish Laboratory.

The attenuation of a beam of slow neutrons passing through a specimen of hydrogen gas was measured by moving the specimen in and out of the beam. The specimen, 80 cm long was maintained at a temperature of 20.4°K. Neutrons with various energies between 0.002 and 0.014 ev were selected with the slow neutron velocity selector.

Measurements were made first with specimens of normal hydrogen, 75 percent *ortho* and 25 percent *para*, and secondly with specimens of 99.8 percent *para*-hydrogen, the equilibrium mixture at 20.4°K. Considerable attention was paid to the determination, via thermal conductivity analysis, of the *ortho-para* composition of the specimens.

Absorption and *para*-hydrogen scattering contribute about 3 percent to the normal hydrogen cross section; hence relatively approximate values of these cross sections are sufficient to determine the *ortho*-hydrogen cross section. In the almost pure *para*-hydrogen, however, absorption accounts for about 30 percent of the total so that the value chosen for the absorption cross section affects considerably the value obtained for the *para* cross section.

The elastic scattering cross section of *para*-hydrogen is proportional to f^2 where f, the coherent scattering amplitude, is given by

$$f=2(\tfrac{3}{4}a_t+\tfrac{1}{4}a_s).$$

a_t and a_s are the triplet and singlet scattering amplitudes respectively.

If the absorption cross section σ_{abs}, at 2200 m/sec, is taken[5] to be $\sigma_{abs}=(0.330\pm0.007)\times10^{-24}$ cm², our results give a value of the coherent scattering amplitude:

$$f=-(3.80\pm0.05)\times10^{-13}\text{ cm}.$$

The quoted error of 1.2 percent is the combination of 0.5 percent from the uncertainty in σ_{abs} and 1.1 percent from our experimental measurements. Our value of f may be compared with $f=-(3.90\pm0.12)\times10^{-13}$ cm obtained by Sutton *et al.* in a *para*-hydrogen experiment, and with the value $f=-(3.78\pm0.02)\times10^{-13}$ cm given by Burgy, Ringo, and Hughes[6] from liquid mirror experiments.

The free proton cross section,

$$\sigma_f=4\pi(\tfrac{3}{4}a_t^2+\tfrac{1}{4}a_s^2),$$

calculated from our results for the *ortho*-hydrogen cross section, is

$$\sigma_f=(20.41\pm0.14)\times10^{-24}\text{ cm}^2,$$

which may be compared with the value $\sigma_f=(20.36\pm0.10)\times10^{-24}$ cm² obtained by Melkonian.[7]

A more detailed account of the experiment will be published elsewhere.

We wish to thank Dr. Ashmead and Mr. Sadler of the Mond Laboratory, Cambridge, for valuable assistance with the low temperature aspects of the experiment.

* Now at Atomic Energy of Canada, Ltd., Chalk River, Ontario, Canada.
† Now at Atomic Energy Research Establishment, Harwell, England.
[1] J. Schwinger and E. Teller, Phys. Rev. **52**, 286 (1937).
[2] Sutton, Hall, Anderson, Bridge, DeWire, Lavatelli, Long, Snyder, and Williams, Phys. Rev. **72**, 1147 (1947).
[3] Halpern, Estermann, Simpson, and Stern, Phys. Rev. **52**, 142 (1937).
[4] Brickwedde, Dunning, Hoge, and Manley, Phys. Rev. **54**, 266 (1938).
[5] *Neutron Cross Sections*, U. S. Atomic Energy Commission Report AECU 2040 (Technical Services Division, Department of Commerce, Washington, D. C., 1952).
[6] Burgy, Ringo, and Hughes, Phys. Rev. **84**, 1160 (1951).
[7] E. Melkonian, Phys. Rev. **76**, 1744 (1949).

Noncentral Force Matrix Elements for the Nuclear d^2 Configuration

L. W. LONGDON*
Department of Mathematics, The University, Southampton, England
(Received April 22, 1953)

A STUDY by the writer of the tensor operator algebra of Racah[1] has led to the derivation of expressions for the matrix elements, between two-nucleon states, of the purely orbital operators of the two-body tensor and spin orbit interaction operators:

$$\text{Tensor:}\quad J_t(r)T_{12}\{(\boldsymbol{\sigma}_1\cdot\mathbf{r})(\boldsymbol{\sigma}_2\cdot\mathbf{r})/r^2-\tfrac{1}{3}(\boldsymbol{\sigma}_1\cdot\boldsymbol{\sigma}_2)\}.$$
$$\text{Spin-orbit:}\quad J_s(r)T_{12}\{(\boldsymbol{\sigma}_1+\boldsymbol{\sigma}_2)\cdot(\mathbf{r}\times\mathbf{p})\}.$$

The Slater method of expanding the distance dependence has been used, and the results obtained involve linear combinations of radial integrals in which no particular wave functions or interactions are specified.

In their most general form these results are cumbersome because the coefficients of the radial integrals are Wigner coefficients and the W functions of Racah. Considerable reduction, however, is possible under a restriction to equivalent nucleons or direct and exchange matrix elements. It is hoped that a more detailed report on these formulas will appear elsewhere.

The noncentral force matrix elements for the $(3d)^2$ configuration[2]

have been calculated using harmonic oscillator radial wave functions. Results for diagonal and nondiagonal elements in states of lowest total angular momentum J, using a charge symmetric operator, $T_{12}=(\tau_1\cdot\tau_2)$, are expressed in Table I in terms of radial integrals defined later.

TABLE I. Noncentral force matrix elements for $(3d)^2$ configuration with harmonic oscillator wave functions and symmetric charge operator.

	Tensor force				Spin-orbit force			
$\langle^{2T+1,2S+1}L_J\|^{2T+1,2S+1}L_{J'}\rangle$	I_1	I_2	I_3	I_4	I_1	I_2	I_3	I_4
$\langle^{33}P_0\|^{33}P_0\rangle$	$\frac{7}{6}$	$-\frac{5}{3}$	$+\frac{7}{6}$		-7	$+10$	-7	
$7^{-\frac{1}{2}}\langle^{13}S_1\|^{13}D_1\rangle$	$-\frac{31}{60}$	$+\frac{19}{12}$	$-\frac{17}{12}$	$+\frac{3}{4}$				
$\langle^{13}D_1\|^{13}D_1\rangle$	$\frac{14}{15}$	$-\frac{65}{84}$	$-\frac{7}{6}$	$+\frac{3}{4}$		$\frac{51}{2}$	-21	$\frac{27}{2}$
$7^{\frac{1}{2}}2^{-\frac{1}{2}}\langle^{33}P_2\|^{33}F_2\rangle$		1	$-\frac{7}{5}$					
$\langle^{33}F_2\|^{33}F_2\rangle$	$\frac{1}{5}$		$-\frac{1}{5}$		$-\frac{2}{3}$		$-\frac{22}{3}$	
$3^{-\frac{1}{2}}\langle^{13}D_4\|^{13}G_4\rangle$	$-\frac{3}{10}$	$+\frac{33}{98}$	$-\frac{1}{2}$	$+\frac{9}{14}$				
$(28)^{-1}\langle^{13}G_4\|^{13}G_4\rangle$		$+\frac{55}{7}$		$+15$		210		630

1. The corresponding matrix elements for the remaining allowed values of J are given by the relations:

Tensor force	Spin orbit force
$\langle^{33}P_0\rangle=-2\langle^{33}P_1\rangle=10\langle^{33}P_2\rangle$	$\langle^{33}P_0\rangle=2\langle^{33}P_1\rangle=-2\langle^{33}P_2\rangle$
$2\langle^{13}D_1\rangle=-2\langle^{13}D_2\rangle=7\langle^{13}D_3\rangle$	$2\langle^{13}D_1\rangle=6\langle^{13}D_2\rangle=-3\langle^{13}D_3\rangle$
$5\langle^{33}F_2\rangle=-4\langle^{33}F_3\rangle=12\langle^{33}F_4\rangle$	$3\langle^{33}F_2\rangle=12\langle^{33}F_3\rangle=-4\langle^{33}F_4\rangle$
$28\langle^{13}G_3\rangle=-20\langle^{13}G_4\rangle=55\langle^{13}G_5\rangle$.	$4\langle^{13}G_3\rangle=20\langle^{13}G_4\rangle=-5\langle^{13}G_5\rangle$.

2. Results for a neutral charge operator $T_{12}=1$ may be derived from the above by multiplying matrix elements involving singlet charge states by -3^{-1}, and leaving triplet charge state elements unaltered.

3. The radial integrals $I_l(a,b)$ are functions of the force range a and wave function parameter b, and are defined as follows:

$$I_l(a,b)=\int_0^\infty R_l^2(r,b)V(r,a)dr.$$

The single particle wave functions,

$$R_l(r,b)=N_l\exp[-(r/2b)^2]r^{l+1},$$

are subject to the normalizing condition

$$\int_0^\infty R_l^2(r,b)dr=1,$$

which yields

$$N_l^2=2[(2l+1)!!b^{2l+3}(2\pi)^{\frac{1}{2}}]^{-1}.$$

4. For a Yukawa type distance dependence, i.e., $V(r,a)=Be^{-r/a}(r/a)^{-1}$, the integrals $I_l(ab)$ may be calculated either by the method of Talmi[3] or from the Hh functions tabulated in the British Association Mathematical Tables, Vol. I (1931), by using the relation

$$I_l(a,b)=2^{l+1}l!\exp(b^2/2a^2)(a^2/2\pi b^2)^{\frac{1}{4}}Hh_{2l+1}(b/a).$$

Values of the $I_l(a,b)$ for the distance dependence suggested by Case and Pais,

$$V(r,a)=\frac{-Ba^2}{r}\frac{d}{dr}(e^{-r/a}(r/a)^{-1}),$$

may be obtained from those evaluated for Yukawa by using a relation established by Elliott:[4] Replace each function $Hh_{2l+1}(b/a)$ by $(a^2/b^2)\{(2l)^{-1}Hh_{2l-1}(b/a)-Hh_{2l+1}(b/a)\}$.

* Present address: Department of Mathematics, Royal Military College of Science, Shrivenham, Nr. Swindon, Wilts, England.

[1] G. Racah, Phys. Rev. **62**, 438 (1942).

[2] An account of an application of these results to early d shell nuclei is given in a thesis for the degree of PhD (London) which the author proposes to submit shortly.

[3] I. Talmi, Helv. Phys. Acta **25**, 185 (1952).

[4] J. P. Elliott, Ph.D. thesis, London, 1952 (unpublished).

Observation of V^0 Particles Produced at the Cosmotron*

W. B. FOWLER, R. P. SHUTT, A. M. THORNDIKE, AND W. L. WHITTEMORE
Brookhaven National Laboratory, Upton, New York
(Received April 29, 1953)

TWO definite examples of V^0 particles similar to those found in cosmic rays by many workers[1] have been observed in a cloud chamber exposed to a neutron beam from the Cosmotron. These two cases, in addition to several other less definite ones, were found in a total of about 4000 photographs scanned up to date. Further work is in progress.

The events were observed when the machine was operating with a circulating beam of 10^8 to 10^9 protons per pulse, reaching an energy of about 2.2 Bev. The protons were allowed to strike carbon targets 1.25 in. and 2.5 in. thick. Neutrons emerged through a 1-in.×2-in. hole in the shielding wall, located at 0° to the proton beam direction. The number of the neutrons can only be estimated very roughly, and their energy distribution is not known at the present time except that the maximum energy is 2.2 Bev. The neutron beam passed through a permanent magnet which deflected charged particles away from the cloud chamber, and then through 1.5 in. or 3 in. of lead into the cloud chamber. A diffusion cloud chamber was used, filled with hydrogen at 18 atmospheres and methyl alcohol vapor. A pulsed magnetic field of 11 000 gauss was applied.

The V^0 particles show the characteristic inverted V-shaped track originating in the cloud-chamber gas. Their identification follows from the usual arguments.[1] In this case the identification is especially certain because neutron-proton collision processes in hydrogen can only result in events with an odd number of prongs rather than 2-prong events such as V particles. The amount of alcohol present is less than that used in expansion cloud chambers, very few stars produced in the alcohol were seen, and it is very unlikely that "alcohol stars" could have the appearance of V particles.

The photographs are shown in Figs. 1 (event A) and 2 (event B).

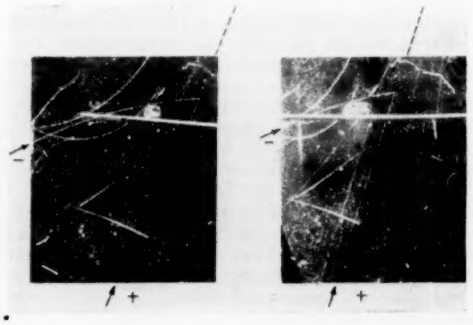

FIG. 1. Stereoscopic photograph of V^0 decay "A." Its apex is just above the horizontal bar across the picture, which is a sweeping field electrode suspended above the sensitive layer of the cloud chamber. The tracks pass underneath this electrode, not through it. The dashed line at the top of the picture points toward the part of the lead shield struck by the neutron beam. Information concerning the V^0 is given in Table I.

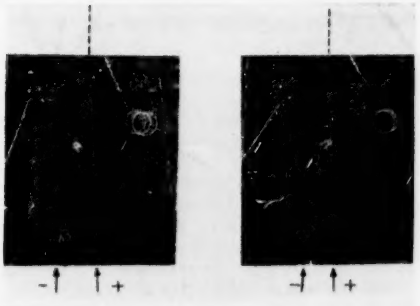

FIG. 2. Stereoscopic photograph of V^0 decay "B." Its apex is just below the horizontal bar across the picture, which is a sweeping field electrode suspended above the sensitive layer of the cloud chamber. The apex of the V^0 particle is vertically separated from the sweeping field electrode by about 5 cm in depth. The dashed line at the top of the picture points toward the part of the shield struck by the neutron beam. Information concerning the V^0 is given in Table I.

The details of the events are given in Table I. For both cases the given momenta and ionization densities show that the negative particles are light particles, most probably π-mesons.[1] The identification of the positive particles is not definite, although in both cases their ionization densities appear to be somewhat larger than minimum. If this were certain, these particles could be identified as protons, and V_1^0 particles ($V_1^0 \rightarrow p+\pi^-+Q_1$) would

TABLE I. Data on V^0 particles.

		Event A	Event B
Positive particle	Momentum, P_+	910 ±230 Mev/c	1200 ±180 Mev/c
	Estimated density of ionization	>1 (?), <2 ×minimum	>1 (?), <2 ×minimum
Negative particle	Momentum, P_-	72 ±3 Mev/c	270 ±30 Mev/c
	Estimated density of ionization	3 ×minimum	1 ×minimum
Angle between tracks		61.5 ±1°	26 ±1°
V^0 momentum, P_0		940 ±240 Mev/c	1450 ±210 Mev/c
Manchester parameter, $\alpha=(P_+^2-P_-^2)/P_0^2$		0.92	0.65
If V_1^0	Q value	39 ±16 Mev	37 ±8 Mev
	Lifetime (10^{-10} sec)	>8, <12	>5, <8
	Range for possible values of α	0.40 to 0.98	0.45 to 0.93
If V_2^0	Q value	236 ±55 Mev	157 ±30 Mev
	Lifetime (10^{-10} sec)	>3, <5	>2, <3
	Range for possible values of α	−0.90 to +0.90	−0.85 to +0.85

be involved. The Q values calculated for this assumption are given in Table I. They agree with the generally accepted $Q_1=35$ to 40 Mev. Assuming that these particles were produced in the lead or possibly in the steel wall of the chamber, lower and upper limits for their lifetimes are also given. These lifetimes are high compared to the lifetime of the V_1^0 of 3×10^{-10} sec given in the literature.[1] The parameter $\alpha=(P_+^2-P_-^2)/P_0^2$ may have any value between the limits given with equal probability. Both computed values for α fall within these ranges.

If one assumes that V_2^0 particles ($V_2^0 \rightarrow \pi^+ + \pi^- + Q_2$) are involved, the calculated Q values are also consistent with the value of $Q_2=190$ Mev given in the literature.[1] The lifetimes are again higher than the mean lifetime of 10^{-10} sec for V_2^0. Here both of the computed values for α lie at the upper end of the possible ranges for α. This fact, the particularly good agreement of the calculated Q values with Q_1, and the apparently somewhat higher-than-minimum ionization density of the positive decay products, make it more probable that the observed particles are V_1^0 rather than V_2^0.

Assuming that the V^0 is produced in a collision of an incident neutron of maximum energy of 2.2 Bev with a nucleon in a nucleus, which may have itself an energy of 20 Mev, the maximum energy available in the center-of-mass system of the two nucleons is 1.11 Bev, which would be just sufficient to produce the total mass of a V_1^0. But then the kinetic energy of the V_1^0 in the laboratory system could be at most 400 Mev. The actual kinetic energies observed (assuming V_1^0) are 349±140 and 714±150 Mev for events A and B, respectively. The high kinetic energy observed for B, if not in error, rules out this possibility experimentally. Production of V_1^0 from pre-existing nucleons, singly or in pairs,[2] or of (V_1^0, V_2^0) pairs, would still be consistent with the present observations. The possibility of single V_1^0 production by 230-Mev π^- mesons has already been indicated by Schein.[3]

* Work performed under the auspices of the U. S. Atomic Energy Commission.

[1] *Progress in Cosmic Ray Physics*, edited by J. G. Wilson (Interscience Publishers, Inc., New York, 1952), Chapter II by C. C. Butler, pp. 65–123; Leighton, Wanlass, and Anderson, Phys. Rev. **89**, 148 (1953); Fretter, May, and Nakada, Phys. Rev. **89**, 168 (1953); Bridge, Peyrou, Rossi, and Safford (to be published); Thompson, Buskirk, Etter, Karzmark, and Rediker, Phys. Rev. **90**, 329 (1953). All references to previous work are cited in these articles.

[2] A. Pais, Phys. Rev. **86**, 663 (1952). References to previous work are cited in this article.

[3] M. Schein, *Proceedings of the Third Annual Rochester Conference on High Energy Physics* (Interscience Publishing Company, New York, 1953).

K Mesons

J. CRUSSARD, L. LEPRINCE-RINGUET, D. MORELLET, A. ORKIN-LECOURTOIS, AND J. TREMBLEY
Laboratoire de l'Ecole Polytechnique, Paris, France
(Received April 24, 1953)

SIX K mesons[1] coming to rest in the emulsion have been observed in a series of 600 μ Ilford G5 plates exposed to the cosmic radiation at balloon altitude (140 cm³ of emulsion×hours of flight above 70 000 feet). Most of the plates were exposed under a copper absorber 3 cm thick. Among these K mesons, three are ejected from stars (see Fig. 1);[2] their ranges are sufficiently long (5000μ, 6000μ, and 9000μ) to allow accurate measurements of their masses. Two of the three remaining mesons are observed in favorable conditions to give some indication of the nature of the secondary particles.

(1) *Mass measurements of the K mesons emitted from stars.*—Scattering-range measurements have been carried out by several observers using different methods. One observer derives the scattering angle from measurements made with continously variable cell-lengths, as suggested by the Brussel group; while others employ the method indicated by the Bristol group.[3] All the measurements yield results in good agreement.

Ionization measurements have been made with a specially designed set-up to determine the opacity of the track by means of a photomultiplier associated to a microscope.[4,5] Appropriate corrections have been made to take into account the depth as well as the dip of the track. The results thus obtained are perfectly consistent, allowing good precision. This precision has been controlled by means of particles of known mass.

The measurements are listed in Table I. If we put together

TABLE I. Mass measurements for the three events.

		K meson[b]			Secondary	
	Star[a]	Length μ	Mass from scatt. range	Mass from ioniza. range	Length μ	Ionization[c]
K_{P2}	$13+18p$	4950	850 ±150	902 ±80	155	0.85 ±0.2
K_{P3}	$9+2p$	6040	1065 ±160	1015 ±85	a few grains	
K_{P4}	$6+1p$	9000	920 ±130	910 ±75	850	1.0 ±0.1

[a] The notation $m+np$ is used to describe a star initiated by a singly charged primary: m indicates the number of heavy tracks (black and gray) and n that of minimum ionization.
[b] The masses are expressed in terms of electron rest-mass.
[c] The ionizations are relative to the plateau.

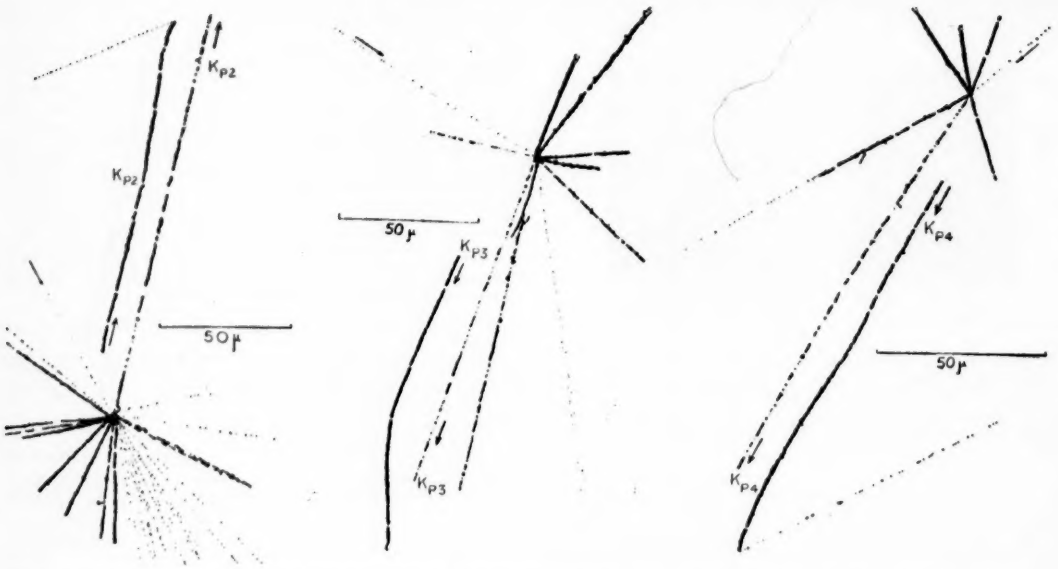

FIG. 1. Tracks of three K mesons emitted from stars. Since the K-meson tracks are very long, only the beginning and end are shown in each case.

the results of these six independent measurements of the mass of the K meson (three by scattering range, three by ionization range), we find

$$M_K = 940 \pm 40.$$

None of the mass measurements of K mesons made in other laboratories disagree with this value. The longest tracks, giving the best measurements, yield the following results:

K_{B2}	1125 ± 150 (5670μ)[6]
K_{B12}	870 ± 100 ($13\,300\mu$)[6]
K_{M2}	1040 ± 90 (5260μ)[7]
K_O	950 ± 50 ($14\,000\mu$)[8]

We see that they are not significantly different from the value given above. Therefore, we will assume tentatively that all the K mesons hitherto observed in emulsions have the same mass, $M_K = 940 \pm 40$.

(2) *Indications on two secondary particles.*—Table II summarizes the measurements of secondary particles having sufficient lengths, observed in this laboratory.

(a) If we analyze the measurements concerning the secondary of K_{P1} using the calibration and method established by the Bristol group,[9] the results strongly suggest a μ-meson, rather than a π-meson.

(b) The mass of K_{P6} (1400μ long) is found to be 900 ± 160. The measurement, though not very accurate, agrees with the adopted value, 940 ± 40. Assuming this mass, if we take into account: (1)—the upper limit of the energy of the secondary particle for a given value of the mass of the K, and (2)—the results of the measurement of $p\beta c$ and ionization of the secondary, we arrive at the conclusion that for the secondary particle, a μ-meson is more probable than a π-meson.

TABLE II.

	Length	$p\beta c$ Mev	Grain-density[a]
K_{P1}	$20\,000\mu$	197 ± 14	0.97 ± 0.03
K_{P4}	3400μ	290 ± 60	0.975 ± 0.05

[a] Grain density is relative to that of the plateau.

(3) *Discussion.*—We mentioned above that all the measurements on K mesons agree with a unique mass of 940 ± 40. This suggests the possibility of trying also a unique scheme of decay. In this case the secondary particle would have to be a μ-meson, and the decay would involve three particles, since the Bristol group has observed with certainty two events in which secondary μ-mesons are emitted with low energies.

The main objection to this assumption is the observation by the Bristol group of three or four secondaries identified by scattering-ionization measurement, most probably, as π-mesons having the same energy.[6] We know also that among the heavy charged particles observed in cloud chambers (charged V's), there is one which emits a π-meson secondary[10] (identified by nuclear scattering).

It may be interesting to investigate whether there is another objection raised by the energy of the secondary: is it possible that K mesons of such a small mass could give rise to energetic secondaries as observed? Assuming the decay scheme $K \rightarrow \mu + 2$ neutral particles of zero mass, we deduce from the conservation laws the limit of the energy spectrum of μ-mesons:

$$p\beta c = 200 \text{ Mev} \quad \text{for} \quad M_K = 940,$$
$$p\beta c = 220 \text{ Mev} \quad \text{for} \quad M_K = 1000.$$

Actually several secondaries have been found with a $p\beta c$ of the order of 250 Mev, greater than these limit values. However, if we consider only the published cases of secondaries longer than 2000μ, we have

$$K_{B1} = p\beta c = 250 \pm 35 \text{ (length: } 2200\mu),^6$$
$$K_{P6} = p\beta c = 290 \pm 60 \text{ (length: } 3400\mu).$$

The lower limit of these measures lies not far from the grouping observed around $p\beta c = 185$ Mev (K_{P1}: 197 ± 14 Mev, K_{B7}: 174 ± 29 Mev, K_{B8}: 192 ± 18, K_{B9}: 179 ± 18). There is therefore no real disagreement between the most energetic secondaries observed and the limit of the spectrum calculated above.

If another decay scheme is adopted, $K \rightarrow \pi^0 + \mu + \nu$, the limit of

the spectrum turns out to be

$$p\beta c = 180 \text{ Mev} \quad \text{for} \quad M_K = 940,$$
$$p\beta c = 200 \text{ Mev} \quad \text{for} \quad M_K = 1000.$$

Agreement with the experimental results is still possible, though somewhat more difficult.

Hence the main argument against the hypothesis of a unique K meson arises from the observations mentioned above of the Bristol group.

One may note that any decay scheme involving a neutral particle heavier than π^0, such as V_2^0, is excluded on account of the small value of the mass of the parent particle.

To sum up, the great majority of K particles observed until now in photographic emulsions can be interpreted as due to the decay of a particle of 940 ± 40 electron masses into at least three particles, one of which is a μ; the upper limit of the energy spectrum of the μ is about $p\beta c = 200$ Mev; among the neutral products, at most one could be a π^0, and none could be heavier than a π^0. We suggest the name "kappa" (first introduced by O'Ceallaigh and the Bristol group[11]) to designate the parent particle.

[1] The term K meson is used to designate any unstable particle of unit charge which has a mass lying between those of π-meson and proton and emits a charged secondary particle at the end of its range. K_B, K_M, K_O, K_P = observations from Bristol, Milano, Oslo, Paris.
[2] Crussard, Leprince-Ringuet, Morellet, Orkin-Lecourtois, and Trembley, Compt. rend. **236**, 872 (1953).
[3] M. G. K. Menon and O. Rochat, Phil. Mag. **42**, 1232 (1951).
[4] G. Kayas and D. Morellet, Compt. rend. **234**, 1359 (1952).
[5] G. Kayas and D. Morellet, J. phys. et radium (to be published).
[6] M. G. K. Menon, Thesis, University of Bristol, 1952 (unpublished).
[7] R. Levi Setti and G. Tomasini, Nuovo cimento **9**, 1244 (1952).
[8] Isachsen, Vangen, and Sörensen, Phil. Mag. **44**, 224 (1953).
[9] L. Voyvodic, Conference on V particles and Heavy Mesons, Bristol, 1951 (unpublished).
[10] H. S. Bridge and M. Annis, Phys. Rev. **81**, 445 (1951).
[11] C. O'Ceallaigh, Phil. Mag. **42**, 1032 (1951).

Energy Levels of C^{12} from the $Be^9(\alpha,n)C^{12}$ Reaction

L. E. Beghian, H. H. Halban, T. Husain, and L. G. Sanders
Clarendon Laboratory, Oxford, England
(Received April 21, 1953)

ENERGY levels of C^{12} have been studied by examining the gamma-radiation from the reaction $Be^9(\alpha,n)C^{12}$. The α-particles were emitted from a thin polonium source (strength 80 mC) deposited on a 1-cm square of thin platinum foil. The foil was placed adjacent to a 1-cm square of beryllium foil (33 mg/cm²) and the whole enclosed in an evacuated copper box with sides 1 mm thick. The gamma-radiation was analyzed with a pair spectrometer similar to that described by Johansson[1] and the spectrum displayed on a 25-channel kicksorter.

Apart from the well-known energy level of C^{12} at 4.43 ± 0.05 Mev (the mean value of a number of observations)[2–6] with $J=2^+$, the existence of a level at 7.5 Mev is indicated by the neutron spectrum from this reaction,[7] and also by the discovery of pair emission [energy (7.0 ± 0.6) Mev] from this reaction.[8] This evidence, together with the absence of gamma-radiation of 7.5 Mev from such an excited level to the ground state of C^{12} ($J=0$), suggested that its spin is also zero. It is to be expected that the de-excitation of this level could also take place by a gamma-cascade via the 4.43-Mev level, resulting in the emission of a gamma-ray of energy about 3 Mev. Previous measurements do not exclude the existence of such a line and place an upper limit of 30 percent on its intensity.[9] (All intensities refer to the 4.43-Mev line as 100 percent.)

We have detected gamma-radiation of energy 3.16 ± 0.05 Mev and intensity ~3 percent in addition to the 4.43-Mev line (see Fig. 1). Together with the evidence obtained from internal pairs,[8] this suggests the existence in C^{12} of a level with energy 7.59 ± 0.07 Mev rather than a level at 3.16 Mev. To show that this radiation was not due to secondary effects caused by neutrons from the reaction (i.e., interaction of the neutrons with the copper of the source box or with the sodium and iodine nuclei of the central crystal of the spectrometer) the following two tests were made. First a run was made with $\frac{1}{2}$ cm of extra copper surrounding the source box. The intensity of the line was not enhanced, thus eliminating the first possibility. Again if the radiation is due to secondary effects in the central crystal, then

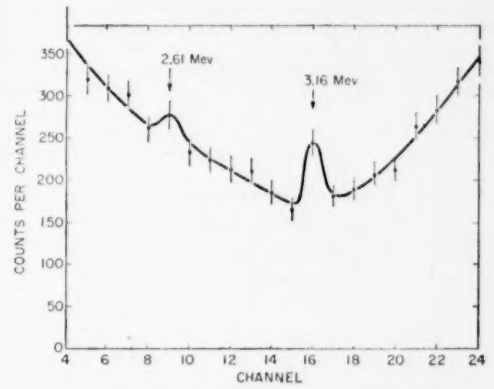

FIG. 1. 3.16-Mev line from $Be^9(\alpha,n)C^{12}$.

intensity (relative to the 4.43-Mev line) would vary as the linear dimensions of the crystal. Measurements made of the intensity with two crystals of different sizes (1 in. cube and 1.5 cm×1 cm ×1 cm) definitely exclude this possibility.

A very weak gamma-ray of energy 2.61 ± 0.08 Mev and intensity ~1.5 percent was also detected but on repeating the copper test its intensity increased to ~7 percent. This line was therefore attributed to interaction of the neutrons with copper (probably inelastic scattering).

We have also examined the region in the neighborhood of 7.5 Mev but no evidence was found for radiation of this energy (upper limit of intensity 1 part in 2500). Previous measurements have placed an upper limit of 1 part in 500.[5]

We wish to thank Dr. W. B. Mims for his help and advice in constructing the spectrometer, Mr. D. Hicks for his help in the initial stages of this experiment, and Professor Lord Cherwell for extending to us the facilities of his laboratory.

[1] S. A. E. Johansson, Phil. Mag. **43**, 249 (1952).
[2] J. Terrell, Phys. Rev. **80**, 1076 (1950).
[3] P. R. Bell and W. H. Jordan, Phys. Rev. **79**, 392 (1950).
[4] Pringle, Roulston, and Standil, Phys. Rev. **78**, 627 (1950).
[5] K. P. Artemov and N. A. Vlasov, Doklady Akad. Nauk. S.S.S.R. **77**, 225 (1951).
[6] D. E. Alburger, Phys. Rev. **87**, 194 (1952).
[7] Guier, Bertini, and Roberts, Phys. Rev. **85**, 426 (1952).
[8] G. Harries and W. T. Davies, Proc. Phys. Soc. (London) **A65**, 564 (1952).
[9] B. Arakatsu *et al.*, J. Phys. Soc. Japan **6**, 66 (1951).

Proton-Proton Scattering at 32.0 Mev

Bruce Cork
Radiation Laboratory, Department of Physics, University of California, Berkeley, California
(Received April 27, 1953)

CALCULATIONS have been made[1] of the differential cross section for proton-proton scattering at 18.3 and 32 Mev. The pseudoscalar meson theory was analyzed and comparison was made with the 18.3-Mev data[2] and the 32-Mev data.[3–4]

The purpose of this letter is to point out that later data have been published[5] supplementing the earlier data.[3] These data are plotted in Fig. 1 transformed to 32.0 Mev assuming a $1/E$ de-

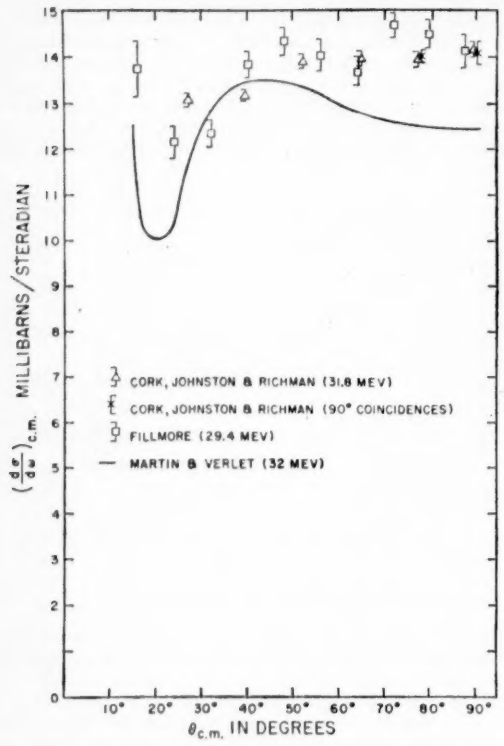

FIG. 1. The differential cross section for proton-proton scattering, normalized to 32.0 Mev assuming a $1/E$ dependence, and comparison with the calculated values of Martin and Verlet.

pendence. Also the calculated curve of Martin and Verlet is shown on the same graph.

The probable errors indicated are those assigned by the experimenters. The more recent data[5] are observed to be in better agreement with the calculated curve,[1] and the proportional counter data.[4]

[1] A. Martin and L. Verlet, Phys. Rev. **89**, 519 (1953).
[2] J. L. Yntema and M. G. White, Technical Report NYO-3478, Princeton University (unpublished).
[3] W. K. H. Panofsky and F. Fillmore, Phys. Rev. **79**, 57 (1950).
[4] Cork, Johnston, and Richman, Phys. Rev. **79**, 71 (1950).
[5] F. Fillmore, Phys. Rev. **83**, 1252 (1951).

The Spin and Magnetic Moment of Ca^{43}

C. D. JEFFRIES
Department of Physics, University of California, Berkeley, California
(Received April 21, 1953)

THE magnetic resonance of Ca^{43} has been observed at a frequency of 2.85 Mc/sec in a magnetic field of 10 000 gauss, using a recording nuclear induction spectrometer somewhat similar to that described by Proctor.[1] The sample consisted of a 0.7-molar aqueous solution of $CaBr_2$, enriched to 68 percent Ca^{43}, mixed with a 4.5-molar aqueous solution of $MnCl_2$ containing a few percent D_2O. The D_2O provided a deutron magnetic resonance signal for reference and the Mn^{++} ions acted as a paramagnetic catalyst to shorten the relaxation time. The ratio of the resonance frequency of Ca^{43} to that of D in the same magnetic field has been observed to be

$$R=\nu(Ca^{43})/\nu(D)=0.43832\pm0.00004. \quad (1)$$

By comparing the sign of the Ca^{43} signal to that of the D signal it was furthermore observed that the magnetic moment of Ca^{43} is negative.

According to Bloch's phenomenological theory of nuclear induction,[2] the spin of a nucleus can be determined in principle by comparing its signal amplitude and width with the amplitude and width of the signal from a nucleus whose spin is known. By this means the spins of several nuclei have been measured by Proctor,[1] Alder and Yu,[3] and others. For slow passage conditions it can be shown that if the radiofrequency field H_1 is much smaller than the saturation value, and the modulation field H_s small compared to the line width, then the observed signal amplitude h is proportional to $\gamma^3W^{-2}NI(I+1)H_1H_s\omega^2$, where γ is the gyromagnetic ratio, W is the line width, N is the number of nuclei per unit volume, I is the spin, and ω is the Larmor frequency.

In the present case it was observed that the variation of the Ca^{43} signal amplitude with the magnitude of the radiofrequency field had the behavior predicted by Bloch's theory; a similar behavior was observed for the D signal amplitude. Slow passage conditions were achieved by shortening the relaxation times by the use of the Mn^{++} ions and by using a low spectrometer modulation frequency. The line shapes were normal, and there was no evidence of any structure which are due to chemical effects. Thus there is good evidence that the expression for the signal amplitude as given above is applicable to both the Ca^{43} and the D signals. For nine sets of data we have measured h and W for both the Ca^{43} and the D signals obtained for the same values of H_1, H_s, and ω. Using the above expression, we find

$$[I(\mathrm{Ca})][I(\mathrm{Ca})+1]=2\left[\frac{1}{R}\right]^2\left[\frac{W(\mathrm{Ca})}{W(\mathrm{D})}\right]^2\left[\frac{h(\mathrm{Ca})}{h(\mathrm{D})}\right]\left[\frac{N(\mathrm{D})}{N(\mathrm{Ca})}\right]$$
$$=15.8\pm2,$$

from which we conclude that the spin of Ca^{43} is

$$I(Ca^{43})=7/2, \quad (2)$$

considering that the nearest other possible spin values of 5/2 and 9/2 give values of $I(I+1)$ well outside this measured value.

Using this spin value and the frequency ratio (1), we obtain for the magnetic moment of Ca^{43}, without diamagnetic correction,

$$\mu(Ca^{43})=-1.3152\pm0.0002 \text{ nm}, \quad (3)$$

where we have used in this calculation the ratio $\mu(D)/\mu(H)=0.307015$ as given by Mack,[4] and $\mu(H)=2.7925$ as determined by Bloch and Jeffries.[5]

This experiment assigns an $f_{7/2}$ orbit to the odd neutron in Ca^{43}, which is in agreement with the nuclear shell model proposed by Mayer[6] and Haxel, Jensen, and Suess.[7] It should also be pointed out that the values of the magnetic moment of Ca^{43} as predicted by the schemes of Schawlow and Townes,[8] and of Davidson,[9] which are -1.38 nm and -1.17 ± 0.12 nm, respectively, agree well with the above measured value.

The author wishes to express his appreciation to the Stable Isotopes Division of the Oak Ridge National Laboratory for the loan of the enriched Ca^{43}, which made these measurements possible.

[1] W. G. Proctor, Phys. Rev. **79**, 35 (1950).
[2] F. Bloch, Phys. Rev. **70**, 406 (1950).
[3] F. Alder and F. C. Yu, Phys. Rev. **81**, 1067 (1951).
[4] J. E. Mack, Revs. Modern Phys. **22**, 64 (1950).
[5] F. Bloch and C. D. Jeffries, Phys. Rev. **80**, 305 (1950).
[6] M. G. Mayer, Phys. Rev. **78**, 16 (1950).
[7] Haxel, Jensen, and Suess, Z. Physik **128**, 295 (1950).
[8] A. L. Schawlow and C. H. Townes, Phys. Rev. **82**, 268 (1951).
[9] J. P. Davidson, Phys. Rev. **85**, 432 (1952).

Errata for Vol. 90

The Abundances of the Elements, HAROLD C. UREY [Phys. Rev. **88**, 248 (1952)]. On page 252, the abundances of bismuth are given incorrectly by a factor of 10. The percent should be 2×10^{-5}, and the atomic abundance in the third column should be 0.0014. This atomic abundance is also given incorrectly in *The Planets* (Yale University Press, New Haven, 1952), second edition. Also, Kuiper's atomic abundance for argon should be 25 000 instead of 2500.

Spherical Model of a Ferromagnet, H. W. LEWIS AND G. H. WANNIER [Phys. Rev. **88**, 682 (1952)]. In this Letter, we presented an alternative derivation of the results of T. H. Berlin and M. Kac [Phys. Rev. **86**, 821 (1952)], using a different statistical ensemble. We stated in the Letter that all their results could be derived by our method. We want to amend this to say that all thermodynamic properties can be so derived. For other averages this may or may not be the case; discrepancies are particularly apt to occur in those averages which are connected with the fluctuations in the assumed constraints. A discrepancy of this sort does indeed arise in connection with $\Sigma_i\epsilon_i^4$ which, in our derivation, equals $3N$ at all temperatures, while in the original paper, it drops to N near absolute zero. The quantity in question is one of the sums which determines the fluctuation of the thermodynamic variable $D=\Sigma_i\epsilon_i^2$ (assumed equal to N). In the original paper, the fluctuation of D was assumed exactly zero, while in our Letter, its value is controlled through its conjugate function s. The discovered discrepancy makes a contribution of $(2/N)^{\frac{1}{2}}$ to the relative fluctuation of D; this is the normal order of magnitude to be expected.

Activation Cross Sections for 14-Mev Neutrons, STUART G. FORBES [Phys. Rev. **88**, 1309 (1952)]. The caption to Fig. 1 is incorrect. The data are for Cu^{62} beta-rays, not for Cu^{64}.

Nuclear Mass Determinations from Disintegration Energies: Oxygen to Sulfur, C. W. LI [Phys. Rev. **88**, 1038 (1952)]. In Table III, Table of atomic masses, the value of $M-A$ for Mg^{27} should be -6.633 ± 0.028 Mev, instead of -8.633 ± 0.028 Mev. The value of M is correct. In Table I, footnote a, the words "p. 000" should be replaced by "p. 1040."

Theory of the Response of Organic Scintillation Crystals to Short-Range Particles, J. B. BIRKS [Phys. Rev. **86**, 569 (1952)]. The probability of an exciton traveling a distance a from 0 is $\exp(-a/a_0)/a^2$, and not $\exp(-a/a_0)$. This modifies the expression for ϕ to

$$\phi=1-\tfrac{1}{2}[\exp(-r/a_0)-(r/a_0)\mathrm{Ei}(r/a_0)], \qquad (2)$$

where $\mathrm{Ei}(r/a_0)$ is the exponential integral. This expression has a similar form to that previously given, though it falls more sharply to 0.5 at $r=0$.

Conversion of an Amplified Dirac Equation to an Approximately Relativistic Form, W. A. BARKER AND Z. V. CHRAPLYVY [Phys. Rev. **89**, 446 (1953)]. Two second-order terms in Table I are dimensionally incorrect. The fourth spin-field term in the tensor column should read

$$\frac{\beta i\hbar^2}{8m^2c^2}\boldsymbol{\sigma}\cdot\nabla\times\frac{\partial\mathbf{P}}{\partial t}.$$

The first spin-orbit term in the pseudovector column should read

$$\frac{1}{2m^2c}\{\boldsymbol{\sigma}\cdot(\mathbf{S}\times\mathbf{p})\times\mathbf{p}\}.$$

A Third Rydberg Series of N_2, R. EDWIN WORLEY [Phys. Rev. **89**, 863 (1953)]. On page 864, column 1, the paragraph beginning with "Professor Mulliken . . ." should *begin* with its *last* sentence.

The Macroscopic Theory of Superfluid He^3-He^4 Mixtures, P. J. PRICE [Phys. Rev. **89**, 1209 (1953)]. Equation (15′) was printed incorrectly. It should read

$$w'=\epsilon wS'/S. \qquad (15')$$

Impurity Diffusion and Space Charge Layers in "Fused Impurity" *p-n* Junctions, J. S. SABY AND W. C. DUNLAP, JR. [Phys. Rev. **90**, 630 (1953)]. The above title and authors were inadvertently omitted from the May 15, 1953 Table of Contents. They should replace "Scattering of Protons by Protons"—H. H. Hall and J. L. Powell (p. 630).

PHYSICAL REVIEW VOLUME 90, NUMBER 6 JUNE 15, 1953

Proceedings of the American Physical Society

MINUTES OF THE 1953 SPRING MEETING OF THE OHIO SECTION AT THE OHIO STATE UNIVERSITY, COLUMBUS, OHIO, APRIL 24 AND 25, 1953

THE regular spring meeting of the Ohio Section of The American Physical Society was held at The Ohio State University, Columbus, Ohio, on April 24–25, 1953. This was a joint session with Section F of the Ohio Academy of Science. Ninety-three were present at the first paper and fifty-three were in the room at the end of the contributed papers on Saturday. Five invited papers and two films were presented which dealt with current knowledge of high altitudes and problems arising from rocket flight.

The invited papers presented were "The Proposed Artificial Satellite," Dr. J. Allen Hynek, The Ohio State University; "Contributions of Astrophysics to Our Knowledge of the Upper Atmosphere," Dr. Geoffrey Kellar, The Perkins Observatory; "The Physics of the Earth's Atmosphere," Dr. David T. Williams, Battelle Memorial Institute; "Human Factors in Space Travel," Dr. F. A. Hitchcock, Physiology Department, The Ohio State University; and "The Physics of Propulsion in the Upper Atmosphere," Lt. Col. R. W. Hoffman, U. S. Air Force, Wright Field.

The two recently released films shown were "Living Animals in Rocket Flight," through the courtesy of the Wright Air Development Center, and "The Viking" through the Naval Research Laboratory. The Saturday morning program was devoted to the contributed papers: "A Simplified Derivation of Formulas for Refraction at a Spher-

ical Boundary," by Dr. R. L. Edwards, Miami University, Oxford, Ohio; and "A Course Called Space Travel," by Thomas D. Phillips, Marietta College, Marietta, Ohio.

Officers for the year 1953–1954 were chosen as follows: Chairman, DR. CHARLES M. SCHWARTZ, Battelle Memorial Institute, Columbus, Ohio; Vice-Chairman, DR. WILLIAM H. GRAN, Miami University, Oxford, Ohio; Secretary-Treasurer, LEON E. SMITH, Denison University, Granville, Ohio.

Abstracts of the contributed papers follow.

LEON E. SMITH, *Secretary*
Ohio Section
Denison University
Granville, Ohio

A Vector Addition Coefficient Identity. R. L. GUERNSEY AND G. B. ARFKEN, *Miami University.*—Published results on the angular correlation of mixed multiple gamma-rays using electromagnetic theory[1] and group theory[2] imply the existence of a vector addition coefficient identity. The identity has the form $2M(LLM-M|J\ O)-(L-M)\ (LLM+1-M-1|J\ O)+(L+M)\ (LLM-1-M+1|J\ O)=F\ (L+1\ LM-M|J\ O)(L+M+1)^{-\frac{1}{2}}\ (L-M+1)^{-\frac{1}{2}}$. The function F is found to be $[J(J+1)(2L-J+1)(2L+J+2)]^{\frac{1}{2}}$, independent of magnetic quantum numbers. A generalization to cover unequal values of the L's has been obtained. Application of the identity is made in the construction of convenient expressions for $(LL2-2|J\ O)$.

[1] D. S. Ling, Jr., and D. L. Falkoff, Phys. Rev. **76**, 1639 (1949).
[2] S. P. Lloyd, Phys. Rev. **85**, 904 (1952); also L. C. Biedenharn and M. E. Rose, (review article, to be published). The implied existence of this identity was first recognized in the course of an earlier investigation, Rose, Biedenharn, and Arfken, Phys. Rev. **85**, 5 (1952).

Method for Measuring the Half-Lives of Positron Emitters.* DONALD W. GREEN, J. C. HARRIS, AND JOHN N. COOPER, *Ohio State University.*—Apparatus has been designed and constructed for measuring half-lives between two and fifteen seconds. It is being used for the study of positron emitters produced by proton-capture reactions. The apparatus consists of two units. The first contains the target and Geiger tube with a mechanism for moving the target from bombarding position to counting position and back. The second consists of a distributor and timing shaft. The distributor receives the output signal from the G-M tube and feeds it to five scalers in sequence, with each scaler counting for 3.5 seconds. The timing shaft is geared to the distributor and correlates the motion of the target with the distributor. Preliminary measurements have been made on Al^{26}, which has a half-life of approximately six[1] seconds. This isotope was produced by the bombardment of natural magnesium with protons of energies for which the reaction $Mg^{25}(p,\gamma)Al^{26}$ is known[2] to be excited.

* Supported in part by the U. S. Atomic Energy Commission through a contract with the Ohio State University Research Foundation.
[1] L. Katz and A. G. W. Cameron, Phys. Rev. **84**, 1115 (1951).
[2] Russell, Taylor, and Cooper, Phys. Rev. **86**, 653A (1952).

Author Index to Volume 90

References with (A) are to abstracts of papers presented at meetings of the American Physical Society, and those with (T) designate title only; references with (L) are to Letters to the Editor; references to (E) are to Errata.

Aarons, M. W., J. Ashkin, F. Feiner, J. G. Gorman, and L. Smith. Nuclear cross sections of negative and positive pions—342(A)

Abe, Hidetaro and Junji Shimada. Anomalous magnetic resonance absorption of Cu acetate at 40 kMc/sec—317(L)

Abragam, A. Indirect interaction between nuclear spins in Cu acetate—358(A)

—— (see Kambe, K.)—348(A)

—— (see Pound, R. V.)—993(L)

Abraham, Bernard M., Darrell W. Osborne, and Bernard Weinstock. Nuclear alignment and entropy of liquid He^3—347(A)

Abrahams, Elihu (see Kittel, C.)—238

Acquista, N. (see Mann, D. E.)—359(A)

Adel, Arthur. Absorption line-width in infrared spectrum of atmospheric CO_2—1024

Ahrens, Tino. Pseudoscalar interaction in theory of β-decay—974

Akeley, E. S. (see Jacobs, Ira)—386(A)

Albers-Schönberg, H., F. Hänni, E. Heer, T. B. Novey, and P. Scherrer. Effect of electric quadrupole interaction on γ-γ directional correlation in Cd^{111}—322(L)

Albrecht, H. O. (see Mandeville, C. E.)—25; 364(A); 992(L)

Alford, W. L. and R. B. Leighton. Mean lifetimes of V-particles and heavy mesons—622

Allen, H. C., Jr. (see Meal, H. C.)—348(A)

Allison, Samuel K. and Harvey Casson. Scintillation response from NaI(Tl) crystals under bombardment with 60–600 kev positive ions—354(A); 880

Allred, J. C. (see Armstrong, A. H.)—340(A)

Alperovitch, E. (see Lidofsky, L.)—387(A)

Amdur, I. and W. T. Lindsay. Scattering of fast N_2 molecules by N_2—344(A)

Anderson, Carl E., George W. Wheeler, and W. W. Watson. Inner bremsstrahlung associated with K-capture in A^{37}—606

Anderson, E. C. (see Cowan, C. L., Jr.)—493(L)

Anderson, J. M. (see Goldstein, L.)—151(L); 486(L)

Anderson, James L. Use of functionals in evaluating S matrix—373(A)

Angell, C. E. and J. P. Perry. Total cross sections of 37-Mev pions in H—724(L)

Antonoff, George. Methods for advancing subject of liquid—385(A)

—— (see Madrazo, Raymond, Jr.)—385(A)

Appleton, G. L. (see Halpern, O.)—869

Arase, E., Gerson Goldhaber, and S. Goldhaber. Elastic pion-deuteron scattering—160(L)

—— (see Goldhaber, S.)—344(A)

Arfken, G. B. (see Guernsey, R. L.)—1132(A)

Armstrong, A. H., J. C. Allred, and L. Rosen. Interaction of 14-Mev neutrons with protons and deuterons—340(A)

Arnold, James R. and Thomas Sugihara. Decay scheme of natural Lu^{176}—332(L)

Artman, J. O. and J. P. Gordon. Pressure broadening of O_2 lines in mm wavelength region—338(A)

Ascoli, Giulio. Mass of cosmic-ray mesons at mountain altitudes—1079

Ashkin, J. (see Aarons, M. W.)—342(A)

Auluck, F. C. and D. S. Kothari. Fermi's theory of nucleon collisions and zero-point energy of pions—1002(L)

Austern, N. and S. T. Butler. Coulomb effects in deuteron stripping—365(A)

Baerg, A. P. Neutron capture cross section of Em^{239}—1121(L)

Bainbridge, Kenneth T., M. Goldhaber, and Elizabeth Wilson. Influence of chemical state on lifetime of nuclear isomer, Tc^{99m}—430

—— (see Kraushaar, J. J.)—610

Bair, J. K., J. D. Kington, and H. B. Willard. N^{14} level structure from $C^{13}(p,n)N^{13}$—575

—— (see Willard, H. B.)—865

Ballam, J., D. R. Harris, A. L. Hodson, R. Ronald Rau, G. T. Reynolds, and Marcello Vidale. Magnetic field cloud chamber for studying nuclear interactions in cosmic radiation. I. Equipment—369(A)

—— (see Rau, R. Ronald)—369(A)

Ballard, Stanley S. and Kathryn A. McCarthy. Thermal conductivity values for $BaTiO_3$—375(A)

Bame, S. J., Jr. (see Perry, J. E., Jr.)—380(A)

Band, William and Raymond A. Nelson. Cluster theory of saturated vapor pressure of He isotope mixtures—744

Barbour, Ian. Z-dependence of cross section and energy in cosmic-ray stars—361(A)

Barker, W. A. and Z. V. Chraplyvy. Conversion of amplified Dirac equation to approximately relativistic form, erratum—1131(E)

Barnes, R. G. (see Harrick, N. J.)—260

Barnett, C. F. (see Evans, G. E.)—825

Barnett, S. J. Gyromagnetic ratios of microcrystalline and macrocrystalline materials—315(L)

Barschall, H. H. (see Walt, M.)—714(L)

Bartell, L. S. and L. O. Brockway. Investigation of electron distribution in atoms by electron diffraction—833

Bartholomew, G. A. and B. B. Kinsey. γ-rays produced by neutron capture in Cd^{113}—355(A)

Bay, Z., V. P. Henri, and F. McLernon. Lifetimes of excited states of Ni^{60}—371(A)

—— (see Kanner, H.)—371(A)

Beach, E. H. (see King, J. S.)—381(A)

Becker, Robert A. (see Bendel, W. L.)—888

—— (see Brown, Hugh N.)—323(L)

Beers, Y. (see Weisbaum, S.)—338(A)

Beghian, L. E., H. H. Halban, T. Husain, and L. G. Sanders. Energy levels of C^{12} from $Be^9(\alpha,n)C^{12}$—1129(L)

—— (see Hicks, D.)—163(L)

Bekefi, G. Diffraction of electromagnetic waves by aperture in infinite screen—385(A)

Belinfante, F. J. and J. C. Swihart. Special-relativistic linear theory of gravitation—357(A)

Bell, George I. Capture and loss of electrons by fission fragments—548

Bell, R. E. and R. L. Graham. Time distribution of positron annihilation in liquids and solids—644

Bendel, W. L., F. J. Shore, H. N. Brown, and R. A. Becker. Disintegration of 24-min Ag^{108}—888

Benenson, R. E. Energy levels in N^{14} and C^{14} from deuteron bombardment of C^{13}—420

Bennett, Clarence and Victor H. Coffin. Molar refraction of CO_2 as function of density and age of gas—344(A)

Bennett, Willard H. Magnetically self-focusing discharges—387(A)

Bergmann, Otto. Conservation laws in classical electrodynamics—315(L)

Bergmann, Peter G. Self-consistency of Lagrangian quantization—357(A)

—— (see Thomson, Robb M.)—357(A)

Berko, Stephen and Frank L. Hereford. Deflection of high energy electrons in magnetized Fe—341(A)
Berman, Arthur I. Total Compton and pair production cross sections at 19.5 Mev—210
Bernardini, G., R. Reitz, and E. Segrè. Photomesonic fission of Bi—573
Bernstein, W. (see Chase, R. L.)—353(A)
—— (see Schardt, A. W.)—353(A)
Bethe, H. A. Sign of phase shifts in meson-nucleon scattering—994(L)
—— **and F. J. Dyson.** Asymptotic behavior and differential equation of meson wave function—372(A)
Bever, R. S. (see Sproull, R. L.)—352(A)
Beyster, J. R. (see Carter, R. E.)—389(A)
Bichsel, H. and R. F. Mozley. Range of protons in Al—354(A)
—— (see Mozley, R. F.)—354(A)
Biedenharn, L. C. and John M. Blatt. Variational principle for n-p scattering with tensor forces—365(A)
Biondi, Manfred A. Processes involving ions and metastable atoms in Hg afterglows—730
Birks, J. B. Response of organic scintillation crystals to short-range particles, erratum—1131(E)
Bitter, Francis. Magneto-resonance and magnetic optics—358(T)
Bjornerud, E. K. (see York, C. M.)—167(L)
Black, Clayton F. Angular distributions of (d,p) reactions—381(A)
Blair, J. S. and G. F. Chew. Fourth order corrections to scattering of pions by non-relativistic nucleons—1065
Blatt, John M., A. K. Stebbins, and D. J. Tendam. (α,n) and $(\alpha,2n)$ cross sections of Ag^{109}—460
—— (see Biedenharn, L. C.)—365(A)
Bleuler, E., J. W. Blue, S. A. Chowdary, A. C. Johnson, and D. J. Tendam. Isomerism of In^{110} and In^{112}—464
Blewett, J. P. Accelerators incorporating alternating-gradient focusing—347(T)
Bloom, A. L. and J. N. Shoolery. High resolution of nuclear resonance signals in flowing samples—358(A)
Bloom, Stanley. Spectral line broadening by electrons—382(A)
—— **and Henry Margenau.** Quantum theory of spectral line broadening—791
Blue, J. W. (see Bleuler, E.)—464
Bockelman, C. K., C. P. Browne, A. Sperduto, and W. W. Buechner. Inelastic scattering of protons and deuterons from B^{10}—340(A)
—— (see Browne, C. P.)—340(A)
Bodansky, D., A. Sachs, and J. Steinberger. Differential cross sections for scattering of 58-Mev π^+ mesons in H—996(L)
——, **A. M. Sachs, and J. Steinberger.** Phase-shift analysis of scattering of positive mesons at 58 Mev—997(L)
Boehm, F., D. C. Peaslee, and V. Perez-Mendez. Search for 1-Mev γ from N^{16} decay—1119(L)
—— **and C. S. Wu.** Inner bremsstrahlung and ionization of atom accompanying β-decay—369(A)
—— (see Wu, C. S.)—388(A)
Bohr, Aage and Ben R. Mottelson. Rotational states in even-even nuclei—717(L)
Boley, F. I. and D. S. Dunavan. Radioactive decay of Y^{91}—158(L)
Boorse, H. A. (see Smith, B.)—156(L)
Booth, E. C. (see Rasetti, F.)—388(A)
Borowitz, Sidney (see Boyet, Howard)—341(A)
—— (see Mostov, Philip M.)—376(A)
Borst, L. B. Resonance scattering in In—354(A); 859
Bortner, T. E. and G. S. Hurst. Energy per ion pair for 5-Mev α-particles in He—160(L)
Bots, G. J. C. and C. J. Gorter. Fountain effect in He II below 1°K—1117(L)
Boyd, A. W. (see MacKenzie, D. R.)—327(L)
Boyet, Howard and Sidney Borowitz. Scattering of electrons by H atoms—341(A)
Braams, R. and C. L. Smith. Photoneutron reaction in Ca^{40}—995(L)
Bracci, A., U. Facchini, and A. Malvicini. Spectrum of γ-radiation emitted in reaction $n+p \rightarrow d+\gamma$—162(L)
Braid, T. H. Measurements of neutron capture γ-rays with scintillation spectrometer—355(A)
Bramson, H. J. (see Seifert, A. M.)—349(A)
Branin, Franklin H., Jr. Bi-directional electronic counter for use in optical interferometry—345(A)
Brattain, W. H. (see Portis, A. M.)—988(L)
Braunstein, R. and J. W. Trischka. Nuclear-molecular interactions of Li^7F^{19}—348(A)
Bray, P. J. (see Harrick, N. J.)—260
Breckenridge, R. G. Semiconducting intermetallic compounds—488(L)
Breit, G. (see Gluckstern, R. L.)—1026
Brentano, J. C. M. and T. L. Thourson. X-ray investigation on effect of mechanical surface treatment on lattice regularity of quartz and calcite—351(A)
Brice, M. K. (see Cork, J. M.)—444; 579
Bridge, H. S., C. Peyrou, B. Rossi, and R. Safford. Cloud chamber observations of heavy charged unstable particles in cosmic rays—921
—— (see Peyrou, C.)—368(A)
—— (see Safford, R.)—369(A)
Bridgman, P. W. Recent results at high pressures—367(T)
Brockman, F. G. (see Corliss, L. M.)—1013
Brockway, L. O. (see Bartell, L. S.)—833
Broder, Jacob (see Keck, Paul H.)—521
Brolley, J. E., Jr. (see Dickinson, W. C.)—388(A)
Bronzo, Joseph (see Truell, Rohn)—152(L)
Brooks, Harvey. Diffusion of injected carriers in semiconductor of mixed conductivity type—336(A)
—— (see Ham, Frank)—383(A)
Brosi, A. R. (see Ketelle, B. H.)—567
Brower, D. (see Hinman, G.)—370(A)
Brown, Harry B. and Robert Stump. Continuous γ-radiation accompanying internal conversion in Ba^{137m}—1061
Brown, Hugh N. and Robert A. Becker. Excitation of 16-μsec state in Ta^{181} by capture of bremsstrahlung—328(L)
—— (see Bendel, W. L.)—888
Brown, L. Carlton (see Manring, Edward)—348(A)
—— (see Schwarz, Guenter)—351(A)
Brown, Laurie M. Grain density in nuclear emulsions—95
Brown, N. L. (see Cole, R. H.)—352(A)
Brown, Sanborn C. (see Goldey, James M.)—336(A)
Brown, W. L., R. C. Fletcher, and S. Machlup. Annealing of bombardment damage in solids—709(L)
—— **and W. Shockley.** n-type conduction on p-type Ge surfaces—336(A)
Browne, C. P., C. K. Bockelman, W. W. Buechner, and A. Sperduto. Inelastic scattering of protons and deuterons from N^{14} and Li^6—340(A)
—— (see Bockelman, C. K.)—340(A)
Brownell, L. E. (see Meinke, W. W.)—353(A)
Brueckner, K. A. Damping of virtual nucleon-pair formation in pseudoscalar meson theory—476
—— Elastic scattering of pions in D—715(L)
—— **and K. M. Watson.** Construction of potentials in quantum field theory—699
Brysk, Henry. Extreme single-particle model and β-decay—365(A)
Bube, Richard H. Electronic transitions in luminescence of ZnS phosphors—70

Buechner, W. W. (see Bockelman, C. K.)—340(A)
—— (see Browne, C. P.)—340(A)
Bunbury, D. StP. β-decay of Li^8—1121(L)
Burgess, R. E., H. Kroemer, and J. M. Houston. Corrected values of Fowler-Nordheim field emission functions $v(y)$ and $s(y)$—515
Burke, B. F. and M. W. P. Strandberg. Zeeman effect in rotational spectra of asymmetric-rotor molecules—303; 338(A)
Burson, S. B. (see Jordan, W. C.)—862
Buskirk, A. V., H. O. Cohn, L. R. Etter, C. J. Karzmark, R. H. Rediker, and R. W. Thompson. New magnet chamber for study of V particles—369(A)
—— (see Thompson, R. W.)—329(L)
Butler, S. T. (see Austern, N.)—365(A)
Byfield, H. (see Kessler, J.)—343(A)
—— (see Lederman, L.)—344(A)

Calhoun, B. A. Electrical conductivity of magnetite at low temperatures—374(A)
Callen, Herbert B. (see Offenbacher, Elmer L.)—401
Cameron, John R. Elastic scattering of α-particles by oxygen—839
Carlson, B. C. (see Rohrlich, F.)—378(A)
Carr, E. F. and R. D. Spence. Influence of magnetic field on microwave dielectric constant of liquid crystal—339(A)
Carr, W. J., Jr. Spin-dependent couplings in many electron system—383(A)
Carter, D. E. and M. P. Givens. Soft x-ray absorption of Fe and Fe_2O_3—379(A)
Carter, R. E. and J. R. Beyster. Inelastic collision cross sections for fission spectrum neutrons—389(A)
Caspar, D. L. and C. R. Woese. Inactivation of dysentery toxin with ionizing radiation—384(A)
Casson, Harvey (see Allison, Samuel K.)—354(A); 880
Caswell, R. S. (see Nelson, C. M.)—364(A)
Cavallo, L. (see Seliger, H. H.)—443
Chamberlain, Joseph W. and Norman J. Oliver. OH in airglow at high latitudes—1118(L)
Champion, K. S. W. Constriction of high power discharges by intense magnetic field—387(A)
Chang, C. H., C. S. Cook, and H. Primakoff. Transmission of electrons through thin metallic foils—544
Chang, W. Y., W. Bernstein, and A. W. Schardt. Versatile coincidence gray wedge pulse-height analyzer—353(A)
—— (see Grodzins, L.)—361(A)
—— (see Schardt, A. W.)—353(A)
Cheka, J. S. Fast neutron film dosimeter—353(A)
Ch'en, Shang-Yi and Donald A. Kohler. Broadening and shift of second doublet of Rb absorption series under different pressures of A and He—1019
Cheng, L. S. and M. L. Pool. Disintegration of Sc^{47}—886
Chew, G. F. (see Blair, J. S.)—1065
Chisholm, R. and B. Touschek. Spin orbit coupling and mesonic Lamb shift—763
Chou, C. N. Energy spectra of cosmic ray photons and electrons from plastic scintillation counter measurements—473
Chowdary, S. A. (see Bleuler, E.)—464
Chrapylvy, Z. V. (see Barker, W. A.)—1131(E)
Chu, Sheng To (see Tifford, Arthur N.)—377(A)
Clapp, Roger E. Elementary particle structure—356(A)
Clark, G. L. (see Goldstein, L.)—151(L); 486(L)
Clark, G. W. Scintillation counter measurements of absorption of N-component—368(A)
Clarke, R. L. (see Paul, E. B.)—381(A)
Clauser, F. H. Turbulent boundary layers having equilibrium velocity profiles in adverse pressure gradients—379(T)
Coffin, Victor (see Bennett, Clarence)—344(A)
Cohen, B. L., E. Newman, T. H. Handley, and A. Timnick. Angular distribution of deuterons from $Be^7(p,d)Be^8$—328(L)
—— (see Neidigh, R. V.)—340(A)
Cohen, M. H. Nuclear quadrupole coupling in solids—348(A)
Cohn, H. O. (see Buskirk, A. V.)—369(A)
Cole, R. H., R. W. Swenson, and N. L. Brown. Dielectric constants of solid HCl and HBr—352(A)
Coleman, E. W. (see Meinke, W. W.)—353(A)
Coleman, John W. Electron gun—386(A)
Colladay, G. S. (see Juenker, D. W.)—772
Collins, S. C. and F. J. Zimmerman. Cyclic adiabatic demagnetization—991(L)
Colton, E. T. (see Lees, S.)—346(A)
Conklin, G. L. (see Zucker, E. R.)—387(A)
Conwell, E. M. High field mobility in Ge with impurity scattering dominant—769
Cook, C. Sharp and Fred T. Porter. $Zn^{64}(d,\alpha n)Cu^{63}$—429
—— (see Chang, C. H.)—544
Cook, L. G. and K. D. Shafer. Neutron activation of Ca^{46}—1121(L)
Cook, W. R., Jr., and Hans Jaffe. Ferro-electricity in oxides of fluorite structure—375(A)
Coomes, E. A. (see Juenker, D. W.)—772
Cooper, D. I., D. H. Frisch, and R. L. Zimmerman. p-p scattering in interference minimum region—339(A)
—— (see Zimmerman, R. L.)—339(A)
Cooper, John N. (see Green, Donald W.)—1132(A)
Corey, H. E. (see Vogel, F. L.)—489(L)
Cork, Bruce, p-p scattering at 32.0 Mev—1129(L)
Cork, J. M., J. M. LeBlanc, D. W. Martin, W. H. Nester, and M. K. Brice. Nuclear levels associated with Zr^{95} and Nb^{95}—579
——, **J. M. LeBlanc, W. H. Nester, D. W. Martin, and M. K. Brice.** Radioactive decay of Cs^{134}, Os^{185}, Os^{193}, and Os^{193}—444
—— (see Jordan, W. C.)—862
Corliss, L. M., J. M. Hastings, and F. G. Brockman. Neutron diffraction study of $MgFe_2O_4$—1013
Corrsin, S. Propagation of turbulence into irrotational flow ——376(A)
Corson, Dale R. Radiation by electrons in large orbits—748
Coryell, Charles D. (see Richter, Harold G.)—389(A)
Coté, R. E. and P. Kusch. Low frequency resonances in spectra of diatomic molecules—103
Cowan, C. L., Jr., F. Reines, F. B. Harrison, E. C. Anderson, and F. N. Hayes. Large liquid scintillation detectors —493(L)
—— (see Reines, F.)—492(L)
Cowen, J. A. and R. D. Spence. Temperature dependence of ferromagnetic resonance in (Ni-Fe) alloy—359(A)
Crandall, W. E. (see Schecter, L.)—633
Crasemann, Bernd. Decay of Ga^{64} and Ga^{65}—995(L)
—— **and Harry T. Easterday.** Decay of Cr^{49}—1124(L)
Cronemeyer, D. C. (see Rank, D. H.)—202
Crosbie, Edwin A. Relative energy levels of P-shell nuclei in intermediate coupling—138
Crouch, M. F. and D. E. Diller. Method for absolute neutron source calibration—361(A)
Crussard, J., L. Leprince-Ringuet, D. Morellet, A. Orkin-Lecourtois, and J. Trembley. K-mesons—1127(L)
Culpepper, S. V. (see Seliger, H. H.)—443
Curie, Daniel. Mechanism of phosphorescence in crystal phosphors—154(L)
Cutler, M. Effect of surface states in diode rectification theory—337(A)

Dacey, G. C. Space-charge limited hole current in Ge—759
Dailey, B. P. Rotational spectrum and molecular structure of $C_2H_5Cl^{35}$—337(A)
Damm, C. C. (see Smith, Lincoln G.)—324(L)
Damon, P. E. and R. R. Edwards. Electromagnetic spectrum of RaD—280
Darlington, Lillian E., Jack Haugsnes, Harry M. Mann, and James H. Roberts. Angular distribution of $Li^6(n,\alpha)H^3$ for neutrons of 200, 270, 400, and 600 kev—1049
Dash, William C. Additive coloration of single crystals of BaO—352(A)
Daubin, Scott M. (see Pipkin, Francis M.)—353(A)
Daunt, J. G. (see Horowitz, M.)—379(A)
Davis, Marguerite. Biological determination of range of low voltage electrons—384(A)
deBretteville, A., Jr. (see Lefker, R.)—345(A)
Dehmelt, H. G. Nuclear quadrupole resonance—348(T)
Déjardin, G., J. Janin, and M. Peyron. Vibration-rotation band system of OH in near infrared—359(A)
Del Castillo, G. (see Grodzins, L.)—361(A)
del Rio, C. S. and Valentine L. Telegdi. Inelastic nuclear scattering of photons by Rh^{103}—439
Dempster, J. R. Hugh. Calculations on μ-meson capture in nuclei—349(A)
der Mateosian, E. and Luke C. L. Yuan. Surface effect of NaI scintillators—868
Deser, Stanley and Paul C. Martin. Covariant meson-nucleon equation—1075
de-Shalit, A. Effects of departure from single particle model on nuclear magnetic moments—83
Deutsch, R. W. Secondary particles resulting from 375-Mev α-bombardment of nuclei—499(L)
DeWitt, Bryce S. Pair production by curved metric—357(A)
Dexter, D. L. Small angle scattering of x-rays from cold-worked solids—1007
Dicke, R. H. Excitation of superradiant states: New technique for high resolution microwave spectroscopy—337(T)
Dickinson, W. C. and J. E. Brolley, Jr. Angular distribution of fragments from neutron-induced fission—388(A)
Dieterich, Ernest J. Excitation of light by H ions—386(A)
Diller, D. E. (see Crouch, M. F.)—361(A)
Dodd, J. S. (see Lefker, R.)—345(A)
Draper, J. E. and B. D. McDaniel. Pulsed source of fast neutrons—362(A)
Drell, S. D. (see King, William C.)—326(L)
Dudziak, Walter F. π^+ meson production cross sections from C by 341-Mev protons—342(A)
Duller, N. M. (see Walker, W. D.)—320(L)
DuMond, Jesse W. M. (see Hoyt, Harry C.)—169(L)
Dunavan, D. S. (see Boley, F. I.)—158(L)
Dunlap, W. C., Jr. (see Saby, John S.)—630; 1131(E)
Dutta, Ajit Kumar. Electrical conductivity of single crystals of graphite—187
Dutton, David and Robert Maurer. Color centers and trapped charge in KCl and KBr—126
Dvorak, H. R. and R. N. Little, Jr. Total cross sections of Cl, Na, Ti, and Br for fast neutrons—618
Dyson, Freeman J. Use of Tamm-Dancoff method in field theory—994(L)
——, **S. S. Schweber, and W. M. Visscher.** Theoretical analysis of meson-proton scattering—372(A)
—— (see Bethe, H. A.)—372(A)
—— (see Mitra, A. N.)—372(A)

Easterday, Harry T. (see Crasemann, Bernd)—1124(L)
Edwards, R. R. (See Damon, P. E.)—280
Edwards, S. F. Non-perturbation approach to quantum electrodynamics—284
Elson, R., P. A. Sellers, and E. R. John. Thermal neutron capture cross sections of Pa^{231} and Pa^{233}—102
Emrich, R. J., J. E. Mack, and R. A. Shunk. Variation with time of flow variables in shock tube—375(A)
Engelder, Theodore C. Search for short-lived nuclear isomers—259
Engelkemeir, D. W., P. P. Fields, and J. R. Huizenga. Radiations of Pu^{243}—6
Erickson, R. A. Neutron diffraction studies of antiferromagnetism in MnF_2 and some isomorphous compounds—779
Eschenfelder, A. H. and R. T. Weidner. Saturation effects in paramagnetic resonance absorption and spin-lattice relaxation time—358(A)
Eshelby, J. D. Equation of motion of a dislocation—248
Etter, L. R. (see Buskirk, A. V.)—369(A)
—— (see Thompson, R. W.)—329(L); 1122(L)
Evans, G. E., P. M. Stier, and C. F. Barnett. Stopping of heavy ions in gases—825
Evett, Arthur A. and Henry Margenau. Forces between H_2 molecules—1021

Facchini, U. (see Bracci, A.)—162(L)
Fagot, W. C. (see Simpson, J. A.)—1068
Fairbank, Henry A. (see King, J. C.)—347(A); 989(L)
Fano, U. Geometrical characterization of nuclear states and theory of angular correlations—577
Farnsworth, H. E. (see Schlier, Robert E.)—351(A)
Faust, W. R., V. E. Scherrer, and R. B. Theus. γ-radiation from interaction of 14-Mev neutrons with matter—355(A)
Feiner, F. (see Aarons, M. W.)—342(A)
Feld, B. T. Analysis of photomeson production data—342(A)
—— (see Wattenberg, A.)—380(A)
Ferguson, R. C. and E. B. Wilson, Jr. Microwave spectrum and structure of SOF_2—338(A)
Feshbach, Herman, Charles E. Porter, and Victor F. Weisskopf. Formation of compound nucleus in neutron reactions—166(L)
Feynman, R. P. λ-transition in liquid He—1116(L)
Fields, P. R. (see Engelkemeir, D. W.)—6
Findley, D. E. (see Worthington, H. R.)—899
Fiora, Verna C. (see Turner, T. E.)—338(A)
Fleming, W. H. and H. G. Thode. A^{38} in pitchblende minerals and nuclear processes in nature—857
Fletcher, R. C. (see Brown, W. L.)—709(L)
Flint, H. T. and E. Marjorie Williamson. Coordinate operators and fundamental lengths—318(L)
Fonger, W. (see Simpson, J. A.)—934
Foote, H. L., Jr., V. L. Sailor, and H. H. Landon. Low energy neutron resonance cross sections for Ho, Er, Lu, and Tm—362(A)
—— (see Landon, H. H.)—363(A)
Forbes, Stuart G. Activation cross sections for 14-Mev neutrons, erratum—1131(E)
Ford, Kenneth W. First excited states of even-even nuclei—29; 366(A)
—— (see Wilets, L.)—366(A)
Forsthoff, C. W., R. H. Goeckermann, and R. A. Naumann. Formation and decay of Mo^{99m}—1004(L)
Foss, Martyn H. Rotating condenser for synchrocyclotron oscillator—353(A)
Foster, Bruce P. (see May, John E.)—243; 370(A)
Fowler, W. B., R. P. Shutt, A. M. Thorndike, and W. L. Whittemore. Observation of V^0 particles produced at cosmotron—1126(L)
Fox, J. G. (see Grove, D. J.)—378(A)
—— (see Mott, W. E.)—712(L)
Fox, R. E. (see Hickam, W. M.)—386(A)
—— (see Kjeldaas, T., Jr.)—386(A)

Frankl, D. R. and T. A. Read. Internal friction of rocksalt single crystals—351(A)
Franklin, R., M. Friedman, and R. Setlow. Ultraviolet action spectrum of bacillus megatherium bacteriophage—384(A)
Fraser, J. S. and J. C. D. Milton. Distribution of prompt neutron emission probability for fission fragments of U^{233}—389(A)
—— (see Milton, J. C. D.)—388(A)
Friedman, M. and E. Pollard. Ionizing radiation evidence for internal structure in bacterial virus—384(A)
—— (see Franklin, R.)—384(A)
Frisch, David H. *S*-wave two-body interaction in nuclei—367(A)
—— (see Cooper, D. I.)—339(A)
—— (see Storrs, C. L.)—339(A)
—— (see Zimmerman, R. L.)—339(A)
Fry, W. F. Evidence for emission of neutrino following nuclear capture of μ-meson—999(L)
—— **and George R. White.** Range distribution of μ-mesons from π-meson decay in photographic emulsions—207
—— (see White, George R.)—349(A)
Frye, G. M. and L. Rosen. Angular distribution and energy spectrum of charged particles produced by 14-Mev neutrons on Li^6 and Li^7—381(A)
Fumi, F. G. and L. Wolfenstein. Allowed final states for annihilation into 3 photons—498(L)
Furuichi, Jiro (see Mitsui, Toshito)—193

Garwin, R. L. Search for V^0 particles produced by 450-Mev protons—274
Geller, M. (see von Hippel, A.)—364(A)
Geltman, Sydney. Mobility of He molecular ions in He—808
Gerjuoy, E. (see Saxon, David S.)—373(A)
Ghiorso, Albert (see Hyde, Earl K.)—267
Gilleo, M. A. Photoemission from Ag into AgCl, KBr, NaCl, and new bands of photosensitivity in AgCl—364(A)
Ginther, Robert J. (see Schulman, James H.)—351(A)
Givens, M. P. (see Carter, D. E.)—379(A)
Glass, Neel W., Louis K. Jensen, and J. Reginald Richardson. Short-lived radioisotopes P^{28} and Cl^{32}—320(L)
Glasser, R. G. and Marcel Schein. Energy of nucleon-nucleon collisions—218
Glaubman, Michael J. Spins and parities of excited states in even-even nuclei—1000(L)
Glazer, Herbert and Howard Reiss. Application of Fermi-Thomas model in computing dipole moment of ICl—360(A)
Gluckstern, R. L. and M. H. Hull, Jr. Polarization dependence of integrated bremsstrahlung cross section—1030
——, **M. H. Hull, Jr., and G. Breit.** Polarization of bremsstrahlung radiation—1026
Godbole, R. D. (see Wattenberg, A.)—380(A)
Goeckermann, R. H. (see Forsthoff, C. W.)—1004(L)
Goldberg, Joshua N. Gravitational radiation—356(A)
Goldberg, M. D. (see Hughes, D. J.)—497(L)
Goldemberg, J. and L. Katz. High energy γ-γ cross section of In^{115}—308
Goldey, James M. and Sanborn C. Brown. Microwave determination of electrical properties of Ge—336(A)
Goldhaber, Gerson and Leon Lederman. Positive pion scattering in H—343(A)
—— (see Arase, E.)—160(L)
—— (see Goldhaber, S.)—344(A)
Goldhaber, M. Families of fundamental particles—369(A)
—— (see Bainbridge, Kenneth T.)—430
Goldhaber, S., E. Arase, and Gerson Goldhaber. Elastic pion-deuteron scattering—344(A)
—— (see Arase, E.)—160(L)
Goldman, J. E. Theory of resistance minimum in metals—379(A)
Goldschmidt-Clermont, Y., L. S. Osborne, and M. B. Scott. Photoproduction of neutral mesons in H—350(A)
Goldstein, J. S. (see Salpeter, E. E.)—983
Goldstein, L., J. M. Anderson, and G. L. Clark. Interaction of microwaves propagated through gaseous discharge plasma—151(L)
——, **J. M. Anderson, and G. L. Clark.** Quenching of afterglow in gaseous discharge plasmas by low power microwaves—486(L)
Goldwasser, E. L., F. E. Mills, and T. R. Robillard. Direct measurement of effect of polarization on energy losses of fast electrons—378(A)
Good, R. H., Jr. Generalization of WKB method to radial wave equations—131
Goodman, Clark (see Kiehn, R. M.)—362(A)
Gordon, J. P. (see Artman, J. O.)—338(A)
Gordon, W. L. and J. A. Soules. Ross filter design for x-ray scattering experiments—346(A)
Gordy, Walter (see King, William C.)—319(L)
Gorman, J. G. (see Aarons, M. W.)—342(A)
Gorter, C. J. (see Bots, G. J. C.)—1117(L)
—— (see Kramers, H. C.)—1117(L)
Gorter, E. W. and J. A. Schulkes. Reversal of spontaneous magnetization as function of temperature in LiFeCr spinels—487(L)
Gove, H. E. p-γ angular correlations in $C^{13}(p,p'\gamma)$—370(A)
Grad, Harold (see Mostov, Philip M.)—376(A)
Graham, R. L. (see Bell, R. E.)—644
Grant, F. A. and A. D. Krumbein. Effect of temperature on duration of $^3P_2$ metastable level of Ne—59
Green, Donald W., J. C. Harris, and John N. Cooper. Method for measuring the half-lives of positron emitters—1132(A)
Green, G. K. Brookhaven cosmotron—347(T)
Green, H. S. Generalized method of field quantization—270
Green, J. B. and R. A. Loring. Zeeman effect in spectra of Te—80
Green, Melville S. Statistical mechanics of irreversible processes in fluids—376(A)
Green, Thomas A. Elastic scattering of π-mesons by deuterons—161(L)
Green, W. D. (see Lees, S.)—346(A)
Greenwald, Selma (see McGuire, T. R.)—373(A)
Greisen, K. and W. D. Walker. Ratio of neutral to charged particles in nuclear interacting component of cosmic rays—915
Grodzins, L., G. Del Castillo, and W. Y. Chang. Two-particle showers from Be—361(A)
Gross, E. P. (see von Hippel, A.)—364(A)
Grove, D. J. and J. G. Fox. e/m for 385-Mev protons—378(A)
Guernsey, R. L. and G. B. Arfken. Vector addition coefficient identity—1132(A)
Gunst, S. B. (see Page, L. A.)—377(A)
Gurney, I. D. C. Lattice sums: Validity of Evjen's method—316(L)

Haber, Agnes (see Sugarman, Nathan)—342(A)
Hahn, E. L. Spin-echo pulse technique in nuclear resonance studies—348(T)
Halban, H. H. (see Beghian, L. E.)—1129(L)
Hall, G. G. Electronic structure of diamond—316(L)
Hall, H. H. and J. L. Powell. Scattering of protons by protons—912

Halpern, O. and G. L. Appleton. Scattering of slow neutrons by O_2 molecules—869
Ham, Frank and Harvey Brooks. Effect of boundary states on free electron diamagnetism—383(A)
Hamermesh, Bernard and Clyde Kimball. Photodisintegration cross section of Be at 2.185 Mev—1063
——, **G. R. Ringo, and S. Wexler.** Thermal neutron capture cross section of H—603
Hamilton, Donald R. β-γ polarization correlations—370(A)
—— (see Pipkin, Francis M.)—353(A)
Hammer, C. L., E. C. Raka, and R. W. Pidd. Scattering of high energy electrons by nuclei—341(A)
—— (see Raka, E. C.)—341(A)
Hammond, William R., D. N. Kundu, and M. L. Pool. Activity assignment to Ti^{51}—157(L)
Handley, Thomas H. and Elmer L. Olson. Dy^{159}—500(L)
—— (see Cohen, B. L.)—323(L)
Hänni, F. (see Albers-Schönberg, H.)—322(L)
Hansen, K. F. (see Kiehn, R. M.)—362(A)
Harrick, N. J., R. G. Barnes, P. J. Bray, and N. F. Ramsey. Nuclear rf spectra of D_2 and H_2 in intermediate and strong magnetic fields—260
Harris, D. R. (see Ballam, J.)—369(A)
—— (see Rau, R. Ronald)—369(A)
Harris, Edward G. and Michel A. Melkanoff. Quadrupole moment of Li^7—585
Harris, F., B. Rossi, and I. Escobar Vallejo. East-west asymmetry for positive and negative mesons near equator —360(A)
Harris, J. C. (see Green, Donald W.)—1132(A)
Harrison, F. B. (see Cowan, C. L., Jr.)—493(L)
Harrison, G. R. Echelle spectroscopy—367(T)
Hartzler, A. J. and R. T. Siegel. Measurements with 390-Mev neutrons—362(A)
Harvey, J. A. (see Hughes, D. J.)—497(L)
Hastings, J. M. (see Corliss, L. M.)—1013
Haugsnes, Jack (see Darlington, Lillian E.)—1049
Havens, W. W., Jr. (see Seifert, A. M.)—349(A)
Hayes, F. N. (see Cowan, C. L., Jr.)—493(L)
Hayes, S., R. Smoluchowski, and R. W. Turner. Small angle x-ray scattering in deformed crystals—350(A)
Haynes, J. R. and J. A. Hornbeck. Temporary traps in Si and Ge—152(L)
Hazen, W. E., C. A. Randall, Jr., and R. W. Williams. Experiments on air showers—361(A)
—— (see Heineman, R. E.)—496(L)
—— (see Williams, R. W.)—361(A)
Heer, C. V. and C. Rauch. Magnetic susceptibility of colored KCl from 1°K to 300°K—530
Heer, E. (see Albers-Schönberg, H.)—322(L)
Heineman, R. E. and W. E. Hazen. Density distribution within 2 meters of large air shower axes—496(L)
Heller, Jack. Theory of nonhomogeneous turbulence—376(A)
Heller, W. and W. J. Pangonis. Refractive index corrections for molecular weight determined from light scattering —345(A)
—— (see Pangonis, W. J.)—345(A)
Hellund, E. J. Inner bremsstrahlung and magnetic moment of the neutrino—721(L)
Henley, E. M. and M. A. Ruderman. Recoil effects in meson-nucleon scattering—719(L)
Henri, V. P. (see Bay, Z.)—371(A)
—— (see Kanner, H.)—371(A)
Henry, Warren E. Magnetic saturation and apparent molecular fields of $MnCl_2 \cdot 4H_2O$—492(L)
Hereford, Frank L. and Jerome P. Keuper. Azimuthal distribution of photoelectrons produced by 0.5-Mev polarized photons—1043
—— **and Jerome P. Keuper.** Photoelectron ejection by 0.51-Mev polarized photons—382(A)
—— (see Berko, Stephen)—341(A)
Hermans, J. J. and Robert Ullman. Statistics of stiff chains—384(A)
Herrmann, G. (see Weisbaum, S.)—338(A)
Herschman, A. (see Hull, M. H., Jr.)—482
Heydenburg, N. P. (see Talbott, F. L.)—186
—— (see Temmer, G. M.)—340(A)
Hickam, W. M., R. E. Fox, and T. Kjeldaas, Jr. Ionization probability near threshold for formation of Xe^{++}, Kr^{++}, A^{++}, and Ne^{++}—386(A)
—— (see Kjeldaas, T., Jr.)—386(A)
Hicks, B. L. (see Turner, T. E.)—338(A)
Hicks, D. A., T. Husain, L. G. Sanders, and L. E. Beghian. Levels in N^{14} from $C^{13}(p,\gamma)N^{14}$—163(L)
—— (see Schecter, L.)—633
Hildebrand, B. Energy loss distribution of 624-kev electrons in thin foils—378(A)
Hill, David L. (see Wheeler, John A.)—366(A)
—— (see Wilets, L.)—366(A)
Hill, R. D. (see Swan, J. B.)—257
Hill, Richard William. Elastic scattering of α-particles by C—845
Hiller, Dale M. and Don S. Martin, Jr. Radiochemical studies on photofission of Th—581
Hillman, Peter and R. H. Stahl. Total cross section of He for high energy neutrons—362(A)
Hinman, G., D. Brower, and R. Leamer. Internal conversion in Na^{22} and Fe^{59}—370(A)
Hodson, A. L. (see Ballam, J.)—369(A)
—— (see Rau, R. Ronald)—369(A)
Hofmann, J. A. and K. Strauch. Interaction of 95-Mev protons with D, Li, Be, C, Al, Cu, and Pb nuclei—449
Holmes, John R. (see Parker, Lee W.)—142
Horan, John R. Non-uniform track shrinkage in nuclear emulsions—717(L)
Hornbeck, J. A. Trapping of injected carriers in semiconductors—336(T)
—— (see Haynes, J. R.)—152(L)
Horowitz, M. and J. G. Daunt. Specific heat measurements on pure metals at low temperatures—379(A)
Horton, G. K. (see Sharp, R. T.)—316(L)
Horton, J. and R. Sherr. α-γ angular correlation in ThC—388(A)
Houston, J. M. (see Burgess, R. E.)—515
Howe, Horace A. and K. R. MacKenzie. Positron-electron scattering at 1.3 Mev—678
Howling, D. H., E. Mendoza, and J. E. Zimmerman. Method of measuring specific heats at very low temperatures—347(A)
Hoyt, Harry C., Joseph J. Murray, and Jesse W. M. DuMond. Comparison of γ-ray reflections from (550) and (310) planes of quartz—169(L)
Hsiao, C. A. and V. L. Telegdi. Mechanism of $O^{16}+h\nu \rightarrow 4He^4$—494(L)
Hughes, D. J., J. A. Harvey, M. D. Goldberg, and Marilyn J. Stafne. Neutron-electron interaction—497(L)
——, **F. G. P. Seidl, H. Palevsky, and J. S. Levin.** Neutron resonance measurements with Brookhaven fast chopper—363(A)
—— (see Levin, J. S.)—363(A)
Hughes, Francis J. (see Jensen, Erling N.)—557
Hughes, Vernon W. (see Weinreich, Gabriel)—377(A)
Hugo, T. J. (see Naudé, S. M.)—318(L)
Huizenga, J. R. (see Engelkemeir, D. W.)—6
Hull, G. F., Sr. Experimental discoveries announced in programme of meeting of fifty years ago—367(T)

Hull, M. H., Jr., and A. Herschman. Effect of short range repulsion on low energy singlet nucleon-nucleon scattering—482
—— (see Gluckstern, R. L.)—1026; 1030
Hulm, J. K. Thermal resistivity of Hg in intermediate state—1116(L)
Hulthén, Lamek and Bengt C. H. Nagel. Photodisintegration of the deuteron—62
Humphrey, J. N., Frances L. Lummis, and W. W. Scanlon. Capacitance effects in thin conductive films—111
Hurst, G. S. (see Bortner, T. E.)—160(L)
Husain, T. (see Beghian, L. E.)—1129(L)
—— (see Hicks, D.)—163(L)
Hyde, Earl K. and Albert Ghiorso. α-branching of AcK and presence of As in nature—267

Ingram, D. J. E. Paramagnetic resonance in Mn formate—711(L)
Inn, Edward C. Y. (see Watanabe, K.)—155(L);—359(A)
—— (see Zelikoff, Murray)—359(A)

Jackson, J. David and D. I. Wanklyn. Disintegration of C by fast neutrons—381(A)
Jackson, J. M. and W. A. Rense. Origin of zodiacal light—345(A)
—— (see Pietenpol, W. B.)—156(L)
Jacobs, Ira and E. S. Akeley. Transverse motion of electron in constant wave speed section of linear accelerator—386(A)
Jacobs, James A. (see Schrader, Carlton D.)—159(L)
Jaffe, Hans (see Cook, W. R., Jr.)—375(A)
Jagger, John. Particle size of α-amylase—384(A)
Janes, G. S. and W. L. Kraushaar. Photoproduction of π^+ mesons from H—341(A)
Janin, J. (see Déjardin, G.)—359(A)
Jankus, V. Z. Radiative correction for collision loss of heavy particles—4
Jeffries, C. D. Spin and magnetic moment of Ca^{43}—1130(L)
Jelatis, J. G. (see von Hippel, A.)—364(A)
Jen, C. K. Classical model for rotational magnetic moments in molecules—359(A)
Jensen, Erling N., L. Jackson Laslett, Don S. Martin, Jr., Francis J. Hughes, and William W. Pratt. Radiations from Se^{75}—557
Jensen, Louis K. (see Glass, Neel W.)—320(L)
Jesse, William P. and John Sadauskis. α-particle ionization in pure gases and average energy to make ion pair—1120(L)
John, E. R. (see Elson, R.)—102
Johnson, A. C. (see Bleuler, E.)—464
Johnson, N. R. (see Sheline, R. K.)—325(L)
Johnson, P. D. Recent advances in interpretation of luminescence in solids—363(T)
Johnson, V. A. and F. M. Shipley. Adiabatic Hall effect in semiconductors—523
Jones, G. A. and D. H. Wilkinson. Purity of isotopic spin of charge parity states—722(L)
Jones, John W. and Truman P. Kohman. Synchrocyclotron production and properties of Mg^{28}—495(L)
Jongenburger, P. Extra resistivity due to vacancies in Cu—710(L)
Jordan, W. C., J. M. Cork, and S. B. Burson. Decay of Rh^{104m} (4.3-min) and Rh^{104} (44-sec)—862
Juenker, D. W., G. S. Colladay, and E. A. Coomes. Surface barrier analysis for highly refractory metals by means of Schottky deviations—772

Kahn, David. Energy loss of protons in metallic foils and mica—503
Kallmann, H. K. Continuous layer formation in atmosphere under influence of solar radiation—153(L)
Kambe, K. and A. Abragam. Line width in pure quadrupole resonance experiments in crystals—348(A)
Kane, J. A. (see Mott, W. E.)—712(L)
Kane, R. P. (see Sarabhai, V.)—204
Kanner, H., Z. Bay, and V. P. Henri. Accuracy of time measurements by delayed coincidences—371(A)
Kantrowitz, Arthur. Studies of thermally ionized gases produced by shock waves.—368(T)
Kaplon, M. F., D. M. Ritson, and W. D. Walker. High energy nuclear interactions in Pb and light elements—716(L)
—— (see Ritson, D. M.)—360(A)
Karplus, Robert, Margaret Kivelson, and Paul C. Martin. Meson-nucleon scattering—1072
Karzmark, C. J. (see Buskirk, A. V.)—369(A)
—— (see Thompson, R. W.)—329(L); 1122(L)
Kash, S. W. and D. C. Woods. Measurement of transport mean free path of thermal neutrons in D_2O by B poisoning method—564
Kasnitz, Harold L. and Kurt Sitte. Structure and composition of air shower cores—361(A)
Kato, W. Y. (see Levin, J. S.)—363(A)
Katz, L. (see Goldemberg, J.)—308
Keck, Paul H. Solubility of Si in Ga and In—379(A)
—— **and Jacob Broder.** Solubility of Si and Ge in Ga and In—521
Kellogg, D. A. Cross sections for products of 90-Mev neutrons on C—224
Kendrick, W. M. (see Turner, T. E.)—338(A)
Kessler, J., H. Byfield, L. M. Lederman, and K. Rogers. Production of high energy photons in pion collisions—343(A)
—— (see Lederman, L.)—344(A)
Ketelle, B. H., A. R. Brosi, and F. M. Porter. Gallium 67—567
Keuffel, J. W. (see Meyer, A. J.)—349(A)
Keuper, Jerome P. (see Hereford, Frank L.)—382(A); 1043
Kiehn, R. M., Clark Goodman, and K. F. Hansen. Total neutron cross sections of Cl and C—362(A)
Kimball, Clyde (see Hamermesh, Bernard—1063
King, J. C. and Henry A. Fairbank. Second sound velocity in mixtures of He^3—He^4—347(A); 989(L)
King, J. S. and E. H. Beach. Angular distributions of (d,p) reactions on P^{31}, Cl^{35}, V^{51}, and Sc^{45}—381(A)
King, R. W. and D. C. Peaslee. Odd-odd spins and *j-j* coupling—1001(L)
King, William C. and Walter Gordy. One to two mm wave spectroscopy—319(L)
Kington, J. D. (see Bair, J. K.)—575
—— (see Willard, H. B.)—865
Kinsey, B. B. (see Bartholomew, G. A.)—355(A)
Kip, A. F. Paramagnetic resonance resulting from conduction-electrons in metals—348(T)
—— (see Portis, A. M.)—988(L)
Kirk, Russell D. (see Schulman, James H.)—351(A)
Kittel, C. and Elihu Abrahams. Dipolar broadening of magnetic resonance lines in magnetically-diluted crystals—238
—— (see Portis, A. M.)—988(L)
Kivel, B. Pressure broadening by electron impacts—382(A)
Kivelson, D. and E. B. Wilson, Jr. Constants of centrifugal distortion—338(A)
Kivelson, Margaret (see Karplus, Robert)—1072
Kjeldaas, T., Jr., W. M. Hickam, and R. E. Fox. Relative ionization probability of He near threshold—386(A)
—— (see Hickam, W. M.)—386(A)

Klein, Abraham. Lamb shift for spinless electrons—372(A)
—— Tamm-Dancoff formalism and symmetric pseudoscalar theory of nuclear forces—1101
Kleiner, W. H. Orbital effect in neutron-electron magnetic scattering—168(L)
Kleinman, David A. Energy distribution of slow neutrons scattered in crystals—355(A)
Klick, Clifford C. and James H. Schulman. Luminescence of divalent Mn in solids—363(A)
Koehler, W. C. and E. O. Wollan. Paramagnetic scattering of neutrons by trivalent ions of Nd and Er—354(A)
Kohler, Donald A. (see Ch'en, Shang-Yi)—1019
Kohman, Truman P. (see Jones, John W.)—495(L)
Kohn, W. Adiabatic treatment of slow atomic collisions—383(A)
Kolb, E. D. (see Slichter, W. P.)—987(L)
Kotani, M. (see Miller, S. L.)—542
Kothari, D. S. (see Auluck, F. C.)—1002(L)
Kothari, L. S. Production of heavy mesons—1087
Kramers, H. C., F. A. W. van den Burg, and C. J. Gorter. Heat pulses in He II between 0.1°K and 1.0°K—1117(L)
Kranz, A. Z. and W. W. Watson. Thermal diffusion constant of HCl—344(A)
Kraushaar, J. J., Elizabeth D. Wilson, and Kenneth T. Bainbridge. Disintegration constant of Be^7 in Be, BeO, and BeF_2—610
Kraushaar, W. L. (see Janes, G. S.)—341(A)
Kriessman, C. J. and T. R. McGuire. Magnetic susceptibilities of Hf, Gd, and Mn—374(A)
Kroemer, H. (see Burgess, R. E.)—515
Kronheimer, Erwin H. Calculation of nuclear binding energies with single-particle oscillator wave-functions—1003(L)
Kruger, Paul and Nathan Sugarman. Evidence for 25.5-day Sr—76-sec Rb chain—158(L)
Krumbein, A. D. (see Grant, F. A.)—59
Kruse, U. E. (see Malenka, B. J.)—365(A)
Kulp, J. Laurence and Herbert L. Volchok. Constancy of cosmic ray flux over past 30,000 years—713(L)
Kundu, D. N. (see Hammond, William R.)—157(L)
Kusch, P. (see Coté, R. E.)—103
Kusumoto, Osamu, Saburo Miyake, Koichi Suga, and Yuzuru Watase. Example of multiple meson production observed with high pressure H_2-filled cloud chamber—998(L)

Laitone, E. V. and Helmer Nielsen. Transonic flow past wedge profiles by hydraulic analogy—375(A)
Lakin, W. and L. Wolfenstein. Nuclear reactions involving polarized deuterons—365(A)
Lamb, Willis E., Jr. (see Yergin, Paul F.)—377(A)
Landon, H. H., V. L. Sailor, and H. L. Foote, Jr. Neutron resonance energy measurements with Brookhaven crystal spectrometer—363(A)
—— (see Foote, H. L., Jr.)—362(A)
Laslett, L. Jackson (see Jensen, Erling N.)—557
Lawson, R. D. and S. D. Drell. Double meson photoproduction—326(L)
Lax, Melvin. Transition temperatures for spherical model ferromagnets—374(A)
—— (see Levitas, Alfred)—374(A)
Leaf, Boris. Continuum in special relativity—1090
Leamer, R. (see Hinman, G.)—370(A)
LeBlanc, J. M. (see Cork, J. M.)—444; 579
Lederman, Leon, H. Byfield, J. Kessler, and K. Rogers. Pion scattering and absorption cross sections in Pb and C—344(A)
—— (see Goldhaber, Gerson)—343(A)
—— (see Kessler, J.)—343(A)
Lee, T. D., F. E. Low, and D. Pines. Motion of slow electrons in polar crystal—297
—— (see Pines, D.)—382(A)
Lees, S., W. D. Green, and E. T. Colton. Low frequency oscillator, circular sweep generator, and direct reading phase measuring instrument—346(A)
Lefker, R., A. deBretteville, Jr., and J. S. Dodd. Single crystal high temperature heater for x-ray spectrometer—345(A)
Lehovec, Kurt. Space charge layer and distribution of lattice defects at surface of ionic crystals—350(A)
Leighton, R. B. (see Alford, W. L.)—622
—— (see York, C. M.)—167(L)
Lemonick, Aaron (see Pipkin, Francis M.)—353(A)
Lenard, A. Inner bremsstrahlung in μ decay—372(A); 968
Leprince-Ringuet, L. (see Crussard, J.)—1127(L)
Levin, J. S., W. Y. Kato, N. G. Sjostrand, and D. J. Hughes. Neutron resonances in Ag, Th, and Mn—363(A)
—— (see Hughes, D. J.)—363(A)
Levinger, J. S. Effects of radioactive disintegrations on inner electrons of the atom—11
Levitas, Alfred and Melvin Lax. Improved spherical treatment of Ising model—374(A)
Lew, Hin and Günter Wessel. Hfs of $3p\ ^3P_{1/2}$ state of Al^{27}—1
Lewis, H. W. and G. H. Wannier. Spherical model of a ferromagnet, erratum—1131(E)
Li, C. W. Nuclear mass determinations from disintegration energies: O to S, erratum—1131(E)
Lidofsky, L., E. Alperovitch, and C. S. Wu. β-spectrum of Cs^{135}—387(A)
Liepmann, H. W. Skin friction in supersonic and high subsonic flow—379(T)
Lin, C. C. Stability of boundary layer at supersonic speeds—379(T)
Lindenfeld, P. (see Steinberger, J.)—343(A)
Lindsay, W. T. (see Amdur, I.)—344(A)
Lindström, Gunnar. Establishment of absolute energy scale in β-spectroscopy—369(T)
Lipworth, Edgar (see Yergin, Paul F.)—377(A)
Littauer, R. M., A. M. Perry, and W. M. Woodward. Photomesons from H—342(A)
Little, R. N., Jr. (see Dvorak, H. R.)—618
Livingston, M. S. Strong focusing synchrotron—368(T)
Livingston, Ralph and Henry Zeldes. Quadrupole moment ratio of I^{129} and I^{127} from pure quadrupole spectra—609
Locher, K. and P. Stoll. (γ,α) reaction of B^{11} and B^{10}—164(L)
Loeb, Leonard B. Current increase at constant amplification factor in steady corona with coaxial cylindrical geometry—144
Longdon, L. W. Non-central force matrix elements for nuclear d^2 configuration—1125(L)
Lönsjö, O. (see Roderick, H.)—371(A)
Loring, R. A. (see Green, J. B.)—80
Lounsbury, M. (see MacKenzie, D. R.)—327(L)
Lovberg, R. H. (see Yarnell, J. L.)—292
Low, F. E. (see Lee, T. D.)—297
—— (see Pines, D.)—382(A)
Löwdin, Per-Olov. Atomic self-consistent fields. I. Calculation of Slater functions—120
Luckey, David. Excitation curve for photomesons from Be—711(L)
Lummis, Frances L. (see Humphrey, J. N.)—111

MacDonald, J. Ross. Polarization capacitance effects in photoconductors and semiconductors—364(A)
—— (see Thickens, R. W.)—375(A)
Machlup, S. (see Brown, W. L.)—709(L)
Mack, J. E. (see Emrich, R. J.)—375(A)

MacKenzie, D. R., M. Lounsbury, and A. W. Boyd. β^- half-life of Pu^{241}—327(L)
—— (see Howe, Horace A.)—678
Madrazo, Raymond, Jr., and George Antonoff. Interpolation of vapor pressures—385(A)
Maita, J. P. (see Morin, F. J.)—337(A)
Malenka, B. J., U. E. Kruse, and N. F. Ramsey. Polarizability of deuteron—365(A)
Malkus, Willem V. R. Discrete transitions in thermal turbulence—376(A)
Malvicini, A. (see Bracci, A.)—162(L)
Mandeville, C. E. and H. O. Albrecht. α-particle induced phosphorescence of Ag-activated NaCl—25; 364(A)
—— **and H. O. Albrecht.** Phosphorescence of thoria—992(L)
—— (see Zucker, E. R.)—387(A)
Mann, D. E. and N. Acquista. Vibrational spectrum of CTFE—359(A)
Mann, Harry M. (see Darlington, Lillian E.)—1049
Mann, L. G. (see West, H. I.)—370(A)
Manring, Edward, Carlton Brown, and Dudley Williams. Nuclear quadrupole transitions in paradibromobenzene—348(A)
Marcus, Paul M. Statistical basis of 2-fluid models of superconductivity—346(A)
—— (see Maxwell, E.)—346(A)
Margenau, Henry (see Bloom, Stanley)—791
—— (see Evett, Arthur A.)—1021
Marmo, Frederick (see Watanabe, K.)—155(L)
Marquez, Luis. β-spectrum of Mg^{28}—330(L)
Marshall, John H. Liquid A ionization chamber measurement of shape of β-ray spectrum of K^{40}—371(A)
Martin, D. W. (see Cork, J. M.)—444; 579
Martin, Don S., Jr. (see Hiller, Dale M.)—581
—— (see Jensen, Erling N.)—557
Martin, Paul C. (see Deser, Stanley)—1075
—— (see Karplus, Robert)—1072
Marton, L., J. Arol Simpson, and J. A. Suddeth. Electron beam interferometer—490(L)
Matossi, Frank. Vibrational emission spectra in glow discharges—359(A)
—— (see Nudelman, Sol)—363(A)
Matthias, B. T. Superconducting compounds of non-superconducting elements—487(L)
—— (see Salam, Abdus)—690
Maurer, Robert (see Dutton, David)—126
Maxwell, E. and P. M. Marcus. Aspects of 2-fluid model of superconductivity—346(A)
May, John E. and Bruce P. Foster. γ-rays from Mg^{28}—243; 340(A)
McCarthy, John A. Search for double β-decay in Sn^{124} and Zr^{96}—853
McCarthy, Kathryn A. (see Ballard, Stanley S.)—375(A)
McClure, Gordon W. Specific primary ionization of H_2, He, Ne, and A by high energy electrons—796
McDaniel, B. D. (see Draper, J. E.)—362(A)
—— (see Weil, J. W.)—380(A)
McGruer, J. N. (see Worthington, H. R.)—899
McGuire, T. R. and Selma Greenwald. Magnetic susceptibility and x-ray diffraction measurements of VO and TiO—373(A)
—— (see Kriessman, C. J.)—374(A)
McLernon, F. (see Bay, Z.)—371(A)
Meal, H. C. and H. C. Allen, Jr. Pure quadrupole spectra of HCl and DCl—348(A)
Meinke, W. Wayne. Half-life of Pd^{109} and neutron activation cross section of Pd^{108}—410
——, **E. W. Coleman, J. V. Nehemias, and L. E. Brownell.** 10-kC Co^{60} source—353(A)
Meissner, H. (see Meissner, W.)—709(L)
Meissner, W., F. Schmeissner, and H. Meissner. Temperature, current, magnetic field phase diagram of superconductivity—709(L)
Melkanoff, Michel A. (see Harris, Edward G.)—585
Melkonian, Edward. Recent developments in methods of analysis of slow neutron transmission data in neighborhood of nuclear energy levels—362(A)
Melvin, M. Avramy. Derivation of gauge condition in new electrodynamics—389(A)
—— Generalization of new classical electrodynamics—357(A)
Mendenhall, R. I. (see Zucker, E. R.)—387(A)
Mendoza, E. (see Howling, D. H.)—347(A)
Merz, Walter J. Double hysteresis loop of $BaTiO_3$ at Curie point—375(A)
Metzger, Franz R. Spin and parity of 2.3-Mev excited state of Te^{123}—328(L)
—— (see Schiff, D.)—849
Meyer, A. J. and J. W. Keuffel. μ-meson capture probabilities for intermediate Z elements—349(A)
Meyerhof, W. E. (see Roderick, H.)—371(A)
Michaelis, R. P. and C. E. Violet. Ratio of plateau to minimum grain density for electrons—723(L)
Millburn, G. P. (see Schecter, L.)—633
Miller, Park H. (see Wahlig, Charles F.)—337(A)
Miller, S. L. and C. H. Townes. Microwave absorption spectrum of O_2^{18} and $O^{16}O^{17}$—537
—— **C. H. Townes, and M. Kotani.** Electronic structure of O_2—542
Mills, F. E. (see Goldwasser, E. L.)—378(A)
Milton, J. C. D. and J. S. Fraser. Response of NaI(Tl), KI(Tl), and stilbene phosphors to fission fragments—388(A)
—— (see Fraser, J. S.)—389(A)
Mitra, A. N. and F. J. Dyson. Evidence for direct meson-meson interaction—372(A)
Mitra, S. K. Active nitrogen—516
Mitsui, Toshito and Jiro Furuichi. Domain structure of rochelle salt and KH_2PO_4—193
Miyake, Saburo (see Kusumoto, Osamu)—998(L)
Morellet, D. (see Crussard, J.)—1127(L)
Morin, F. J. and J. P. Maita. Comparison of Cu-doped Ge with heat treated Ge—337(A)
Morita, Masato. Interference terms of electron-neutrino angular correlation—1005(L)
Morrish, A. H. Nuclear interactions of 210-Mev π^- mesons in emulsions—674
Morse, Philip M. Excitation of molecular rotation-vibration by electron impact—51
Moshinsky, Marcos. Poles of S matrix for nuclear reactions—365(A)
Moskowitz, Marvin. Apparatus for measuring thermal conductivity of metals in vacuum at high temperatures—379(A)
Mostov, Philip M., Harold Grad, and Sidney Borowitz. Moment method solution of Boltzmann equation for rough sphere molecular model—376(A)
Moszkowski, S. A. and V. L. Telegdi. Nuclear double γ-emission—366(A)
Mott, W. E. and R. B. Sutton. p-p scattering at 435 Mev—339(A)
—— **R. B. Sutton, J. G. Fox, and J. A. Kane.** Differential cross section for elastic p-p scattering at 435 Mev—712(L)
Mottelson, Ben R. (see Bohr, Aage)—717(L)
Motz, Henry T. Prompt γ-rays from slow neutron capture—355(A)
Mozley, R. F. and H. Bichsel. Analyzing magnet—354(A)
—— (see Bichsel, H.)—354(A)
Murray, Joseph J. (see Hoyt, Harry C.)—169(L)

Nagel, Bengt C. H. (see Hulthén, Lamek)—62
Nagel, E. (see Wu, C. S.)—388(A)
Naudé, S. M. and T. J. Hugo. Emission spectrum of AlF—318(L)
Naumann, R. A. (see Forsthoff, C. W.)—1004(L)
Nedzel, V. Alexander. Total cross sections for 400-Mev neutrons—169(L)
Nehemias, J. V. (see Meinke, W. W.)—353(A)
Neher, H. V. Fluctuations and latitude-effect of cosmic rays at high altitudes and latitudes—360(T)
——, **V. Z. Peterson, and E. A. Stern.** Fluctuations and latitude effect of cosmic rays at high altitudes and latitudes—655
—— **and E. A. Stern.** Energy distribution of cosmic rays—360(A)
Neidigh, R. V. and B. L. Cohen. Angular distributions of 21-Mev protons elastically scattered by various nuclei—340(A)
Nelson, C. M., R. L. Sproull, and R. S. Caswell. Conductivity changes in KCl produced by γ and n irradiation—364(A)
Nelson, Edward B. (see Schrader, Carlton D.)—159(L)
Nelson, Raymond A. (see Band, William)—744
Nergaard, L. S. Studies in oxide-coated cathodes—368(T)
Nester, W. H. (see Cork, J. M.)—444; 579
Neugebauer, H. E. J. Generalization of Kirchhoff's theorem to electromagnetic fields—385(A)
Neuman, Maurice. Radiation of a high energy electron in constant magnetic field—682
Newman, E. (see Cohen, B. L.)—323(L)
Niday, James B. (see Turkevich, A.)—342(A)
Nielsen, Helmer (see Laitone, E. V.)—375(A)
Novey, T. B. (see Albers-Schönberg, H.)—322(L)
Novick, Robert (see Yergin, Paul F.)—377(A)
Nudelman, Sol and Frank Matossi. Influence of electric fields on luminescence—363(A)

O'Day, Marcus. Electron physics in upper atmosphere—368(T)
Offenbacher, Elmer L. and Herbert B. Callen. Directional effects in electric breakdown of ionic crystals—401
Ohtsuka, T. (see Waniek, R. W.)—355(A)
Olbert, S. Atmospheric effects on cosmic-ray intensity at sea level—360(A)
Oldenberg, O. Active nitrogen, airglow—727
Oliver, Norman J. (see Chamberlain, Joseph W.)—1118(L)
Orkin-Lecourtois, A. (see Crussard, J.)—1127(L)
Olson, Elmer L. (see Handley, Thomas H.)—500(L)
O'Rourke, R. C. Deviations from Brillouin's free-spin theory in $MnSiF_6 \cdot 6H_2O$—786
Ortel, William C. G. Neutrons produced in cosmic-ray stars—368(A)
Osborne, Darrell W. (see Abraham, Bernard M.)—347(A)
Osborne, L. S. Photomeson production from H—349(T)
—— (see Goldschmidt-Clermont, Y.)—350(A)
Overhauser, Albert W. Isothermal annealing effects in irradiated Cu—393

Page, L. A., P. Stehle, and S. B. Gunst. Direct comparison of m/e for positron and electron—377(A)
Palevsky, H. (see Hughes, D. J.)—363(A)
Pangonis, W. J. and W. Heller. Solid angle corrections for light scattering measurements—345(A)
—— (see Heller, W.)—345(A)
Parker, Eugene N. Acoustical radiation from velocity field in compressible fluid—240
—— Extension of Heisenberg's model of turbulence to critical Reynolds numbers—221
Parker, Lee W. and John R. Holmes. New fine structure in neutral oxygen—142
Paul, E. B., R. L. Clarke, and W. T. Sharp. Angular distribution of long range α-particles from $F^{19}(p,\alpha)O^{16}$—381(A)
Paul, William. Pressure dependence of resistivity of Ge—336(A)
Pearson, G. L. High impedance field-effect Si transistor—336(A)
—— **and M. Tanenbaum.** Magneto-resistance effect in InSb—153(L)
Pease, Jane S. (see Pease, Robert L.)—371(A)
Pease, Robert L. and Jane S. Pease. Exact interaction of scalar and electrostatic fields—371(A)
Peaslee, D. C. (see Boehm, F.)—1119(L)
—— (see King, R. W.)—1001(L)
Pell, E. M. Recombination rate in Ge by observation of pulsed reverse characteristic—278
Perez-Mendez, V. (see Boehm, F.)—1119(L)
Perry, A. M. (see Littauer, R. M.)—342(A)
Perry, J. E., Jr., and S. J. Bame, Jr. $T(p,\gamma)$ reaction—380(A)
Perry, J. P. (see Angell, C. E.)—724(L)
Peterson, V. Z. (see Neher, H. V.)—655
Petschek, Albert G. Absorption of slow π^- mesons by He^4 nuclei—959
Peyron, M. (see Déjardin, G.)—359(A)
Peyrou, C., R. Safford, and H. Bridge. Experimental results on V^0 particles—368(A)
—— (see Bridge, H. S.)—921
—— (see Safford, R.)—369(A)
Pfann, W. G. (see Vogel, F. L.)—489(L)
Phillips, James A. Energy loss of low energy protons in some gases—532
Picus, Gerald S. Transfer rate of liquid He II film near zero level difference—719(L)
Pidd, R. W. (see Hammer, C. L.)—341(A)
—— (see Raka, E. C.)—341(A)
Pietenpol, W. B. and W. A. Rense. Observations of zodiacal light during total solar eclipse—345(A)
——, **W. A. Rense, F. C. Walz, D. S. Stacey, and J. M. Jackson.** Lyman-α line photographed in sun's spectrum—156(L)
Pines, D., F. Low, T. D. Lee, and C. N. Yang. Motion of slow electrons in polar crystals—382(A)
—— (see Lee, T. D.)—297
Pipkin, Francis M., Scott M. Daubin, Aaron Lemonick, and Donald R. Hamilton. Fast triple coincidence circuit—353(A)
Pollard, E. C. Physical studies on viruses—367(T)
—— (see Friedman, M.)—384(A)
Pool, M. L. (see Cheng, L. S.)—886
—— (see Hammond, William R.)—157(L)
Porter, Charles E. (see Feshbach, Herman)—166(L)
Porter, F. M. (see Ketelle, B. H.)—567
Porter, Fred T. (see Cook, C. Sharp)—429
—— (see Whittle, Charles E.)—498(L)
Portis, A. M., A. F. Kip, C. Kittel, and W. H. Brattain. Electron spin resonance in Si semiconductor—988(L)
Portnoy, W. M. (see Swan, J. B.)—257
Pound, R. V. and A. Abragam. Angular correlations from liquid sources—993(L)
Powell, J. L. (see Hall, H. H.)—912
Pratt, William W. (see Jensen, Erling N.)—557
Price, P. J. Macroscopic theory of superfluid He^3-He^4 mixtures, erratum—1131(E)
Prim, R. C. (see Shockley, W.)—753
Primakoff, H. (see Chang, C. H.)—544
Purcell, E. M. Nuclear magnetism—367(T)

Rainwater, James. Mesonium—349(T)
Raka, E. C., C. L. Hammer, and R. W. Pidd. Scattering of high energy electrons by nuclei—341(A)
—— (see Hammer, C. L.)—341(A)
Ramsey, Norman F. Spin interactions of accelerated nuclei in molecules—232; 382(A)
—— (see Harrick, N. J.)—260
—— (see Malenka, B. J.)—365(A)
Randall, C. A., Jr. (see Hazen, W. E.)—361(A)
Rank, D. H. and D. C. Cronemeyer. Infrared absorption characteristics of thermiated Ge—202
Raphael, R. B. and J. Schwinger. High energy nucleon scattering and isobars—373(A)
Rasetti, F. and E. C. Booth. γ-ray spectrum of ionium—388(A)
Rau, R. Ronald, Marcello Vidale, G. T. Reynolds, D. R. Harris, A. L. Hodson, and J. Ballam. Magnetic field cloud chamber for studying nuclear interactions in cosmic radiation. II. Preliminary results—369(A)
—— (see Ballam, J.)—369(A)
Rauch, C. (see Heer, C. V.)—530
Read, T. A. (see Frankl, D. R.)—351(A)
Rediker, R. H. (see Buskirk, A. V.)—369(A)
Rediker, R. H. (see Thompson, R. W.)—329(L); 1122(L)
Reines, F. and C. L. Cowan, Jr. Proposed experiment to detect free neutrino—492(L)
—— (see Cowan, C. L., Jr.)—493(L)
Reiss, Howard. Chemical equilibria involving electrons as independent chemical entities in impurity semi-conductors—336(A)
—— (see Glazer, Herbert)—360(A)
Reitz, R. (see Bernardini, G.)—573
Rense, W. A. (see Jackson, J. M.)—345(A)
—— (see Pietenpol, W. B.)—156(L); 345(A)
Reynolds, G. T. (see Ballam, J.)—369(A)
—— (see Rau, R. Ronald)—369(A)
Reynolds, John H. Isotopic constitution of Si, Ge, and Hf—1047
—— **and T. J. Ypsilantis.** Techniques in isotopic abundance measurements on elements of Group IV—378(A)
Rice, O. K. and Benjamin Widom. Thermodynamics of He film—987(L)
Richardson, J. Reginald (see Glass, Neel W.)—320(L)
Richter, Harold G. and Charles D. Coryell. Fission of U with 16-Mev x-rays—389(A)
Rinehart, M. C. (see Sargent, C. P.)—343(A)
Ringo, G. R. (see Hamermesh, B.)—603
Ritson, D. M., M. F. Kaplon, and W. D. Walker. High energy cosmic-ray interactions in photographic emulsion and Pb—360(A)
—— (see Kaplon, M. F.)—716(L)
Roberts, A., W. Spry, and J. Tinlot. Charge exchange scattering of 40-Mev π-mesons in H and D—343(A)
—— **and J. Tinlot.** Charge-exchange scattering of 34-Mev π-mesons in H and D—951
Roberts, James H. (see Darlington, Lillian E.)—1049
Roberts, Shepard. Dielectric changes of electroluminescent phosphor during illumination—364(A)
Robillard, T. R. (see Goldwasser, E. L.—378(A)
Robinson, Lawrence Baylor. Production of fissionable isotopes in thermal reactor—1054
Roderick, H., O. Lönsjö, and W. E. Meyerhof. Decay scheme of P^{32}—371(A)
Rogers, K. (see Kessler, J.)—343(A)
—— (see Lederman, L.)—344(A)
Rogosa, G. L. and Guenter Schwarz. Extent of perfect single crystal regions within imperfect single crystals—351(A)
—— (see Schwarz, Guenter)—351(A)
Rohrlich, F. and B. C. Carlson. Energy loss of positrons and electrons—378(A)
Rorschach, H. E., Jr. (see Teasdale, Tom S.)—709(L)
Rose, M. E. O^{14} β-decay and Fermi interaction—1123(L)
—— **and C. L. Terry.** Effect of finite DeBroglie wavelength in theory of β-decay—479
—— (see Armstrong, A. H.)—340(A)
—— (see Frye, G. M.)—381(A)
Rosenstock, Herbert B. Response of pulsed Geiger tube—352(A)
Ross, M. (see Sundaresan, M. K.)—372(A)
Rossi, B. (see Bridge, H. S.)—921
—— (see Harris, F.)—360(A)
—— (see Safford, R.)—369(A)
Rothstein, Jerome. Concept of physical object—356(A)
Rubin, Robert J. Propagation of "plastic" wave in material exhibiting strain-rate effect—346(A)
Ruby, Stanley L. (see Rustad, Brice M.)—370(A)
Ruderman, M. A. Nuclear forces from pseudoscalar meson theory—183
—— Pseudoscalar β-decay and RaE—366(A)
—— (see Henley, E. M.)—719(L)
Rustad, Brice M. and Stanley L. Ruby. β-recoil correlation in decay of He^6—370(A)
Ryder, E. J. Mobility of holes and electrons in high electric fields—766

Saby, John S. and W. C. Dunlap, Jr. Impurity diffusion and space charge layers in fused-impurity p-n junctions—630; 1131(E)
Sachs, A. (see Bodansky, D.)—996(L); 997(L)
—— (see Steinberger, J.)—343(A)
Sachs, Mendel. Nuclear hfs of Mn^{++}—1058
Sadauskis, John (see Jesse, William P.)—1120(L)
Safford, R., C. Peyrou, H. Bridge, and B. Rossi. Cloud-chamber observations on unstable heavy charged particles in cosmic rays—369(A)
—— (see Bridge, H. S.)—921
—— (see Peyrou, C.)—368(A)
Sagane, Ryokichi. Pion production ratios by proton bombardment—1003(L)
Sailor, V. L. (see Foote, H. L., Jr.)—362(A)
—— (see Landon, H. H.)—363(A)
Salam, Abdus and P. T. Matthews. Fredholm theory of scattering in given time-dependent field—690
Salkovitz, E. I. and P. L. Smith. Plastic deformation in ADP crystals—350(A)
Salpeter, E. E. and J. S. Goldstein. Momentum space wave functions. II. Deuteron ground state—983
—— (see Sundaresan, M. K.)—372(A)
Sanders, L. G. (see Beghian, L. E.—1129(L)
—— (see Hicks, D.)—163(L)
Sarabhai, V. and R. P. Kane. Worldwide effects of continuous emission of cosmic rays from the sun—204
Sargent, C. P. and M. C. Rinehart. Absorption of negative pions in H—343(A)
Satchler, G. R. Angular distribution of γ-rays from stripping reactions—722(L)
Saxon, David S. and E. Gerjuoy. Variational calculation of high energy scattering by Yukawa potential—373(A)
Scanlon, W. W. (see Humphrey, J. N.)—111
Schardt, A. W., W. Bernstein, and R. L. Chase. Gray wedge time delay analyzer—353(A)
—— (see Chase, R. L.)—353(A)
Scharff-Goldhaber, Gertrude. Excited states of even-even nuclei—587
Schawlow, A. L. Nuclear quadrupole resonances in Br and I compounds—348(A)

Schecter, L., W. E. Crandall, G. P. Millburn, D. A. Hicks, and A. V. Shelton. High energy charged particles from targets bombarded by 190-Mev deuterons—633
Schein, Marcel (see Glasser, R. G.)—218
Scherrer, P. (see Albers-Schönberg, H.)—322(L)
Scherrer, V. E. (see Faust, W. R.)—355(A)
Schiff, D. and F. R. Metzger. γ-γ directional correlations in Co^{58}, Xe^{133}, and Hg^{198}—849
Schlier, Robert E. and H. E. Farnsworth. Studies of gas adsorption on (100) faces of Cu and Ni crystals by low speed electron diffraction—351(A)
Schmeissner, F. (see Meissner, W.)—709(L)
Schrader, Carlton D., Edward B. Nelson, and James A. Jacobs. Angular correlation of cascade γ-rays from decay of Au^{198}—159(L)
Schubauer, G. B. Turbulent processes as observed in boundary layer and type—379(T)
Schulkes, J. A. (see Gorter, E. W.)—487(L)
Schulman, James H., Robert J. Ginther, and Russell D. Kirk. Enhancement of x-ray-induced absorption bands in alkaline-earth compounds—351(A)
—— (see Klick, Clifford C.)—363(A)
Schwarz, Guenter, L. Carlton Brown, and G. L. Rogosa. X-ray path through calcite for anomalous transmission—351(A)
—— (see Rogosa, G. L.)—351(A)
Schweber, S. S. (see Dyson, F. J.)—372(A)
Schwinger, Julian (see Raphael, R. B.)—373(A)
Scott, M. B. (see Goldschmidt-Clermont, Y.)—350(A)
Scovil, Georgiana. Hall effect in Ti—337(A)
Segrè, E. (see Bernardini, G.)—573
Seidl, F. G. P. (see Hughes, D. J.)—363(A)
Seifert, A. M., H. J. Bramson, and W. W. Havens, Jr. Photographic study of muon range spectrum from $\pi \rightarrow \mu$ decay—349(A)
Seliger, H. H., L. Cavallo, and S. V. Culpepper. Half-life of I^{131}—443
Sellers, P. A. (see Elson, R.)—102
Selove, W., K. Strauch, and F. Titus. n-p scattering near 180° at 94 Mev—339(A)
Senitzky, I. R. Transition from classical to quantum interaction between electron and high frequency field—386(A)
Setlow, Richard. Quantum yield for inactivation of dry chymotrypsin—383(A)
—— (see Franklin, R.)—384(A)
Shafer, K. D. (see Cook, L. G.)—1121(L)
Shanks, Daniel. Blasius and Weyl constants in boundary layer theory—377(A)
Shapiro, E. (see Zucker, E. R.)—387(A)
Shapiro, Mathew M. Cross sections for formation of compound nucleus by charged particles—171
Sharp, R. T. and G. K. Horton. Variational approach to uni-potential many-electron problem—316(L)
Sharp, W. T. (see Paul, E. B.)—381(A)
Sheline, R. K. and N. R. Johnson. Decay scheme of Mg^{28}—325(L)
Shelton, A. V. (see Schecter, L.)—633
Sherman, Dora F. Production of μ-mesons and their behavior in nuclear research emulsions—469
Sherr, R. (see Horton, J.)—388(A)
Shimada, Junji (see Abe, Hidetaro)—317(L)
Shipley, F. M. (see Johnson, V. A.)—523
Shockley, W. Cyclotron resonances, magnetoresistance, and Brillouin zones in semiconductors—491(L)
—— **and R. C. Prim.** Space charge limited emission in semiconductors—753
—— (see Brown, W. L.)—336(A)
Shoolery, J. N. (see Bloom, A. L.)—358(A)
Shore, F. J. (see Bendel, W. L.)—888
Shull, C. G. (see Wilkinson, M. K.)—374(A)
Shunk, R. A. (see Emrich, R. J.)—375(A)
Shutt, R. P. (see Fowler, W. B.)—1126(L)
Siegel, R. T. (see Hartzler, A. J.)—362(A)
Siegert, Arnold J. F. Theory of condensation—344(A)
—— Theory of fusion and condensation—97
Simon, Albert. Higher spin polarizations in nuclear reactions—325(L)
—— Theory of polarized particles in nuclear reactions—991(L)
—— **and T. A. Welton.** Production of polarized particles in nuclear reactions—1036
Simon, Ivan. Structure of SiO_2 and B_2O_3 glasses compacted by very high pressures—350(A)
Simons, Lennart. Existence of positronium chloride—165(L)
Simpson, J. Arol and W. C. Fagot. Properties of low energy nucleonic component at large atmospheric depths—1068
——, **W. Fonger, and S. B. Treiman.** Cosmic-ray intensity-time variations and origin. I. Neutron intensity variation method and meteorological factors—934
—— **and R. B. Uretz.** Cosmic-ray neutron production in elements as function of latitude and altitude—44
—— (see Marton, L.)—490(L)
Singer, S. F. Meteorites as cosmic-ray meters—168(L)
Sitte, Kurt (see Kasnitz, Harold L.)—361(A)
Sjostrand, N. G. (see Levin, J. S.)—363(A)
Slichter, W. P. and E. D. Kolb. Solute distribution in Ge crystals—987(L)
Smart, J. Samuel. Magnetic structure transitions—55
—— Specific heats of ferrites—374(A)
Smith, B. and H. A. Boorse. He II film transport rates over various surfaces—156(L)
Smith, Cyril L. Inactivation of desoxyribonuclease by particle bombardment and by heat—383(A)
—— (see Braams, R.)—995(L)
Smith, L. (see Aarons, M. W.)—342(A)
Smith, Lincoln G. and C. C. Damm. Mass synchrometer doublet measurement at masses 28 and 30—324(L)
Smith, P. L. (see Salkovitz, E. I.)—350(A)
Smoluchowski, R. (see Hayes, S.)—350(A)
Snowdon, S. C. and W. D. Whitehead. Total neutron cross sections of Au, Cl, and P—615
Snyder, H. S. Alternating-gradient focusing principle—347(T)
Soules, J. A. (see Gordon, W. L.)—346(A)
Spence, R. D. (see Carr, E. F.)—339(A)
—— (see Cowen, J. A.)—359(A)
Spencer, L. V. Calculation of peaked angular distributions from Legendre polynomial expansions and application to multiple scattering of charged particles—146
—— **and Charles Wolff.** Penetration and diffusion of hard x-rays: Polarization effects—510
Sperduto, A. (see Bockelman, C. K.)—340(A)
—— (see Browne, C. P.)—340(A)
Spetner, L. M. Fade-time of Rayleigh distributed random function—346(A)
Sproull, R. L. and R. S. Bever. O vacancies in BaO crystals—352(A)
—— (see Nelson, C. M.)—364(A)
Spry, W. (see Roberts, A.)—343(A)
Squires, G. L. (see Stewart, A. T.)—1125(L)
Stacey, D. S. (see Pietenpol, W. B.)—156(L)
Stafne, Marilyn J. (see Hughes, D. J.)—497(L)
Stahl, R. H. (see Hillman, Peter)—362(A)
Stebbins, A. K. (see Bleuler, E.)—460
Steffen, Rolf M. Evidence of mixed $E1+M2$ transition and angular momenta of Sr^{88} levels—321(L)

—— Interaction of electric field gradients and nuclear electric quadrupole moments in angular correlation—1119(L)
Stehle, P. (see Page, L. A.)—377(A)
Stein, Richard and John J. Keane. Scattering of light from polymer films—384(A)
Steinberger, J., A. Sachs, and P. Lindenfeld. Internal pair production of γ-rays of mesonic origin: Alternate modes of π^0 decay—343(A)
—— (see Bodansky, D.)—996(L); 997(L)
Stern, E. A. (see Neher, H. V.)—360(A); 655
Sternglass, E. J. Temperature dependence of secondary electron emission from Ta, Pt, and graphite—380(A)
Sternheimer, R. M. Double-focusing by system of two magnets with nonuniform fields—352(A)
Stewart, A. T. and G. L. Squires. Scattering of slow neutrons by ortho- and para-hydrogen—1125(L)
Stewart, John Q. Kinds of energy—356(A)
Stier, P. M. (see Evans, G. E.)—825
Stoll, P. (see Locher, K.)—164(L)
Storrs, C. L. and D. H. Frisch. Total neutron scattering cross sections of polyethylene and C at 1.32 Mev—339(A)
Strandberg, M. W. P. (see Burke, B. F.)—303; 338(A)
Stratton, W. R. (see Yarnell, J. L.)—292
Strauch, K. (see Hofmann, J. A.)—449
—— (see Selove, W.)—339(A)
Stump, Robert (see Brown, Harry B.)—1061
Suddeth, J. A. (see Marton, L.)—490(L)
Suga, Koichi (see Kusumoto, Osamu)—998(L)
Sugarman, Nathan and Agnes Haber. Interaction of negative pions with Hg—342(A)
—— (see Kruger, Paul)—158(L)
Sugihara, Thomas (see Arnold, James R.)—332(L)
Sugita, T. (see Yamaka, E.)—992(L)
Sundaresan, M. K., E. E. Salpeter, and M. Ross. Theoretical analysis of meson-proton scattering—372(A)
Sunyar, A. W. Disintegration of W^{187}: Evidence for slow $E1$ transition—387(A)
Sutton, R. B. (see Mott, W. E.)—339(A); 712(L)
Sutton, R. M. Response of Oersted medallist: Heritage of physics teacher—367(T)
Swan, J. B., W. M. Portnoy, and R. D. Hill. Radioactivity of Pt^{191} and Pt^{193m}—257
Swenson, R. W. (see Cole, R. H.)—352(A)
Swihart, J. C. (see Belinfante, F. J.)—357(A)

Talbott, F. L. and N. P. Heydenburg. γ-ray resonances in the α-particle bombardment of Be and B—186
Talmi, Igal. Spins and parities of excited states in even-even nuclei—1001(L)
Tanaka, K. Radiation emitted by uniformly moving particles—358(A)
Tanenbaum, M. (see Pearson, G. L.)—153(L)
Tchen, C. M. Transfer processes in isotropic turbulence—376(A)
Teasdale, Tom S. and H. E. Rorschach, Jr. Paramagnetic effect in superconductors—709(L)
Telegdi, Valentine L. (see del Rio, C. S.)—439
—— (see Hsiao, C. A.)—494(L)
—— (see Moszkowski, S. A.)—366(A)
Temmer, G. M. and N. P. Heydenburg. Precision α-α scattering at low energies—340(A)
Tendam, D. J. (see Bleuler, E.)—460; 464
Tenney, F. and J. Tinlot. Low energy π^+ interactions in Be—342(A)
Terry, C. L. (see Rose, M. E.)—479
Theus, R. B. (see Faust, W. R.)—355(A)
Thickens, R. W. and J. R. MacDonald. Electret-like behavior in polarized $BaTiO_3$ ceramic—375(A)
Thode, H. G. (see Fleming, W. H.)—857
—— (see Walker, W. H.)—447
Thomas, E. E. (see Vogel, F. L.)—489(L)
Thomas, L. H. (see Zondek, B.)—738
Thompson, R. W., A. V. Buskirk, L. R. Etter, C. J. Karzmark, and R. H. Rediker. Disintegration of V^0 particles—329(L)
——, **A. V. Buskirk, L. R. Etter, C. J. Karzmark, and R. H. Rediker.** Unusual example of V^0 decay—1122(L)
—— (see Buskirk, A. V.)—369(A)
Thomson, Robb M. and Peter G. Bergmann. Spin and statistics of general-relativistic Dirac field—357(A)
Thorndike, A. M. (see Fowler, W. B.)—1126(L)
Thourson, T. L. (see Brentano, J. C. M.)—351(A)
Tietz, T. Movable critical points of nonlinear wave equation—495(L)
Tifford, Arthur N. and Sheng To Chu. Boundary layer on spinning axisymmetric bodies—377(A)
Timnick, A. (see Cohen, B. L.)—323(L)
Tinlot, J. (see Roberts, A.)—343(A); 951
—— (see Tenney, F.)—342(A)
Tittman, Jay. Thermal energy relaxation length of Ra-Be neutrons in water—256
Titus, F. (see Selove, W.)—339(A)
Tolhoek, H. A. Theory of directional distribution and polarization of β- and γ-rays emitted by oriented nuclei—366(A)
Toll, John S. Radiative corrections to forward Compton scattering—372(A)
Tompkins, Althea (see Turkevich, A.)—247
Touschek, B. (see Chisholm, R.)—763
Townes, C. H. (see Miller, S. L.)—537; 542
Trammell, G. T. Elastic scattering of neutrons from paramagnetic rare earth atoms—355(A)
Trefftz, Eleanor. Energy bands in Nb metal—380(A)
Treiman, S. B. (see Simpson, J. A.)—934
Trembley, J. (see Crussard, J.)—1127(L)
Trischka, J. W. (see Braunstein, R.)—348(A)
Truell, Rohn and Joseph Bronzo. Ultrasonic attenuation measurements in Ge—152(L)
Turkevich, A. and James B. Niday. Radioactive products of interaction of π^- with As^{75}—342(A)
—— and Althea Tompkins. Search for Si^{28} in natural Si—247
Turner, R. W. (see Hayes, S.)—350(A)
Turner, T. E., Verna C. Fiora, W. M. Kendrick, and B. L. Hicks. Preliminary analysis of microwave spectrum of C_2H_4NH—338(A)

Uehling, Edwin A. (see Young, J. A., Jr.)—990(L)
Ullman, Robert (see Hermans, J. J.)—384(A)
Uretz, R. B. (see Simpson, J. A.)—44
Urey, Harold C. Abundances of elements, erratum—1131(E)

Vaidya, P. C. Spherically symmetric solutions in nonsymmetrical field theories. I. Skew symmetric tensor—695
Vallejo, I. Escobar (see Harris, F.)—360(A)
van den Burg, F. A. W. (see Kramers, H. C.)—1117(L)
Van Vleck, J. H. Two barrier phenomena—367(T)
van Wieringen, J. S. Anomalous behavior of g-factor of LiFeCr spinels as function of temperature—488(L)
Vidale, Marcello (see Ballam, J.)—369(A)
—— (see Rau, R. Ronald)—369(A)
Violet, C. E. (see Michaelis, R. P.)—723(L)
Visscher, W. M. (see Dyson, F. J.)—372(A)
Vogel, F. L., W. G. Pfann, H. E. Corey, and E. E. Thomas. Observations of dislocations in lineage boundaries in Ge—489(L)
Volchok, Herbert L. (see Kulp, J. Laurence)—713(L)

von Hippel, A., E. P. Gross, J. G. Jelatis, and M. Geller. Photocurrent space charge build-up and field emission in alkali halide crystals—364(A)

Wahlig, Charles F. and Park H. Miller. Photo-Hall-Voltaic effect—337(A)
Wakely, P. G. Binding energy calculation on He^4 with single particle wave functions—724(L)
Walchli, H. E. Nuclear magnetic resonance measurements of Se—331(L)
Walker, William D. Interactions of μ-mesons—234; 349(A)
—— **and N. M. Duller.** Unstable particles from penetrating showers—320(L)
—— (see Greisen, K.)—915
—— (see Kaplon, M. F.)—716(L)
—— (see Ritson, D. M.)—360(A)
Walker, W. H. and H. G. Thode. Relative abundances and neutron capture cross sections of Nd isotopes—447
Walt, M. and H. H. Barschall. Angular distribution of elastically scattered 1-Mev neutrons—714(L)
Walz, F. C. (see Pietenpol, W. B.)—156(L)
Waniek, R. W. and T. Ohtsuka. Stars initiated by neutrons—355(A)
Wanklyn, D. I. Fast neutron reactions in O and Ne—381(A)
—— (see Jackson, J. David)—381(A)
Wannier, Gregory H. Threshold law for single ionization of atoms or ions by electrons—817
—— (see Lewis, H. W.)—1131(E)
Watanabe, K., Edward C. Y. Inn, and Murray Zelikoff. Absorption coefficients of O_2 in vacuum uv—359(A)
——, **Frederick Marmo, and Edward C. Y. Inn.** Formation of D layer—155(L)
—— (see Zelikoff, Murray)—359(A)
Watase, Yuzuru (see Kusumoto, Osamu)—998(L)
Watson, K. M. (see Brueckner, K. A.)—699
Watson, W. W. (see Anderson, Carl E.)—606
—— (see Kranz, A. Z.)—344(A)
Wattenberg, A., B. T. Feld, and R. D. Godbole. High energy photoproton production—380(A)
Weaver, Albert B. Search for penetrating showers from H_2 at sea level using a cloud chamber—86
Weber, J. Quantum effects in noise—357(A)
—— Quantum theory of damped electrical oscillator and noise—977
Weidner, R. T. (see Eschenfelder, A. H.)—358(A)
Weil, J. W. and B. D. McDaniel. Photoproduction of protons by monoenergetic 190-Mev γ-rays—380(A)
Weinreich, Gabriel and Vernon W. Hughes. Atomic beam magnetic resonance experiments on He^3—377(A)
Weinstock, Bernard (see Abraham, Bernard M.)—347(A)
Weisbaum, S., Y. Beers, and G. Herrmann. S-band spectrum of HDO—338(A)
Weisskopf, Victor F. (see Feshbach, Herman)—166(L)
Welton, T. A. Theory of Lamb shift—373(A)
—— (see Simon, A.)—1036
Wessel, Günter (see Lew, Hin)—1
West, H. I. and L. G. Mann. Measurement of γ-ray spectra using three-crystal pair spectrometer—370(A)
Wexler, S. (see Hamermesh, B.)—603
Weyl, Peter K. Energy loss of heavy charged particles in gases—378(A)
Wheeler, George W. (see Anderson, Carl E.)—606
Wheeler, John A. and David L. Hill. Collective model of nucleus—366(A)
White, George R. and W. F. Fry. Range distribution of μ-mesons from π-meson decays in photographic emulsions—349(A)
—— (see Fry, W. F.)—207
Whitehead, W. D. (see Snowdon, S. C.)—615
Whittemore, W. L. (see Fowler, W. B.)—1126(L)
Whittle, Charles E. and Fred T. Porter. γ-ray cascade following decay of Sc^{46}—498(L)
Widgoff, M. Multiplicity of neutrons from interaction of μ^- mesons at rest in Pb, Bi, Sn, and Al—891
Widom, Benjamin (see Rice, O. K.)—987(L)
Wilets, L., D. Hill, and K. W. Ford. Contribution of nuclear distortion to isotope shifts—366(A)
Wilkinson, D. H. Possible breakdown of isotopic spin and charge parity selection rules—721(L)
—— (see Jones, G. A.)—722(L)
Wilkinson, M. K. and C. G. Shull. Neutron diffraction studies on various ferromagnetic alloys—374(A)
Willard, H. B., J. K. Bair, and J. D. Kington. $T(p,n)He^3$ and $T(p,\gamma)He^4$—865
—— (see Bair, J. K.)—575
Williams, A. O., Jr. Two-electron self-consistent field—803
Williams, Dudley (see Manring, Edward)—348(A)
Williams, R. W. and W. E. Hazen. Experiments on air showers—361(A)
—— (see Hazen, W. E.)—361(A)
Williamson, E. Marjorie (see Flint, H. T.)—318(L)
Wilson, E. B., Jr. (see Ferguson, R. C.)—338(A)
—— (see Kivelson, D.)—338(A)
Wilson, Elizabeth (see Bainbridge, Kenneth T.)—430
—— (see Kraushaar, J. J.)—610
Wilson, Robert R. Scattering of 1.3-Mev γ-rays by electric field—720(L)
Winsberg, Lester. Interaction of π^- mesons with I^{127}—343(A)
Woese, C. R. (see Caspar, D. L.)—384(A)
Wolfenstein, L. Tensor operators in isotopic spin space—371(A)
—— (see Fumi, F. G.)—498(L)
—— (see Lakin, W.)—365(A)
Wolff, Charles (see Spencer, L. V.)—510
Wollan, E. O. (see Koehler, W. C.)—354(A)
Woods, D. C. (see Kash, S. W.)—564
Woodward, W. M. (see Littauer, R. M.)—342(A)
Woonton, G. A. Diffraction field of circular aperture—385(A)
Worley, R. Edwin. Third Rydberg series of N_2, erratum—1131(E)
Worthington, H. R., J. N. McGruer, and D. E. Findley. p-p scattering from 1.8 to 4.2 Mev—899
Wright, Byron T. Spectrometer measurement on high energy positrons of Na^{22}—159(L)
Wu, C. S., F. Boehm, and E. Nagel. Radiations from RaD and RaE—388(A)
—— (see Boehm, F.)—369(A)
—— (see Lidofsky, L.)—387(A)

Yadoff, Oleg. Free electron emission in atmosphere—387(A)
Yamaka, E. and T. Sugita. Energy band structure in Si crystal—992(L)
Yang, C. N. (see Pines, D.)—382(A)
Yarnell, J. L., R. H. Lovberg, and W. R. Stratton. Angular distribution of $He^3(d,p)He$ between 240 kev and 3.56 Mev—292
Yergin, Paul F., Willis E. Lamb, Jr., Edgar Lipworth, and Robert Novick. Fine structure of singly ionized He—377(A)
Yevick, George J. Pines-Bohm theory of many particles with long-range forces—383(A)
York, C. M., R. B. Leighton, and E. K. Bjornerud. Direct experimental evidence for existence of heavy V^0 particle—167(L)

Young, J. A., Jr., and Edwin A. Uehling. Energy absorption in ferromagnetic resonance—990(L)
Young, R. A. (see Ziegler, W. T.)—115
Ypsilantis, T. J. (see Reynolds, J. H.)—378(A)
Yuan, Luke C. L. (see der Mateosian, E.)—868

Zeldes, Henry (see Livingston, Ralph)—609
Zeldes, Nissan. Spark spectrum of Gd II—413
—— spins of Li^8 and B^{10} in shell-model—416
Zelikoff, Murray, Edward C. Y. Inn, and K. Watanabe. Absorption coefficients of N_2O and CO_2 in vacuum uv—359(A)
—— (see Watanabe, K.)—359(A)
Ziegler, W. T. and R. A. Young. Studies of compounds for superconductivity—115
Zimmerman, F. J. (see Collins, S. C.)—991(L)
Zimmerman, J. E. (see Howling, D. H.)—347(A)
Zimmerman, R. L., D. I. Cooper, and D. H. Frisch. *n-d* and *p-d* scattering in *S*-wave region—339(A)
—— (see Cooper, D. I.)—339(A)
Zirin, Harold. Exchange potential in electron gas at nonzero temperature—795
Zondek, B. and L. H. Thomas. Stability of limiting case of plane Couette flow—738
Zucker, Alexander. Nuclear reactions with 25-Mev nitrogen nuclei—380(T)
Zucker, E. R., C. E. Mandeville, E. Shapiro, R. I. Mendenhall, and G. L. Conklin. γ-radiation from Zr^{96} and Nb^{95}—387(A)
Zucker, Francis J. Guided surface waves on lossy structures—385(A)

PHYSICAL REVIEW VOLUME 90, NUMBER 6 JUNE 15, 1953

Analytic Subject Index to Volume 90

References with (A) are to abstracts of papers presented at meetings of the American Physical Society; references with (L) are to Letters to the Editor; references with (E) are to Errata. Items are listed under the following categories:

Acoustics
Astrophysics
Atomic and Molecular Beams
Atomic Mass and Abundance
Atomic Structure and Spectra
Biophysics
Chemical Effects and Properties
Constants, Standards, Units
Cosmic Radiation
Crystalline State
Dielectrics and Dielectric Properties
Diffraction
Diffusion
Elasticity and Plasticity
Electrical Conductivity and Resistance
Electrical Discharges
Electrical Properties
Electromagnetic Theory and Electrodynamics
Electrons and Positrons
Elementary Particle Interactions
Errata
Field Theory
Films, Properties
Fluid Dynamics
Gamma-Rays
Gases
Geophysics
Helium, Liquid
Imperfections in Solids
Ionization
Ions
Ions and Electrons, Mobility
Liquids
Luminescence
Magnetic Properties
Magnetic Resonance Absorption
Mathematical Methods
Mechanics
Mesons
Methods and Instruments
Microwaves
Miscellaneous
Molecular Aggregates
Molecular Structure and Spectra
Neutrino
Noise
Nuclear Fission
Nuclear Moments and Spin
Nuclear Photoeffects
Nuclear Reactions, General
Nuclear Reactions Induced by α-Particles
Nuclear Reactions Induced by Deuterons
Nuclear Reactions Induced by Mesons
Nuclear Reactions Induced by Neutrons
Nuclear Reactions Induced by Protons
Nuclear Spectra
Nuclear Structure Theory
Optical Properties
Proceedings of the American Physical Society
Quantum Electrodynamics
Quantum Mechanics
Radiation
Radioactivity
Range and Energy Loss of Particles
Relativity and Gravitation
Scattering, General
Scattering of α-Particles
Scattering of Deuterons
Scattering of Electrons and Positrons
Scattering of Mesons
Scattering of Neutrons
Scattering of Protons
Semiconductors
Spectra, General
Statistical Mechanics and Thermodynamics
Superconductivity
Thermal Properties
X-Rays

Absorption of Radiation (see **Radiation**)
Acoustics
Acoustical radiation from velocity field in compressible fluid, Eugene N. Parker—240
Ultrasonic attenuation in Ge, Rohn Truell and Joseph Bronzo—152(L)
Adsorption (see **Gases**)
Aerodynamics (see **Fluid Dynamics**)
Afterglow (see **Electrical Discharges**)
Alloys (see **Crystalline State**)
Annihilation (see **Electrons and Positrons**)
Antiferroelectric Phenomena (see **Dielectrics and Dielectric Properties**)
Antiferromagnetism (see **Magnetic Properties**)
Arcs (see **Electrical Discharges**)
Astrophysics
Lyman-α line in sun's spectrum, W. B. Pietenpol, W. A. Rense, F. C. Walz, D. S. Stacey, and J. M. Jackson—156(L)
Origin of zodiacal light, J. M. Jackson and W. A. Rense—345(A)
Zodiacal light during total solar eclipse, W. B. Pietenpol and W. A. Rense—345(A)

Atmosphere (see **Geophysics**)
Atomic and Molecular Beams
Atomic beam magnetic resonance experiments on He^3, Gabriel Weinreich and Vernon W. Hughes—377(A)
Scattering of fast N_2 molecules by N_2, I. Amdur and W. T. Lindsay—344(A)
Atomic Mass and Abundance
Abundances of elements, erratum, Harold C. Urey—1131(E)
Isotopic constitution of Si, Ge, and Hf, John H. Reynolds—1047
Mass synchrometer doublet measurements at masses 28 and 30, Lincoln G. Smith and C. C. Damm—324(L)
Nuclear mass determinations from disintegration energies: O to S, erratum, C. W. Li—1131(E)
Nuclear rf spectra of D_2 and H_2 in intermediate and strong magnetic fields, N. J. Harrick, R. G. Barnes, P. J. Bray, and N. F. Ramsey—260
Relative abundances of Nd isotopes, W. H. Walker and H. G. Thode—447
Techniques in isotopic abundance measurements on elements of Group IV, J. H. Reynolds and T. J. Ypsilantis—378(A)
Atomic Structure and Spectra
Atomic self-consistent fields. I. Calculation of Slater functions, Per-Olov Löwdin—120
Broadening and shift of second doublet of Rb absorption series under different pressures of A and He, Shang-Yi Ch'en and Donald A. Kohler—1019
Effect of temperature on duration of $^3P_2$ metastable level of Ne, F. A. Grant and A. D. Krumbein—59
Effects of radioactive disintegrations on inner electrons of the atom, J. S. Levinger—11
Electron distribution in atoms by electron diffraction, L. S. Bartell and L. O. Brockway—833
Fine structure of singly ionized He, Paul F. Yergin, Willis E. Lamb, Jr., Edgar Lipworth, and Robert Novick—377(A)
Gd spark spectrum, Nissan Zeldes—413
Hfs of $3p\ ^2P_{1/2}$ state of Al^{27}, Hin Lew and Günter Wessel—1
Lyman α-line in sun's spectrum, W. B. Pietenpol, W. A. Rense, F. C. Walz, D. S. Stacey, and J. M. Jackson—156(L)
Mn^{++} hfs, Mendel Sachs—1058
Orbital effect in neutron-electron magnetic scattering, W. H. Kleiner—168(L)
Oxygen fine structure, Lee W. Parker and John R. Holmes—142
Positronium chloride, Lennart Simons—165(L)
Pressure broadening by electron impacts, B. Kivel—382(A)
Spectral line broadening by electrons, S. Bloom—382(A)
Spin orbit coupling and mesonic Lamb shift, R. Chisholm and B. Touschek—763
Two-electron self-consistent field, A. O. Williams, Jr.—803
Zeeman effect in spectra of Te, J. B. Green and R. A. Loring—80
Aurora (see **Astrophysics; Geophysics**)

Barkhausen Effect (see **Magnetic Properties**)
Biophysics
Biological determination of range of low voltage electrons, Marguerite Davis—384(A)
Inactivation of desoxyribonuclease by particle bombardment and by heat, Cyril L. Smith—383(A)
Inactivation of dysentery toxin with ionizing radiation, D. L. Caspar and C. R. Woese—384(A)
Ionizing radiation evidence for internal structure in bacterial virus, M. Friedman and E. Pollard—384(A)
Particle size of α-amylase, John Jagger—384(A)
Quantum yield for inactivation of dry chymotrypsin, Richard Setlow—383(A)
Ultraviolet action spectrum of bacillus megatherium bacteriophage, R. Franklin, M. Friedman, and R. Setlow—384(A)
Boson Theory (see **Field Theory**)
Bremsstrahlung (see **Radiation**)
Broadening of Spectral Lines (see **Atomic Structure and Spectra; Molecular Structure and Spectra; Spectra, General**)

Capture Cross Sections (see **Electrons and Positrons; Nuclear Reactions; Radiation**)
Chemical Effects and Properties
Chemical Reactions (see **Chemical Effects and Properties**)
Chemiluminescence (see **Luminescence**)
Cold Emission (see **Electrical Properties**)
Colloids (see **Chemical Effects and Properties; Molecular Aggregates**)
Conductivity, Electrical (see **Electrical Conductivity and Resistance**)
Conductivity, Thermal (see **Thermal Properties**)
Constants, Standards, Units
Direct comparison of m/e for positron and electron, L. A. Page, P. Stehle, and S. B. Gunst—377(A)
e/m for 385-Mev protons, D. J. Grove and J. G. Fox—378(A)
Cosmic Radiation
Air shower experiments, W. E. Hazen, C. A. Randall, Jr., and R. W. Williams—361(A); R. W. Williams and W. E. Hazen—361(A)
Atmospheric effects on cosmic-ray intensity at sea level, S. Olbert—360(A)
Cloud-chamber observations of heavy charged unstable particles, H. S. Bridge, C. Peyrou, B. Rossi, and R. Safford—921
Constancy of cosmic-ray flux over past 30 000 years, J. Laurence Kulp and Herbert L. Volchok—713(L)
Cosmic-ray neutron production in elements as function of latitude and altitude, J. A. Simpson and R. B. Uretz—44
Density distribution within 2 meters of large air shower axes, R. E. Heineman and W. E. Hazen—496(L)
Disintegration of V^0 particles, R. W. Thompson, A. V. Buskirk, L. R. Etter, C. J. Karzmark, and R. H. Rediker—329(L)
East-west asymmetry for positive and negative mesons near equator, F. Harris, B. Rossi, and I. Escobar—360(A)
Energy distribution, H. V. Neher and E. A. Stern—360(A)
Energy spectra of cosmic-ray photons and electrons from plastic scintillation counter measurements, C. N. Chou—473
Families of fundamental particles, M. Goldhaber—369(A)
Fluctuations and latitude effect at high altitudes and latitudes, H. V. Neher, V. Z. Peterson, and E. A. Stern—655
Heavy V^+ particle, C. M. York, R. B. Leighton, and E. J. Bjornerud—167(L)
High energy cosmic-ray interactions in photographic emulsion and Pb, D. M. Ritson, M. F. Kaplon, and W. D. Walker—360(A)
High energy nuclear interactions in Pb and light elements, M. F. Kaplon, D. M. Ritson, and W. D. Walker—716(L)

K mesons, J. Crussard, L. Leprince-Ringuet, D. Morellet, A. Orkin-Lecourtois, and J. Trembley—1127(L)
Low energy nucleonic component at large atmospheric depths, J. A. Simpson and W. C. Fagot—1068
Magnetic field cloud chamber for studying nuclear interactions in cosmic radiation. I. Equipment, J. Ballam, D. R. Harris, A. L. Hodson, R. Ronald Rau, G. T. Reynolds, and Marcello Vidale—369(A); II. Preliminary results, R. Ronald Rau, Marcello Vidale, G. T. Reynolds, D. R. Harris, A. L. Hodson, and J. Ballam —369(A)
Mass of cosmic-ray mesons at mountain altitudes, Giulio Ascoli—1079
Mean lifetimes of *V* particles and heavy mesons, W. L. Alford and R. B. Leighton—622
Meteorites as cosmic-ray meters, S. F. Singer—168(L)
Multiple meson production observed with high pressure hydrogen-filled cloud chamber, Osamu Kusumoto, Saburo Miyake, Koichi Suga, and Yuzuru Watase—998(L)
Neutron intensity variation method and meteorological factors, J. A. Simpson, W. Fonger, and S. B. Treiman—934
Neutrons produced in cosmic-ray stars, William C. G. Ortel—368(A)
New magnet chamber for study of *V* particles, A. V. Buskirk, H. O. Cohn, L. R. Etter, C. J. Karzmark, R. H. Rediker, and R. W. Thompson—369(A)
Ratio of neutral to charged particles in nuclear interacting component of cosmic rays, K. Greisen and W. D. Walker —915
Scintillation counter measurements of absorption of *N* component, G. W. Clark—368(A)
Search for penetrating showers from H_2 at sea level using a cloud chamber, Albert B. Weaver—86
Structure and composition of air shower cores, Harold L. Kasnitz and Kurt Sitte—361(A)
Two-particle showers from Be, L. Grodzins, G. Del Castillo, and W. Y. Chang—361(A)
Unstable heavy charged particles, R. Safford, C. Peyrou, H. Bridge, and B. Rossi—369(A)
Unstable particles from penetrating showers, W. D. Walker and N. M. Duller—320(L)
V^0 decay, unusual example, R. W. Thompson, A. V. Buskirk, L. R. Etter, C. J. Karzmark, and R. H. Rediker —1122(L)
V^0 particles, C. Peyrou, R. Safford, and H. Bridge—368(A)
Worldwide effects of continuous emission of cosmic rays from the sun, V. Sarabhai and R. P. Kane—204
Z dependence of cross section and energy in cosmic-ray stars, Ian Barbour—361(A)

Cosmology (see **Astrophysics; Relativity and Gravitation**)
Critical Potentials (see **Atomic Structure and Spectra; Molecular Structure and Spectra**)
Cross Section (see **Electrons and Positrons; Nuclear Reactions; Radiation; Scattering**)
Crystal Counters (see **Methods and Instruments**)
Crystalline State (see also **Electrical Properties; Imperfections in Solids; Magnetic Properties; Semiconductors;** etc.)
Deviations from Brillouin's free-spin theory in $MnSiF_6 \cdot 6H_2O$, R. C. O'Rourke—786
Directional effects in electric breakdown of ionic crystals, Elmer L. Offenbacher and Herbert B. Callen—401
Domain structure of rochelle salt and KH_2PO_4, Toshito Mitsui and Jiro Furuichi—193
Effect of mechanical surface treatment on lattice regularity of quartz and calcite, J. C. M. Brentano and T. L. Thourson—351(A)
Electronic structure of diamond, G. G. Hall—316(L)
Energy band structure in Si crystal, E. Yamaka and T. Sugita—992(L)
Energy bands in Nb metal, Eleanor Trefftz—380(A)
Enhancement of x-ray-induced absorption bands in alkaline-earth compounds, James H. Schulman, Robert J. Ginther, and Russell D. Kirk—351(A)
Exchange potential in electron gas at nonzero temperature, Harold Zirin—795
Extent of perfect single crystal regions within imperfect single crystals, G. L. Rogosa and Guenter Schwarz—351(A)
Gas adsorption on (100) faces of Cu and Ni crystals studied by low speed electron diffraction, Robert E. Schlier and H. E. Farnsworth—351(A)
Gyromagnetic ratios of microcrystalline and macrocrystalline materials, S. J. Barnett—315(L)
Improved spherical treatment of Ising model, Alfred Levitas and Melvin Lax—374(A)
Indirect interaction between nuclear spins in Cu acetate, A. Abragam—358(A)
Internal friction of rocksalt single crystals, D. R. Frankl and T. A. Read—351(A)
Lattice sums: Validity of Evjen's method, I. D. C. Gurney —316(L)
Magnetic susceptibility and x-ray diffraction measurements of VO and TiO, T. R. McGuire and Selma Greenwald 373(A)
Motion of slow electrons in polar crystal, T. D. Lee, F. E. Low, and D. Pines—297; D. Pines, F. E. Low, T. D. Lee, and C. N. Yang—382(A)
Neutron diffraction study of $MgFe_2O_4$, L. M. Corliss, J. M. Hastings, and F. G. Brockman—1013
Nuclear quadrupole coupling in solids, M. H. Cohen—348(A)
Observations of dislocations in lineage boundaries in Ge, F. L. Vogel, W. G. Pfann, H. E. Corey, and E. E. Thomas—489(L)
Pines-Bohm theory of many particles with long-range forces, George J. Yevick—383(A)
Small angle scattering of x-rays from cold-worked solids, D. L. Dexter—1007
Small angle x-ray scattering in deformed crystals, S. Hayes, R. Smoluchowski, and R. W. Turner—350(A)
Solubility of Si and Ge in Ga and In, Paul H. Keck and Jacob Broder—521
Solubility of Si in Ga and In, Paul H. Keck—379(A)
Solute distribution in Ge crystals, W. P. Slichter and E. D. Kolb—987(L)
Space charge layer and distribution of lattice defects at surface of ionic crystals, Kurt Lehovec—350(A)
Spin-dependent couplings in many-electron system, W. J. Carr, Jr.—383(A)
Surface barrier analysis for highly refractory metals by Schottky deviations, D. W. Juenker, G. S. Colladay, and E. A. Coomes—772
X-ray path through calcite for anomalous transmission, Guenter Schwarz, L. Carlton Brown, and G. L. Rogosa —351(A)

Diamagnetism (see **Magnetic Properties**)
Dielectrics and Dielectric Properties
Dielectric changes of electroluminescent phosphor during illumination, Shepard Roberts—364(A)
Dielectric constants of solid HCl and HBr, R. H. Cole, R. W. Swenson, and N. L. Brown—352(A)
Directional effects in electric breakdown of ionic crystals, Elmer L. Offenbacher and Herbert B. Callen—401
Domain structure of rochelle salt and KH_2PO_4, Toshito Mitsui and Jiro Furuichi—193

Dielectrics and Dielectric Properties (Continued)
Double hysteresis loop of $BaTiO_3$ at Curie point, Walter J. Merz—375(A)
Electret-like behavior in polarized $BaTiO_3$ ceramic, R. W. Thickens and J. R. MacDonald—375(A)
Ferroelectricity in oxides of fluorite structure, W. R. Cook, Jr., and Hans Jaffe—375(A)
Influence of magnetic field on microwave dielectric constant of liquid crystal, E. F. Carr and R. D. Spence—339(A)
Diffraction (see also **Scattering**)
Diffraction field of circular aperture, G. A. Woonton—385(A)
Of electromagnetic waves by aperture in infinite screen, G. Bekefi—385(A)
Electron beam interferometer, L. Martin, J. Arol Simpson, and J. A. Suddeth—490(L)
Gamma-ray reflections from (550) and (310) planes of quartz, Harry C. Hoyt, Joseph J. Murray, and Jesse W. M. DuMond—169(L)
Generalization of Kirchhoff's theorem to electromagnetic fields, H. E. J. Neugebauer—385(A)
Investigation of electron distribution in atoms by electron diffraction, L. S. Bartell and L. O. Brockway—833
Neutron diffraction studies of antiferromagnetism in MnF_2 and some isomorphous carbons, R. A. Erickson—779
Neutron diffraction studies on various ferromagnetic alloys, M. K. Wilkinson and C. G. Shull—374(A)
Neutron diffraction study of $MgFe_2O_4$, L. M. Corliss, J. M. Hastings, and F. G. Brockman—1013
Diffusion
Impurity diffusion and space charge layers in fused-impurity *p-n* junctions, John S. Saby and W. C. Dunlap, Jr.—630; 1131(E)
Of injected carriers in semiconductor of mixed conductivity type, Harvey Brooks—336(A)
Measurement of transport mean free path of thermal neutrons in D_2O by B poisoning method, S. W. Kash and D. C. Woods—564
Penetration and diffusion of hard x-rays: polarization effects, L. V. Spencer and Charles Wolff—510
Thermal diffusion constant of HCl, A. Z. Kranz and W. W. Watson—344(A)
Thermal energy relaxation length of Ra-Be neutrons in water, Jay Tittman—256
Discharge of Electricity in Gases (see **Electrical Discharges**)
Disintegration and Excitation of Nucleus (see **Nuclear Reactions**)
Dynamics (see **Mechanics**)

Elasticity and Plasticity
Internal friction of rocksalt single crystals, D. R. Frankl and T. A. Read—351(A)
Plastic deformation in ADP crystals, E. I. Salkovitz and P. L. Smith—350(A)
Propagation of "plastic" wave in material exhibiting strain-rate effect, Robert J. Rubin—346(A)
Electrical Breakdown (see **Dielectrics and Dielectric Properties; Electrical Discharges**)
Electrical Conductivity and Resistance (see also **Semiconductors; Superconductors**)
Capacitance effects in thin conductive films, J. N. Humphrey, Frances L. Lummis, and W. W. Scanlon—111
Conductivity changes in KCl produced by γ and *n* irradiation, C. M. Nelson, R. L. Sproull, and R. S. Caswell—364(A)
Electrical conductivity of magnetite at low temperatures, B. A. Calhoun—374(A)
Electrical conductivity of single crystals of graphite, Ajit Kumar Dutta—187
Extra resistivity due to vacancies in Cu, P. Jongenburger—710(L)
Isothermal annealing effects in irradiated Cu, Albert W. Overhauser—393
Magnetoresistance effect in InSb, G. L. Pearson and M. Tanenbaum—153(L)
Motion of slow electrons in polar crystal, T. D. Lee, F. E. Low, and D. Pines—297; D. Pines, F. E. Low, T. D. Lee, and C. N. Yang—382(A)
Photocurrent space charge build-up and field emission in alkali halide crystals, A. von Hippel, E. P. Gross, J. G. Jelatis, and M. Geller—364(A)
Photoemission from Ag into AgCl, KBr, NaCl, and new bands of photosensitivity in AgCl, M. A. Gilleo—364(A)
Polarization capacitance effects in photoconductors and semiconductors, J. Ross MacDonald—364(A)
Theory of resistance minimum in metals, J. E. Goldman—379(A)
Electrical Discharges
Active nitrogen, S. K. Mitra—516
Active nitrogen, airglow, O. Oldenberg—727
Constriction of high power discharges by intense magnetic field, K. S. W. Champion—387(A)
Current increase at constant amplification factor in steady corona with coaxial cylindrical geometry, Leonard B. Loeb—144
Interaction of microwaves propagated through gaseous discharge plasma, L. Goldstein, J. M. Anderson, and G. L. Clark—151(L)
Ionization probability near threshold for formation of Xe^{++}, Kr^{++}, A^{++}, and Ne^{++}, W. M. Hickam, R. E. Fox, and T. Kjeldaas, Jr.—386(A)
Magnetically self-focusing discharges, Willard H. Bennett—387(A)
Mobility of He molecular ions in He, Sydney Geltman—808
Processes involving ions and metastable atoms in Hg afterglows, Manfred A. Biondi—730
Quenching of afterglow in gaseous discharge plasmas by low power microwaves, L. Goldstein, J. M. Anderson, and G. L. Clark—486(L)
Relative ionization probability of He near threshold, T. Kjeldaas, Jr., W. M. Hickam, and R. E. Fox—386(A)
Vibrational emission spectra in glow discharges, Frank Matossi—359(A)
Electrical Properties (see also **Dielectrics and Dielectric Properties; Electrical Conductivity and Resistance; Semiconductors; Superconductors**)
Adiabatic Hall effect in semiconductors, V. A. Johnson and F. M. Shipley—523
Azimuthal distribution of photoelectrons produced by 0.5-Mev polarized photons, Frank L. Hereford and Jerome P. Keuper—1043
Corrected Fowler-Nordheim field emission functions $v(y)$ and $s(y)$, R. E. Burgess, H. Kroemer, and J. M. Houston—515
Free electron emission in atmosphere, Oleg Yadoff—387(A)
Hall effect in Ti, Georgiana Scovil—337(A)
Photoelectron ejection by 0.51-Mev polarized photons, Frank L. Hereford and Jerome P. Keuper—382(A)
Photo-Hall-voltaic effect, Charles F. Wahlig and Park H. Miller—337(A)
Surface barrier analysis for highly refractory metals by means of Schottky deviations, D. W. Juenker, G. S. Colladay, and E. A. Coomes—772
Temperature dependence of secondary electron emission from Ta, Pt, and graphite, E. J. Sternglass—380(A)

Electrodynamics (see **Electromagnetic Theory and Electrodynamics**)
Electrolysis (see **Chemical Effects and Properties**)
Electromagnetic Theory and Electrodynamics
Conservation laws in classical electrodynamics, Otto Bergmann—315(L)
Diffraction field of circular aperture, G. A. Woonton—385(A)
Diffraction of electromagnetic waves by aperture in infinite screen, G. Bekefi—385(A)
Double-focusing by system of two magnets with nonuniform fields, R. M. Sternheimer—352(A)
e/m for 385-Mev protons, D. J. Grove and J. G. Fox—378(A)
Electron beam interferometer, L. Marton, J. Arol Simpson, and J. A. Suddeth—490(L)
Electron gun, John W. Coleman—386(A)
Generalization of Kirchhoff's theorem to electromagnetic fields, H. E. J. Neugebauer—385(A)
Generalization of new classical electrodynamics, M. Avramy Melvin—357(A)
Guided surface waves on lossy structures, Francis J. Zucker—385(A)
Radiation by electrons in large orbits, Dale R. Corson—748
Transition from classical to quantum interaction between electron and high frequency field, I. R. Senitzky—386(A)
Transverse motion of electron in constant wave speed section of linear accelerator, Ira Jacobs and E. S. Akeley—386(A)
Electron Diffraction (see **Diffraction; Scattering of Electrons and Positrons**)
Electron Optics (see **Electromagnetic Theory and Electrodynamics**)
Electronic Tubes (see **Methods and Instruments**)
Electrons and Positrons (see also **Electromagnetic Theory and Electrodynamics; Elementary Particle Interactions; Scattering of Electrons and Positrons**)
Allowed final states for annihilation into 3 photons, F. G. Fumi and L. Wolfenstein—498(L)
Direct comparison of m/e for positron and electron, L. A. Page, P. Stehle, and S. B. Gunst—377(A)
Energy loss of positrons and electrons, F. Rohrlich and B. C. Carlson—378(A)
Exchange potential in electron gas at nonzero temperature, Harold Zirin—795
Internal pair production of γ-rays of mesonic origin: Alternate models of π^0 decay, J. Steinberger, A. Sachs, and P. Lindenfeld—343(A)
Positronium chloride, Lennart Simons—165(L)
Time distribution of positron annihilation in liquids and solids, R. E. Bell and R. L. Graham—644
Total Compton and pair production cross sections at 19.5 Mev, Arthur I. Berman—210
Electrons, Mobility (see **Ions and Electrons, Mobility**)
Electrons, Scattering of (see **Scattering of Electrons and Positrons**)
Electrons, Secondary (see **Electrical Properties**)
Electrons, Thermionic (see **Electrical Properties**)
Electro-Optical Effects (see **Optical Properties**)
Electrostriction (see **Dielectrics and Dielectric Properties**)
Elementary Particle Interactions
Absorption of π^- mesons in H, C. P. Sargent and M. C. Rinehart—343(A)
Charge exchange scattering of 40-Mev π mesons in H and D, A. Roberts, W. Spry, and J. Tinlot—343(A)
Covariant meson-nucleon equation, Stanley Deser and Paul C. Martin—1075
Differential cross section for elastic p-p scattering at 435 Mev, W. E. Mott, R. B. Sutton, J. G. Fox, and J. A. Kane—712(L)
Differential cross section for scattering of 58-Mev π^+ mesons in H, D. Bodansky, A. Sachs, and J. Steinberger—996(L)
Effect of short-range repulsion on low energy singlet nucleon-nucleon scattering, M. H. Hull, Jr., and A. Herschman—482
Elementary particle structure, Roger E. Clapp—356(A)
Energy of nucleon-nucleon collisions, R. G. Glasser and Marcel Schein—218
Evidence for direct meson-meson interaction, A. N. Mitra and F. J. Dyson—372(A)
Fermi's theory of nucleon collisions and zero-point energy of pions, F. C. Auluck and D. S. Kothari—1002(L)
Fourth-order corrections to scattering of pions by nonrelativistic nucleons, J. S. Blair and G. F. Chew—1065
High energy nucleon scattering and isobars, R. B. Raphael and J. Schwinger—373(A)
Interaction of 14-Mev neutrons with protons and deuterons, A. H. Armstrong, J. C. Allred, and L. Rosen—340(A)
Meson-nucleon scattering, Robert Karplus, Margaret Kivelson, and Paul C. Martin—1072
Meson-proton scattering, theoretical analysis, F. J. Dyson, S. S. Schweber, and W. M. Visscher—372(A); M. K. Sundaresan, E. E. Salpeter, and M. M. Ross—372(A)
Multiple meson production observed with high pressure hydrogen-filled cloud chamber, Osamu Kusumoto, Saburo Miyake, Koichi Suga, and Yuzuru Watase—998(L)
n-e interaction, D. J. Hughes, J. A. Harvey, M. D. Goldberg, and Marilyn J. Stafne—497(L)
n-p scattering near 180° at 94 Mev, W. Selove, K. Strauch, and F. Titus—339(A)
Nuclear forces from pseudoscalar meson theory, M. Ruderman—183
Orbital effect in neutron-electron magnetic scattering, W. H. Kleiner—168(L)
p-p scattering, H. H. Hall and J. L. Powell—912
p-p scattering at 32.0 Mev, Bruce Cork—1129(L)
p-p scattering at 435 Mev, W. E. Mott and R. B. Sutton—339(A)
p-p scattering from 1.8 to 4.2 Mev, H. R. Worthington, J. N. McGruer, and D. E. Findley—899
p-p scattering in interference minimum region, D. I. Cooper, D. H. Frisch, and R. L. Zimmerman—339(A)
Phase-shift analysis of scattering of positive mesons at 58 Mev, D. Bodansky, A. M. Sachs, and J. Steinberger—997(L)
Positive pion scattering in H, Gerson Goldhaber and Leon Lederman—343(A)
Positron-electron scattering at 1.3 Mev, Horace A. Howe and K. R. MacKenzie—678
Recoil effects in meson-nucleon scattering, E. M. Henley and M. A. Ruderman—719(L)
Scattering of slow neutrons by ortho- and para-hydrogen, A. T. Stewart and G. L. Squires—1125(L)
Sign of phase shifts in meson-nucleon scattering, H. A. Bethe—994(L)
Spectrum of γ-radiation emitted in reaction $n+p \rightarrow d+\gamma$, A. Bracci, U. Facchini, and A. Malvincene—162(L)
Tamm-Dancoff formalism and symmetric pseudoscalar theory of nuclear forces, Abraham Klein—1101
Thermal neutron capture cross section of H, B. Hamermesh, G. R. Ringo, and S. Wexler—603

Elementary Particle Interactions (Continued)
Variational calculation of high-energy scattering by Yukawa potential, David S. Saxon and E. Gerjuoy—373(A)
Variational principle for n-p scattering with tensor forces, L. C. Biedenharn and John M. Blatt—365(A)
Elements (see **Atomic Mass and Abundance**)
Energy Loss of Particles (see **Range and Energy Loss of Particles**)
Energy States of Atoms (see **Atomic Structure and Spectra**)
Energy States of Molecules (see **Molecular Structure and Spectra**)
Energy States of Nucleus (see **Nuclear Reactions; Nuclear Spectra; Nuclear Structure Theory**)
Equations of State (see **Chemical Effects and Properties**)
Errata
Abundances of elements, Harold C. Urey—1131(E)
Activation cross sections for 14-Mev neutrons, Stuart G. Forbes—1131(E)
Conversion of amplified Dirac equation to approximately relativistic form, W. A. Barker and Z. V. Chraplyvy—1131(E)
Impurity diffusion and space charge layers in "fused-impurity" p-n junctions, John S. Saby and W. C. Dunlap, Jr.—1131(E)
Macroscopic theory of superfluid He^3-He^4 mixtures, P. J. Price—1131(E)
Nuclear mass determinations from disintegration energies: O to S, C. W. Li—1131(E)
Response of organic scintillation crystals to short-range particles, J. B. Birks—1131(E)
Spherical model of a ferromagnet, H. W. Lewis and G. H. Wannier—1131(E)
Third Rydberg series of N_2, R. Edwin Worley—1131(E)
Errors of Measurement (see **Methods and Instruments**)
Evaporation (see **Liquids**)
Excitation of Atoms (see **Atomic Structure and Spectra**)
Excitation of Molecules (see **Molecular Structure and Spectra**)
Excitation of Nucleus (see **Nuclear Reactions; Nuclear Spectra; Nuclear Structure Theory**)
Explosion Phenomena (see **Fluid Dynamics**)

Faraday Effect (see **Optical Properties**)
Ferroelectric Phenomena (see **Dielectrics and Dielectric Properties**)
Ferromagnetism (see **Magnetic Properties**)
Field Emission (see **Electrical Properties**)
Field Theory (see also **Quantum Electrodynamics**)
Conservation laws in classical electrodynamics, Otto Bergmann—315(L)
Construction of potentials in quantum field theory, K. A. Brueckner and K. M. Watson—699
Damping of virtual nucleon-pair formation in pseudoscalar meson theory, K. A. Brueckner—476
Exact interaction of scalar and electrostatic fields, Robert L. Pease and Jane S. Pease—371(A)
Fourth-order corrections to scattering of pions by non-relativistic nucleons, J. S. Blair and G. F. Chew—1065
Generalization of new classical electrodynamics, M. Avramy Melvin—357(A)
Generalized method of field quantization, H. S. Green—270
Nuclear forces from pseudoscalar meson theory, M. Ruderman—183
Pair production by curved metric, Bryce S. DeWitt—357(A)
Poles of S matrix for nuclear reactions, Marcos Moshinsky—365(A)
Self-consistency of Lagrangian quantization, Peter G. Bergmann—357(A)
Spherically symmetric solutions in nonsymmetrical field theories. I. Skew symmetric tensor, P. C. Vaidya—695
Spin and statistics of general-relativistic Dirac field, Robb M. Thompson and Peter G. Bergmann—357(A)
Use of functionals in evaluating S matrix, James L. Anderson—373(A)
Use of Tamm-Dancoff method in field theory, Freeman J. Dyson—994(L)
Films, Properties
Capacitance effects in thin conductive films, J. N. Humphrey, Frances L. Lummis, and W. W. Scanlon—111
Soft x-ray absorption of Fe and Fe_2O_3, D. E. Carter and M. P. Givens—379(A)
Thermodynamics of He film, O. K. Rice and Benjamin Widom—987(L)
Fine Structure (see **Atomic Structure and Spectra**)
Fission of Nucleus (see **Nuclear Fission**)
Fluctuation Phenomena (see **Noise**)
Fluid Dynamics
Acoustical radiation from velocity field in compressible fluid, Eugene N. Parker—240
Blasius and Weyl constants in boundary layer theory, Daniel Shanks—377(A)
Boundary layer on spinning axisymmetric bodies, Arthur N. Tifford and Sheng To Chu—377(A)
Discrete transitions in thermal turbulence, Willem V. R. Malkus—376(A)
Extension of Heisenberg's model of turbulence to critical Reynold's numbers, Eugene N. Parker—221
Moment method solution of Boltzmann equation for rough sphere molecular model, Philip M. Mostov, Harold Grad, and Sidney Borowitz—376(A)
Propagation of turbulence into irrotational flow, S. Corrsin—376(A)
Stability of limiting case of plane Couette flow, B. Zondek and L. H. Thomas—738
Statistical mechanics of irreversible processes in fluids, Melville S. Green—376(A)
Theory of nonhomogeneous turbulence, Jack Heller—376(A)
Transfer processes in isotropic turbulence, C. M. Tchen—376(A)
Transonic flow past wedge profiles, E. V. Laitone and Helmer Nielsen—375(A)
Variation with time of flow variables in shock tube, R. J. Emrich, J. E. Mack, and R. A. Shunk—375(A)
Fluorescence (see **Luminescence**)
Friction (see **Mechanics**)

Galvanomagnetic Effect (see **Magnetic Properties**)
Gamma-Rays (see also **Nuclear Reactions; Nuclear Spectra**)
γ-ray reflections from (550) and (310) planes of quartz, Harry C. Hoyt, Joseph J. Murray, and Jesse W. M. DuMond—169(L)
Gases
Gas adsorption on (100) faces of Cu and Ni crystals studied by low speed electron diffraction, Robert E. Schlier and H. E. Farnsworth—351(A)
Geophysics
Absorption line-width in infrared spectrum of atmospheric CO_2, Arthur Adel—1024
Abundance of elements, erratum, Harold C. Urey—1131(E)

Continuous layer formation in atmosphere under influence of solar radiation, H. K. Kallmann—153(L)
Formation of *D*-layer, K. Watanabe, Frederick Marmo, and Edward C. Y. Inn—155(L)
Isotopic constitution of Si, Ge, and Hf, John H. Reynolds —1047
OH in airglow at high latitudes, Joseph W. Chamberlain and Norman J. Oliver—1118(L)
Techniques in isotopic abundance measurements in elements of Group IV, J. H. Reynolds and T. J. Ypsilantis —378(A)

Glasses (see **Molecular Aggregates**)
Gravitation (see **Relativity and Gravitation**)
Gyromagnetization (see **Magnetic Properties**)

Hall Effect (see **Electrical Conductivity and Resistance**)
Heat Capacity (see **Thermal Properties**)
Heat Conduction (see **Thermal Properties**)
Heat of Dissociation and Formation (see **Molecular Structure and Spectra**)
Heat of Fusion (see **Thermal Properties**)
Heat of Vaporization (see **Thermal Properties**)
Helium, Liquid
Cluster theory of saturated vapor pressure of He isotope mixtures, William Band and Raymond A. Nelson—744
Fountain effect in He II below 1°K, G. J. C. Bots and C. J. Gorter—1117(L)
He II film transport rates over various surfaces, B. Smith and H. A. Boorse—156(L)
Heat pulses in He II between 0.1°K and 1.0°K, H. C. Kramers, F. A. W. van den Burg, and C. J. Gorter—1117(L)
λ-transition in liquid He, R. P. Feynman—1116(L)
Macroscopic theory of superfluid He^3-He^4 mixtures, erratum, P. J. Price—1131(E)
Nuclear alignment and entropy of liquid He^3, Bernard M. Abraham, Darrell W. Osborne, and Bernard Weinstock —347(A)
Second sound velocity in mixtures of He^3-He^4, J. C. King and Henry A. Fairbank—347(A); 989(L)
Thermodynamics of He film, O. K. Rice and Benjamin Widom—987(L)
Transfer rate of liquid He II film near zero level difference, Gerald S. Picus—719(L)
High Voltage Tubes and Machines (see **Methods and Instruments**)
Hydrodynamics (see **Fluid Dynamics**)
Hyperfine Structure (see **Atomic Structure and Spectra; Molecular Structure and Spectra; Nuclear Moments and Spin**)

Imperfections in Solids (see also **Crystalline State; Electrical Conductivity and Resistance; Luminescence; Semiconductors**)
Additive coloration of single crystals of BaO, William C. Dash—352(A)
Annealing of bombardment damage in solids, W. L. Brown, R. C. Fletcher, and S. Machlup—709(L)
Color centers and trapped charge in KCl and KBr, David Dutton and Robert Maurer—126
Conductivity changes in KCl produced by γ and n irradiation, C. M. Nelson, R. L. Sproull, and R. S. Caswell—364(A)
Equations of motion of dislocation, J. D. Eshelby—248
Extra resistivity due to vacancies in Cu, P. Jongenburger —710(L)
Internal friction of rocksalt single crystals, D. R. Frankl and T. A. Read—351(A)
Isothermal annealing effects in irradiated Cu, Albert W. Overhauser—393
Magnetic susceptibility of colored KCl from 1°K to 300°K, C. V. Heer and C. Rauch—530
O vacancies in BaO crystals, R. L. Sproull and R. S. Bever—352(A)
Observations of dislocations in lineage boundaries in Ge, F. L. Vogel, W. G. Pfann, H. E. Corey, and E. E. Thomas—489(L)
Photocurrent space charge build-up and field emission in alkali halide crystals, A. von Hippel, E. P. Gross, J. G. Jelatis, and M. Geller—364(A)
Polarization capacitance effects in photoconductors and semiconductors, J. Ross MacDonald—364(A)
Solute distribution in Ge crystals, W. P. Slichter and E. D. Kolb—987(L)
Space charge layer and distribution of lattice defects at surface of ionic crystals, Kurt Lehovec—350(A)
Inelastic Scattering (see **Nuclear Reactions; Scattering**)
Instruments (see **Methods and Instruments**)
Internal Conversion (see **Nuclear Spectra**)
Ionization (see also **Electrical Discharges; Range and Energy Loss of Particles**)
α-particle ionization in pure gases and average energy to make ion pair, William P. Jesse and John Sadauskis—1120(L)
Ionization probability near threshold for formation of Xe^{++}, Kr^{++}, A^{++}, and Ne^{++}, W. M. Hickam, R. E. Fox, and T. Kjeldaas—386(A)
Ratio of plateau to minimum grain density for electrons, R. P. Michaelis and C. E. Violet—723(L)
Relative ionization probability of He near threshold, T. Kjeldaas, Jr., W. M. Hickam, and R. E. Fox—386(A)
Specific primary ionization of H_2, He, Ne, and A by high energy electrons, Gordon W. McClure—796
Threshold law for single ionization of atoms or ions by electrons, Gregory H. Wannier—817
Ionization Potentials of Atoms (see **Atomic Structure and Spectra**)
Ionization Potentials of Molecules (see **Molecular Structure and Spectra**)
Ionosphere (see **Geophysics**)
Ions (see also **Electrical Discharges**)
Excitation of light by H ions, Ernest J. Dieterich—386(A)
Processes involving ions and metastable atoms in Hg afterglows, Manfred A. Biondi—730
Scintillation response from NaI(Tl) crystals under bombardment with 60–600 kev positive ions, Samuel K. Allison and Harvey Casson—354(A); 880
Stopping of heavy ions in gases, G. E. Evans, P. M. Stier, and C. F. Barnett—825
Ions and Electrons, Mobility (see also **Semiconductors**)
High field mobility in Ge with impurity scattering dominant, E. M. Conwell—769
Mobility of He molecular ions in He, Sydney Geltman—808
Mobility of holes and electrons in high electric fields, E. J. Ryder—766
Isobars (see **Atomic Mass and Abundance**)
Isomers, Molecular (see **Molecular Structure and Spectra**)
Isomers, Nuclear (see **Nuclear Spectra**)
Isotopes (see **Atomic Mass and Abundance; Radioactivity**)

Kerr Effect (see **Optical Properties**)
Kinetic Theory of Gases (see **Gases**)

Liquid Helium (see **Helium, Liquid**)
Liquids
Methods for advancing subject of liquid, George Antonoff —385(A)

Luminescence
α-particle induced phosphorescence of Ag-activated NaCl, C. E. Mandeville and H. O. Albrecht—25; 364(A)
Dielectric changes of electroluminescent phosphor during illumination, Shepard Roberts—364(A)
Electronic transitions in luminescence of ZnS phosphors, Richard H. Bube—70
Influence of electric fields on luminescence, Sol Nudelman and Frank Matossi—363(A)
Luminescence of divalent Mn in solids, Clifford C. Klick and James H. Schulman—363(A)
Mechanism of phosphorescence in crystal phosphors, Daniel Curie—154(L)
Phosphorescence in thoria, C. E. Mandeville and H. O. Albrecht—992(L)
Response of NaI(Tl), Ki(Tl), and stilbene phosphors to fission fragments, J. C. D. Milton and J. S. Fraser—388(A)
Response of organic scintillation crystals to short-range particles, erratum, J. B. Birks—1131(E)
Surface effect of NaI scintillators, E. der Mateosian and Luke C. L. Yuan—868

Magnetic Fields (see **Electromagnetic Theory and Electrodynamics**)

Magnetic Properties
Anomalous behavior of g factor of LiFeCr spinels as function of temperature, J. S. van Wieringen—488(L)
Cyclic adiabatic demagnetization, S. C. Collins and F. J. Zimmerman—991(L)
Deflection of high energy electrons in magnetized Fe, Stephen Berko and Frank L. Hereford—341(A)
Deviations from Brillouin's free-spin theory in $MnSiF_6 \cdot 6H_2O$, R. C. O'Rourke—786
Double hysteresis loop of $BaTiO_3$ at Curie point, Walter J. Merz—375(A)
Effect of boundary states on free electron diamagnetism, Frank Ham and Harvey Brooks—383(A)
Electrical conductivity of magnetite at low temperatures, B. A. Calhoun—374(A)
Gyromagnetic ratios of microcrystalline and macrocrystalline materials, S. J. Barnett—315(L)
Improved spherical treatment of Ising model, Alfred Levitas and Melvin Lax—374(A)
Magnetic saturation and apparent molecular fields of $MnCl_2 \cdot 4H_2O$, Warren E. Henry—492(L)
Magnetic structure transitions, J. Samuel Smart—55
Magnetic susceptibilities of Hf, Gd, and Mn, C. J. Kriessman and T. R. McGuire—374(A)
Magnetic susceptibility and x-ray diffraction measurements of VO and TiO, T. R. McGuire and Selma Greenwald—373(A)
Magnetic susceptibility of colored KCl from 1°K to 300°K, C. V. Heer and C. Rauch—530
Neutron diffraction studies of antiferromagnetism in MnF_2 and some isomorphous compounds, R. A. Erickson—779
Neutron diffraction studies on various ferromagnetic alloys, M. K. Wilkinson and C. G. Shull—374(A)
Paramagnetic effect in superconductors, Tom S. Teasdale and H. E. Rorschach, Jr.—709(L)
Reversal of spontaneous magnetization as function of temperature in LiFeCr spinels, E. W. Gorter and J. A. Schulkes—487(L)
Specific heats of ferrites, J. Samuel Smart—374(A)
Spherical model of a ferromagnet, erratum, H. W. Lewis and G. H. Wannier—1131(E)
Transition temperatures for spherical model ferromagnets, Melvin Lax—374(A)

Magnetic Resonance Absorption (see also **Nuclear Moments and Spin**)
Anomalous magnetic resonance absorption of Cu acetate at 40 kMc/sec, Hidetaro Abe and Junji Shimada—316(L)
Atomic beam magnetic resonance experiments on He^3, Gabriel Weinreich and Vernon W. Hughes—377(A)
Dipolar broadening of magnetic resonance lines in magnetically-diluted crystals, C. Kittel and Elihu Abrahams—238
Electron spin resonance in Si semiconductor, A. M. Portis, A. F. Kip, C. Kittel, and W. H. Brattain—988(L)
Energy absorption in ferromagnetic resonance, J. A. Young, Jr., and Edwin A. Uehling—990(L)
High resolution of nuclear resonance signals in flowing samples, A. L. Bloom and J. N. Shoolery—358(A)
Indirect interaction between nuclear spins in Cu acetate, A. Abragam—358(A)
Line width in pure quadrupole resonance experiments in crystals, K. Kambe and A. Abragam—348(A)
Nuclear magnetic resonance measurements of Se, H. E. Walchli—331(L)
Nuclear quadrupole coupling in solids, M. H. Cohen—348(A)
Nuclear quadrupole resonances in Br and I compounds, A. L. Schawlow—348(A)
Nuclear quadrupole transitions in paradibromobenzene, Edward Manring, Carlton Brown, and Dudley Williams—348(A)
Nuclear rf spectra of D_2 and H_2 in intermediate and strong magnetic fields, N. J. Harrick, R. G. Barnes, P. J. Bray, and N. F. Ramsey—260
Paramagnetic resonance in Mn formate, D. J. E. Ingram—711(L)
Pure quadrupole spectra of HCl and DCl, H. C. Meal and H. C. Allen, Jr.—348(A)
Saturation effects in paramagnetic resonance absorption and spin-lattice relaxation time, A. H. Eschenfelder and R. T. Weidner—358(A)
Temperature dependence of ferromagnetic resonance in (Ni-Fe) alloy, J. A. Cowen and R. D. Spence—359(A)

Magneto-Optical Effects (see **Optical Properties**)

Magnetoresistance (see **Electrical Conductivity and Resistance**)

Magnetostriction (see **Magnetic Properties**)

Mass Defects (see **Atomic Mass and Abundance**)

Mass Spectroscopy (see **Atomic Mass and Abundance; Methods and Instruments**)

Mathematical Methods
Movable critical points of nonlinear wave equation, T. Tietz—495(L)
Vector addition coefficient identity, R. L. Guernsey and G. B. Arfken—1132(A)

Measurements (see **Methods and Instruments**)

Mechanics

Mechanics, Quantum—Atomic Structure and Spectra (see **Atomic Structure and Spectra**)

Mechanics, Quantum—General (see **Quantum Mechanics**)

Mechanics, Quantum—Molecular Structure and Spectra (see **Molecular Structure and Spectra**)

Mechanics, Quantum—Nuclear (see **Nuclear Structure Theory**)

Mechanics, Quantum—of Solid Bodies (see **Crystalline State**)

Mechanics, Statistical (see **Statistical Mechanics and Thermodynamics**)

Meson Field Theory (see **Field Theory**)

Mesons (see also **Cosmic Radiation; Elementary Particle Interactions; Nuclear Reactions Induced by Mesons; Scattering of Mesons**)
Analysis of photomeson production data, B. T. Feld—342(A)
Asymptotic behavior and differential equation of meson wave function, H. A. Bethe and F. J. Dyson—372(A)
Cloud chamber observations of heavy charged unstable particles in cosmic rays, H. S. Bridge, C. Peyrou, B. Rossi, and R. Safford—921; R. Safford, C. Peyrou, and B. Rossi—369(A)
Disintegration of V^0 particles, R. W. Thompson, A. V. Buskirk, L. R. Etter, C. J. Karzmark, and R. H. Rediker—329(L)
Double meson photoproduction, R. D. Lawson and S. D. Drell—326(L)
Excitation curve for photomesons from Be, David Luckey—711(L)
Families of fundamental particles, M. Goldhaber—369(A)
Fermi's theory of nucleon collisions and zero-point energy of pions, F. C. Auluck and D. S. Kothari—1002(L)
Heavy V^+ particle, C. M. York, R. B. Leighton, and E. K. Bjornerud—167(L)
Inner bremsstrahlung in μ-decay, A. Lenard—372(A); 968
Interactions of μ-mesons, W. D. Walker—234
Internal pair production of γ-rays of mesonic origin: Alternate modes of π^0 decay, J. Steinberger, A. Sachs, nd P. Lindenfeld—343(A)
K mesons, J. Crussard, L. Leprince-Ringuet, D. Morellet, A. Orkin-Lecourtois, and J. Trembley—1127(L)
Mass of cosmic-ray mesons at mountain altitudes, Guilio Ascoli—1079
Mean lifetimes of V-particles and heavy mesons, W. L. Alford and R. B. Leighton—622
Muon range spectrum from $\pi \rightarrow \mu$ decay, A. M. Seifert, H. J. Bramson, and W. W. Havens, Jr.—349(A)
Multiple meson production observed with high pressure hydrogen-filled cloud chambers, Osamu Kusumoto, Saburo Miyake, Koichi Suga, and Yuzuru Watase—998(L)
New magnet chamber for study of V particles, A. V. Buskirk, H. O. Cohn, L. R. Etter, C. J. Karzmark, R. H. Rediker, and R. W. Thompson—369(A)
Photomesons from H, R. M. Littauer, A. M. Perry, and W. M. Woodward—342(A)
Photoproduction of neutral mesons in H, Y. Goldschmidt-Clermont, L. S. Osborne, and M. B. Scott—350(A)
Photoproduction of π^+ mesons from H, G. S. Janes and W. L. Kraushaar—341(A)
$\pi^\pm$ meson production cross sections from C by 341-Mev protons, Walter F. Dudziak—342(A)
Pion production ratios by proton bombardment, Ryokichi Sagane—1003(L)
Production of heavy mesons, L. S. Kothari—1087
Production of μ-mesons and their behavior in nuclear emulsions, Dora F. Sherman—469
Range distribution of μ-mesons from π-meson decay in photographic emulsions, W. F. Fry and George R. White—207; George R. White and W. F. Fry—349(A)
Search for V^0 particles produced by 450-Mev protons, R. L. Garwin—274
Spin orbit coupling and mesonic Lamb shift, R. Chisholm and B. Touschek—763
Tensor operators in isotopic spin space, L. Wolfenstein—371(A)
Unstable particles from penetrating showers, W. D. Walker and N. M. Duller—320(L)
V^0 decay, unusual example, R. W. Thompson, A. V. Buskirk, L. R. Etter, C. J. Karzmark, and R. H. Rediker—1122(L)
V^0 particles, C. Peyrou, R. Safford, and H. Bridge—368(A)
V^0 particles produced at Cosmotron, W. B. Fowler, R. P. Shutt, A. M. Thorndike, and W. L. Whittemore—1126(L)
Metals (see **Crystalline State**)
Metastable Atoms (see **Atomic Structure and Spectra**)
Metastable Molecules (see **Molecular Structure and Spectra**)
Meteorology (see **Geophysics**)
Methods and Instruments
Accuracy of time measurements by delayed coincidences, H. Kanner, Z. Bay, and V. P. Henri—371(A)
Analyzing magnet, R. F. Mozley and H. Bichsel—354(A)
Apparatus for measuring thermal conductivity of metals in vacuum at high temperatures, Marvin Moskowitz—379(A)
Bi-directional electronic counter for use in optical interferometry, Franklin H. Branin, Jr.—345(A)
Cyclic adiabatic demagnetization, S. C. Collins and F. J. Zimmerman—991(L)
Double-focusing by system of two magnets with nonuniform fields, R. M. Sternheimer—352(A)
Electron beam interferometer, L. Marton, J. Arol Simpson, and J. A. Suddeth—490(L)
Electron gun, John W. Coleman—386(A)
Fade-time of Rayleigh distributed random function, L. M. Spetner—346(A)
Fast neutron film dosimeter, J. S. Cheka—353(A)
Fast triple coincidence circuit, Francis M. Pipkin, Scott M. Daubin, Aaron Lemonick, and Donald R. Hamilton—353(A)
γ-ray reflections from (550) and (310) planes of quartz, Harry C. Hoyt, Joseph J. Murray, and Jesse W. M. DuMond—169(L)
Grain density in nuclear emulsions, Laurie M. Brown—95
Gray wedge time-delay analyzer, A. W. Schardt, W. Bernstein, and R. L. Chase—353(A)
Large liquid scintillation detectors, C. L. Cowan, Jr., F. Reines, F. B. Harrison, E. C. Anderson, and F. N. Hayes—493(L)
Low frequency oscillator, circular sweep generator, and direct reading phase measuring instrument, S. Lees, W. D. Green, and E. T. Colton—346(A)
Magnetic field cloud chamber for studying nuclear interactions in cosmic radiation, J. Ballam, D. R. Harris, A. L. Hodson, R. Ronald Rau, G. T. Reynolds, and Marcello Vidale—369(A); R. Ronald Rau, Marcello Vidale, G. T. Reynolds, D. R. Harris, A. L. Hodson, and J. Ballam—369(A)
Measurement of γ-ray spectra using three-crystal pair spectrometer, H. I. West and L. G. Mann—370(A)
Meteorites as cosmic-ray meters, S. F. Singer—168(L)
Method for absolute neutron source calibration, M. F. Crouch and D. E. Diller—361(A)
Method for measuring the half-lives of positron emitters, Donald W. Green, J. C. Harris, and John M. Cooper—1132(A)
Methods of analysis of slow neutron transmission data in neighborhood of nuclear energy levels, Edward Melkonian—362(A)
Methods of measuring specific heats at very low temperatures, D. H. Howling, E. Mendoza, and J. E. Zimmerman—347(A)
Neutron resonance energy measurements with Brookhaven crystal spectrometer, H. H. Landon, V. L. Sailor, and H. L. Foote, Jr.—363(A)
Neutron resonance measurements with Brookhaven fast chopper, D. J. Hughes, F. G. P. Seidl, H. Palevsky, and J. S. Levin—363(A)

Methods and Instruments (Continued)
Neutron resonances in Ag, Th, and Mn, J. S. Levin, W. Y. Kato, N. G. Sjostrand, and D. J. Hughes—363(A)
New magnet chamber for study of V particles, A. V. Buskirk, H. O. Cohn, L. R. Etter, C. J. Karzmark, R. H. Rediker, and R. W. Thompson—369(A)
Non-uniform track shrinkage in nuclear emulsions, John R. Horan—717(L)
Pulsed source of fast neutrons, J. E. Draper and B. D. McDaniel—362(A)
Ratio of plateau to minimum grain density for electrons, R. P. Michaelis and C. E. Violet—723(L)
Response of NaI(Tl), KI(Tl), and stilbene phosphors to fission fragments, J. C. D. Milton and J. S. Fraser—388(A)
Response of organic scintillation crystals to short-range particles, erratum, J. B. Birks—1131(E)
Response of pulsed Geiger tube, Herbert B. Rosenstock—352(A)
Ross filter design for x-ray scattering experiments, W. L. Gordon and J. A. Soules—346(A)
Rotating condenser for synchrocyclotron oscillator, Martyn H. Foss—353(A)
Scintillation response from NaI(Tl) crystals under bombardment with 60-600 kev positive ions, Samuel K. Allison and Harvey Casson—354(A); 880
Single crystal high temperature heater for x-ray spectrometer, R. Lefker, A. deBretteville, Jr., and J. S. Dodd—345(A)
Surface effect of NaI scintillators, E. der Mateosian and Luke C. L. Yuan—868
Techniques in isotopic abundance measurements on elements of Group IV, J. H. Reynolds and T. J. Ypsilantis—378(A)
10-kC Co^{60} source, W. W. Meinke, E. W. Coleman, J. V. Nehemias, and L. E. Brownell—353(A)
Versatile coincidence gray wedge pulse-height analyzer, R. L. Chase, W. Bernstein, and A. W. Schardt—353(A)
Microwaves (see also **Atomic Structure and Spectra; Magnetic Resonance Absorption; Molecular Structure and Spectra; Nuclear Moments and Spin**)
Influence of magnetic field on microwave dielectric constant of liquid crystals, E. F. Carr and R. D. Spence—339(A)
Interaction of microwaves propagated through gaseous discharge plasma, L. Goldstein, J. M. Anderson, and G. L. Clark—151(L)
One to two mm wave spectroscopy, William C. King and Walter Gordy—319(L)
Miscellaneous
Concept of physical object, Jerome Rothstein—356(A)
Kinds of energy, John Q. Stewart—356(A)
Mobility of Ions and Electrons (see **Ions and Electrons, Mobility**)
Molecular Aggregates
Scattering of light from polymer films, Richard Stein and John J. Keane—384(A)
Statistics of stiff chains, J. J. Hermans and Robert Ullman—384(A)
Structure of SiO_2 and B_2O_3 glasses compacted by very high pressures, Ivan Simon—350(A)
Molecular Beams (see **Atomic and Molecular Beams**)
Molecular Structure and Spectra
Absorption coefficients of N_2O and CO_2 in vacuum uv, Murray Zelikoff, Edward C. Y. Inn, and K. Watanabe—359(A)
Absorption coefficients of O_2 in vacuum uv, K. Watanabe, Edward C. Y. Inn, and Murray Zelikoff—359(A)
Absorption line-width in infrared spectrum of atmospheric CO_2, Arthur Adel—1024
Active nitrogen, S. K. Mitra—516
Active nitrogen, airglow, O. Oldenberg—727
AlF emission spectrum, S. M. Naude and T. J. Hugo—318(L)
Application of Fermi-Thomas model in computing dipole moment of ICl, Herbert Glazer and Howard Reiss—360(A)
C_5H_5NH microwave analysis, T. E. Turner, Verna C. Fiora, W. M. Kendrick, and B. L. Hicks—338(A)
Classical model for rotational magnetic moments in molecules, C. K. Jen—359(A)
Constants of centrifugal distortion, D. Kivelson and E. B. Wilson, Jr.—338(A)
Excitation of molecular rotation-vibration by electron impact, Philip M. Morse—51
Forces between H_2 molecules, Arthur A. Evett and Henry Margenau—1021
HDO S-band spectrum, S. Weisbaum, Y. Beers, and G. Herrmann—338(A)
Low frequency resonances in spectra of diatomic molecules, R. E. Coté and P. Kusch—103
Nuclear-molecular interactions of Li^7F^{19}, R. Braunstein and J. W. Trischka—348(A)
Nuclear rf spectra of D_2 and H_2 in intermediate and strong magnetic fields, N. J. Harrick, R. G. Barnes, P. J. Bray, and N. F. Ramsey—260
O_2 electronic structure, S. L. Miller, C. H. Townes, and M. Kotani—542
$(O^{18})_2$ and $O^{16}O^{17}$ microwave absorption spectra, S. L. Miller and C. H. Townes—537
OH in airglow at high latitudes, Joseph W. Chamberlain and Norman J. Oliver—1118(L)
One to two mm wave spectroscopy, William C. King and Walter Gordy—319(L)
Pressure broadening of O_2 lines in mm wavelength region, J. O. Artman and J. P. Gordon—338(A)
Pure quadrupole spectra of HCl and DCl, H. C. Meal and H. C. Allen, Jr.—348(A)
Quadrupole moment of Li^7 and dissociation energy of Li_2, Edward G. Harris and Michel A. Melkanoff—585
Quantum theory of spectral line broadening, Stanley Bloom and Henry Margenau—791
Rotational spectrum and molecular structure of $C_2H_5Cl^{35}$, B. P. Dailey—337(A)
SOF_2 microwave spectrum and structure, R. C. Ferguson and E. B. Wilson, Jr.—338(A)
Spin interactions of accelerated nuclei in molecules, Norman F. Ramsey—232; 382(A)
Third Rydberg series of N_2, erratum, R. Edwin Worley—1131(E)
Vibration-rotation band system of OH in near infrared, G. Déjardin, J. Janin, and M. Peyron—359(A)
Vibrational emission spectra in glow discharges, Frank Matossi—359(A)
Vibrational spectrum of chlorotrifluoroethylene, D. E. Mann and N. Acquista—359(A)
Zeeman effect in rotational spectra of asymmetric-rotor molecules, B. F. Burke and M. W. P. Strandberg—303; 338(A)
Moments, Nuclear (see **Nuclear Moments and Spin**)
Moments of Molecules (see **Molecular Structure and Spectra**)

Neutrino (see also **Nuclear Spectra; Radioactivity**)
Evidence for emission of neutrino following nuclear capture of μ^- meson, W. F. Fry—999(L)
Inner bremsstrahlung and magnetic moment of the neutrino, E. J. Hellund—721(L)
Proposed experiment to detect free neutrino, F. Reines and C. L. Cowan, Jr.—492(L)

Neutron Diffraction (see **Diffraction; Scattering of Neutrons**)
Neutrons (see **Elementary Particle Interactions**)
Noise
Quantum effects in noise, J. Weber—357(A)
Quantum theory of damped electrical oscillator and noise, J. Weber—977
Nuclear Fission
Angular distribution of fragments from neutron-induced fission, W. C. Dickinson and J. E. Brolley, Jr.—388(A)
Capture and loss of electrons by fission fragments, George I. Bell—548
Distribution of prompt neutron emission probability for fission fragments of U^{233}, J. S. Fraser and J. C. D. Milton—389(A)
Fission of U with 16-Mev x-rays, Harold G. Richter and Charles D. Coryell—389(A)
Inelastic collision cross sections for fission spectrum neutrons, R. E. Carter and J. R. Beyster—389(A)
Photomesonic fission of Bi, G. Bernardini, R. Reitz, and E. Segrè—573
Production of fissionable isotopes in thermal reactor, Lawrence Baylor Robinson—1054
Response of NaI(Tl), KI(Tl), and stilbene phosphors to fission fragments, J. C. D. Milton and J. S. Fraser—388(A)
Th photofission, Dale M. Hiller and Don S. Martin, Jr.—581
Nuclear Forces (see **Elementary Particle Interactions; Field Theory; Nuclear Structure Theory**)
Nuclear Induction (see **Magnetic Resonance Absorption; Nuclear Moments and Spin**)
Nuclear Isomers (see **Nuclear Spectra; Radioactivity**)
Nuclear Moments and Spin
Ca^{43} spin and magnetic moment, C. D. Jeffries—1130(L)
Effects of departure from single particle model on nuclear magnetic moments, A. de-Shalit—83
Hfs of $3p\ ^2P_{1/2}$ state of Al^{27}, Hin Lew and Günter Wessel—1
Indirect interaction between nuclear spins in Cu acetate, A. Abragam—358(A)
Interaction of electric field gradients and nuclear electric quadrupole moments in angular correlation, Rolf M. Steffen—1119(L)
Line width in pure quadrupole resonance experiments in crystals, K. Kambe and A. Abragam—348(A)
Nuclear molecular interactions of Li^7F^{19}, R. Braunstein and J. W. Trischka—348(A)
Nuclear quadrupole coupling in solids, M. H. Cohen—348(A)
Nuclear quadrupole resonances in Br and I compounds, A. L. Schawlow—348(A)
Nuclear quadrupole transitions in paradibromobenzene, Edward Manring, Carlton Brown, and Dudley Williams—348(A)
Pure quadrupole spectra of HCl and DCl, H. C. Meal and H. C. Allen, Jr.—348(A)
Quadrupole moment of Li^7, Edward G. Harris and Michel A. Melkanoff—585
Quadrupole moment ratio of I^{129} and I^{127} from pure quadrupole spectra, Ralph Livingston and Henry Zeldes—609
Spin interactions of accelerated nuclei in molecules, Norman F. Ramsey—232; 382(A)
Spins of Li^8 and B^{10} in shell model, Nissan Zeldes—416
Nuclear Photoeffects
Analysis of photomeson production data, B. T. Feld—342(A)
Double meson photoproduction, R. D. Lawson and S. D. Drell—326(L)
Excitation curve for photomesons from Be, David Luckey—711(L)
Excitation of 16-μsec state in Ta^{181} by capture of bremsstrahlung, Hugh N. Brown and Robert A. Becker—328(L)
(γ,α) reaction of B^{11} and B^{10}, K. Locher and P. Stoll—164(L)
High energy γ-γ cross section of In^{115}, J. Goldemberg and L. Katz—308
High energy photoproton production, A. Wattenberg, B. T. Feld, and R. D. Godbole—380(A)
Inelastic nuclear scattering of photons by Rh^{103}, C. S. del Rio and Valentine L. Telegdi—439
Mechanism of $O^{16}+h\nu\rightarrow 4He^4$, C. A. Hsiao and V. L. Telegdi—494(L)
Photodisintegration cross section of Be at 2.185 Mev, Bernard Hamermesh and Clyde Kimball—1063
Photodisintegration of the deuteron, Lamek Hulthén and Bengt C. H. Nagel—62
Photomesonic fission of Bi, G. Bernardini, R. Reitz, and E. Segrè—573
Photomesons from H, R. M. Littauer, A. M. Perry, and W. M. Woodward—342(A)
Photoneutron reaction in Ca^{40}, R. Braams and C. L. Smith—995(L)
Photoproduction of neutral mesons in H, Y. Goldschmidt-Clermont, L. S. Osborne, and M. B. Scott—350(A)
Photoproduction of π^+ mesons from H, G. S. Janes and W. L. Kraushaar—341(A)
Photoproduction of protons by monoenergetic 190-Mev γ-rays, J. W. Weil and B. D. McDaniel—380(A)
Radiochemical studies on Th photofission, Dale M. Hiller and Don S. Martin, Jr.—581
Nuclear Reactions, General (see also **Elementary Particle Interactions; Scattering**)
Angular distribution of γ-rays from stripping reactions, G. R. Satchler—722(L)
Coulomb effects in deuteron stripping, N. Austern and S. T. Butler—365(A)
Cross sections for formation of compound nucleus by charged particles, Mathew M. Shapiro—171
Energy of nucleon-nucleon collisions, R. G. Glasser and Marcel Schein—218
Formation of compound nucleus in neutron reactions, Herman Feshbach, Charles E. Porter, and Victor F. Weisskopf—166(L)
Higher spin polarizations in nuclear reactions, Albert Simon—325(L)
Nuclear mass determinations from disintegration energies: Q to S, erratum, C. W. Li—1131(E)
Nuclear reactions involving polarized deuterons, W. Lakin and L. Wolfenstein—365(A)
Poles of S matrix for nuclear reactions, Marcos Moshinsky—365(A)
Production of polarized particles in nuclear reactions, A. Simon and T. A. Welton—1036
Tensor operators in isotopic spin space, L. Wolfenstein—371(A)
Theory of polarized particles in nuclear reactions, Albert Simon—991(L)
Nuclear Reactions Induced by α-Particles (see also **Scattering of α-Particles**)
Ag^{109} (α,n) and $(\alpha,2n)$ cross sections, E. Bleuler, A. K. Stebbins, and D. J. Tendam—460
Energy levels of C^{13} from $Be^9(\alpha,n)C^{13}$, L. E. Beghian, H. H. Halban, T. Husain, and L. G. Sanders—1129(L)
γ-ray resonances in α-particle bombardment of Be and B, F. L. Talbott and N. P. Heydenburg—186
Secondary particles resulting from 375-Mev α-bombardment of nuclei, R. W. Deutsch—499(L)

Nuclear Reactions Induced by Deuterons (see also **Scattering of Deuterons**)
Angular distribution of $He^3(d,p)He^4$ between 240 kev and 3.56 Mev, J. L. Yarnell, R. H. Lovberg, and W. R. Stratton—292
Angular distributions of (d,p) reactions, Clayton F. Black—381(A)
Angular distributions of (d,p) reactions on P^{31}, Cl^{35}, V^{51}, and Sc^{45}, J. S. King and E. H. Beach—381(A)
High energy charged particles from targets bombarded by 190-Mev deuterons, L. Schecter, W. E. Crandall, G. P. Millburn, D. A. Hicks, and A. V. Shelton—633
Inelastic scattering from B^{10}, C. K. Bockelman, C. P. Browne, A. Sperduto, and W. W. Buechner—340(A)
Inelastic scattering from N^{14} and Li^6, C. P. Browne, C. K. Bockelman, W. W. Buechner, and A. Sperduto—340(A)
N^{14} and C^{14} energy levels from deuteron bombardment of C^{13}, R. E. Benenson—420
$Zn^{64}(d,\alpha n)Cu^{63}$, C. Sharp Cook and Fred T. Porter—429
Nuclear Reactions Induced by Mesons (see also **Elementary Particle Interactions; Mesons; Scattering of Mesons**)
Charge exchange scattering of 40-Mev π-mesons in H and D, A. Roberts, W. Spry, and J. Tinlot—343(A)
Evidence for direct meson-meson interaction, A. N. Mitra and F. J. Dyson—372(A)
Evidence for emission of neutrino following nuclear capture of μ-meson, W. F. Fry—999(L)
Interactions of μ-mesons, William D. Walker—349(A)
Interactions of negative pions with Hg, Nathan Sugarman and Agnes Haber—342(A)
Interactions of π^- mesons with I^{127}, Lester Winsberg—343(A)
Low energy π^+ interactions in Be, F. Tenney and J. Tinlot—342(A)
μ-meson capture in nuclei, calculations, J. R. Hugh Dempster—349(A)
μ-meson capture probabilities for intermediate Z elements, A. J. Meyer and J. W. Keuffel—349(A)
Multiplicity of neutrons from interaction of μ^- mesons at rest in Pb, Bi, Sn, and Al, M. Widgoff—891
Nuclear cross sections of π^- and π^+ mesons, M. W. Aarons, J. Ashkin, F. Feiner, J. G. Gorman, and L. Smith—342(A)
Nuclear interactions of 210-Mev π^- mesons in emulsions, A. H. Morrish—674
Pion scattering and absorption cross sections in Pb and C, L. Lederman, H. Byfield, J. Kessler, and K. Rogers—344(A)
Production of high energy photons in pion collisions, J. Kessler, H. Byfield, L. M. Lederman, and K. Rogers—343(A)
Radioactive products of interaction of π^- with As^{75}, A. Turkevich and James B. Niday—342(A)
Total cross sections of 37-Mev pions in H, C. E. Angell and J. P. Perry—724(L)
Nuclear Reactions Induced by Neutrons (see also **Elementary Particle Interactions; Scattering of Neutrons**)
Activation cross sections for 14-Mev neutrons, erratum, Stuart G. Forbes—1131(E)
Analysis of slow neutron transmission data in neighborhood of nuclear energy levels, Edward Melkonian—362(A)
Angular distribution and energy spectrum of charged particles produced by 14-Mev neutrons on Li^6 and Li^7, G. M. Frye and L. Rosen—381(A)
Angular distribution of fragments from neutron-induced fission, W. C. Dickinson and J. E. Brolley, Jr.—388(A)
Angular distribution of $Li^6(n,\alpha)H^3$ for neutrons of 200, 270, 400, and 600 kev, Lillian E. Darlington, Jack Haugsnes, Harry M. Mann, and James H. Roberts—1049
Cross sections for products of 90-Mev neutrons on C, D. A. Kellogg—224
Disintegration of C by fast neutrons, J. David Jackson and D. I. Wanklyn—381(A)
Fast neutron reactions in O and Ne, D. I. Wanklyn—381(A)
γ-radiation from interaction of 14-Mev neutrons with matter, W. R. Faust, V. E. Scherrer, and R. B. Theus—355(A)
γ-rays produced by neutron capture in Cd^{113}, G. A. Bartholomew and B. B. Kinsey—355(A)
Inelastic collision cross sections for fission spectrum neutrons, R. E. Carter and J. R. Beyster—389(A)
Low energy neutron resonance cross sections for Ho, Er, Lu, and Tm, H. L. Foote, Jr., V. L. Sailor, and H. H. Landon—362(A)
Measurements of neutron capture γ-rays with scintillation spectrometer, T. H. Braid—355(A)
Measurements with 390-Mev neutrons, A. J. Hartzler and R. T. Siegel—362(A)
Neutron activation cross section of Pb^{102}, W. Wayne Meinke—410
Neutron activation of Ca^{40}, L. G. Cook and K. D. Shafer—1121(L)
Neutron capture cross section of Em^{222}, A. P. Baerg—1121(L)
Neutron capture cross sections of Nd isotopes, W. H. Walker, and H. G. Thode—447
Neutron resonance energy measurements with Brookhaven crystal spectrometer, H. H. Landon, V. L. Sailor, and H. L. Foote, Jr.—363(A)
Neutron resonance measurements with Brookhaven fast chopper, D. J. Hughes, F. G. P. Seidl, H. Palevsky, and J. S. Levin—363(A)
Neutron resonances in Ag, Th, and Mn, J. S. Levin, W. Y. Kato, N. G. Sjostrand, and D. J. Hughes—363(A)
Prompt γ-rays from slow neutron capture, Henry T. Motz—355(A)
Resonance scattering in In, L. B. Borst—859
Spectrum of γ-radiation emitted in reaction $n+p\rightarrow d+\gamma$, A. Bracci, U. Facchini, and A. Malvicini—162(L)
Stars initiated by neutrons, R. W. Waniek and T. Ohtsuka—355(A)
Thermal neutron capture cross section of H, B. Hamermesh, G. R. Ringo, and S. Wexler—603
Thermal neutron capture cross sections of Pa^{231} and Pa^{233}, R. Elson, P. A. Sellers, and E. R. John—102
Total cross section of He for high energy neutrons, Peter Hillman and R. H. Stahl—362(A)
Total cross sections for 400-Mev neutrons, V. Alexander Nedzel—169(L)
Total cross sections of Cl, Na, Ti, and Br for fast neutrons, H. R. Dvorak and R. N. Little, Jr.—618
Total neutron cross sections of Au, Cl, and P, S. C. Snowdon and W. D. Whitehead—615
Total neutron cross sections of Cl and C, R. M. Kiehn, Clark Goodman, and K. F. Hansen—362(A)
Nuclear Reactions Induced by Protons (see also **Elementary Particle Interactions; Scattering of Protons**)
Angular distribution of deuterons from $Be^9(p,d)Be^8$, B. L. Cohen, E. Newman, T. H. Handley, and A. Timnick—328(L)
Angular distribution of long range α-particles from $F^{19}(p,\alpha)O^{16}$, E. B. Paul, R. L. Clarke, and W. T. Sharp—381(A)

Inelastic scattering from B^{10}, C. K. Bockelman, C. P. Browne, A. Sperduto, and W. W. Buechner—340(A)
Inelastic scattering from N^{14} and Li^6, C. P. Browne, C. K. Bockelman, W. W. Buechner, and A. Sperduto—340(A)
Interactions of 95-Mev protons with D, Li, Be, C, Al, Cu, and Pb nuclei, J. A. Hofmann and K. Strauch—449
Levels in N^{14} from $C^{13}(p,\gamma)N^{14}$, D. Hicks, T. Husain, L. G. Sanders, and L. E. Beghian—163(L)
Multiple meson production observed with high pressure hydrogen filled cloud chamber, Osamu Kusumoto, Saburo Miyake, Koichi Suga, and Yuzuru Watase—998(L)
N^{14} level structure from $C^{13}(p,n)N^{13}$, J. K. Bair, J. D. Kington, and H. B. Willard—575
$\pi^{\pm}$ meson production cross sections from C by 341-Mev protons, Walter F. Dudziak—342(A)
Pion production ratios by proton bombardment, Ryokichi Sagane—1003(L)
Proton-γ angular correlations in $C^{13}(p,p'\gamma)$, H. E. Gove—370(A)
Search for V^0 particles produced by 450-Mev protons, R. L. Garwin—274
Synchrocyclotron production and properties of Mg^{28}, John W. Jones and Truman P. Kohman—495(L)
$T(p,\gamma)$ reaction, J. E. Perry, Jr. and S. J. Bame, Jr.—380(A)
$T(p,n)He^3$ and $T(p,\gamma)He^4$, H. B. Willard, J. K. Bair, and J. D. Kington—865
Nuclear Scattering (see **Scattering**)
Nuclear Spectra (see also **Nuclear Isomers; Nuclear Reactions; Radioactivity**)
Angular correlation of cascade γ-rays from decay of Au^{198}, Carlton D. Schrader, Edward B. Nelson, and James A. Jacobs—159(L)
Angular correlations from liquid sources, R. V. Pound and A. Abragam—993(L)
β-γ polarization correlations, Donald R. Hamilton—370(A)
β-recoil correlation in decay of He^6, Brice M. Rustad and Stanley L. Ruby—370(A)
Continuous γ-radiation accompanying internal conversion in Ba^{137m}, Harry B. Brown and Robert Stump—1061
Cr^{49} decay, Bernd Crasemann and Harry T. Easterday—1124(L)
Cs^{134}, Os^{193}, Os^{191}, and Os^{192} decay, J. M. Cork, J. M. LeBlanc, W. H. Nester, D. W. Martin, and M. K. Brice—444
Cs^{135} β-spectrum, L. Lidofsky, E. Alperovitch, and C. S. Wu—387(A)
Decay of Rh^{104m} (4.3-min) and Rh^{104} (44-sec), W. C. Jordan, J. M. Cork, and S. B. Burson—862
Dy^{157}, Thomas H. Handley and Elmer L. Olson—500(L)
Effect of electric quadrupole interaction on γ-γ directional correlation in Cd^{111}, H. Albers-Schönberg, F. Hänni, E. Heer, T. B. Novey, and P. Scherrer—322(L)
Effect of finite DeBroglie wavelength in theory of β-decay, M. E. Rose and C. L. Terry—479
Energy levels of C^{13} from $Be^9(\alpha,n)C^{13}$, L. E. Beghian, H. H. Halban, T. Husain, and L. G. Sanders—1129(L)
Excitation of 16-sec state in Ta^{181} by capture of bremsstrahlung, Hugh N. Brown and Robert A. Becker—328(L)
Excited states of even-even nuclei, Gertrude Scharff-Goldhaber—587
Extreme single-particle model and β-decay, Henry Brysk—365(A)
First excited states of even-even nuclei, Kenneth W. Ford—29; 366(A)
Ga^{64} and Ga^{65} decay, Bernd Crasemann—995(L)
Ga^{67}, B. H. Ketelle, A. R. Brosi, and F. M. Porter—567
γ-γ directional correlations in Co^{60}, Xe^{131}, and Hg^{198}, D. Schiff and F. R. Metzger—849
γ-radiation from interaction of 14-Mev neutrons with matter, W. R. Faust, V. E. Scherrer, and R. B. Theus—355(A)
γ-ray cascade following decay of Sc^{46}, Charles E. Whittle and Fred T. Porter—498(L)
γ-rays produced by neutron capture in Cd^{113}, G. A. Bartholomew and B. B. Kinsey—353(A)
In^{110} and In^{112} isomerism, E. Bleuler, J. W. Blue, S. A. Chowdary, A. C. Johnson, and J. Tendam—464
Inner bremsstrahlung and ionization of atom accompanying β-decay, F. Boehm and C. S. Wu—369(A)
Inner bremsstrahlung associated with K capture in A^{37}, Carl E. Anderson, George W. Wheeler, and W. W. Watson—606
Interaction of electric field gradients and nuclear electric quadrupole moments in angular correlation, Rolf M. Steffen—1119(L)
Interference terms of electron-neutrino angular correlation, Masato Morita—1005(L)
Internal conversion in Na^{22} and Fe^{59}, G. Hinman, D. Brower, and R. Leamer—370(A)
Ionium γ-ray spectrum, F. Rasetti and E. C. Booth—388(A)
Levels in N^{14} from $C^{13}(p,\gamma)N^{14}$, D. Hicks, T. Husain, L. G. Sanders, and L. E. Beghian—163(L)
Li^8 β-decay, D. StP. Bunbury—1121(L)
Liquid A ionization chamber measurement of shape of β-ray spectrum of K^{40}, John H. Marshall—371(A)
Measurement of γ-ray spectra using three-crystal pair spectrometer, H. I. West and L. G. Mann—370(A)
Measurements of neutron capture γ-rays with scintillation spectrometer, T. H. Braid—355(A)
Mg^{28} γ-rays, John E. May and Bruce P. Foster—243; 340(A)
Mg^{25} β-spectrum, Luis Marquez—330(L)
Mg^{28} decay scheme, R. K. Sheline and N. R. Johnson—325(L)
Mo^{97m} formation and decay, C. W. Forsthoff, R. H. Goeckermann, and R. A. Naumann—1004(L)
N^{14} and C^{14} energy levels from deuteron bombardment of C^{13}, R. E. Benenson—420
N^{14} level structure from $C^{13}(p,n)N^{13}$, J. K. Bair, J. D. Kington, and H. B. Willard—575
Na^{22} high energy positrons, Byron T. Wright—159(L)
Natural Lu^{176} decay scheme, James R. Arnold and Thomas Sugihara—332(L)
Ni^{60}, lifetimes of excited states, Z. Bay, V. P. Henri, and F. McLernon—371(A)
Noncentral force matrix elements for nuclear d^3 configuration, L. W. Longdon—1125(L)
Nuclear double γ-emission, S. A. Moszkowski and V. L. Telegdi—366(A)
O^{14} β-decay and Fermi interaction, M. E. Rose—1123(L)
P^{30} decay scheme, H. Roderick, O. Lönsjö, and W. E. Meyerhof—371(A)
Prompt γ-rays from slow neutron capture, Henry T. Motz—355(A)
Pseudoscalar β-decay and RaE, M. Ruderman—366(A)
Pseudoscalar interaction in theory of β-decay, Tino Ahrens—974
Pt^{191} and Pt^{193m} radioactivity, J. B. Swan, W. M. Portnoy, and R. D. Hill—257
Pu^{242} radiations, D. W. Engelkemeir, P. R. Fields, and J. R. Huizenga—6
RaD and RaE radiations, C. S. Wu, F. Boehm, and E. Nagel—388(A)
RaD electromagnetic spectrum, P. E. Damon and R. R. Edwards—280

Nuclear Spectra (Continued)
Sc^{47} disintegration, L. S. Cheng and M. L. Pool—886
Of Se^{75}, Erling N. Jensen, L. Jackson Laslett, Don S. Martin, Jr., Francis J. Hughes, and William W. Pratt—557
Search for double β-decay in Sn^{124} and Zr^{96}, John A. McCarthy—853
Search for 1-Mev γ from N^{16} decay, F. Boehm, D. C. Peaslee, and V. Perez-Mendez—1119(L)
Search for short-lived nuclear isomers, Theodore C. Engelder—259
Short-lived radioisotopes P^{30} and Cl^{32}, Neel W. Glass, Louis K. Jensen, and J. Reginald Richardson—320(L)
Spectrum of γ-radiation emitted in reaction $n+p \rightarrow d+\gamma$, A. Bracci, U. Facchini, and A. Malvicini—162(L)
Spin and parity of 2.3-Mev excited state of Te^{124}, Franz R. Metzger—328(L)
Spins and parities of excited states in even-even nuclei, Michael J. Glaubman—1000(L); Igal Talmi—1001(L)
Sr^{88}, mixed $E1+M2$ transition and angular momenta, Rolf M. Steffen—321(L)
Synchrocyclotron production and properties of Mg^{28}, John W. Jones and Truman P. Kohman—495(L)
ThC α-γ angular correlation, J. Horton and R. Sherr—388(A)
Theory of directional distribution and polarization of β- and γ-rays emitted by oriented nuclei, H. A. Tolhoek—366(A)
Ti^{51} activity, William R. Hammond, D. N. Kundu, and M. L. Pool—157(L)
Of 24-min Ag^{106}, W. L. Bendel, F. J. Shore, H. N. Brown, and R. A. Becker—888
W^{187} disintegration: Slow $E1$ transition, A. W. Sunyar—387(A)
Y^{91} decay, F. I. Boley and D. S. Dunavan—158(L)
Zr^{95} and Nb^{95} γ-radiation, E. R. Zucker, C. E. Mandeville, E. Shapiro, R. I. Mendenhall, and G. L. Conklin—387(A)
Zr^{95} and Nb^{95} nuclear levels, J. M. Cork, J. M. LeBlanc, D. W. Martin, W. H. Nester, and M. K. Brice—579

Nuclear Structure Theory
Binding energy calculations on He^4 with single particle wave functions, P. G. Wakely—724(L)
Calculation of nuclear binding energies with single-particle oscillator wave-functions, Erwin H. Kronheimer—1003(L)
Collective model of nucleus, John A. Wheeler and David L. Hill—366(A)
Contribution of nuclear distortion to isotope shifts, L. Wilets, D. Hill, and K. W. Ford—366(A)
Effects of departure from single particle model on nuclear magnetic moments, A. de-Shalit—83
Elementary particle structure, Roger E. Clapp—356(A)
First excited states of even-even nuclei, Kenneth W. Ford—29; 366(A)
Geometrical characterization of nuclear states and theory of angular correlations, U. Fano—577
Interference terms of electron-neutrino angular correlation, Masato Morita—1005(L)
Momentum space wave functions. II. Deuteron ground state, E. E. Salpeter and J. S. Goldstein—983
Nuclear double γ-emission, S. A. Moszkowski and V. L. Telegdi—366(A)
Odd-odd spins and j-j coupling, R. W. King and D. C. Peaslee—1001(L)
Polarizability of deuteron, B. J. Malenka, U. E. Kruse, and N. F. Ramsey—365(A)
Pseudoscalar β-decay and RaE, M. Ruderman—366(A)
Relative energy levels of P-shell nuclei in intermediate coupling, Edwin A. Crosbie—138
Rotational states in even-even nuclei, Aage Bohr and Ben R. Mottelson—717(L)
S-wave two-body interaction in nuclei, David H. Frisch—367(A)
Spins and parities of excited states in even-even nuclei, Michael J. Glaubman—1001(L); Igal Talmi—1001(L)
Spins of Li^8 and B^{10} in shell-model, Nissan Zeldes—416

Optical Instruments (see **Methods and Instruments**)
Optical Properties
Bi-directional electronic counter for use in optical interferometry, Franklin H. Branin, Jr.—345(A)
Molar refraction of CO_2 as function of density and age of gas, Clarence Bennett and Victor H. Coffin—344(A)

Pair Production (see **Electrons and Positrons**)
Phosphors and Phosphorescence (see **Luminescence**)
Photoconductivity (see **Electrical Conductivity and Resistance**)
Photodisintegration (see **Nuclear Photoeffects**)
Photoelasticity (see **Elasticity and Plasticity**)
Photoelectric Effect (see **Electrical Properties**)
Photography and Photographic Emulsions (see **Methods and Instruments**)
Photometry (see **Methods and Instruments**)
Photons (see **Radiation**)
Photovoltaic Effect (see **Electrical Properties**)
Piezoelectric Effect (see **Dielectrics and Dielectric Properties**)
Plasmoidal Discharges (see **Electrical Discharges**)
Plasticity (see **Elasticity and Plasticity**)
Polarization, Electrical (see **Dielectrics and Dielectric Properties**)
Polymers (see **Molecular Aggregates**)
Positrons (see **Electrons and Positrons**)
Probability (see **Mathematical Methods**)
Proceedings of the American Physical Society
Annual Meeting, Cambridge, Massachusetts, January 22–24, 1953 [Bull. Am. Phys. Soc. **28**, No. 1 (1953)]—333
Ohio Section Meeting, Ohio State University, Columbus, Ohio, April 24 and 25, 1953—1131
Protons (see **Elementary Particle Interactions**)

Quantum Electrodynamics (see also **Field Theory**)
Absorption of π^- mesons in H, C. P. Sargent and M. C. Rinehart—343(A)
Absorption of slow π^- mesons by He^4 nuclei, Albert G. Petschek—959
Derivation of gauge condition in new electrodynamics, M. Avramy Melvin—389(A)
Fredholm theory of scattering in given time-dependent field, Abdus Salam and P. T. Matthews—690
Lamb shift for spinless electrons, Abraham Klein—372(A)
Non-perturbation approach, S. F. Edwards—284
Polarizability of deuterons, B. J. Malenka, U. E. Kruse, and N. F. Ramsey—365(A)
Radiation of high energy electron in constant magnetic field, Maurice Neuman—682
Radiative corrections to forward Compton scattering, John S. Toll—372(A)
Self-consistency of Lagrangian quantization, Peter G. Bergmann—357(A)
Theory of Lamb shift, T. A. Welton—373(A)
Transition from classical to quantum interaction between electron and high frequency field, I. R. Senitzky—386(A)
Use of functionals in evaluating S matrix, James L. Anderson—373(A)

Quantum Mechanics
Atomic self-consistent fields. I. Calculation of Slater functions, Per-Olov Löwdin—120
Conversion of amplified Dirac equation to approximately relativistic form, erratum, W. A. Barker and Z. V. Chraplyvy—1131(E)
Coordinate operators and fundamental lengths, H. T. Flint and E. Marjorie Williamson—318(L)
Effect of boundary states on free electron diamagnetism, Frank Ham and Harvey Brooks—383(A)
Exchange potential in electron gas at nonzero temperature, Harold Zirin—795
Generalization of WKB method to radial wave equations, R. H. Good, Jr.—131
Movable critical points of nonlinear wave equation, T. Tietz—495(L)
Pines-Bohm theory of many particles with long-range forces, George J. Yevick—383(A)
Quantum effects in noise, J. Weber—357(A)
Quantum theory of damped electrical oscillator and noise, J. Weber—977
Quantum theory of spectral line broadening, Stanley Bloom and Henry Margenau—791
Spin-dependent couplings in many-electron system, W. J. Carr, Jr.—383(A)
Two-electron self-consistent field, A. O. Williams, Jr.—803
Variational approach to uni-potential many-electron problem, R. T. Sharp and G. K. Horton—316(L)
Quenching of Radiation (see **Radiation**)

Radar (see **Methods and Instruments; Radiation**)
Radiation
Acoustical radiation from velocity field in compressible fluid, Eugene N. Parker—240
Continuous layer formation in atmosphere under influence of solar radiation, H. K. Kallmann—153(L)
Excitation of light by H ions, Ernest J. Dieterich—386(A)
Fade-time of Rayleigh distributed random function, L. M. Spetner—346(A)
Gravitational radiation, Joshua N. Goldberg—356(A)
Guided surface waves on lossy structures, Francis J. Zucker—385(A)
Inner bremsstrahlung and ionization of atom accompanying β-decay, F. Boehm and C. S. Wu—369(A)
Inner bremsstrahlung and magnetic moment of neutrino, E. J. Hellund—721(L)
Inner bremsstrahlung associated with K capture in A^{37}, Carl E. Anderson, George W. Wheeler, and W. W. Watson—606
Inner bremsstrahlung in μ-decay, A. Lenard—372(A); 968
Polarization dependence of integrated bremsstrahlung cross section, R. L. Gluckstern and M. H. Hull, Jr.—1030
Polarization of bremsstrahlung radiation, R. L. Gluckstern, M. H. Hull, Jr., and G. Breit—1026
Radiation by electrons in large orbits, Dale R. Corson—748
Radiation emitted by uniformly moving particles, T. Tanaka—358(A)
Radiation of high energy electron in constant magnetic field, Maurice Neuman—682
Radiative corrections to forward Compton scattering, John S. Toll—372(A)
Refractive index corrections for molecular weight determined from light scattering, W. Heller and W. J. Pangonis—345(A)
Scattering of light from polymer films, Richard Stein and John J. Keane—384(A)
Scattering of 1.3[3] Mev γ-rays by electric field, Robert R. Wilson—720(L)
Solid angle corrections for light scattering measurements, W. J. Pangonis and W. Heller—345(A)
Total Compton and pair production cross sections at 19.5 Mev, Arthur I. Berman—210
Transition from classical to quantum interaction between electron and high frequency field, I. R. Senitzky—386(A)
Radio Waves (see **Radiation**)
Radioactivity (see also **Nuclear Spectra**)
A^{39} in pitchblende minerals and nuclear processes in nature, W. H. Fleming and H. G. Thode—857
Accuracy of time measurements by delayed coincidences, H. Kanner, Z. Bay, and V. P. Henri—371(A)
α-branching of AcK and presence of As in nature, Earl K. Hyde and Albert Ghiorso—267
β^- half-life of Pu^{241}, D. R. MacKenzie, M. Lounsbury, and A. W. Boyd—327(L)
Disintegration constant of Be^7 in Be, BeO, and BeF_2, J. J. Kraushaar, Elizabeth D. Wilson, and Kenneth T. Bainbridge—610
Dy^{157}, Thomas H. Handley and Elmer L. Olson—500(L)
Effects of radioactive disintegrations on inner electrons of the atom, J. S. Levinger—11
Ga^{64} and Ga^{66} decay, Bernd Crasemann—995(L)
I^{131} half-life, H. H. Seliger, L. Cavallo, and S. V. Culpepper—443
Influence of chemical state on lifetime of nuclear isomer, Tc^{99m}, Kenneth T. Bainbridge, M. Goldhaber, and Elizabeth Wilson—430
Inner bremsstrahlung and ionization of atom accompanying β-decay, F. Boehm and C. S. Wu—369(A)
Method for measuring the half-lives of positron emitters, Donald W. Green, J. C. Harris, and John N. Cooper—1132(A)
Pd^{109} half-life, W. Wayne Meinke—410
Phosphorescence of thoria, C. E. Mandeville and H. O. Albrecht—992(L)
Search for double β-decay in Sn^{124} and Zr^{96}, John A. McCarthy—853
Search for short-lived nuclear isomers, Theodore C. Engelder—259
Search for Si^{29} in natural Si, A. Turkevich and Althea Tompkins—247
Short-lived radioisotopes P^{28} and Cl^{32}, Neel W. Glass, Louis K. Jensen, and J. Reginald Richardson—320(L)
Synchrocyclotron production and properties of Mg^{28}, John W. Jones and Truman P. Kohman—495(L)
10-kC Co^{60} source, W. W. Meinke, E. W. Coleman, J. V. Nehemias, and L. E. Brownell—353(A)
Ti^{51} activity, William R. Hammond, D. N. Kundu, and M. L. Pool—157(L)
25.5-day Sr—76-sec Rb chain, Paul Kruger and Nathan Sugarman—158(L)
Raman Spectra (see **Molecular Structure and Spectra**)
Range and Energy Loss of Particles (see also **Scattering**)
α-particle ionization in pure gases and average energy to make ion pair, William P. Jesse and John Sadauskis—1120(L)
Biological determination of range of low voltage electrons, Marguerite Davis—384(A)
Capture and loss of electrons by fission fragments, George I. Bell—548
Direct measurement of effect of polarization on energy losses of fast electrons, E. L. Goldwasser, F. E. Mills, and T. R. Rubillard—378(A)
Energy loss distribution of 624-kev electrons in thin foils, B. Hildebrand—378(A)
Energy per ion pair for 5-Mev α-particles in He, T. E. Bortner and G. S. Hurst—160(L)

Range and Energy Loss of Particles (Continued)
Grain density in nuclear emulsions, Laurie M. Brown—95
Of heavy charged particles in gases, Peter K. Weyl—378(A)
Of low energy protons in some gases, James A. Phillips—532
Nonuniform track shrinkage in nuclear emulsions, John R. Horan—717(L)
Photographic study of muon range spectrum from $\pi \rightarrow \mu$ decay, A. M. Seifert, H. J. Bramson, and W. W. Havens, Jr.—349(A)
Of positrons and electrons, F. Rohrlich and B. C. Carlson—378(A)
Of protons in metallic foils and mica, David Kahn—503
Radiative correction for collision loss of heavy particles, V. Z. Jankus—4
Range distribution of μ-mesons from π-meson decay in photographic emulsions, W. F. Fry and George R. White—207; George R. White and W. F. Fry—349(A)
Range of protons in Al, H. Bichsel and R. F. Mozley—354(A)
Ratio of plateau to minimum grain density for electrons, R. P. Michaelis and C. E. Violet—723(L)
Specific primary ionization of H_2, He, Ne, and A by high energy electrons, Gordon W. McClure—796
Stopping of heavy ions in gases, G. E. Evans, P. M. Stier, and C. F. Barnett—825
Transmission of electrons through thin metallic foils, C. H. Chang, C. S. Cook, and H. Primakoff—544
Recombination (see **Molecular Structure and Spectra**)
Rectifiers (see **Electrical Conductivity and Resistance; Semiconductors**)
Relativity and Gravitation
Continuum in special relativity, Boris Leaf—1090
Gravitational radiation, Joshua N. Goldberg—356(A)
Pair production by curved metric, Bryce S. DeWitt—357(A)
Special-relativistic linear theory of gravitation, F. J. Belinfante and J. C. Swihart—357(A)
Spin and statistics of general-relativistic Dirac field, Robb M. Thomson and Peter G. Bergmann—357(A)
Resistance, Electrical (see **Electrical Conductivity and Resistance**)
Resonance Radiation (see **Radiation**)

Scattering, General (see also **Diffraction; Nuclear Reactions; Range and Energy Loss of Particles**)
Adiabatic treatment of slow atomic collisions, W. Kohn—383(A)
Calculation of peaked angular distributions from Legendre polynomial expansions and application to multiple scattering of charged particles, L. V. Spencer—146
Effect of short-range repulsion on low energy singlet nucleon-nucleon scattering, M. H. Hull, Jr., and A. Herschman—482
Energy of nucleon-nucleon collisions, R. G. Glasser—218
Fredholm theory of scattering in given time-dependent field, Abdus Salam and P. T. Matthews—690
High energy nucleon scattering and isobars, R. B. Raphael and J. Schwinger—373(A)
Scattering of fast N_2 molecules by N_2, I. Amdur and W. T. Lindsay—344(A)
Variational calculation of high energy scattering by Yukawa potential, David S. Saxon and E. Gerjuoy—373(A)
Scattering of α-Particles
Elastic scattering of α-particles by C, Richard William Hill—845; By O, John R. Cameron—839
Precision α-α scattering at low energies, G. M. Temmer and N. P. Heydenburg—340(A)
Scattering of Atoms and Molecules (see **Atomic and Molecular Beams**)
Scattering of Deuterons
Inelastic scattering from B^{10}, C. K. Bockelman, C. P. Browne, A. Sperduto, and W. W. Bueckner—340(A); From N^{14} and Li^6, C. P. Browne, C. K. Bockelman, W. W. Buechner, and A. Sperduto—340(A)
n-d and *p-d* scattering in *S* wave region, R. L. Zimmerman, D. I. Cooper, and D. H. Frisch—339(A)
Scattering of Electrons and Positrons
Deflection of high energy electrons in magnetized Fe, Stephen Berko and Frank L. Hereford—341(A)
Excitation of molecular rotation-vibration by electron impact, Philip M. Morse—51
Investigation of electron distribution in atoms by electron diffraction, L. S. Bartell and L. O. Brockway—833
Scattering of electrons by H atoms, Howard Boyet and Sidney Borowitz—341(A)
Scattering of high energy electrons by nuclei, E. C. Raka, C. L. Hammer, and R. W. Pidd—341(A); C. L. Hammer, E. C. Raka, and R. W. Pidd—341(A)
Transmission of electrons through thin metallic foils, C. H. Chang, C. S. Cook, and H. Primakoff—544
Scattering of Mesons (see also **Mesons; Nuclear Reactions Induced by Mesons**)
Charge-exchange scattering of 40-Mev π-mesons in H and D, A. Roberts and J. Tinlot—951
Covariant meson-nucleon equation, Stanley Deser and Paul C. Martin—1072
Differential cross sections for scattering of 58-Mev π^+ mesons in H, D. Bodansky, A. Sachs, and J. Steinberger—996(L)
Elastic scattering of π-mesons by deuterons, Thomas A. Green—161(L)
Elastic scattering of pions in D, K. A. Brueckner—715(L)
Fourth order corrections to scattering of pions by non-relativistic nucleons, J. S. Bair and G. F. Chew—1065
Interactions of μ-mesons, W. D. Walker—234
Meson-nucleon scattering, Robert Karplus, Margaret Kivelson, and Paul C. Martin—1072
Meson-proton scattering, theoretical analysis, F. J. Dyson, S. S. Schweber, and W. M. Visscher—372(A); M. K. Sundaresan, E. E. Salpeter, and M. M. Ross—372(A)
Phase-shift analysis of scattering of positive mesons at 58 Mev, D. Bodansky, A. M. Sachs, and J. Steinberger—997(L)
Pion scattering and absorption cross sections in Pb and C, L. Lederman, H. Byfield, J. Kessler, and K. Rogers—344(A)
Positive pion scattering in H, Gerson Goldhaber and Leon Lederman—343(A)
Recoil effects in meson-nucleon scattering, E. M. Henley and M. A. Ruderman—719(L)
Sign of phase shifts in meson-nucleon scattering, H. A. Bethe—994(L)
Scattering of Neutrons
Angular distribution of elastically scattered 1-Mev neutrons, M. Walt and H. H. Barschall—714(L)
Elastic scattering of neutrons from paramagnetic rare earth atoms, G. T. Trammell—355(A)
Energy distribution of slow neutrons scattered in crystals, David A. Kleinman—355(A)
Interaction of 14-Mev neutrons with protons and deuterons, A. H. Armstrong, J. C. Allred, and L. Rosen—340(A)
Measurement of transport mean free path of thermal neutrons in D_2O by B poisoning method, S. W. Kash and D. C. Woods—564
n-d and *p-d* scattering in *S* wave region, R. L. Zimmerman, D. I. Cooper, and D. H. Frisch—339(A)

n-p scattering near 180° at 94 Mev, W. Selove, K. Strauch, and F. Titus—339(A)
Neutron diffraction studies of antiferromagnetism in MnF_2 and some isomorphous carbons, R. A. Erickson—779
Neutron diffraction studies on various ferromagnetic alloys, M. K. Wilkinson and C. G. Shull—374(A)
Neutron diffraction study of $MgFe_2O_4$, L. M. Corliss, J. M. Hastings, and F. G. Brockman—1013
Neutron-electron interaction, D. J. Hughes, J. A. Harvey, M. D. Goldberg, and Marilyn J. Stafne—497(L)
Orbital effect in neutron-electron magnetic scattering, W. H. Kleiner—168(L)
Paramagnetic scattering of neutrons by trivalent ions of Nd and Er, W. C. Keohler and E. O. Wollan—354(A)
Resonance scattering in In, L. B. Borst—354(A); 859
Scattering of slow neutrons by O_2 molecules, O. Halpern and G. L. Appleton—869
Scattering of slow neutrons by *ortho-* and *para*-hydrogen, A. T. Stewart and G. L. Squires—1125(L)
Thermal energy relaxation length of Ra-Be neutrons in water, Jay Tittman—256
Total neutron scattering cross sections of polyethylene and C at 1.32 Mev, C. L. Storrs and D. H. Frisch—339(A)
Variational principle for n-p scattering with tensor forces, L. C. Biedenharn and John M. Blatt—365(A)

Scattering of Protons
Angular distributions of 21-Mev protons elastically scattered by various nuclei, R. V. Neidigh and B. L. Cohen—340(A)
Differential cross section for elastic p-p scattering at 435 Mev, W. E. Mott, R. B. Sutton, J. G. Fox, and J. A. Kane—712(L)
Inelastic scattering from B^{10}, C. K. Bockelman, C. P. Browne, A. Sperduto, and W. W. Buechner—340(A); From N^{14} and Li^6, C. P. Browne, C. K. Bockelman, W. W. Buechner, and A. Sperduto—340(A)
n-d and p-d scattering in S wave region, R. L. Zimmerman, D. I. Cooper, and D. H. Frisch—339(A)
p-p scattering, H. H. Hall and J. L. Powell—912
p-p scattering at 32.0 Mev, Bruce Cork—1129(L)
p-p scattering at 435 Mev, W. E. Mott and R. B. Sutton—339(A)
p-p scattering from 1.8 to 4.2 Mev, H. R. Worthington, J. N. McGruer, and D. E. Findley—899
p-p scattering in interference minimum region, D. I. Cooper, D. H. Frisch, and R. L. Zimmerman—339(A)
Possible breakdown of isotopic spin and charge parity selection rules, D. H. Wilkinson—721(L)
Purity of isotopic spin of charge parity states, G. A. Jones and D. H. Wilkinson—722(L)

Scattering of Radiation (see **Radiation; X-Rays**)
Scintillation Counters (see **Methods and Instruments**)
Secondary Emission (see **Electrical Properties**)

Semiconductors
Adiabatic Hall effect in semiconductors, V. A. Johnson and F. M. Shipley—523
Chemical equilibria involving electrons as independent chemical entities in impurity semiconductors, Howard Reiss—336(A)
Comparison of Cu-doped Ge with heat treated Ge, F. J. Morin and J. P. Maita—337(A)
Cyclotron resonances, magnetoresistance, and Brillouin zones in semiconductors, W. Shockley—491(L)
Diffusion of injected carriers in semiconductor of mixed conductivity type, Harvey Brooks—336(A)
Effect of surface states in diode rectification theory, M. Cutler—337(A)
Electron spin resonance in Si semiconductor, A. M. Portis, A. F. Kip, C. Kittel, and W. H. Brattain—988(L)
High field mobility in Ge with impurity scattering dominant, E. M. Conwell—769
High impedance field-effect Si transistor, G. L. Pearson—336(A)
Impurity diffusion and space charge layers in fused-impurity p-n junction, John S. Saby and W. C. Dunlap, Jr.—630; 1131(E)
Infrared absorption characteristics of thermiated Ge, D. H. Rank and D. C. Cronemeyer—202
Microwave determination of electrical properties of Ge, James M. Goldey and Sanborn C. Brown—336(A)
Mobility of holes and electrons in high electric fields, E. J. Ryder—766
n-type conduction on p-type Ge surfaces, W. L. Brown and W. Shockley—336(A)
Polarization capacitance effects in photoconductors and semiconductors, J. Ross MacDonald—364(A)
Pressure dependence of resistivity of Ge, William Paul—336(A)
Recombination rate in Ge by observation of pulsed reverse characteristic, E. M. Pell—278
Semiconducting intermetallic compounds, R. G. Breckenridge—488(L)
Space-charge limited emission, W. Shockley and R. C. Prim—753
Space-charge limited hole current in Ge, G. C. Dacey—759
Temporary traps in Si and Ge, J. R. Haynes and J. A. Hornbeck—152(L)
Ultrasonic attenuation in Ge, Rohn Truell and Joseph Bronzo—152(L)

Shock Waves (see **Fluid Dynamics**)
Solid State (see **Crystalline State**)
Solutions (see **Liquids**)
Sound (see **Acoustics**)
Spallation (see **Nuclear Reactions**)
Spark Discharge (see **Electrical Discharges**)
Specific Heat (see **Thermal Properties**)
Spectra, Atomic (see **Atomic Structure and Spectra**)

Spectra, General
Quantum theory of spectral line broadening, Stanley Bloom and Harry Margenau—791

Spectra, Molecular (see **Molecular Structure and Spectra**)
Spectra, Nuclear (see **Nuclear Spectra**)
Spectroscopy Technique (see **Methods and Instruments**)
Spinor Fields (see **Field Theory**)
Standards (see **Constants, Standards, Units**)
Stark Effect (see **Atomic Structure and Spectra**)

Statistical Mechanics and Thermodynamics
Cluster theory of saturated vapor pressure of He isotope mixtures, William Band and Raymond A. Nelson—744
Interpolation of vapor pressures, Raymond Madrazo, Jr., and George Antonoff—385(A)
Statistical mechanics of irreversible processes in fluids, Melville S. Green—376(A)
Theory of condensation, A. J. F. Siegert—344(A)
Theory of fusion and condensation, Arnold J. F. Siegert—97
Thermodynamics of He film, O. K. Rice and Benjamin Widom—987(L)

Statistical Methods (see **Mathematical Methods**)

Superconductivity
Aspects of 2-fluid model of superconductivity, E. Maxwell and P. M. Marcus—346(A)
Paramagnetic effect in superconductors, Tom S. Teasdale and H. E. Rorschach, Jr.—709(L)
Statistical basis of 2-fluid models of superconductivity, Paul M. Marcus—346(A)
Studies of compounds for superconductivity, W. T. Ziegler and R. A. Young—115

Superconductivity (Continued)
Superconducting compounds of nonsuperconducting elements, B. T. Matthias—487(L)
Temperature, current, magnetic field phase diagram, W. Meissner, F. Schmeissner, and H. Meissner—709(L)
Supersonics (see **Fluid Dynamics**)

Thermal Conductivity (see **Thermal Properties**)
Thermal Diffusion (see **Diffusion**)
Thermal Expansion (see **Thermal Properties**)
Thermal Properties
Apparatus for measuring thermal conductivity of metals in vacuum at high temperatures, Marvin Moskowitz—379(A)
Method of measuring specific heats at very low temperatures, D. H. Howling, E. Mendoza, and J. E. Zimmerman—347(A)
Specific heat measurements on pure metals at low temperatures, M. Horowitz and J. G. Daunt—379(A)
Specific heats of ferrites, J. Samuel Smart—374(A)
Thermal conductivity values for $BaTiO_3$, Stanley S. Ballard and Kathryn A. McCarthy—375(A)
Thermal resistivity of Hg in intermediate state, J. K. Hulm—1116(L)
Thermal Radiation (see **Radiation**)
Thermionic Emission (see **Electrical Properties**)
Thermodynamics (see **Statistical Mechanics and Thermodynamics**)
Thermoelectric Effect (see **Electrical Properties**)
Thermoluminescence (see **Luminescence**)
Thermomagnetic Effect (see **Magnetic Properties**)
Total Cross Sections (see **Electrons and Positrons; Nuclear Reactions**)
Transmutation (see **Nuclear Reactions**)

Uncertainty Principle (see **Quantum Mechanics**)
Units (see **Constants, Standards, Units**)

Vacuum Tubes (see **Methods and Instruments**)
Van der Waals Forces (see **Molecular Structure and Spectra**)
Viscosity (see **Liquids**)

Wave Mechanics (see **Quantum Mechanics**)
Work Function (see **Electrical Properties**)

X-Rays
Enhancement of x-ray induced absorption bands in alkaline-earth compounds, James H. Schulman, Robert J. Ginther, and Russell D. Kirk—351(A)
Fission of U with 16-Mev x-rays, Harold G. Richter and Charles D. Coryell—389(A)
Magnetic susceptibility and x-ray diffraction measurements of VO and TiO, T. R. McGuire and Selma Greenwald—373(A)
Penetration and diffusion of hard x-rays: Polarization effects, L. V. Spencer and Charles Wolff—510
Ross filter design for x-ray scattering experiments, W. L. Gordon and J. A. Soules—346(A)
Single crystal high temperature heater for x-ray spectrometer, R. Lefker, A. deBretteville, Jr., and J. S. Dodd—345(A)
Small angle scattering of x-rays from cold worked solids, D. L. Dexter—1007
Small angle x-ray scattering in deformed crystals, S. Hayes, R. Smoluchowski, and R. W. Turner—350(A)
Soft x-ray absorption of Fe and Fe_2O_3, D. E. Carter and M. P. Givens—379(A)
X-ray investigation on effect of mechanical surface treatment on lattice regularity of quartz and calcite, J. C. M. Brentano and T. L. Thourson—351(A)
X-ray path through calcite for anomalous transmission, Guenter Schwarz, L. Carlton Brown, and G. L. Rogosa—351(A)

Zeeman Effect (see **Atomic Structure and Spectra**)

CONTENTS—*Continued*

Letters to the Editor:

Thermal Resistivity of Mercury in the Intermediate State . . . . . J. K. Hulm 1116

λ-Transition in Liquid Helium . . . . . R. P. Feynman 1116

Heat Pulses in Helium II between 0.1°K and 1.9°K . . . . . H. C. Kramers, F. A. W. van den Burg, and C. J. Gorter 1117

Fountain Effect in Helium II below 1°K . . . . . G. J. C. Bots and C. J. Gorter 1117

OH in the Airglow at High Latitudes . . . Joseph W. Chamberlain and Norman J. Oliver 1118

Influence of the Interaction of Electric Field Gradients and Nuclear Electric Quadrupole Moments in Angular Correlation . . . . . Rolf M. Steffen 1119

Search for 1-Mev Gamma from F^{18} Decay . F. Boehm, D. C. Peaslee, and V. Perez-Mendez 1119

Alpha-Particle Ionization in Pure Gases and the Average Energy to Make an Ion Pair . . . . . William P. Jesse and John Sadauskis 1120

Neutron Activation of Ca^{48} . . . . . L. G. Cook and K. D. Shafer 1121

Neutron Capture Cross Section of Rn^{220} . . . . . A. P. Baerg 1121

β-Decay of Li^9 . . . . . D. S. Bunbury 1121

Unusual Example of F^{18} Decay . . . . . R. W. Thompson, A. V. Buskirk, L. R. Etter, C. J. Karzmark, and R. H. Rediker 1122

O^{14} β-Decay and the Fermi Interaction . . . . . M. E. Rose 1123

Decay of Cr^{49} . . . . . Bernd Crasemann and Harry T. Easterday 1124

Scattering of Slow Neutrons by *Ortho-* and *Para*-Hydrogen . . . . . A. T. Stewart and G. L. Squires 1125

Noncentral Force Matrix Elements for the Nuclear d^n Configuration . . . L. W. Longdon 1125

Observation of F^{18} Particles Produced at the Cosmotron . . . . . W. B. Fowler, R. P. Shutt, A. M. Thorndike, and W. L. Whittemore 1126

K Masses . . . . . J. Crussard, L. Leprince-Ringuet, D. Morellet, A. Orkin-Lecourtois, and J. Tremoley 1127

Energy Levels of C^{13} from the $Be^9(\alpha,n)C^{13}$ Reaction . . . . . L. E. Beghian, H. H. Halban, T. Hussin, and L. G. Sanders 1129

Proton-Proton Scattering at 32.0 Mev . . . . . Bruce Cork 1129

Spin and Magnetic Moment of Ca^{43} . . . . . C. D. Jeffries 1130

Errata 1131

Proceedings of the American Physical Society:

Minutes of the 1953 Spring Meeting of the Ohio Section at The Ohio State University, Columbus, Ohio, April 24 and 25, 1953 1131

Author Index to Volume 90 1133

Analytic Subject Index to Volume 90 1147

CONTENTS

THE PHYSICAL REVIEW SECOND SERIES, VOLUME 93, NO. 6 JUNE 15, 1954

Small Angle Scattering of X-Rays from Cold-Worked Gold . . . . . D. L. Dexter 1407

Neutron Diffraction Study of Magnetism in Cerium . . . L. M. Corliss, J. M. Hastings, and F. G. Brockhouse 1413

Broadening and Shift of the Second Doublet of the Rubidium Absorption Series under Increased Pressures of Argon and Helium . . . . . Shang-Yi Ch'en and Donald A. Keller 1419

Forces Between Hydrogen Molecules . . . . . Arthur A. Evett and Henry Margenau 1421

Absorption Line Width in the Infrared Spectrum of Atmospheric Carbon Dioxide . . . . . Arthur Adel 1426

Polarization of Bremsstrahlung Radiation . . . . . R. L. Gluckstern, M. H. Hull, Jr., and G. Breit 1426

Polarization Dependence of the Integrated Bremsstrahlung Cross Section . . . . . R. L. Gluckstern and M. H. Hull, Jr. 1430

Production of Polarized Particles in Nuclear Reactions . . . . . A. Simon and T. A. Welton 1436

Azimuthal Distribution of Photoelectrons Produced by 0.5-Mev Polarized Photons . . . . . Frank L. Hereford and James P. Kesper 1443

Isotopic Constitution of Silicon, Germanium, and Hafnium . . . . . John H. Reynolds 1447

Angular Distribution of $Li^6(n,\alpha)H^3$ for Neutrons of 200, 270, 400, and 600 kev . . . . . Lillian E. Darlington, Jack Hanna, Henry M. Mann, and James H. Roberts 1449

Production of Fissionable Isotopes in a Thermal Reactor . . . . . Lawrence Baylor Robinson 1454

Nuclear Hyperfine Structure of Mn^{55} . . . . . Mendel Sachs 1456

Continuous Gamma-Radiation Accompanying Internal Conversion in Sn^{119} . . . . . Harry R. Brown and Robert Spence 1461

Photodisintegration Cross Section of Beryllium at 2.189 Mev . . Bernard Hamermesh and Clyde Hurwitz 1463

Fourth-Order Corrections in the Scattering of Fluxs by Ferromagnetic Nucleons . . . . . J. S. Blair and G. F. Chew 1465

Properties of the Low Energy Nucleonic Component at Large Atmospheric Depths . . . . . J. A. Simpson and W. C. Fagot 1468

Note on Meson-Nucleon Scattering . . . . . Robert Karplus, Margaret Klevansz, and Paul C. Martin 1472

Covariant Meson-Nucleon Equation . . . . . Stanley Deser and Paul C. Martin 1473

Mass of Cosmic-Ray Mesons at Mountain Altitudes . . . . . Giulio Accoli 1479

Production of Heavy Mesons . . . . . L. S. Rothenberg 1487

Continuum in Special Relativity. II . . . . . Rudy Lurd 1489

Tamm-Dancoff Formalism and the Symmetric Pseudoscalar Theory of Nuclear Forces . Abraham Klein 1491

(continued on cover three)

LANCASTER PRESS, INC., LANCASTER, PA.